RESPONSE, ANALYSIS, AND DESIGN OF PILE GROUPS SUBJECTED TO STATIC & DYNAMIC LATERAL LOADS

By: Kyle Rollins, Ph.D.
Ryan Olsen
Jeffery Egbert
Kimball Olsen
Derek Jensen
Brian Garrett

Civil & Environmental
Engineering Department
Brigham Young University

Utah Department of Transportation
Research Division

June 2003

UDOT RESEARCH & DEVELOPMENT REPORT ABSTRACT

1. Report No. UT-03.03	2. Government Accession No.	3. Recipient's Catalog No.
4. Title and Subtitle RESPONSE, ANALYSIS, AND DESIGN OF PILE GROUPS SUBJECTED TO STATIC & DYNAMIC LATERAL LOADS	**5. Report Date** June 18, 2003	
	6. Performing Organization Code	
7. Author(s) Rollins, K.M., Olsen, R.J., Egbert, J.J., Olsen, K.G., Jensen, D.H., and Garrett, B.H.	**8. Performing Organization Report No.** BYU Report No. CEG 2003-02	
9. Performing Organization Name and Address Civil & Environmental Engineering Department Brigham Young University 368 CB, Provo, UT 84602	**10. Work Unit No.**	
	11. Contract No. 009171	
12. Sponsoring Agency Name and Address Douglas I. Anderson, P. E. Utah Department of Transportation 4501 So. 2700 W. Salt Lake City, Utah 84114-8410	**13. Type of Report and Period Covered** Final, 1999-2003	
	14. Sponsoring Agency Code	

15. Supplementary Notes

16. Abstract

Static and dynamic lateral load tests were performed on four full-scale pile groups driven at four different spacings. P-multipliers to account for group interaction effects were back-calculated for each test. P-multipliers were found to be a function of row position within the group but were independent of position within a row. Curves were developed to define p-mulipliers as a function of pile spacing. Using these p-multipliers along with soil properties obtained from site characterization work, excellent agreement between measured and computed response could be obtained. Dynamic load tests were performed using the Statnamic load system. Dynamic lateral resistance was consistently higher than the measured static resistance, however, resistance was dynamic resistance was greater for the virgin load than for reloading. Simple one degree-of-freedom models were successfully used to interpret the static load-deflection curve from the dynamic load-deflection curves. These analyses indicate that the increased dynamic lateral resistance was largely due to damping.

17. Key Words Laterally Loaded Pile Groups, Lateral Load Tests, Statnamic Load Tests, Dynamic Loading, Cyclic Loading	**18. Distribution Statement** Available: UDOT Research Division Box 148410 Salt Lake city, Utah 84114-8410 www.dot.state.ut.us/res	
19. Security Classification (of this report) N/A	**20. Security Classification (of this page)** N/A	**21. No. of Pages** **22. Price**

ACKNOWLEDGEMENTS

TABLE OF CONTENTS

IMPLEMENTATION SUMMARY

When pile groups are driven with center-to-center spacings less than eight pile diameters, interaction between shear zones produced by adjacent piles leads to a decrease in lateral pile resistance. As a result, the deflection and bending moments for piles in the group are significantly greater than would be expected for a single isolated pile at the same average load. In addition, maximum bending moments occur at greater depths than for a single isolated pile.

To account for these group interaction effects, the p-y curves used to define the lateral soil resistance (p) vs. lateral deflection (y) for a single pile must be reduced. This can be accomplished by multiplying the p value by a constant multiplier, known as a p-multiplier (P_m) as shown in Figure IS-1. As the pile spacing increases, there is less group interaction and the p-multiplier increases. Full-scale test results indicate that the appropriate P_m is a function of row location and that lateral resistance is independent of location within a row. Based on the results
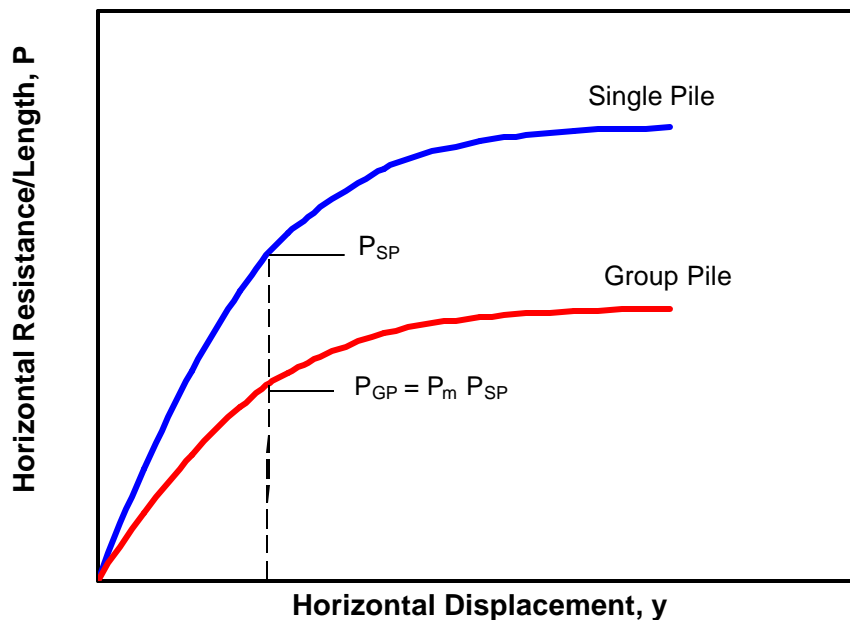
Figure IS-1 Use of P-multiplier to reduce single pile p-y curve to produce p-y curve for a pile within a group.

of the full-scale tests performed in this study, curves have been developed to define the relationship between P_m and pile spacing divided by pile diameter as shown in Figure IS-2. Separate curves are provided for piles in (1) the first or (lead) row, (2) the second row, and (3) the third or higher rows. The P_m values in Figure IS-2 are higher than those recommended by AASHTO for groups of drilled shafts.
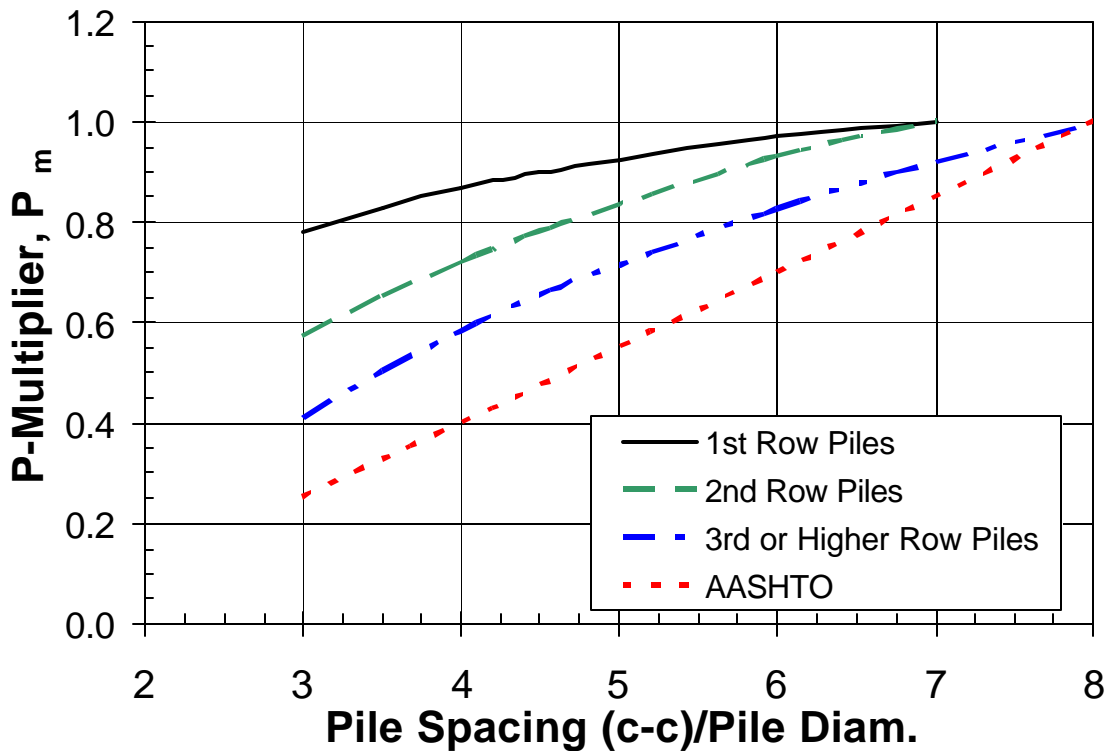
Figure IS-2 Recommended design curves for selecting p-multipliers (P_m) as a function of normalized pile spacing for 1st row piles, 2nd row piles and 3rd row or higher row piles.

Although these curves were developed based on tests in clay, they appear to give reasonable estimates of the behavior of pile groups in sand based on available full-scale and centrifuge testing (McVay et al, 1995). This study also suggests that the curves are not significantly affected by the pile diameter or pile head boundary condition.

Equations have also been developed to compute the p-multiplier (P_m) for each of the curves shown in Figure IS-2. The equations for each case are:

First (Lead) Row Piles: $P_m = 0.26\ln(s/d)+0.5 = 1.0$ (IS.1)

Second Row Piles: $P_m = 0.52\ln(s/d) = 1.0$ (IS.2)

Third or Higher Row Piles: $P_m = 0.60\ln(s/d)-0.25 = 1.0$ (IS.3)

where s is the center-to-center spacing between piles in the direction of loading and d is the width or outside diameter of the pile. An example problem demonstrating the use of the curves in Figure IS-2 is provided below.

EXAMPLE OF P-MULTIPLIER APPROACH

The total lateral load resistance of a group of 12 piles is to be determined. The piles are arranged in four rows of three piles each as shown in Figure IS-3 with a spacing of 1143 mm center to center in the direction of loading. Each pile is a 324 mm outside diameter steel pipe pile. Therefore, the s/d ratio is 1143/324 or 3.53. The p-multiplier values for this spacing were determined using equations IS.1, IS.2, and IS.3 and the results are shown below.
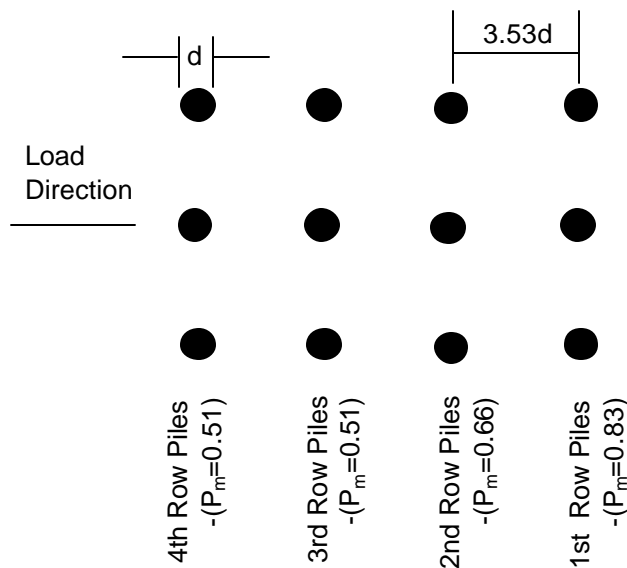
Figure IS-3 Arrangement of piles in the pile group for example problem.

First (Lead) Row Piles: $P_m = 0.26\ln(3.53)+0.5 = 0.83$ $= 1.0$ OK

Second Row Piles: $P_m = 0.52\ln(3.53) = 0.66$ $= 1.0$ OK

Third and Higher Row Piles: $P_m = 0.60\ln(3.53)-0.25 = 0.51$ $= 1.0$ OK

Lateral load analyses can be performed using the computer program LPILE (Reese and Wang, 1997) or COM624 with these three P_m values to account for group effects. The computed load vs. deflection curves for a single pile with P_m values of 1.0, 0.83, 0.66 and 0.51 are shown in Figure IS-4. As the P_m value decreases, the computed deflection increases for a given load.
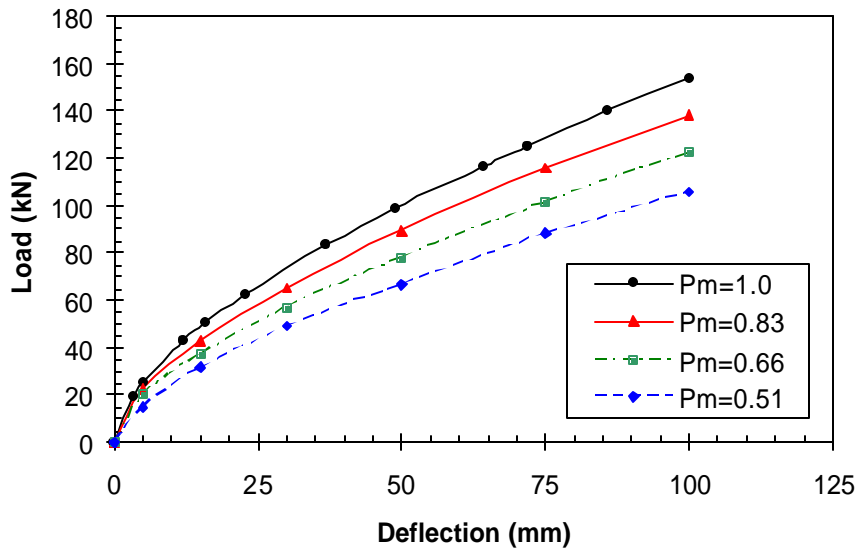
Figure IS-4 Computed load-deflection curves for single piles with various P_m values.

To obtain the total load-deflection curve for the group, the resistance for each pile is summed at a given displacement using the appropriate single pile load-deflection curve in Figure IS-4. An example calculation of the total group load for a deflection of 75 mm is shown below.

Example Calculation of Total Group Load at 75 mm Displacement

1st (Lead) Row Load = 116 kN at 75 mm
2nd Row Load = 101.5 kN at 75 mm
3rd and 4th Row Load = 88 kN at 75 mm

Total Load = 3 piles x 116 kN + 3 piles x 101.5 kN + 6 piles x 88 kN = 1180.5 kN
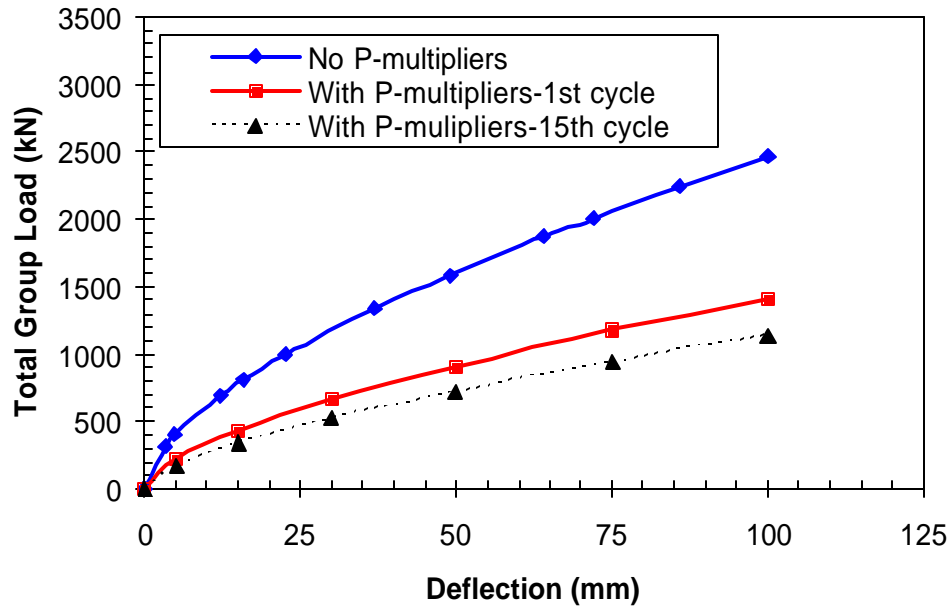
Figure IS-5 Total group load vs deflection curves computed using LPILE with p-multipliers along with curve with no P-multiplier to account for group interaction effects.

The total group load vs. deflection curve computed using LPILE with consideration of appropriate p-multipliers is shown in Figure IS-5. The total load vs. deflection curve assuming no group interaction (no p-multipliers) is also shown in Figure IS-5. In this case, failure to account for group interaction effects would lead to a 75% overestimation of lateral resistance. The results of this study suggest that the peak load vs. deflection curve after 15 cycles of loading (typical of a M7.5 earthquake) would decrease the peak load to about 80% of its original value as shown in Figure IS-5. Computer programs such as GROUP (Reese et al, 1996) and PBPier handle the summation process and allow the user to define the p-multipliers for each row in the group.

The maximum bending moment versus load or bending moment versus depth curves can also be determined for piles in the group using the appropriate p-mulipliers. In general, the worst case curves should be used for all piles since the load direction may reverse, changing 1st row piles into 3rd row piles.

DYNAMIC RESISTANCE

The statnamic load tests conducted during this study consistently showed that the dynamic lateral resistance was higher than that measured during static loading. Dynamic resistance was significantly higher during virgin loading than during reloading. Simplified analyses indicate that the difference is largely attributable to damping. Additional analyses are necessary to develop damping coefficients as a function of depth along the length of the pile. Using a one-degree-of-freedom model, the dynamic load-deflection curves measured during the statnamic testing can be used to determine the static load-deflection curves with reasonable accuracy for design work.

RESEARCH SUMMARY

BACKGROUND

The lateral load capacity of pile foundations is critically important in the design of highway structures which may be subjected to earthquake motions. Although fairly reliable methods have been developed for predicting the lateral capacity of single piles under static loads, there is very little information to guide engineers in the design of closely spaced pile groups with spacings less than about 6 pile diameters particularly under dynamic loads. Because of the high cost and logistical difficulty of conducting lateral load tests on pile groups, only a few full-scale load test results are available that show the distribution of load within a pile group (Brown et al, 1987; Brown et al, 1988; Meimon et al, 1986; Rollins et al, 1998; Ruesta and Townsend, 1997). These tests have all involved static or quasi-static loadings.

Nevertheless, the data from these limited field tests indicate that piles in groups will undergo significantly more displacement and higher bending moments for a given load per pile than will a single isolated pile (Brown et al, 1987; Brown et al, 1988; Meimon et al, 1986; Rollins et al, 1998; Ruesta and Townsend, 1997). The tendency for a pile in a trailing row to exhibit less lateral resistance because of interference with the failure surface of the pile in front of it is commonly referred to as "shadowing". This shadowing or group interaction effect is thought to become less significant as the spacing between piles increases and there is less overlap between adjacent failure planes.

The lateral response of piles is typically analyzed using finite-difference methods. The pile is modeled as a beam and the soil is modeled using non-linear springs that are attached to the pile. The non-linear springs are defined using p-y curves at regular depth intervals, where p represents the lateral soil resistance per unit length of the pile and the y is the lateral deflection of

the pile. One method of accounting for the shadowing or group reduction effects is to reduce the single pile p-y curve using a p-multiplier as suggested by Brown et al (1988). With this approach, the soil resistance, p, is scaled down by a constant factor. The appropriate p-multiplier is likely dependent on a number of factors such as pile spacing, row position in the group, deflection level and soil type.

Because of the dearth of experimental data, computer programs for pile groups have not been thoroughly validated and empirical methods such as those using p-multipliers are extremely restricted in their application. For example, p-multipliers from full-scale tests are only available for spacings of three pile diameters and typically for three rows or less. As a result, engineers are forced to design pile groups in a very conservative manner to deal with the uncertainty. Although numerical and centrifuge models can provide some guidance regarding these issues, a reasonable number of full-scale load tests are necessary to verify these models and provide ground truth information.

RESEARCH OBJECTIVES

This pile group load testing research had the following objectives:

1. Evaluate the effect of pile spacing on measured p-multipliers and develop design curve for p-multipliers as a function of pile spacing.
2. Determine the validity of the p-multiplier concept for a larger (5-row) pile group and determine if p-multiplier values remain constant beyond the third row.
3. Examine the influence of pile diameter on lateral load resistance and p-multiplier values.
4. Determine the effect of cyclic loading and gap formation in clays on the measured group effects and p-multipliers.
5. Examine the effect of cyclic loading and gap formation in clays on the measured dynamic resistance.
6. Evaluate the effect of pile diameter and stiffness on p-multiplier values for pile groups.
7. Evaluate the effect of axial tension and compression on the lateral resistance of pile groups.

8. Provide a well-documented case histories for use in evaluating and calibrating computer and physical models.

To achieve the objectives of the study, a series of full-scale static and dynamic lateral load tests were conducted on two single piles and four pile groups at different center to center spacings at a test site on the Interstate 15 alignment in Salt Lake City as shown in Figure RS-1.
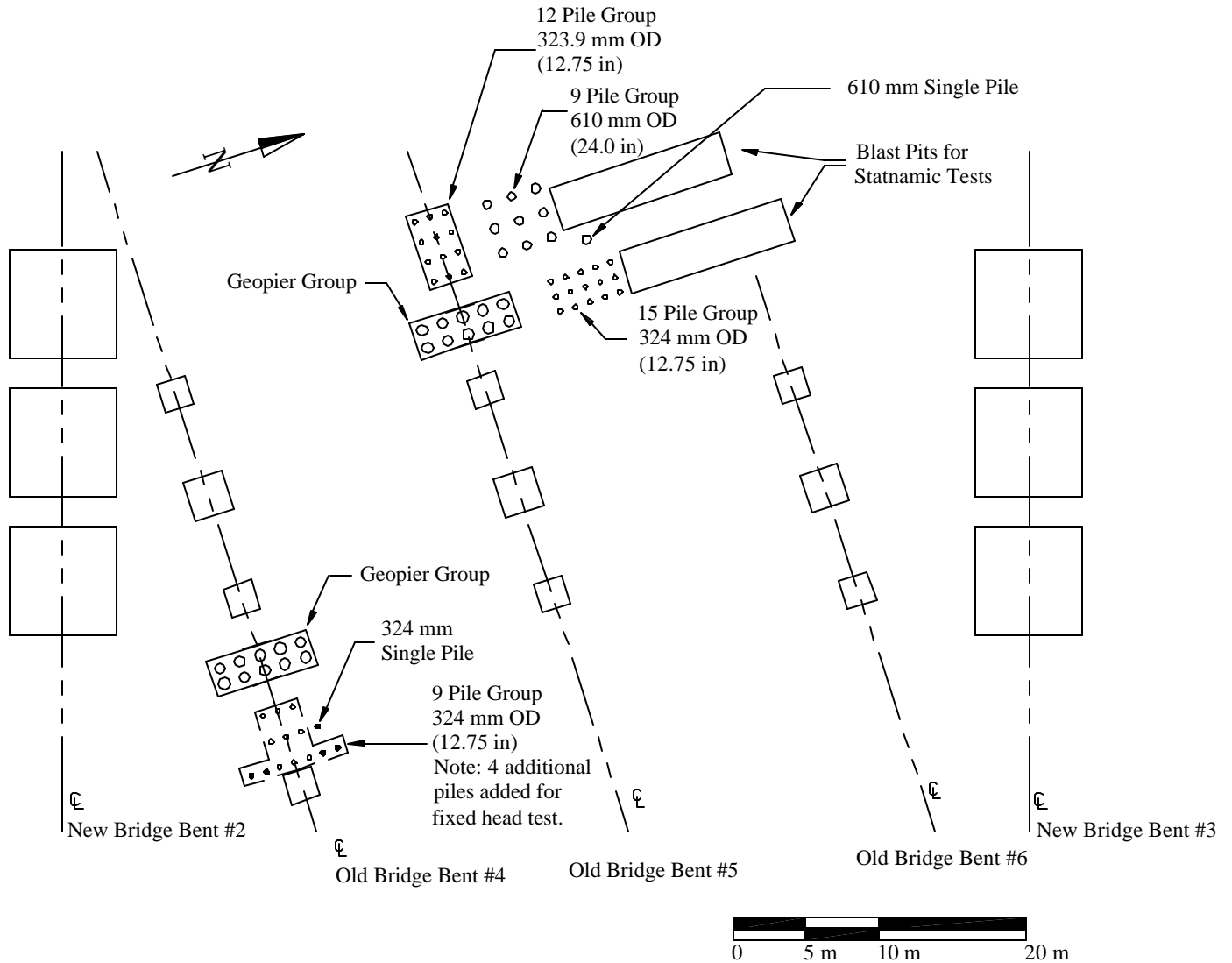
Figure RS-1 Layout of two single piles and four pile groups at site below South Temple overpass on I-15 corridor.

SITE CHARACTERIZATION

The subsurface profile was characterized using a variety of methods to provide basic geotechnical data for use in subsequent computer analyses of the test results. Based on the results of the field and laboratory testing the soil profile shown in Figure RS-2 was developed. The soil profile generally consists of medium stiff clays with some sand layers near the surface. The sand layers were in a medium compact density state. The medium stiff clay was underlain by soft sensitive clays which were in turn underlain by interbedded layers of silty clay and sand. Cone penetration test (CPT) soundings were performed at each test foundation to define the stratigraphy and the variations across the site. These tests confirmed that the profiles were very similar at each site. Logs of the average CPT cone tip resistance and friction ratio for the site are presented in Figure RS-2. Additional in-situ testing included borehole shear tests, vane shear tests, standard penetration tests, cone pressuremeter tests, and shear wave velocity tests. Undisturbed samples and disturbed samples were also obtained for laboratory strength, consolidation and index testing.

The vane shear test was the primary means for evaluating the undrained shear strength of the clay and the results from these tests are also shown in Figure RS-2. In addition, undrained shear strength was obtained from unconfined compression tests on undisturbed samples and from correlations with the CPT cone resistance. In general, the agreement between the strength evaluation methods was very good. The undrained strength values used subsequently in the analysis are also identified in Figure RS-2 and are in good agreement with the measured strength. The pre-consolidation pressures obtained from the consolidation testing indicate that the clay is overconsolidated near the ground surface but that overconsolidation decreases with depth. The water table was typically located 1.07 m below the ground surface during the testing.
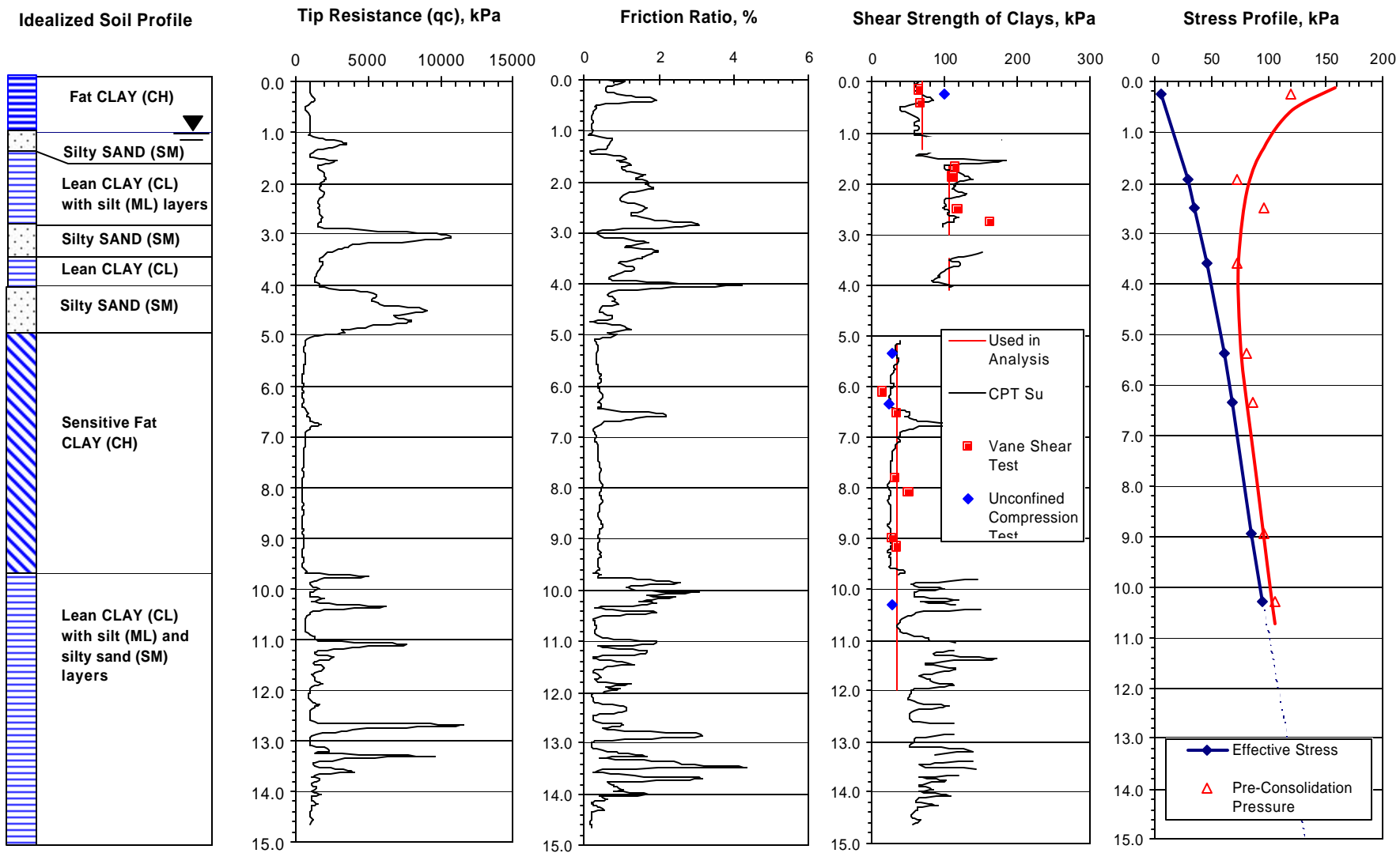
Figure RS-2 Interpreted soil profile along with results from field and laboratory testing.

RS-5

CYCLIC LATERAL LOAD TESTING OF SINGLE PILES

Initially, cyclic load tests were performed on two isolated single piles driven to a depth of approximately 11.5 m. These tests were necessary to provide a comparison to the behavior of the pile groups. One test pile was a closed-end 324 mm OD steel pipe pile (9 mm wall thickness) while the other was an open-end 610 mm OD steel pipe pile (12.7 mm wall thickness). Strain gages were placed on opposite faces of the pile at 10 depth levels to determine bending moment profiles versus depth. Load was applied in approximately 10 increments with a hydraulic jack. Applied loads were measured with a load cell while pile head deflection and rotation were measured with LVDTs. For each deflection increment, 15 load cycles were applied to simulate the cyclic loading typical of an earthquake and to evaluate the change in lateral resistance due to cyclic loading.

The peak load-deflection curves for the 1st and 15th cycles for the two single pile tests are presented in Figures 3 and 4. For a given deflection, the drop in peak load from the 1st to the 15th cycle is about 15%. Most of this drop occurs in two to three cycles. Although the difference in the peak load-deflection curves for the 1st and 15th cycles is relatively small, these curves are deceptive because they do not show the full load-deflection curve before the peak load. The complete load-deflection curves for each fifteenth cycle are included in Figure RS-3. At deflections short of the previous peak deflection, the load during the 15th cycle is significantly below that for the 1st cycle. The curves for the fifteenth cycle appear to be composed of two segments. The lower part of the curve is relatively linear. The slope of the upper part of the curve increases rapidly and the curve becomes parabolic with a concave upward shape.

This change in slope of the load versus deflection curve is readily explained by presence of the gap which developed around the pile. During the first cycle, the applied load is resisted by
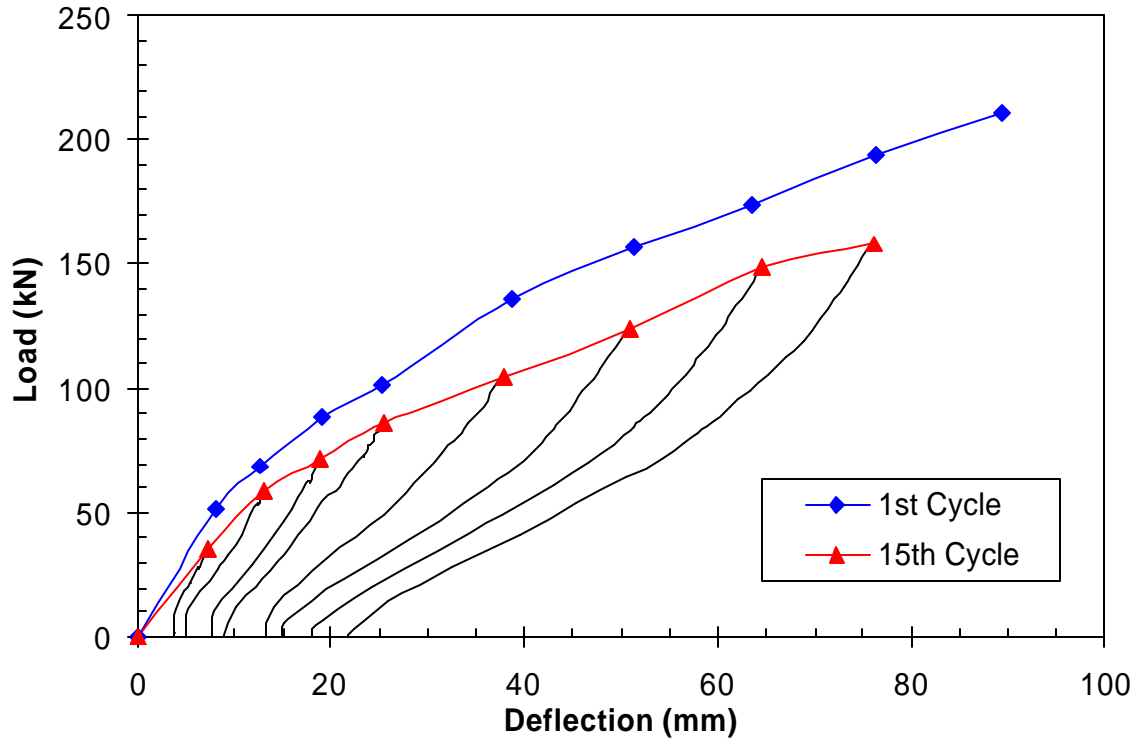
Figure RS-3 Load-deflection curves for the peak points on the first and fifteenth cycles along with the complete load-deflection curve for each fifteenth cycle on the 324 mm pile test.
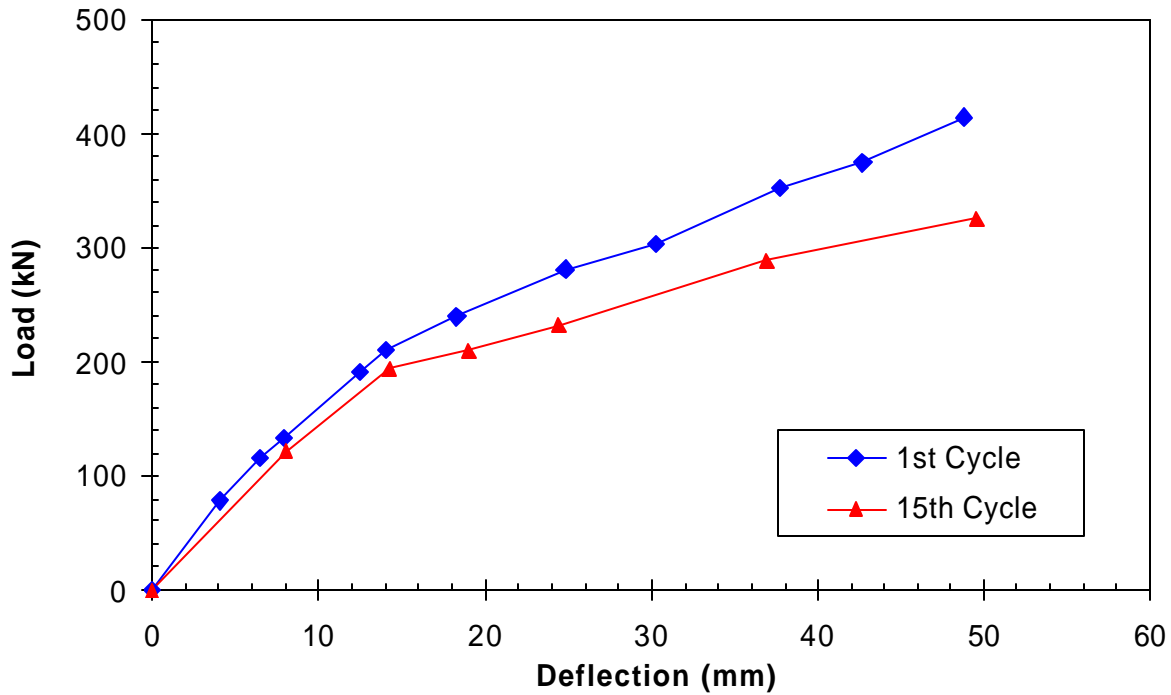
 Figure RS-4 Load versus deflection curves for the peak points during 1st and 15th cycles of load during lateral load test on 610 mm OD pipe pile.
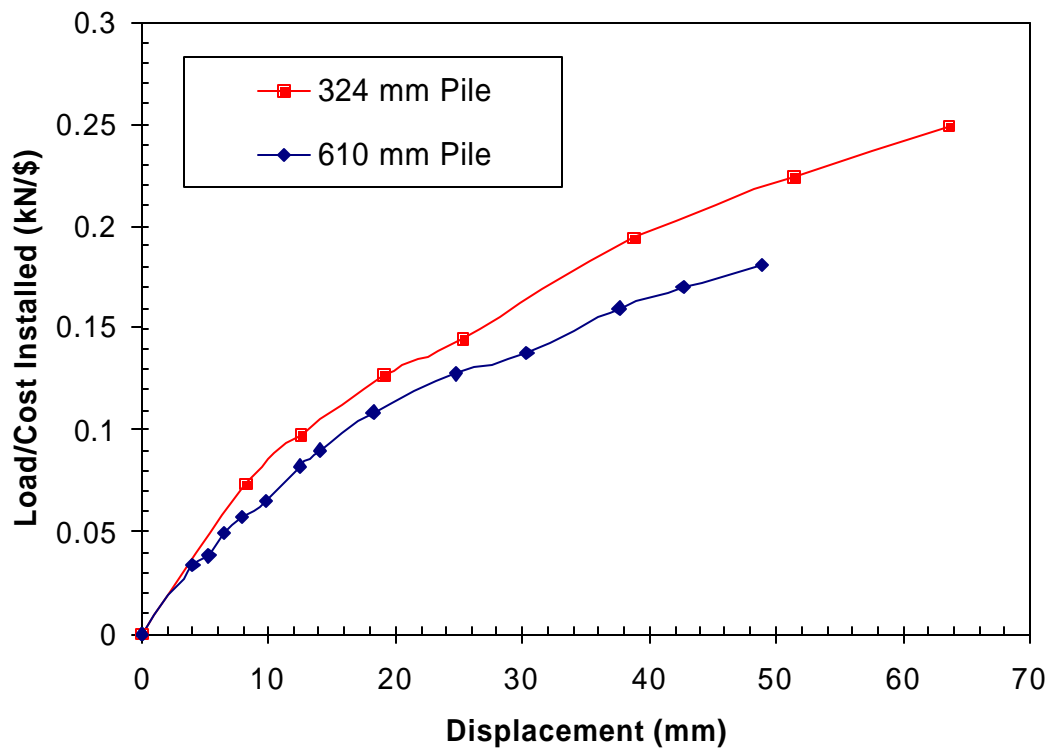
Figure RS-5 Comparison of lateral load per installed cost versus displacement curves for the 324 and 610 mm diameter single pipe piles.
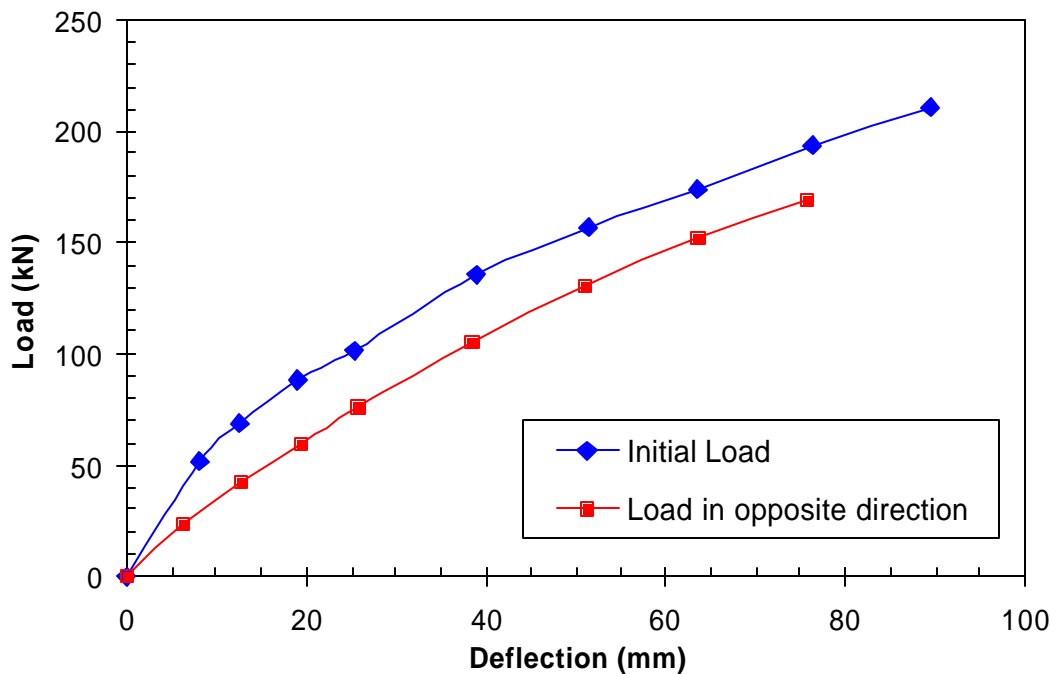
Figure RS-6 Comparison of initial laod versus deflection curve for 324 mm single pile with curve for subsequent test in the opposite direction.

both the pile and the soil near the ground surface. During the subsequent loadings, a gap developed between the soil and pile due to the previous loading. For deflections less than the width of that gap, the primary resistance to loading is due to the pile stiffness. This explains the approximately linear relationship between load and deflection when the pile is pushed through the gapped region. As the deflection approached the previously achieved maximum deflection, the load-deflection relationship became non-linear with a concave upward shape. This increase in slope of the upper part of the curve is due to the pile engaging the soil and receiving progressively more lateral soil resistance.

Although the lateral load carried by the 610 mm diameter pile was about two times higher than that carried by the 324 mm diameter pile at the same deflection, the cost to buy and install the 610 mm pile was more than two times greater than that for the 324 mm pile. When the lateral load in each case was normalized by the cost, as shown in Figure RS-5, the 324 mm pile was somewhat more efficient than the 610 mm pile. This may be due to the fact that strength decreases with depth in this case and may not be true in all cases.

A load test was also performed on a 324 mm single pile to evaluate the lateral resistance that would be provided if the pile were loaded in the opposite direction from the direction of the initial loading. This test was necessary to provide a comparison single pile for the 15 pile group which was also loaded in the opposite direction from the initial direction of loading. The load deflection curves for the two tests are shown in Figure RS-6 and the curve for the reloading test is considerably softer and more linear than the curve for the initial load test. At greater deflections the curves tend to converge. These features are a result of of gaps around the entire perimeter of the pile which reduce the soil resistance particularly at small deflection levels even when the pile is loaded in a direction that is different from the initial direction of loading.

CYCLIC LATERAL LOAD TESTING OF FOUR FREE-HEAD PILE GROUPS

Cyclic load testing was also performed on four separate pile groups at different spacings. Three of the pile groups involved 324 mm diameter piles. One group consisted of piles in a 3 x 3 arrangement with a longitudinal spacing of 5.6 pile diameters on centers. A second group consisted of piles in 3 x 4 arrangement with a spacing of 4.4 pile diameters and the third group consisted of piles in a 3 x 5 arrangement with a spacing of 3.3 pile diameters. The fourth pile group consisted of 610 mm diameter piles in a 3 x 3 arrangement with a spacing of 3.0 pile diameters on centers. The load was applied to a load frame using two 1300 kN hydraulic jacks and measured with load cells.

The load frame was designed to provide the same displacement at each pile location and be essentially rigid in comparison with the stiffness of the piles. Each pile was attached to the load frame by a tie-rod with a moment free connection. Strain gages attached to each tie-rod provided a continuous readout of the load carried by each individual pile during the test. Pile head deflection and rotation was measured using LVDT's attached to an independent reference frame. Strain gages were placed on opposite faces of one pile in each row at 10 depth levels. The same sequence of loading described for the single pile test was employed for the pile group tests.

Load versus Deflection Relationships

Plots of average pile load versus average group deflection for each pile group are presented in Figures 7 through 10 for each pile group. The curves are grouped by row with row

.
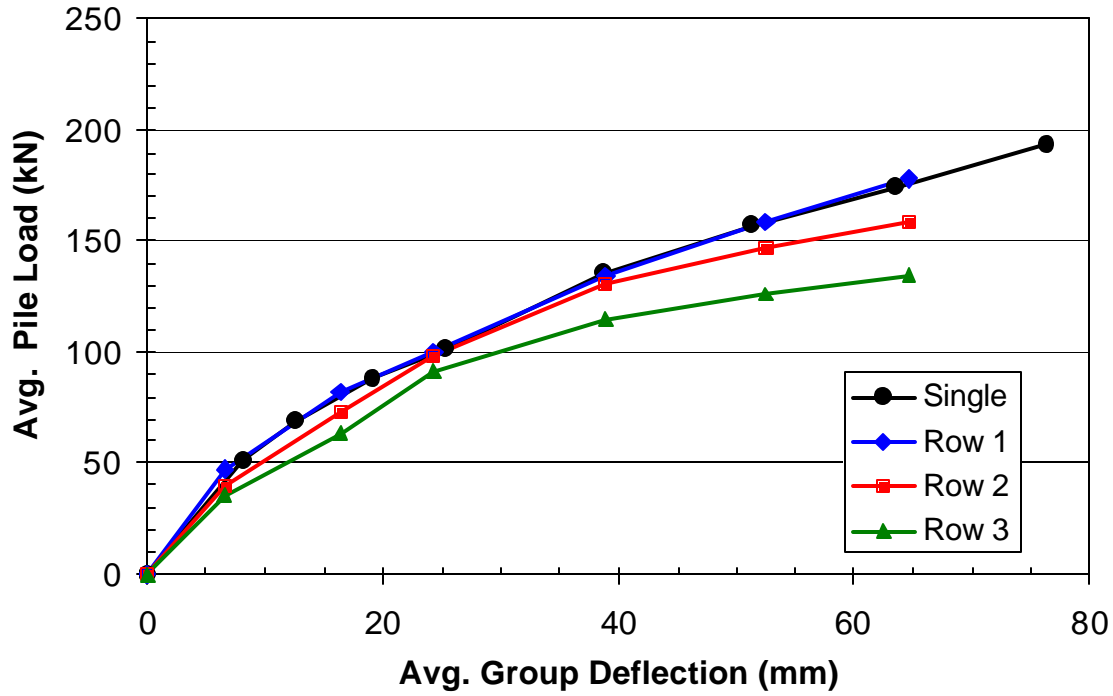
Figure RS-7 Comparison of average load versus deflection curves for piles in the three rows of the nine pile group at 5.6 pile diameter spacing relative to the single pile curve.
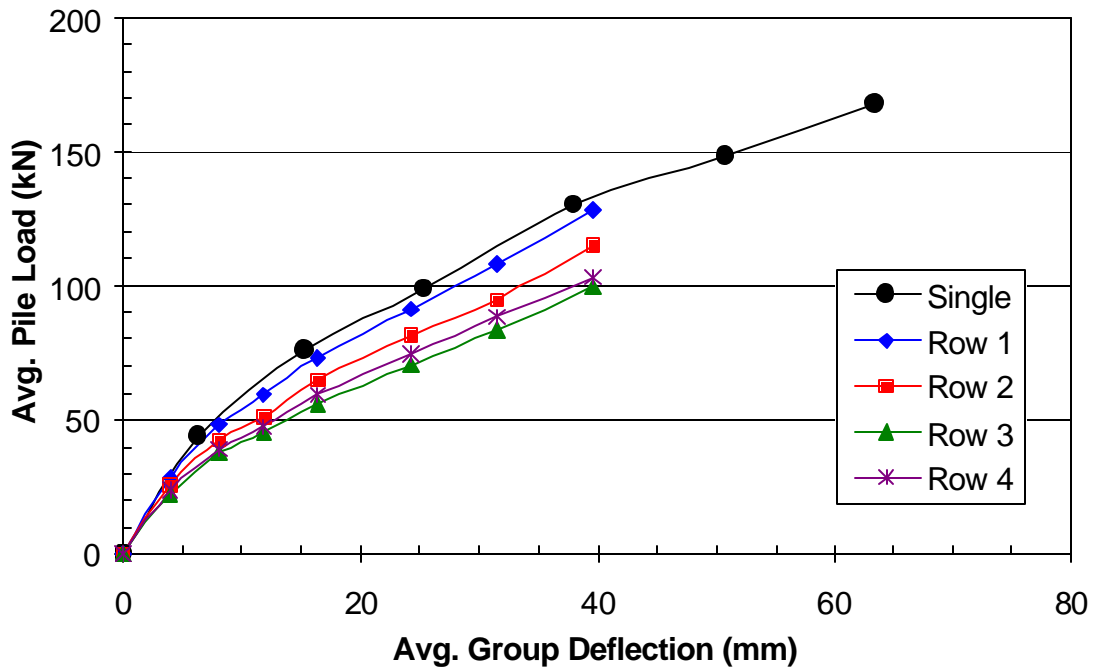
Figure RS-8 Comparison of average load versus deflection curves for piles in the four rows of the 12 pile group at 4.4 pile diameter spacing relative to the single pile curve.
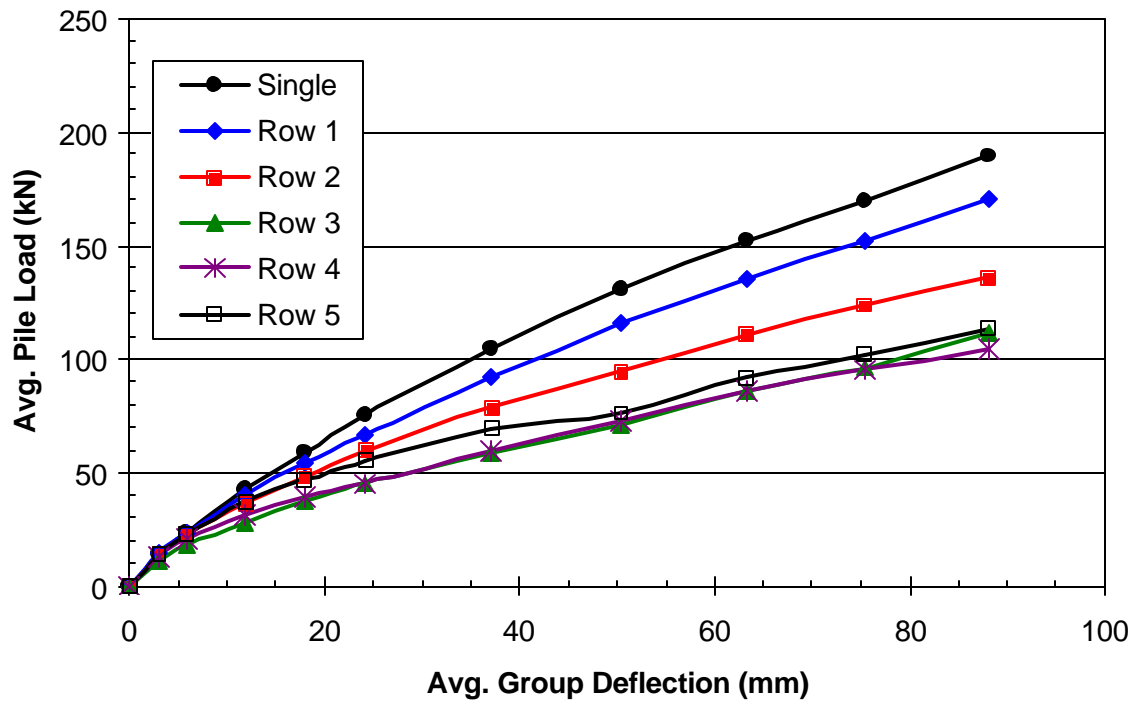
Figure RS-9 Comparison of average load versus deflection curves for piles in the five rows of the 15 pile group at 3.3 pile diameter spacing relative to single pile curve.
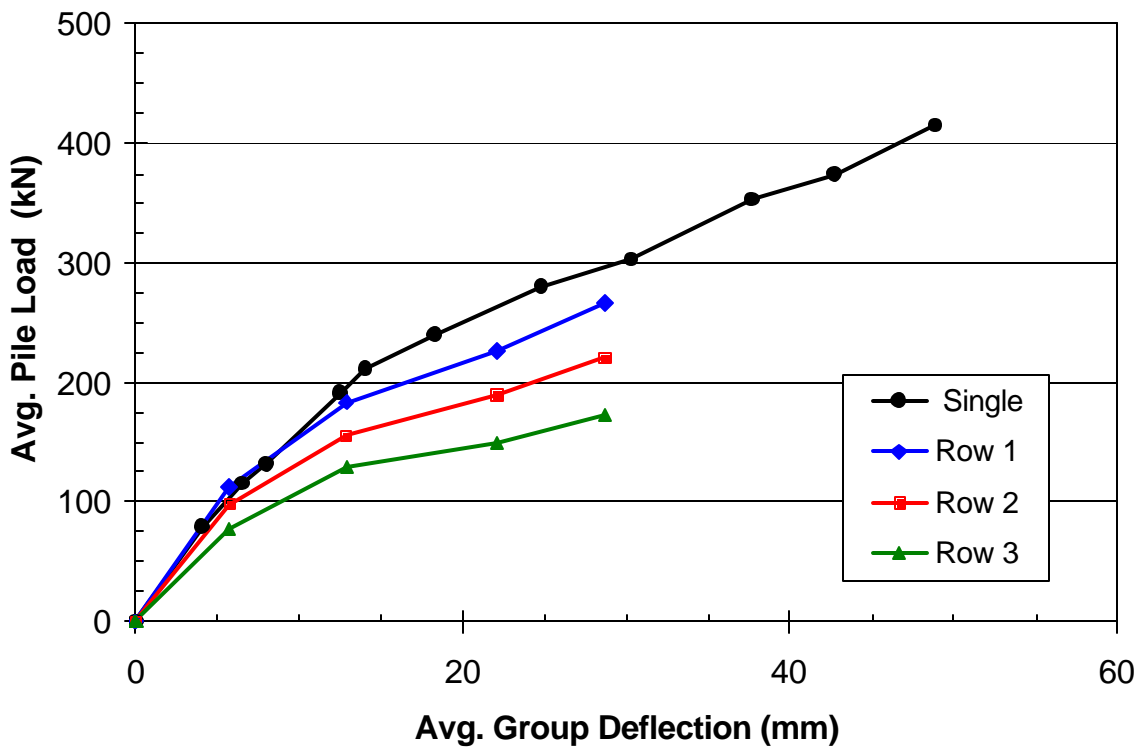
Figure RS-10 Comparison of average load versus deflection curves for piles in the three rows of the nine pile group (610 mm piles) at 3.0 pile diameter spacing relative to the single pile curve.

1 being the front or lead row in the group. The load versus deflection curve for the appropriate single pile test is also shown in each plot for comparison.

The lateral resistance of the piles in the group was a function of row location within the group, rather than location within a row. Contrary to expectations based on the elastic theory, the piles located on the edges of a row did not consistently carry more load than the center piles for a given deflection. The front row piles in the groups carried the greatest load, while the second and third row piles carried successively smaller loads for a given displacement. However, the fourth and fifth row piles, when present, typically carried about the same load as the third row piles. The back row piles often carried a slightly higher load than that in the piles in the preceding row. This finding is consistent with full-scale test results previously reported by Rollins et al (1998) and centrifuge tests reported by McVay et al (1998).

Average lateral load resistance was a function of pile spacing. Very little decrease in lateral resistance due to group effects was observed for the pile group spaced at 5.6 pile diameters; however, the lateral resistance consistently decreased for pile groups spaced at 4.4, 3.3 and 3.0 pile diameters on centers. Group reduction effects typically increased as the load and deflections increased up to a given deflection but then remained relatively constant beyond this deflection. The deflection necessary to fully develop the group effects increased as the pile spacing increased. This increase in required deflection is likely related to the increased movement necessary to cause interaction between failure zones.

Bending Moment versus Load

Bending moment versus load curves are shown for the 9 pile group (324 mm) at 5.6 diameter spacing and the 9 pile group (610 mm) at 3.0 diameter spacing in Figures 11 and 12, respectively. Curves are separated out by row and compared with the single pile curve.
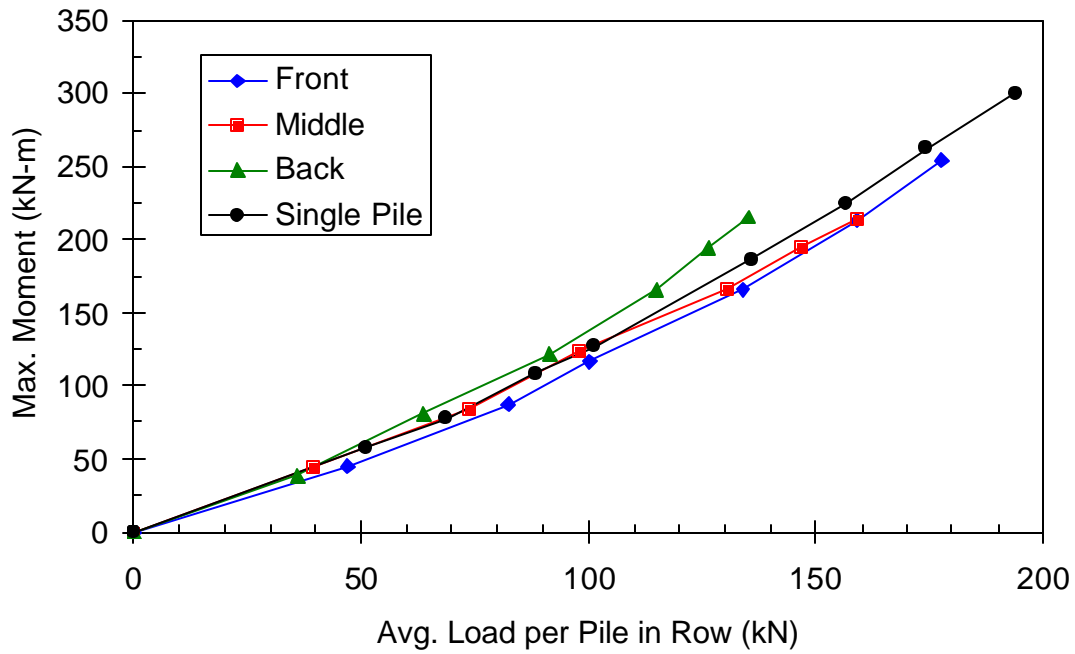
Figure RS-11 Curves showing maximum bending moment versus average load for each row in the nine pile group (324 mm) at 5.6 diameter spacing with curve for single pile.
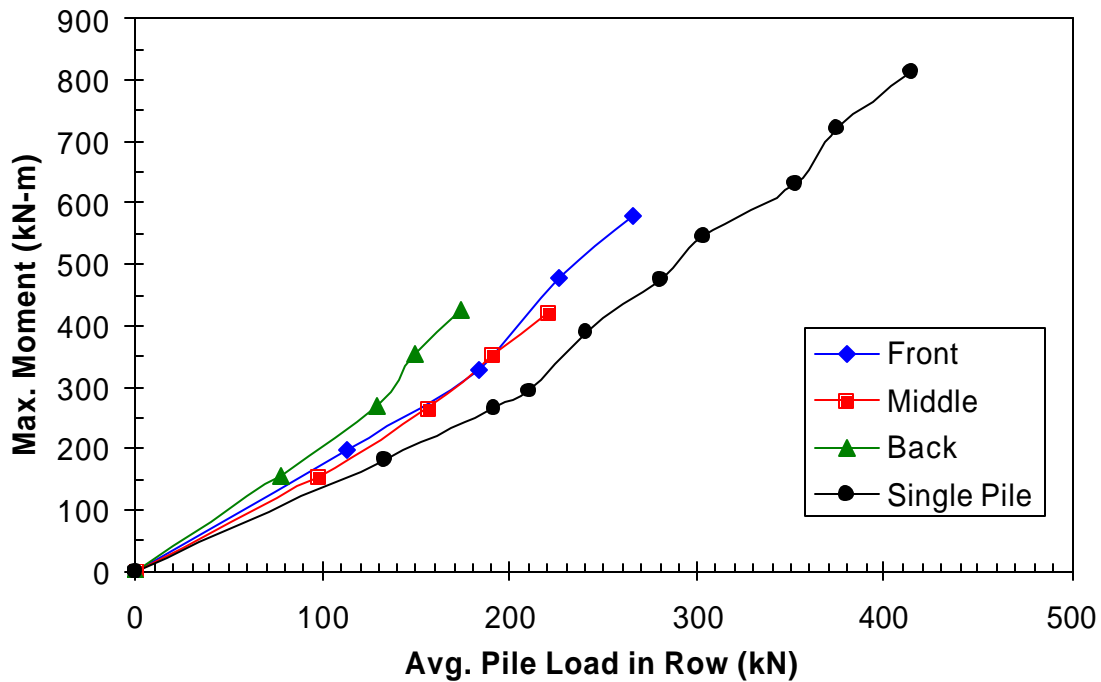
Figure RS-12 Curves showing maximum bending moment versus average load for each row in the nine pile group (324 mm) at 3.0 diameter spacing along with curve for single pile.
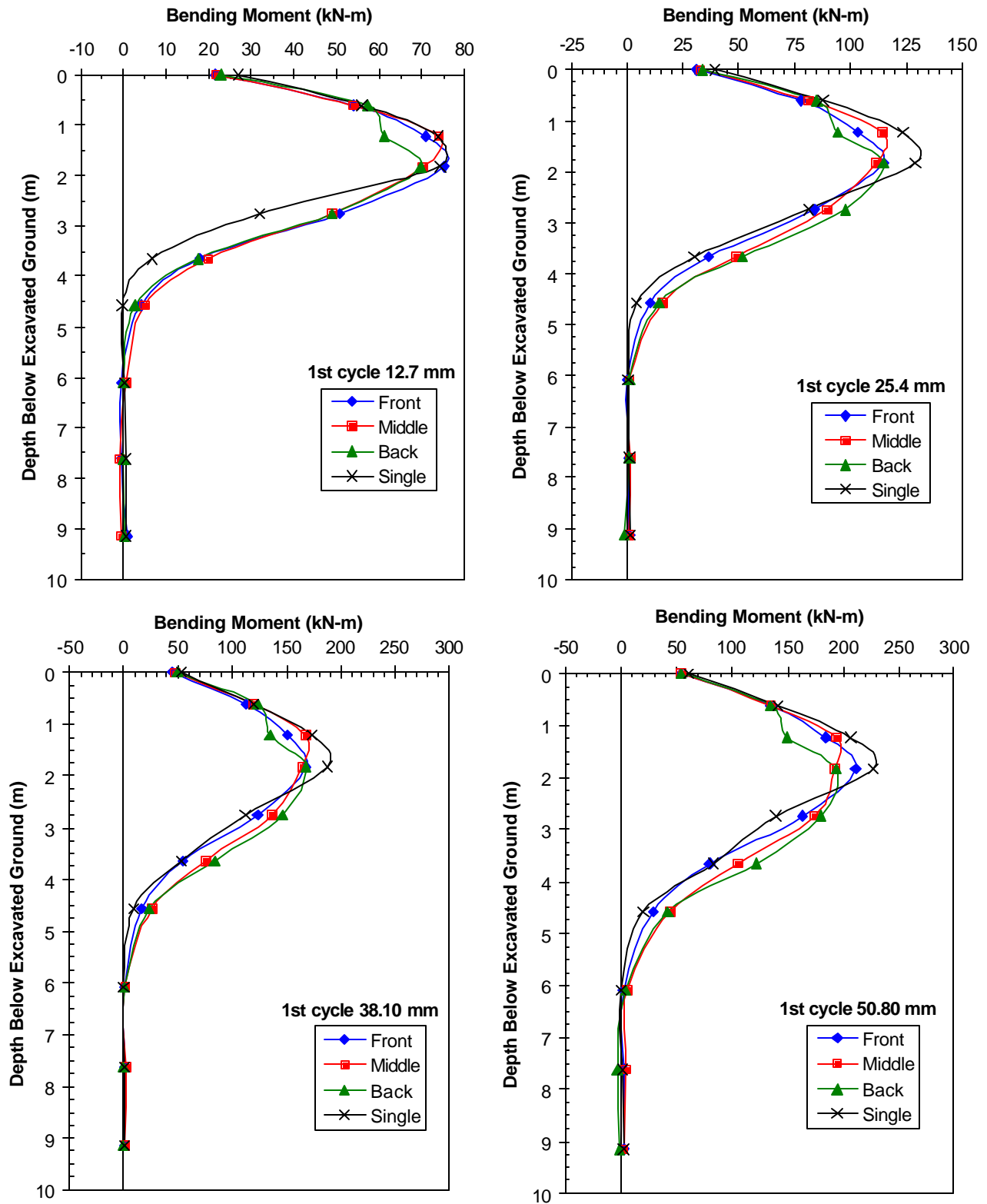
Figure RS-13 Bending moment versus depth curves for the front, middle and back row of the 9 pile group (5.6 pile diameter spacing) at various deflection levels along with the curve for the single pile at the same deflection
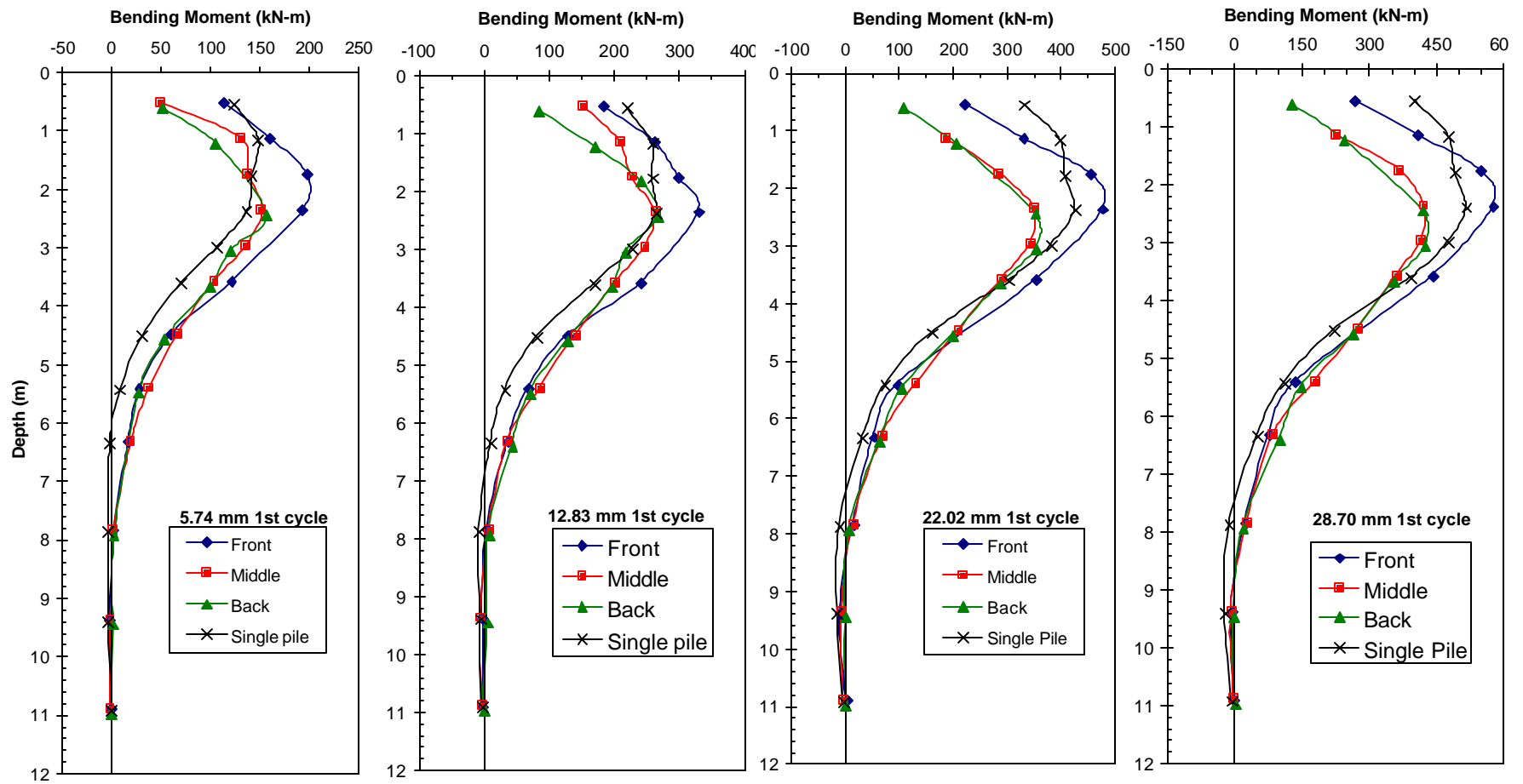
Figure RS-14 Bending moment versus depth curves for the front, middle and back row of the 9 pile group (3 pile diameter spacing) at various deflection levels along with the curve for the single pile at the same deflection.

The curves for the group at the largest spacing (5.6 pile diameters) are relatively close to that for the single pile; however the curves for the group at the closest spacing (3 pile diameters) are all higher that for the single pile at a given load. This is a result of group interaction which has the effect of softening the soil resistance in the trailing rows and causing greater bending moment for a given load.

Bending Moment versus Depth

Bending moment versus depth curves are shown for the nine pile group with 5.6 diameter spacing and the nine pile group with 3.0 pile diameter spacing in Figures 13 and 14. Curves are shown for each row in the group at the four deflection levels along with a curve for the single pile at the same deflection level for comparison. For the pile group with the largest spacing the curves for the three rows are quite close to one another and to the single pile curve; however, for the pile group with the closest spacing the lead row develops the greatest bending moment while the trailing row piles develop considerably less moment at the same deflection. This results from the fact that the trailing row piles, which receive less lateral soil resistance due to group interaction effects, carry lower loads at the same deflection level. Because the loads are lower, the bending moments and also lower.

CYCLIC LATERAL LOAD TESTING OF FIXED-HEAD PILE GROUP

Following the free head tests conducted on the 12 pile group, the frame was removed and the pile group was encased in a 1.12 m thick reinforced concrete cap that was 5.22 m long and 3.04 m wide as shown in Figure RS-15. The pile cap produced a "fixed-head" boundary condition at the pile head, although some rotation did still occur. Bent load tests were performed by Profs. Pantelides and Lawton from the Univ. of Utah in which the fixed-head pile and Geopier groups served as foundations for the load frame as shown in Figure RS-15.
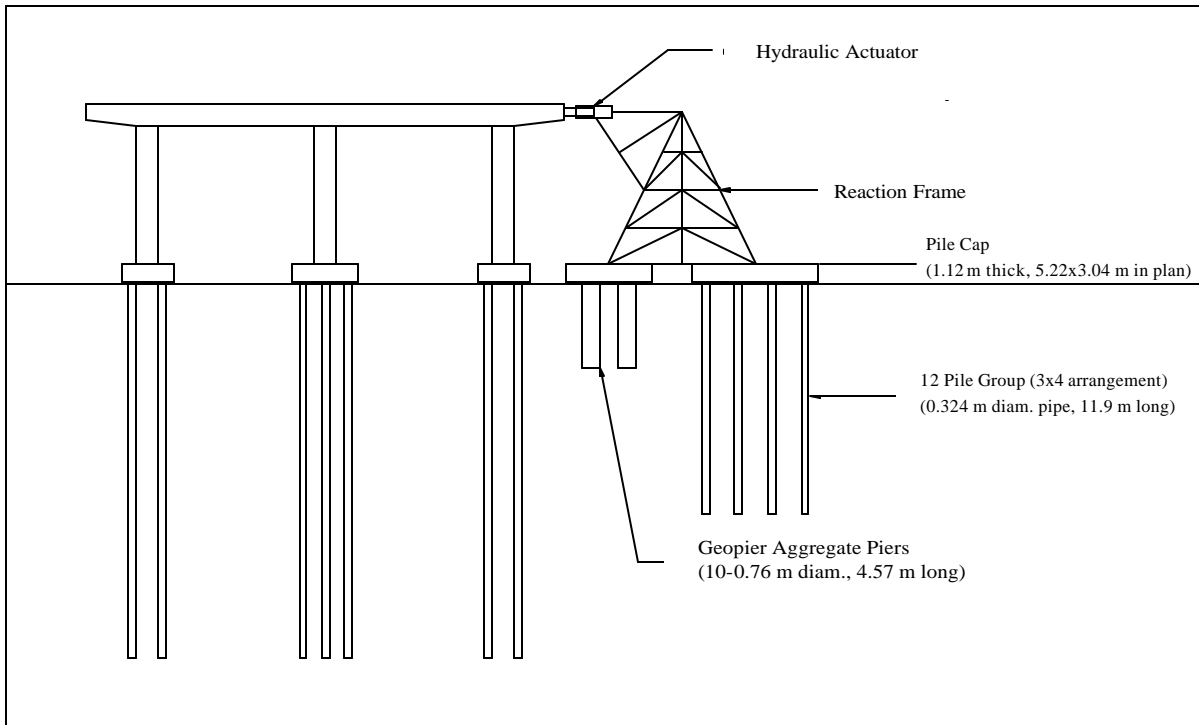
Figure RS-15 Schematic drawing of the bent test setup with reaction frame supported by fixed-head pile group and Geopier group.
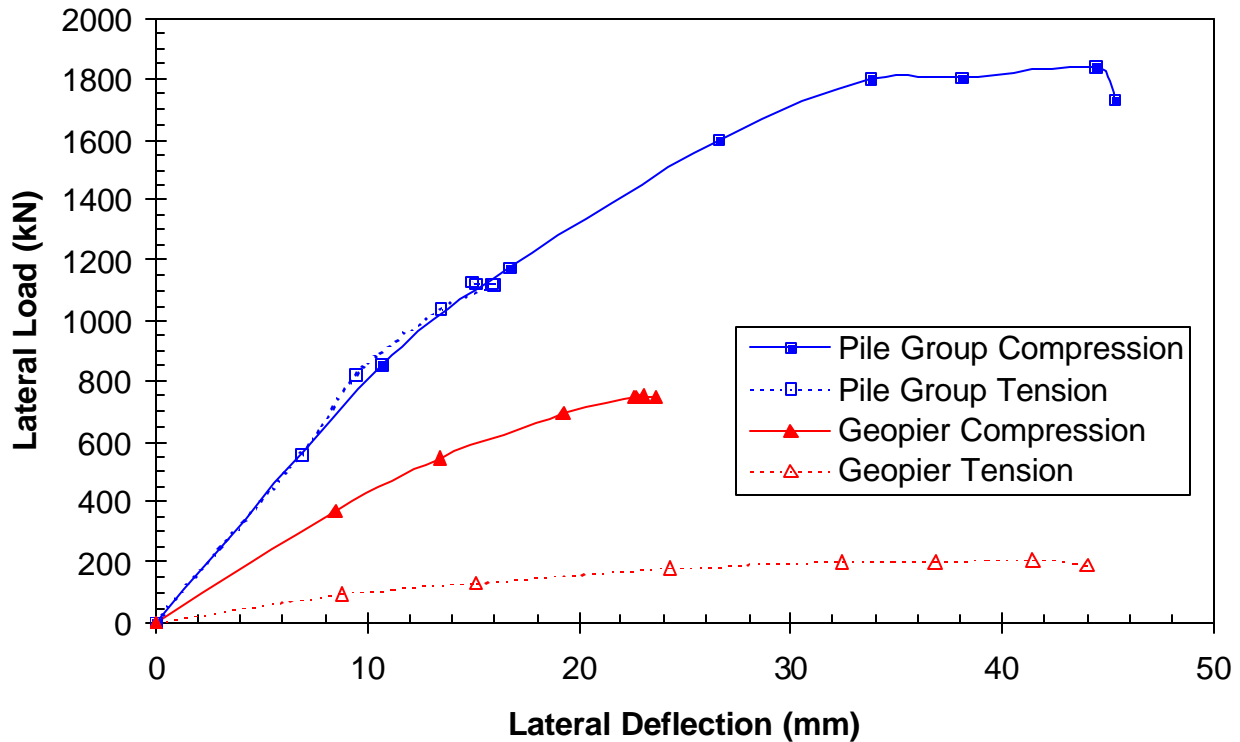
Figure RS-16 Comparison of load-deflection curves for the fixed-head pile group and geopier foundations under tension and compression loads.

As the bent was pushed, the load frame produced axial compression force and a lateral force on the pile cap. As the bent was pulled in the opposite direction, the frame produced an axial tension force and a lateral force in the other direction. The load applied to both foundations was determined from strain gages mounted on the load frame. Figure RS-16 shows the load versus deflection curves for both the pile cap and Geopier group under both tension and compression loads. The pile group carried approximately 85% of the total lateral load when the pile group was in compression and the Geopier group was in tension. When the pile group was in tension and the Geopier group was in compression the pile group carried approximately 60% of the lateral load.

The lateral load-deflection relationship for the pile group remained essentially the same even when significant axial compression or tension forces were applied to the group. In contrast, the lateral resistance of the Geopier group increased when an axial compressive force was applied and decreased when an axial tensile force was applied. The load deflection curve for the fixed-head pile group was 60 to 70% stiffer than that for the same pile group under free-head conditions even though gaps had formed around the piles due to previous loadings. This result points out the importance of the pile head boundary condition in evaluating the lateral resistance of a pile group.

ANALYSIS OF STATIC LOAD TESTS & DETERMINATION OF P-MULTIPLIERS

The idealized soil profile presented in Figure RS-16 was developed for the computer analysis based on the results of the field and laboratory testing. Analyses were made using the computer programs LPILE (Reese and Wang, 1997) and FLPIER (Hoit et al, 2001). The load versus deflection and bending moment versus load curves computed using these two programs are compared with the measured curves in Figures RS-18 and 19. Very little manipulation of the
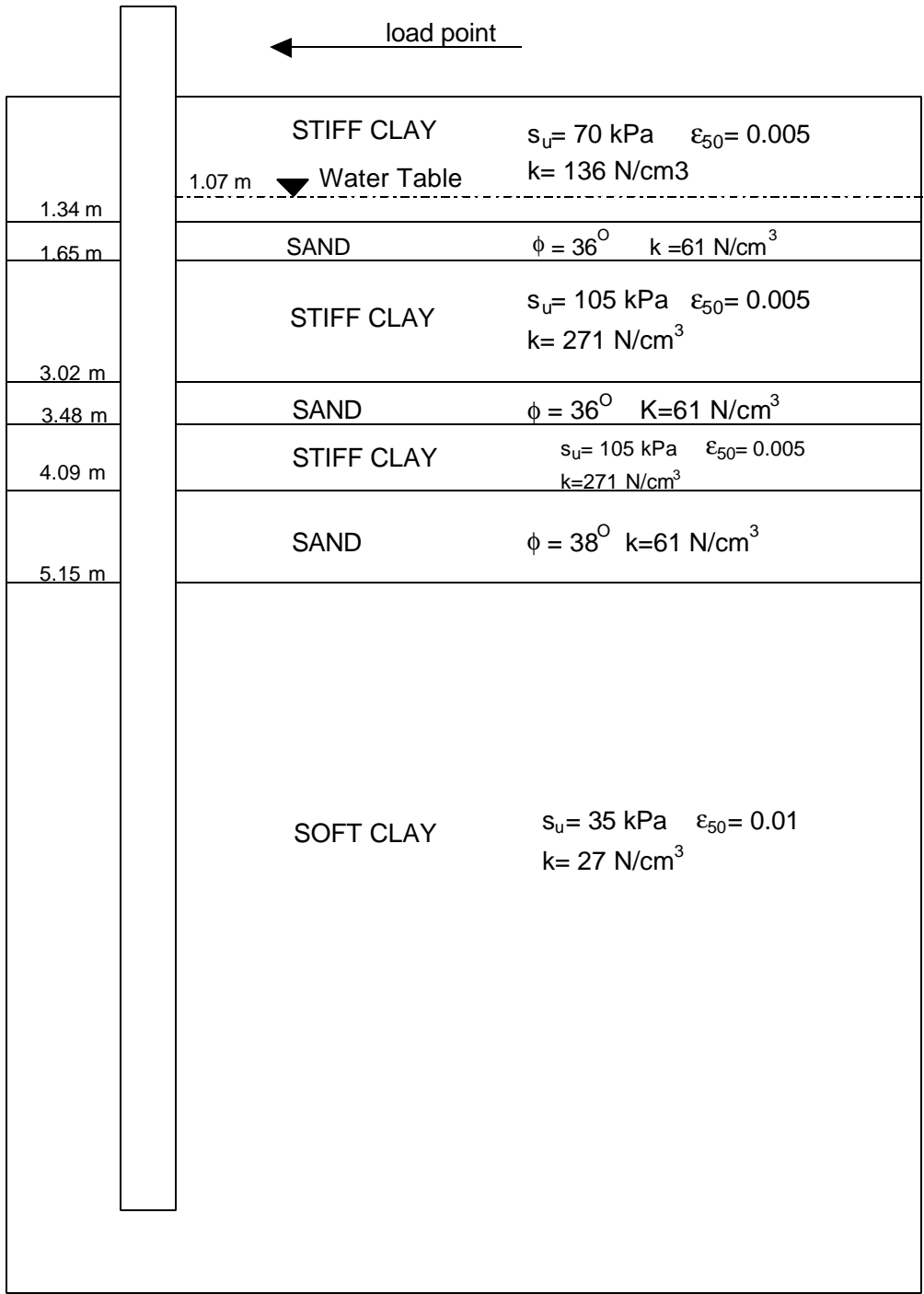
Figure RS-17 Idealized soil profile with soil properties used in the computer analysis.
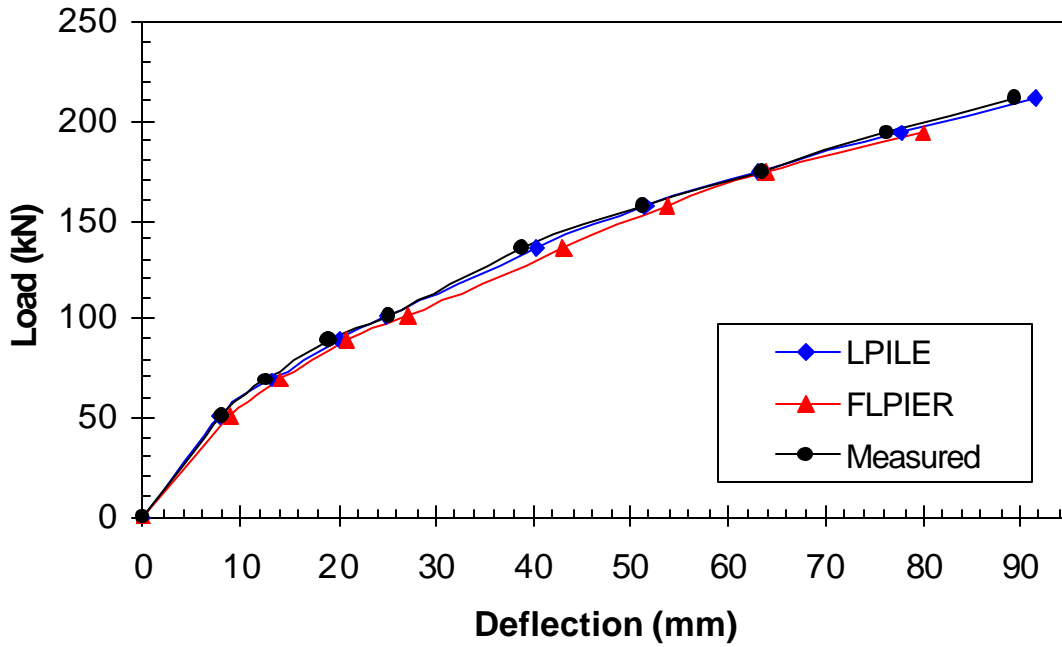
Figure RS-18 Comparison of measured load versus deflection curve for 324 mm diameter single pile with curves computed using computer programs LPILE and FLPIER.
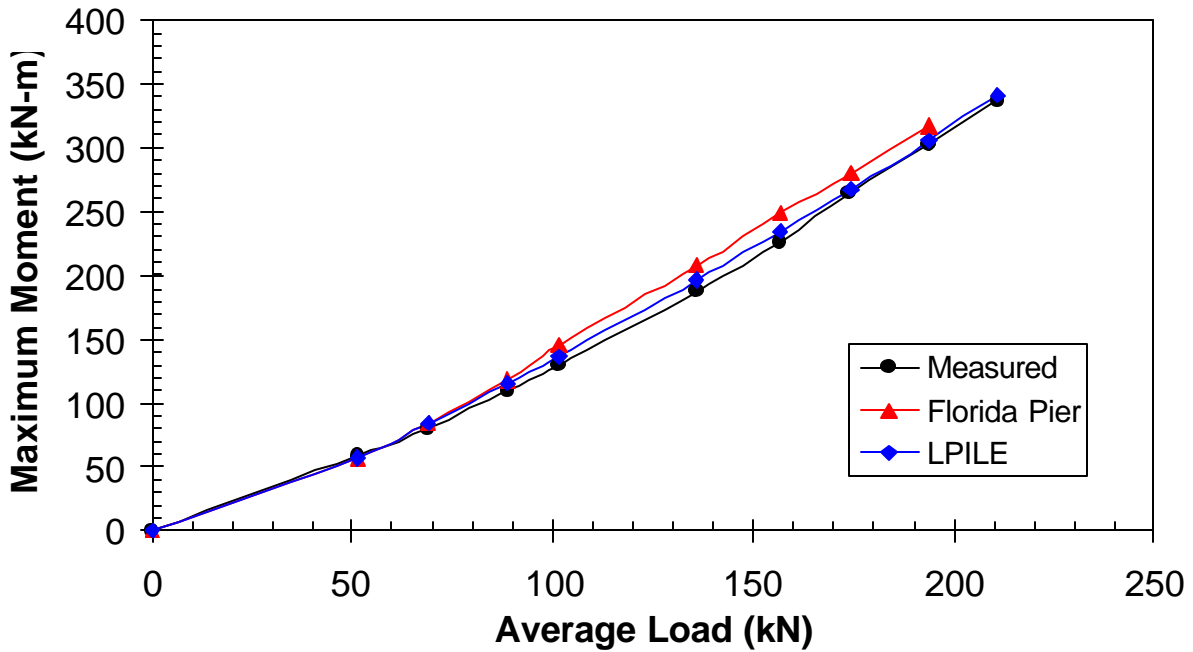
Figure RS-19 Comparison of measure d maximum bending moment versus load curve with curves computed using computer programs LPILE and FLPIER.

input parameters was required to achieve this match. In general, changes in the properties were less than about 10% of the measured values which is within the typical error range for most measured geotechnical properties. Despite the excellent agreement shown in Figures RS-18 and 19 for virgin load conditions, neither of the computer programs was capable of matching the complete load-deflection curve for the re-load conditions without significant manipulation of the input parameters. This result points out the need for improved models to account for pile behavior when gaps are present.

Once the soil profile had been established based on the single pile analysis, the same profile and properties were used in the pile group analysis with the computer program GROUP to back-calculate appropriate p-multipliers. Initial p-multipliers were estimated based on the average ratio of row loads to the single pile load. The p-multipliers were then adjusted, generally using a common factor, to obtain the best match between the measured and computed total load-deflection curves for the group. These p-multipliers were then used in computing load versus deflection curves and bending moment versus load curves for each row without further adjustment. The use of these simple p-multipliers generally provided a very good match with measured response for each row. The back-calculated p-multipliers for each group test are summarized in Table RS-1.

Table RS-1 Summary of row spacing, pile diameter and p-multipliers back-calculated for each pile group during this study.

Row Spacing Center-to-Center	Pile Diameter	P-Multipliers				
		Row 1	Row 2	Row 3	Row 4	Row 5
5.6	324 mm	0.94	0.88	0.77	--	--
4.4	324 mm	0.90	0.80	0.69	0.73	--
3.3	324 mm	0.82	0.61	0.45	0.45	0.51 to 0.46
3.0	610 mm	0.82	0.61	0.45	--	--

A review of the results in Table RS-1 and those for other full-scale load tests indicates that the p-multipliers for the leading row piles are significantly higher than those for the trailing row piles. In addition, the results from this study suggest that the p-multipliers for the second row of piles are also noticeably higher than those for the third and subsequent rows. For design purposes, the p-multipliers tend to remain about the same for the third and subsequent rows.

The back-calculated p-multipliers for the leading row piles in each group are plotted versus pile spacing in Figure RS-20(a) while the p-multipliers for the trailing row piles are shown in Figure RS-20(b). P-multipliers obtained from previous full-scale load testing are also shown in Figure RS-20 for comparison. The p-multipliers from this series of tests are within the middle of the range from previous tests at the closest spacings.

Proposed design curves, which show p-multiplier values as a function of pile spacing, have been developed based on the results from this study and the curves for leading and trailing row pile are presented in Figure RS-20 (a) and (b), respectively. For both leading and trailing row piles, there is a clear trend for the p-multipliers to increase as the spacing increases; however, the relationship does not appear to be linear. The p-multipliers tend to change more gradually as the spacing increases. Extrapolation of the curves suggests that the p-multipliers will go to one at a spacing of 6.5 diameters for the leading row and 7 to 8 diameters for the trailing rows. Two curves are provided for trailing row piles in Figure RS-20 (b). The upper curve gives p-multipliers for the second row (or first trailing row) in the group, while the lower curve gives the p-multiplier for all other trailing rows in the group.

The p-multiplier versus pile spacing curves recommended in GROUP (Reese and Wang, 1996) and by AASHTO (2000) are also presented in Figures RS-20 (a) and (b) for comparison. The p-multipliers based on the results from this and previous full-scale group load tests are
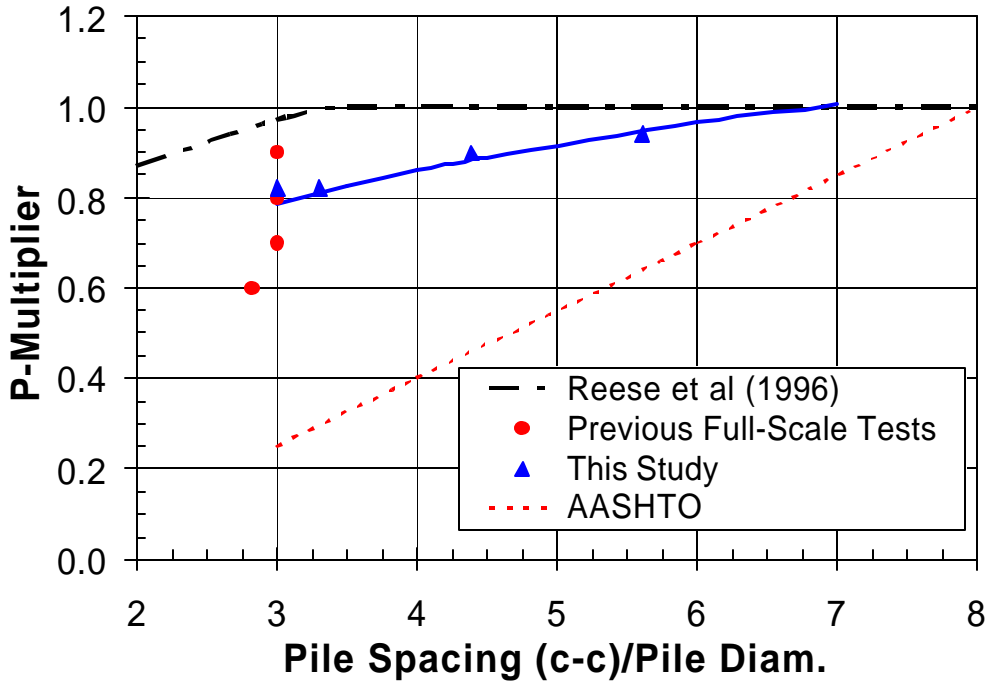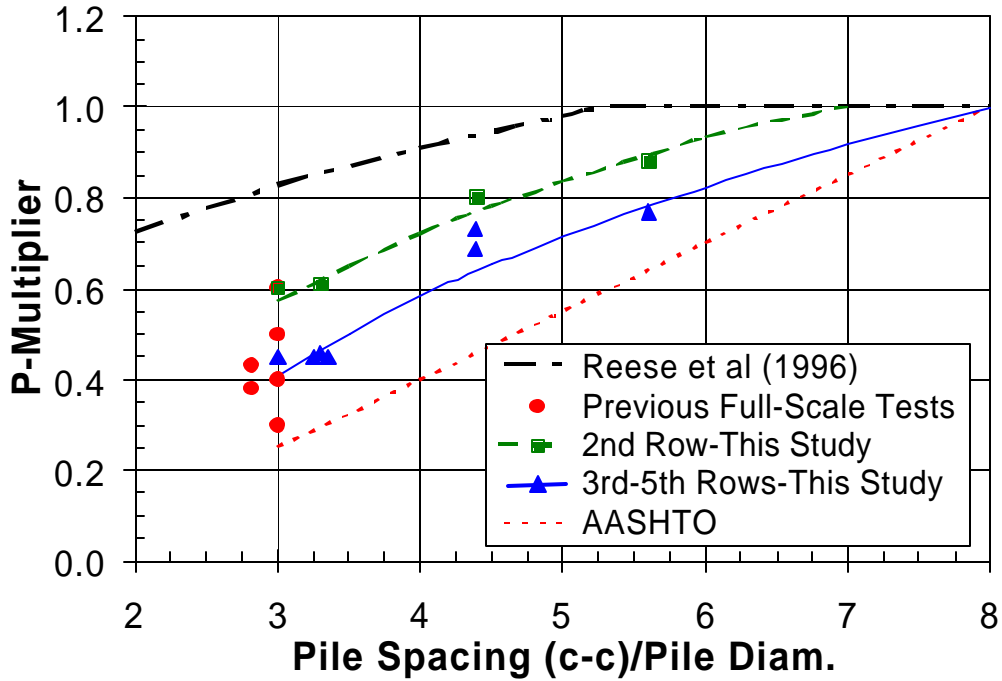
Figure RS-20 Back-calculated p-multipliers for (a) leading row and (b) trailing row piles from this study and previous full-scale load tests along with recommended design curves.

significantly lower than the curves used in GROUP but significantly higher than the curves recommended by AASHTO. In addition, the curves used in GROUP assume that group interaction effects are eliminated at smaller spacings than are indicated by this series of tests

A summary plot of the curves recommended for determining p-multipliers for pile groups based on the results of this study is provided in Figure RS-21. Curves are provided for three separate cases, namely: (1) first row piles sometimes referred to as leading row piles, (2) second row piles, and (3) third or higher row piles. The AASHTO curve is also provide in Figure RS-20 for comparison purposes only.
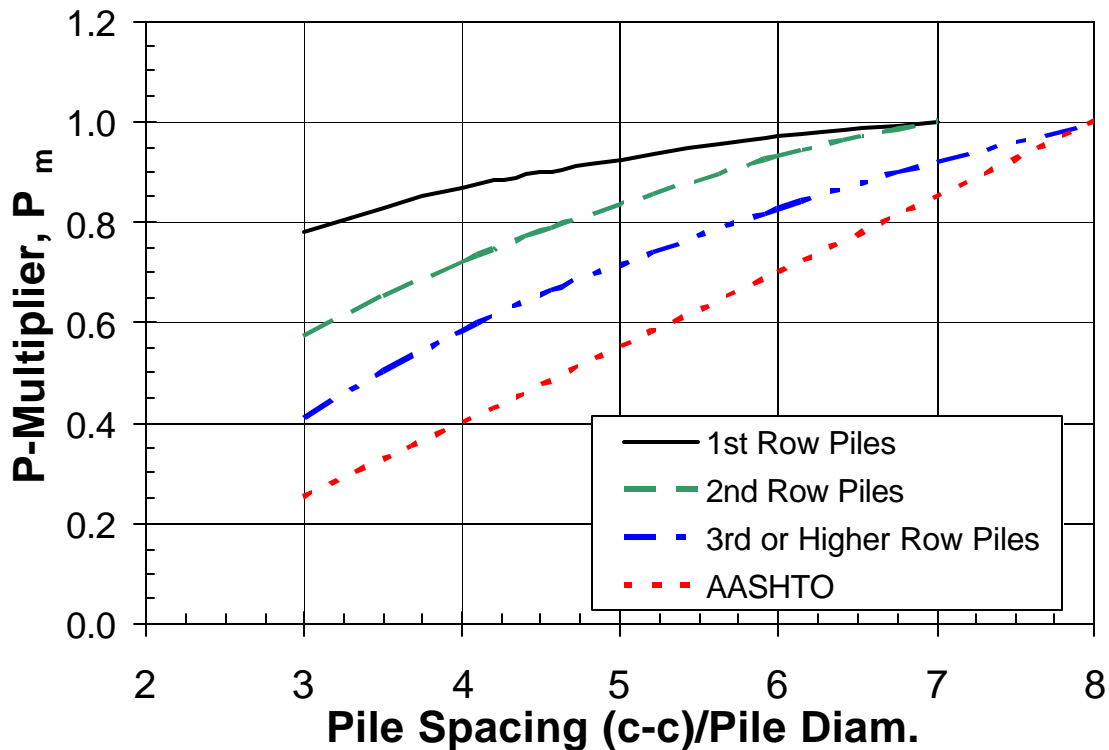
Figure RS-21 Recommended design curves for selecting p-multipliers (P_m) as a function of normalized pile spacing for 1st row piles, 2nd row piles and 3rd row or higher row piles

Equations have also been developed to compute the p-multiplier (P_m) for each of the curves shown in Figure RS-20. The equations for each case are:

First (Lead) Row Piles: $P_m = 0.26\ln(s/d)+0.5$ = 1.0 (RS.1)

Second Row Piles: $P_m = 0.52\ln(s/d)$ = 1.0 (RS.2)

Third or Higher Row Piles: $P_m = 0.60\ln(s/d)-0.25$ = 1.0 (RS.3)

where s is the center to center spacing between piles in the direction of loading and d is the width or outside diameter of the pile.

STATNAMIC LATERAL LOAD TESTS

Statnamic load testing was also performed on the nine pile group consisting of 610 mm test piles and the 15 pile group consisting of 324 mm test piles both with free-head conditions. Statnamic tests were initially performed after 15 cycles of static loading had been applied to the pile group and subsequently statnamic tests were performed for virgin loading conditions where deflections exceeded the deflections of the static tests. This approach provided a comparison between the dynamic resistance offered before and after cyclic loading. The statnamic loading system was capable of applying loads as great as 3600 kN with rise times between 0.05 and 0.3 seconds. Velocities were between 0.3 and 1.5 m/sec, which is similar to what would be produced by a large earthquake having peak accelerations between 0.5 and 1.5 g. A high-speed data acquisition system was used to record data for over 150 channels at 1500 samples per second.

Figure RS-22 presents the load versus deflection curves obtained for two statnamic tests conducted after fifteen static load cycles in comparison with the load versus deflection curve based on the 15th cycle of static loading. For these conditions, the statnamic curves are close to the static curves. Figure RS-23 presents the load versus deflection curves obtained from three
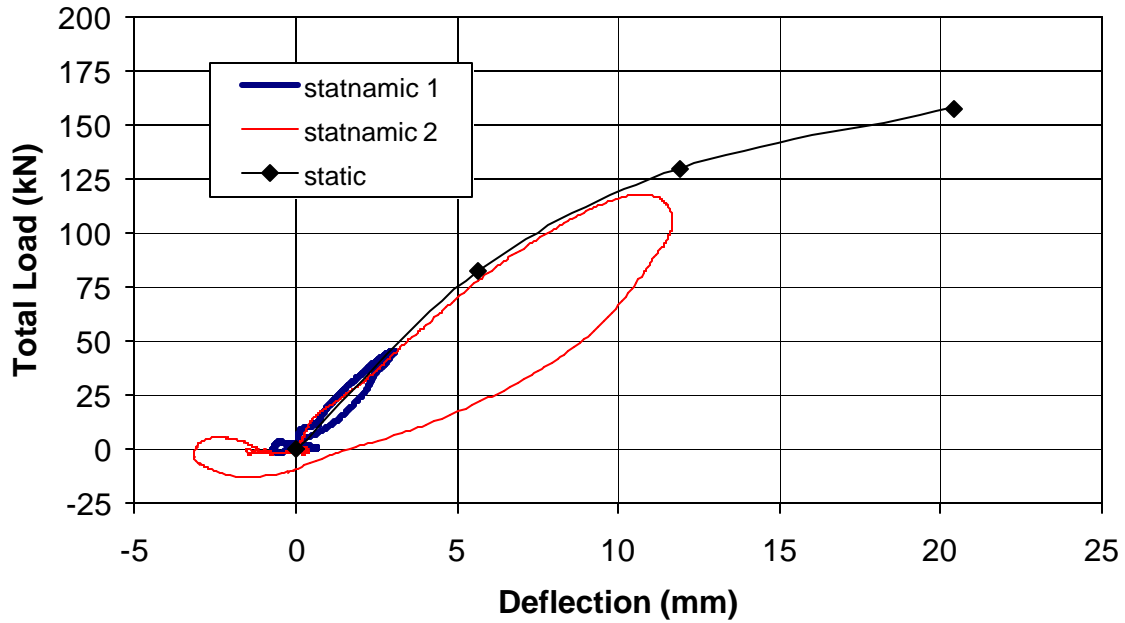
Figure RS-22 Load vs. deflection curves for statnamic tests conducted after previous cyclic static loadings relative to 15th cycle static load vs. deflection curve.
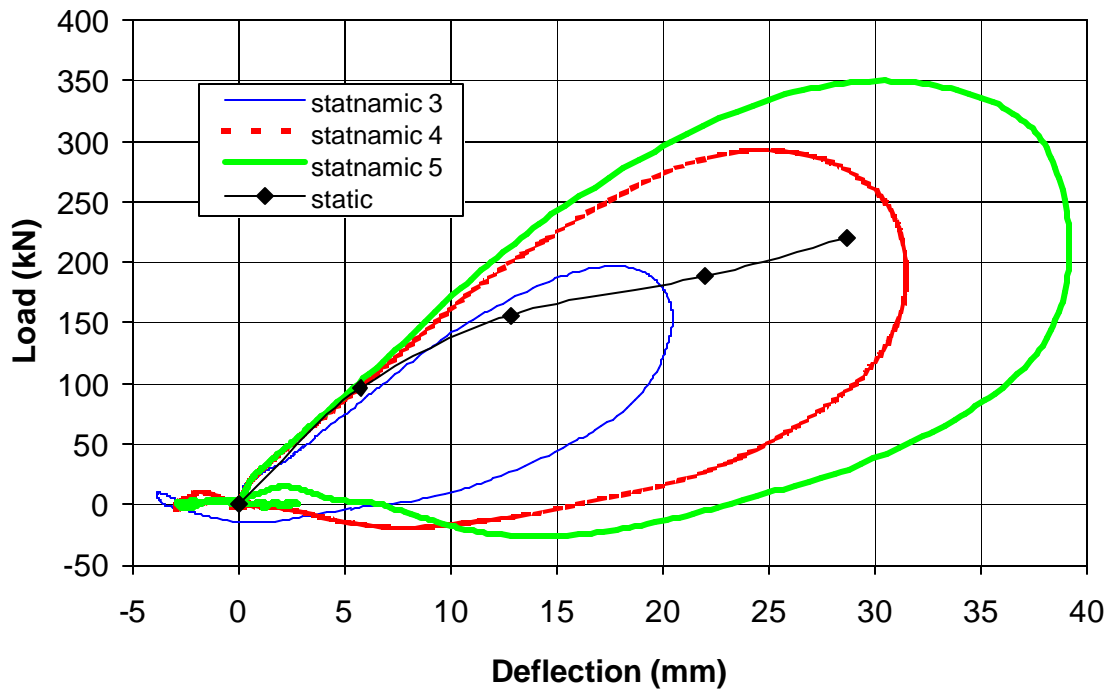
Figure RS-23 Load vs. deflection curves for statnamic tests conducted before static loading along with first cycle static load vs. deflection curve.

statnamic tests conducted prior to any static load application. In contrast to the curves in Figure

RS-22, the load-deflection curves from the statnamic test are considerably stiffer than those from

the static test. These results indicate that the dynamic resistance can drop significantly when

cyclic loads form gaps around the piles in contrast to the virgin load condition.

Figure RS-24 presents statnamic load versus deflection curves for six tests conducted on

the 15 pile group in comparison with a static load versus deflection curve obtained by loading the

pile group in the opposite direction. As was the case for the nine pile group, during virgin

loading the statnamic tests develop significantly greater load for a given deflection than the

corresponding static test.
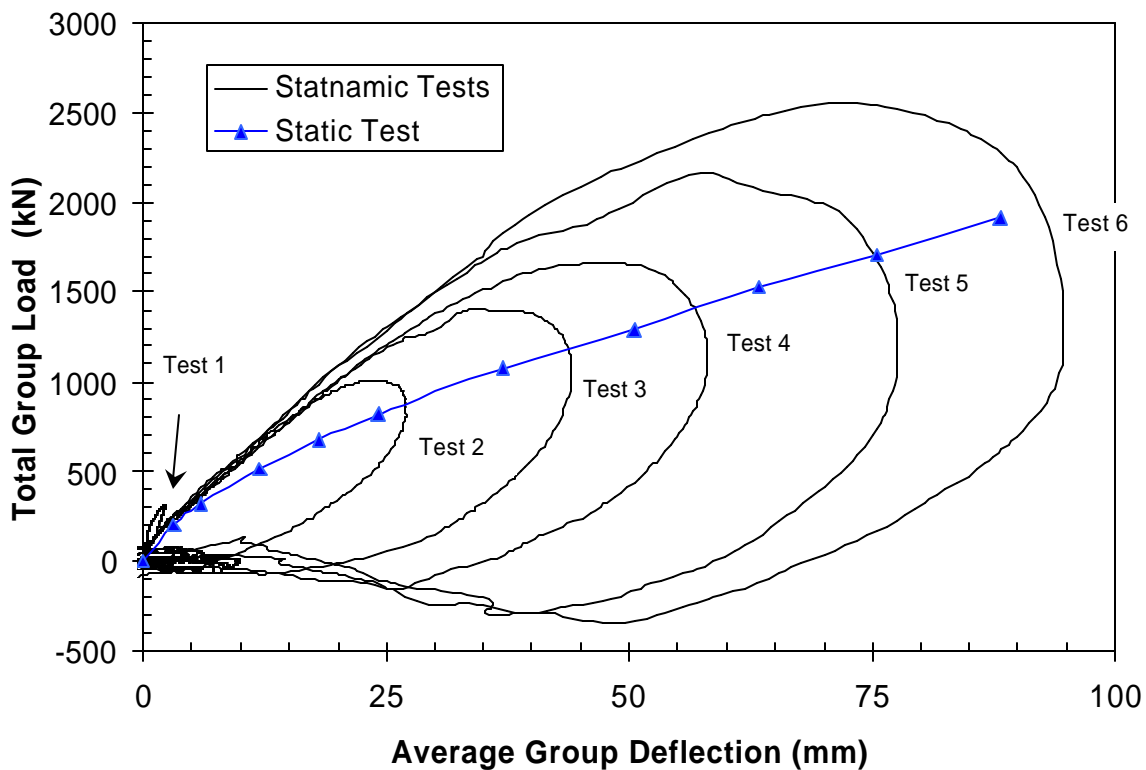
RS-24 Load vs. deflection curves for statnamic tests in comparison with static load vs. deflection curve obtained by loading the pile group in the opposite direction

COMPUTER ANALYSIS OF STATNAMIC LOAD TESTS

As part of this study, an effort was also made to separate out the components of lateral resistance developed during the statnamic testing. These components include static "spring" stiffness, damping, and inertia forces. The Unloading Point method, introduced by Middendorp et al (1992) for axial statnamic load tests, was used to analyze the statnamic tests that were performed on the 9 pile and 15 pile groups. This method treats the pile foundation as an equivalent single degree of freedom system and is admittedly a simplification of a complex reality. Nevertheless, the results from this analysis technique have proven useful. The analyses suggest that inertia forces are relatively small for the free-head pile groups involved where the mass is assumed to be the weight of the pile sections above the ground surface. The increased dynamic resistance was determined to be primarily due to damping. Damping resistance was significantly greater for virgin loading than for reloading because the pile was in contact with the soil and gaps had not formed.

Figure RS-25 shows the derived static load (F_u) versus deflection curves for four statnamic tests on the nine pile group along with the load versus deflection curve for the last cycle of the maximum static load. The consistency in the derived curve shapes for the various statnamic tests is very good. During the virgin loading segment of a given load-deflection curve, there is a clear indication of greater resistance. However, for repeated loadings, the load-deflection curves for the various tests lie nearly on top of each other. The derived load-deflection curves are also in very good agreement with the measured static load-deflection curve.

Figure RS-26 provides a similar comparison between the derived static load (F_u) versus deflection curves from the statnamic tests on the 15 pile group and the measured load versus deflection curve for a static test performed in the opposite direction. As in the case with the tests
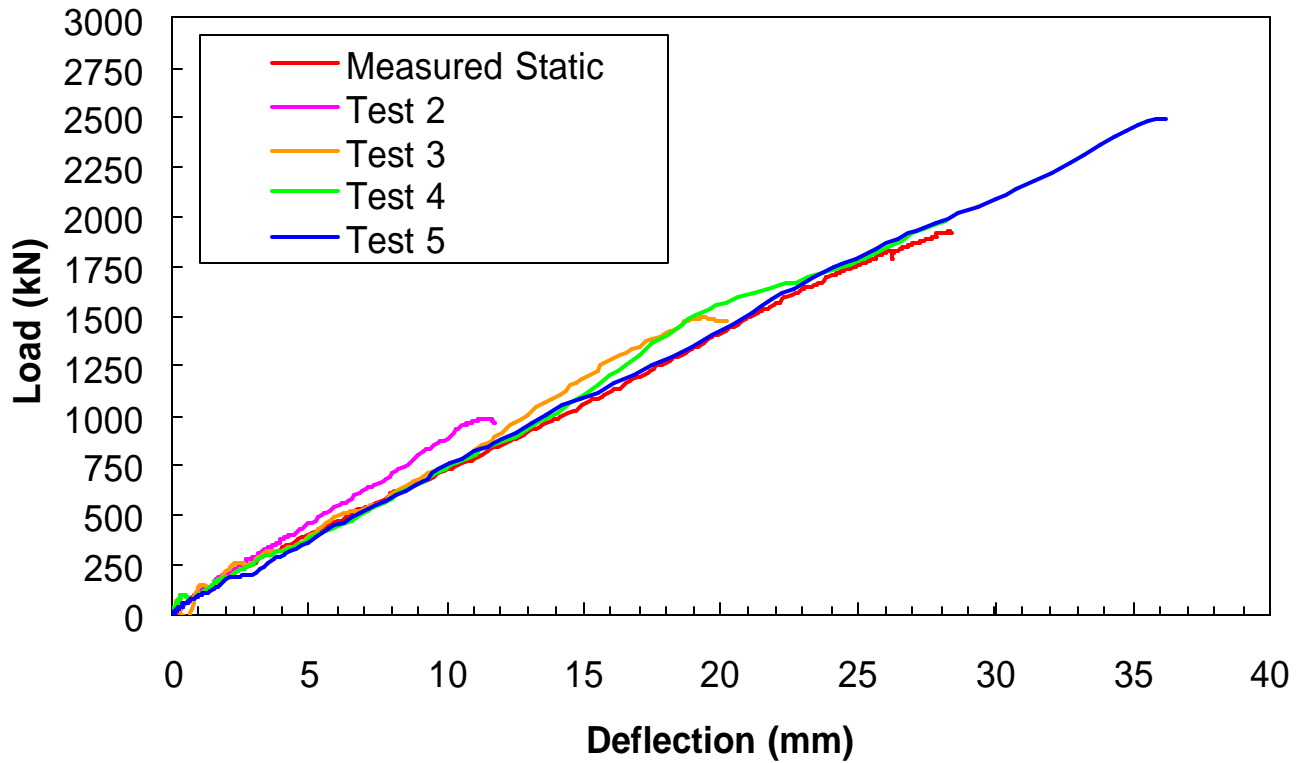
Figure RS-25 Comparison of derived static load-deflection curves from four statnamic tests on the nine pile group with measured static load-deflection curve from last cycle.
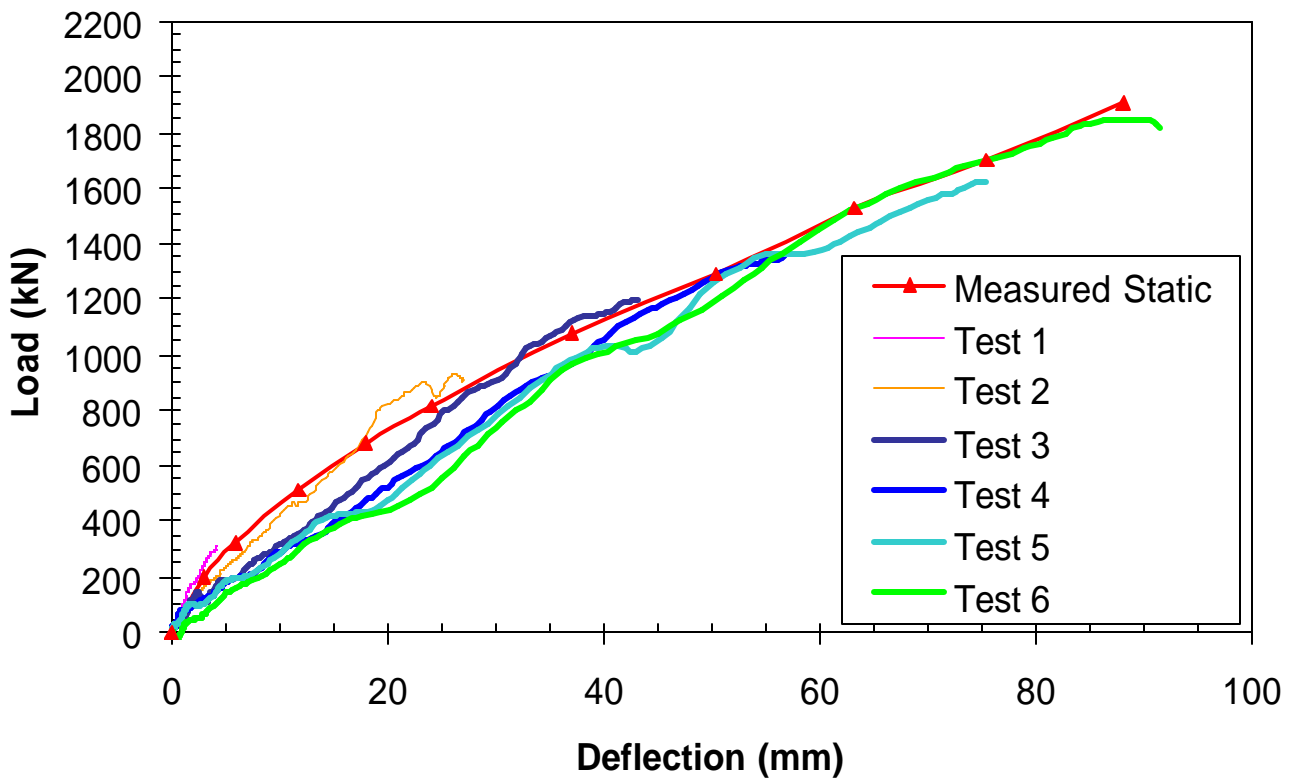
Figure RS-26 Comparison of derived static load-deflection curves from six statnamic tests on the 15 pile group with measured static load-deflection curve.

on the nine pile group, the derived curves match the static curve reasonably well in the region where virgin loading is occurring. However, for intervals where reloading is occurring, the derived curve is considerably softer than the static curve due to the presence of gaps around the pile. In the re-load intervals the derived curves tend to lie fairly close to one another since the resistance is largely due to the pile stiffness only.

CHAPTER 1 INTRODUCTION, TEST OBJECTIVES AND SCOPE OF WORK

BACKGROUND

The lateral load capacity of pile foundations is critically important in the design of buildings and highway structures which may be subjected to earthquake motions. Although fairly reliable methods have been developed for predicting the lateral capacity of single piles under static loads, there is very little information to guide engineers in the design of closely spaced pile groups (i.e. spacings less than about 6 to 8 pile diameters), particularly under dynamic loads. Because of the high cost and logistical difficulty of conducting lateral load tests on pile groups, only a few full-scale load test results are available that show the distribution of load within a pile group (Brown et al, 1987; Brown et al, 1988; Meimon et al, 1986; Rollins et al, 1998; Ruesta and Townsend, 1997). These tests have all involved static or quasi-static loadings.

Nevertheless, the data from these limited field tests indicate that piles in groups will undergo significantly more displacement and higher bending moments for a given load per pile than will a single isolated pile (Brown et al, 1987; Brown et al, 1988; Meimon et al, 1986; Rollins et al, 1998; Ruesta and Townsend, 1997). The tendency for a pile in a trailing row to exhibit less lateral resistance because of interference with the failure surface of the pile in front of it, as illustrated in Figure 1.1, is commonly referred to as "shadowing". This shadowing or group interaction effect becomes less significant as the spacing between piles increases and there is less overlap between adjacent failure planes.

The lateral response of piles is typically analyzed using finite-difference methods. This method was developed based on early work performed by McClelland and Focht (1958). The pile is modeled as a beam and the soil is modeled using non-linear springs that are attached to the pile. The non-linear springs are defined using p-y curves at regular depth intervals, where the p

Leading Row Piles
(Front Row or Row 1)

Shear Zones

Trailng Row Piles
(Row 2)

Trailng Row Piles
(Row 3)

Test Piles

Trailng Row Piles
(Back Row or Row 4)

Direction of Applied Force
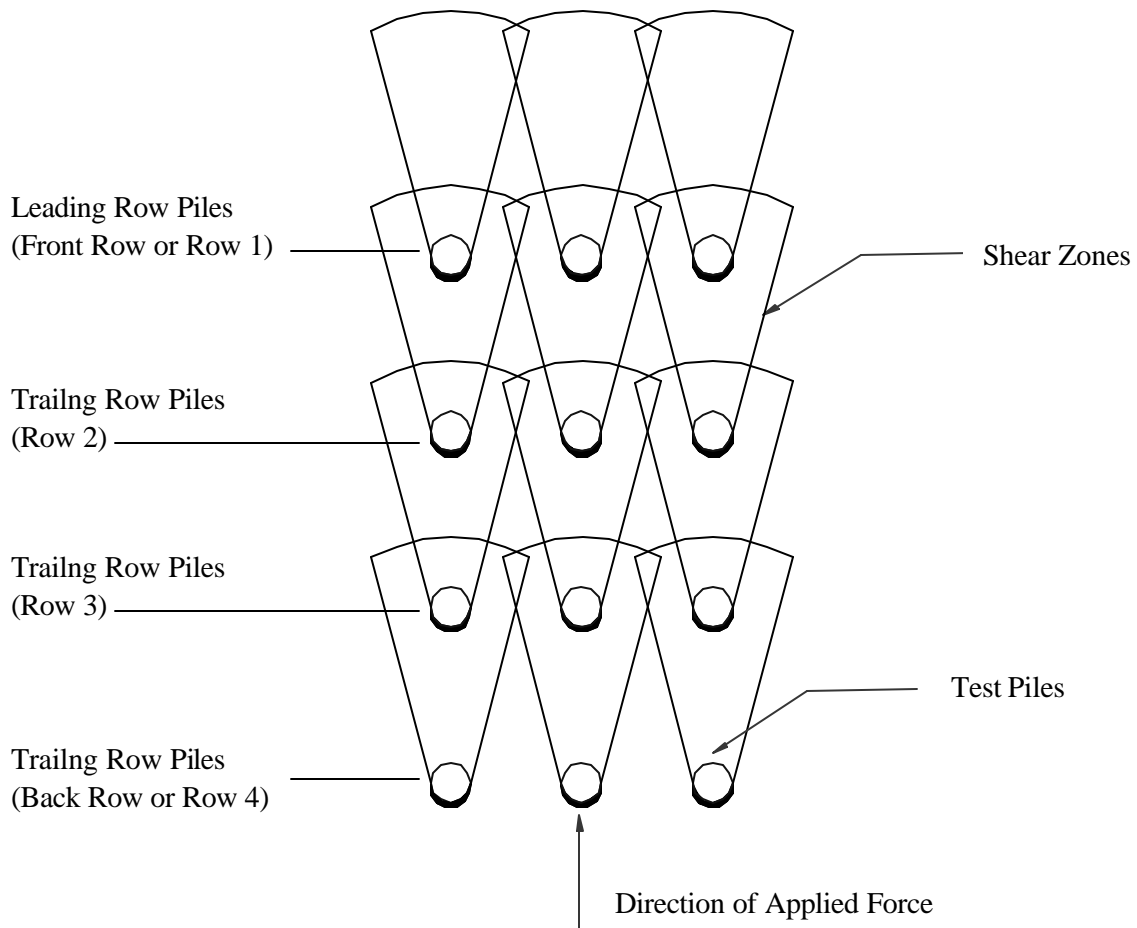
Figure 1.1 Reduction in lateral resistance due to overlapping shear zones ("shadowing" or "group interaction") in closely spaced groups.

represents the lateral soil resistance per unit length of the pile and the *y* is the lateral deflection of

the pile. One method of accounting for the shadowing or group reduction effects is to reduce the

single pile p-y curve (horizontal soil resistance vs displacement curve) using a p-multiplier as

suggested by Brown et al (1987). With this approach, the soil resistance, p, is scaled down by a

constant factor as shown in Figure 1.2. The appropriate p-multiplier is likely dependent on a

number of factors such as pile spacing, row position in the group, deflection level and soil type.
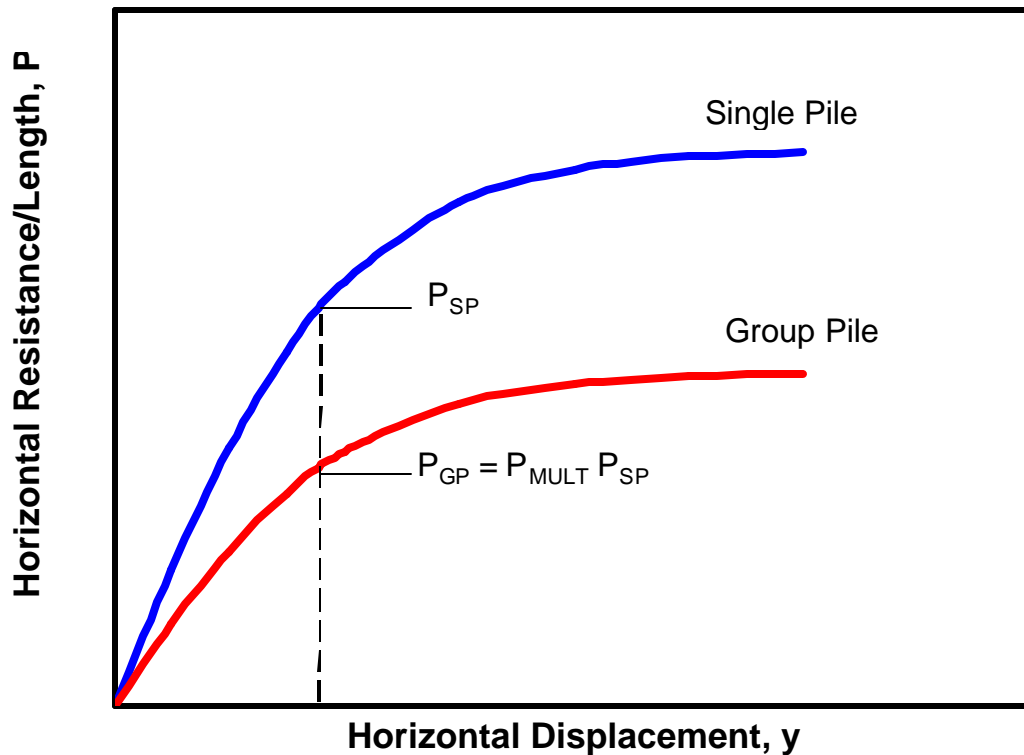
Figure 1.2 Use of P-multiplier to reduce single pile p-y curve to produce p-y curve for a pile within a group.

Because of the dearth of experimental data, computer programs for pile groups have not been thoroughly validated and empirical methods such as those using p-multipliers are extremely restricted in their application. As a result, engineers are forced to design pile groups in a very conservative manner to deal with the uncertainty. Although numerical and centrifuge models can provide some guidance regarding these issues, a reasonable number of full-scale load tests are necessary to verify these models and provide ground truth information.

Rollins and his co-workers recently conducted a series of static and dynamic lateral load tests on a full-scale pile group at the Salt Lake International Airport (Rollins et al, 1998; Weaver et al, 1998). The piles were 324 mm outside diameter steel pipe piles driven to a depth of approximately 10 m in a soil profile consisting of soft to medium clay. The piles were driven in

a 3 x 3 pattern with a nominal spacing of 2.8 pile diameters center to center. Static loads were applied in one direction with conventional hydraulic jacks and subsequently dynamic loads were applied in the opposite direction with a Statnamic loading device. The Statnamic device produced loads of up to 2700 kN with peak accelerations between 0.5 and 2.0 g and durations of about 300 msec. These parameters are similar to what might be expected for an earthquake loading. The load in each of the nine piles was measured during both loadings so that the distribution of loading in the pile group could be determined. Tests were also performed with a pile cap to create a fixed-head boundary condition.

As a result of the lateral load tests at the Salt Lake City Airport, significant insight has been provided regarding group reduction factors (p-multipliers), large-strain dynamic resistance, and the accuracy of several computer analysis methods (Rollins et al, 1998; Weaver et al, 1998). There are, however, several unresolved issues that need to be explored with supplemental full-scale load testing.

The first unresolved issue involves the effect of pile spacing on group interaction effects. Almost all of the available full-scale pile group tests where load distribution was measured, including the Utah tests, involve pile groups spaced at about three pile diameters center to center. The p-multipliers obtained from these full-scale group load tests are significantly <u>lower</u> than those obtained from model tests. Although group effects would likely become less important as spacing increases. Current AASHTO specifications (AASHTO, 2000) recommend relatively conservative group reduction factors based on tests at three diameter spacing. These factors could lead to overly costly designs. Design charts are needed to show appropriate p-multipliers as a function of pile spacing based on full-scale tests.

A second unresolved issue involves the selection of appropriate p-multipliers for large

pile groups. In fact, some question the validity of the p-multiplier concept for larger pile groups. Four of the five available full-scale pile group tests have been performed on groups with only two or three rows. The results from these tests generally show that the p-multiplier decreases from the front row to the back row although there was some increase in the p-multiplier for the back row in the Utah tests. It is unclear at this point whether the p-multipliers developed for the third row in a group is appropriate for subsequent rows in a large pile group or whether the p-multipliers will continue to gradually decrease with each additional trailing row. Tests on larger groups are necessary to answer this question.

Third, there is presently significant uncertainty about the importance of group effects in earthquake events. For example (ATC-32 Applied Technology Council, 1996) suggests that "group effects can be neglected for earthquake loading at three-diameter center–to-center spacing or higher" because "for softer soils, cyclic loading tends to remold a zone immediately around the pile, with the weakened soil becoming less effective in transferring induced stresses to the neighboring piles." This issue will continue to be unresolved unless cyclic full-scale static and dynamic load tests are performed in softer silts and clays. These tests would make it possible to evaluate the effects of remolding and gapping on the p-multipliers in these materials and determine if p-multipliers really should be neglected.

Fourth, some state DOTs, such as Caltrans, are moving to the use of larger diameter pile foundations (610 to 1000 mm) to resist large lateral loads. Some testing on large diameter drilled shafts suggests that group effects will be less pronounced for stiffer pile foundations in comparison to 250 to 300 mm diameter pile groups which have been tested in the past. Additional testing of large diameter pile groups will help resolve this question.

Finally, the lateral Statnamic testing previously conducted on the pile group at the Salt

Lake Airport indicated that the dynamic resistance was significantly higher than the static resistance. The increased resistance was determined to be primarily due to damping, however this testing involved only a few load cycles. Damping may decrease significantly as gaps develop behind the pile with increased number of cycles. Statnamic testing, conducted after various numbers of cycles have taken place, would provide an indication of the effect of gapping on the dynamic capacity.

RESEARCH OBJECTIVES

The driven pile research described in this report had the following objectives:

1. Evaluate the effect of pile spacing on measured p-multipliers and develop design curve for p-multipliers as a function of pile spacing.
2. Determine the validity of the p-multiplier concept for a larger (5-row) pile group and determine if p-multiplier values remain constant beyond the third row.
3. Examine the influence of pile diameter on lateral load resistance and p-multiplier values.
4. Determine the effect of cyclic loading and gap formation in clays on the measured group effects and p-multipliers.
5. Examine the effect of cyclic loading and gap formation in clays on the measured dynamic resistance.
6. Evaluate the effect of pile diameter and stiffness on p-multiplier values for pile groups.
7. Evaluate the effect of uplift and compression on the lateral resistance of pile groups.
8. Provide well-documented case histories for use in evaluating and calibrating computer and physical models.

SCOPE OF WORK

To achieve the objectives of the research investigation, a series of static and dynamic lateral load tests were conducted on two single piles and four pile groups at a test site below the South Temple Street overpass on the Interstate 15 alignment in Salt Lake City, Utah, as shown in Figure 1.3. Work tasks included (a) Site Characterization, (b) Cyclic Lateral Load Testing of
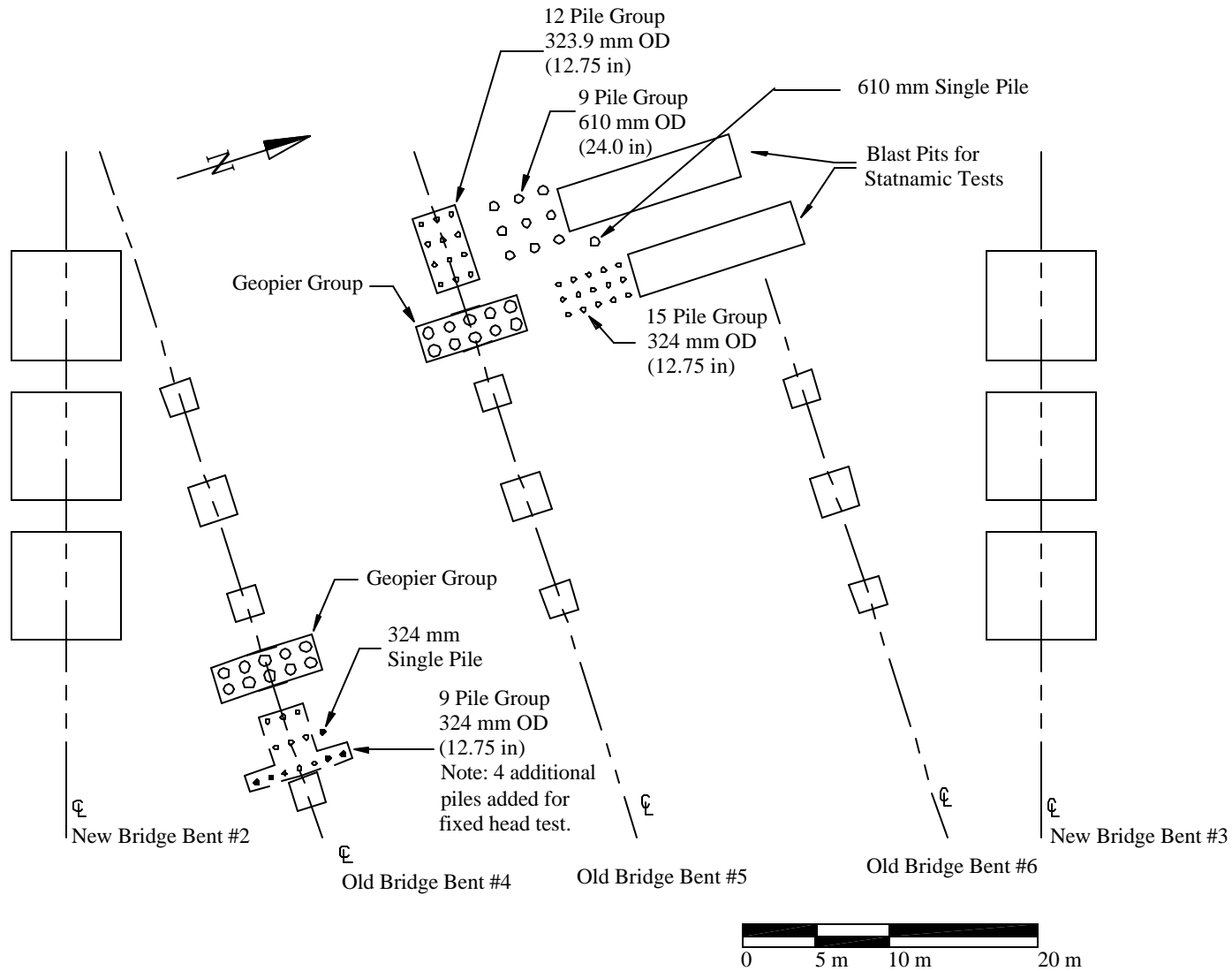
Figure 1.1 Layout of two single test piles and four pile groups at site below South Temple overpass on I-15 corridor.

Single Piles, (c) Cyclic Lateral Load Testing of Four Free-Head Pile Groups (d) Dynamic Lateral Load Testing of Two Free-Head Pile Groups, (e) Cyclic Lateral Load Testing of a Fixed-Head Pile Group. (f) Data Reduction and Analysis. A summary of each work task is provided below.

Site Characterization

Proper characterization of the subsurface materials was necessary to ensure that the foundation and instrumentation were designed properly and to provide input data for use in the numerical analyses. Cone penetration test (CPT) soundings were performed at each test foundation to define the stratigraphy and variations across the site. Additional in-situ testing included vane shear tests, standard penetration tests, cone pressuremeter tests, and shear wave velocity tests. Undisturbed samples and disturbed samples were also obtained for laboratory strength, consolidation and index testing. The soil profile generally consists of medium stiff clay with some sand layers. The water table was typically located 1.2 m below the ground surface.

Cyclic Lateral Load Testing of Two Single Piles

Cyclic load tests were performed on two isolated single piles driven to a depth of approximately 11.5 m. These tests were necessary to provide a comparison to the behavior of the pile groups. One test pile was a closed-end 324 mm OD pipe pile while the other was an open-end 610 mm OD steel pipe pile. Strain gages were placed on opposite faces of each pile at 10 depth levels to determine bending moment profiles versus depth. Load was applied in approximately 10 increments with a hydraulic jack. Applied load was measured with a load cell while pile head deflection and rotation were measured with LVDTs. For each deflection increment, 15 load cycles were applied to simulate the cyclic loading typical of an earthquake and to evaluate the change in lateral resistance due to cyclic loading.

Cyclic Lateral Load Testing of Four Free-Head Pile Groups

Cyclic load testing was also performed on four separate pile groups at different spacings. Three of the pile groups involved 324 mm diameter piles. One group consisted of piles in a 3 x 3 arrangement with a longitudinal spacing of 5.6 pile diameters on centers. A second group consisted of piles in 3 x 4 arrangement with a spacing of 4.4 pile diameters and the third group consisted of piles in a 3 x 5 arrangement with a spacing of 3.3 pile diameters. The fourth pile group consisted of 610 mm diameter piles in a 3 x 3 arrangement with a spacing of 3.0 pile diameters on centers. The load was applied to a load frame using two 1300 kN hydraulic jacks and measured with load cells.

The load frame was designed to provide the same displacement at each pile location and to be essentially rigid in comparison with the stiffness of the piles. Each pile was attached to the load frame by a tie-rod with a moment free connection. Strain gages attached to each tie-rod provided a continuous readout of the load carried by each individual pile during the test. Pile head deflection and rotation were measured using LVDTs attached to an independent reference frame. Strain gages were placed on opposite faces of one pile in each row at 10 depth levels. The same sequence of loading described for the single pile test was employed for the pile group tests.

Dynamic Lateral Load Testing of Two Free-Head Pile Groups

Statnamic load testing was also performed on the 3 x 5 pile group consisting of 324 mm test piles and the 3 x 3 pile group consisting of 610 mm test piles. At small deflections, statnamic tests were performed after 15 cycles of static loading had been applied to the pile group; however, at larger deflection levels, the statnamic device was used to produce the first cycle of loading. This approach provided a comparison between the dynamic resistances offered

before and after cyclic loading under dynamic loading. The statnamic loading system was capable of applying loads as great as 3600 kN with rise times between 0.1 and 0.3 seconds. A high-speed data acquisition system was used to record data for over 150 channels at 2000 samples per second.

Cyclic Lateral Load Testing of a Fixed-Head Pile Group

As part of a cooperative effort, pushover testing of a bridge deck was performed by researchers at the University of Utah during this study (Lawton, 2003) The load was applied to the bridge deck using a hydraulic actuator mounted atop a structural steel frame. The footings for the steel frame consisted of a pile cap supported by Geopier foundations and a pile cap supported by steel pipe piles. A reinforced concrete pile cap was constructed around the 3 x 4 pile group to provide a one reaction footing for the pushover test. During this loading process the fixed-head pile group was subjected to simulated cyclic earthquake loads consisting of a horizontal force (alternating in direction) along with a vertical force (alternating compression and uplift), and a moment (alternating direction) generated by the horizontal force acting on top of the pile cap. Comparison of the results for the nearly identical testing conditions and similar subsurface conditions allowed determination of the relative performance of the pile and Geopier foundation systems under simulated earthquake loads.

Data Reduction and Analysis of Test Results

The results from the testing program were reduced in an effort to produce the following basic test plots:

- Average pile head load versus deflection curves for the first and last cycle for the single pile and pile groups.

- Normalized load versus deflection curves to show average load carried by piles in each row relative to that carried by a single pile.

- Maximum bending moment versus applied load for the first and last cycle for the single single pile and the pile groups.

- Bending moment versus depth curves for each load cycle at each load increment for the single pile and the pile groups.

- Reduction in pile group stiffness as a function of the number of cycles

- Statnamic load versus deflection curves relative to static load versus deflection curves.

- Time histories of static spring force, damping force and inertia force for each statnamic test.

Based on the results of the testing, p-multipliers were back-calculated using computer analysis programs. The results for the pile group testing made it possible to develop p-multipliers as a function of row position. In addition, p-multipliers were developed as a function of center to center pile spacing.

Finally, studies were conducted to evaluate the ability of several computer programs for analyzing laterally loaded piles and pile groups to match the behavior observed in the testing. These programs included LPILE and GROUP (Reese et al, 1996) and FLPIER (Hoit, 1997). The GROUP program uses the finite difference method and is widely used in practice. The FLPIER program uses the finite element method and was developed at the Univ. of Florida. This program is distributed by the Florida DOT at no cost and will likely see increased use as a result of FHWA support. Both of these programs employ the p-y concept and allow the user to define p-multipliers. These programs were found to provide reasonable estimates of the lateral load behavior of a pile group in a previous testing program. Validation studies of this type are crucial

in providing designers and researchers with "ground truth" information regarding the ability of

computer programs to model real conditions.

CHAPTER 2 LITERATURE REVIEW

INTRODUCTION

Previous research conducted on the lateral response of pile groups has involved full-scale tests, centrifuge model tests, 1-g models tests and numerical analyses. This chapter contains a review of previous research, a discussion of the limitation of existing research and a discussion of the need for further research.

Full-scale lateral pile group test results were reported by six investigators including: Brungraber, et al, (1976), Meimon, et al (1986), Brown, et al (1987), Brown, et al (1988), Townsend, et al (1997), and Rollins, et al (1998). These tests provide the best indication of pile group behavior since they involve real piles in real soils.   Pile group tests involving small-scale physical models were reported by Prakash and Saran (1967), Dunnavant and O'Neill (1986) and Cox et al (1984); however, these tests suffer from questions regarding scale and stress level effects. Later, centrifuge pile group tests were performed by a number of investigators including Kotthaus, et al (1994), McVay, et al (1998), McVay et al (1994), McVay, et al (1995) and Remaud, et al (1998). Although centrifuge tests eliminate stress level concerns, questions still exist regarding their direct applicability to full-scale behavior. Finally, numerical analyses involving pile group behavior were reported by Brown and Shie (1991). They identified and modeled the reduction in resistance as a function of pile spacing. However, numerical analysis methods in general suffer from difficulties in defining the soil stress-strain properties and in accounting for slippage between the pile and the surrounding soil.

FULL-SCALE TESTS

Full-Scale Lateral Load Tests on Pile Groups (Brungraber and Kim, 1976)

A series of lateral load tests were performed on two pile groups and isolated single piles at a site at Bucknell University near Lewisburg, Pennsylvania. The 10BP42 steel H-piles were approximately 12.2 meters (40 feet) in length. Each pile group was designed to have two rows containing three piles each. The pile rows were spaced at 1.2 meters (4 feet) in Group I and 0.9 meters (3 feet) in Group II. Each pile group was capped with a 1.2-meter (4-foot) thick concrete footing. The soil profile consisted of clay and clay loam underlain by limestone at a depth of 12.2 meters (40 feet). The water table was at 10.7 meters (35 feet) below the ground surface.

Three series of vertical and lateral load tests were conducted. Two calibrated 534-kN (60-ton) jacks were used to apply the lateral load. Strain gauges were placed along the length of each pile, which enabled the calculation of the bending moments. The displacements at each corner of the pile cap were measured with 12 dial gauges.

A comparison of the Group I (1.2 meter spacing) and Group II (0.9 meter spacing) results revealed that an increase in spacing between the rows increased the lateral load resistance of the group. At a given load, the deflection of the Group II piles was twice that of the Group I piles. This increase in deflection in Group II was a result of decreased soil resistance because of group interaction effects. In addition, the reduced soil resistance led to greater bending moments in Group II.

The cyclic loading of the group resulted in increased deflections as the cycles progressed. The soil resistance decreased as the soil was moved and gaps formed around the piles. For loads up to 59 kN (13 kips) the increase in deflection was about 29%. For subsequently greater loads the increase was only about 4%. Similar increases were noted in the bending moments.

Groups I and II were capped with a concrete footing. This essentially rigid cap influenced the behavior of the pile group. Interaction between the fixed cap and the ground created difficulties in analyzing the load capacities of the two groups with the isolated single pile test results. Although this test does show group effects resulting from variations in spacing, due to the capped pile groups the distribution of loading is unknown.

Pile Group Behavior Under Long Time Lateral Monotonic and Cyclic Loading (Meimon, et al, 1986).

Full-scale lateral load tests were performed at a site in Brittany, France on a 6-pile group as well as a single pile. The pile group was composed of six piles hinged in a rigid cap and aligned in two rows spaced three pile diameters apart center-to-center. Within each row, the spacing was two pile diameters. The closed ended H piles were 284 mm by 270 mm with a stiffness (EI) of 3×10^4 kN-m^2. Each pile was driven to a depth of 7.5 m (24.6 ft).

The initial soil profile consisted of high and low plasticity clays underlain with silt. After excavation of one meter of highly plastic clay around the piles, the soil profile consisted of four meters of low plasticity clay and four meters of silty sand. The water table was located at the ground surface.

A double-acting hydraulic jack was used to apply the lateral load to the pile cap. The lateral displacement of the pile group was measured with two gauges that were attached to the excavated wall. Bending moments were calculated based on measurements obtained from strain gauges located along the entire depth of four of the piles. The testing also included two long-term creep tests and five cyclic tests. The cyclic tests were composed of 1,000 to 10,000 cycles.

The displacement at the top of the pile group was about 40% greater than the single pile, which can be attributed to several factors. The three-pile diameter spacing resulted in pile-soil interaction, which reduced the soil resistance. In addition, the time between the driving of the

piles and the testing was different for the group and the single pile. Nine months had passed between the driving and testing of the single pile. The time between the driving and the testing of the pile group was only one month. This difference in time was an uncontrolled variable in the experiment and introduced some uncertainty into the results.

The load history also influenced the pile group behavior. Following the initial static test and three cyclic tests, the subsequent static test showed a stiffer group behavior. A reduction in the group effect was noticed as the cyclic loading progressed. This could indicate that a uniform degradation of the soil around the piles in the group occurred due to gap formation so that the contribution of soil resistance became less important.

Characteristic signs of the group effect or shadowing were noticed in this test. The front row supported a greater load than the trailing row. This was due to greater soil resistance in front of the first row. The trailing row was subjected to an overlapping of shear zones and consequently experienced decreased soil resistance. The group effect was most pronounced in the initial portion of the test. As the test progressed, the reduction due to the group effect reached a constant value.

Cyclic Lateral Loading of a Large-Scale Pile Group (Brown et al, 1987; Brown et al, 1988).

A lateral load test was conducted on a group of nine piles. The soil profile consisted of stiff over-consolidated clays and silty clays (CL, CH) to a depth of 7.3 m (24 feet), underlain by sandy clay and silt (CL, ML). The 3x3 group had rows spaced at three pile diameters center to center. The piles were steel pipes, 273 mm (10.75 in.) in outside diameter, with a wall thickness of 9.27 mm (0.365 in.).

All nine piles were instrumented with strain gauges to allow for the computation of bending moments and load cells to measure the applied load. A double-acting hydraulic cylinder

applied the lateral load, and pin connection load cells transferred the load from the frame to the piles. The loading was cyclic and bi-directional with 5 series of load applications (100 to 200 cycles per series). Two linear potentiometers spaced 1.5 m (5 ft) apart monitored both deflection and rotation.

The deflection in the group was significantly greater than the deflection of the single pile when subjected to the same average load per pile. As the load increased the group effect increased. At large loads the group effect was significantly more apparent and a "collapse" load for the group would most likely appear at a significantly lower load per pile than would occur for the single pile.

The load supported by each pile was a function of the position of the pile within the group. As shown in Figure 2.1, the front row piles supported the greatest load while each successive row supported a smaller load at the same deflection. As the load increased, the difference between the load in each row became more pronounced. In addition, as the group was subjected to multiple cycles the load required to reach the same deflection decreased.

The load was measured at each pile to determine the importance of the position within the group. The distribution of the load within the group was a function of the row position and not the individual position of the pile within a row. This pattern does not agree with elasticity-based methods in which corner piles carry the greatest load regardless of the position of the row (Brown et al, 1987). The importance of row position became more apparent as the loads and deflections increased and stabilized at large loads and deflections. The row position seemed to be less important after many cycles. This was most likely due to the creation of gaps around the piles.
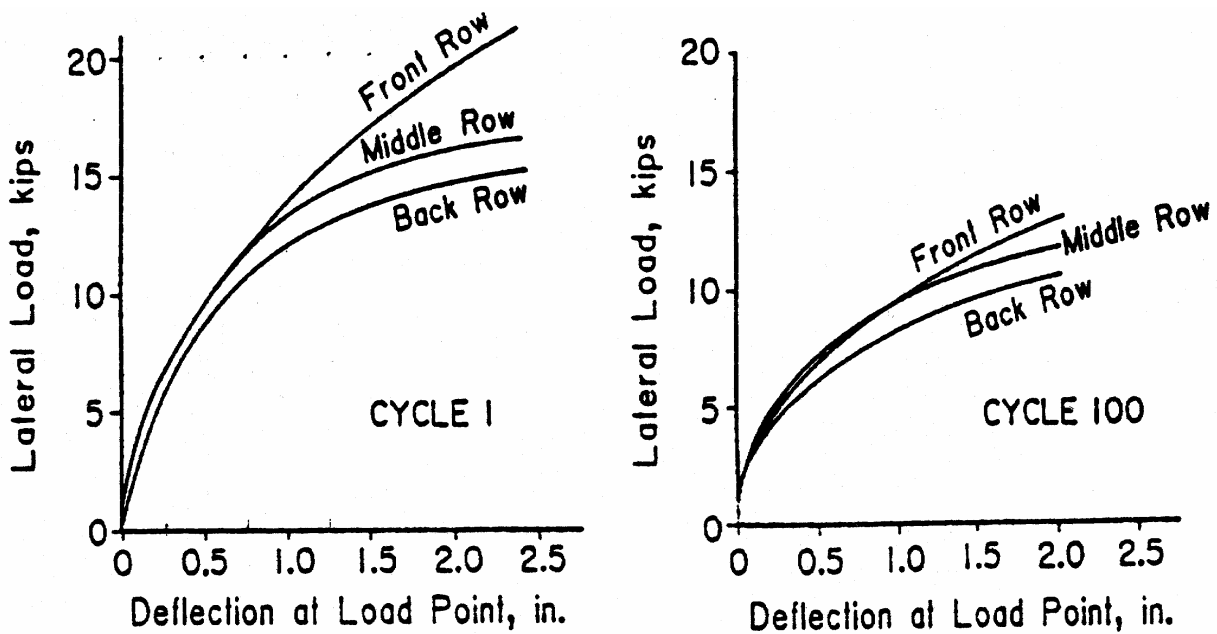
Figure 2.1 The load supported by each row of the group (Brown et al, 1987).

Bending moments in the piles located in the group were greater and occurred at deeper depths than those experienced by the single pile. The largest moment occurred in the front row at a shallower depth than those of the trailing rows. This was due to the group effect. As the piles interacted with the soil the resistance in the upper layers decreased.

Following the testing described above the clay was excavated to a depth of 2.9 m (9.5 ft) and backfilled with medium dense sand. The sand was compacted in 0.15 m thick lifts to a relative density of about 50%. The same piles and test setup that were used in the previous clay test were used in the sand test.

As was observed in the experiment involving clay, the leading row experienced the greatest soil resistance. The behavior of the leading row was similar to the isolated pile. An overlapping of the shear zones of the piles in the trailing rows resulted in a reduction of the soil

resistance. The effect of shadowing appeared to be more significant in the sand experiment than in the clay experiment. (Brown et al, 1988).

Cyclic loading in two opposite directions had a relatively small effect on the pile response relative to similar tests conducted in clays. Some softening of the response of the piles in the group was observed at large loads (approaching pile failure); almost no effect occurred at small loads.

Significant densification apparently occurred in the sand due to two-way cyclic loading and may explain the relatively small loss in soil resistance due to cyclic loading. It is probable that one-directional cyclic loading would have produced greater loss of soil resistance and less densification. These observations underscore the importance of load history on the behavior of laterally loaded piles in sand.

Bending moments in the piles in the leading row were very similar to those of the isolated single pile under the same load per pile. The maximum bending moments in the trailing rows occurred at greater depths than in the leading row. The total load on the group was distributed in greater proportion to the piles in the leading row, therefore the maximum bending moments for a given load occurred in the leading row piles as shown in Figure 2.2.

Brown et al (1988) developed p-multipliers that took into account the loss of soil resistance in piles located in trailing rows. The soil properties influence p-multipliers and therefore they are site specific. As shown in Figure 2.3, the p-multipliers for this group were 0.8 for the front row 0.4 and 0.3 for the middle and back row, respectively.
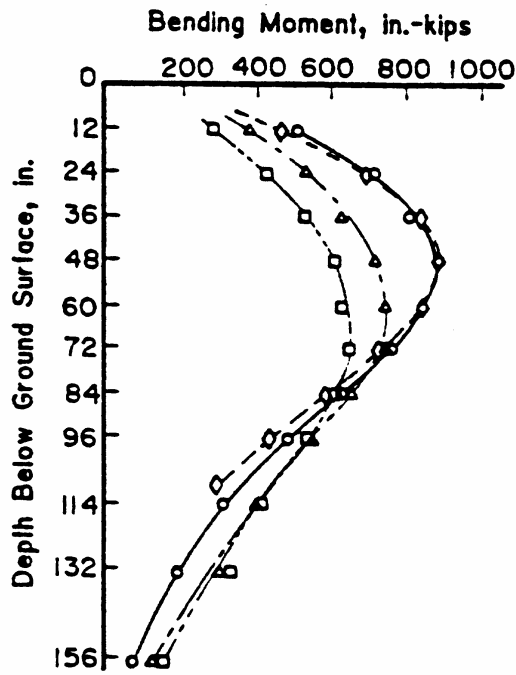
Figure 2.2 Bending moment versus depth (Brown et al, 1988).
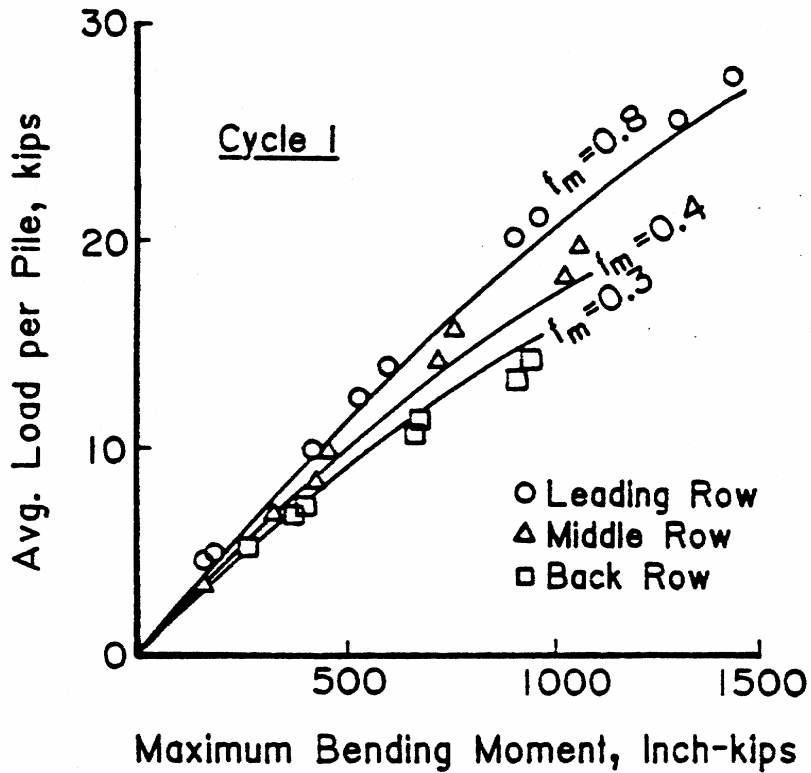
Figure 2.3 P-multipliers for the 9-pile group in sand (Brown et al, 1988).

Lateral Load Behavior of Full -Scale Pile Group in Clay (Rollins et al, 1998)

Rollins et al (1998) conducted a full-scale static lateral load test of a 3 X 3 pile group at the Salt Lake City International Airport in Salt Lake City, Utah. The piles were 305 mm I.D. closed-end steel pipe piles with a 9.5-mm wall thickness that were filled with concrete.

The soil profile consisted of about 8.5 meters of soft to medium-stiff clays (CL) and silts (ML) underlain by sand (SP, SM). The water table was located at the ground surface.

Six of the nine piles were fully instrumented with inclinometers and strain gauges. A load frame with lubricated steel casters that traveled on steel beams placed on the ground was used in the test to reduce friction. Load was applied to the group using a 1.34 MN (150 ton) hydraulic jack. A W36X150 beam was used to distribute the force to a sheet pile reaction wall. The load was transferred from the load frame to the piles by pin-connected tie rods. Linear variable differential transducers (LVDTs) were used in the test to measure the displacement of the pile group. Strain gauges attached to each tie rod acted as load cells and measured the resistance provided by each pile. A load cell placed behind the hydraulic jack measured the total load applied to the frame.

The group deflected 2 to 2.5 times as much as the single pile under the same average per pile loading. The load distribution in the pile group was not uniform. As previously noted by Brown et al (1987) the front row carried the greatest portion of the load for a given group deflection. The load per pile was always less than that of the single pile for equivalent deflections due to the group effect. In contrast to previous tests, Rollins et al found that the back row carried a greater load than the middle row as shown in Figure 2.4. No consistent trends were found in the load distribution among piles in the same row.

A difference in pore water pressures seems to be the explanation for the increased load carrying capability of the back row.   During the lateral movement of the pile group the material

right behind the pile would be in tension resulting in negative pore water pressure in soft clays. This negative pore water pressure would increase the soil resistance and strength in the trailing row. In stiff overconsolidated clays positive pore water pressure would have been developed and therefore a decrease in strength would be observed. For sands the pore water pressure would dissipate quickly and have little effect on the strength of the soil (Rollins et al. 1998).

Bending moments for piles in the group were significantly higher than those of the isolated single pile for the same average load. Increases between 50 and 100 % were observed. The reduction in soil resistance in the top layers also increased the depth at which the maximum moment occurred. This finding of greater moments at deeper occurrence is similar to previous findings.

The computer software GROUP was used in the analysis of the data (Reese and Wang, 1996). For this pile group the p-multipliers were found to be 0.6, 0.38, and 0.43 for the front, middle and back rows respectively. These values were significantly lower than the default p-multipliers used by the GROUP program. As can be seen in Figure 2.5, adjusting the p-multipliers of the program provided good agreement between the computer-derived load versus deflection curve and the measured load versus deflection curve. Design charts can be developed to obtain estimates of p-multipliers for other spacings.
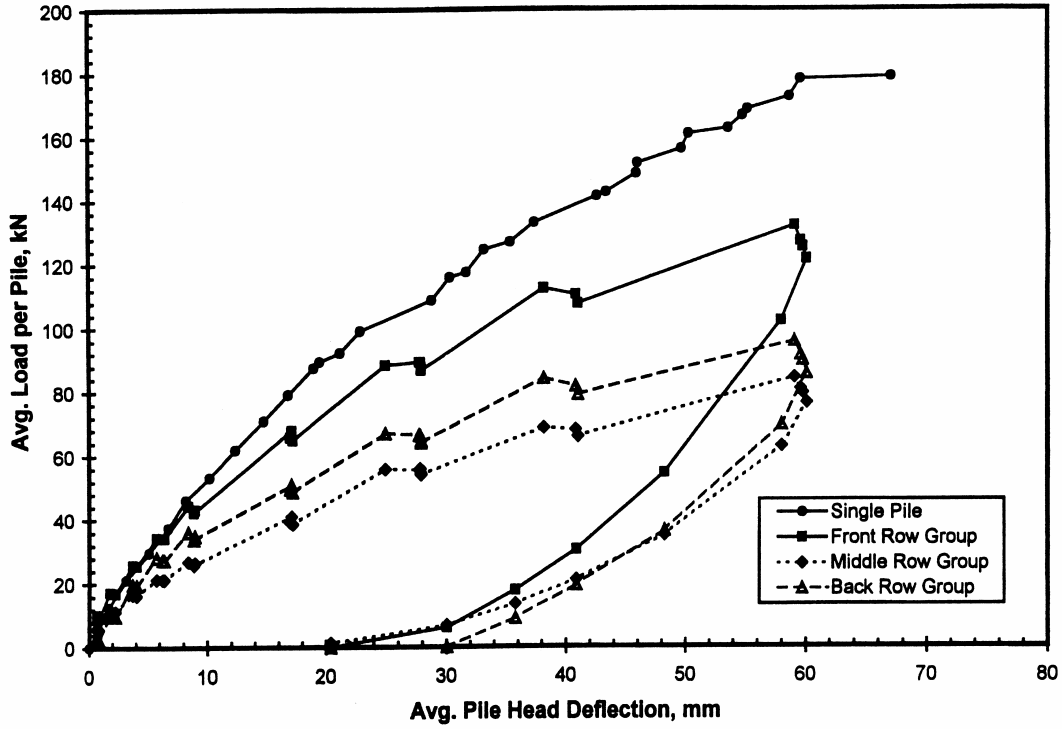
Figure 2.4 Average load versus average deflection (Rollins et al. 1998).
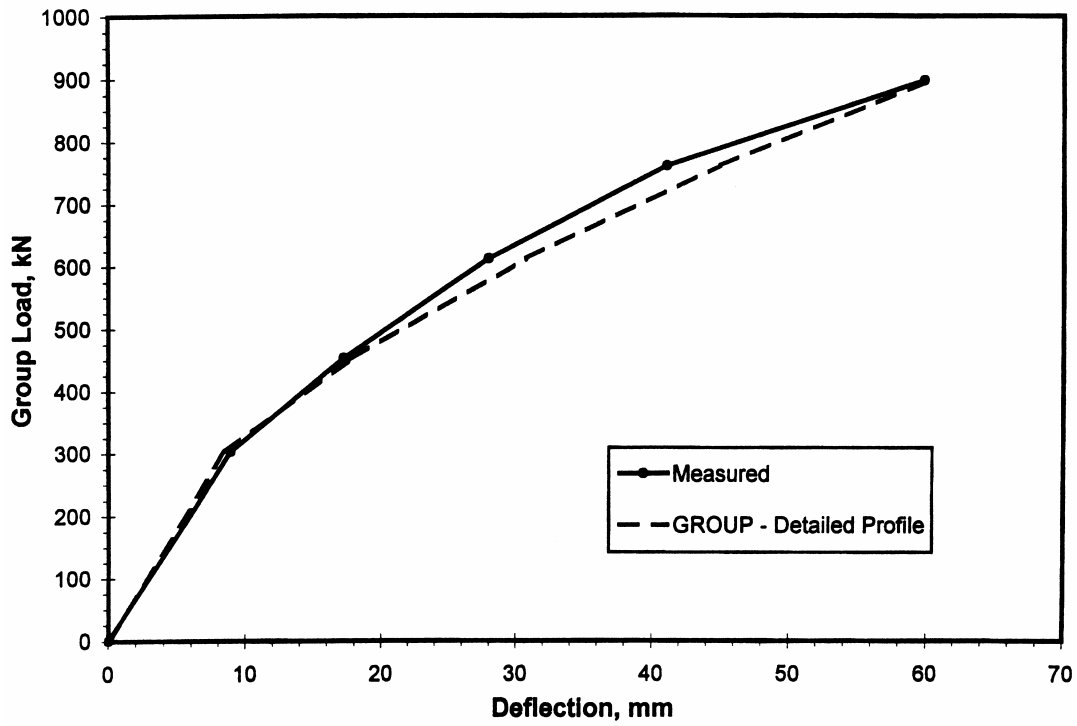
Figure 2.5 Comparison of measured load versus deflection curves and those computed with GROUP program (Rollins et al. 1998).

Evaluation of Laterally Loaded Pile Group at Roosevelt Bridge (Ruesta and Townsend, 1997)

Ruesta and Townsend (1997) studied the lateral load behavior of a 16-pile group in Stuart, Florida. The group was composed of pre-stressed concrete piles in a 4 x 4 arrangement that were spaced at 3 pile diameters. The piles were 760 mm (29.92 in) in diameter and 16.5 m (54.1 ft) long. The ground surface was 2 meters below the water level and the soil profile consisted of two well-defined layers of cohesionless soil made up of 4 m of fine loose sand underlain by partially cemented sand.

The test instrumentation consisted of strain gauges attached to a 350 mm (13.8 in) diameter steel pipe (9.5 mm thick (0.37 in)) inserted and grouted into each instrumented pile. In addition, a slope inclinometer casing was used. Ten piles of the test group, six piles of the reaction group, and the single pile were instrumented with strain gauges and inclinometers. A strain gauge was placed on each side of the pipe at eight different levels. One load cell was used to measure the load applied to the entire group and separate load cells were attached to each of the ten fully instrumented piles. Spherical bearing connections were used for both the individual load cells and the main load cell to minimize loading eccentricity. The loading consisted of static loads up to 320 kN (71.9 kip) for the single pile and 4,800 kN (1079 kip) for the pile group.

The load versus deflection curves showed that the load per pile was lower than that measured in the single pile for the same deflection. The leading row behaved similarly to the single pile and carried more load than the trailing rows.

The p-multiplier concept worked well for predicting the behavior of the group. The p-multipliers obtained were 0.8, 0.7, 0.3, and 0.3 for the leading, middle leading, middle trailing and trailing rows respectively. The bending moments in the group were greater than those of the

single pile for the same average load due to the decreased soil resistance. All of the above

differences can be attributed to the group effect as explained previously.

Summary of Full-Scale Pile Group Testing

Tables 2.1 and 2.2 are summaries of the lateral load tests conducted on full-scale pile

groups and the p-multipliers that were back-calculated from the test results.

Table 2.1 Summary of previous full-scale lateral pile group tests.

Reference	Location	Pile Type	Group Geometry	Soil Type
Kim and Brungraber (1976)	Lewisburg, PA	0.254 m H-piles	2-2x3, s=3.5d and s=4.7d	Clay w/ Gravel
Meimon et al (1986)	Brittany, France	0.284 m H-piles	3x2, s=3d long., but 4d transverse	Silty Clay
Brown et al (1987)	Houston, TX	0.273 m pipe piles	3x3, s=3d	Stiff OC Clay
Brown et al (1988)	Houston, TX	0.273 m pipe piles	3x3, s=3d	Uniform Clean Sand
Ruesta and Townsend, (1997)	Stuart, FL	0.76 m square pre-stressed concrete	4x4, s=3d	Loose Fine Sand
Rollins et al (1998)	Salt Lake City, UT	0.324 m pipe piles	3x3, s=3d	Clayey Silt

Table 2.2 Back-calculated P-multipliers based on previous full-scale lateral pile group tests.

Reference	P-multipliers by Row				Load-Carrying Characteristics
	1	2	3	4	
Kim and Brungraber (1976)	NA	NA	NA	NA	Piles spaced at 3.5d deflected twice as much as piles spaced at 4.7d for same load
Meimon et al (1986)	0.9	0.5	-	-	Trailing row piles carried 65 to 85% of front row piles at 15 mm deflection
Brown et al (1987) (30 mm) (50 mm)	0.7 0.7	0.6 0.5	0.5 0.4	- -	Trailing row piles carried 70 to 80% of front row piles after 25 mm deflection
Brown et al (1988)	0.8	0.4	0.3	-	Trailing row piles carried 55 to 75% of front row piles at 25 mm deflection
Ruesta and Townsend, (1997)	0.8	0.7	0.3	0.3	Trailing row piles carried 50 to 75% of front row piles at 30 mm deflection
Rollins et al (1998)	0.6	0.38	0.43	-	Trailing row piles carried 60 to 75% of front row piles at 30 mm deflection

ONE-G MODEL TESTS

Model tests have also been used to study lateral pile group behavior and the reduction in resistance due to group interaction. The concept of p-multipliers as a function of pile spacing has also been investigated and the findings are summarized below.

Line-By-Line Reduction Factors (Dunnavant and O'Neill 1986; Cox et al, 1984)

The line-by-line reduction factors that are used in GROUP version 4.0 (Reese and Wang, 1996) are based on work by Cox et al (1984) that was formalized by Dunnavant and O'Neill (1986). Cox et al (1984) studied pile behavior with 25 mm diameter model piles. The reduction factors used in GROUP for the leading and trailing row can be found in Figures 2.6 and 2.7.
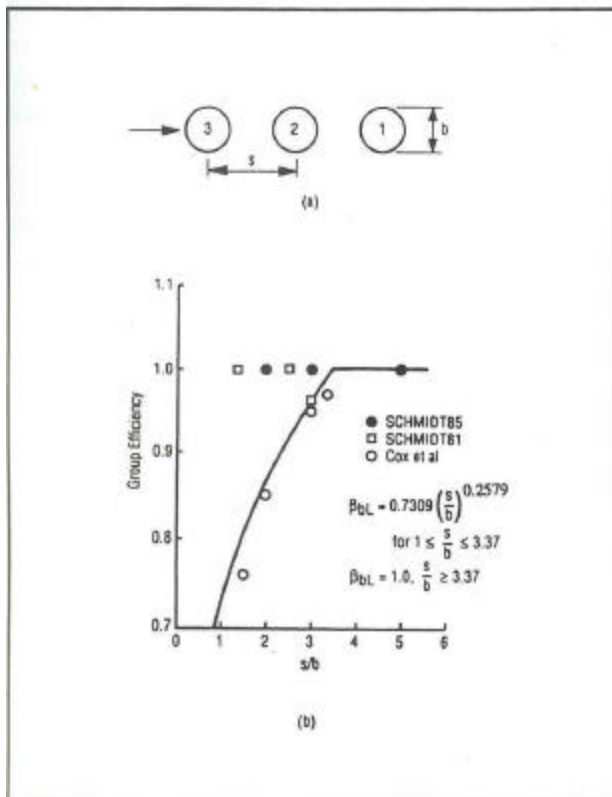
Figure 2.6 Reduction factors used in GROUP Program for the leading row piles (Reese and Wang, 1996).
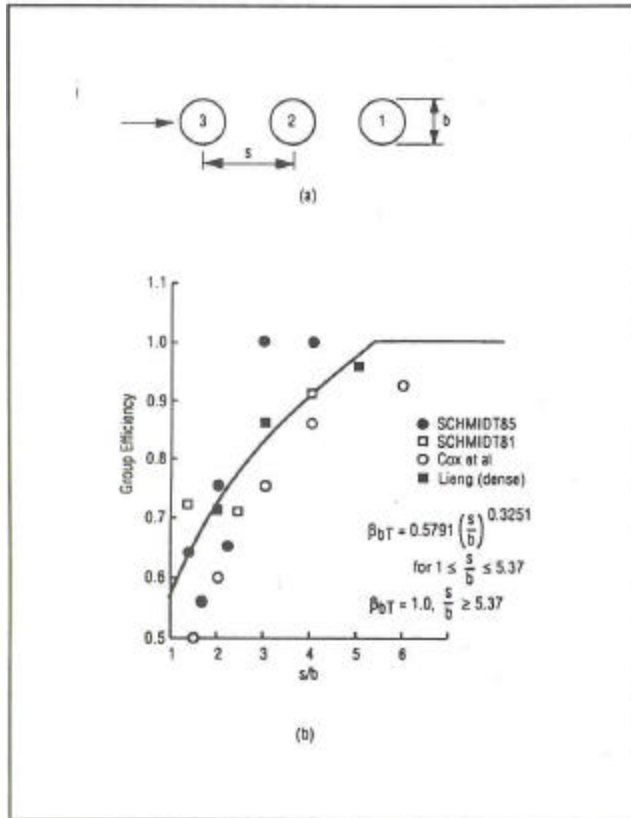
Figure 2.7 Reduction factors used in GROUP Program for the trailing row piles (Reese and Wang, 1996).

These results suggest that group interaction is insignificant for center-to-center spacings larger than 3.5 pile diameters in the leading row and 5.5 diameters in the trailing rows.

Behavior of Laterally Loaded Piles in Cohesive Soil (Prakash and Saran, 1967 and 1990)

Prakash and Saran (1967) presented results of lateral load tests conducted on groups of model piles in clay. Seven fixed head tests were conducted on 2x2 and 3x3 pile groups in prepared soil. Each set of piles was tested to determine the group efficiency, G_e, of the pile groups. Aluminum piles 29 cm in length with outside diameters of 9 mm (0.35 inches) and inside diameters of 5.9 mm (0.23 in) were used in the tests. Loads were applied to the pile caps at the ground level and lateral deflections were measured at the load point.

2-15

Prakash and Saran (1967) concluded that the group interference decreased with increased spacing in the load direction and vanished altogether at spacings greater than six diameters. In 1990, Parakash and Saran summarized the group efficiency results from the 1967 paper and revised the recommendations somewhat. These results can be found in Table 2.3.

Table 2.3 Group efficiency G_e, for piles in cohesive soils[a]

S/B	G_e 2x2 Group	3x3 Group	Recommended
3.0	0.42	0.39	0.40
3.5	0.50	0.42	0.45
4.0	0.57	0.44	0.50
4.5	0.61	0.47	0.55
5.0	0.63	0.48	0.55
6.0[b]	-	-	0.65
8.0[b]	-	-	1.00

S = Center-to-center pile spacing
B = Pile diameter or width
[a] These values have been obtained from curves provided by Prakash and Saran (1967).
[b] These values are extrapolated.

The results indicated that at the spacing of eight pile diameters center to center, the group effect becomes negligible. Tests, however, were not conducted at this spacing. The results come from extrapolating the data acquired at smaller spacings. The suggested eight-diameter spacing was only a conservative estimation of the same results that led to the previous six-diameter estimate (Personal communication, Prakash, 2000). Prakash and Saran (1990), while summarizing the findings of the 1967 paper, state that there is a limited amount of ultimate lateral load resistance data available from pile groups and there is a need for further testing 90).

CENTRIFUGE MODEL TESTS

The principle behind centrifuge testing is to use scale model piles and subject them to an artificially high acceleration field. This field reproduces the in-situ stresses that the full-scale pile would experience. For example, at a centrifuge acceleration of 45 g a full-scale pile 15 m

(49.2 ft) long and 0.61 m (2 ft) in diameter can be modeled by a 0.33 m (13 in) long, 13.5 mm (0.53 in) diameter pile (McVay 1995). To more accurately model field conditions, innovative devices have been developed that can drive and laterally load the piles in flight at full test acceleration. The results can then be scaled up to "prototype" or full-scale conditions.

Single Piles and Pile Rows Subjected to Static and Dynamic Lateral Load (Kotthaus et al, 1994)

Kotthaus et al (1994) conducted tests on a single pile and a group of three piles in a line. The model piles were aluminum tubes with an external diameter of 3 cm (1.2 in). The piles were 60 cm (23.6 in) long and the load was applied at 8.5 cm (3.4 in) above the soil surface. The soil was a fine-grained sand with a relative density of 98% and was placed around the arranged piles by pluvial deposition. Row spacings of 3 and 4 pile diameters were used. Load was applied with a hydraulic actuator attached to the container rim. The piles were coupled to the actuator by a rigid bar which was hinge connected to the pile head and the actuator. Applied load was measured by a pair of strain gauges attached to opposite sides of each pile at the soil surface. Moments were observed on two of the piles equipped with 9 additional strain gauges along the embedded length. The test acceleration was 50 g and tests were performed with as many as 1000 load cycles.

The group effects lead to a reduction in the load carrying capacity of the piles in the group. The load in each pile divided by the load in the single pile is shown as a function of normalized deflection (deflection, u, divided by pile width, D) in Figure 2.8. The lead pile carried the highest load followed by the trailing and middle rows, respectively. As load cycles increased, the maximum bending moments were reduced. In addition, the location of the maximum moment shifted upwards indicating an increase in soil stiffness.
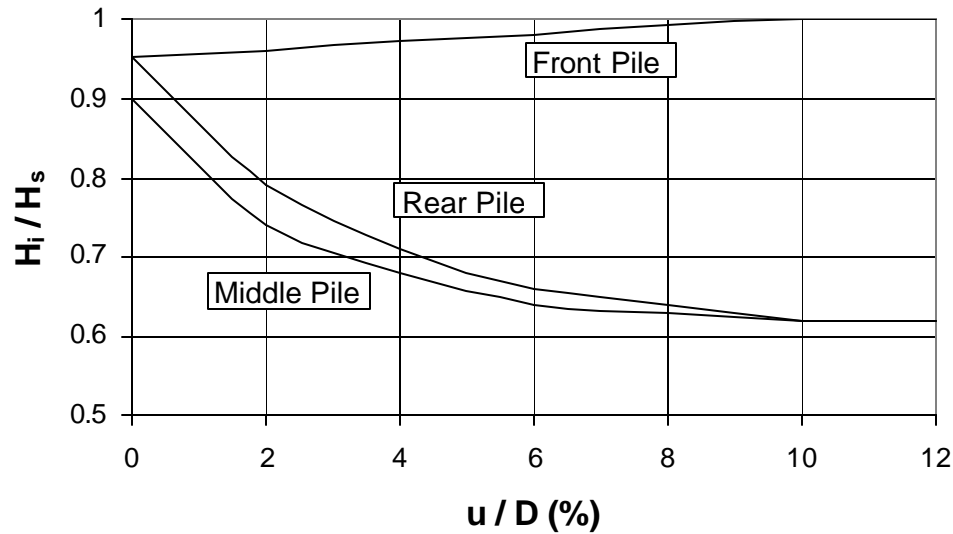
Figure 2.8 Ratio of load carried by pile in group to that carried by the single pile (H_i/H_s) as a function of deflection normalized by pile width, (u/D).

Overall, the group efficiency was significantly reduced due to group interaction. At the four diameter spacing the efficiency was approximately 80% while at the three diameter spacing efficiency was about 70%.

Centrifuge Modeling of Laterally Loaded Pile Groups in Sands (McVay et al, 1994)

The piles in this study were made of high strength aluminum tubing with an outside diameter of 9.5 mm (0.37 in). They were 279.4 mm (11 in) in length from the bottom of the pile cap with a clear distance of 44.5 mm (1.75 in) between the bottom of the pile cap and the soil surface. The nine piles were arranged in a 3 x 3 group. Row spacings of 3 and 5 pile diameters were investigated.

An innovative apparatus was developed and used to drive and laterally load the piles at a full test acceleration of 48 g. Lateral load was applied with a 5.3 kN (1200 lb) air cylinder. A load cell and a linear variable displacement transducer (LVDT) were attached to the cylinder to measure applied loads and lateral movement. The pile cap consisted of three separate aluminum

2-18

blocks that transferred the load to one another through four load cells. Two loads cells were located between the lead and middle rows and two between the middle and trailing rows. The load transmitted to each row was found by subtraction from the total applied load. The soil was a Reid-Bedford sand placed at relative densities of 16 and 45%.

At the three-pile diameter spacing the lead row carried more load than the other two rows (37, 33, and 30% respectively for a relative density of 16%). At the five diameter spacing the load distribution was much more uniform with the lead row carrying 35% of the total followed by the middle and trailing rows with 33 and 31%, respectively at the same relative density. At the increased spacing of five diameters the average lateral resistance increased by 22% relative to the pile group at three pile diameter spacing. This indicates a reduction in the group effect at increased spacing as suggested by Reese (1986). At a higher relative density the soil showed a stiffer response and carried higher ultimate loads.

Lateral Response of Three-Row Groups in Loose to Dense Sands at Three and Five Pile Spacings (McVay et al, 1995)

The piles in this test were chosen to simulate a full-scale pile driven open ended with an overall length of 13.3 m (43.2 ft) and a diameter of 0.43 m (16.88 in). The piles were grouped and spaced the same as the test by McVay et al (1994). An isolated single pile was also tested and all piles were tested in the free-head condition. The piles were again driven "in flight". The Reid-Bedford sand was used in this test at relative densities of 33 and 55%.

Load distributions were virtually identical to the McVay et al (1994) test. At the three diameter spacing soil density was found to have an effect on row contributions to the total load while at the five diameter spacing there was no significant variation. At the three diameter spacing the group efficiency for both relative densities was approximately 73% while at the five

diameter spacing the efficiency was approximately 93%. The p-multipliers for the three diameter spacing were 0.8, 0.45, and 0.3 at a relative density of 55% and 0.65, 0.45, and 0.35 at a relative density of 33%. At the five diameter spacing the p-multipliers were 1, 0.85, and 0.7 for both relative densities. Numerical calculations of lateral pile response using the p-multipliers matched well with the measured results.

Laterally Loaded Piles: Investigation of Group Effects (Remaud et al, 1998)

The test piles in this study were AU4G aluminum hollow pipes with an outside diameter of 18 mm (0.71 in) and a total length of 380 mm (15 in). A single pile and a pair of piles spaced at 2, 4, and 6 pile diameters were tested with a free head boundary condition. The piles were equipped with 20 pairs of strain gauges placed every 15 mm (0.6 in) down the length of the piles. The first pair of gauges was at the soil surface. Lateral loading was done by a hydraulic servo-actuator. The loading device was attached to the piles with a metallic cable 40 mm (1.6 in) above the soil surface. Two displacement transducers at heights of 20 and 65 mm (0.8 and 2.6 in) measured pile head deflections and rotation. The soil was fine white Fontainebleau sand with a dry density of 16.3 kN/m^3 (103.8 lb/ft^3).

The group effects were pronounced at pile spacing less than six pile diameters. The loads on the lead pile, determined from the bending moments at the soil surface, were 59% of the total applied load at the two pile diameter spacing, 56% at the four diameter spacing, and 51% at six diameter spacing. Bending moments in the lead pile were very similar to those in the single pile. For the trailing pile the moments approached the single pile values as spacing increased. The p-multipliers calculated for the trailing pile were 0.52 at two diameter spacing, 0.82 at four diameter spacing, and 0.93 at six diameter spacing.

Centrifuge Testing of Large Laterally Loaded Pile Groups in Sands (McVay et al, 1998)

The piles used in this test were solid square aluminum (alloy 6061) bars with a width of 9.5 mm (0.38 in) and an overall length of 304.8 mm (12 in). The group layouts consisted of 3x3, 3x4, 3x5, 3x6, and 3x7 groups with all rows spaced at three pile diameters on center. A pile cap was constructed with rows of solid square aluminum bars containing slots machined for each pile. The pile groups were laterally loaded using an air piston. A miniature load cell measured lateral loads and an LVDT measured deflection. Sets of four strain gauges on each side of the pile above ground were used to measure applied loads on each pile. The soil was mixed sand made from a blend of different gradation sands so as to closely approximate the Reid-Bedford sand used in the authors' other experiments. The two relative soil densities used in all of the tests were 36 and 55%.

The load carried by an individual pile row was a function of the number of rows in the pile group. In the 3 x 3 group the lead row carried approximately 45% of the total load and dropped to 23% for the 3 x 7 group. The load carried by each row of the five different tests is shown in Table 2.4. Row contributions to total load were shown to be independent of soil density. The decrease in load carrying capacity appeared to stabilize after the fourth row in the groups containing more than four rows.

Table 2.4 Percent of Total Lateral Load by Row for Pile Groups (McVay 1998).

Row Position	3 X 3 Dense Sand	Loose Sand	3 X 4 Dense Sand	Loose Sand	3 X 5 Dense Sand	Loose Sand	3 X 6 Dense Sand	Loose Sand	3 X 7 Dense Sand	Loose Sand
Lead Row %	43.3	46.6	37.8	36.7	30.4	29.0	26.4	25.0	23.0	22.7
Second Row %	31.5	29.3	24.4	23.9	22.6	22.6	18.3	18.3	16.9	16.8
Third Row %	25.2	24.1	19.2	19.2	16.6	17.2	16.3	15.7	13.9	13.4
Fourth Row %	---	---	18.6	20.2	15.1	15.1	12.9	13.1	12.2	12.6
Fifth Row %	---	---	---	---	15.2	16.1	12.9	13.0	11.0	11.0
Sixth Row %	---	---	---	---	---	---	13.2	15.0	11.2	11.0
Seventh Row %	---	---	---	---	---	---	---	---	11.8	12.6

Summary of Results from One G and Centrifuge Testing of Pile Groups

Table 2.5 is a summary of all the centrifuge tests discussed in this chapter. It provides a comparison of the tests based on type of pile used, geometry, and soil type. P-multipliers were determined in several of the tests. Table 2.6 is a comparison of the p-multipliers that were calculated as well as the load carrying characteristics that were observed during the tests.

Table 2.5: Summary of centrifuge lateral load tests.

Summary of Lateral Pile Tests				
Reference	Location	Pile Type	Group Geometry	Soil
Kotthaus et al. (1994)	Germany	30mm pipe	1x3, s=3d, 4d	Fine sand
McVay et al. (1994)	University of Florida	9.5mm pipe	3x3 square, s=3d	Reid-Bedford Sand Dr = 16 and 45%
McVay et al. (1995)	University of Florida	9.5mm pipe	3x3 square, s=3d, 5d	Reid-Bedford Sand Dr = 33 and 55%
Garnier et al. (1998)	France	18mm pipe	1x2, s=2d, 4d, 6d	Fine sand
McVay et al. (1998)	University of Florida	9.5 mm Solid Al. Square	3x3 to 3x7, s=3d	Mixed Sand Dr = 36 and 55%

Table 2.6: Summary of *p*-multipliers based on previous centrifuge tests.

Reference	*p*-multipliers (by row)							Load Carrying Characteristics
	1	2	3	4	5	6	7	
Kotthaus et al. (1994)	N/a	-	-	-	-	-	-	3d space deflected 10% more than 4d for equal loads
McVay et al. (1994)	N/a	-	-	-	-	-	-	22% increase in lateral resistance as spacing increased from 3d to 5d
McVay et al. (3d at Dr=33%)	0.65	0.45	0.35	-	-	-	-	group effects negligible at 5d
(1995)　　 (3d at Dr=55%)	0.80	0.45	0.30	-	-	-	-	affect of soil density significant
(5d at both Dr%)	1.0	0.85	0.70	-	-	-	-	at 3d spacing
Garnier et al. (1998) (2d)	-	0.52	-	-	-	-	-	total group load reduced about
(4d)	-	0.82	-	-	-	-	-	20% at 2d spacing
(6d)	-	0.93	-	-	-	-	-	
McVay et al. (1995)　(3x3)	0.80	0.40	0.30	-	-	-	-	slight increase in trail row % for
(3x4)	0.80	0.40	0.30	0.30	-	-	-	groups larger than 4 rows
(3x5)	0.80	0.40	0.30	0.20	0.30	-	-	trailing rows after four reach
(3x6)	0.80	0.40	0.30	0.20	0.20	0.30	-	limiting reduced load value
(3x7)	0.80	0.40	0.30	0.20	0.20	0.20	0.30	

NUMERICAL ANALYSIS
Modification of P-Y Curves to Account for Group Effects on Laterally Loaded Piles (Brown and Shie, 1991)

The effect of pile spacing on lateral pile groups was analyzed by Brown and Shie (1991). The analysis was performed using a three-dimensional finite element computer model. To model clay soils, the total stress approach was employed using an elastic-plastic constant yield strength model. Sands were modeled with the effective stress approach using a modified Drucker-Prager model with non-associated flow. Analyses were performed on models with two rows spaced at 3 and 5 pile diameter spacing center- to-center. A single pile test was also modeled under the same conditions. A pile spacing of 10 diameters was assumed adequate to eliminate all group effects.

The analyses indicate that the front row piles in clay would behave similarly to the single pile model. The back row piles, however, had a reduction in lateral resistance because of the shadowing effects of the piles ahead of them. Because the piles in the front row required higher load to produce the same deflection as the back row piles, the front row piles had higher bending moments. Yield occurred at a greater depth for the back row piles than for the front row piles.

Evaluation of group effects was done using *p-y* curves derived from pile stresses. Pile spacing effects were expressed in terms of p-multipliers and related y-multiplier scaling factors that were applied to single pile *p-y* curves. Values used as p-multipliers were determined, and then y-multipliers were selected to best fit the sloped portion at the beginning of the *p-y* curve. The p-multipliers determined based on these analyses are shown in Fig. 2.9 as a function of pile spacing. The results indicate that group effects would be insignificant at a center-to-center spacing of 5 pile diameters for the leading row piles and at a spacing of 6 pile diameters for the trailing row piles.
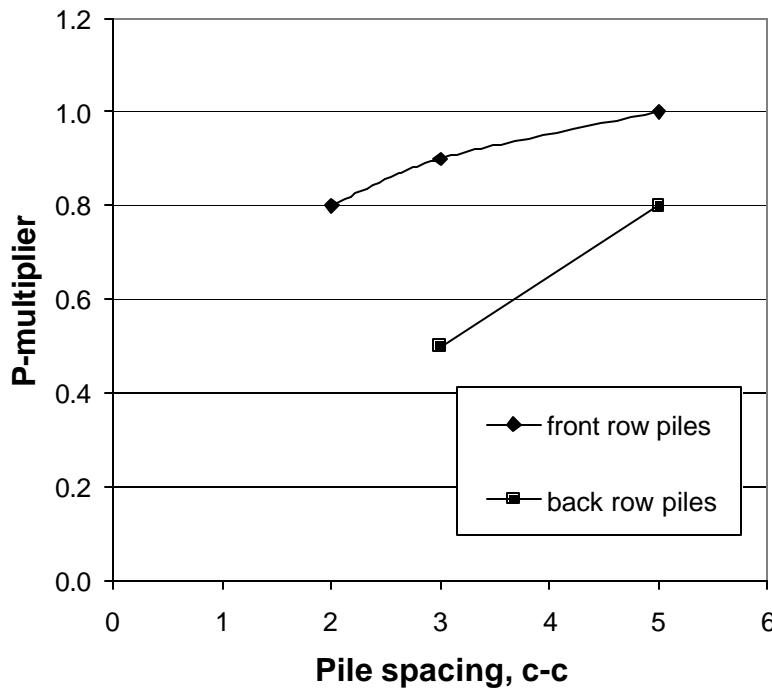
Figure 2.9 P-multiplier values from numerical analysis (Brown and Shie, 1991).

SUMMARY AND CONCLUSIONS BASED ON PREVIOUS TESTING AND ANALYSIS

1. Piles in a group will experience more deflection than a single isolated pile when subjected to the same load per pile.

2. The load distribution in the pile group placed the largest loads on the piles of the leading row.

3. The load distribution is not a function of pile position within a row, as the elasticity-based model would suggest but rather a function of the row position within the group.

4. The "shadowing" or group effect increased as the lateral load and deflection increased.

2-24

5. The maximum bending moments for a given load tended to occur in the leading row due to the fact that the leading row was subjected to the greatest load. The moments in trailing rows occurred deeper due to the pile-soil interaction of the preceding row.

6. The bending moments and load versus deflection curves of the leading row were similar to those of the single pile.

7. Comparisons of actual data and computed data from GROUP are in agreement. However, more comparisons must be made to better validate the software programs.

8. The p-multiplier concept is a simple, but effective way of accounting for group interaction effects in closely spaced piles.

LIMITATIONS OF EXISTING DATA AND NEED FOR ADDITIONAL RESEARCH

As shown in Table 2.1, only about five full-scale lateral pile group tests have been performed where the load distribution within the group was actually measured. Within this small data set, all of the pile groups tested have been spaced at three pile diameters on centers and nearly all have involved only three rows of piles. The variation of p-multipliers with row spacing has thus far been determined only through model tests. In addition, the behavior of pile groups with more than three rows of piles must rely on centrifuge test results only because there is no field performance data to support them. Although centrifuge tests can provide useful guidance to engineers, a reasonable number of full-scale tests are also needed to provide "ground truth" information on pile behavior.

Figures 2.10 and 2.11 show the p-multipliers back-calculated from full-scale load tests for leading and trailing row piles, respectively, along with group efficiency reduction factors (R) factors (essentially the same as p-multipliers) recommended by Reese et al (1996), WSDOT

(2000), AASHTO(2000) and the US Army (1993) as a function of normalized pile spacing. The curves recommended by AASHTO (2000) are identical to curves recommended by the US Navy (1982) and the Canadian Geotechnical Society (1985), which suggests that this is the most widely used curve. Nevertheless, the variation in the curves in Figure 2.10 and 2.11 indicates that there is still considerable uncertainty about appropriate reduction factors to account for group effects.

The p-multipliers based on the full-scale test results are significantly lower than the default p-multipliers in GROUP (Reese et al, 1996). Therefore, use of these default p-multipliers is non-conservative and could result in unsafe designs. The AASHTO and US Army curves appear to provide conservative estimates of the p-multipliers based on the available full-scale tests. This is particularly true for the leading row piles. Therefore, use of the AASHTO or US Army curves could lead to unnecessarily expensive pile foundation designs. The WSDOT curve also fits well with the full-scale results at 3D spacing but is higher than the other curves at greater spacings. Considering the variation in p-multiplier recommendations and the potential for either unsafe or unnecessarily costly foundations, additional full-scale tests are clearly needed to develop reliable p-multiplier vs. pile spacing curves that can be used for engineering design.
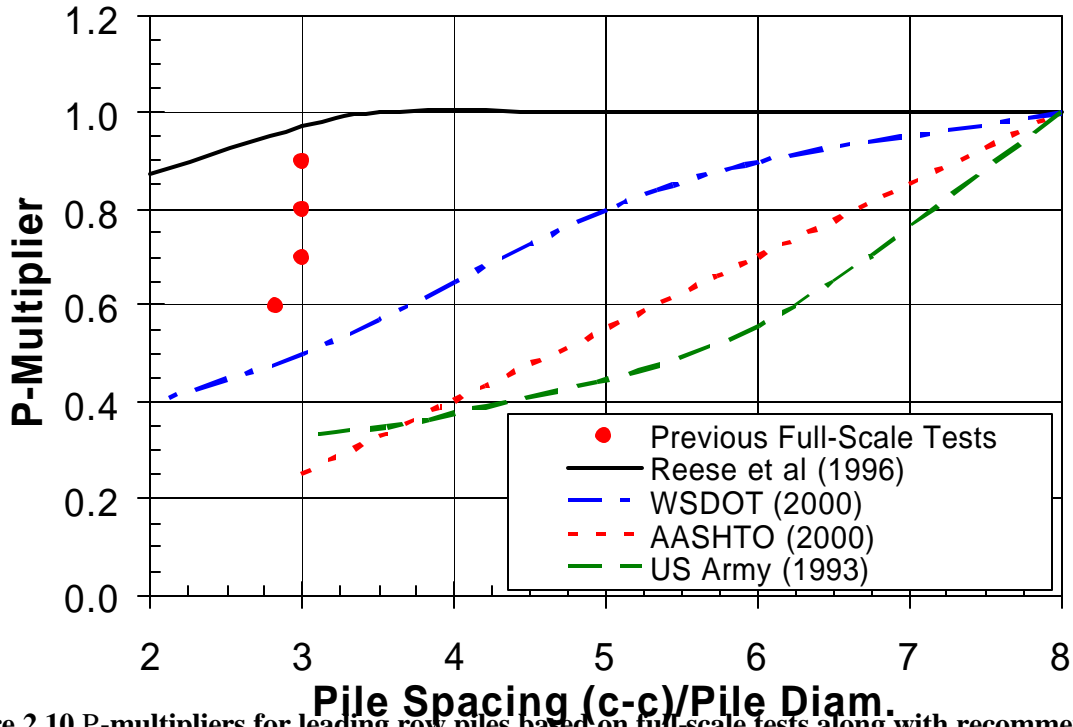
Figure 2.10 P-multipliers for leading row piles based on full-scale tests along with recommendations by various organizations.
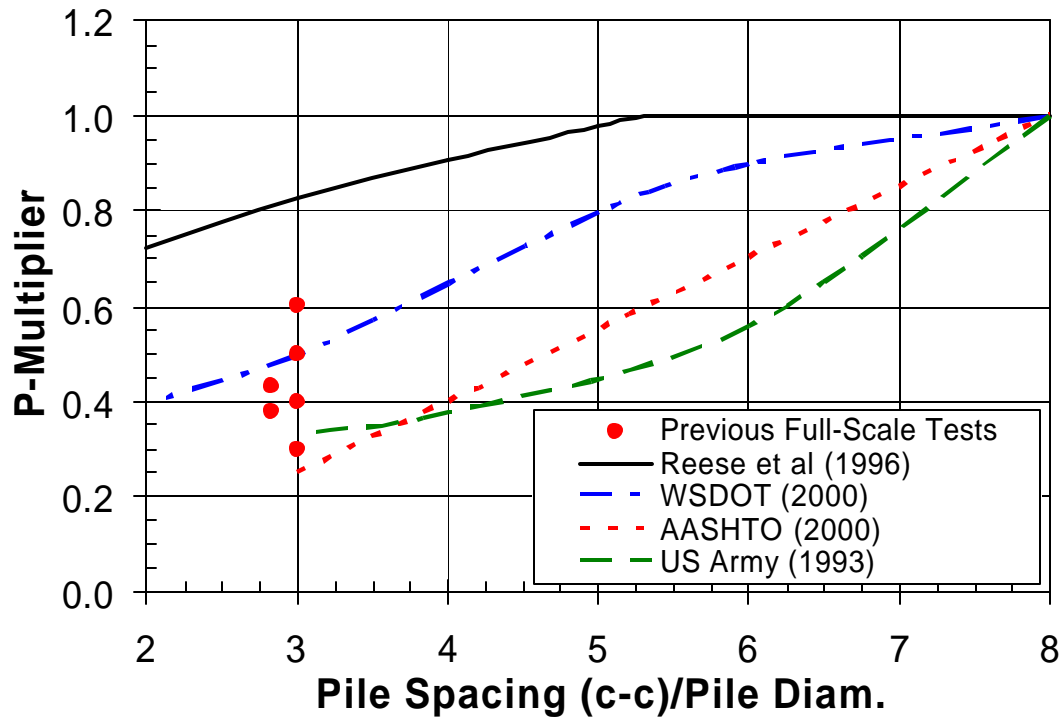
Figure 2.11 P-multipliers for trailing row piles based on full-scale tests along with recommendations from various organizations.

CHAPTER 3 GEOTECHNICAL SITE CHARACTERIZATION

INTRODUCTION

Due to the complex pile-soil-pile interaction anticipated in this series of tests, a comprehensive geotechnical investigation was carried out to define the characteristics of the subsurface materials at the site. This investigation consisted of conventional sampling and laboratory testing as well as in-situ testing. Conventional sampling included undisturbed samples obtained with a thin-walled Shelby tube sampler as well as disturbed soil samples obtained with a standard split-spoon sampler or a hand-auger. In-situ tests included standard penetration (SPT) testing, cone penetrometer (CPT) testing, pressuremeter (PMT) testing, vane shear (VST) testing, borehole shear testing (BST), and shear wave velocity testing. Laboratory testing was performed on the field samples to determine particle size distribution, Atterberg limits, soil classification, shear strength and consolidation characteristics. The locations of the various test holes relative to the test pile groups are shown in Figure 3.1

DRILLING AND SAMPLING

Drilling and sampling was performed by RB&G Engineering using a CME drill rig at three locations (DH-1, 2 & 3) as shown in Figure 3.l. The holes were advanced using a hollow stem auger with a plug in the auger. Undisturbed samples of cohesive soil were obtained by pushing a 76.2 mm diameter, thin-walled Shelby tube using the hydraulic rams on the drill rig. Disturbed samples of cohesionless soil were obtained using a standard 50.8 mm diameter split-spoon sampler. A boring log for drill hole DH-1, representative of both holes, is presented in Figure 3.2. The depth is relative to the excavated ground surface; but, the drill holes were drilled from the original ground surface which was about one meter higher. Locations of the samples and the sampler type used are shown on the boring log along with the recovery in each case.
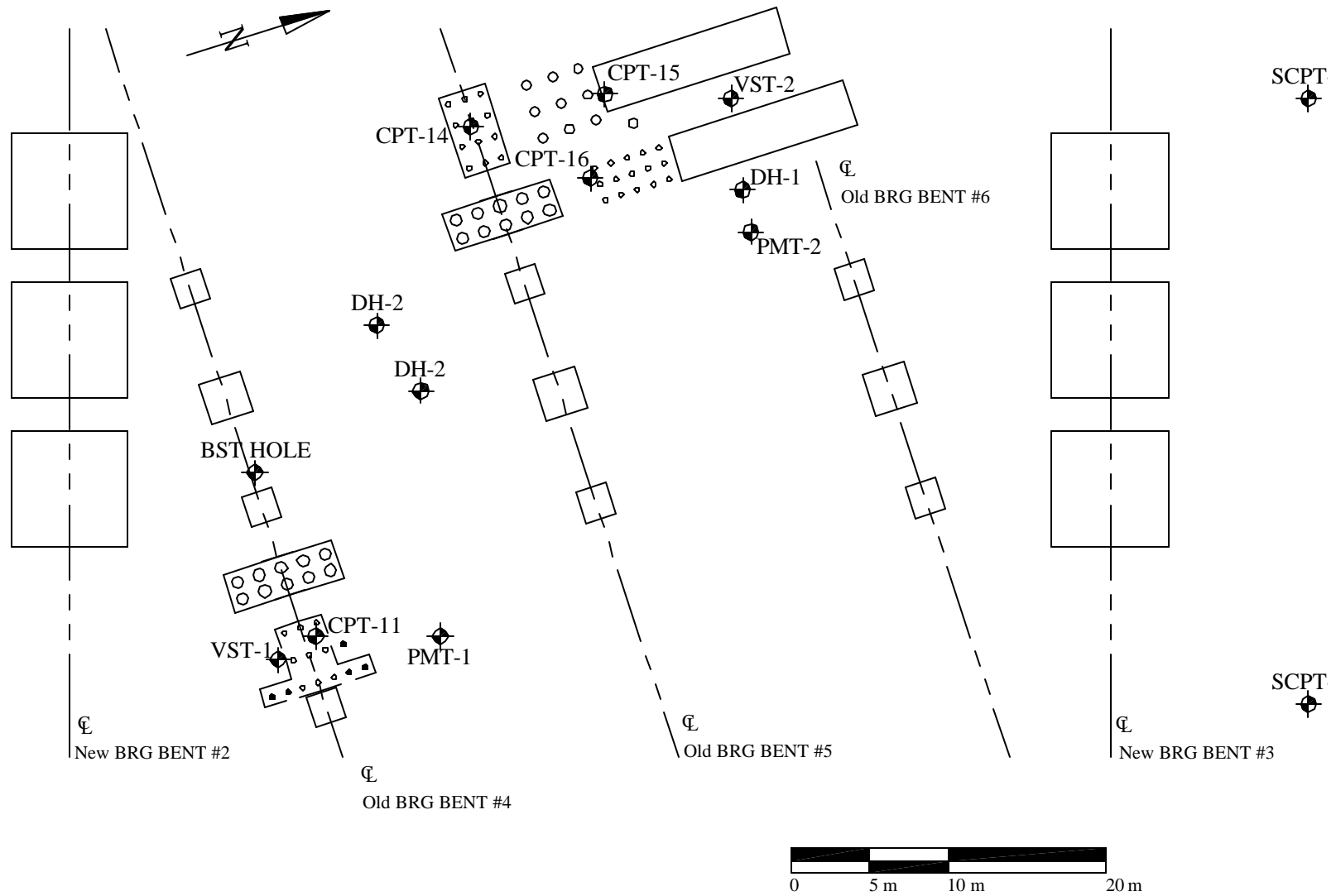
Figure 3.1 Location of drill holes and in-situ tests relative to test pile groups at South Temple site.

DH-1

DATE		
STARTED	3/6/01
COMPLETED	3/6/01
BACKFILLED	3/6/01

South Temple
SLC, UT
Project Number

Rep
Rig Type
Boring Type

LOCATION

NORTHING   EASTING   ELEVATION

Boring with Dr. Rollins 3-6-01

DEPTH										Dry Density (kN/m³)	Moisture Content (%)	Liquid Limit %	Plastic Limit %	Plasticity Index (%)	Fines (%)	Torvane, Su (kPa)	UU, Su (kPa)	<50
METERS	FEET	SAMPLES	UNIFIED SOIL CLASSIFICATION	GRAPHICAL LOG	WATER LEVEL	MATERIAL DESCRIPTION	(N),γₘ	BLOW COUNT 10 20 30 40 50										

Material / data column entries:

- Lean CLAY — CL — 15.4 | 29.0 | 48.7 | | 22 | 90.2 | 69.4 / 43.1 | 100.6
- Sandy SILT — ML — 11.4 | 62.8 | NP | | NP | 51.0
- Lean CLAY — CL — 15.4 | 27.3 | 33.3 | | 12 | 79.7 | | 25.4
-       14.8 | 28.6 | 38.4 | | 15 | 90.2 | 45.5
-       15.5 | 28.8 | 35.9 | | 14 | 97.4 | 60.0 | 22.0
- Silty SAND — SM — 10.3 — | 32.9 | NP | | NP | 32.7
- Fat CLAY — CH — 12.6 | 45.0 | 59.7 | | 30 | 99.4 | 43.1 | 28.0
-       11.4 | 54.1 | 51.5 | | 24 | 96.7 | 28.7 | 22.5
-       9.8 | 62.2 | 58.6 | | 30 | 99.7 | 31.1
- Bottom of Boring @ 35 — 11.6 | 53.1 | 62.5 | | 66 | 97.4 | | 27.8

SAMPLE TYPE
- 2" O.D./1.38 I.D. SPLIT SPOON SAMPLER
- 3" O.D./2.42" I.D. U SAMPLER
- 3" O.D. THIN-WALLED SHELBY SAMPLER

WATER LEVEL
- ▼ - MEASURED
- ▽ - ESTIMATED

NOTES:

Figure 3.2 Log for test hole DH-1 along with laboratory and field test data.

Samples from this borehole were subsequently used for strength and compressibility testing. Samples from the other holes were primarily used for classification purposes.

The soil profile primarily consisted of silty clay or clay layers with occasional thin layers of sand. A soft clay layer was encountered between 5.5 and 10.5 m below the excavated ground surface. The water table was encountered at a depth of 1.06 m below the excavated ground surface.

A hand-auger was also used to obtain disturbed samples at several of the pile group locations immediately following the testing to better define the water content variation in the upper portion of the profile. Samples from the auger holes were typically taken at 0.15 m intervals and the holes were usually less than 1.5 m in depth due to caving sand below the water table.

LABORATORY TESTING

The laboratory tests were performed to determine particle size distribution, Atterberg limits, soil classification, shear strength and consolidation characteristics. The testing procedure and results are described below.

Particle Size Distribution

Particle size distribution curves were developed for some of the sand layers using mechanical (sieve) analysis. Testing was performed in general accordance with ASTM D-2487. The results indicate that the sand between 4 and 5 m below the ground surface is a silty sand with a mean grain size (D_{50}) of 0.083 mm and 44% fines.

Atterberg Limits and Natural Moisture Content

Drill hole samples were tested in accordance with ASTM D-4318 to determine the Atterberg limits (Liquid Limit {LL}, Plastic Limit {PL}, Plasticity Index {PI}) and the natural

Table 3.1 Summary of natural moisture content (w_n), liquid limit (LL), plastic limit (PL),

plasticity index (PI), liquidity index (LI), and Unified Soil Classification System symbol for soil samples from drill holes at South Temple test site.

Drill Hole	Depth (m)	w_n (%)	LL (%)	PL (%)	PI (%)	LI (%)	USCS Symbol
3	0.08	32.4	63.0	20.4	42.6	0.30	CH
1	0.23	34.4	61.2	38.2	23.0	N.A.	MH
3	0.38	30.1	56.5	19.4	37.1	0.29	CH
3	0.53	36.9	36.8	25.5	11.3	1.0	ML
3	0.69	43.8	44.7	19.4	25.3	0.96	CL
3	0.84	39.6	75.5	22.9	52.6	0.32	CH
3	0.99	25.1	29.0	15.7	13.3	0.71	CL
3	1.14	27.9	34.8	20.3	14.5	0.52	CL
3	1.30	28.2	22.7	17.4	5.3	2.0	CL-ML
3	1.42	20.9	NP	NP	NP	NP	SC
3	1.55	29.4	37.3	17.8	19.5	0.59	CL
3	1.68	32.8	30.5	14.6	15.9	1.1	CL
2	1.79	35.0	31.0	18.0	13.0	1.3	CL
1	1.92	27.3	33.3	20.9	12.4	0.52	CL
1	2.47	28.6	38.4	23.4	15.0	0.35	CL
2	2.70	28.0	34.6	21.3	13.3	0.50	CL
1	3.62	34.7	35.9	21.5	14.4	0.92	CL
2	4.53	23.7	NP	NP	NP	NP	SM
1	5.36	45.0	59.7	29.8	29.9	0.51	CH
1	6.34	51.5	54.1	27.8	26.3	0.90	CH
2	8.19	66.0	45.0	27.0	18.0	2.2	CL
1	8.93	62.2	58.6	28.5	30.1	1.1	CH
1	10.3	53.1	62.5	26.7	35.8	0.74	CH

moisture content (w_n). The results of all these tests are tabulated in Table 3.1, sorted in order of depth, and they are also presented graphically in Figure 3.3.

The results indicate that the upper meter of the soil profile consists of high plasticity clay and silt with PIs ranging from 20 to 50%. From 1 to 3 m deep, the soil consists of low to medium plasticity silts and clays (PIs between 10 and 15%) and the natural moisture content is generally lower than the liquid limit indicating that the soil is overconsolidated. Below a depth of 5 m, the PIs increase again and are typically between 20 and 30% indicating that the clays and
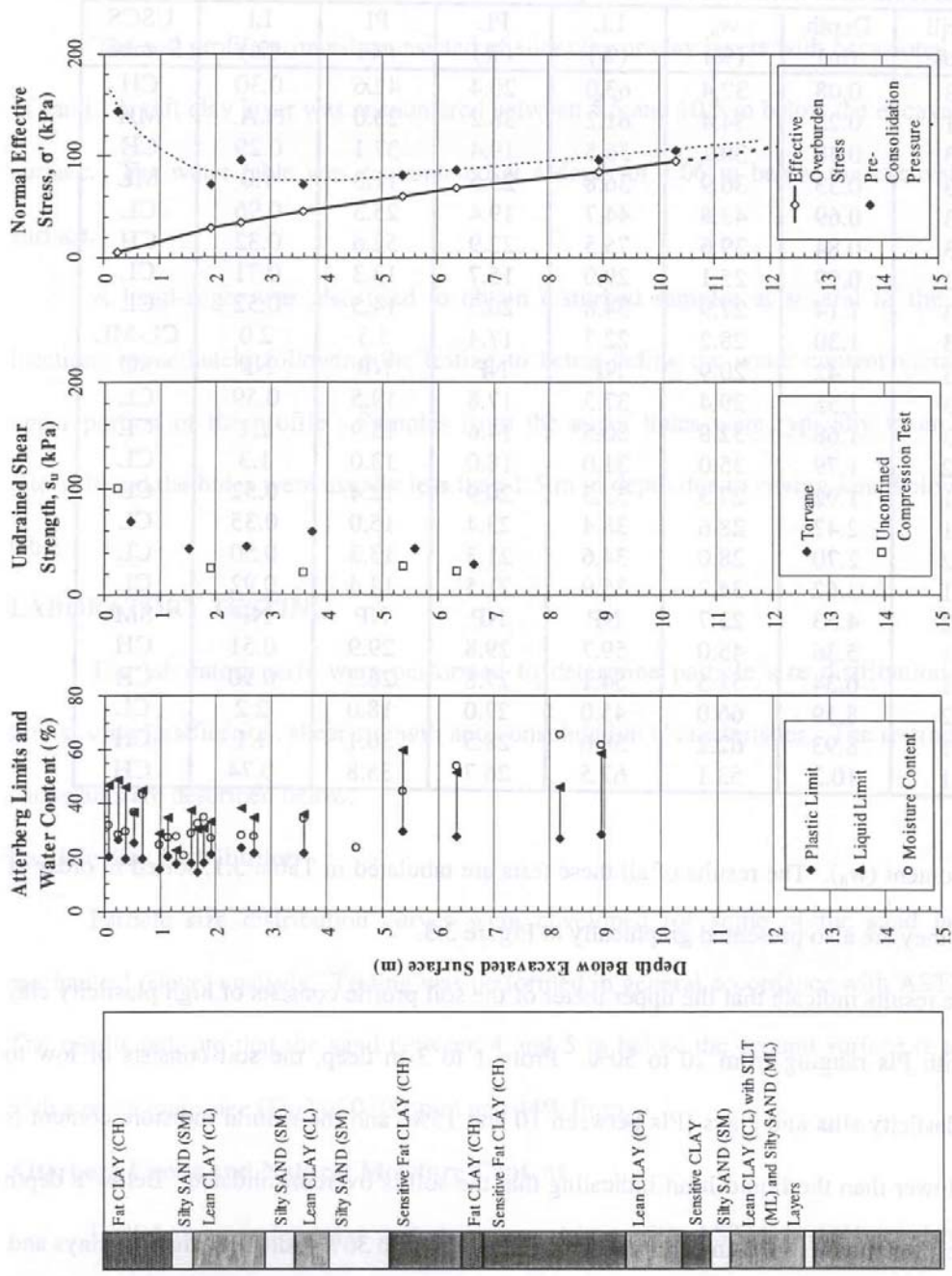
Figure 3.3 Soil profile interpreted from CPT along with Atterberg limits, natural moisture content, undrained shear strength and pre-consolidation pressure profiles from lab tests.

3-6

silts are moderate to high plasticity materials. In a few cases, the natural moisture content is higher than the liquid limit, indicating that the soils may be sensitive.

The natural moisture content after the completion of testing in each pile group was also determined by taking disturbed samples at approximately 0.15 m intervals to depths of 1 to 2 m using a hand auger. Typically, nine holes were drilled within a group to assess the variation of water content. No consistent variation was ever observed in the water content from front to back or side to side. Plots of the average natural moisture content versus depth for the four pile groups are presented in Figures 3.4. The variation in water content at the four sites is typically within ± 3 percentage points in the upper 0.6 m of the profile. The water content drops about 12 percentage points at the transition from the high plasticity surface clay to the lower plasticity clay. This boundary is about 0.15 m deeper at the 9 (324 mm) and 12 pile groups than at the 9 (610 mm) and 15 pile groups.

Soil Classification

The soil samples were classified according to the Unified Soil Classification System (USCS) based on the Atterberg limits and particle size distribution. The symbols designating soil types according to this system are shown on the boring logs. In addition, an idealized soil profile based on the test results is presented in Fig. 3.3. The classifications in the fine-grain soils range from ML to CH materials. The CH materials are typically located from 0 to 1 m in depth and again from 5 to 10 m in depth, while the low to medium plasticity materials are typically located between 1 to 5 m in depth. The coarse-grained soils generally classified as SM materials.

Shear Strength Testing

The laboratory shear strength testing consisted of pocket Torvane shear tests and unconfined compression tests. The strength obtained from the testing is summarized on the

\
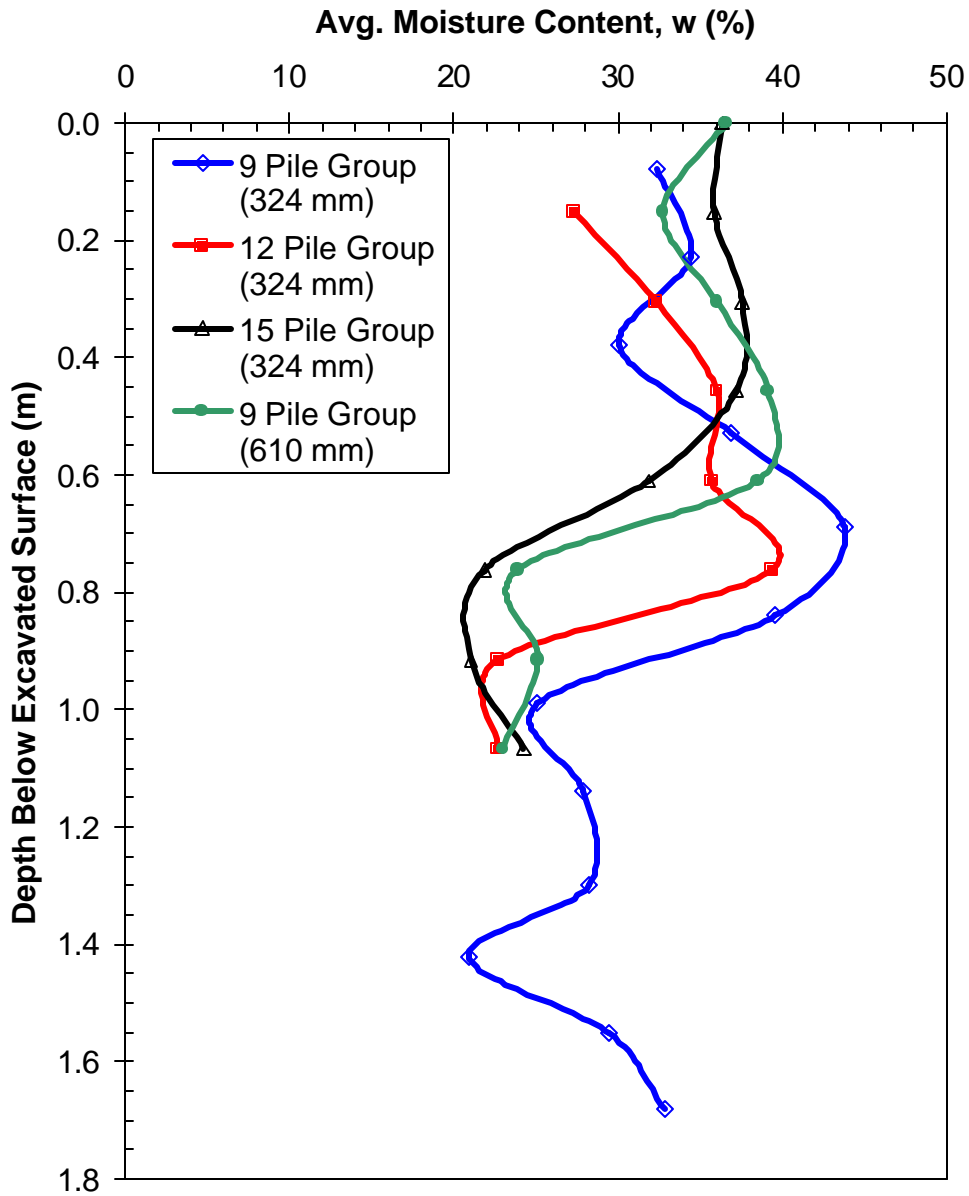
Figure 3.4 Natural moisture content versus depth profiles for each pile group.

boring logs and is also shown as a function of depth in Figure 3.3. The Torvane shear strengths are in good agreement below 5 m but are often twice as high as the unconfined compression values in the range from 1.5 to 4 m deep. This is likely due to sampling disturbance effects in these sensitive materials as discussed subsequently in the section on vane shear testing. In general, the strength of the upper 4 m is significantly higher than that in the clay from 5 to 9 m in depth. This is likely a result of overconsolidation due to desiccation as will be discussed subsequently.

A summary of ε_{50} values obtained from the unconfined compression tests is provided in Table 3.2. The ε_{50} value is the strain at which 50% of the undrained shear strength is mobilized. This value is used in many computer programs for generating p-y curves for cohesive soils.

Table 3.2 e_{50} values from unconfined compression tests on samples from DH-1.

Depth, m	ε_{50}
0.24	0.03
1.92	0.01
3.60	0.013
5.36	0.05
6.34	
10.3	

Consolidation Testing.

Consolidation tests on undisturbed samples from DH-1 were performed in accordance with ASTM D 2435 specifications. Plots of void ratio versus pressure obtained from the consolidation tests are provided in the Appendix. Results from the consolidation tests were used to determine the pre-consolidation pressure, σ'_c, of the soil profile versus depth. The pre-consolidation pressure is plotted along with the overburden pressure (initial vertical effective stress, σ'_o) in Figure 3.3. A comparison of σ'_c and σ'_o shows that the soil profile is generally overconsolidated to a depth of approximately 10 meters (33 feet), but the degree of

overconsolidation decreases substantially with depth. For example, overconsolidation ratios (OCRs) drop from a value of 2.8 at 1.7 meters (5.5 feet) to 1.2 at 10 meters (33 feet) below the excavated ground surface. The shape of the pre-consolidation pressure versus depth curve indicates that the higher overconsolidation ratios near the surface are largely a result of desiccation due to water table fluctuations.

The dry unit weight and natural moisture contents determined for the consolidation test samples are also tabulated on the boring log in Fig 3.2. For the fine-grained soils in the profile between 1.7 to 10 meters in depth, the dry unit weight ranged from 9.8 kN/m^3 (62.4 lb/ft^3) to 15.4 kN/m^3 (98.7 kN/m^3) and saturated unit weight ranged from 15.9 kN/m^3 to 19.9 kN/m^3 (101.2 lb/ft^3 and 126.5 lb/ft^3) with an average of 18.5 kN/m^3 (117.8 lb/ft^3). Nuclear density gauge tests of the surface layer determined the average dry unit weight to be 14.2 kN/m^3 (90.6 lb/ft^3) with an average moisture content of 31.8%. Calculations for the initial vertical stress, σ'_o, shown in Figure 3.3 assumed a moist unit weight of 19.6 kN/m^3 (125.0 lb/ft^3) for the clay above the water table and a saturated unit weight based on the consolidation test data below the water table.

IN-SITU TESTING

Cone Penetration (CPT) Testing

Cone penetration (CPT) soundings were performed at the center of each of the four pile groups as shown in Fig 3.1. The CPT tests were performed by Cone-Tec, Inc, using a 180 kN (20 ton) truck mounted cone rig equipped with an automated data acquisition system. The cone was a piezocone with a 10 cm^2 surface area. The porous filter for the cone was located in position 2, approximately 12 mm from the tip. The tests were conducted in accordance with ASTM D-3441. The soundings typically penetrated to a depth of 15 m below the excavated ground surface and readings were taken at 0.05 m intervals.

The cone (tip) resistance (q_c), sleeve friction (f_s), friction ratio (f_r) and pore water pressure (u) for each of the tests are presented as a function of depth below the excavated ground surface in Figure 3.5. The agreement between the four soundings is very good, indicating that the soil profile and properties are comparable at each test site. The CPT results were used to interpret the soil profile using the correlation with soil behavior type developed by Robertson and Campanella (1988). This soil classification system is based on behavioral rather than gradational characteristics. Therefore, the classification may differ from those established based on laboratory testing only. The interpreted soil behavior profile is also shown in Figure 3.5.

The upper portion of the soil profile (0 to 4.7 m) consisted predominantly of silty clay and clayey silt interbedded with occasional silty sand layers. A soft, sensitive soil layer was consistently located between 4.7 and 9.2 m below depth. Between 9.2 m and 15.0 m the soil profile once again consisted predominantly of silty clay layers interbedded with occasional thin silty sand layers.

Undrained Strength on Clay Based on CPT Results

The undrained shear strength of the fine-grained layers was estimated from the CPT cone resistance using the equation

$$S_u = \left(\frac{q_c - \boldsymbol{S}_o}{N_k} \right) \tag{3.1}$$

where q_c is cone tip resistance, σ_o is the total vertical stress, and N_k is the bearing capacity factor for an electric cone. According to Robertson and Campanella (1998), the N_k value typically ranges from 10 to 20 and was assumed to be equal to 15 for this study. Although the undrained shear strength obtained with equation 3.1 is only an estimate, the approach does provide a continuous profile that shows the consistency of the strength within layers in the profile. The undrained shear strength computed using equation 3.1 is shown as a function of depth in Fig. 3.6.
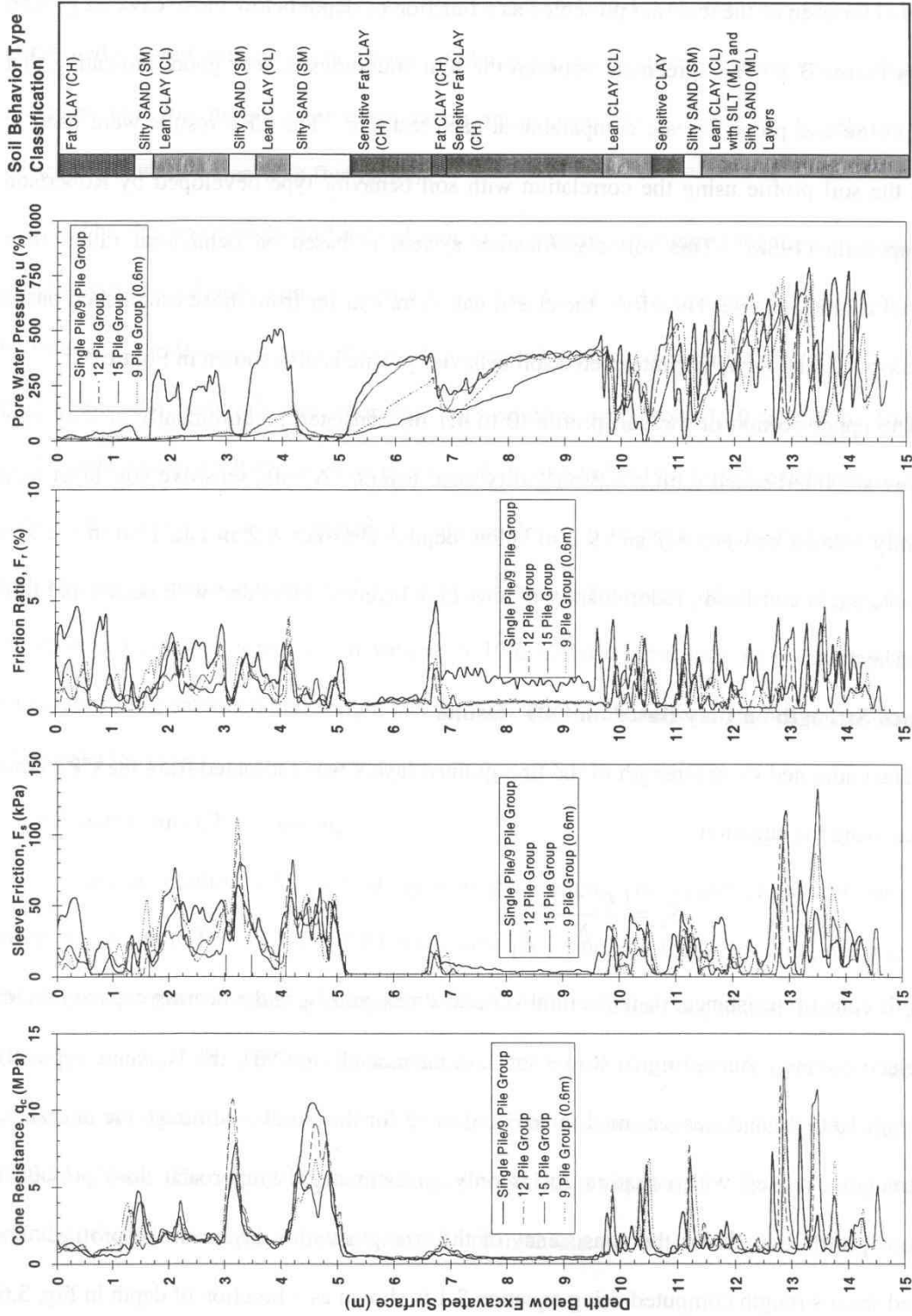
Figure 3.5 Summary of CPT logs and interpreted soil behavior type profile for soundings at each pile group location.

3-12
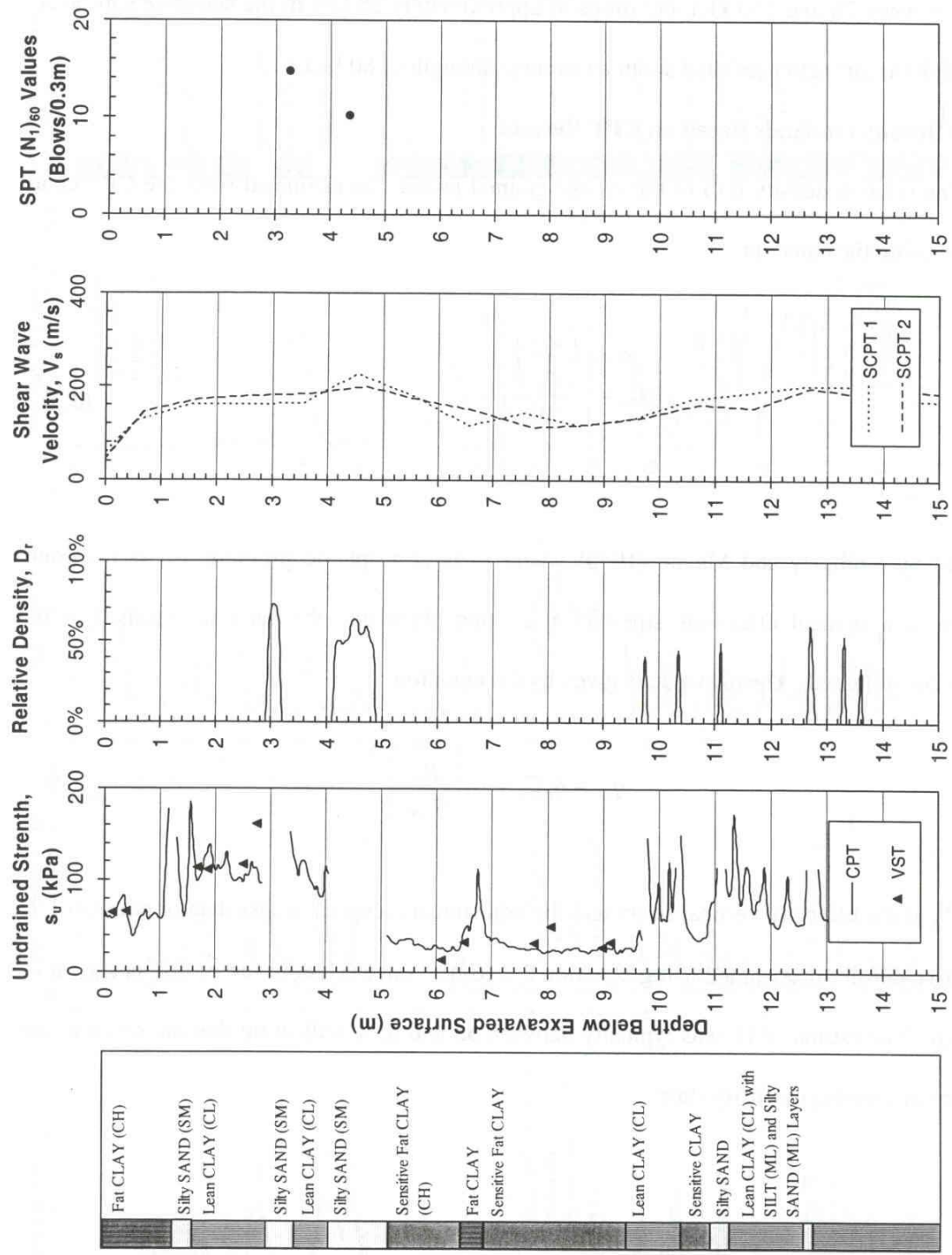
Figure 3.6 Soil profile interpreted from CPT along with undrained shear strength from CPT and VST, relative density in sands, shear wave velocity from seismic CPT and SPT blow counts in sands.

3-13

The strength profile appears to involve three general layers. The upper layer typically has a strength between 70 and 150 kPa, but drops to approximately 35 kPa in the sensitive soil layer. Below 10 m the strength oscillated about an average strength of 80 kPa.

Relative Density on Sands Based on CPT Results

The relative density (D_r) of the coarse-grained layers was estimated from the CPT cone resistance using the equation

$$D_r = \left[\frac{\left(\frac{q_{c1}}{p_a} \right)}{305} \right]^{0.5}$$

(3.2)

developed by Kulhawy and Mayne (1990) where p_a is atmospheric pressure, q_{c1} is the cone resistance at a vertical effectives stress of one atmosphere and the sand is assumed to be normally consolidated. The q_{c1} value is given by the equation

$$q_{c1} = q_c C_n = q_c \left[\frac{p_a}{\sigma'_{vo}} \right]^{0.5}$$

(3.3)

where σ'_{vo} is the effective vertical stress and the adjustment factor C_n is less than or equal to 1.7. The relative density determined using equation 3.2 for the sand layers in the profile is shown in Figure 3.6. The estimated D_r was typically between 55 and 65% indicating that the sands in the profile are in a medium density state.

THIS PAGE LEFT BLANK INTENTIONALLY

Shear Wave (V_s) Velocity Testing

The shear wave velocity profile was measured by Cone-Tec, Inc. using a seismic cone penetrometer at two locations near the site as shown in Figure 3.1. The shear wave velocity profiles for the two tests are plotted in Figure 3.6. The shear wave velocity was typically between 150 and 200 m/sec in the silt and clay zones but dropped to about 120 in the sensitive fines layer.

Standard Penetration (SPT) Testing

Two standard penetration (SPT) tests were performed in the sand layers located between 3 and 5 m below the ground surface. In both cases, the uncorrected N value was 7. The SPT was performed with an automatic trip hammer which applied 80% of the theoretical free-fall energy. The $(N_1)_{60}$ was determined using the equation

$$(N_1)_{60} = N C_n C_E = q_c \left[\frac{p_a}{\boldsymbol{s'}_{vo}} \right]^{0.5} \left[\frac{E_{applied}}{60\%} \right] \tag{3.4}$$

where C_E is the correction for the percent energy applied and $E_{applied}$ is the % of the theoretical energy applied by the hammer. After correction, the $(N_1)_{60}$ values were 14 at 3.2 m and 10 and 4.4 m (see Fig. 3.6). The relative density was computed using the equation

$$D_r = \left[\frac{(N_1)_{60}}{40} \right]^{0.5} \tag{3.5}$$

developed by Kulhawy and Mayne (1990). Using this equation, the relative density of this layer is approximately 60%, which indicates a medium density state. This value is in very good agreement with the relative density estimate for the layer provided by the CPT soundings.

Vane Shear Testing (VST)

A total of 12 vane shear tests were performed in two boreholes located as shown in Figure 3.1. Testing was performed in accordance with ASTM D-2573. The torque arm length was 0.305 m (1 ft) and the diameter of the vane was 63.5 mm (2.5 inches). At each depth, the peak undrained strength $(s_u)_p$ was typically determined along with the residual undrained strength $(s_u)_r$ after rotating the vane 10 times to remold the soil and develop a shear surface. The measured vane shear test results were corrected using the adjustment factor based on plasticity index proposed by Bjerrum (1974). The results of all the vane shear tests are summarized by depth in Table 3.3.

Table 3.3 Summary of undrained shear strength from in-situ vane shear testing.

Test Hole	Depth Below Excavated Ground (m)	Undisturbed $(S_u)_p$ (kN/m^2)	Remolded $(S_u)_r$ (kN/m^2)	Sensitivity S_t
VST 1	0.0	64.7	-	-
VST 2	0.7	78.2	24.8	3.2
VST 2	1.7	133.1	13.4	9.9
VST 1	1.9	110.8	81.6	1.4
VST 1	2.5	117.6	117.6	1
VST 2	2.7	161.0	22.8	7.1
VST 2	6.1	13.4	4.5	3.0
VST 1	6.5	32.7	21.6	1.5
VST 2	7.8	31.9	6.1	5.2
VST 1	8.1	49.8	13.4	3.7
VST 1	9.0	26.8	5.2	5.2
VST 2	9.1	32.7	7.8	4.2

The peak undrained shear strength obtained from the vane shear testing is shown as a function of depth in Figure 3.6 along with the CPT derived shear strength values. The agreement between the measured and estimated values is relatively good. Three general layers appear to be evident based on the shear strength profile. The top layer from the ground surface to a depth of 1.3 m has a strength of 70 kPa; however, the strength increases to approximately 105 kPa from

1.5 to 4.1 m below the excavated ground. Finally, within the sensitive soil, the strength drops to approximately 35 kPa.

The sensitivity was computed by dividing the undisturbed strength by the remolded strength and the results are also listed in Table 3.3. The sensitivity of the cohesive soil typically ranged from 3 to 5, but values of 9.9 and 7.1 were measured at depths of 1.7 and 2.7 m, respectively. These high sensitivity measurements are in the depth range in which the strengths from the torvane and unconfined compression tests were significantly lower than the vane shear values. Therefore, sampling disturbance likely explains the discrepancy. Surprisingly, the soils that were identified as being sensitive by CPT test (soils between 5 and 10 m deep) did not show high sensitivity based on the vane shear test. In addition, the shear strength from the unconfined compression and Torvane shear tests for these materials were nearly identical to the field vane shear results, suggesting that disturbance effects due to sampling and extrusion effects were also minimal.

Borehole Shear Tests (BST)

Borehole shear tests were performed by Prof. Lawton of the University of Utah Civil Engineering Dept. at the location shown in Figure 3.1. These tests allowed the drained strength properties (friction angle and cohesion) to be determined for the subsurface layers. The tests were conducted at intervals of approximately 0.15 m (6 inches) to a depth of 5.1 m. At each test level, a stress was applied normal to the sides of the borehole wall. An upward force was then applied and the force required to cause shear failure was measured. By repeating this process with increased stresses normal to the borehole wall, the friction angle and cohesion intercept were determined. The results from the borehole shear tests are presented in Table 3.4.

Table 3.4 Summary of results from borehole shear tests (BST) conducted by Univ. of Utah.

Depth From Original Ground Surface (m)	Depth from Excavated Ground Surface (m)	Soil Classifications	Strength Properties		Water Table Depth (m)	Vertical Stress (kPa)
			c (kPa)	ϕ		
0.50	-		0	38.57	NO	8.19
0.60	-	ML – Silt	0	37.92	NO	10.92
0.90	0	CH - Fat Clay	3.57	33.99	NO	16.38
1.20	0.3	CH - Fat Clay	0.96	38.49	NO	21.83
1.40	0.5	CH - Fat Clay	1.72	35.37	NO	24.56
1.50	0.6	CH - Fat Clay	0	24.23	3.64	27.29
1.80	0.9	CL - Lean Clay	0	31.90	4.64	32.75
2.10	1.2	SM- Silty Sand	0	35.63	4.64	38.21
2.30	1.4	SM- Silty Sand	0	34.69	3.64	40.94
2.70	1.8	CL-Lean Clay	11.78	28.96	4.64	48.22
2.80	1.9	CL-Lean Clay	5.43	35.26	3.64	50.94
3.00	2.1	CL-Lean Clay	0	26.79	2.64	54.58
3.30	2.4	CL-Lean Clay	6.40	33.02	3.64	58.68
3.50	2.6	CL-ML – Silty Clay	4.14	25.80	3.64	62.77
3.90	3	SM- Silty Sand	7.14	36.21	3.64	69.59
4.10	3.2	SM- Silty Sand	16.69	38.10	3.64	73.69
4.30	3.4	SC – Clayey Sand	0	49.48	3.64	76.42
4.60	3.7	CL-Lean Clay	11.44	31.30	3.64	81.88
4.70	3.8	CL-Lean Clay	0	38.26	3.64	84.60
5.10	4.2	SM- Silty Sand	2.14	33.31	3.64	91.43

Note: Dry unit weight of soil set equal to 14.93 kN/m^3 (95 lbs/ft^3) for determining vertical stress.

Pressuremeter (PMT) Tests

Six cone (push-in) pressuremeter (PMT) tests were performed at two boreholes as shown in Figure 3.1. The cone pressuremeter was a Rocktest Pencell unit which was controlled using a TEXAM actuator and readout unit. The cone was pushed into the ground using the hydraulic rams on the drill rig. Testing was carried out using method B (strain-control approach) as specified in ASTM D4719-87 in which equal volumes of fluid are injected and the resulting pressure is measured. Plots of pressure versus the relative increase in probe radius relative to the initial radius ($\Delta R/R_O$) are shown for each test in Figure 3.7. These curves have been corrected for membrane resistance. The pressuremeter modulus (E_O), net limit pressure (p_l), and the E_O/p_l ratio for each test are summarized in Table 3.5. An indication of the consistency of cohesive soils and the density of cohesionless soils can be obtained from the E_O and p_l values with the aid of Tables 3.6 and 3.7 (Briaud, 1992; Baguelin, 1978). These results indicate that the cohesive surface soils are stiff and the sand layer at a depth of about 3 m is in a medium density state. The E_O/p_l values for the tests suggest that the soils in the upper 4 m of the profile are over-consolidated.

Table 3.5 Summary of pressuremeter modulus (E_O), limit pressure (p_l), and E_O/p_l ratio for push-in pressuremeter tests conducted at the test site.

| Borehole Number	Depth to Center of Probe (m)	Soil Type	Pressuremeter Modulus, E_o (kPa)	Limit Pressure, p_l (kPa)	E_o/p_l
PMT 2	0.9	Clay	4500	360	12.5
PMT 2	1.8	Clay	6700	460	14.5
PMT 1	2.3	Clay	4500	460	9.8
PMT 2	2.7	Clay-Sand	17,900	780	22.9
PMT 1	3.0	Sand	10,300	830	12.4
PMT 2	3.7	Sand-Clay	15900	800	19.9
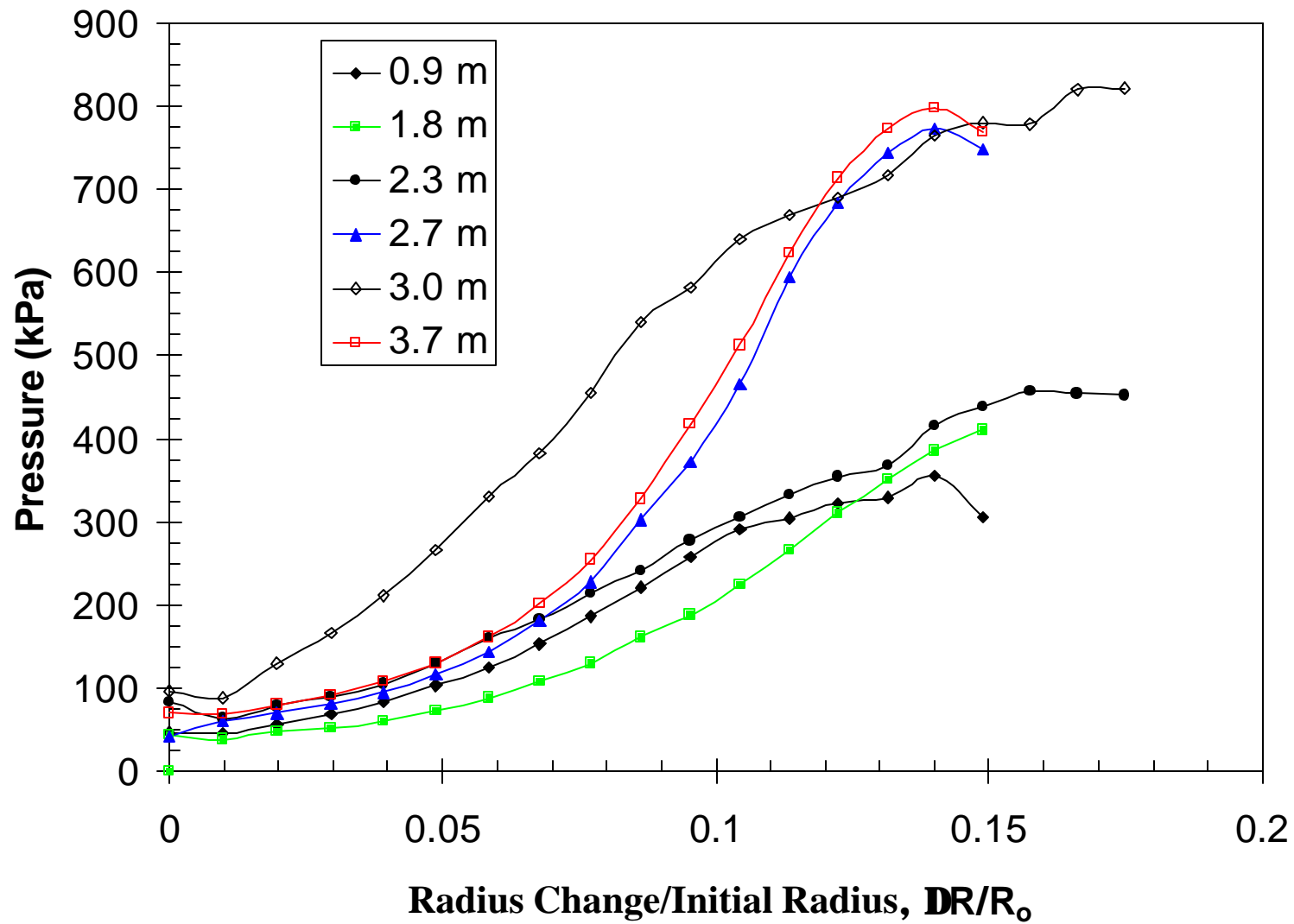
Figure 3.7 Pressure versus normalized radius change for six pressure meter tests conducted in two holes at South Temple site.

Table 3.6 Correlations between soil consistency, pressuremeter modulus (E_0) and limit pressure (p_l) for clays (after Briaud, 1992).

CLAY					
Soil Consistency	Soft	Medium	Stiff	Very Stiff	Hard
p_l (kPa)	0-200	200-400	400-800	800-1600	>1600
E_o (kPa)	0-2500	2500-5000	5000-12000	12000-25000	>25000

Table 3.7 Correlation between density state, pressuremeter modulus (E_0) and limit pressure (p_l) for sands (after Briaud, 1992, Baguelin et al, 1978).

SAND					
Relative Density,	Very Loose	Loose	Medium	Dense	Very Dense
D_r	0 - 15%	15 - 35%	35 – 65%	65 - 85%	85 - 100%
p_l (kPa)	0-200	200-500	500-1500	1500-2500	>2500
E_o (kPa)	0-1400	1400-3500	3500-12000	12000-22500	>22500

Several methods exist to calculate S_u from PMT data, but no one method appears to be definitively more accurate than another. Based on recommendations by Briaud (1992), two correlations with the limit pressure were used to calculate s_u. The first method gives the undrained shear strength as

$$s_u = \frac{p_l}{b} \tag{3.5}$$

where β was assumed to be 7.5 for this study. The second of the methods gives

$$s_u = 0.21 p_a \cdot \left(\frac{p_l}{p_a}\right)^{0.75} \tag{3.6}$$

where p_a is equal to the atmospheric pressure. The strength values obtained for the PMT tests in clay are summarized in Table 3.8. In general, there is good agreement between the strength values estimated by the two methods. However, the strength values estimated with PMT

correlations are 40 to 80% lower than measured with the vane shear test or estimated using the correlation with the cone penetration. Therefore, the correlated strength values should not be given much weight relative to the other test results.

Table 3.8 Summary of undrained shear strength estimated from PMT correlations.

Borehole Location	Depth to Center of Probe (m)	Undrained Shear Strength s_u (kPa) (Eq 3.4)	Undrained Shear Strength s_u (kPa) (Eq 3.5)
PMT 2	0.9	48	54
PMT 2	1.8	61	65
PMT 1	2.3	61	65

IDEALIZED SOIL PROFILE

Based on the results of the field and laboratory testing, an idealized soil profile was constructed as shown in Figure 3.8. The soil profile consists of a surface layer made up of stiff clays with occasional silty sand layers. These layers are underlain by a soft clay layer to the bottom of the pile. The idealized soil profile was constructed primarily based on the stratigraphy identified by the CPT soundings. The water table elevation was measured in a piezometer at the site and was approximately 1.07 m below the excavated ground surface during the testing period.

The undrained shear strength profile used in the analysis is presented along with all the strength data developed during this study for comparison. There is reasonably good agreement between the results from the various tests in many cases. In developing the design strength profile, the greatest weight was given to the field vane shear tests, although the strength profile estimated by the CPT was also helpful. The results from the Torvane, unconfined compression and PMT correlations were considered less reliable due to potential disturbance effects, therefore, these values were often discounted particularly at depths between 1.7 and 4 m. The friction angles for the sand layers were determined by averaging the results from the borehole shear tests in the sand layers. The dry unit weights were based on the relative density values.
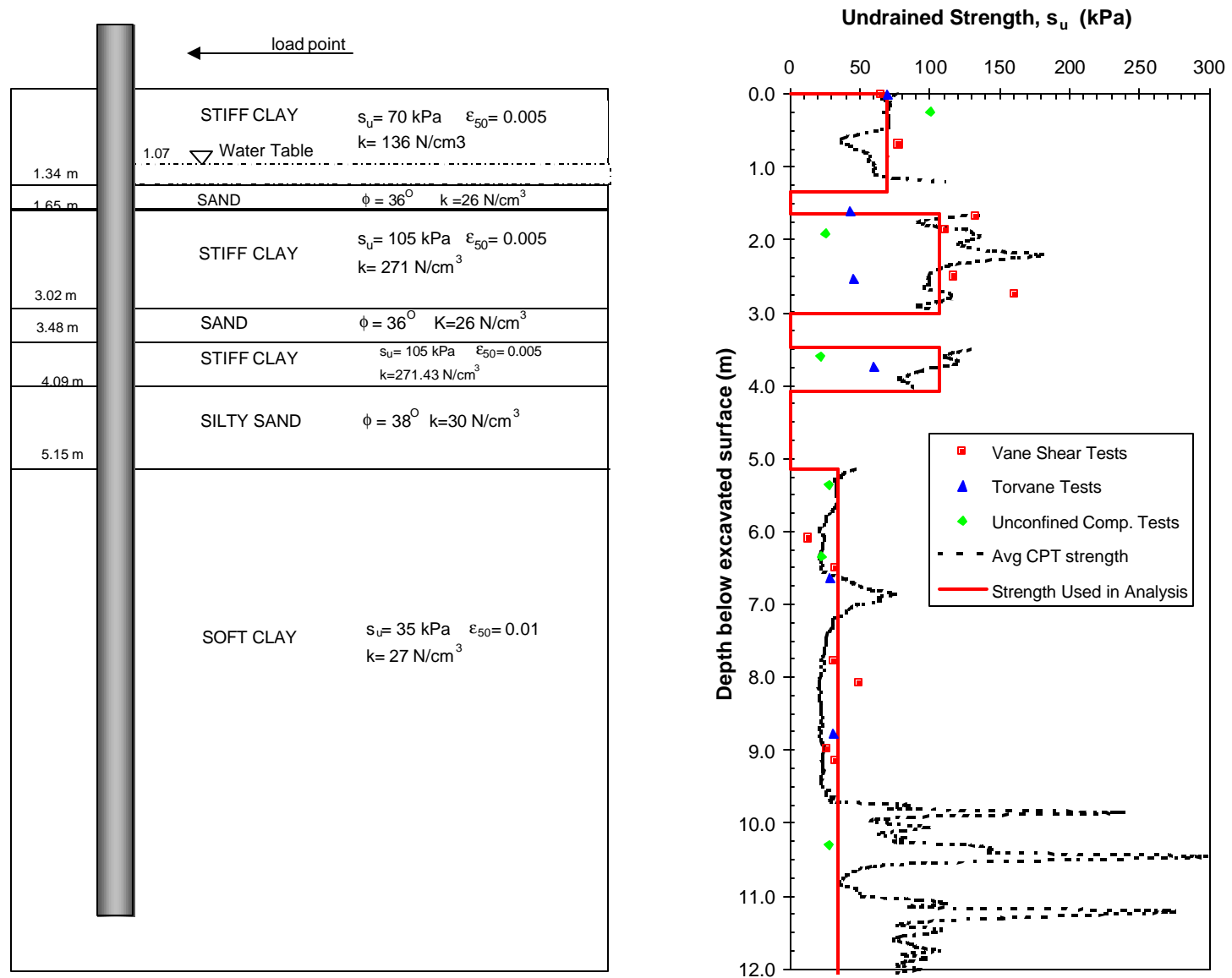
Figure 3.8 Idealized soil profile and strength properties selected for analysis, along with undrained strength determined using several methods

CHAPTER 4 LATERAL LOAD TESTS ON SINGLE PILES

INTRODUCTION

Three separate single pile lateral load tests were conducted in conjunction with this study. The single pile load tests provide a control against which the group load tests can be compared. The results from the single pile load tests were used to normalize the pile group behavior and provide relative performance comparisons.

The first test was performed on a single 324 mm OD pipe pile in virgin ground. This test was used as a comparison with all the group tests involving 324 mm OD pipe piles in virgin soil conditions. A second test was performed on a single 324 mm OD pipe pile in a direction 90 degrees from the direction in which load had been previously applied. This test was subsequently used for comparison with a lateral load test on the 15 pile group where load was applied in the opposite direction subsequent to the first load test. Finally, a lateral pile load test was performed on a 610 mm OD pipe pile. This test was used for comparison with the nine pile group load test involving 610 mm pipe piles. The locations of the various single pile load tests are shown in Figure 1.3.

LATERAL LOAD TEST ON 324 mm SINGLE PILE IN VIRGIN SOIL

Test Layout

The 324 mm single pile test was performed on an isolated single pile located 1.83 meters north of the adjacent nine-pile group near old Bent 4 as shown in Figure 1.3. The single pile was driven closed-ended into undisturbed soil on August 20, 1999 and was tested on November 17, 1999, allowing 86 days for excess pore water pressures generated during driving to dissipate. Using reasonable estimates of the coefficient of consolidation and the clay layer thicknesses involved, we estimate that the excess pore pressures would have fully dissipated within about 25 days.

The test pile had an outside diameter of 324 mm (12.75 inches) and a wall thickness of 9.5 mm (0.375 inch). The steel conformed to ASTM A252 Grade 3 specifications and, based on tests conducted by the manufacturer, Geneva Steel, had a mean yield strength of 404,592 kN/m^2 (58,684 psi), based on the 0.2% offset criteria, with a standard deviation of 15,168 kN/m^2 (2200 psi). The average tensile strength of the pile was 584,087 kN/m^2 (84,715 psi) with a standard deviation of 17,650 kN/m^2 (2,560 psi). The modulus of elasticity (E) for the steel was 200 GPa (29,000 ksi). The moment of inertia (I) of the pile was 1.16×10^8 mm^4 (279 in^4). To protect instrumentation, angle irons were attached to the pile, which increased the moment of inertia to 1.43×10^8 mm^4 (344 in^4). The pile was driven to a depth of approximately 11.9 meters (39 feet) below the excavated ground surface.

The pile was loaded using a 1.34 MN (150 ton) hydraulic jack that reacted against the pile cap constructed around the adjacent pile group after it had been load tested. A schematic drawing of the load test set-up and a photo are provided in Figures 4.1 and 4.2, respectively. The load was applied to the pile at a height of 0.39 m (15.5 inches) above the ground. Although local practice is to fill steel pipe piles with concrete, the test piles were hollow so that the pile would behave in a linear elastic manner. Linear response facilitates analysis of the bending moment.

Instrumentation

The single pile was instrumented to allow the measurement of load, pile head deflection, pile head rotation and strain versus depth along the pile length. The load was measured with a 1.34 MN load cell attached to the hydraulic jack. A spherical endplate was used to prevent eccentric loading and the application of a moment.
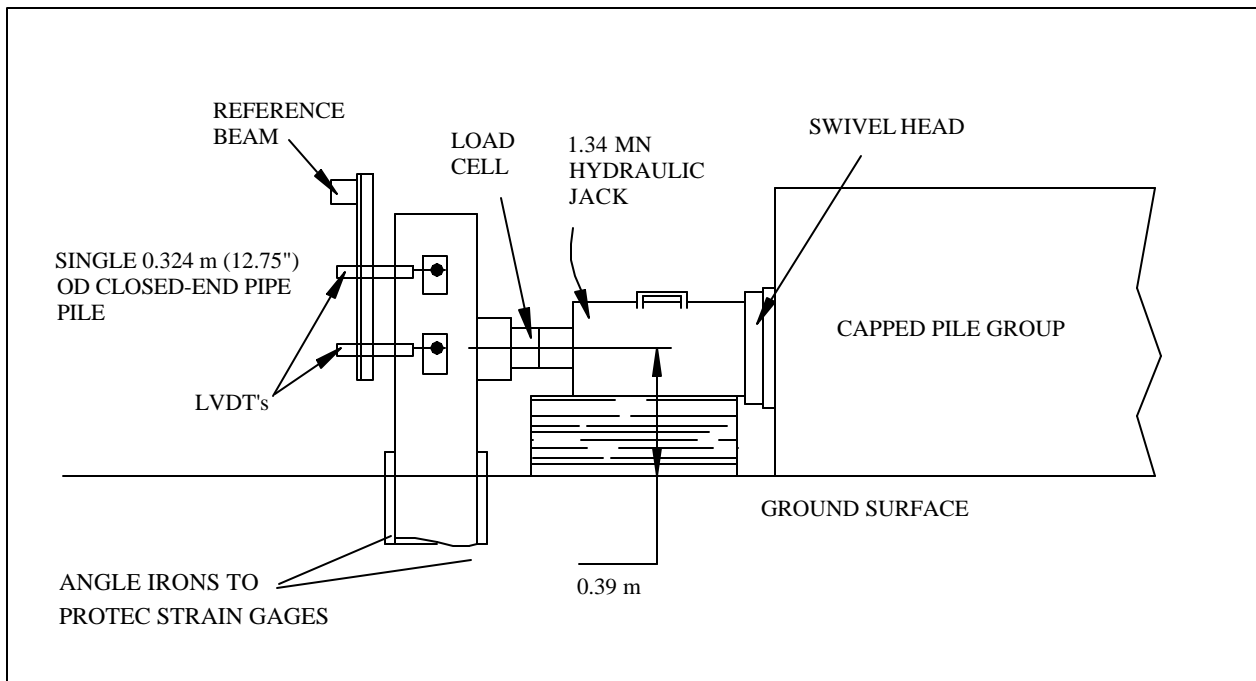
Figure 4.1 Schematic elevation view drawing of the test set-up for the 324 mm OD single pile test.

Figure 4.2 Photograph of the 324 mm OD single pile lateral load test.

The pile head deflection was measured with a linear variable differential transducer (LVDT) that was accurate to 0.127 mm (0.005 inches). The rod portion of the LVDT was pin-connected to an eyehook secured to the pile with epoxy. The housing of the LVDT was fastened to an independent reference frame as shown in Figure 4.2.

Electrical resistance type strain gauges manufactured by Texas Measurements Inc. (model WFLA-6-120) were placed on the front and back outside faces of the pile to measure the tensile and compressive strain that would be produced when the pile was deflected. The strain gauges were located at 9 locations along the length of the pile as shown in Figure 4.3. The gauges and the electrical connections were coated in a waterproof wafer. The lead wires were also coated with waterproof material. The strain gauges were bonded to the outside faces of the piles using epoxy before they were driven into the ground.

A continuous angle iron was used to protect the strain gauges during pile driving. The angle was 5.08 mm (0.2 inch) thick with 38.1 mm (1.5 inch) legs that formed a right angle. The angle iron, shown in Figure 4.3, was spot welded to the pile between each strain gauge and extended to a depth 0.914 meters (3 ft) beyond the final gage.

An Optim Megadac data acquisition system was used throughout the test to continuously record data. The model 5414AC version 7.0.0 system was used with a scanning speed of one sample per second. During the single pile test, 18 channels of strain gauge data, two channels of LVDT data, and one channel of load cell data were recorded.

Procedure

The single pile test was performed using a deflection control approach. The load was applied until the pile head deflection reached a predetermined target. The target deflections consisted of 6.35 mm (0.25 inch) increments to 25.4 mm (1.0 inch) and 12.7 mm (0.5 inch)
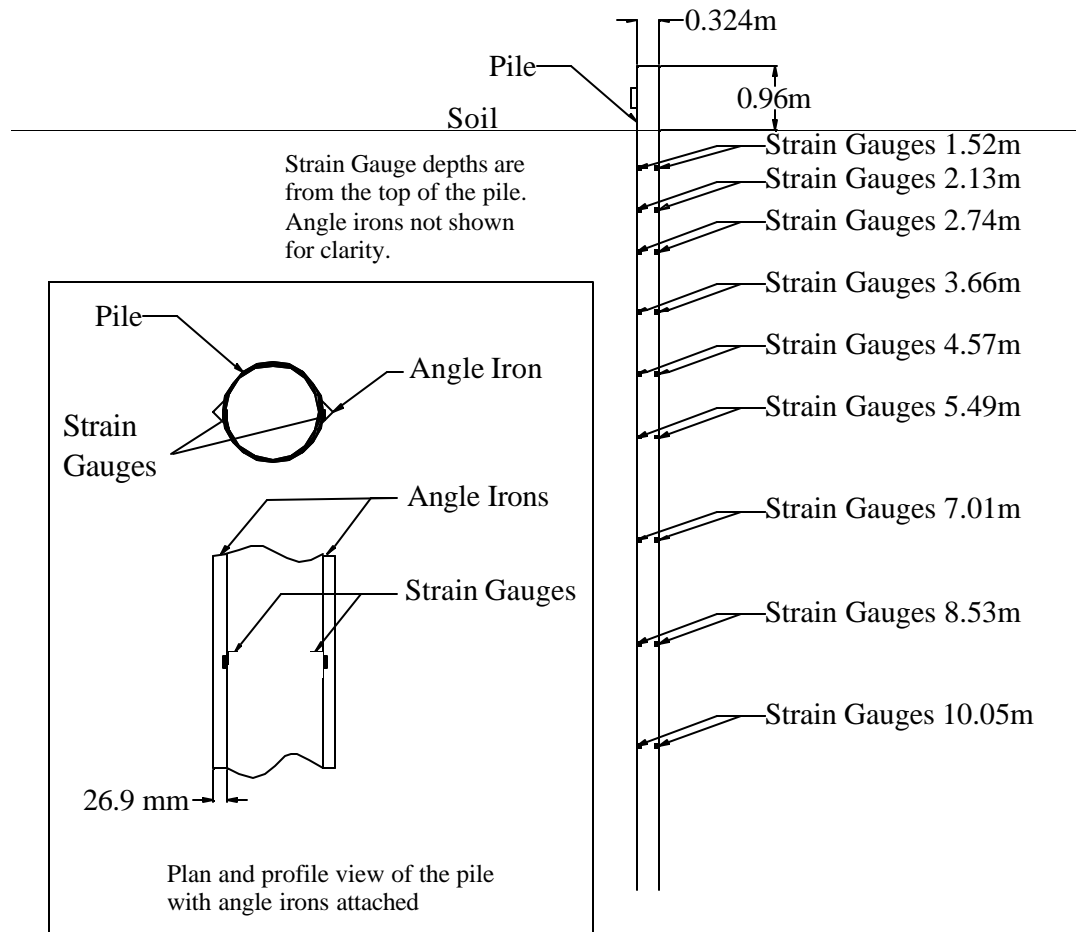
Figure 4.3 Locations of the strain gauges and angle irons with respect to the top of the pile.

increments to 76.2 mm (3 inches). Fifteen cycles were applied at each of the first eight deflections. The final deflection was to 88.9 mm (3.5 in) and only one cycle was carried out at this deflection. The single pile was loaded in one direction only. On the first cycle, the pile was loaded to the target deflection and the deflection was maintained for three minutes to allow recording by hand of peak values and verification of instrumentation functionality. The subsequent cycles followed the same pattern, except that deflection was only maintained at the target level for 10 to 20 seconds while the readings stabilized. After reaching the target

deflection and recording any information, the load was allowed to return to zero between each cycle.

Test Results

Load versus deflection at pile head.

The load versus deflection curve for the entire test is plotted in Figure 4.4. A review of these curves indicates that the deflection did not return to zero after the load was released for each cycle. This occurred even though the load was less than that necessary to cause yielding of the steel permanent pile deflection. One plausible explanation for this behavior is that soil fell into the gap behind the pile as it was loaded and prevented the pile from returning to its original position.
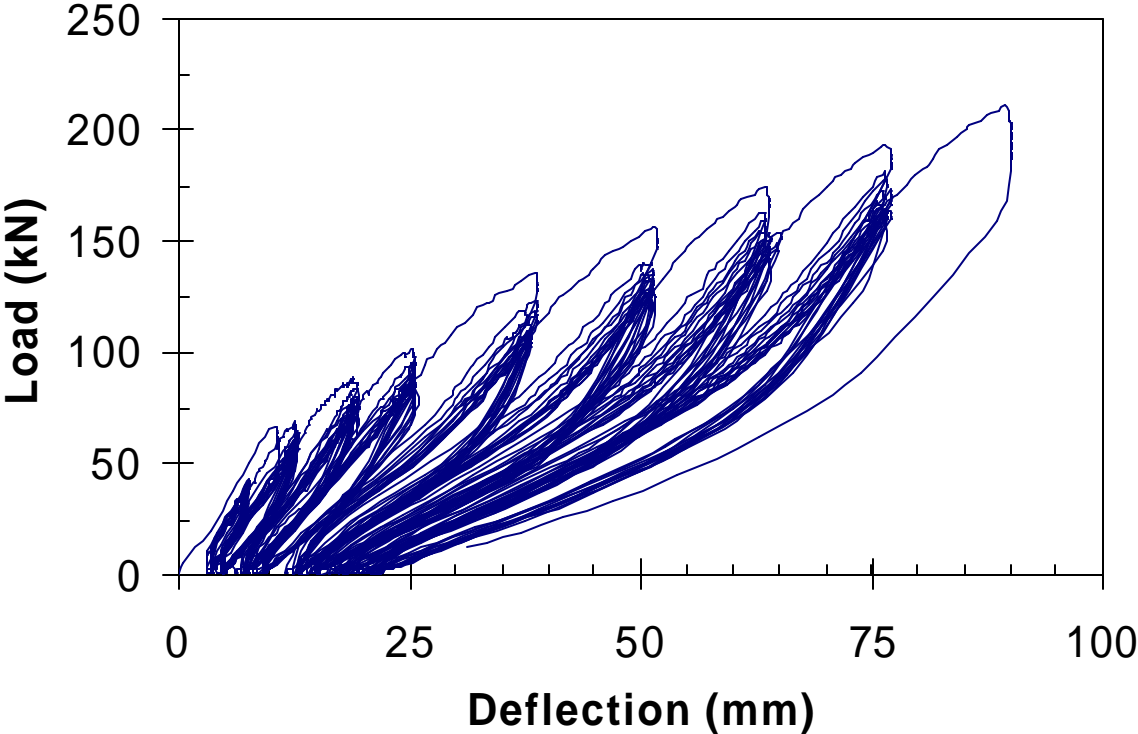
Figure 4.4 Complete load-deflection curve for the 324 mm OD single pile test.

The load cycle curves in Figure 4.4 also show that the shape of the load-deflection curve changes after the first cycle. During the first cycle, the slope of the curve tends to decrease with increasing deflection (concave down shape); however, for subsequent cycles, the slope of the curve appears to increase with increasing deflection (concave upward shape). This behavior is a result of the gap that forms due to permanent deformation of the cohesive soil in front of the pile. The soil was subjected to shear as the pile repeatedly deflected under the applied load. Some of the soil deformation was elastic and was recovered as the pile was unloaded. However, a portion of this deformation was plastic and accumulated throughout the test, resulting in a gap that was formed between the soil and the surface of the pile. The photograph in Figure 4.5 shows the gap that developed in front of the pile due to the plastic deformation in the soil. However, the photograph also shows that a gap develops behind the pile, as soil near the surface falls into the gap formed behind the pile during loading. As a result, near the ground surface a gap developed nearly all the way around the pile although it was much larger in front of the pile.

Even as additional loadings closed the gap and the pile came into full contact with the soil, the lateral resistance was decreased. The graph in Figure 4.6 shows the peak load versus deflection curves for the first and fifteenth cycles of the test.   The peak load for the 15th cycle is typically about 15% lower than the peak load for the 1st cycle. This loss in strength is likely due to soil sensitivity and disturbance caused by repeated shearing of the soil.

Although the difference in the peak load-deflection curves for the 1st and 15th cycles is relatively small, these curves are deceptive because they do not show the full load-deflection of the pile before the peak load is achieved. To better demonstrate the behavior of the pile when subjected to repeated lateral loading, the load versus deflection curve for each fifteenth cycle was also included in Figure 4.6. After an initial target deflection had been obtained, the subsequent

Figure 4.5 Formation of gaps in front of and behind the pile during cyclic loading in cohesive soil.
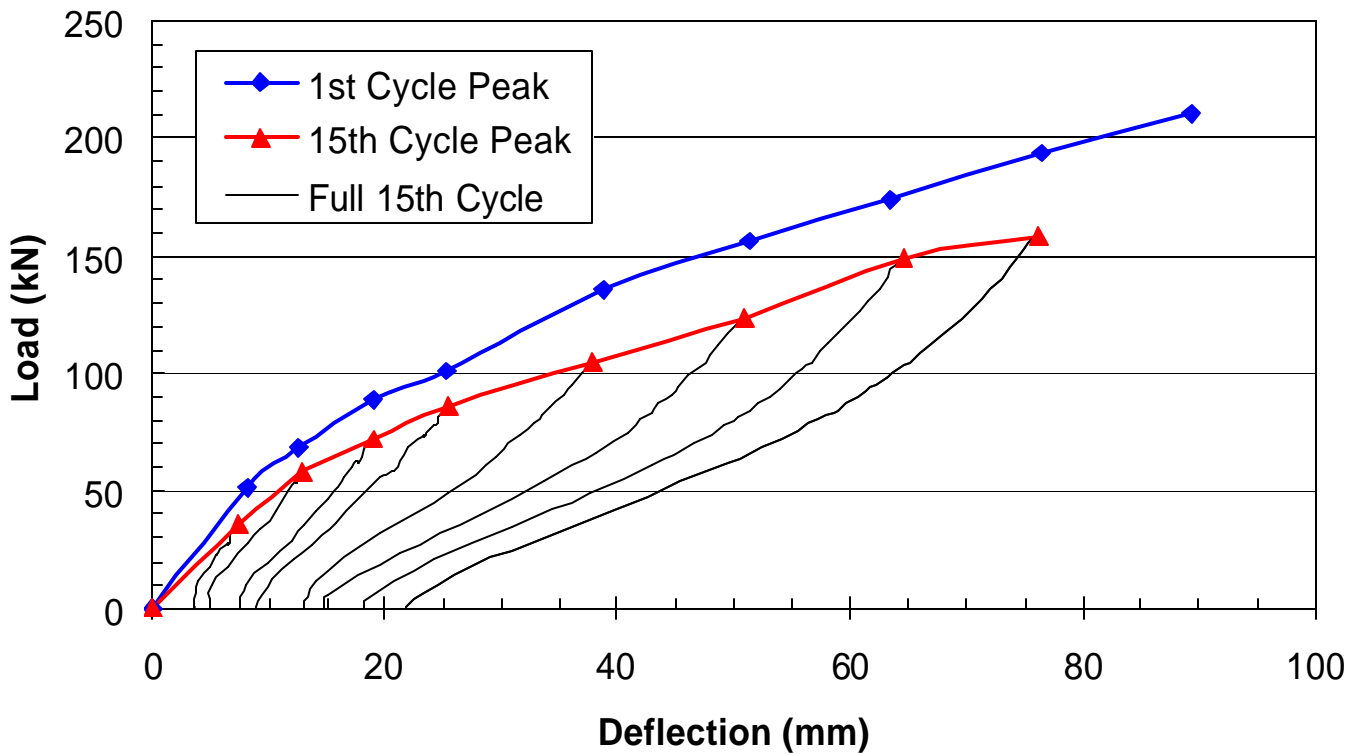
Figure 4.6 Load-deflection curves for the peak points on the first and fifteenth cycles along with the complete load-deflection curve for each fifteenth cycle on the 324 mm pile test.

loading did not actually follow the path suggested by the curve connecting the peak loads and deflections. At deflections short of the previous peak deflection, the load during the 15th cycle is significantly below that for the 1st cycle. The curves for the fifteenth cycle appear to be composed of two segments. The lower part of the curve appears to be relatively linear. The slope of the upper part of the curve increases rapidly and the curve becomes parabolic with a concave upward shape.

This change in slope of the load versus deflection curve is readily explained by the presence of the gap which developed around the pile. During the first cycle, the applied load is resisted by both the pile and the soil near the ground surface. During the subsequent loadings, a gap developed between the soil and pile due to the previous loading. For deflections less than the width of that gap, the primary resistance to loading is flexure of the pile. This explains the

approximately linear relationship between load and deflection when the pile is pushed through the gapped region. As the deflection approaches the previously achieved maximum deflection, the load-deflection relationship becomes non-linear with a concave upward shape. This increase in slope of the upper part of the curve is due to the pile engaging the soil and receiving progressively more lateral soil resistance.

The change in soil stiffness during the fifteen cycles of loading is further examined in Figure 4.7. The soil stiffness (K) was calculated using the equation

$$K = \frac{\Delta F}{\Delta L} \qquad (4.1)$$

where ΔF was the peak force that was applied to the pile during each cycle and ΔL was the pile deflection for each cycle. The stiffness for each cycle was then normalized by the initial stiffness, K_i, for the first cycle for each target deflection.
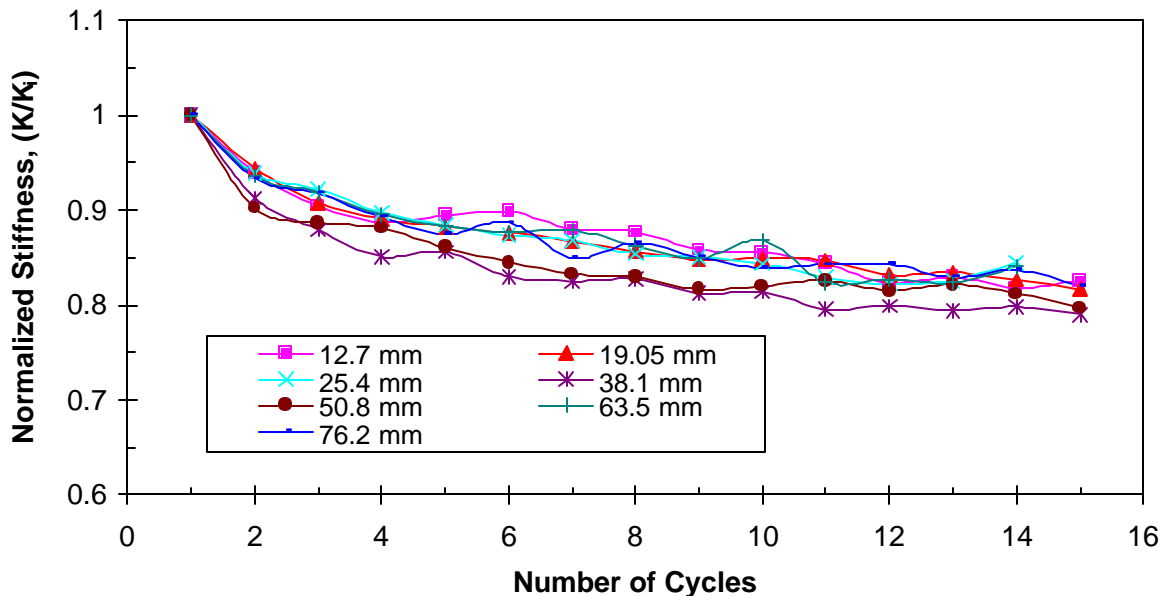
Figure 4.7 Normalized soil stiffness versus the number of load cycles for several displacement increments for the 324 mm single pipe pile.

There was a significant reduction in stiffness for the second cycle, but the rate of decrease in stiffness was more moderate as more cycles were applied. For example, the decrease in

stiffness between the first and second cycle was approximately 10%, but the decrease in stiffness over the next 14 cycles was only between 7.5 and 10%. The rate of decrease in stiffness lessened with each cycle as the number of cycles increased.

Bending Moments

The bending moment was calculated using the strain gauge measurements. The gauges were located at nine depths on opposite sides of the pile (See Figure 4.3). The bending moment was calculated using the equation

$$M = \frac{EI(e_t - e_c)}{h} \tag{4.2}$$

where: ε_t = the change in strain on the tension side of the pile (+ sign)
ε_c = the change in strain on the compression side of the pile (- sign)
h = the horizontal distance between the gauges which was 324 mm (12.75 in)

Some strain gages were damaged during installation or malfunctioned during the test. In these cases, the strain measured by the gauge on the opposite face was assumed to be equal but opposite in sign to the measured value in computing the moment.

Bending Moment versus Depth. A plot of the bending moment versus depth for the various target deflections of the isolated single pile is shown in Figure 4.8. The applied load associated with each deflection level is also indicated in the figure. The depth to the maximum moment gradually increases as the load and deflection levels increase. For example, at the 3.42 mm deflection, the maximum moment occurred at 1.2 meters (3.9 ft) below the surface, however, at a 37.1 mm deflection, the maximum moment occurred at a depth of 1.8 meters (5.9 ft) below the ground surface. The first two deflections produced moment reversals at depths of 3.7 m (12.1 ft). The subsequent deflections had moment reversals at depths of 4.6 to 6.1 meters
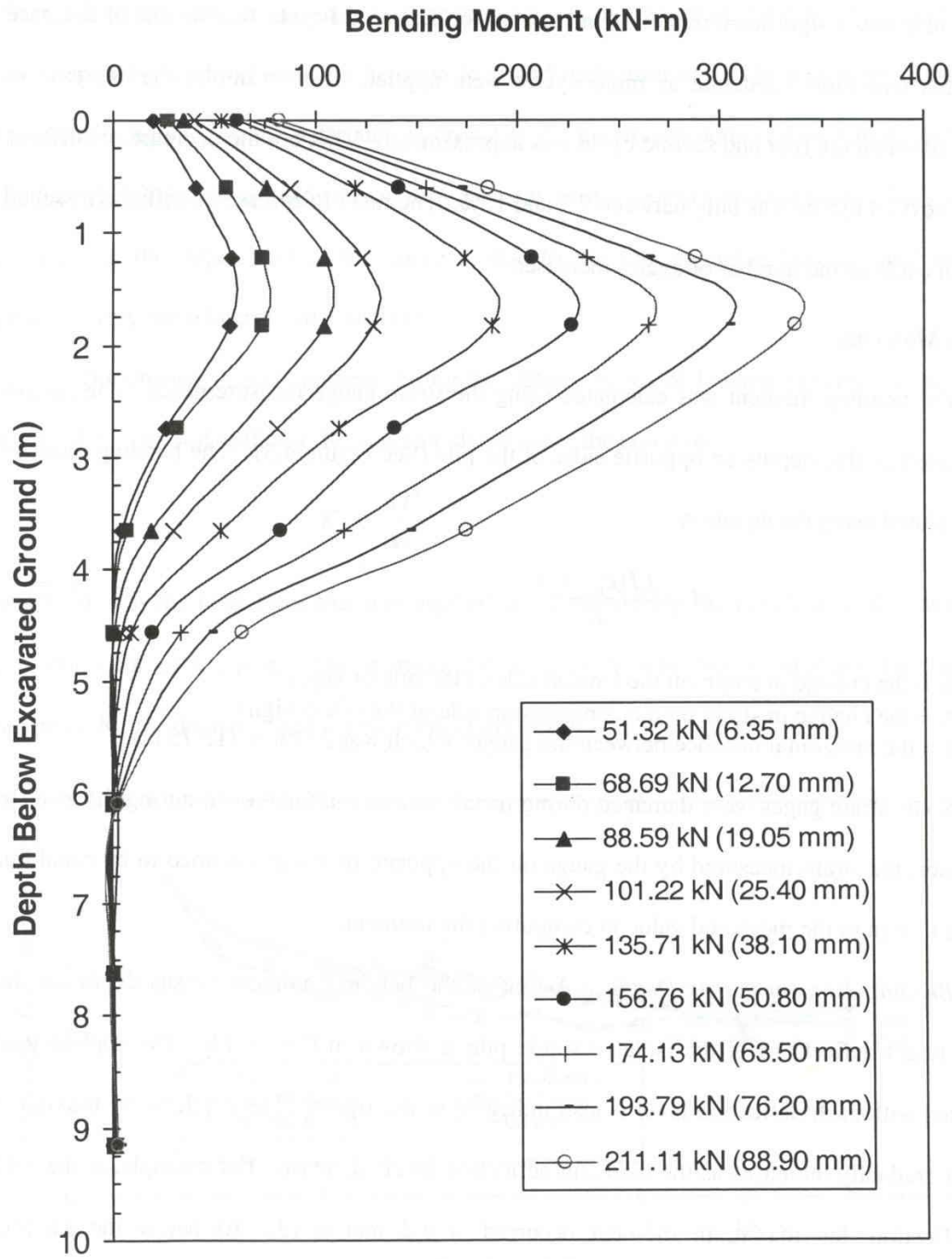
Figure 4.8 Measured bending moment versus depth curves for the first cycles of load on the 324 mm single pipe pile test.

(15.1 ft to 20.0 ft). The depth to the moment reversal increased with each increase in target deflection. The yield moment for the pile was determined to be approximately 330 kN-, (250 kip-ft) using the program LPILE Plus version 3.0 (Reese and Wang, 1997). The maximum moment during the test was 34- kN-m (252 kip-ft). Therefore, yielding likely occurred during the last load cycle.

Maximum Moment versus Load. The maximum bending moments in the single pile for the first and fifteenth cycles are plotted in Figure 4.9 with the applied load on the horizontal axis. The bending moment shown is the greatest moment that occurred along the length of the pile at that deflection level. There is a gradual increase in slope as the load increases. This increase in slope is due to the decrease in soil stiffness and consequential decrease in lateral restraint. As the soil resistance decreases, the pile below the ground level has greater freedom to bend and deflect under lateral load, leading to increasing bending moments.

With the exception of the first target deflection, the bending moments of the first cycle were less than those of the fifteenth cycle for a given deflection. The difference between the two curves was approximately 15%. This difference can be attributed to the softening of the soil and the formation of gaps around the pile from the repeated loading of the pile.

Pile Head Rotation

The pile head rotation for the isolated single pile was determined by placing two LVDTs on one pile at a distance of 0.305 m (1 foot) apart. The pile head rotation is plotted as a function of the load in Figure 4.10. The rotation (ω) in radians was calculated using equation 4.3.

$$\omega = \arctan\left(\frac{\Delta h}{\Delta l}\right)$$
(4.3)
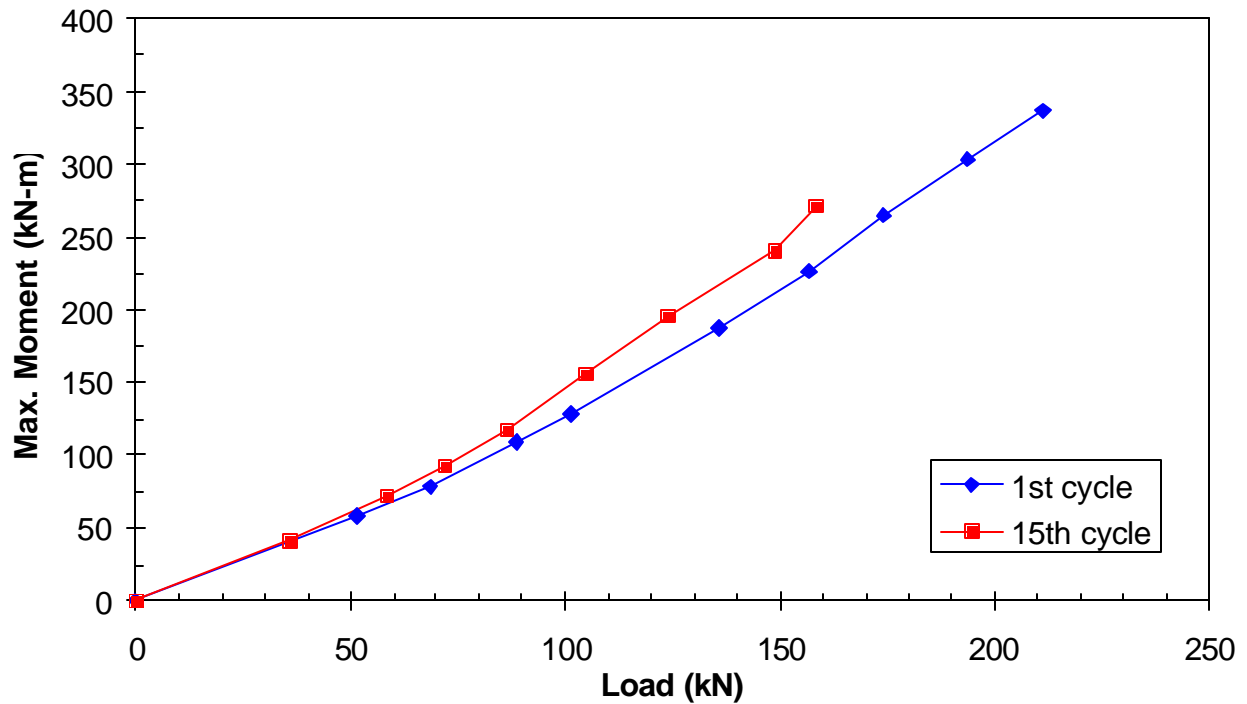
Figure 4.9 Maximum moment versus applied load for the first and fifteenth cycle on the single 324 mm pipe pile load test.
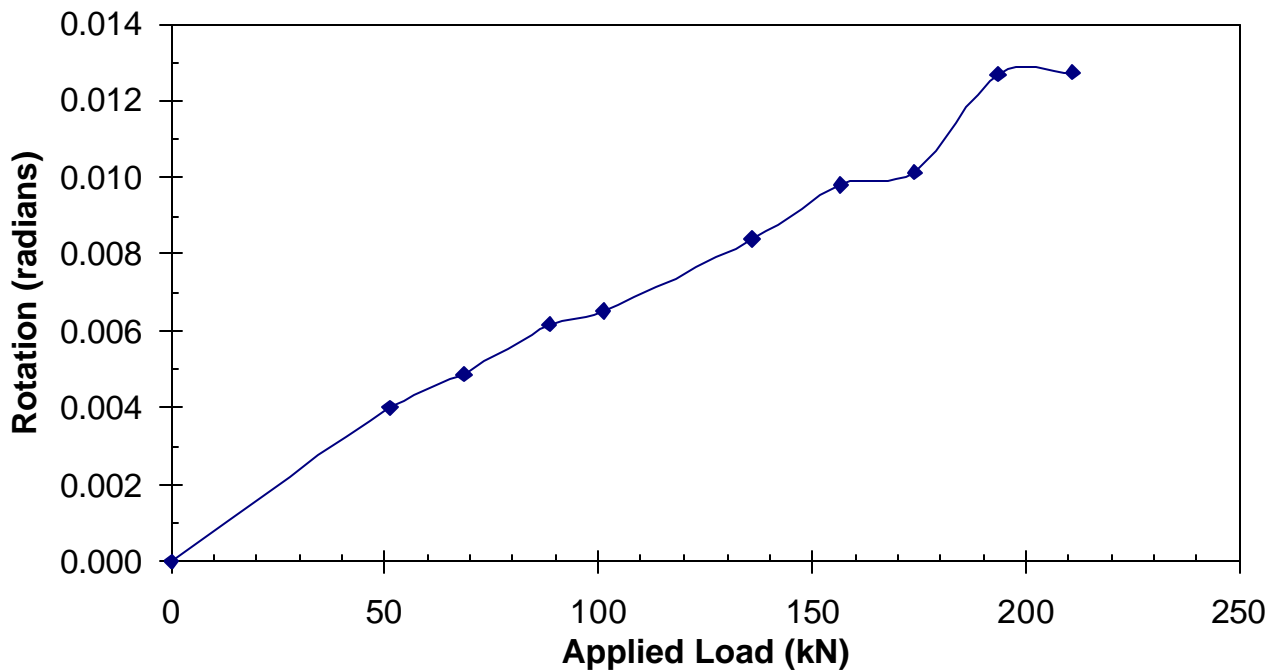

Figure 4.10 Pile head rotation versus applied load for the first load cycles on the single pile test for the single 324 mm pipe pile test.

where: w is the rotation of the pile head in radians

        Δh is the difference in horizontal deflection between two LVDTs

        $\Delta \ell$ is the vertical distance between the LVDTs.

The rotation increased almost linearly with applied load until the maximum rotation of 0.013 radians was attained at a load of 211 kN (47.4 kips). The rotation was 0.007 radians at 25.4 mm (1 inch) deflection and reached a maximum of 0.013 radians at the 76.20 mm (3.0 in) deflection.

LOAD TEST ON 324 mm SINGLE PILE IN PREVIOUSLY LOADED SOIL

A lateral load test was also performed on a single pile that had been previously loaded at 90 degrees to the load test direction during the lateral pile group load test on the 12 pile group. Figure 4.11 provides a schematic drawing showing the layout for the test. The test was performed on a single pile on the outside edge of the group to minimize interaction effects with adjacent piles. The pile was pushed toward the South away from the group. A steel beam distributed the reaction force to three piles in the middle of the group. This test was performed after the pile group had been loaded in the East-West direction to study soil-pile interaction and the group behavior as will be discussed in a subsequent chapter.

The pile was loaded using a 180 kN hand jack, which was operated manually. The load was applied at a height of 0.48 m (19.0 in) above the excavated ground surface. Only one cycle of load was applied at each deflection increment. The load was measured using a load cell and pile head deflection was measured using an LVDT attached to an independent reference frame. No strain gauges were attached to this test pile. Data was recorded using a Labtec notebook data acquisition system running on a laptop computer.

Figure 4.12 shows the load-deflection curve for this test, along with the fist cycle peak load-deflection curve for the single pile in virgin ground previously discussed. The load-
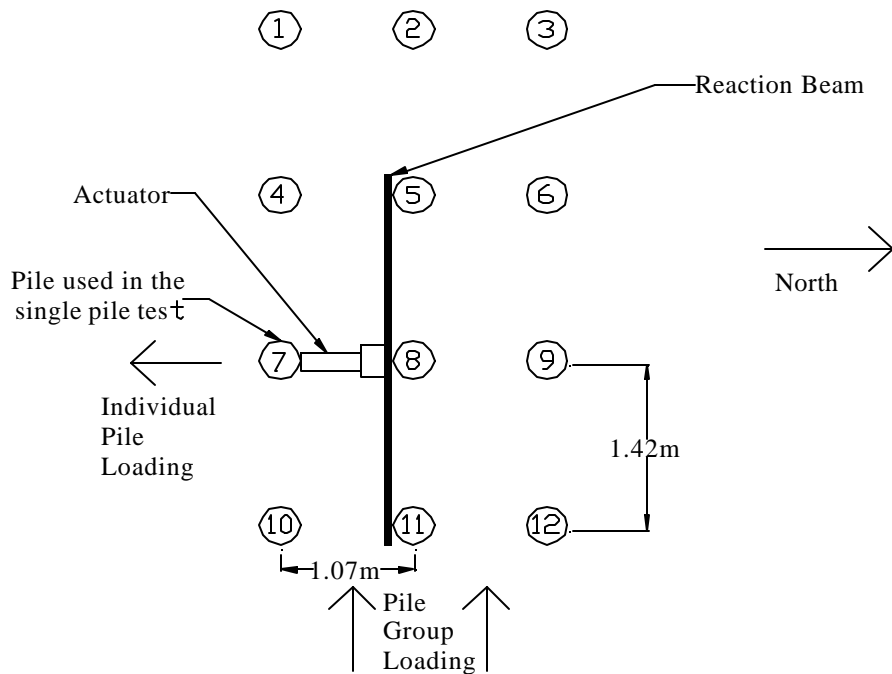
Figure 4.11   Schematic drawing of the load test layout for the single pile test on a pile that was previously loaded at 90 degrees to the test direction.
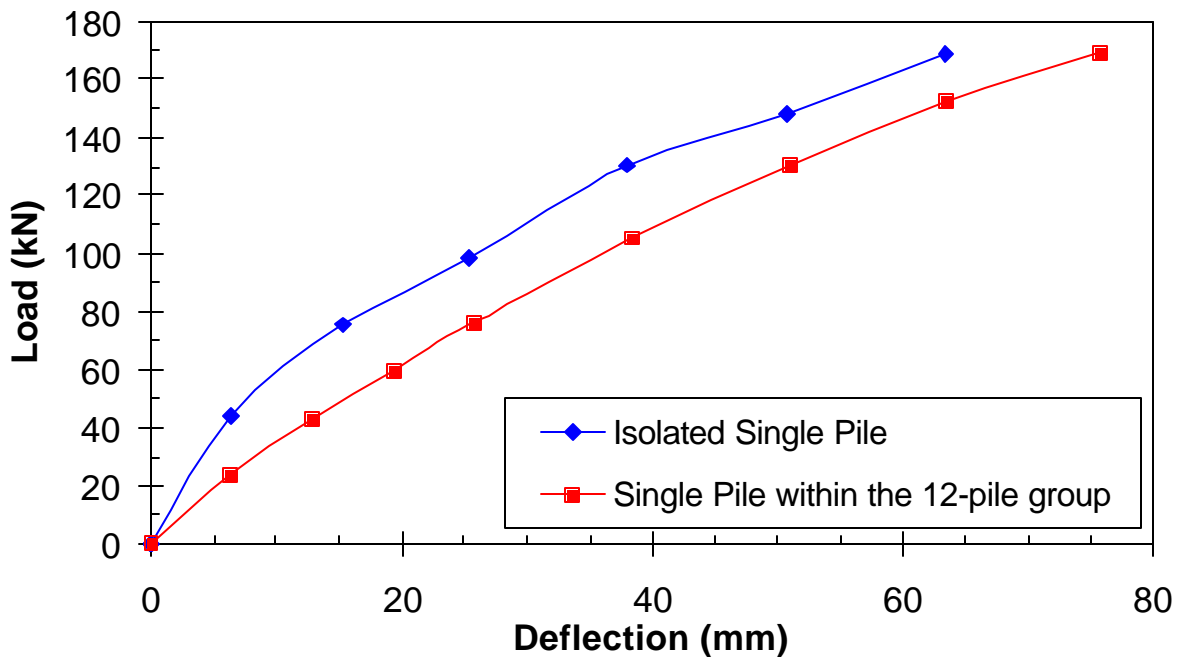

Figure 4.12   Comparison of the load-deflection curves for the single pile load test in virgin soil and the single pile load test performed at 90 degrees to the original load direction.

deflection curve for the reloaded pile is significantly softer and much more linear than that for the pile tested in virgin ground. This difference in the shape of the curve was due to the decreased soil resistance around the pile as a result of the formation of gaps during the previous lateral loading of the pile group. The difference in load at given deflection ranged from 50% at the smaller target deflections to 10% by the higher deflections. As the test progressed to greater deflections, the influence of the gap became less pronounced and the curve shape and slope began to approximate that for the pile in virgin ground. Because the pile chosen was not instrumented with strain gauges, no bending moment curves are presented for this test.

LATERAL LOAD TEST ON 610 mm SINGLE PILE IN VIRGIN SOIL

Test Layout

The 610 mm test pile was driven 2.13 m (7.5 ft) northeast of the companion group of nine piles as shown in Figure 1.3. The pile was driven on August 24, 1999, the same day as the piles in the companion group. The pile was driven open-ended to a depth of 11.2 m (36.8 ft) and, since a plug did not develop in the pile, the soil inside the test pile remained at the same elevation as the excavated ground surface outside the pile. The soil inside the pile remained in place during the test.

The piles used in both the single pile test and the companion group tests were ASTM A252, Grade 3, spiral weld, steel pipe piles. They had a 610 mm (24 in.) outside diameter with a 12.7 mm (0.5 in.) wall thickness. The elastic modulus (E) of the steel was 200 GPa (29,000 ksi), and the moment of inertia (I) for the pile alone was 1.06×10^9 mm^4 (2549 in.^{4}). A 38.1 mm (1.5 in.) angle iron was welded to each side of the pile to protect the strain gauges. These angle irons increased the moment of inertia to 1.15×10^4 mm^4 (2764 in.^{4}). Skyline Steel Corp., the manufacturer of the piles, reported that the piles used in this test had a mean yield strength of

397,600 kN/m^2 (57,670 psi) with a standard deviation of 12,260 kPa (1780 psi). Yield strength was defined using the 0.2% offset method.

The lateral test was performed on May 15, 2000, over nine months after it was driven. This allowed adequate time for pore pressures to dissipate. In addition, the test could only be performed after the completion of the testing of the 15 pile group which provided the reaction for the single pile test. The lateral load was applied to the single pile at a height of 0.495 m (19.5 in.) above the ground using a 1.34 MN (150 ton) hydraulic jack. A spherical end plate was placed behind the jack to prevent eccentric loading. The hydraulic jack was reacted against a steel beam that rested against three piles on the outside edge of the 15 pile group. A photograph of the single pile load test set-up is shown in Figure 4.13.

Figure 4.13 Photograph of lateral load test on 610 mm OD single pile.

Instrumentation

The single pile was instrumented to measure the pile head load, pile head deflection, pile head rotation, and strain versus depth along the length of the pile. The load was measured using a 1.34 MN (150 ton) resistance type strain gauge load cell which was attached to the hydraulic jack. A LVDT accurate to 0.127 mm (0.005 in.) was used to measure pile displacements. The LVDT rod was attached to an independent reference frame with supports placed 1.8 (6 ft) from the edge of the test piles.

The single pile was instrumented with electrical resistance type strain gauges in an identical manner to the piles in the companion pile group. A total of 24 strain gauges were placed on the outside face of the test pile. These gauges were placed at twelve depth intervals on opposite sides of the pile as shown in Figure 4.14. The piles were oriented so that the gauges on one side measured the maximum tension and those on the other side measured maximum compression, so that the maximum bending moment at each depth could be calculated. The strain gauges were 120 ohm electrical resistance type waterproof gauges (Model WFLA-6-120) manufactured by Texas Measurements, Inc. To protect the gauges during driving, 5.08 mm (0.2 in.) thick angle irons with 38.1 mm (1.5 in.) legs were welded above the gauges. The welds were approximately 76 mm (3 in.) long and were placed halfway between each gauge. The angle iron extended to the bottom of the pile, 0.305 m (1 ft) below the last strain gauge.

An Optim Megadac model 5414AC version 7.0.0 computer data acquisition system was used to record all the test data during the test. During the test, readings were taken at one-second intervals. The acquisition system recorded one load cell channel, one LVDT channel, and 24 channels of strain gauge data.

load point

ground surface

0.56*

water table

1.17

1.78

2.39

3.00

3.61

4.52

5.44

6.35

7.87

9.40

10.92
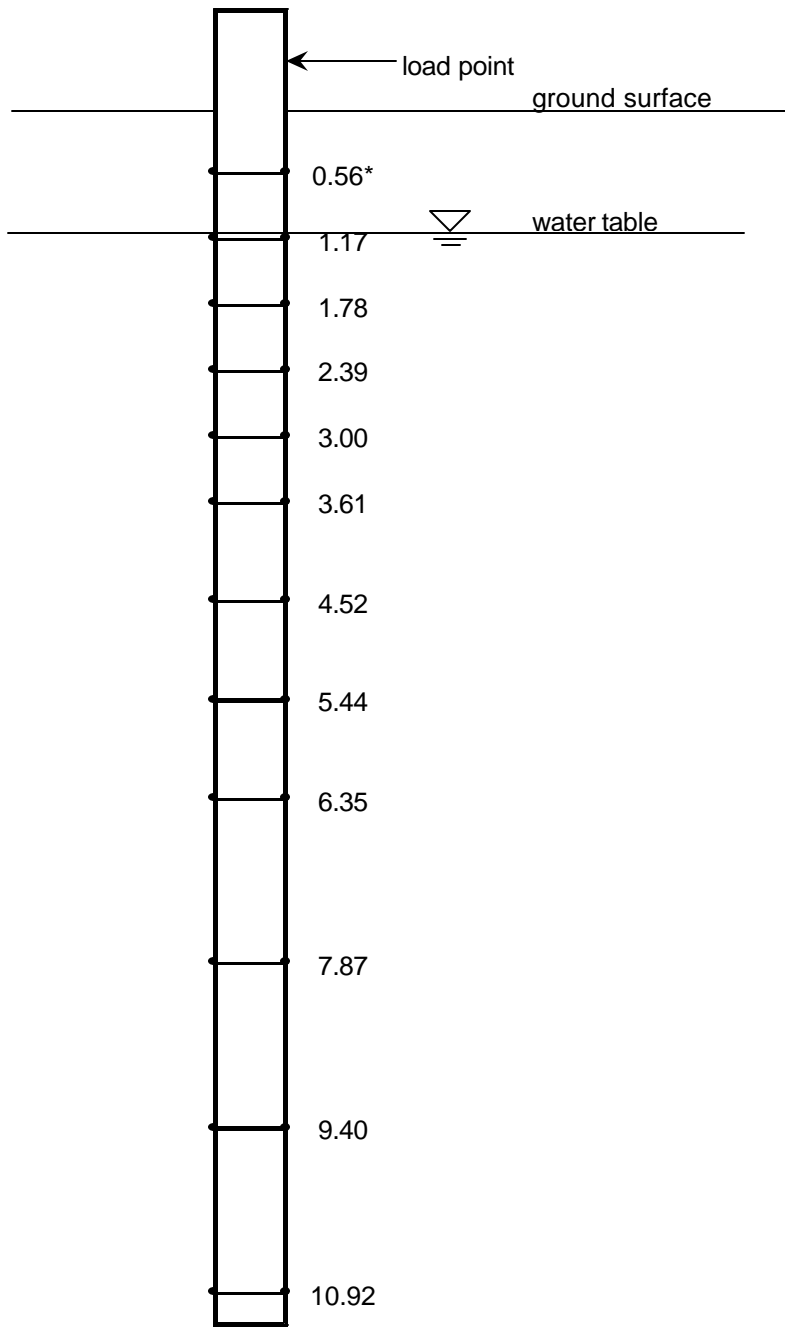
Figure 4.14   Strain gauge locations along the length of the 610 mm OD pipe pile.

Test Procedure

The pile was loaded using a displacement control approach in six increments producing target deflections of 7.62 mm (0.30 in.) to 50.8 mm (2.0 in.) At each increment, the pile loading was cycled fifteen times. The pile was loaded in one direction only, with the load applied by the hydraulic jack and then removed, allowing the pile to return to the unloaded position. On the first cycle of each increment, the load was held for three minutes, as is the procedure for a traditional static lateral load test. During this time, data were read manually, and the instruments were checked. On each of the remaining cycles, the load was held for only about ten seconds until the readings stabilized.

Fifteen static cycles were applied during this testing protocol to simulate the number of lateral load cycles which might be applied by a major earthquake. Based on a statistical study of earthquake records, Seed et al (1975) developed a correlation between earthquake magnitude and the number of equivalent uniform stress cycles for an earthquake time history. Based on this study, an average of 15 cycles corresponds to the number of cycles typically produced by a M7.5 earthquake.

Test Results
Load versus deflection at pile head

A plot of the complete measured pile head load versus deflection curve for the single pile test is shown in Figure 4.15. The single pile was subjected to a maximum load of 414.3 kN (93.1 kips), which corresponded to a deflection of 48.8 mm (1.92 in). The load-deflection curves are very similar to those measured during the single pile test on the 324 mm pipe pile. A drop in strength occurred after the first cycle of loading in each increment. As the pile deflected under
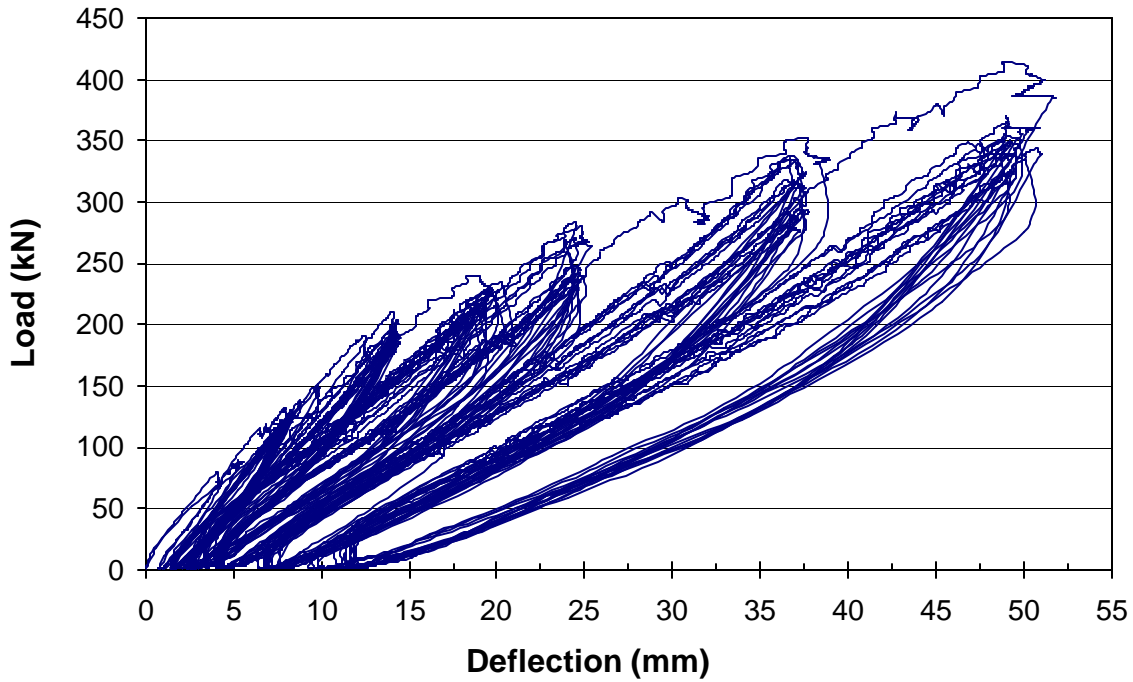
Figure 4.15 Complete load-deflection curve for 610 mm single pile test.
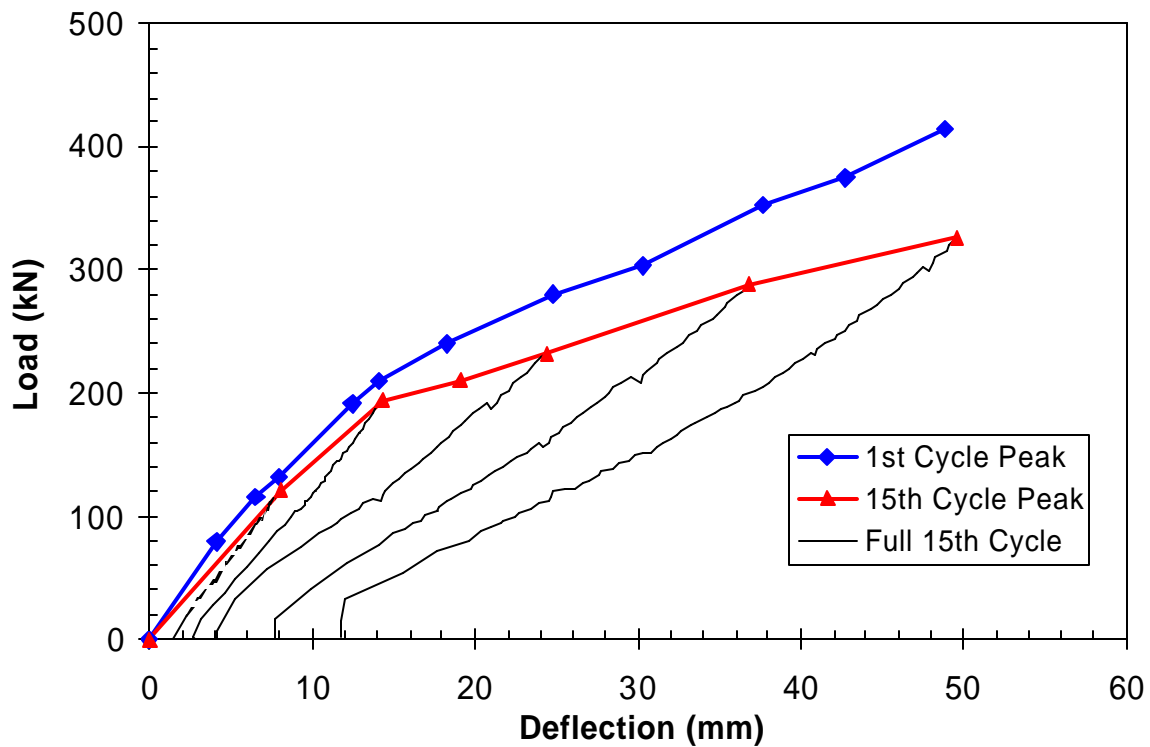
Figure 4.16 Load-deflection curves for the peak points on the first and fifteenth cycles along with the complete load-deflection curve for each fifteenth cycle on the 610 mm pile test.

the first load application, the resisting soil compressed, sheared, and softened, resulting in a reduction of soil resistance to pile movement for all subsequent cycles.

In addition, a gap formed in front of the pile as the cohesive soil was compressed under loading and did not completely rebound. During the first load cycle, the load-deflection curve climbs rapidly but the slope gradually decreases. However, on the remaining cycles, the load-deflection curve initially climbs slowly, because nearly all of the resistance is being provided by the pile itself due to the gaps in the soil. The slope then increases as the pile again starts to react against the soil.

At the completion of the cycles at each deflection increment, some permanent deflection remains. Since the stress level is significantly lower than that necessary to cause yielding in the pile, the permanent deflection is not likely due to plastic deformation of the pile itself. The permanent offset may simply be due to soil falling down the gap between the back wall of the pile and the soil while the load is applied. This soil then prevents the pile from returning back to the original position.

Load-deflection curves for the peak loads of the first and fifteenth cycles of each load increment are plotted in Figure 4.16. The points on this plot are based on the peak load and the corresponding deflection for each load increment. With each cycle, the gaps in the soil grew increasingly larger leading, to a reduction in strength of approximately 20% from the first to the fifteenth cycle.

Bending moment

The strains measured by the strain gauge pairs at each depth interval were used to compute the bending moment according to equation 4.2. In some cases, the strain gauges did not

function properly. In these cases, the reading on the opposite strain gauge was assumed to be equal but opposite in sign to the working strain gauge.

Bending Moment versus Depth. Bending moment versus depth curves are plotted in Figure 4.17 for the peak load during the first cycle for each of the seven load increments. The deflection level associated with this load level is also noted in each case. The maximum bending moment during the test was 812.6 kN-m (7192.2 kip-in). The bending moment causing yield is estimated to be 1129 kN-m, therefore, yield did not occur during the test.

The maximum bending moment during the first load increment occurred at a depth of 1.16 m below the ground surface. For each of the remaining load increments, the gauge at a depth of 2.38 m measured strain correlating to the maximum moment of the single pile. This depth corresponds to approximately 3.9 pile diameters. In contrast, the maximum bending moment for the 324 mm single pile typically occurred at a normalized depth of 5.5 pile diameters. Near the bottom of the pile, negative moments developed for nearly every test. This moment reversal was noted at depths ranging from 6.8 to 7.8 m. Below this depth, all moments were relatively close to zero.

Maximum Bending Moment versus Pile Head Load. The maximum bending moment versus load curves for the first and fifteenth load cycles are plotted in Figure 4.18. The plotted moments correspond to the maximum moment, at any depth along the pile, measured during the peak load for each increment. As the load increased, the slope of each curve gradually increased due to a decrease in soil stiffness. As the stiffness of the soil acting on the pile was reduced, there was less restraint against lateral deformation, leading to an increase in bending moment.

As can be seen in Figure 4.18, the bending moment was larger for the fifteenth cycle than the first cycle, and the two curves separated more as the load increased. This is likely due to the
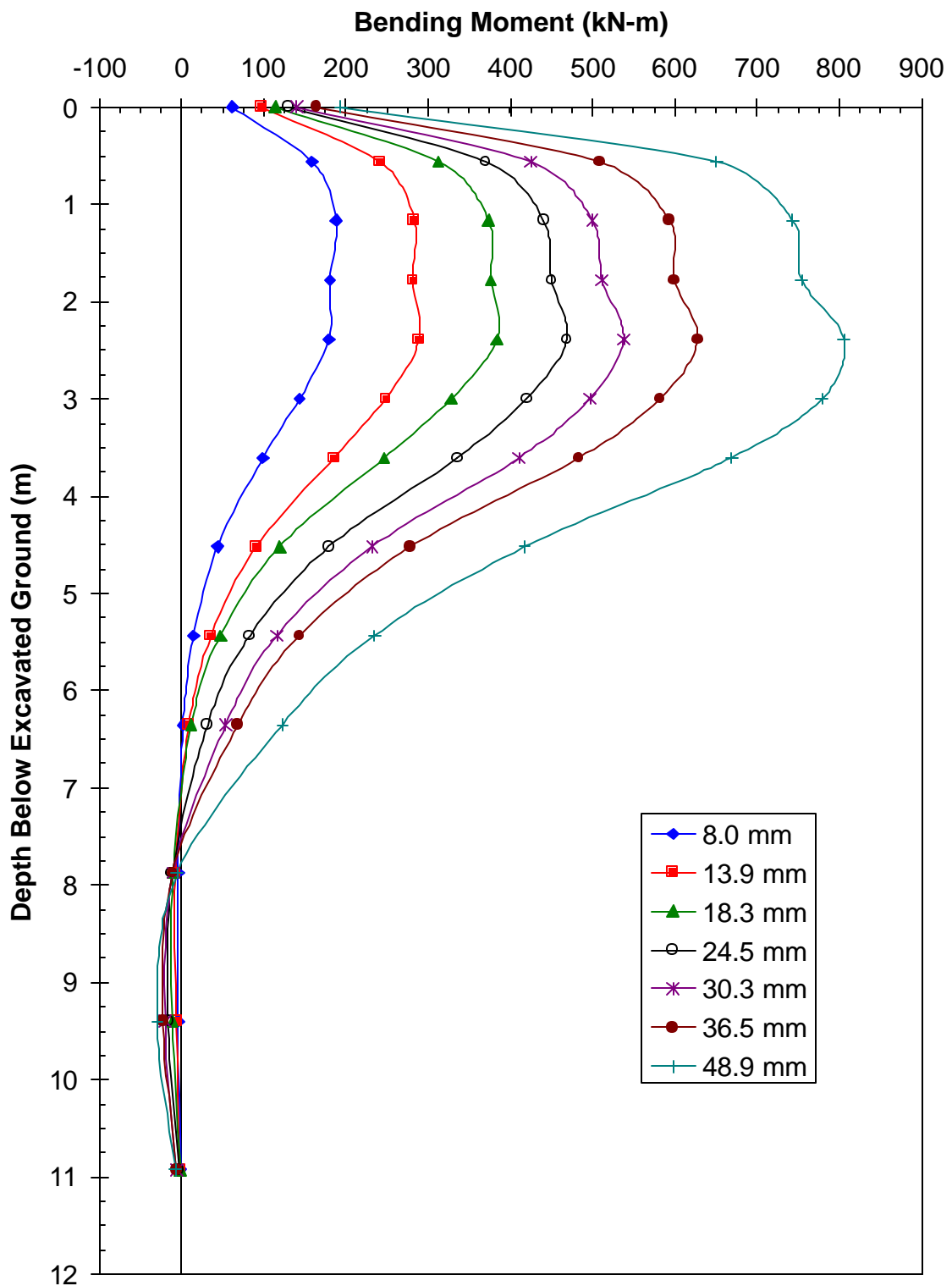
Figure 4.17 Bending moment versus depth curves for each load increment during lateral load test on 610 mm OD single pipe pile.
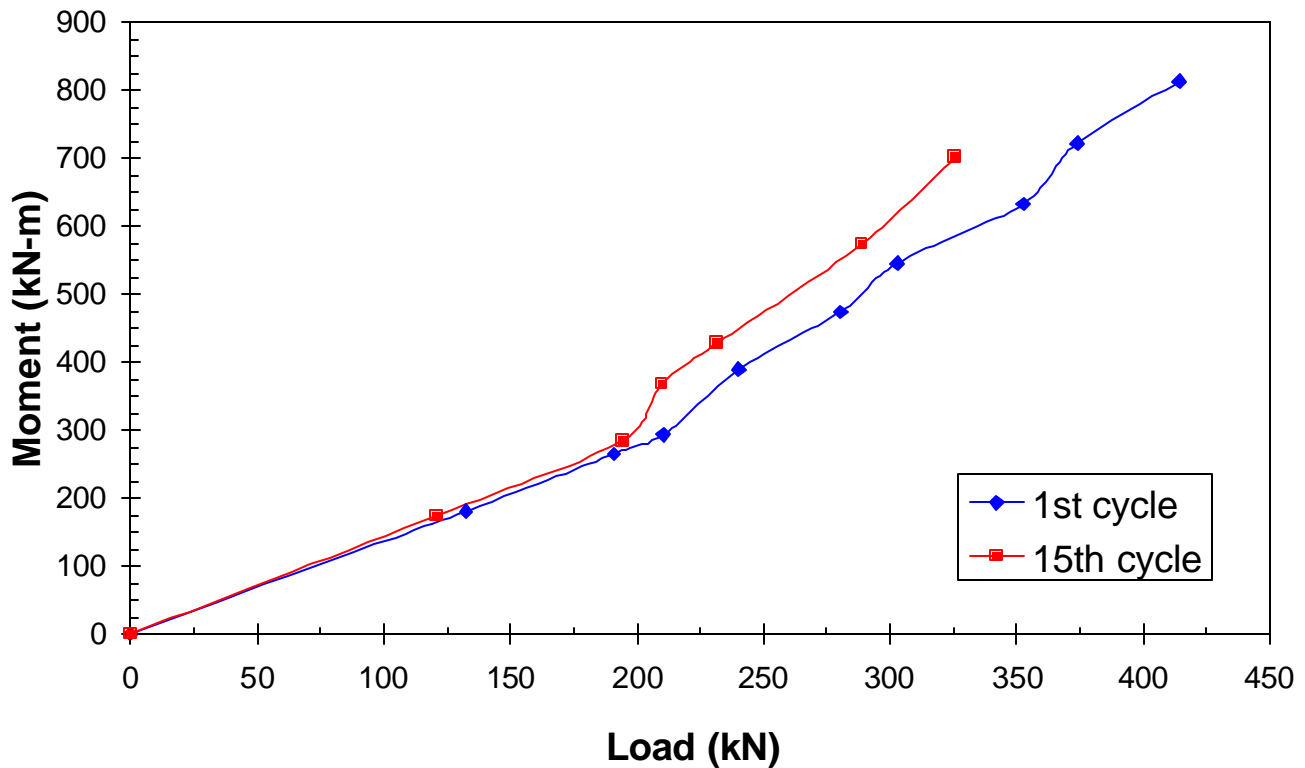
Figure 4.18 Peak bending moment versus load curves for the 1ˢᵗ and 15ᵗʰ load cycles of the single pile test on the 610 mm OD pipe pile.

gap formation and soil softening in the upper soil layers. For example, the difference between the two curves at a load of 132.4 kN was only about 4.5%; however, at a load of 325.7 kN it is about 19%.

COMPARISON OF PERFORMANCE OF SINGLE PILES
The load versus deflection curves obtained from the lateral load tests on the single 324 mm and 610 mm diameter steel pipe piles are presented in Figure 4.19 (a). The load carried by the 610 mm diameter pile is very close to 2.67 times higher than that carried by the 324 mm diameter pile at all deflections levels. This load ratio of 2.67 is higher than the ratio of diameters, which is 1.88 in this case. This result suggests that the increased capacity for these piles in cohesive soil
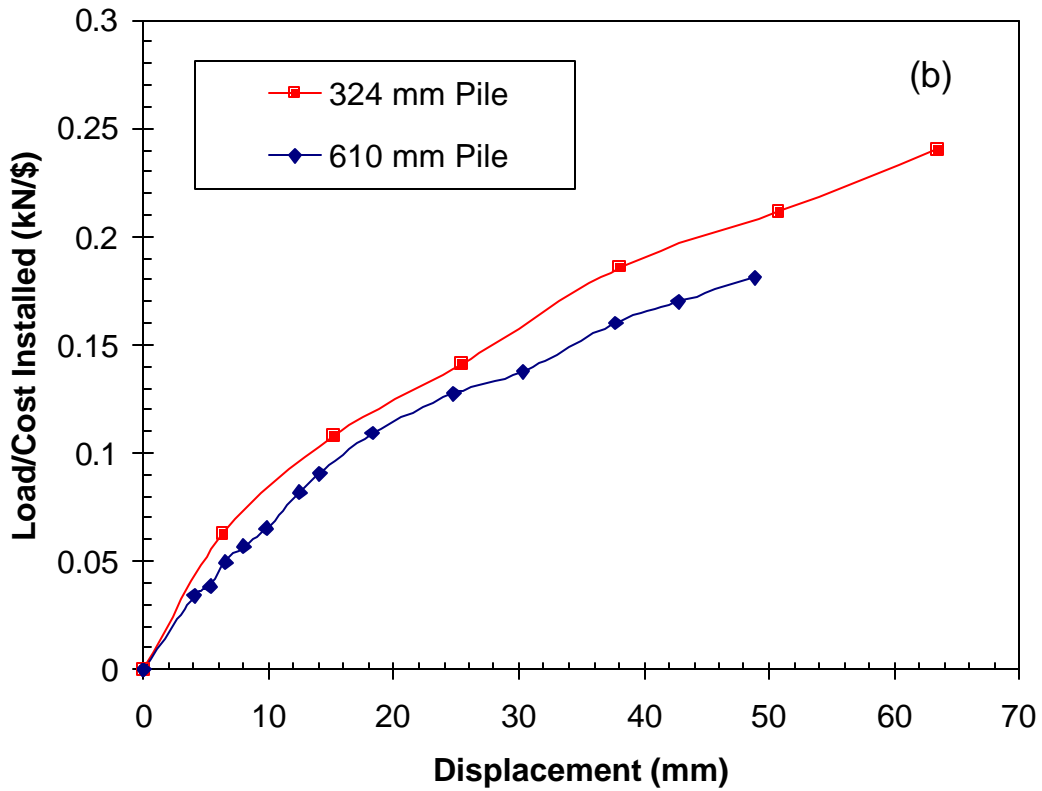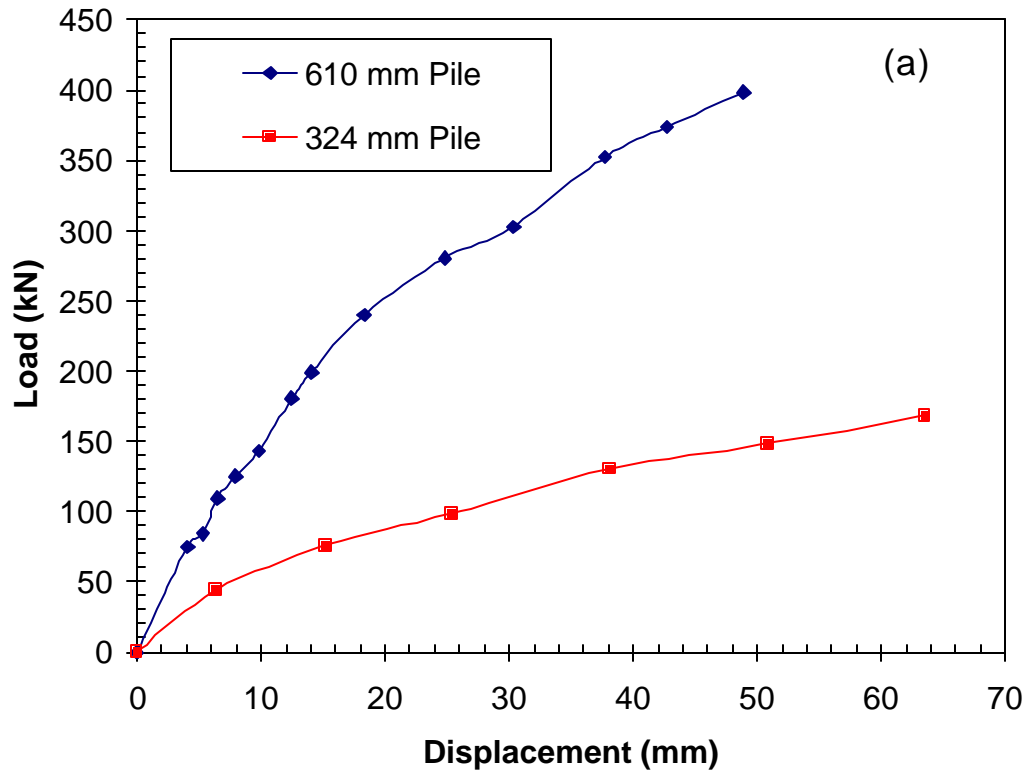
Figure 4.19 Comparison of (a) load vs. displacement curve and (b) load/cost vs. displacement curve for 324 and 610 mm outside diameter steel pipe piles.

is not simply a linear relationship with pile diameter. This conclusion is also confirmed by the basic relationships for p-y curves in cohesive soil developed by Reese and Welch (1975).

Although the larger pile carried 2.67 times more lateral load than the smaller pile, the cost of the larger pile was also greater. The 610 mm diameter pipe piles cost approximately $50 per lineal foot while the 324 mm diameter piles only cost $12.50 per lineal foot. Both piles were driven to a depth of approximately 12.2 m at about the same cost of $5 per lineal foot. To account for the difference in both cost and lateral resistance, the lateral load has been divided by the total cost of installing each pile driven to a depth of 12.2 m, which was $700 for the 324 mm pile and $2200 for the 610 mm pile.

The load per cost is plotted as a function of displacement for both piles in Figure 4.19 (b). At all deflection levels, the smaller diameter pile provides greater lateral resistance per dollar cost than the larger diameter pile. The difference between the two curves is between 10 and 20% based on the relative pile costs at the time of this project and for the soil conditions involved. These results suggest that the use of smaller diameter piles can be economically advantageous when lateral load resistance is a controlling factor in the design, although the difference in cost may be relatively small. This is particularly likely when the soil strength decreases with depth, as in the case where desiccation has produced an overconsolidated soil near the ground surface which becomes normally consolidated at depth. This is true because larger diameter piles tend to derive strength from soils at greater depth than smaller diameter piles. Analyses indicate that this effect would still be observed even if the pile head boundary condition was fixed rather than free. However, for cases where the soil resistance increases with depth, this conclusion may not be valid. Additional testing to evaluate the effect of pile diameter

on lateral resistance would be helpful in answer questions regarding the cost effectiveness of large diameter piles.

CHAPTER 5 STATIC LATERAL LOAD TEST ON NINE-PILE GROUP AT 5.6 DIAMETER SPACING

The static lateral load test on the nine-pile group test was conducted to determine the effects of pile-soil-pile interaction for a pile group spaced at 5.6 pile diameters. At this spacing, group effects were expected to be relatively small. The results of the group test were compared and normalized by the results of the single pile test in virgin soil described in Chapter 4.

TEST LAYOUT

The piles were driven in undisturbed soil adjacent to the geopier pile cap at Bent 4, as shown in Figure 1.3, on August 20 and August 23, 1999. The testing began on September 17, 1999, allowing 25 days for excess pore water pressures to dissipate. The piles were closed-end steel pipes with an outside diameter of 0.324 meters (12.75 inches) and a 12.7 mm (0.5 inch) wall thickness. They were driven to a depth of approximately 12.2 meters (40 feet). The properties of the piles are identical to those given in chapter 4. The piles were arranged in a 3 by 3 pattern as shown in Figure 5.1, with center-to-center spacing of 1.07 meters (3.5 feet) side-to-side and 1.83 meters (6 feet) row-to-row in the direction of loading. For identification purposes, each pile was assigned a number. The piles were driven in the following order: 1, 4, 7, 3, 6, 9, 2, 5, and 8, as shown in Figure 5.1. The order of driving is also shown in Figure 5.2 with designations of 1st through 9th. A photograph of the nine-pile group test setup is shown in Figure 5.2.

Load was applied using two 1.34 MN (150 ton) hydraulic jacks reacting off of an existing pile cap. Spherical end plates were placed at the base of the jacks to prevent eccentric loading. The jacks pushed on a steel load frame, and the load was transferred to the piles by pin-connected (zero moment) tie-rods attached 0.39 meters (15.5 inches) above the ground surface.
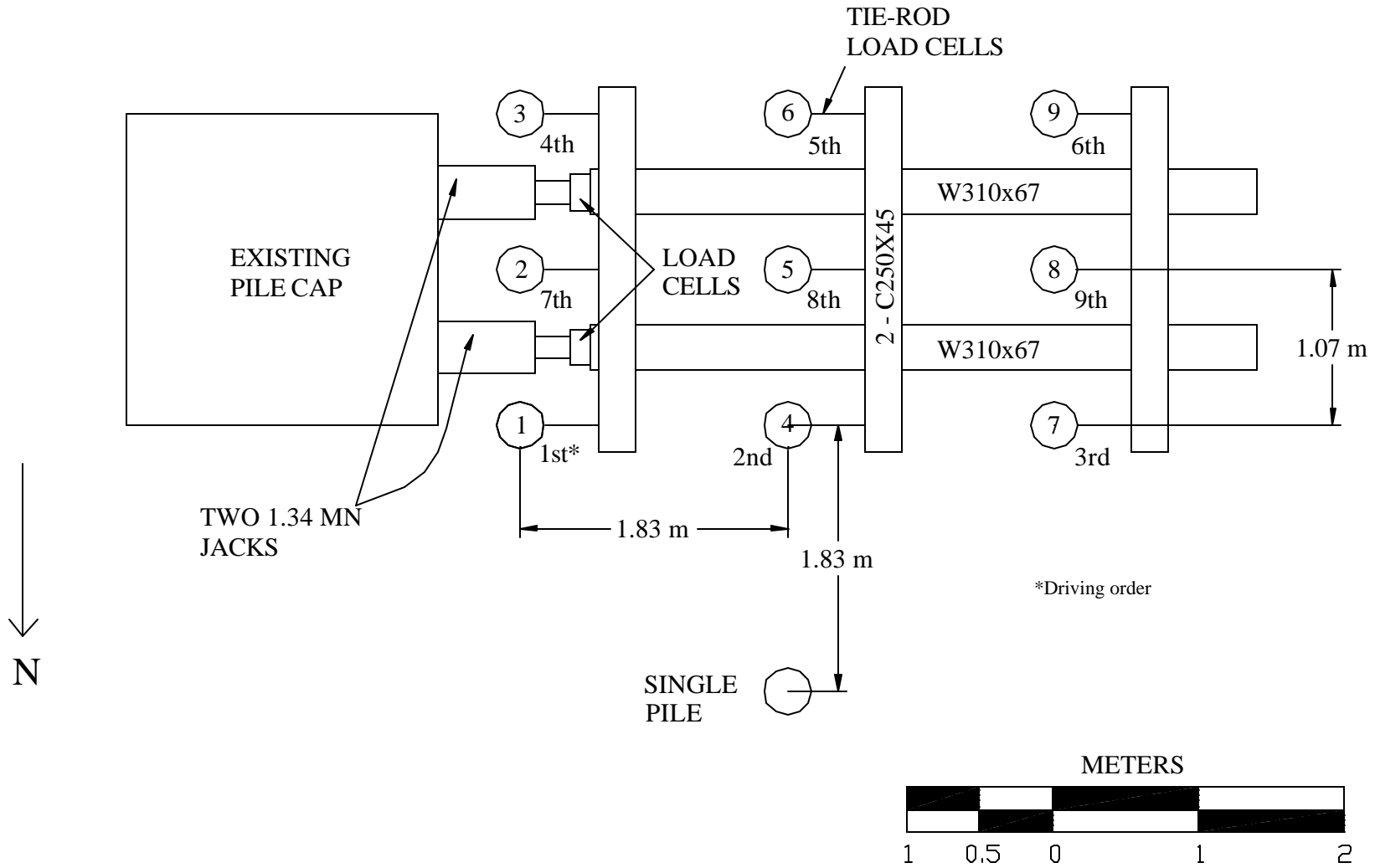
Figure 5.1 Plan view of the single pile and nine-pile group with load frame.

Figure 5.2 Photograph of test-setup for nine-pile group lateral load test.

The steel frame was essentially rigid in comparison with the pile-soil stiffness, therefore, each pile was constrained to have essentially the same deflection.

The load frame was supported by lubricated steel wheels which traveled on steel beams resting on the ground surface. This arrangement minimized any friction forces on the frame. As a result, the force measured by the tie-rod load cells could be compared with the force measured by the load cells on the jacks to provide a rough check on accuracy. Plan and elevation view drawings of the load test set-up are shown in Figures 5.1 and 5.3, with a detail of the pile connection assembly in Figure 5.4.

INSTRUMENTATION

The pile group was instrumented in roughly the same manner as the single pile described in Chapter 4. Instrumentation was designed to measure load, pile head displacement, pile head rotation, and strain along the length of the pile. The tie-rods connecting the piles to the load frame were instrumented with two full-bridge strain gauges on opposite sides of the rod. These gauges made it possible to determine the axial load in each rod and cancel out any strain due to bending. The tie-rod load cells allowed measurement of the load applied to each individual pile. The total group load was also measured by two load cells at the jacking point.

Pile head displacement was measured by eight LVDTs attached to the four corner piles and the middle pile in each row at the load point elevation. In addition, one LVDT was placed 0.305 meters (1 foot) above the load point on pile number 8 to measure the pile head rotation. The displacement measurement system was attached to an independent reference frame by small clamps. Supports for the reference frame were located 1.8 meters (6 feet) away from the piles. Load cells and LVDTs were calibrated prior to and subsequent to testing to confirm accuracy.

1.34 MN
HYDRAULIC
JACKS

0.324 m OD
STEEL
PIPE PILE

PILE CONNECTION
ASSEMBLY

EXISTING
PILE CAP

0.39 m

1.07 m

GROUND LEVEL

WATER TABLE

METERS

1   0.5   0   1   2
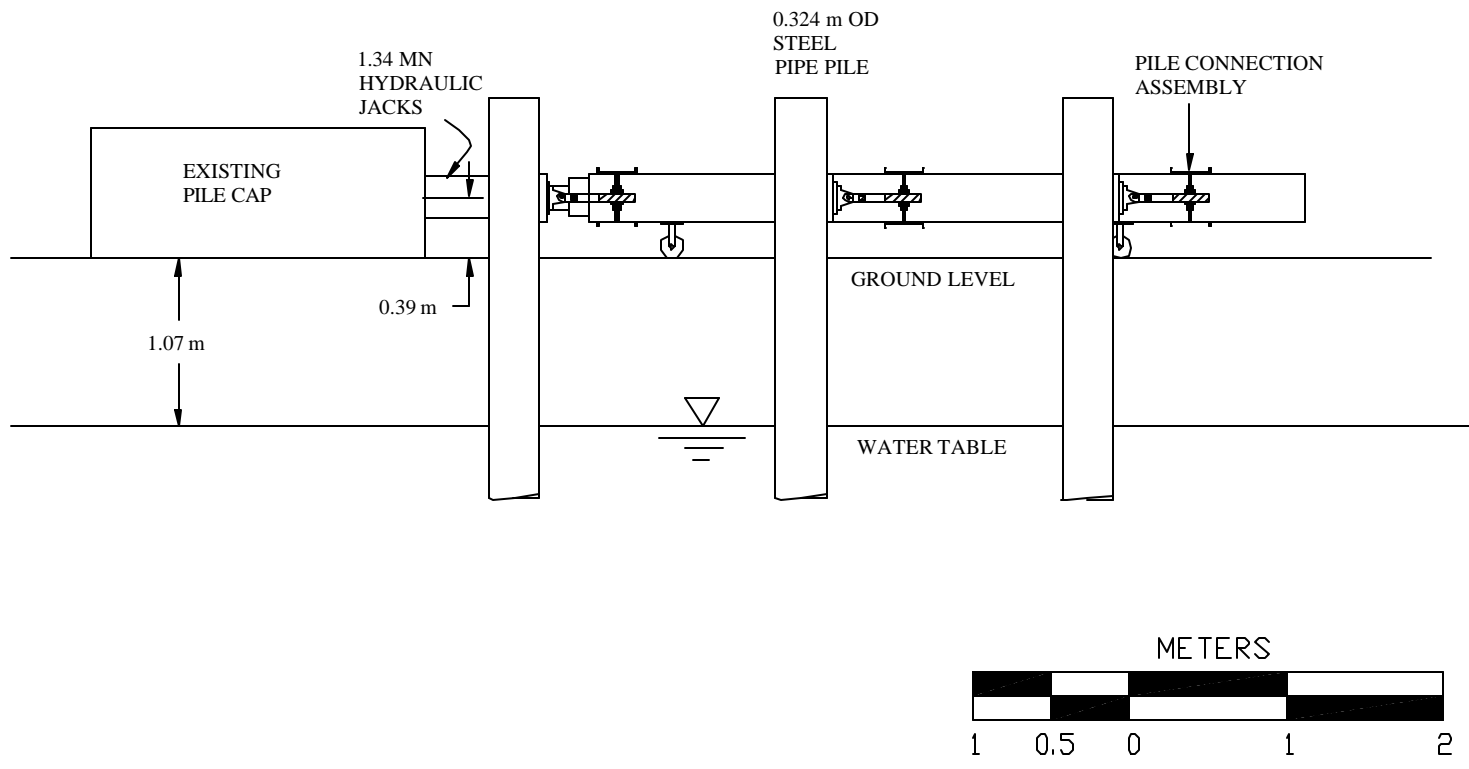
Figure 5.3 Elevation view of load test set-up for lateral load test on 324 mm nine pile group.
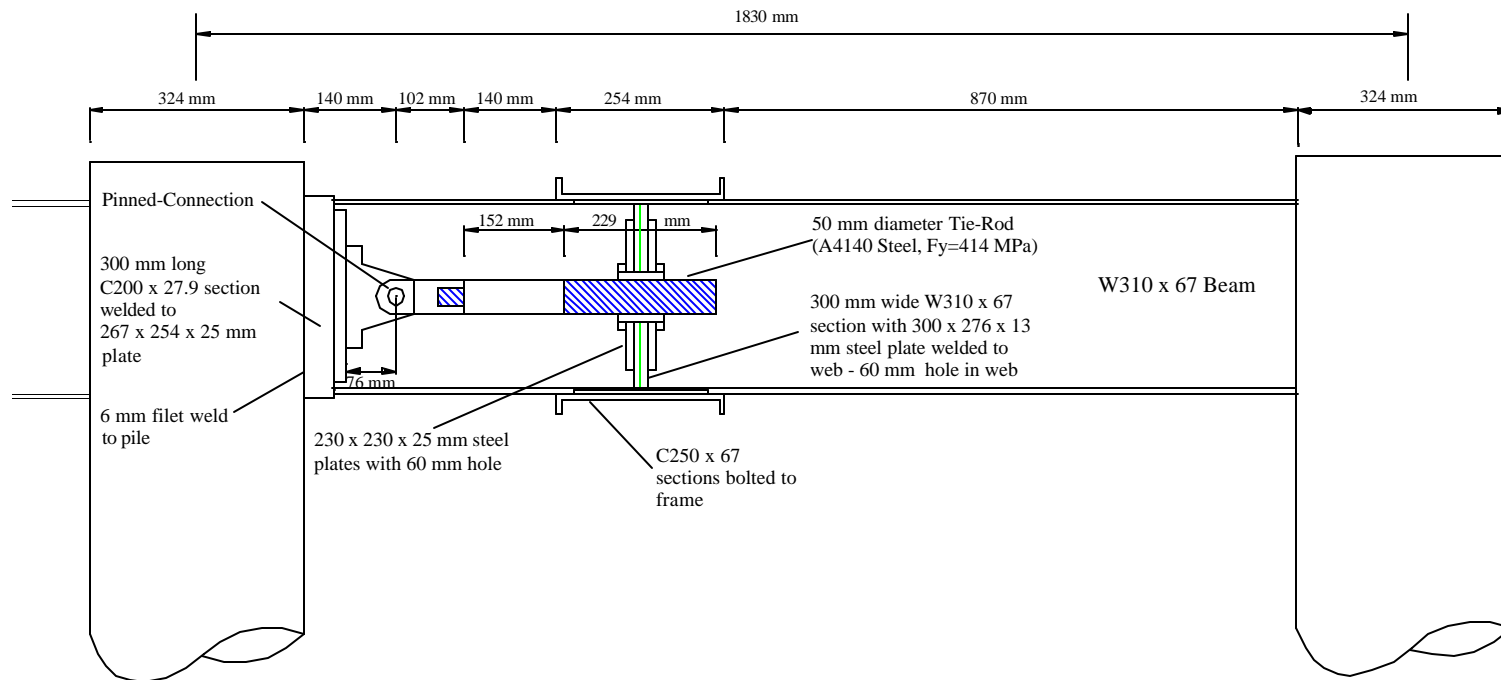
Figure 5.4 Pile-load frame connection assembly detail.

As with the single pile, strain gauges were placed on the tension and compression sides of the middle pile in each row of the group piles at 9 depths (see Figure 4.3). The WFLA-6-120 model resistance type strain gauges from Texas Measurements, Inc. were also used in this test. They were housed in a 5.08 mm (0.2 inch) -thick angle iron that extended to 0.914 meters (3 feet) below the last strain gauge along the sides of the pile.

The Optim Megadac data acquisition system previously described recorded data throughout the testing. The system used 54 channels for strain gauges, 8 for LVDT's, and 11 for load cells. Measurements were taken at one-second intervals throughout the testing.

PROCEDURE

The load testing was performed using a deflection control approach. Fifteen single amplitude cycles of loading (load applied in one direction and then released) were applied for five increments representing target deflections of 6.35 mm (0.25 inches), 12.70 mm (0.50 inches), 25.40 mm (1 inch), 38.10 mm (1.5 inches), and 50.8 mm (2 inches). One cycle was run for a 63.5 mm (2.5 inch) deflection. Loads were held for approximately three minutes on each initial cycle while the readings were recorded manually and for approximately 10-20 seconds on each subsequent cycle at the various increments while the readings stabilized.

During the testing, one LVDT was used to define the applied deflection; however, during data reduction, all the LVDTs were used to define average group deflection in subsequent plots. As a result, there are some variations in the average deflection relative to the target value.

Testing began on September 17, 1999, but problems with the data acquisition system led to a suspension of testing after the first 12.70 mm (0.50 inch) cycle. As a consequence of the data acquisition problems, only four cycles for the 6.35 mm (0.25 inch) target deflection were recorded. Testing resumed on September 21, 1999 with the second 12.70 mm (0.50 inch) cycle.

TEST RESULTS

Load-Deflection at Pile Head

Figure 5.5 presents load versus deflection curves for the first and last cycles of each load increment. The data for these curves was taken from the load-point LVDTs and the tie-rod load cells. The total load from the tie-rod load cells was typically within about 3% (1 or 2% at the peak loads) of that obtained from the load cells attached to the hydraulic jacks. Data points are based on the peak load points for each increment. The continuous load-unload curve for the entire testing sequence is shown in the appendix.

The pile group was subjected to a maximum load of 1420 kN (319.30 kips) for a peak average deflection of 64.61 mm (2.54 inches). A reduction in strength was observed from the first to the fifteenth cycle and the reduction in strength was greater as the applied load increased. For example, the reduction was only about 2% at 12.70 mm (0.5 inch) of deflection, but increased to about 13.5% at 25.40 mm (1 inch) of deflection and to about 17.6 % at 50.80 mm (2 inches) of deflection. This increased strength reduction at higher loads and very small reduction at lower loads is consistent with Brown's findings (Brown et al, 1988). While subsequent loading stiffens the soil, the formation of gaps around the piles decreases the soil resistance. Discontinuities in the load versus deflection curve between the first and third load increments on the first cycle indicate gap formation, accounting for the increased strength reduction from the 25.40 mm (1 inch) deflection onward.

As the testing progressed, cracks developed around the pile group. The approximate locations and orientations of cracks are shown in Figure 5.6 along with the depth of gaps behind each test pile after the test was completed. The deepest gap was 1.42 meters at pile 3 in the front row. The longest crack extended horizontally across the back row of piles.
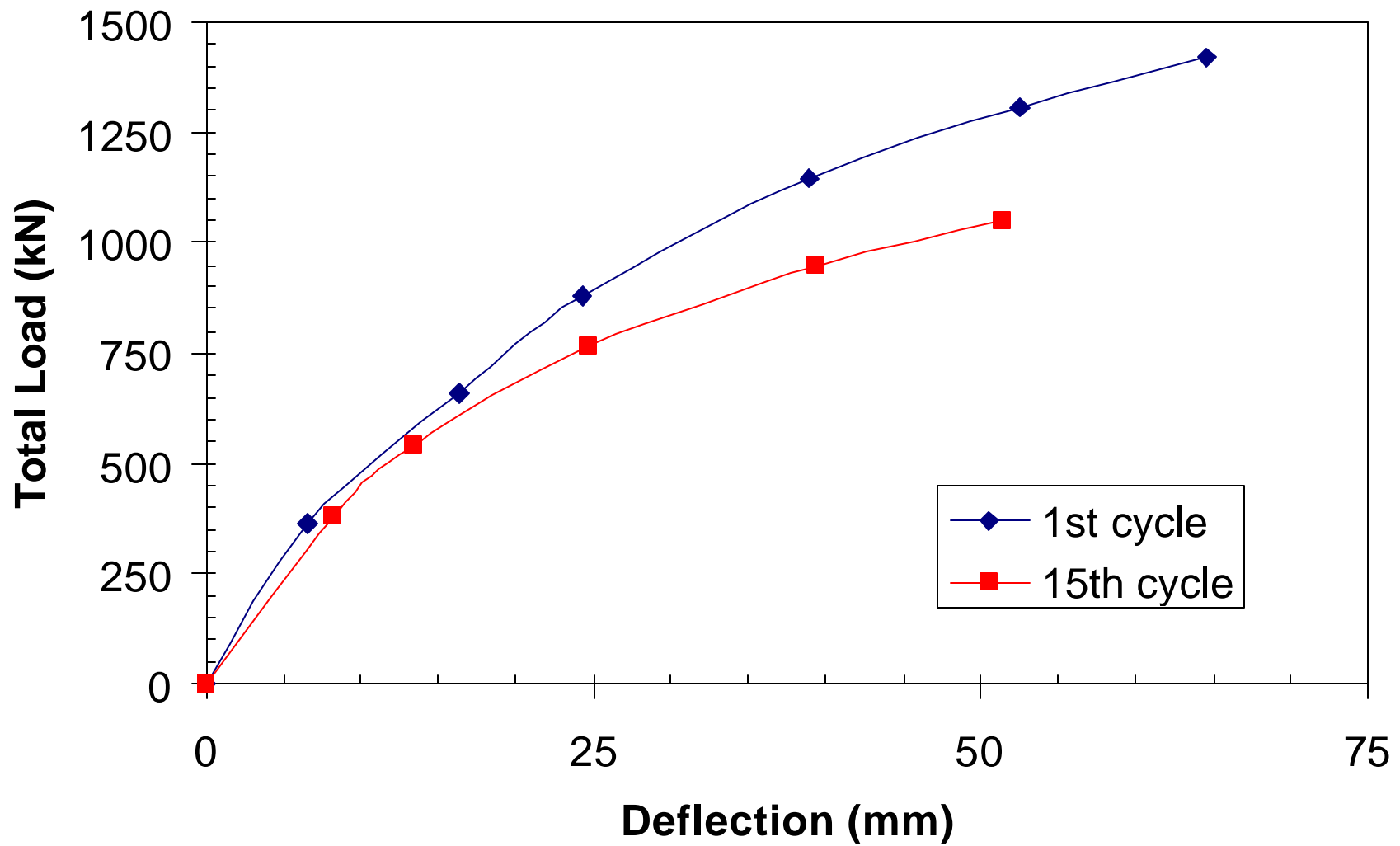
Figure 5.5 Total load versus deflection for 1st and 15th load cycles of nine-pile group lateral load test.

1.42 m

3

1.02 m

6

0.61m

9

EXISTING
PILE CAP

1.22 m

2

0.76 m

5

0.64 m

8

1

0.66 m

4

0.66 m

7

1.22 m*

LOAD DIRECTION

N

* depth of gap

METERS

1   0.5   0   1   2
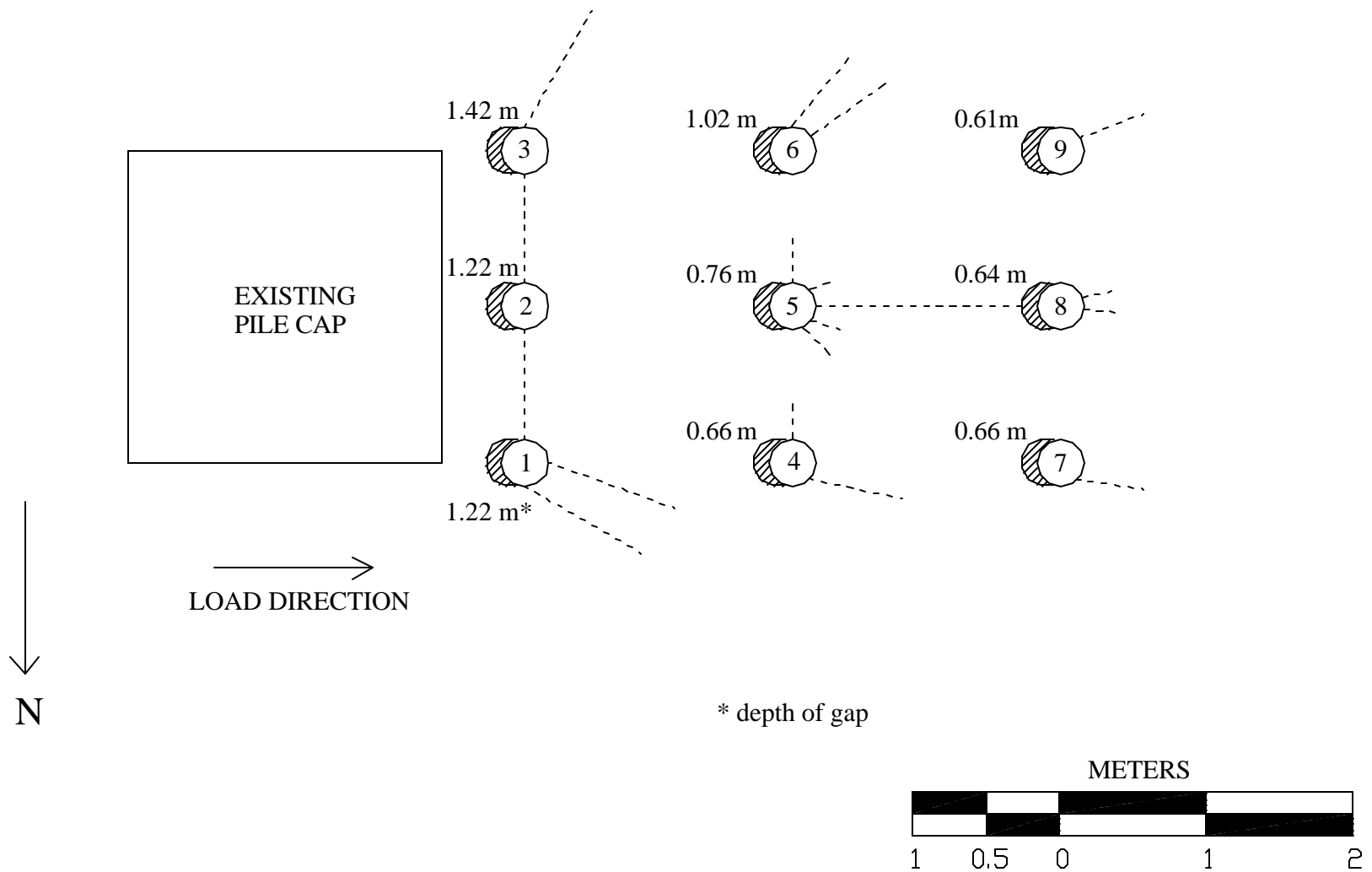
Figure 5.6 Crack pattern and gap depth at the end of the last cycle of loading for nine-pile group test.

The change in soil stiffness over the 15 load cycles is examined in Figure 5.7. Stiffness was determined by the following formula

$$K= DF/DL \hspace{4cm} (5.1)$$

where DF is the change in force applied to the pile group for each cycle, and DL is the change in pile group deflection for each cycle. In Figure 5.7, stiffness is normalized by the initial stiffness for each load increment. The resulting curves initially drop off rapidly and then gradually decrease with further cycles, possibly becoming level when projected to 25 or 30 cycles. For cycles at 12.7 mm (0.5 inch) deflection, the stiffness was still at 87% of its original value for the final cycle, while for cycles at 38.10 mm (1.5 inch) deflection, the stiffness dropped to 82% of its initial value after 15 cycles. Thus, the final stiffness value was between 82 to 87% of the initial value after 15 cycles

Comparisons of individual pile capacity in each row are shown in Figure 5.8. For each row, the pile locations are designated as left, middle and right as viewed in the direction of loading (i.e. pile 3 is the left pile in the front row.) In general, the variation of pile load within a given row is less than 10% of the average pile load in the row. A review of the data also indicates that there is no consistent pattern of load distribution within a row. For example, the middle pile carries the most, the second most, and the least load in the three different rows. This finding is consistent with test results reported by Brown et al (1988) and Rollins et al (1998) but inconsistent with predictions made using the elastic theory.

Elastic theory predicts that the corner piles will carry the highest load and that piles in the middle of a row will carry the least load for a given displacement. Although this pattern is consistent with observed behavior for the back row, it is inconsistent with the behavior of the front and middle rows. These comparisons suggest that the load carrying capacity of piles in a
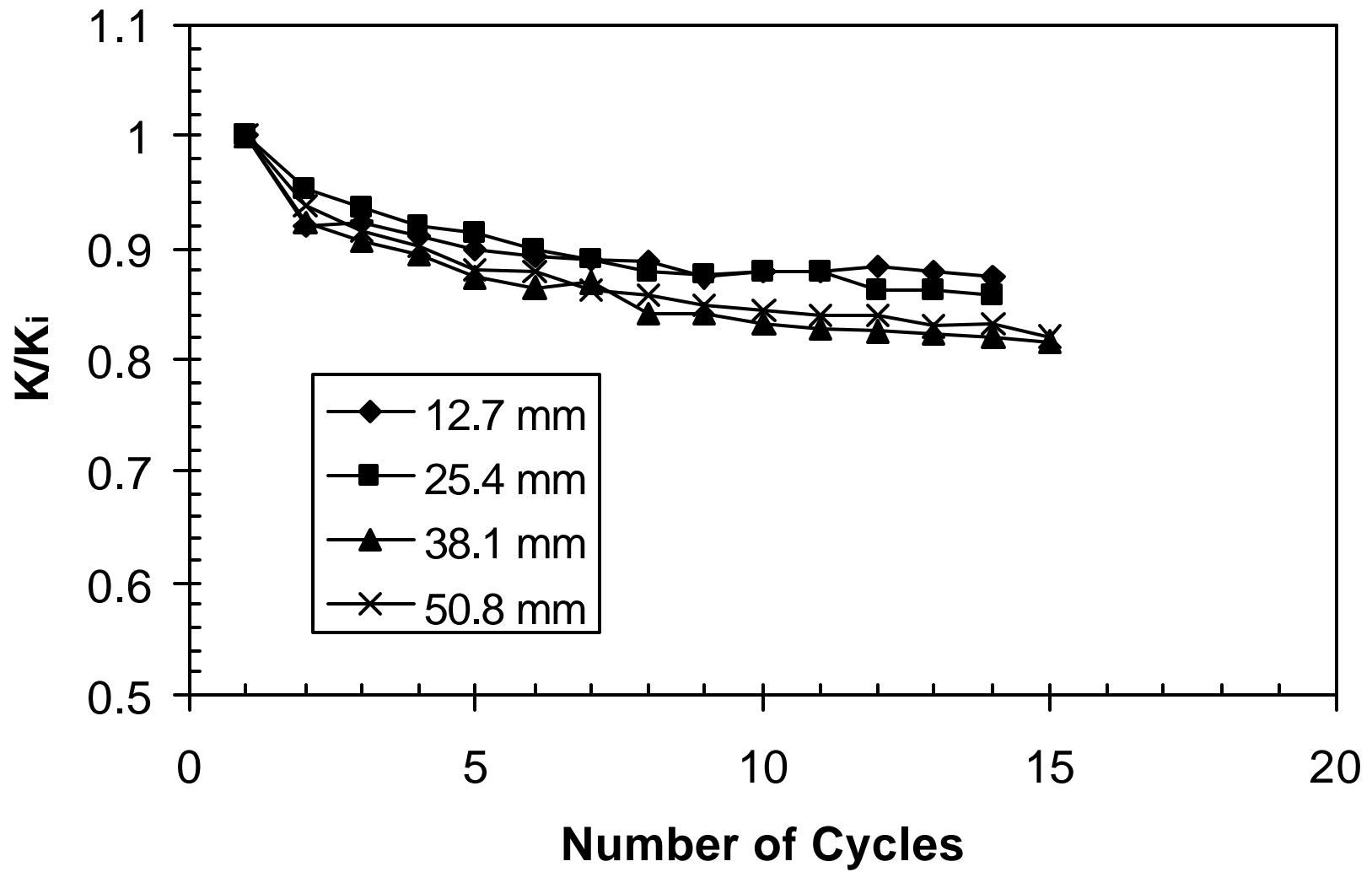
Figure 5.7 Normalized soil-structure stiffness versus number of cycles for four load increments of nine pile group test.
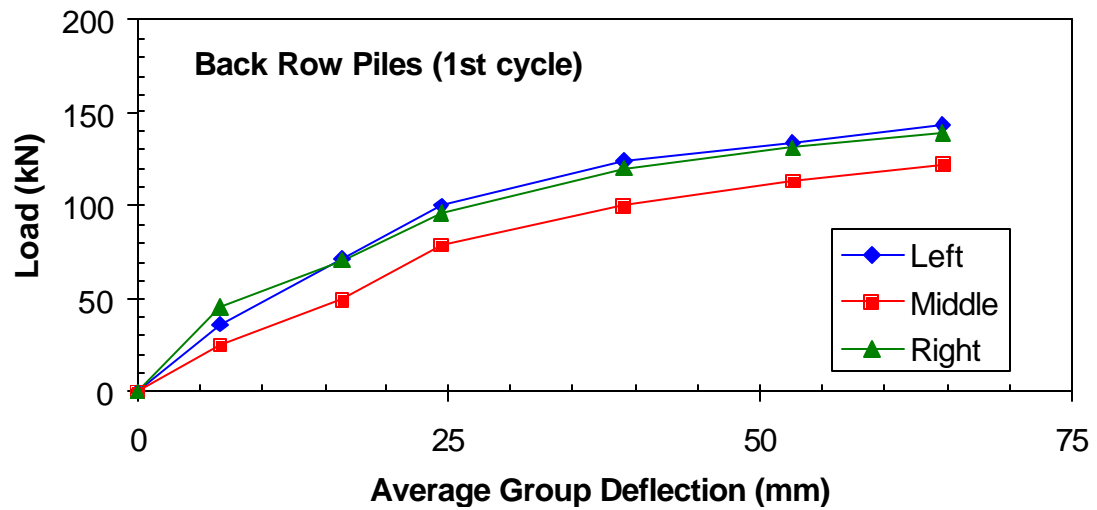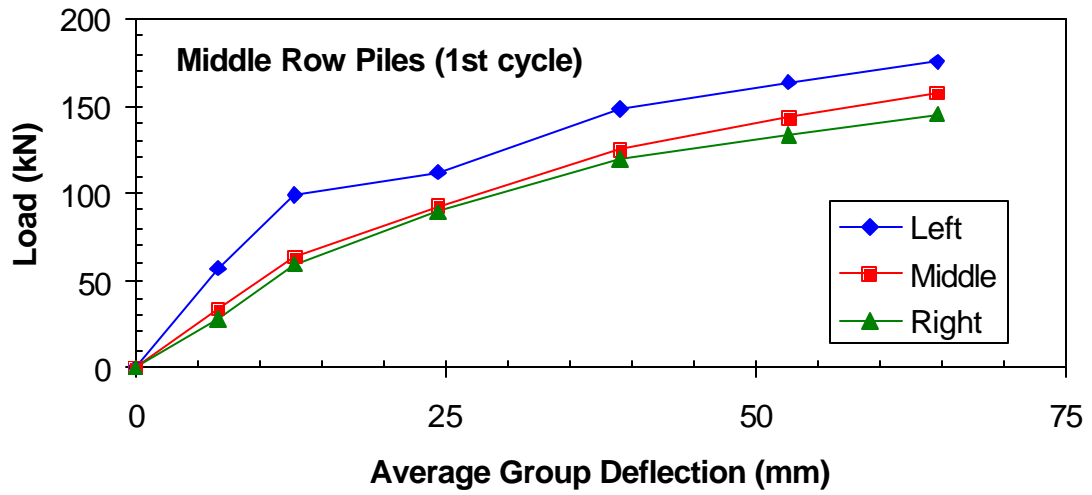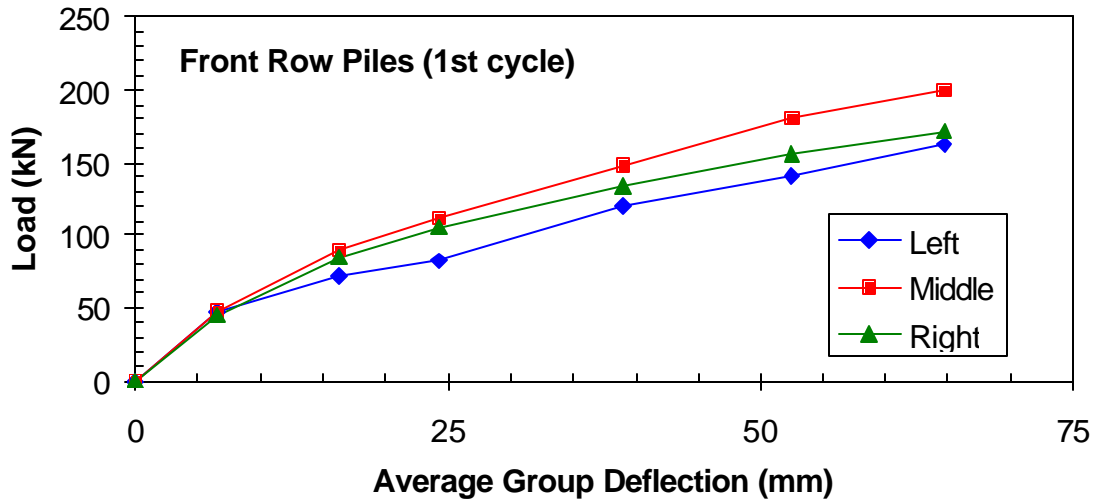
Figure 5.8 Load versus deflection curves for each individual pile, grouped by row location.

group is primarily a function of row location. Therefore, subsequent plots will be presented in terms of average behavior of the front, middle and back row piles.

For comparison with the single pile, the total group load has been divided by the number of piles in the group and the results are shown in Figure 5.9. Figure 5.9 shows the relative change in single pile and group resistance from the first to the fifteenth cycles. The single pile and average group resistance are closer for the fifteenth cycle than for the first cycle, as there was slightly less strength reduction due to cycling in the group. The shadowing effect due to overlapping stress zones in the group is less significant after cycling. After an appreciable amount of plastic deformation of the soil, the overlapping shear zones and overall soil resistance are less important, and load resistance becomes more dependent on the pile. This effect may eventually lead to a p-multiplier of 1.0 for the pile group.

Figure 5.10 shows the average pile load versus deflection curves for each row in the group along with a similar curve for the single pile. Average row loads were determined from the total load carried by the piles in the row divided by the number of piles and deflection was average deflection for the entire pile group. These findings confirm the results of the previous full-scale tests discussed in Chapter 2, with the front row piles carrying about the same load as the single pile and trailing rows carrying less load for the same deflection.

By the fifteenth cycle, load differences between rows at the peak points are slightly less, but still exist as shown in Figure 5.11. However, at deflection levels less than the previous peak deflection, group effects nearly vanish. For example, the 15th cycle load vs. deflection curves at the 52 mm deflection level are shown in Figure 5.12. At deflections less than 40 mm, the curves for each row of the pile group are very similar to the single pile. Group effects are only manifest as the pile closes the gap and contacts the soil at a deflection somewhat less than the maximum.
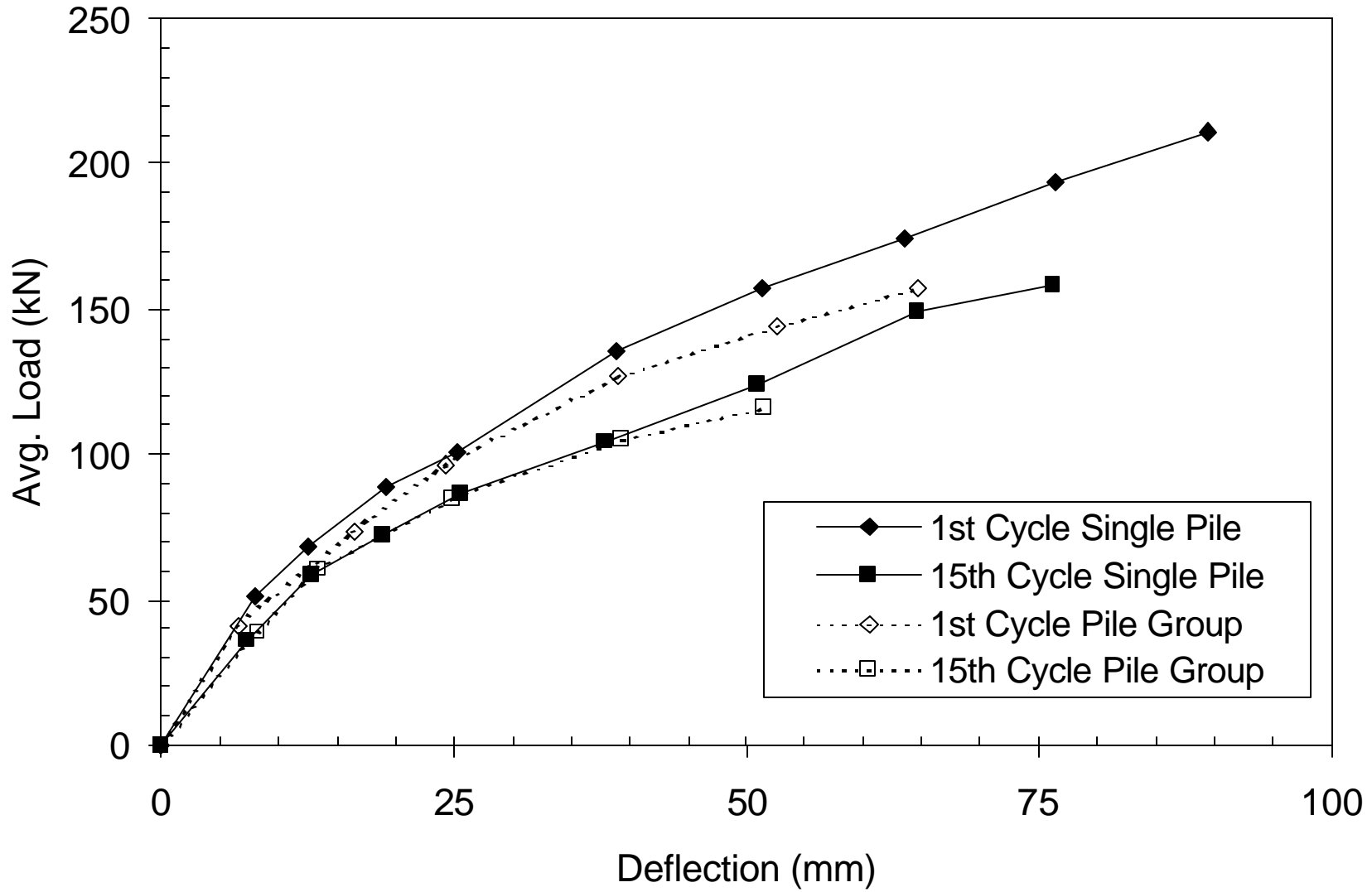
Figure 5.9 Average load versus deflection curves for 1st and 15th load cycles of both single pile and nine-pile group tests.
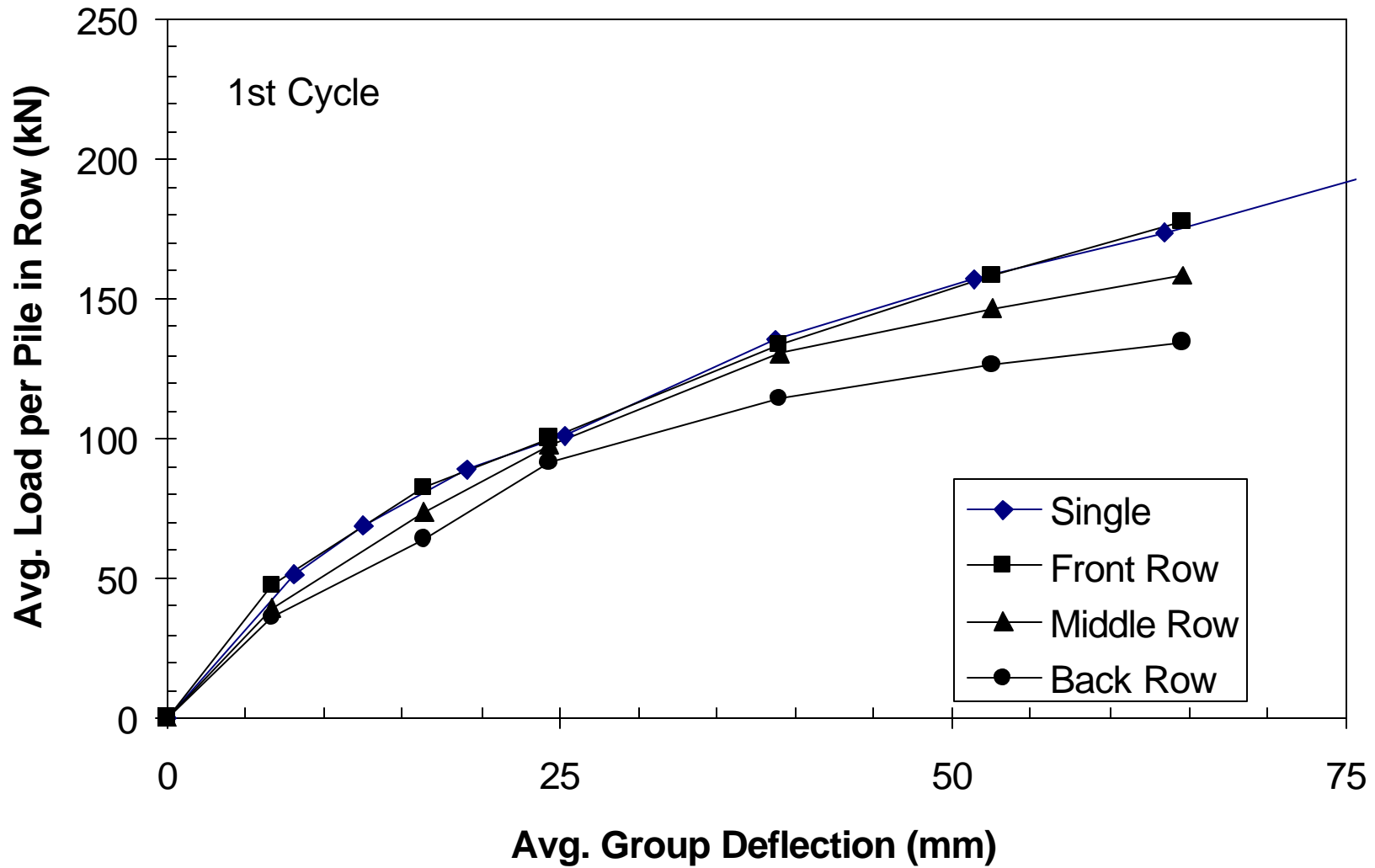
Figure 5.10 Average row load versus group deflection for nine pile group test (1st cycle).
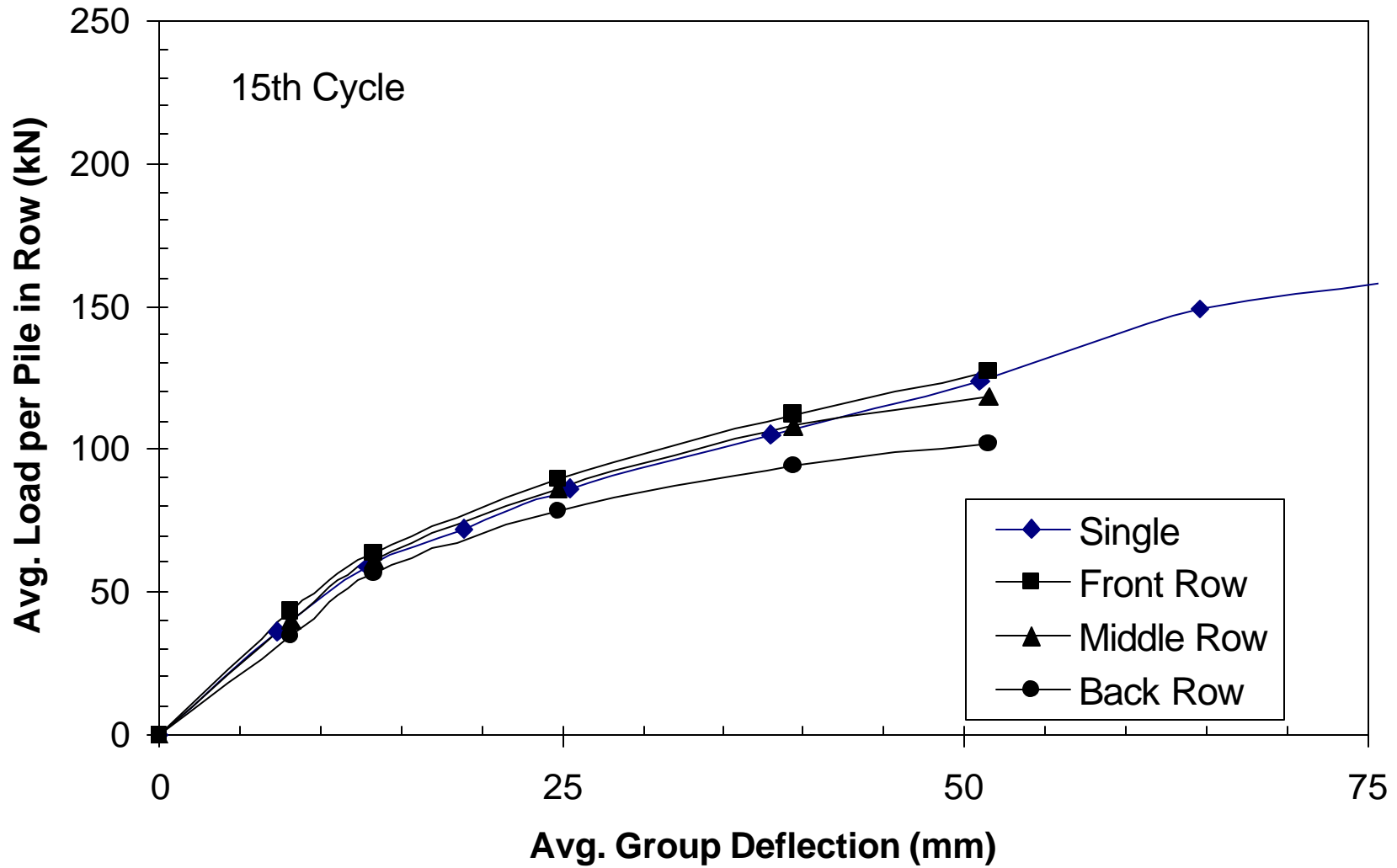
Figure 5.11 Average row load versus group deflection for nine-pile group test (15th cycle).
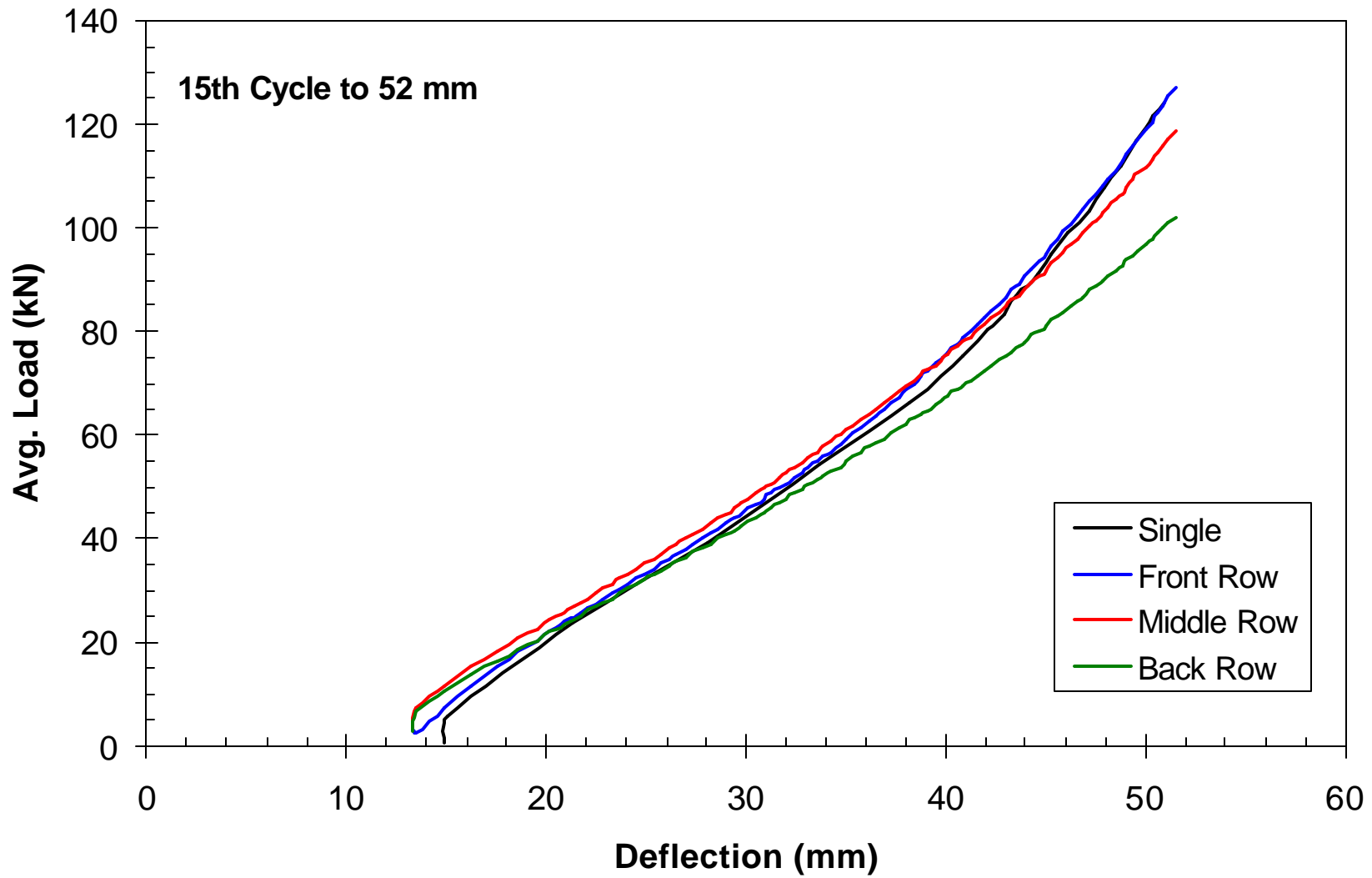
Figure 5.12 Average load versus deflection curves for single pile and rows in nine-pile group during 15th cycle to 52 mm.

Ratios of average row loads carried by piles in the nine-pile group to loads carried by the single pile are shown in Figure 5.13. These load ratios are plotted against the average pile group deflection. Although there is a general trend for the load ratios to decrease slightly as pile deflection increases, there are some unusual peaks and troughs for deflections less than about 25 mm. These fluctuations could be due to local variations in soil properties and variations in gap widths around the piles that were created during driving. As deflection increased during loading, these minor variations became less important and the trends became clearer.

A decrease in resistance with increasing deflection would be expected for closely spaced piles since the shear zones only develop and overlap after significant movement has taken place. In addition, greater movement would be expected to develop overlapping shear zones for piles placed at a six diameter spacing than for a three diameter spacing. Rollins et al (1998) indicate that the load ratios initially decreased rapidly and then remained relatively constant after only about 13 mm of movement for a pile group at three pile diameter spacing. In the current study, movements of over 50 mm appear to be necessary before some stability in the load ratios is achieved. However, the load ratio for the front row piles remains close to 1.0 after deflections of only 13 mm since overlapping shear zones were not developing.

For deflections greater than 25 mm (1 inch), the average load ratios are 1.00, 0.94 and 0.82 for the front, middle and back row piles, respectively. These ratios are substantially higher than have been observed in full-scale load tests on pile groups at three pile diameter spacing. For example, Rollins et al (1998) found the load ratios to be 0.7, 0.5 and 0.4 for the front, middle and back row piles, respectively, in a pile group at three diameter spacing. As expected, these results clearly indicate that group effects become less important as pile spacing increases,.
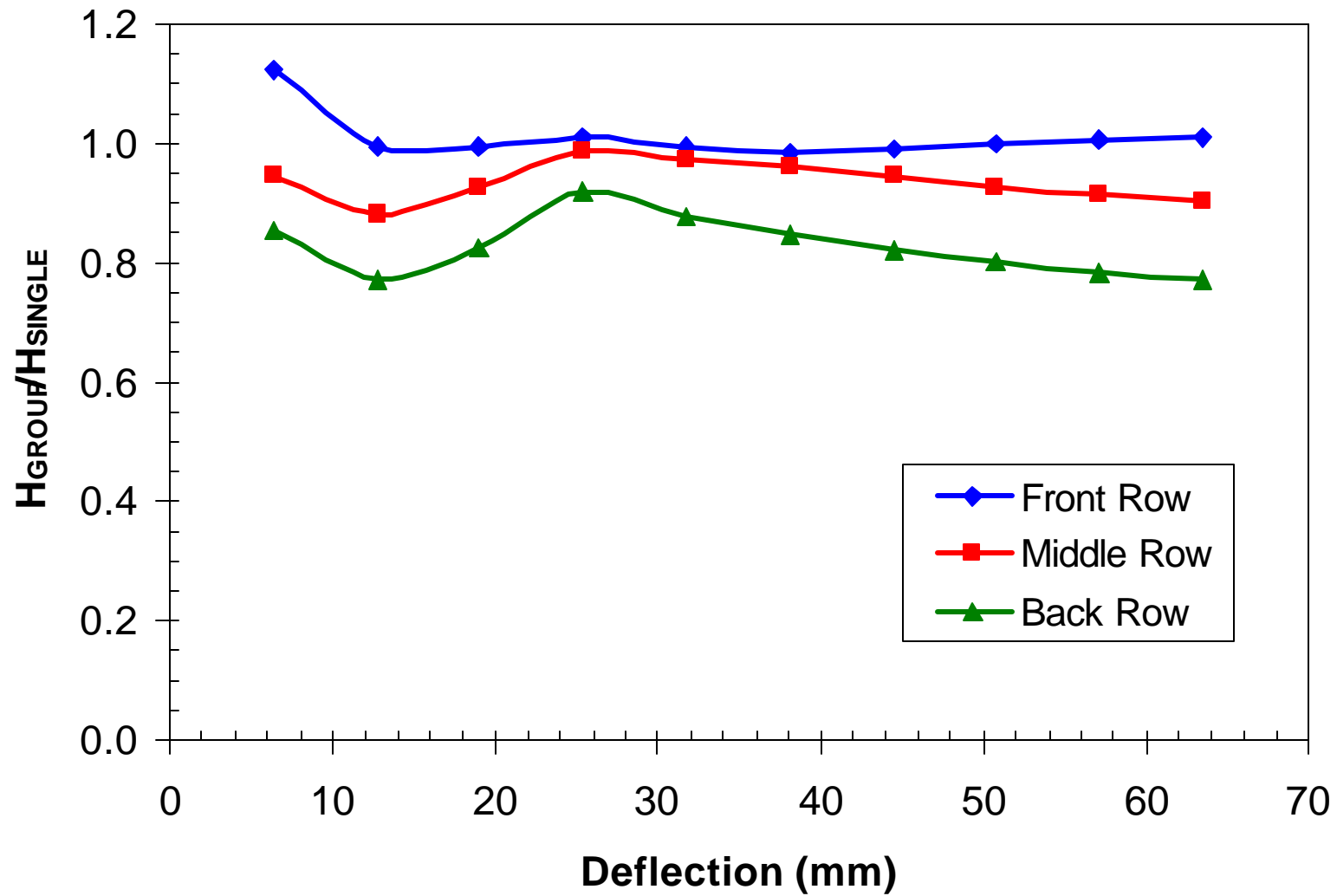
Figure 5.13 Normalized load versus deflection curves for front, middle and back rows during nine-pile group test (1st cycle).

Bending Moment

Bending moment versus depth.

Bending moment versus depth curves are shown for center pile in the front, middle, and back row of the group in Figures 5.14. Curves are shown for the first cycle of loading at average group displacements of 6.35, 12.70, 19.05, 25.40, 38.10, 50.80, and 63.50 mm. For comparison purposes, a bending moment curve is also shown for the single pile at the same pile head deflection. In some cases, the desired deflection level did not correspond to the peak displacement for the first cycle load on the single pile. Therefore, the curves in Figures 5.14 and 5.15 will be somewhat different from those shown for the single pile.

The bending moment curves were formulated from the strain gauge data. The bending moment was calculated using equation 4.2 in the same manner as with the single pile. Maximum bending moments generally occurred at 1.8 meters (6 feet) below the ground surface for the front, middle, and back rows. This corresponds to about 5.6 times the pile diameter. The maximum moment was found at about the same depth for each load increment. The single pile had maximum moments at about 1.6 to 1.7 meters (5.25 to 5.58 feet). Thus, the group piles had maximum moments at slightly greater depths than the single pile. The difference, however, is very small when compared to results for a test on a pile group at three diameter spacing, where the depth to maximum moment in the group was a meter or more below the depth to maximum moment in the single pile (Rollins et al, 1998).

At shallow depths, the single pile had larger moments than any of the group piles, but the single pile moments dropped below any of the group piles at depths of around 2 to 3 meters below the ground. Moment reversals for the group piles were consistently observed at 6.10
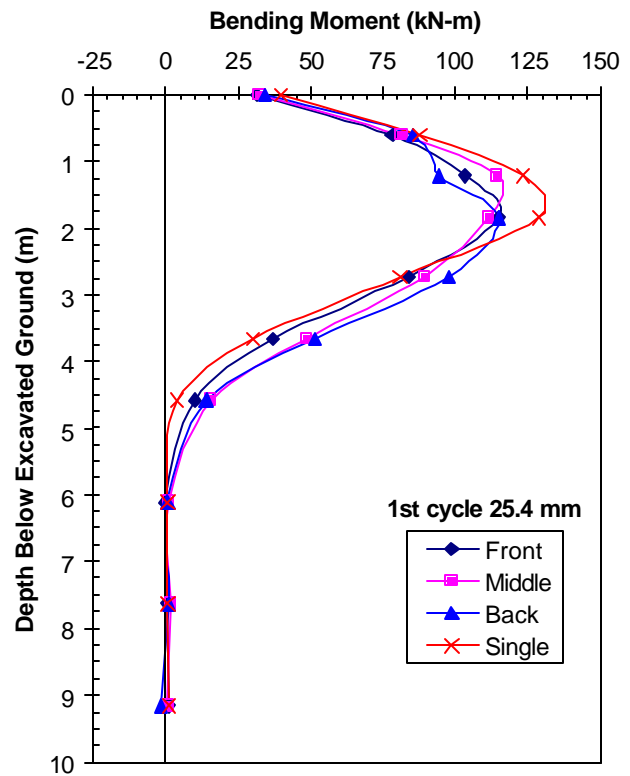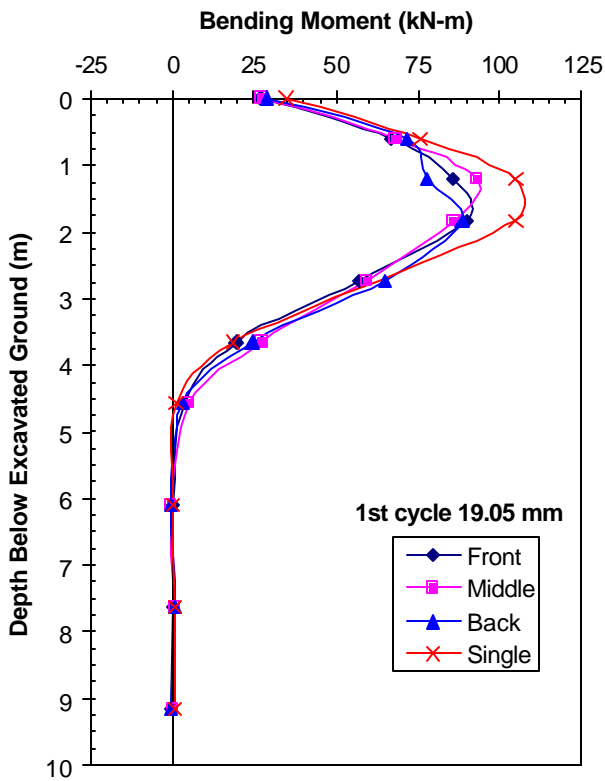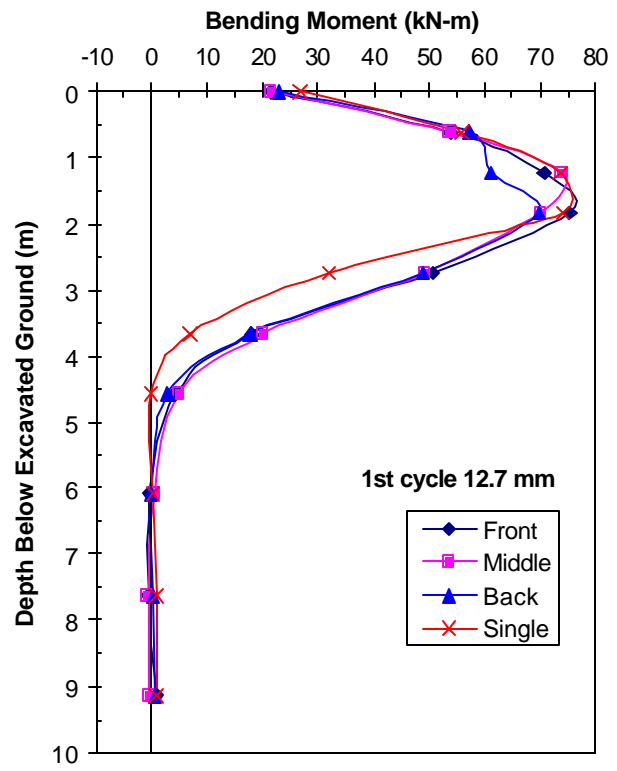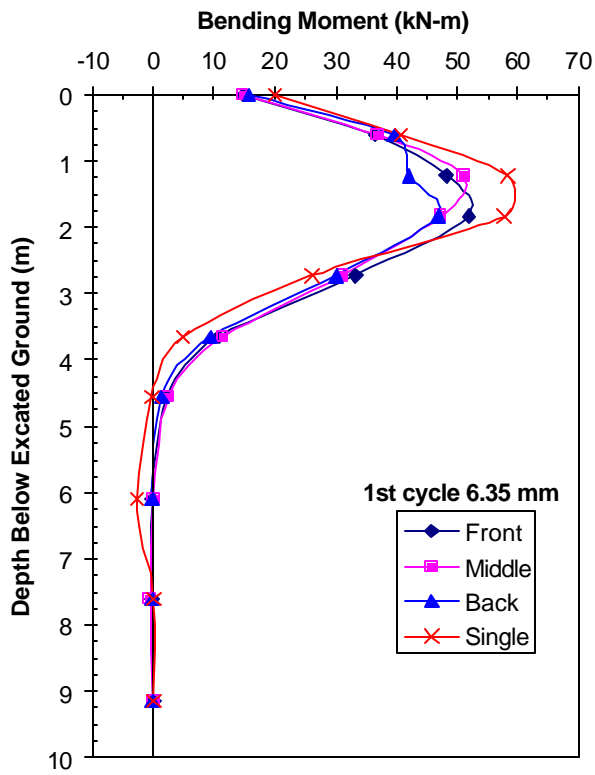
Figure 5.14 Measured bending moment versus depth curves for piles in the group relative to the single pile at various pile head deflections.
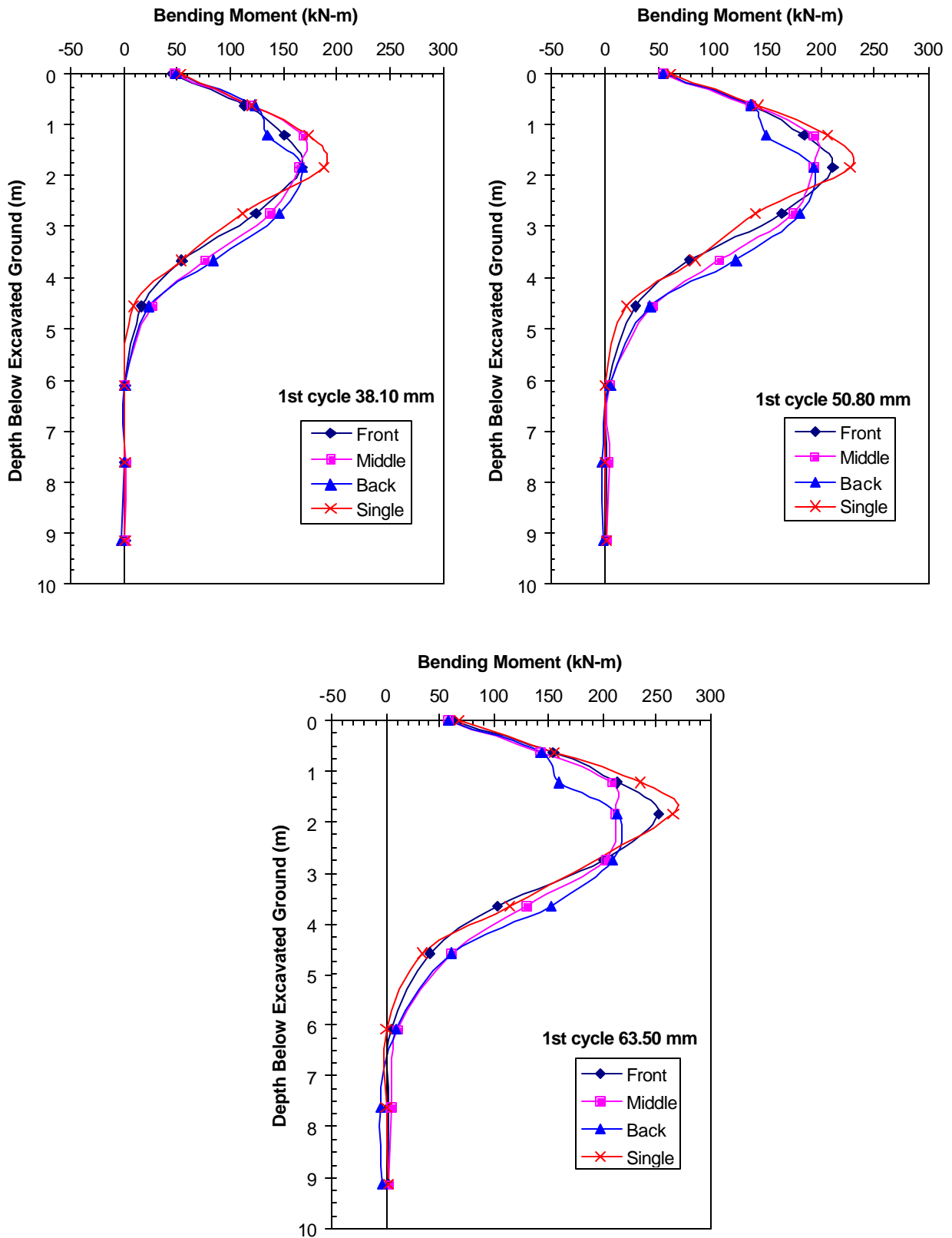
Figure 5.14 (Continued) **Measured bending moment versus depth curves for piles in the group relative to the single pile at various pile head deflections.**
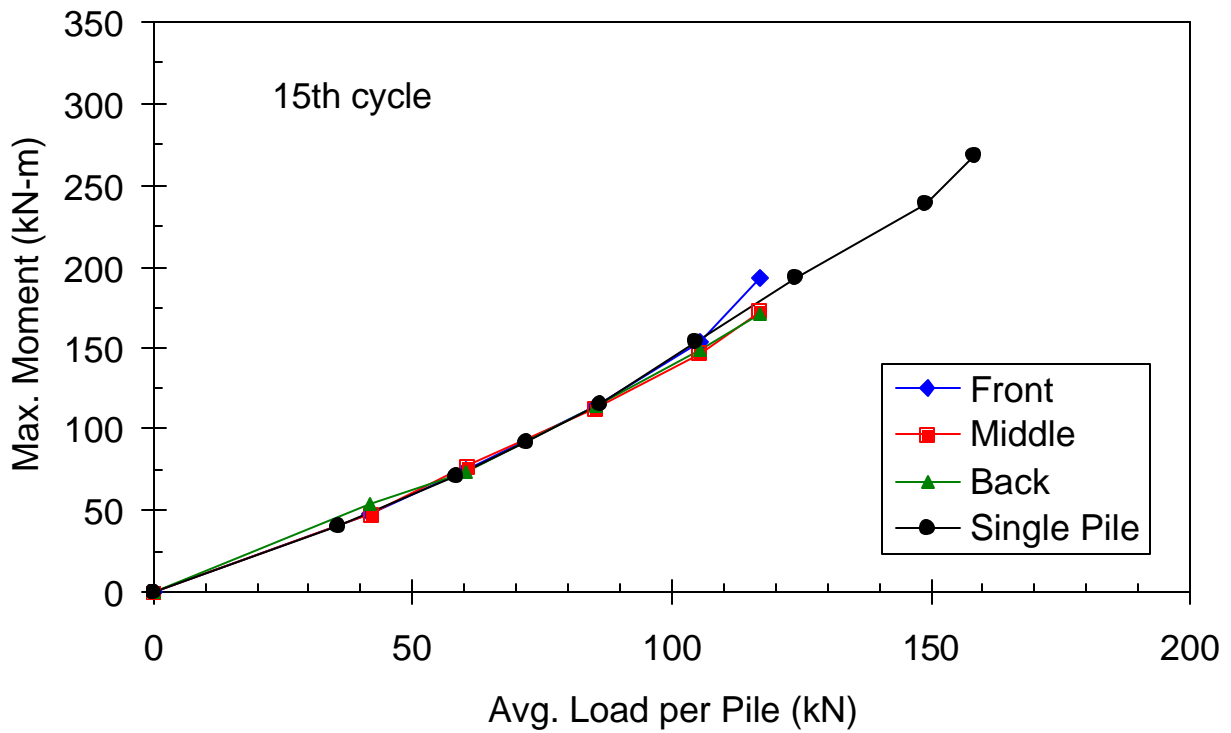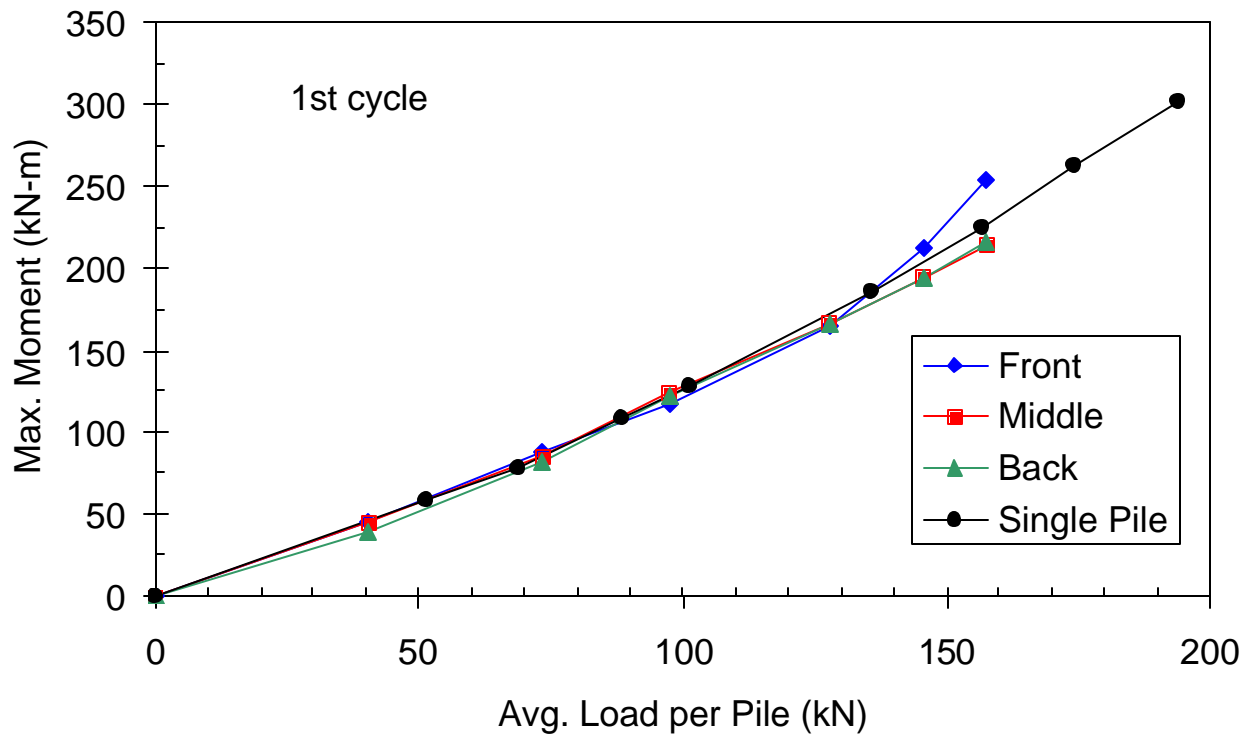
**Figure 5.15 Measured maximum moment versus average load per pile (total load/no. of piles) for each row of the nine pile group relative to that for the single pile meters (20 feet).**

The single pile reached zero moment at progressively deeper depths as the load increased. For example, this depth increased from 4 meters for the 6.35 mm deflection to 6 meters, whereas the group piles generally reached zero moment at around 6.1 m. The front row piles typically developed the greatest moment, but the moments in the middle and back row piles were usually no more than 10 to 15% smaller. The maximum moment generally occurred at a depth of about 1.83 m below the excavated ground surface, which was about the same depth where it occurred in the single pile. From the depth of maximum moment on down, moments in the front row piles tended to decrease more rapidly than in the other rows (following the behavior of the single pile). As a result, for depths greater than about 2.5 meters below the ground surface, the back row pile developed the largest moments In comparison with the other rows.

For the pile spacing involved in this test (5.6 diameter), group effects were small, and maximum moments for the single pile and piles in the group occurred within about 10 to 20% of each other. This agreement in the depth to the maximum moment is in contrast to results from other tests on pile groups at about 3 diameter spacing where the maximum moments in the group typically occurred at greater depths than in the single pile (Brown, 1988; Rollins et al, 1998).

Maximum moment vs. load.

Figure 5.15 presents the maximum bending moment for the middle pile in each row as a function of the average pile load in the group. Curves are presented for both the first cycle and the fifteenth cycle. Once again, the average load was simply determined by dividing the total group load by nine, the number of piles in the group. Generally, for a given load, the maximum moment is very similar for the front, middle and back row piles except at the higher loads. The maximum moment versus load curve for the single pile is also shown in Figure 5.15 and there is very little difference between the curves for the piles in the group and that for the single pile.

Figure 5.16 presents the maximum moment for the middle pile in each row versus the average pile head load on each row (i.e. the total load carried by a row of piles divided by three, the number of piles in the row). Curves are once again presented for the first and fifteenth cycle. When the moments are normalized in this fashion, there is a larger moment per given lateral load in the trailing rows, especially the back row. The soil response in the back row is softer due to group effects, leading to less lateral restraint and thus higher moment per load. The difference between the back and front rows widens from about 20% at a load of 50 kN to 30% at a load of 135 kN. Tests performed on a pile group at three diameter spacing also found higher moments per given load on the back row, with differences of around 50% (Brown et al, 1988).

Pile Head Rotation

The pile head rotation is shown as a function of the applied load in Figure 5.17. The rotation was determined using equation 4.3 in the same manner as with the single pile. The two LVDTs used for measuring rotation were placed on pile number 8, the middle pile in the back row, spaced 0.305 meters (1 foot) apart vertically. There was a rotation of 0.010 radians after 25.4 mm of deflection (1.4 times greater than with the single pile at that deflection) and a peak rotation of 0.019 radians after 63.5 mm of deflection (1.9 times greater than the single pile). This higher rotation for a given load in the group suggests higher bending moment. This may be due to measurement of rotation on the back row, where group effects resulted in a softer soil response.
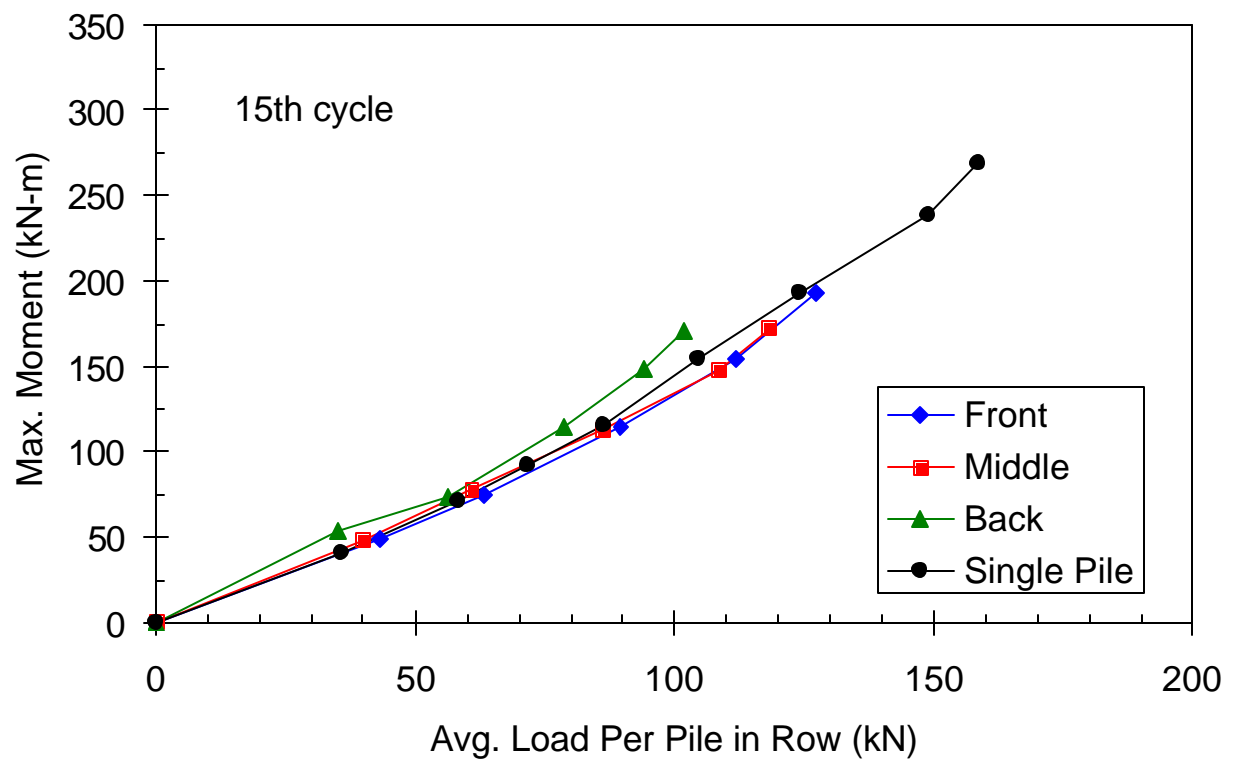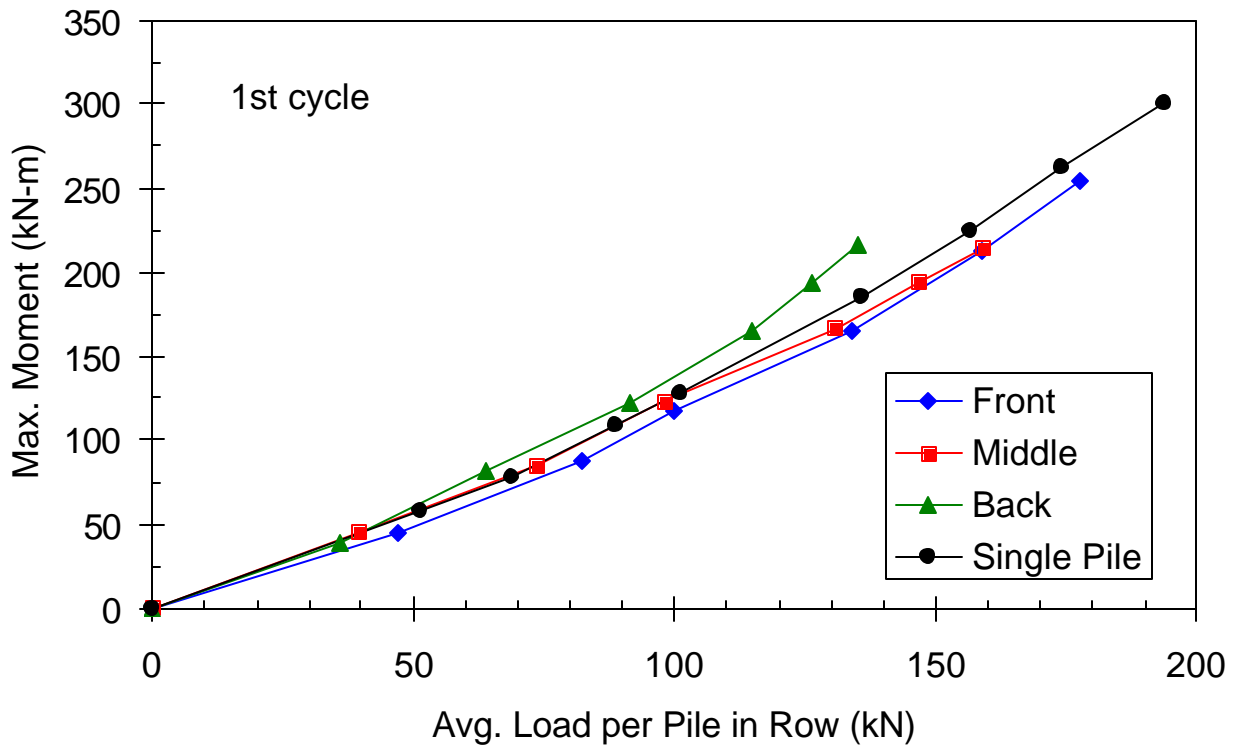
Figure 5.16 Measured maximum moment versus average load per pile in row (total row load/no. of piles) for each row of the nine pile group relative to that for the single pile
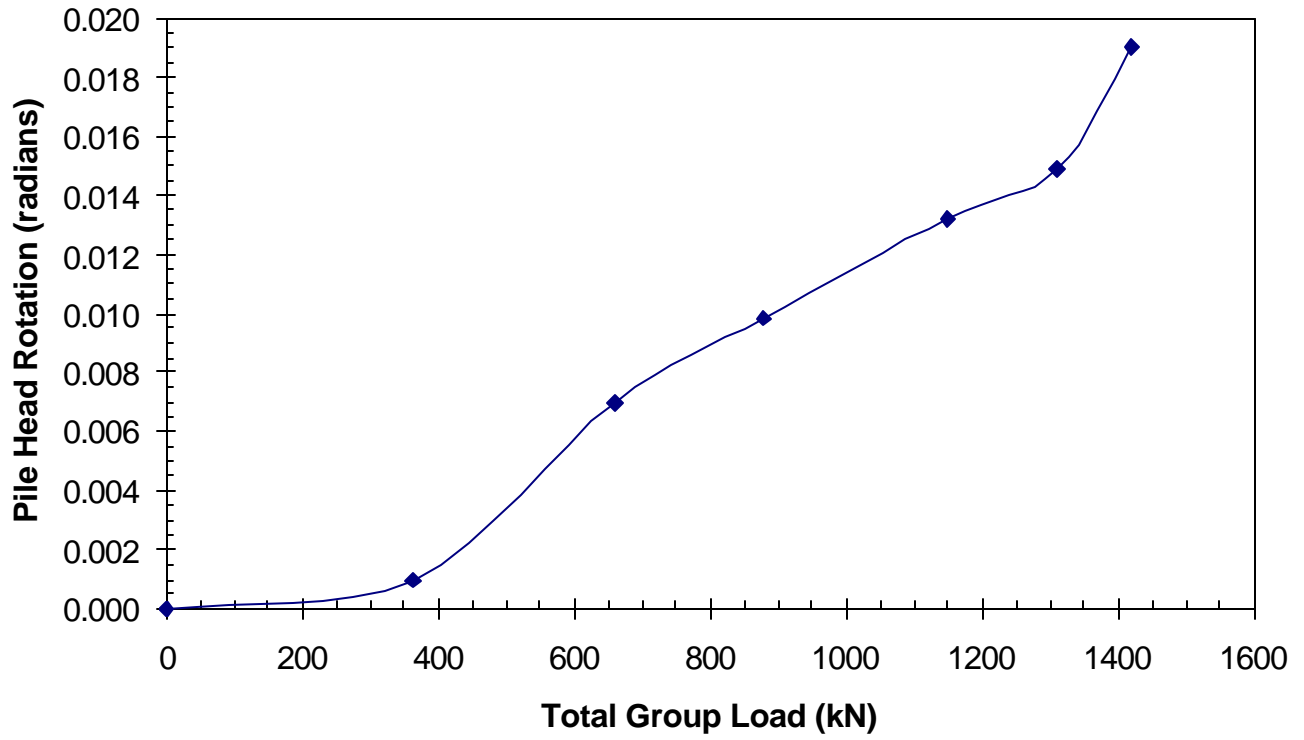
Figure 5.17 Pile head rotation versus total group load (rotation measured on middle pile in back   row).

CHAPTER 6 STATIC LATERAL LOAD TESTS ON TWELVE-PILE GROUP AT 4.4 DIAMETER SPACING

INTRODUCTION

Two static lateral load tests were performed on the pile group consisting of 12 piles spaced at 4.4 pile diameters in the direction of loading. The first test was performed on a free-head group, while the second test was performed after a reinforced concrete pile cap had been placed around the test piles. The tests were conducted to study the effects of pile-soil-pile interaction on the lateral load behavior of the group relative to that of a single isolated pile and to evaluate the effect of pile head fixity on lateral resistance.

FREE-HEAD LOAD TEST

Test Layout

The test site was located west of a geopier footing at Bent 5 along the southbound lanes of the old I-15 alignment at South Temple as shown in Figure 1.3. The 12 piles used in the group test were driven between August 23rd and 25th, 1999. The piles were driven closed-ended to a depth of approximately 12.2 m (40 ft) and the ground heaved about 0.15 m (0.5 ft) at the end of driving in the center of the pile group. The free-head test on the group began on September 29, 1999. However, due to technical problems involving the calibration of the load cells, the testing was suspended following the initial 8.0 mm deflection cycle. The problems were resolved and the test was completed on October 12, 1999. A total of 37 days had passed since the piles were driven, thus, any pore pressures generated by the pile driving would have dissipated.

The pile group consisted of 12 pipe piles arranged in four rows with three piles per row as shown in Figure 6.1. The piles in the group had an outside diameter of 324 mm (12.75 in) and were identical to the single 324 mm steel pipe pile tested previously. The properties of the piles are summarized in Chapter 4. Each row was spaced at 4.4 pile diameters or 1.42 m (4.66 ft) apart in the direction of the loading. The piles within each row were spaced at 1.07 m (3.5 ft)
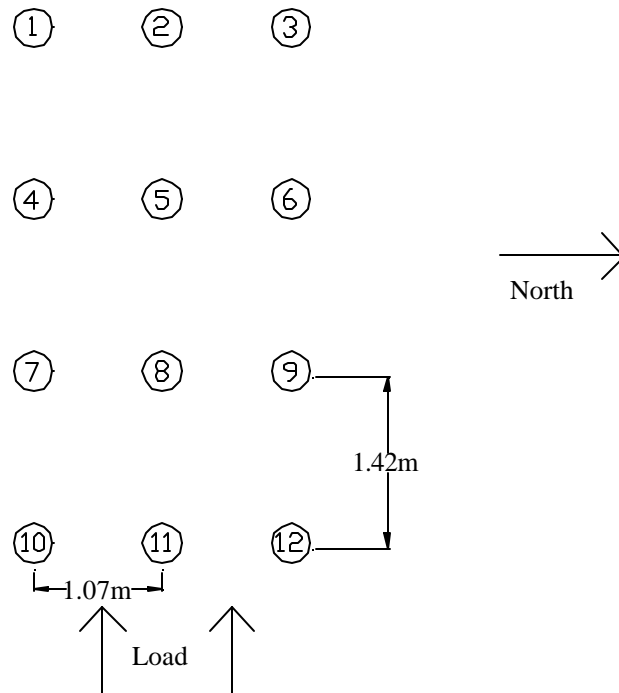

Figure 6.1 Arrangement of piles within the 12-pile group.

perpendicular to the load direction to be consistent with the other pile group tests involving 324 mm diameter piles. The piles were numbered from 1 to 12 in order to facilitate communication. The order of driving by pile number was 2, 5, 8, 11; 1, 4, 7, 10; 3, 6, 9, and 12.

The load was applied using two 1.34 MN (150 ton) hydraulic jacks that reacted against a geopier footing that was constructed by the University of Utah as shown in Figure 6.2. The jacks were connected to a pump with a manifold that produced equal load in each jack. The jacks

pushed against a steel load frame which transferred the load to the piles by pin-connected (zero moment) tie-rods attached 0.48 meters (19.0 inches) above the ground surface as shown in Figure 6.3. A portable electric pump with a maximum pressure of 10,000 psi powered the jacks. The pump was connected to the jacks through a manifold system which produced approximately equal force on each jack. The pumps typically loaded the group at a rate of approximately 20mm/min. In order to prevent eccentric loading, spherical endplates were placed at the base of each jack.

The steel frame consisted of two 6.25 m-long W310x67 (W12x45) beams with four sets of C250x45 (C10x30) channels bolted to the top and bottom of the beams as shown in Figure 6.2. The tie-rods were bolted to a section of I-beam that was bolted to the two channel sections as shown in Figure 6.3. The steel frame was essentially rigid in comparison with the pile-soil stiffness. The load frame was supported by lubricated steel wheels which traveled on steel beams resting on the ground surface. This arrangement minimized any friction forces on the base of the frame. Photographs of the test set up are provided in Figures 6.4 and 6.5.
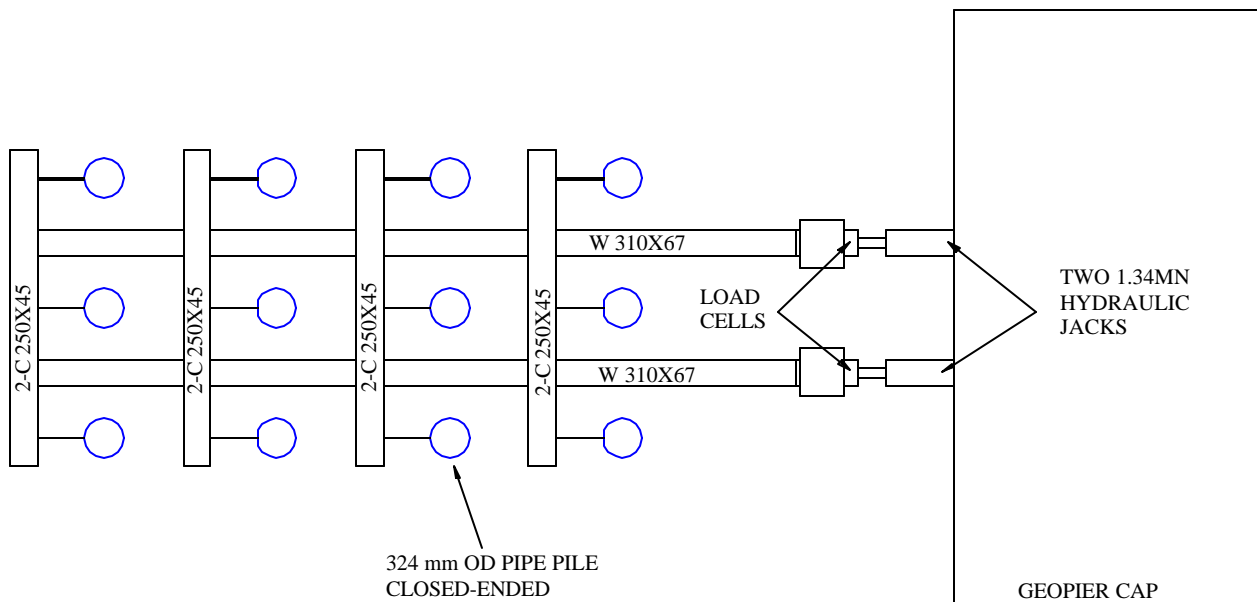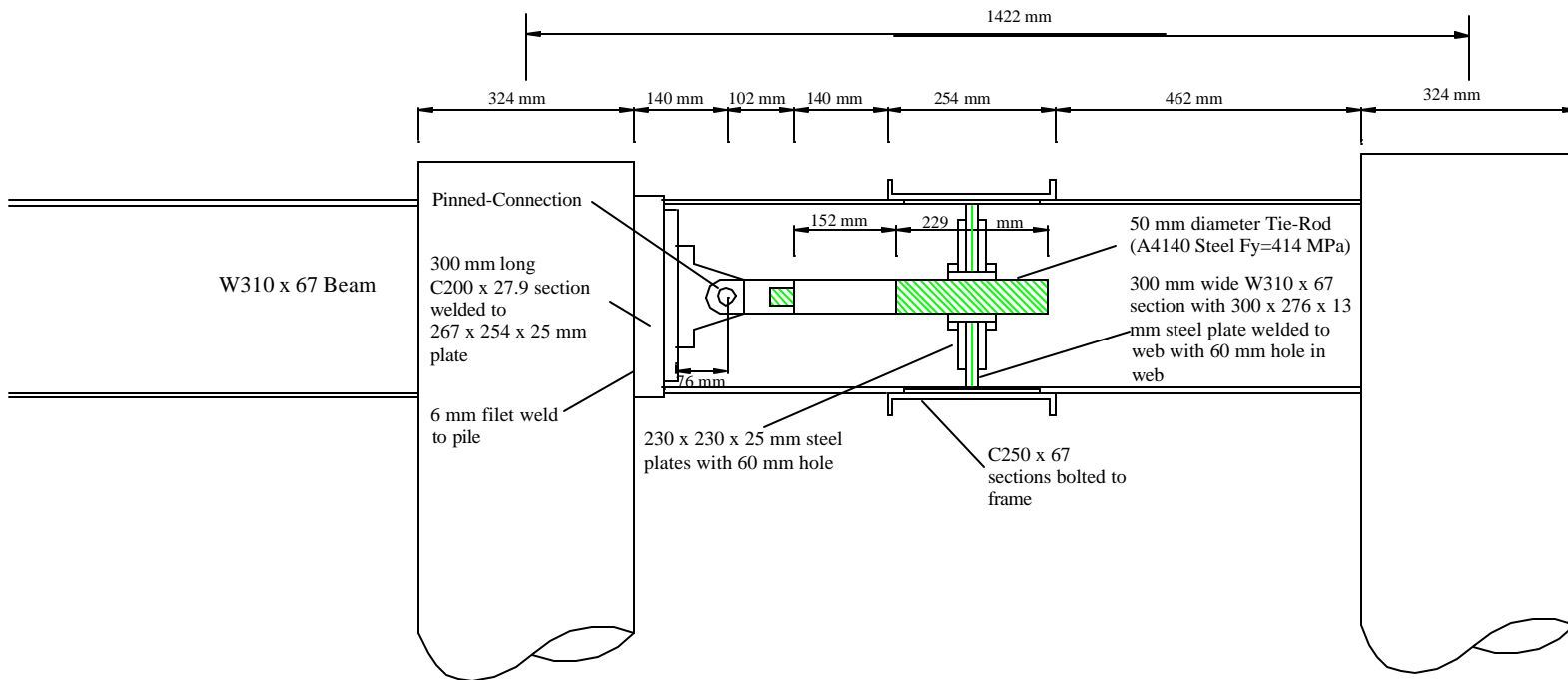
Figure 6.3 Detail of the pinned tie-rod connection from pile to the frame.

Figure 6.4 Photograph of the 12-pile group and load frame during free-head test.

Figure 6.5 Photograph of pinned connection arrangement between frame and pile.

Instrumentation

The pile group was instrumented to measure the load, pile head deflection, pile head rotation, and strain along the length of the pile. Strain gauges were attached to opposite sides of the tie-rod surface so that it acted as a load cell with bending effects being eliminated. The tie-rod load cells were attached to each pile with a pinned connection so that the load carried by each pile could be measured. In addition, two load cells were attached to the hydraulic jacks used during the tests. The forces measured by the tie-rod load cells could be compared to the forces measured by the load cells on the jacks to provide a check on accuracy. The difference was typically less than 2%.

The pile head deflection was measured with 8 linear variable displacement transducers (LVDTs) that were accurate to 0.127 mm (0.005 inches). The LVDTs were connected to an independent reference frame to allow the measurement of the pile head deflection as shown in Figures 6.4 and 6.5. These LVDTs were connected to each corner pile of the group as well as the middle piles of each row. Each of these eight LVDTs was connected at the elevation of the load point. An additional ninth LVDT was placed 0.305 m (1 foot) above the load point on pile 11 to measure pile head rotation.

Four piles in the group were instrumented with waterproof electrical resistance type strain gauges (Texas Measurements, Inc. model WFLA-6-120). The strain gauges were placed on the center pile in each row. As with the single pile, strain gauges were epoxy bonded on opposite sides of the test piles at 9 depths as shown previously in Figure 4.3. The strain gauges were attached to the outside of the piles before they were driven into the ground. To protect them during the driving process, a continous angle iron was placed over the gauges. The piles were oriented during driving so that one set of gauges would be on the side of the pile subjected to tension, while the other set was on the opposite side subjected to compression when the group

was laterally loaded. The angle iron was 5.08 mm (0.2 inch) thick and composed of 38.1 mm (1.5 inch) legs that were connected at a right angle. The angle iron was tack welded to the pile at points midway between each strain gage. The angle iron extended to a depth of 0.914 meters (3 ft) beyond the final gage.

An Optim Megadac data acquisition system was used throughout the test to record data from the load cells, strain gages, and LVDTs. During this group test, 72 channels were allocated to record strain gauge data, 8 channels for LVDT data, and 14 for the load cells. Measurements were taken at one-second intervals throughout the test.

Electrical power for the data acquisition system and the hydraulic pump was provided by a portable gas generator, which supplied 8000 watts and a current of 80 amps. The power was filtered by a universal power system (UPS) to eliminate power surges and to provide temporary power (one-half hour) in the event of a problem with the generator.

Procedure

The group test was performed using a deflection control approach. Six target deflections were chosen for the experiment. The target deflections were 6.35 mm (0.25 inches), 12.70 mm (0.50 inches), 19.1 mm (0.75 inches) 25.40 mm (1.0 inch), 38.10 mm (1.5 inches), 50.8 mm (2 inches), and 63.5 mm (2.5 inches). The load was applied in only one direction until a target deflection was reached at which point the load was released and the piles were allowed to return to an unloaded position. For the first six target deflections, fifteen single amplitude load cycles were applied, but only one cycle was applied for the last target deflection. The first cycle of each target deflection was maintained for two to three minutes. This time period allowed for the manual recording of peak values. Each subsequent loading was only maintained for 10 to 20 seconds to allow the readings to stabilize. The load returned to zero between each cycle.

A single LVDT was used to control the deflection of the pile group during the test. However, in the calculations of the group deflection, an average of all eight LVDTs at the load point elevation were used. Problems with the calibrations of the LVDTs resulted in actual deflections being only 63% of the original target deflections. The actual deflections that were reached were 4.0 mm (0.16 in), 8.5 mm (0.33 in), 13.0 mm (0.51 in), 17.2 mm (0.67 in), 24.8 mm (0.98 in), 31.8 mm (1.25 in), and 39.7 mm (1.56 in). Unfortunately, this problem was discovered after a reinforced concrete pile cap had been poured around the 12-pile group so that additional testing to greater deflections could not be conducted. As a result, the deflection levels are somewhat less than planned, but they are still large enough to provide the required information regarding the behavior of the pile group relative to the single pile.

Test Results

Load- Deflection at Pile Head

LVDT and load cell measurements taken at the load point on the piles were used to obtain the load versus deflection curves. The sum of the loads measured by the individual tie-rod load cells was within one to four percent of that obtained from the two load cells attached to the hydraulic jacks. Load versus deflection plots were typically constructed by extracting data at points of interest such as the target deflections or points of maximum load. A continuous plot of the average pile load (total load divided by 12) versus average group deflection for the entire test is provided in Figure 6.6. The behavior shown in Figure 6.6 is very similar to that described in Chapter 4 for the single pile load test. A gap formed around each pile, significantly reducing the lateral resistance at deflections less than the previous maximum deflection.
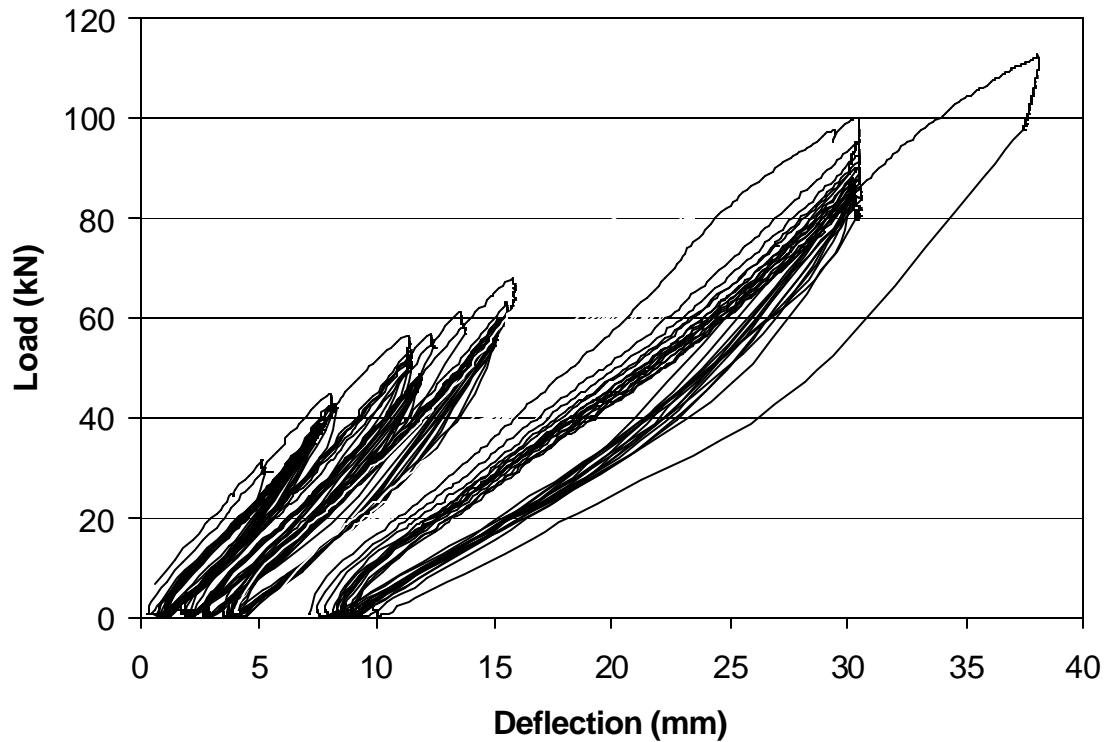
Figure 6.6 Continuous plot of the average pile group load versus average group deflection for the 12 pile group test.

As indicated previously, the group was loaded to seven target deflections. Each target deflection consisted of fifteen single direction load cycles. Figure 6.7 is a plot of average load versus deflection for the first and last cycles of the isolated single pile and the pile group tests. The average load is the maximum total group load for a cycle divided by the number of piles in the group. The group was subjected to a maximum load of 1363 kN (306.4 kips), which resulted in an average deflection of 39.7 mm (1.56 in).

The average load is used in Figure 6.7 to facilitate comparison between the average group pile resistance and that of the isolated single pile. For both the first cycle and fifteenth cycle curves, the average load for the group piles is typically about 15% lower than for the isolated single pile at the same deflection. This suggests that group effects are reducing the lateral resistance at the 4.4 diameter spacing in this pile group in both cases.
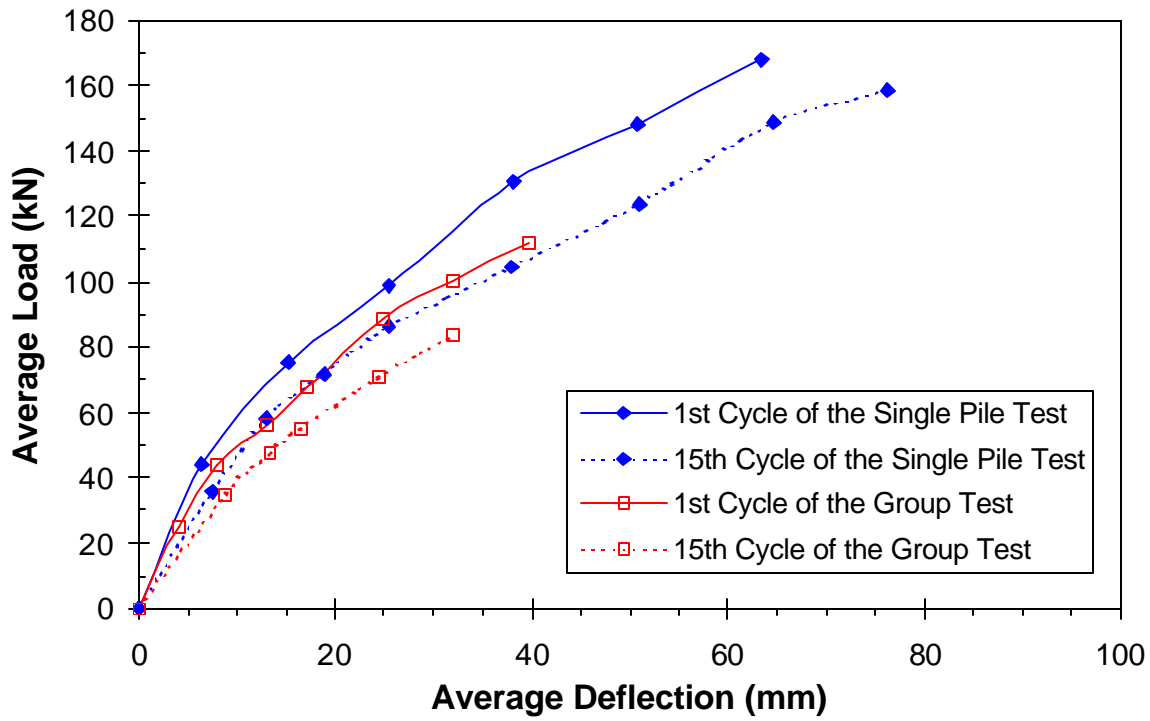
Figure 6.7 Average load per pile versus average pile head deflection for first and last cycles.
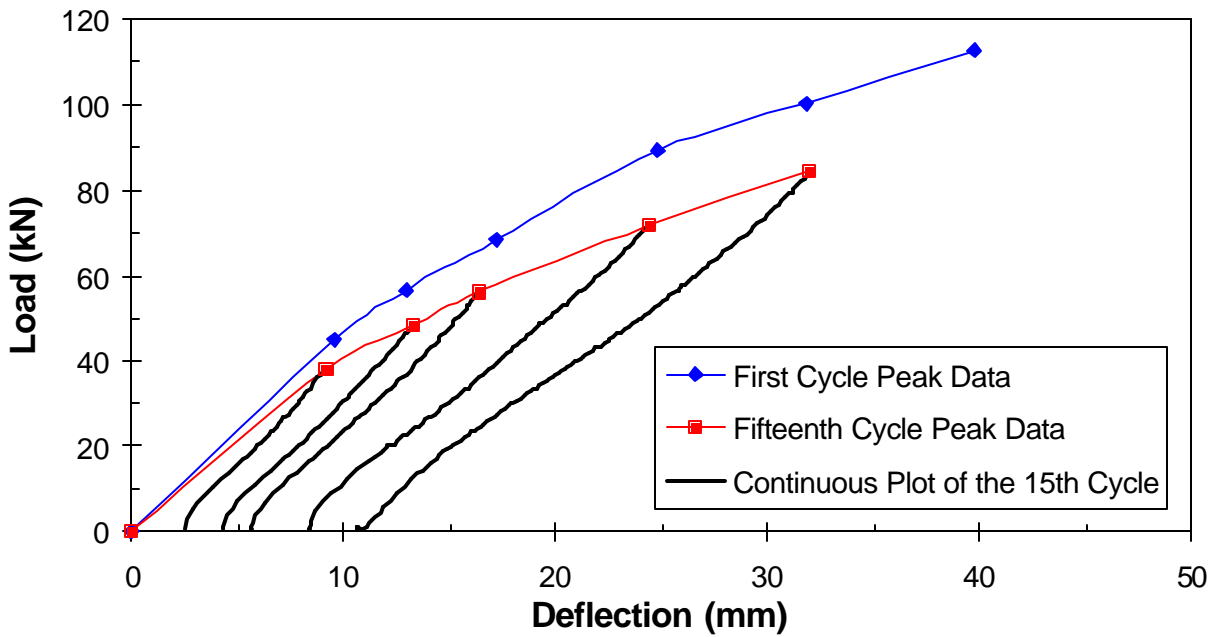
Figure 6.8 Load versus deflection curves for the first and fifteenth cycles of the group test.

As in the case of the single pile, a reduction in soil resistance was observed between the first and last cycle. Repeated loading appears to lead to a reduction in soil strength due to

6-10

remolding. The reduction in soil resistance was manifested in the decreased load necessary to produce the same deflection. This reduction in load from the first to last cycle ranged from 15.7% to 19.4% with an average of 17.6%. In comparison, the reduction in load over the 15 cycles for the isolated single pile averaged 15.0% for the cycles greater than 13.0 mm (0.51 in). Therefore, the reduction due to cyclic loading of the pile group and single pile appear to be approximately the same. The cycles less than 13.0 mm had significantly greater reduction percentages than at higher deflections. The greater percentage reductions occurred at relatively small loads and are not considered indicative of the general behavior of the piles. At these small deflections, local variations in the soil properties immediately around the piles produced by driving can have abnormally large effects.

A plot of the continuous load-deflection curve for each of the 15th load cycles at each deflection increment is presented in Figure 6.8 along with the peak load-deflection curves for the 1st and 15th cycles. As discussed previously for the single pile in Chapter 4, the shape of the reloading curve is substantially lower than that based on the curve defined by connecting the peak points on the curve due to the presence of gaps. Therefore, at deflections much smaller than the maximum previous deflection, the lateral resistance could be as low as 20 or 30% of the initial resistance. The continuous reload curve typically has a "concave up" shape where resistance increases with deflection in contrast to the peak load curves where resistance decreases with deflection.

The change in lateral pile-soil stiffness during the fifteen cycles at each target deflection is examined more closely in Figure 6.9. The stiffness of the lateral soil-pile resistance was again computed using equation 4.1 as was done previously for the isolated single pile test. Stiffness in

each cycle of loading was again normalized by the initial stiffness of the first cycle at each target deflection.

There was a rapid reduction in stiffness initially which leveled out as more cycles were completed. With the exception of the 31.8 mm deflection, all the increments dropped by about 10% from the first to second cycle of the target deflection. By the eighth cycle, the decrease in soil resistance with additional cycles began to level off. In general, the rate of reduction in stiffness decreased as the deflection increased. For example, at the 8.0 mm deflection increment, a 28% reduction in stiffness occurred between the first and last cycles. However, at the 31.8 mm deflection increment the stiffness only decreased by 12% over the fifteen cycles.
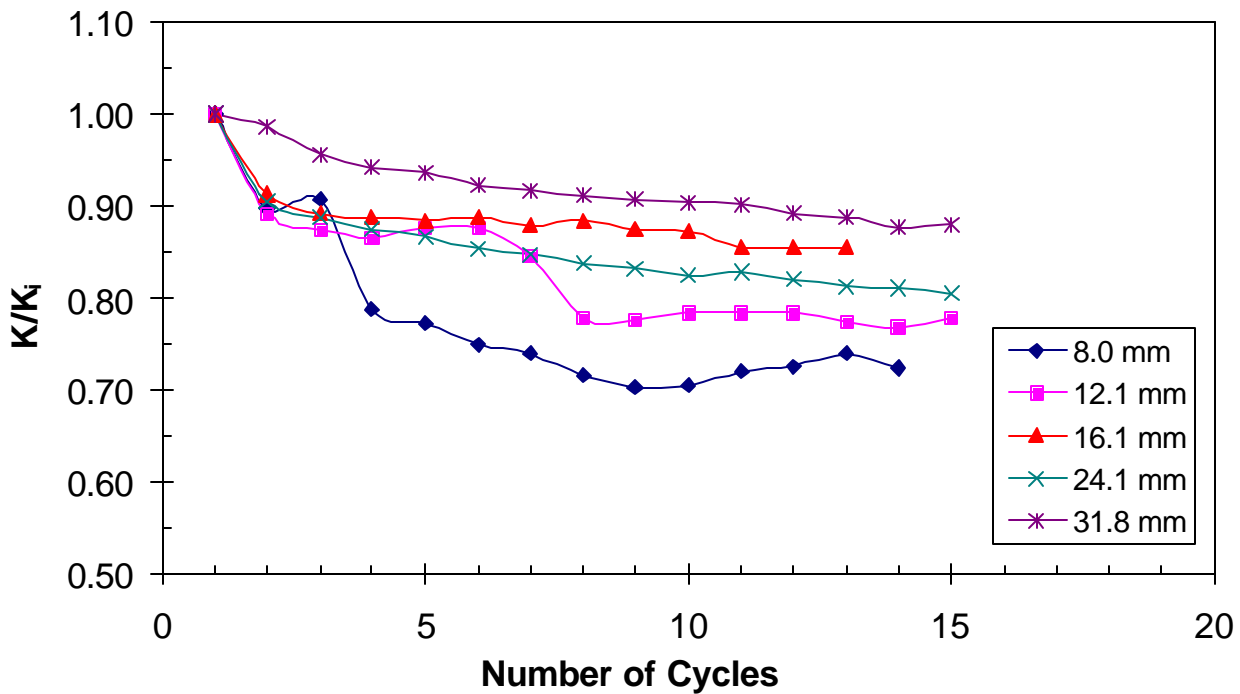
Figure 6.9 Normalized lateral pile group stiffness versus the number of cycles for each deflection increment during the lateral load test.

The load carried by each pile in each row of the pile group is plotted in Figure 6.10. As indicated previously, the group was organized into four rows of three piles. Row 1 is the front or

leading row in the group and row 4 is the back or trailing row in the group. The piles were differentiated as left, middle and right when viewed in the direction of loading. The variation of load in a row was generally less than 10% of the average load for that row. No pile in a row consistently carried more load than any another. Therefore, the position of a pile within a row did not dictate the amount of load it would hold. This finding is consistent with results reported for other full-scale load tests (Brown et al, 1988 and Rollins et al, 1998) but incongruent with predictions made using the elastic theory.

The elastic theory predicts that the corner piles will carry the highest load and that the piles in the middle of a row will carry the lower loads for a given displacement. This lack of agreement with the elastic theory may be a result of driving effects in which the soil around the center piles may be densified more by the driving process than the outer piles. However, since the soil profile largely consists of clay, a significant densification of the soil would not necessary be expected due to pile driving. The elastic theory may simply be inadequate to account for the behavior of the pile as the soil is sheared and exhibits non-linear plastic behavior.

Although no pattern of lateral load resistance was observed within a row, resistance was found to be a function of row location within the group. This result is consistent with results from other full-scale tests in both sands and clays (Brown et al, 1987, 1988; Rollins et al, 1998, and Ruesta and Townsend, 1997).
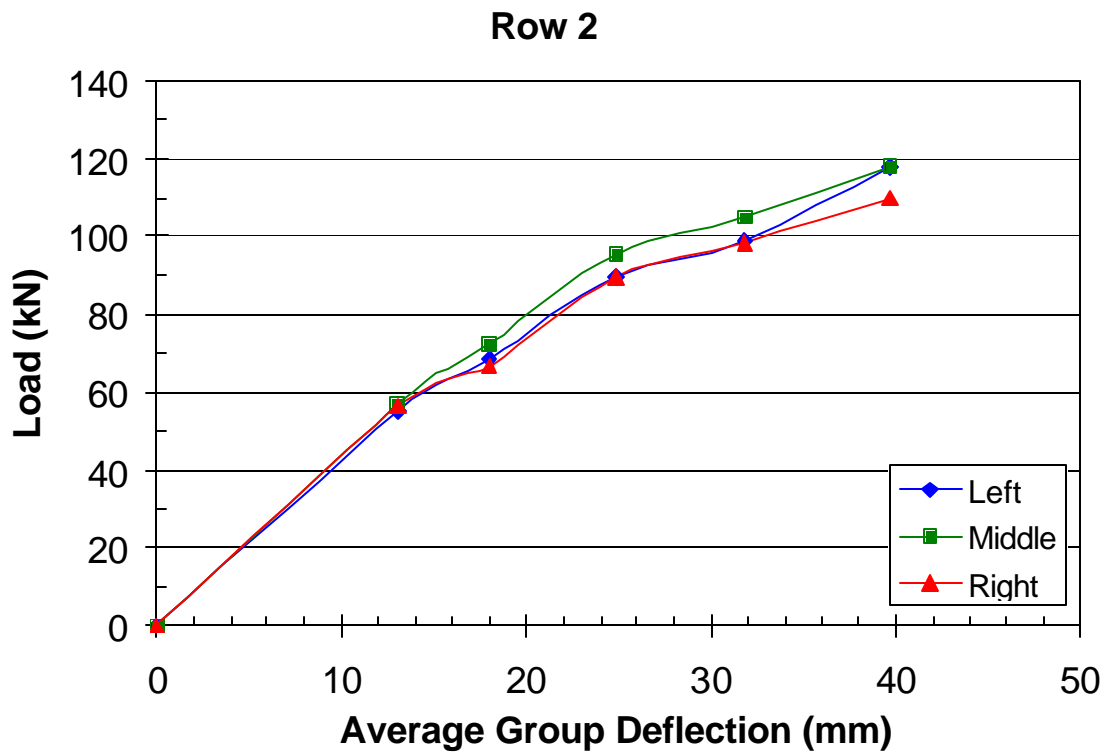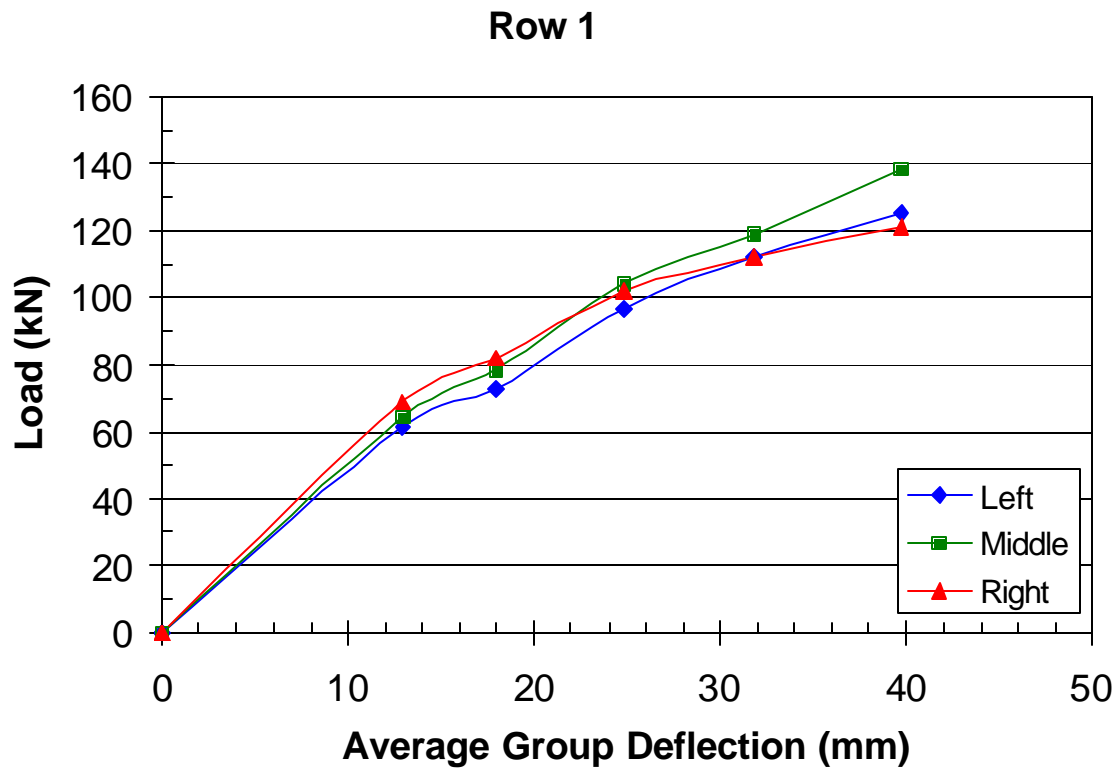
Figure 6.10 Load vs. average group deflection curves for left, middle and right piles in each row in the 12-pile group.
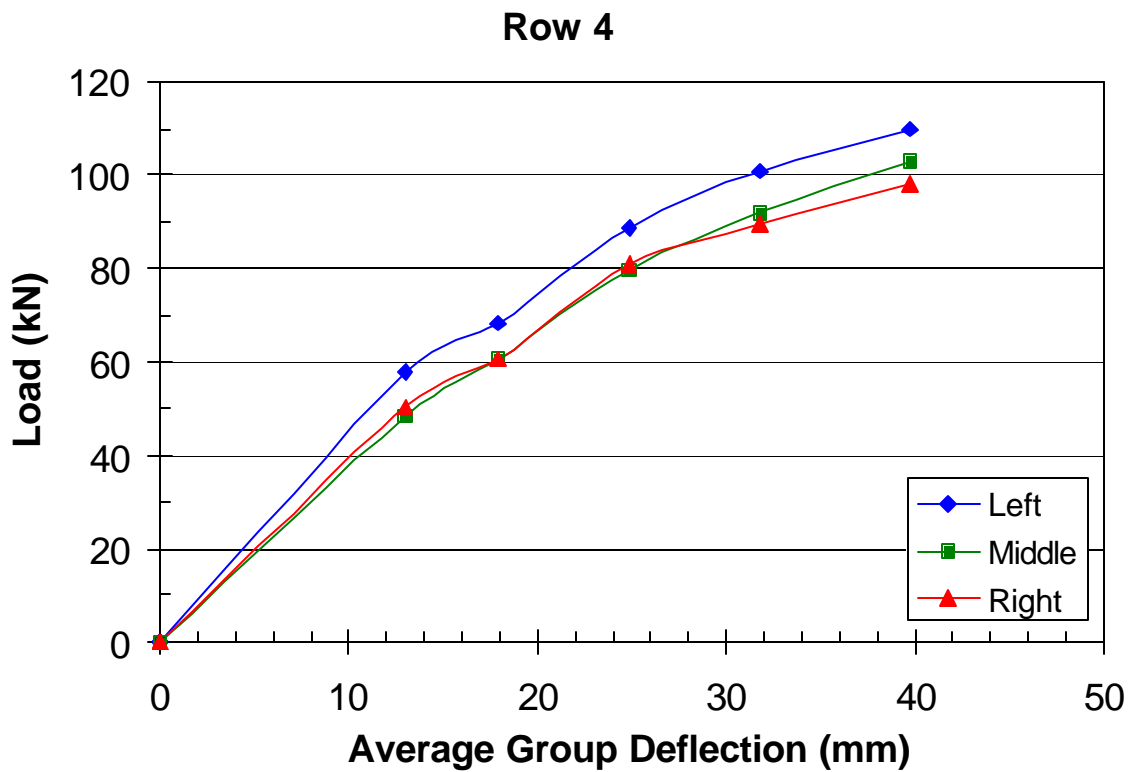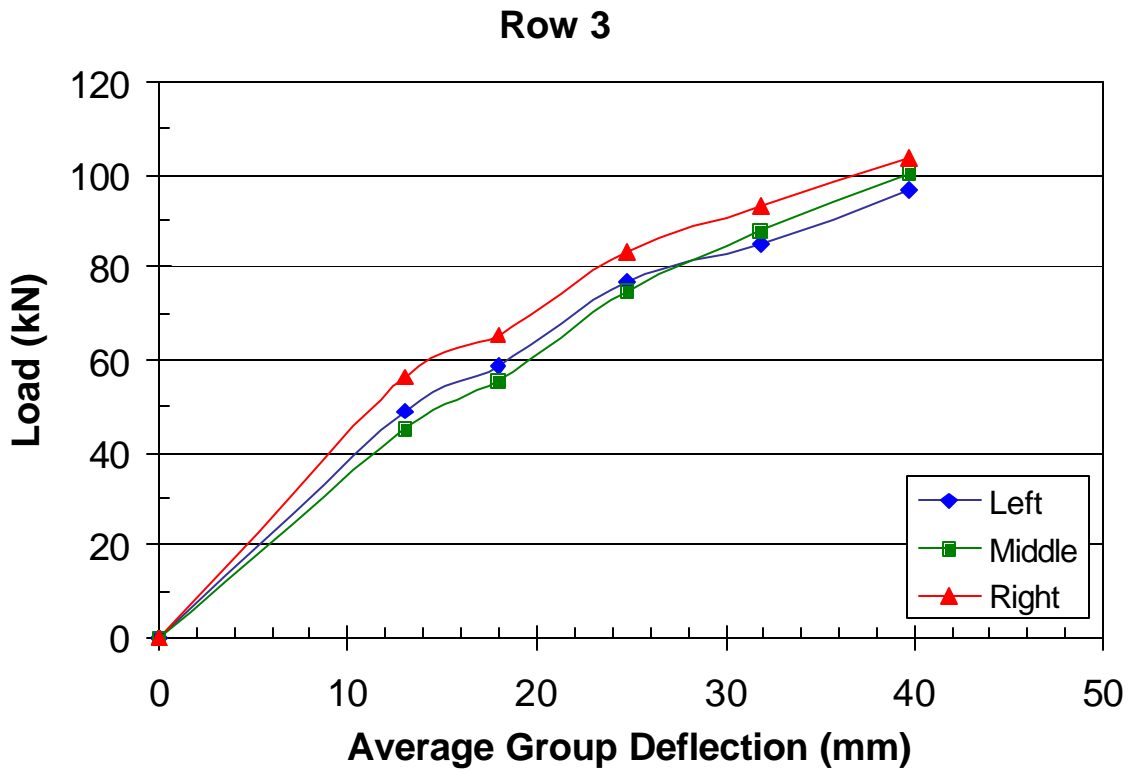
Figure 6.10 (continued) Load vs. average group deflection curves for left, middle and right piles in each row in the 12-pile group.

The average pile load versus deflection curves for each row in the group are shown in Figure 6.11 along with the curve from the single pile test. The average row load was determined by summing the loads recorded by each tie-rod load cell at a given group deflection and dividing the sum by the number of piles in the row. The front row behaved similarly to the single pile; however, the load was slightly lower for a given deflection. The trailing rows carried smaller loads than the front row piles at the same average deflection.

There is a trend for the average load to decrease from the first, to the second to the third row of piles, but this trend is reversed for the fourth or back row of piles. The load carried by the back row of piles is actually slightly higher than that for the piles in the third row. This result suggests that the average row load may stabilize after the third row of piles. This finding is consistent with results from centrifuge tests on pile groups in sand (McVay et al, 1998).
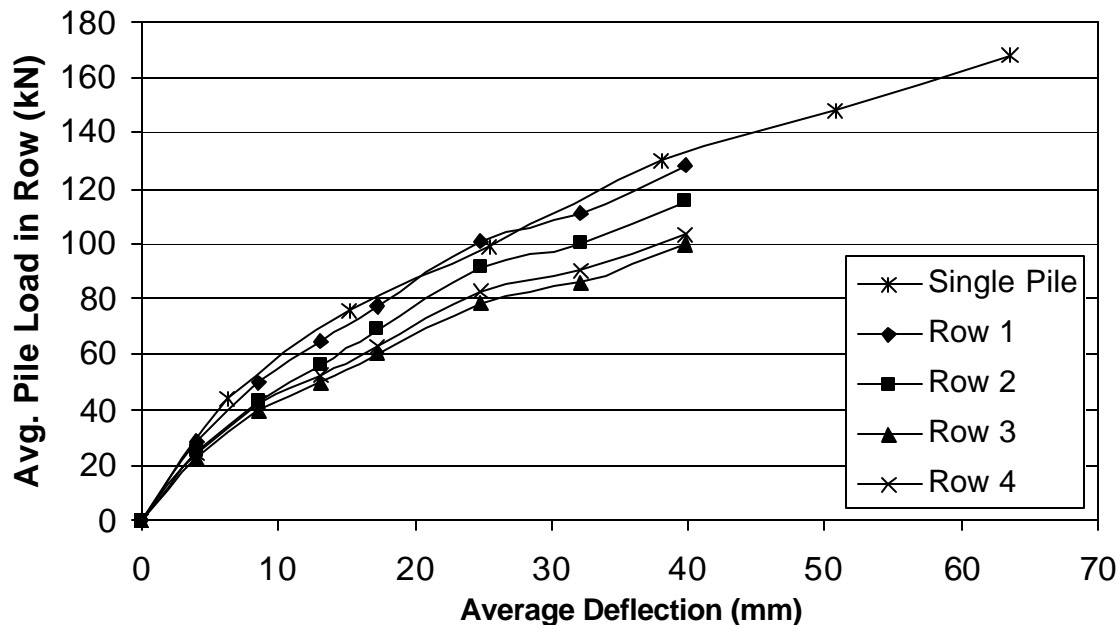
Figure 6.11 Average load versus average deflection curves for each row in the 12 pile group along with the curve for the single pile for peak points during 1st cycle loading.

The average load in each row is plotted in Figures 6.12 and 6.13 for the first and fifteenth cycles at the 32.0 mm deflection level. In addition, the previous target deflection was plotted as

a vertical dashed line. As the deflection increased, the loads carried by each row increased at different rates. Initially, the load was fairly evenly distributed between all twelve piles due to the gap that had formed around the piles from the plastic deformation of the soil. Because there was very little soil resistance, group effects due to soil-pile interaction were relatively unimportant and each pile had essentially the same lateral structural resistance. As deflection increased, the piles made contact with the soil wall and soil resistance developed. Due to group interaction effects, the soil resistance in the trailing rows was smaller than the resistance provided by the first row of piles.

As plotted in Figure 6.12, the slopes of the load-deflection curves began to increase and diverge as the deflection approached the previous target deflection to which the group was cycled (24.8 mm). The curve for the first row showed the greatest increase in slope. The slope was indicative of the increase in soil resistance as the virgin material was encountered. The slope of the third and fourth rows remained relatively constant in comparison to that of the first row. The group effect decreased the soil resistance for these two rows, therefore, the increase in resistance as the deflection passed the previous level was not as noticeable.

By the fifteenth cycle, the gap had widened due to increased plastic deformation of the soil. The slopes of the curves of each row were relatively constant with a small increase as the previous target deflection was reached. However, the first row continued to experience greater soil resistance when compared to the other three rows. The difference in lateral resistance for the three trailing rows was minimal for the majority of the 15th cycle of the test. All three trailing rows experienced a similar amount of soil resistance until the end of the target deflection where
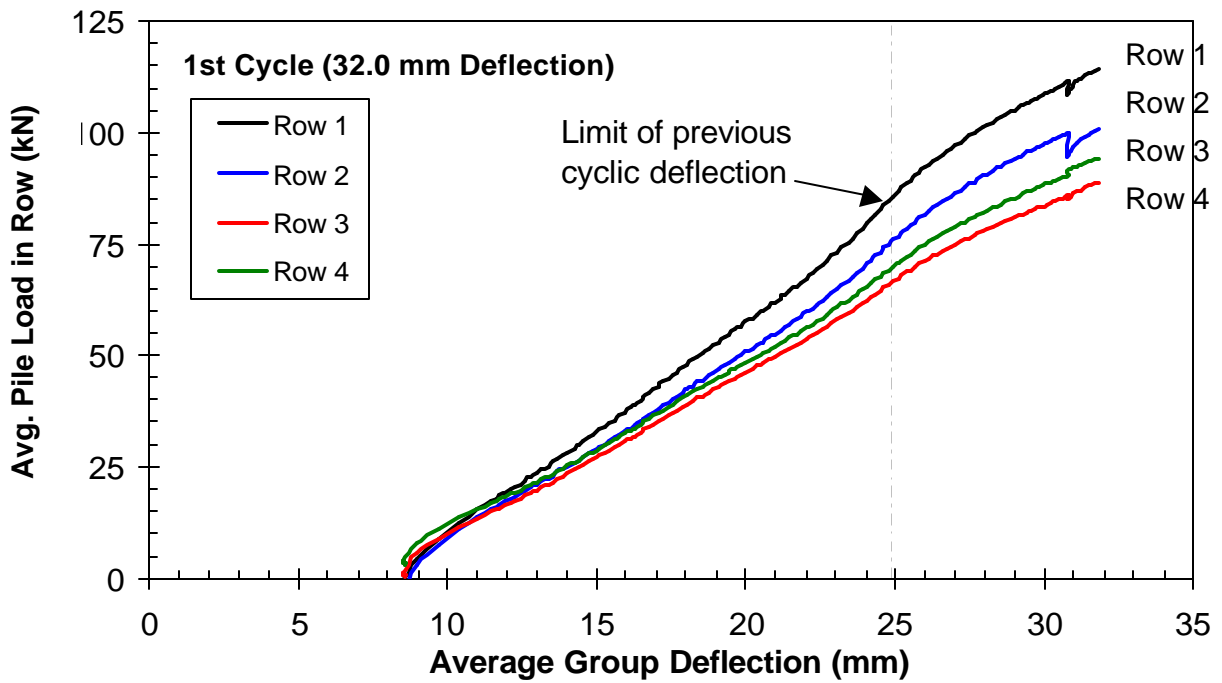
Figure 6.12 Continuous average pile load versus deflection curves for each row in the 12-pile group during the first cycle of loading for the 32 mm deflection level.
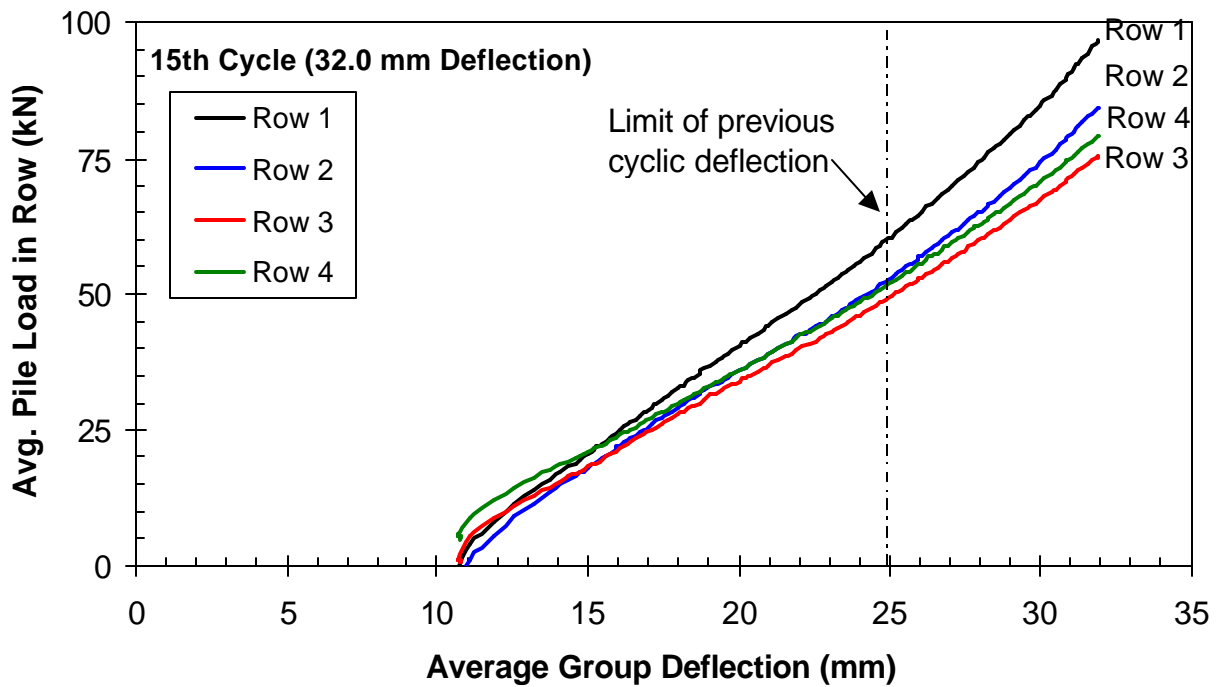

Figure 6.13 Average pile load versus average group deflection for each row in the 12-pile group during the fifteenth cycle of loading for the 32 mm deflection level.

the slopes of the curves increased as they did in the first cycle. For the first cycle the load-deflection curves are concave as the pile first contacts the virgin soil; however, for subsequent

loads the load-deflection curves are concave up in this deflection range. The load required to reach the 32.0 mm deflection on the fifteenth cycle was about 15% less than on the first cycle.

Ratios of the average load carried by a row in the pile group normalized by the load carried by the single pile are plotted in Figure 6.15. There are some abnormalities in the initial part of the graph until the deflection of 20 mm is reached. The troughs that exist in the data may be due to variations in soil properties and disturbance created when the piles were driven. As the test progressed to larger deflections the trends became more consistent. In general, the ratios drop from their initial values, until a deflection level of about 20 mm, where they remain relatively constant. (Rollins et al, 1998).
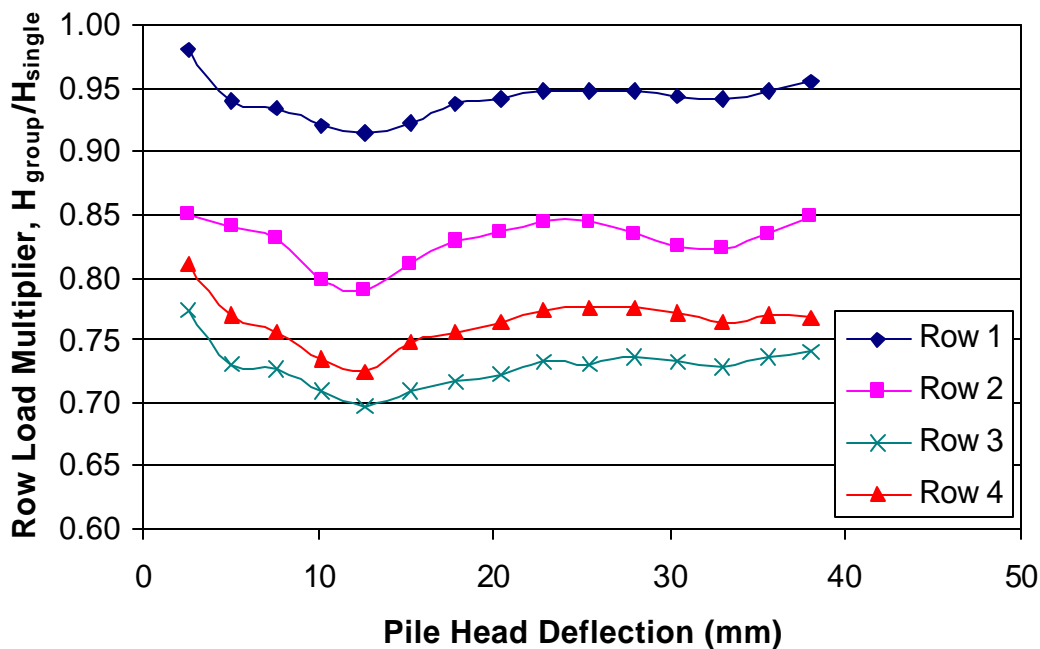
Figure 6.15 Normalized row load versus deflection curves for each row in the 12-pile group (row load normalized by the single pile load).

An initial decrease in resistance with increasing deflection would be expected for closely spaced piles in a group. As the deflections increase, the shear zones begin to develop and start to overlap. As the shear zones overlap, "shadowing" effects develop and the soil resistance

decreases for the piles in the trailing rows. The curves in Figure 6.15 indicate that about 20 mm of deflection was required to develop some sort of stability in the load ratios, whereas about 50 mm of deflection was required for the nine-pile group with 5.6 pile diameter spacing. Full-scale tests on a pile group with piles spaced at 2.8 pile diameters center-to-center indicated that the load ratios initially decreased rapidly and then remained relatively constant after only about 13 mm of movement (Rollins et al., 1998). The deflection at which the decrease in soil resistance remains relatively constant appears to be proportional to the spacing of the rows within a group. In other words, pile groups with smaller row spacings begin to experience this consistency in soil resistance at smaller deflections. Therefore, greater movements were necessary to fully develop overlapping shear zones for the piles spaced at 4.4 diameters than for the piles spaced at 2.8 diameters, but less movement than that for the piles spaced at 5.6 diameters.

For deflections that exceeded 30 mm, the average load ratios were 0.95, 0.84, 0.74, and 0.77 for the first, second, third, and fourth rows, respectively. Rollins et al. (1998) found the load ratios to be 0.7, 0.38 and 0.42 for the front, middle and back row piles, respectively, in a 3x3 pile group at 2.8 diameter spacing. For the group tests reported in Chapter 5 on a 3x3 pile group spaced at 5.6 pile diameter spacing, the load ratios were 1.0, 0.94, 0.82 for the front, middle, and back rows, respectively. As expected, these results indicate that group effect becomes less significant as the piles are spaced farther apart.

Bending Moment versus Depth

Bending moment versus depth curves for the instrumented pile in each row in the group are shown in Figure 6.16 for each of the seven deflection increments. The bending moment versus depth curves for the single pile are also included in the plots in Figure 6.16 for comparison. The bending moment was calculated based on the strain gauge measurements using equation 4.2 as described previously. The gauges were located at nine depths on both sides of the pile as shown in Figure 4.3. The strains associated with the peak load of the first cycle of each deflection increment were used to develop the curves. The maximum bending moment for the first three rows of the group occurred at 1.76 m (5.8 ft) below the ground surface. This depth is equal to 5.4 pile diameters. The maximum moment for the fourth row occurred at the same depth for the 4.0, 8.5, and 13.0 mm deflections. However, at deflections of 17.2, 24.8, 31.8 and 39.7 mm, the maximum bending moment in the fourth row occurred at a depth of 2.5 m (8.2 ft) or 7.7 pile diameters.

An examination of the bending moments at the 1.76 m (5.8 ft) depth reveals that the front row had the maximum moment at every target deflection after the 8.5 mm cycles. At the depth of 2.5 m (8.2 ft), the bending moment of the front row was either the least or very similar to that of the second row. At this depth, the magnitude of the moment in the third row exceeded that in the first two rows in every case. The fourth row bending moment at the 2.5 m (8.2 ft) depth surpassed the moment in the other three rows in all but two instances (the 4.0 and 8.5 mm deflections). This review indicates that the bending moments of the trailing rows are lower at shallow depth but higher at deeper depths than those in the front row piles. The occurrence of deeper bending moments in trailing rows is consistent with the findings of Brown et al (1987) as shown in Figure 6.17.
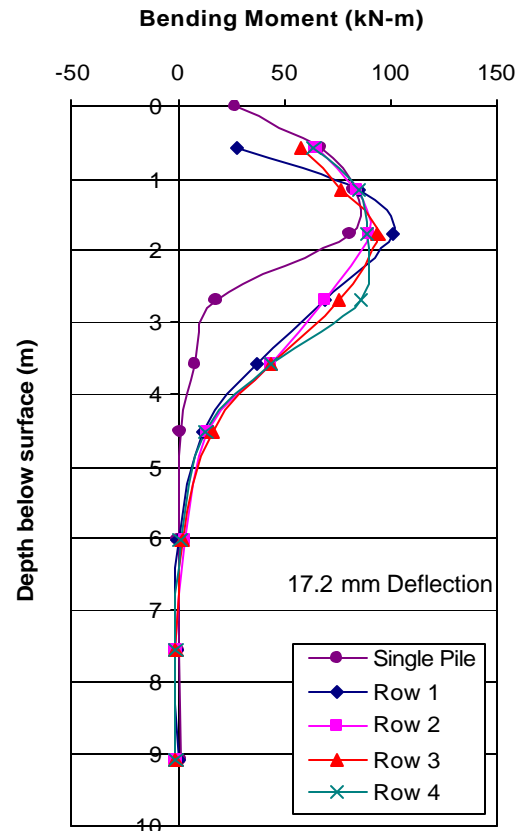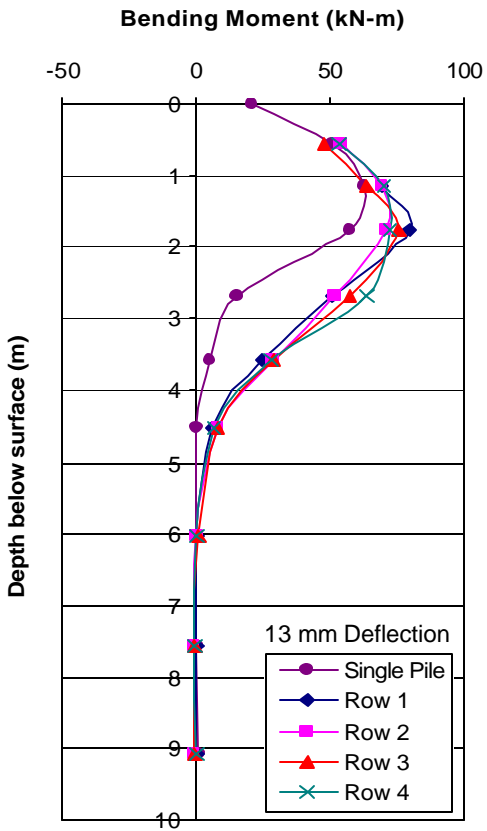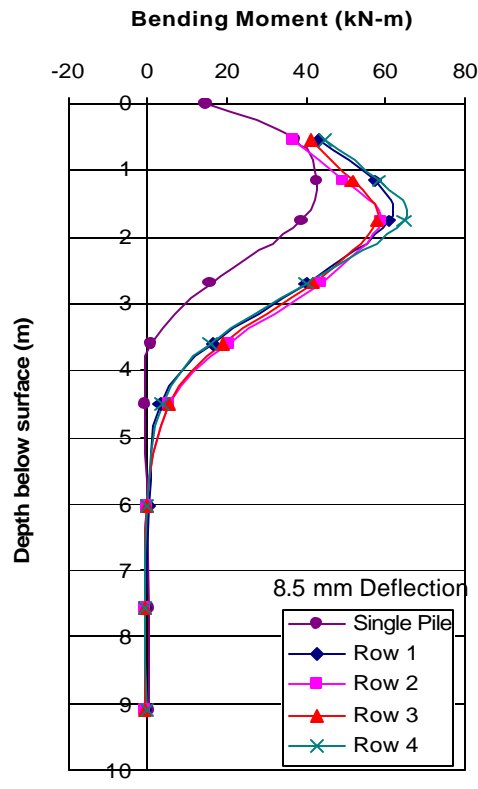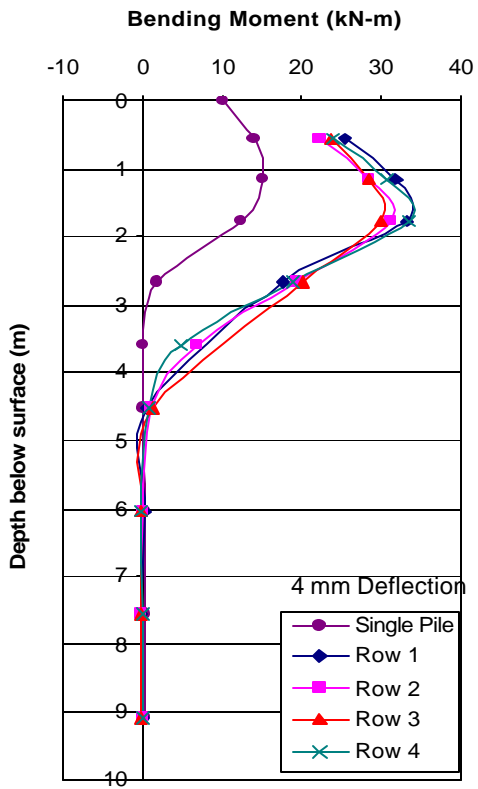
Figure 6.16 Bending moment versus depth curves for various deflection increments.
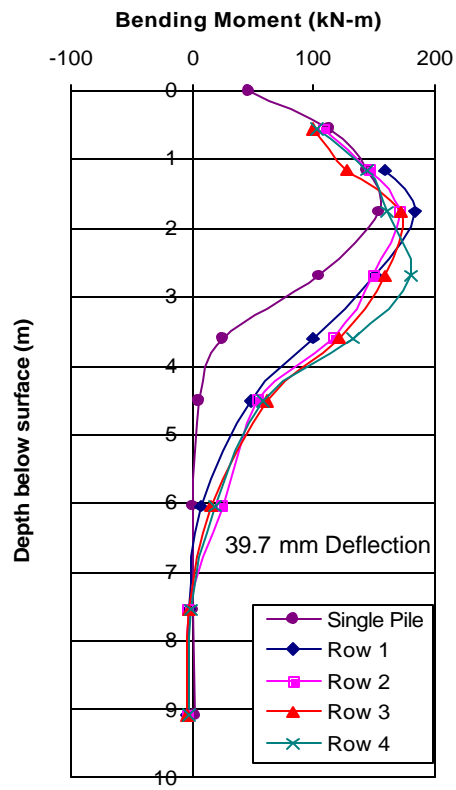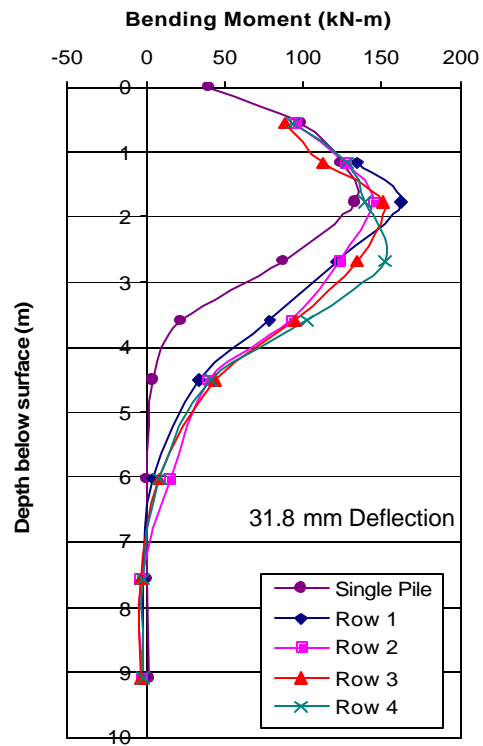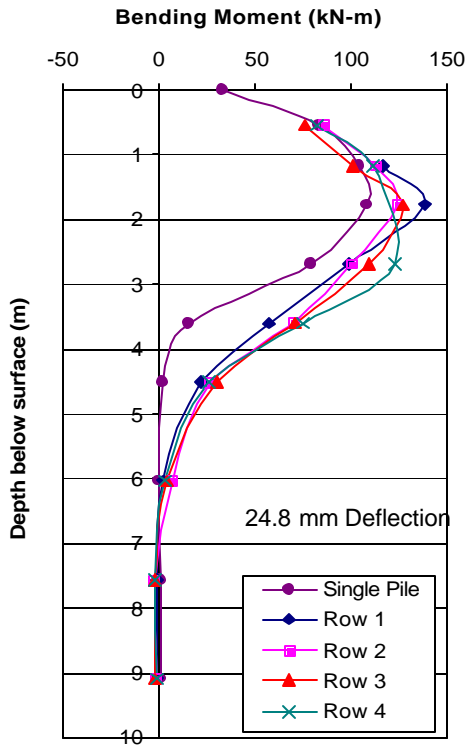
Figure 6.16 (continued) Bending moment versus depth curves for various deflection increments.

The piles were instrumented every 0.61 m to 0.91 m (2 to 3 feet) in the region where the maximum bending moments occurred. Had the piles been instrumented at smaller intervals, the increase in depth of the maximum bending moment for each trailing row would have been better manifested and the results would probably look more similar to those shown in Figure 6.17.

At the larger deflections the maximum moment that occurred in the single pile is relatively consistent in depth and magnitude with those of the pile group. However, the single pile bending moment drops off relatively quickly with depth while the pile group bending moments remain relatively high. This difference in moments, due to the group effect, suggests that the moments for which a pile in a group must be designed may be significantly higher at depth than would be expected based on the single pile load test results. This would require greater reinforcing steel requirements in reinforced concrete piles at depth than would otherwise be used.

The depth to the moment reversal for the first target deflection was 4.5 m (14.8 ft). The moment reversal in the final deflection occurred at 7.5 m (24.6 ft). The depth to the moment reversal increased as the deflection increased. This finding was similar to that observed in the single pile test. The depth to the moment reversal in the group piles, however, was on average about 23% deeper than those of the single pile. The soil in which the pile group was located behaved softer than that of the single pile thus allowing greater bending to occur, which led to a greater depth for moment reversal.
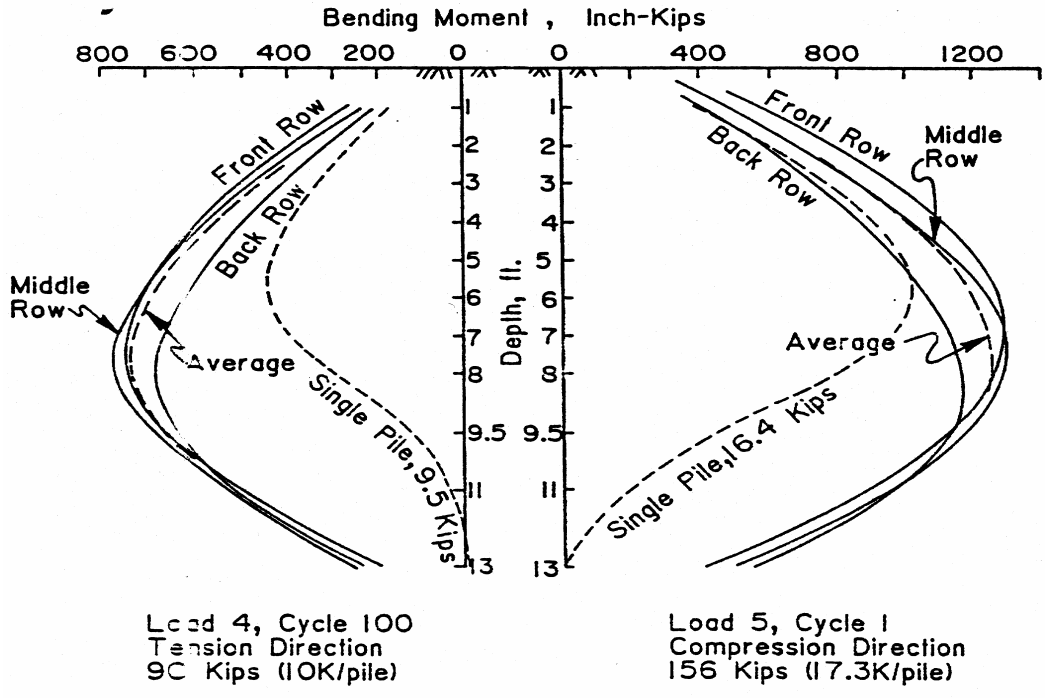
Figure 6.17 Bending moment versus depth for a 3 x 3 pile group in stiff pre consolidated clay. Note the graph is shown in English Units (Brown et al. 1987),

Maximum Moment versus Load

The maximum moment versus the average load per pile in the group is shown in Figure 6.18. The average load was calculated by dividing the total load per row by the number of piles in a row. The maximum moment is the greatest moment along the length of the pile for the load level being considered. The group effect was very apparent in this graph. For a given load, the single pile had the smallest bending moment, while the third row in the group manifested the greatest moment. All of the trailing row piles experienced greater moments at a given load than the first row due to softening of the soil resistance produced by pile group interaction. The overlapping of the shear zones reduced the soil resistance around the piles of the trailing rows. This reduction in soil resistance and lateral restraint led to greater bending moments.
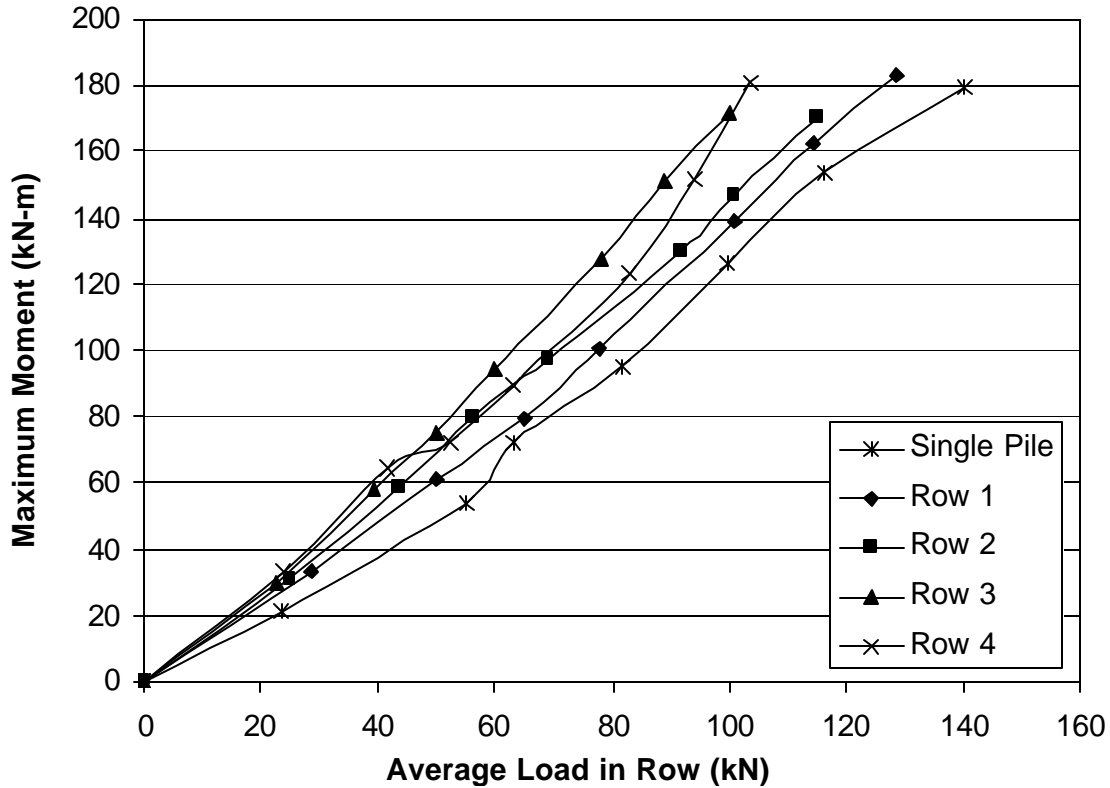
Figure 6.18 Maximum moment versus average load per pile in a row.

Pile Head Rotation

The pile head rotation was determined by placing two LVDTs on one pile at a vertical distance of 0.305 m (1 ft) apart. The pile head rotation is plotted as a function of the total load in Figure 6.19. The rotation was calculated using equation 4.3 given previously. The maximum rotation of 0.032 radians occurred at a total load of 1341 kN. The estimate of the rotation suffers from the fact that it must be obtained by subtracting the deflection at two points relatively close to one another. Since the deflections are relatively small, small errors in the deflection could lead to significant errors in the computed rotation. In future tests, the LVDTs should probably be spaced at greater distances to improve the measurement of rotation.
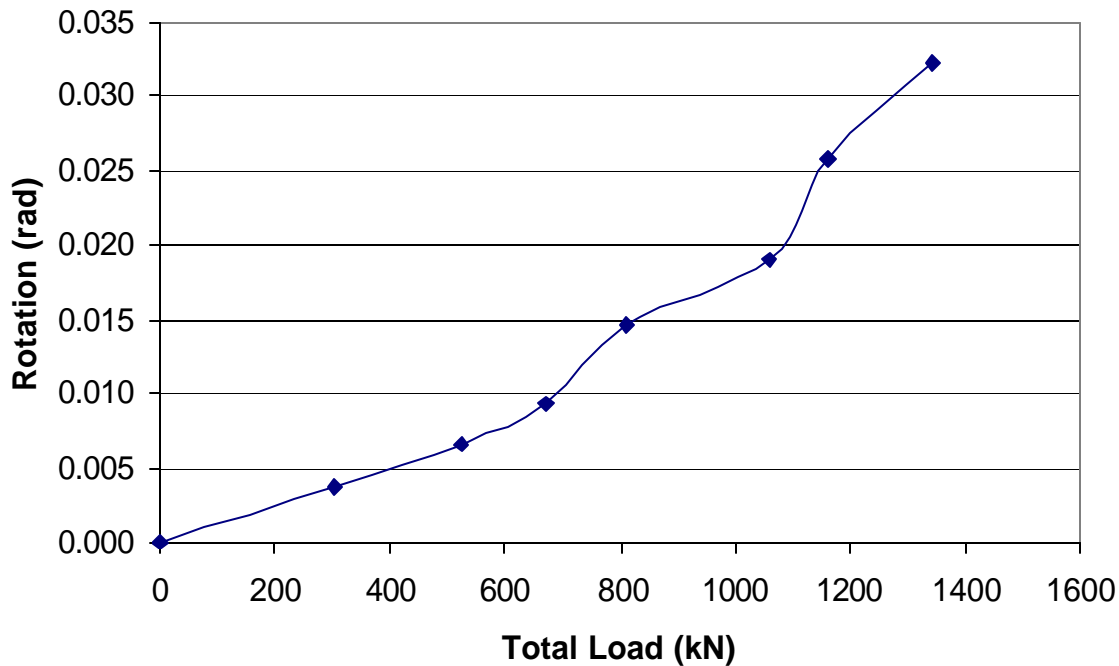
Figure 6.19 Pile head rotation versus total load.

FIXED-HEAD LOAD TEST

Introduction

Following the free head tests conducted on the pile group, the frame was removed and the pile group was encased in a 1.12 m thick (44 inch) reinforced concrete cap that was 5.22 m (17.1 ft) long and 3.04 m (10 ft) wide as shown in Figure 6.20. The pile cap produced what would commonly be considered a "fixed-head" boundary condition at the pile head, although some rotation did still occur. Load tests involving the fixed-head pile group were conducted in April and again in September 2000 in conjunction with the University of Utah (U of U). Dr. Pantelides, a structural engineering professor at the U of U, and his graduate students were performing pull-over testing on several old bridge bents located along the old I-15 alignment at the South Temple Site. On April 26, 2000, the capped pile group was used as one of two reaction footings for a frame used in the bridge bent pullover tests as shown in Figure 6.21.
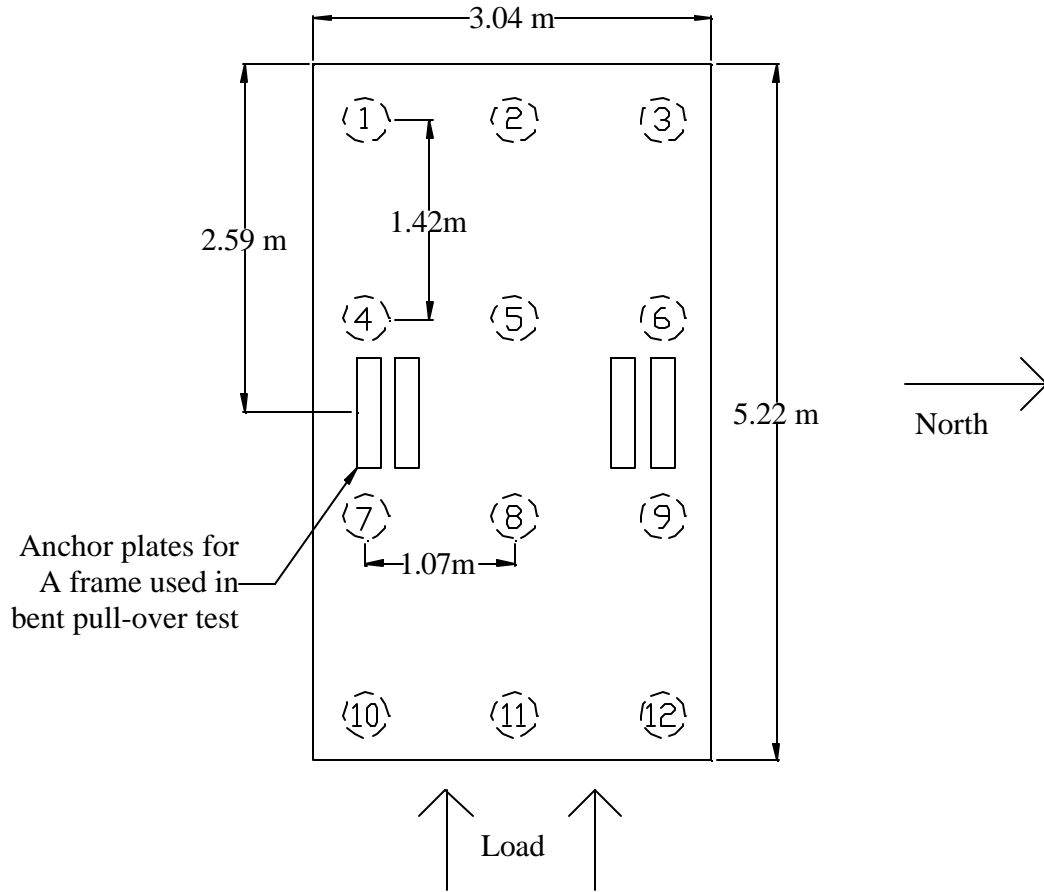
Figure 6.20 Schematic drawing of the capped pile group with anchor plate locations.

The other footing supporting the frame was a geopier group foundation constructed by Dr. Evert Lawton, a geotechnical engineering professor, and his graduate students at the U of U. The geopier foundation consisted of a concrete cap 1 m (3.28 ft) thick and 7.47 m x 2.52 m (24.5 x 8.25 ft) in plan dimension supported by 10 aggregate geopiers (2x5 arrangement) as shown in Figure 6.21. Each geopier was constructed by drilling a 0.76 m (2.5 ft) diameter hole to a depth of 4.57 m (15 ft) and backfilling with a sandy gravel that was compacted inside the hole from the bottom up using a rammer mounted on a telescoping mast. This process typically produces an aggregate column with a friction angle of over 50 degrees. Four high strength steel reinforcing bars were attached to a plate at the base of each aggregate column and extended through to the top of the pile cap.
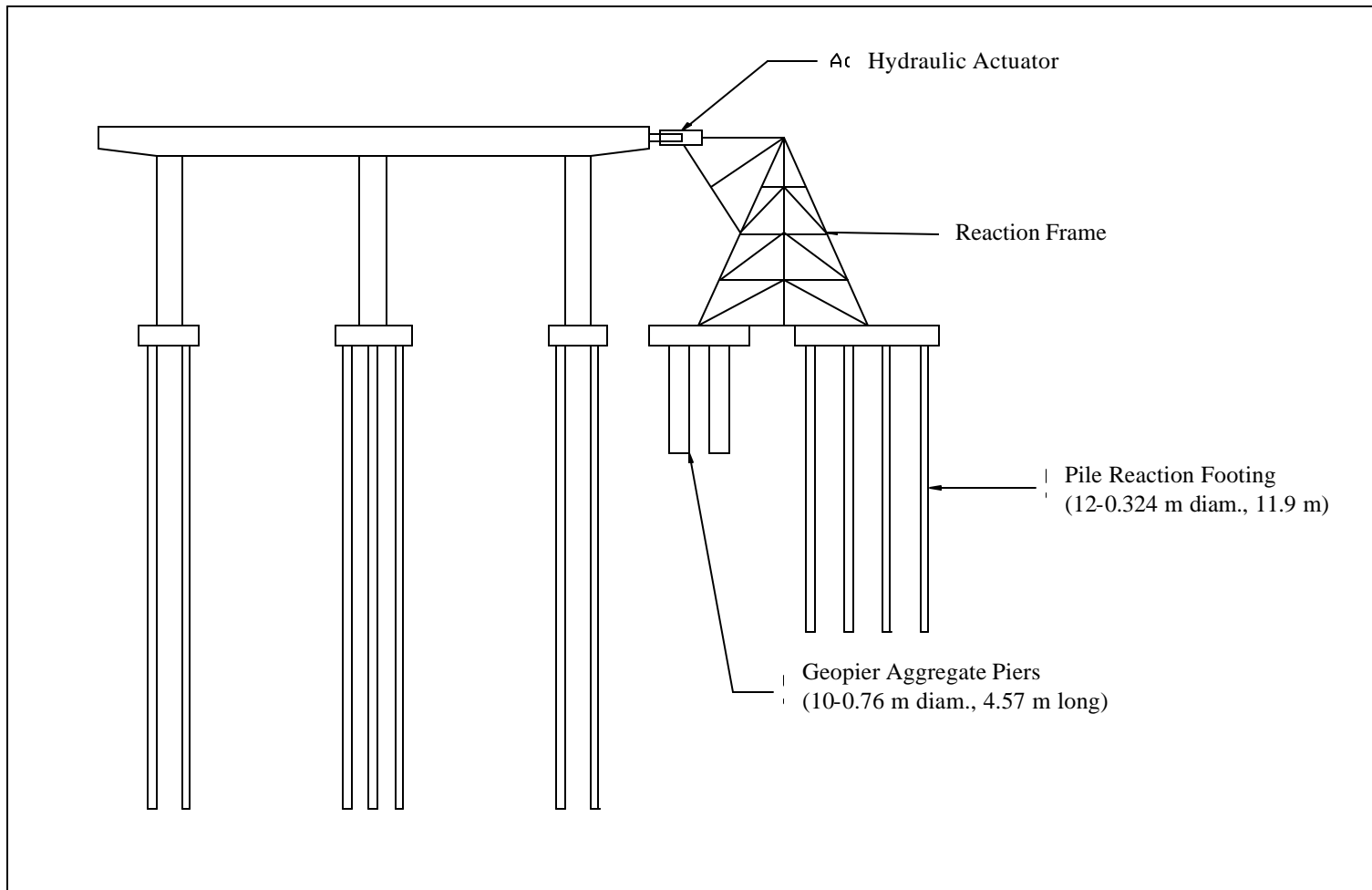
Figure 6.21 Schematic drawing of the bent test setup with reaction frame supported by fixed-head pile group and geopier footings.

Labels in figure:
- Ac Hydraulic Actuator
- Reaction Frame
- Pile Reaction Footing (12-0.324 m diam., 11.9 m)
- Geopier Aggregate Piers (10-0.76 m diam., 4.57 m long)

During the test in April, the pile group and geopier footings were subjected to alternating tension and compression loads along with a lateral load. After completing the pull-over test on the bent, a final lateral load test was performed in which the fixed-head pile group was reacted against the geopier. In this final case there was no vertical load involved.

The testing program had several objectives in addition to simply providing a reaction for the pull-over test. First, the test made it possible to compare the behavior of a fixed-head pile group relative to that of a free-head pile group. Secondly, the test provided an opportunity to evaluate the behavior of a geopier foundation relative to a conventional steel pipe pile group. Third, the lateral resistance of the pile group with and without a vertical load could be evaluated. Finally, the test results could be compared with results computed using computer programs such as GROUP and Florida Pier to evaluate the accuracy of these methods.

Test Layout

The same piles used in the free-head group test were used in the bent pullover test with the addition of a pile cap shown in Figure 6.20. The piles were filled with reinforced concrete prior to construction of the pile cap. The concrete consisted of a five-bag mix with minus 9.25 mm (3/8 inch) aggregate. Tests indicate that the compressive strength at the time of the bent test was between 40 and 41.4 MPa (5800 and 6000 psi). Prior to installation of the pile cap, each pile was cut off a little above the ground surface. The reinforcing cage in the piles consisted of six 2.743 m (9 foot) long 25.4 mm (No. 8) bars that were placed in a circular pattern in each pile with 12.7 mm (No. 4) bars used as circular ties spaced at 304.8 mm (12 inches) on center vertically. Approximately 50 mm (2 in) of concrete cover was provided around the reinforcing bars. The reinforcing cage was placed to a depth of 1.676 m (5.5 feet) in the piles and extended to within 76 mm (3 inches) of the top of the pile cap. The pile cap contained two reinforcing

mats, one 76 mm from the top and the other 76 mm from the base, constructed of 28.6 mm (No. 9) bars on 300 mm (12 in) centers in the North-South direction and 25.4 mm (No. 8) bars placed on 150 mm (6 in) centers in the East-West direction. Prior to the placement of the concrete, 75 mm inclinometer pipes were centered with piles 2, 4, 5, 6, 8, and 11 as shown in Figure 6.20.

The load was applied to the pile cap and geopier cap by a structural frame that was anchored to each foundation and to the bridge bent that it pushed against.   A steel anchor plate assembly was embedded in the pile cap during its construction as shown in Figure 6.20. The load frame for the pullover tests was 7.62 m (25 feet) tall and had a width of 6.10 m (20 ft) at its base. The frame was bolted to the anchor plates at the location shown in Figure 6.20. A hydraulic ram with a capacity of 2222 kN (250 tons) applied load to the bent. The ram was attached to the bridge deck with pre-stressed cables so that load could be applied in both directions.

Instrumentation

The pile cap was instrumented with four string potentiometers. Two of the string pots were placed on the West end measuring vertical deflection. One was placed on the East end also measuring vertical deflection. The fourth string pot was located 292 mm (11 ½ inches) below the top of the pile cap and measured the relative movement between the geopier and the pile cap. The absolute lateral movement was measured with reference to an independent reference frame. Each of the string pots registered deflection continuously which was recorded by the data acquisition system at a sampling rate of two samples per second. Figure 6.22 shows the arrangement of the string pots and the reference frame for the fixed head test in April 2000.

The same electric resistance type strain gauges were still in place from the previous free-head test. These gauges were used to measure the strain along the center piles of each row
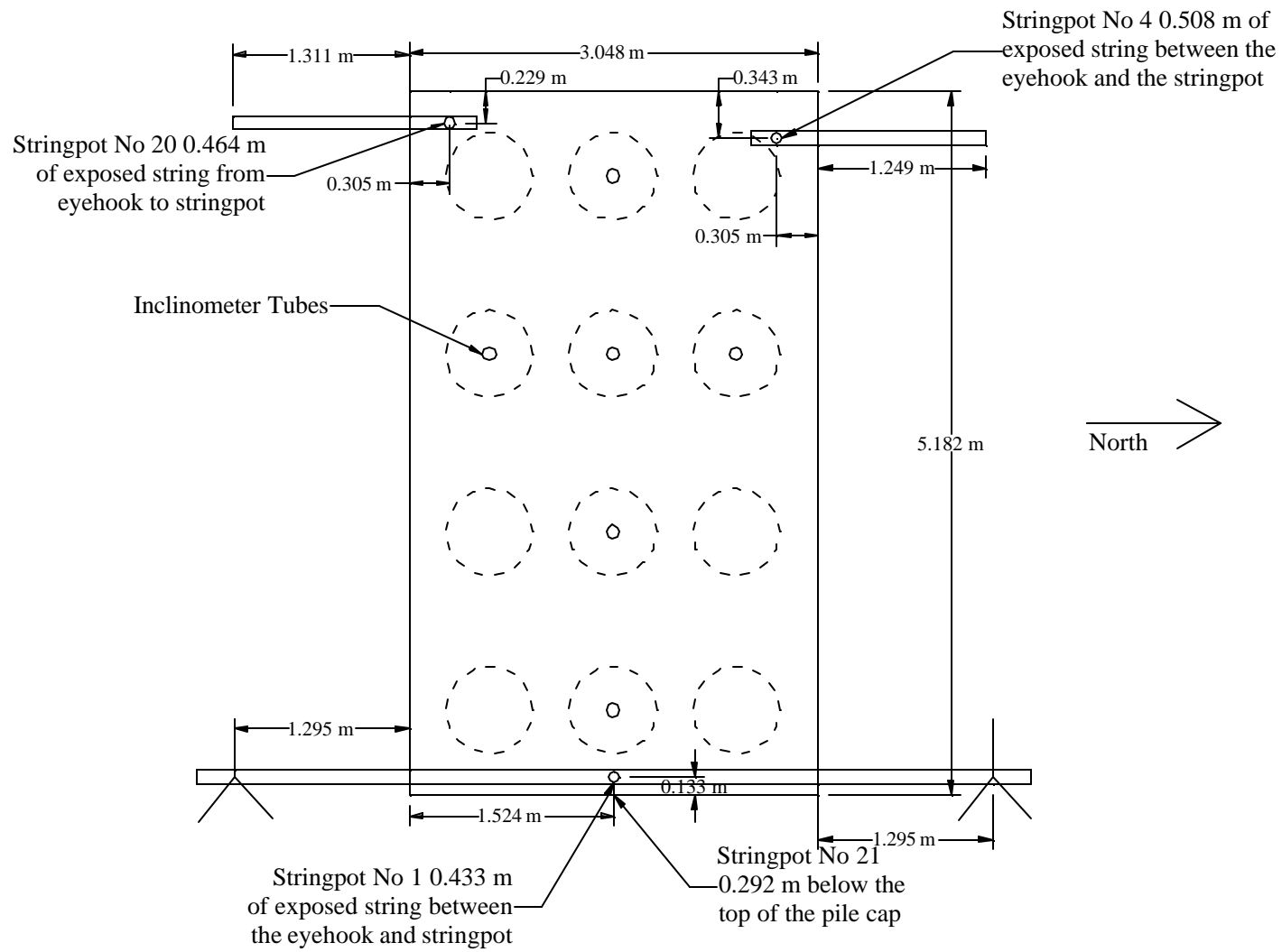
Figure 6.22 Layout of instrumentation around the fixed-head pile group during the bent test.

throughout the test. Unfortunately, some of the strain gauges had either become unattached or were no longer functioning so that the curve shape is not as well-defined as for the free-head tests. Because a vertical load was applied to the pile group along with a lateral load, it was not possible to estimate the strain due to bending alone at depth where only one strain gauge was functioning properly. Therefore, the absence of the strain data from one or both sides made it impossible to calculate the moment. This limited the amount of data available to define bending moment versus depth curves.

The center piles (numbers 2, 5, 8, and 11) as well as the number 4 and 6 piles (see Figure 6.20) were fitted with inclinometer tubes that ran the length of the pile prior to the placement of the cap. These tubes allowed an inclinometer to be used to measure the deflection in the piles. Unfortunately, time did not permit the measurement of the deflection during the maximum deflection of the pile cap. However, inclinometer data was obtained before and after the test so that the residual deflection and bending moment in the pile group could be determined. This data is of some interest when examining the permanent deflection experienced by the pile cap.

The structural members making up the load frame were instrumented with a number of strain gauges on each of the four legs. The strain gauges along with some basic structural analysis allowed the load distribution to the two foundations to be calculated.

Procedure

The pullover testing was performed using a deflection-controlled approach. The hydraulic ram mounted on the frame applied load to the bridge deck in one direction until a specified target deflection was reached and then the load direction was reversed until the same deflection was achieved in the other direction. Three cycles were applied in each direction at each deflection level and then the deflection was increased to a higher increment. A maximum

load of about 2000 kN was applied to the bridge deck during the testing at the highest deflection level.

A final lateral load test involving the geopier and pile cap was conducted on September 16-20, 2000. The test was performed by reacting each foundation against the other. The load was applied using two 1.34 MN (150 ton) hydraulic jacks which were placed between the geopier cap and the pile cap. The pile cap was pushed West and the geopier cap was pushed East. The load was measured using strain gauge load cells and the other instrumentation was essentially the same as for the bent tests. However, inclinometer readings were taken at the maximum load level to define the bending moment versus depth curve for the ultimate load.

Results

Load- Deflection for Previous Free- Head Test

As described in the first part of this chapter, the free-head pile group was initially tested in October 1999 using the geopier cap as a reaction footing. A comparison of the load versus deflection curves for each foundation measured during that test is provided in Figure 6.23. Although the load-deflection curve for the geopier was initially stiffer than that for the pile group, at a deflection of about 20 mm the geopier began to yield and displacements increased rapidly for small increases in lateral load. At the maximum load of 1232 kN, the geopier had deflected 58 mm relative to the 38 mm deflection of the pile group.

Load- Deflection for Fixed-Head Tests

Bent Test (April 2000). Analysis of the strain gauge data on the load frame during the bent tests indicates that the pile group carried 85 to 95% of the total lateral load when the pile group was in compression and the geopier group was in tension. When the pile group was in tension and the geopier was in compression, the pile group took approximately 60% of the lateral
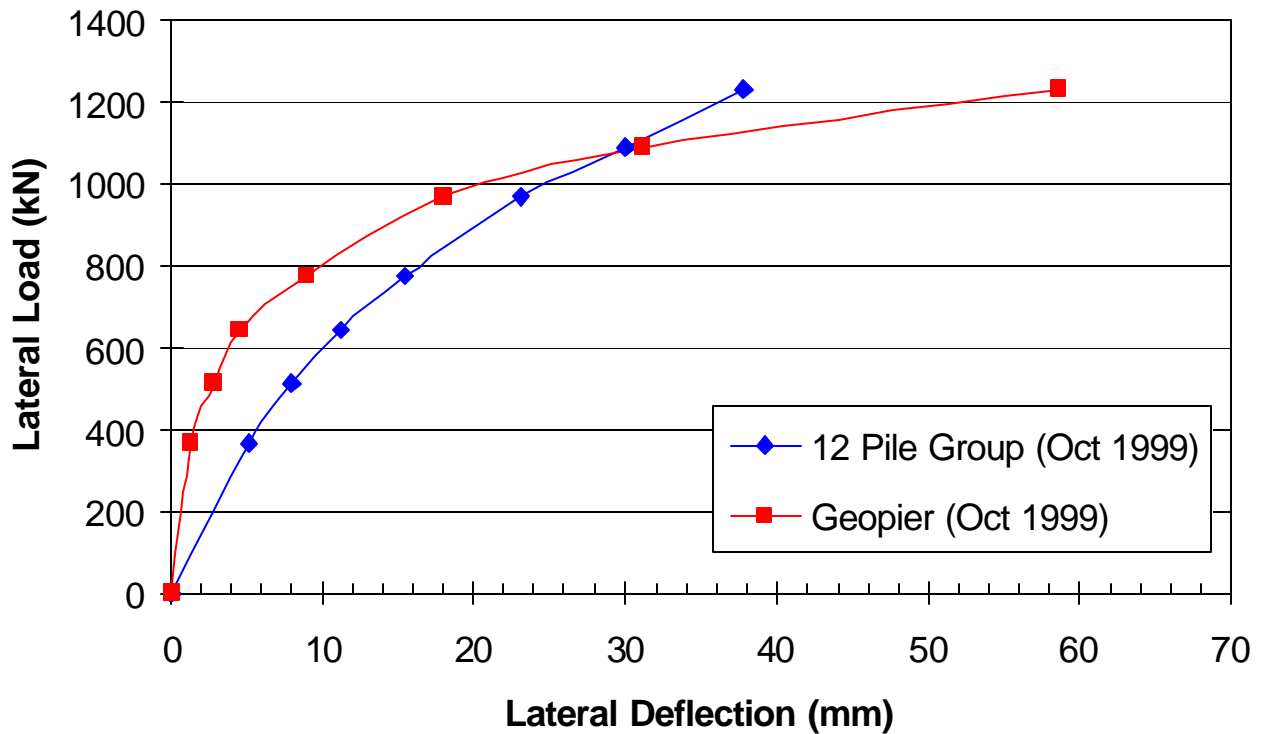
Figure 6.23 **Load versus deflection curves for the geopier and free-head pile group for test conducted in October 1999.**

load and the geopier took 40%. Assuming that the pile group carried 90% of the total lateral

load during the compression cycles, the load versus deflection curves for pile group and geopier

were developed using the peak points in each cycle of loading. The lateral load versus deflection

curves for the fixed-head pile group and the geopier foundation in both tension and compression

are presented in Figure 6.24. The load versus deflection curves for the pile group are nearly

identical for both tension and compression indicating that the variations in axial load had little

effect on the lateral resistance. However, this is not the case for the geopier foundation. The

load versus deflection curve for the geopier was roughly four times stiffer in compression than in

tension. This is likely due to the fact that the geopier derives its resistance from frictional

resistance in the gravel column. When the geopier is in compression, the normal stress on the
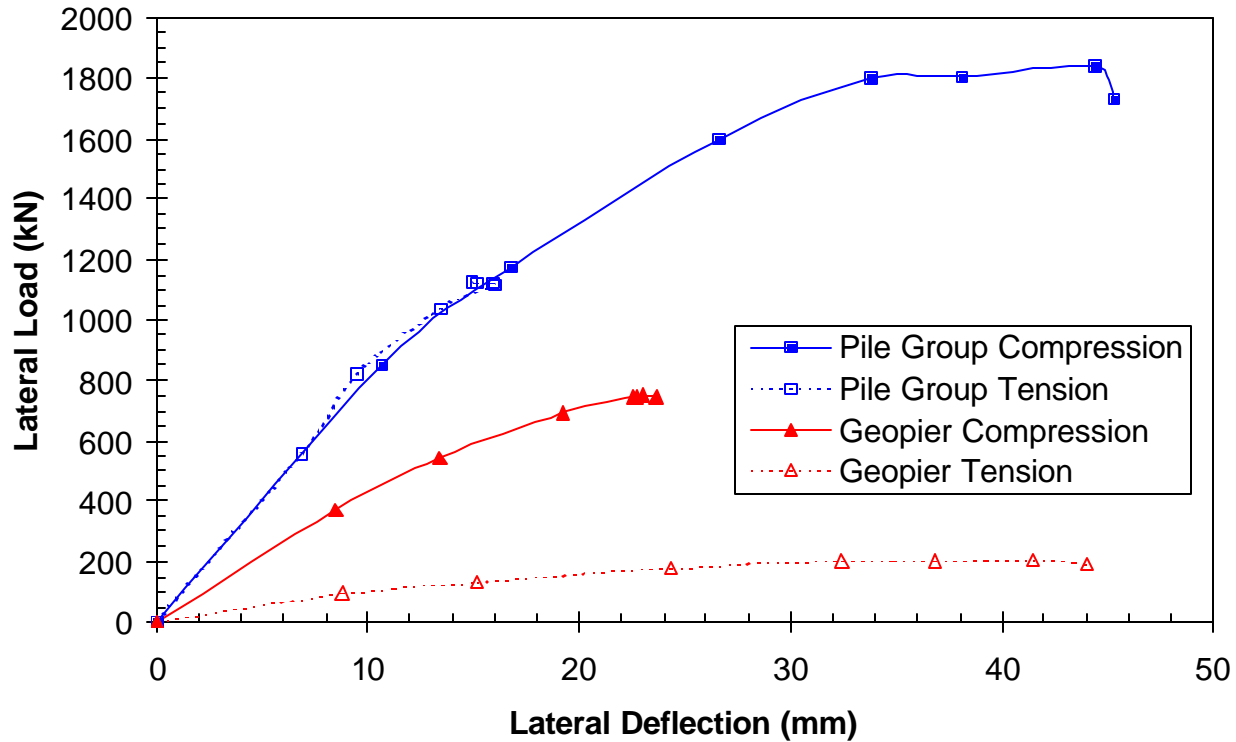
Figure 6.24 Comparison of load-deflection curves for fixed-head pile group and geopier foundations under tension and compression.

gravel increases, which in turn increases the frictional resistance. When the geopier is in tension, the normal stress decreases, which decreases the frictional resistance.

Even when the geopier was in compression the load versus deflection curve was still substantially softer than that for the pile group. Over the deflection range involved in these tests, the load carried by the pile group was typically about 100% higher than that for the geopier for a given deflection.

The load-deflection curves for the 12 pile group under both free-head and fixed-head conditions are presented in Figure 6.25. Even though the fixed-head test was performed after the free-head test when gaps had formed around the piles, the load for the fixed-head test was 40 to 50% higher than that for the free-head test at the same deflection. This result demonstrates the
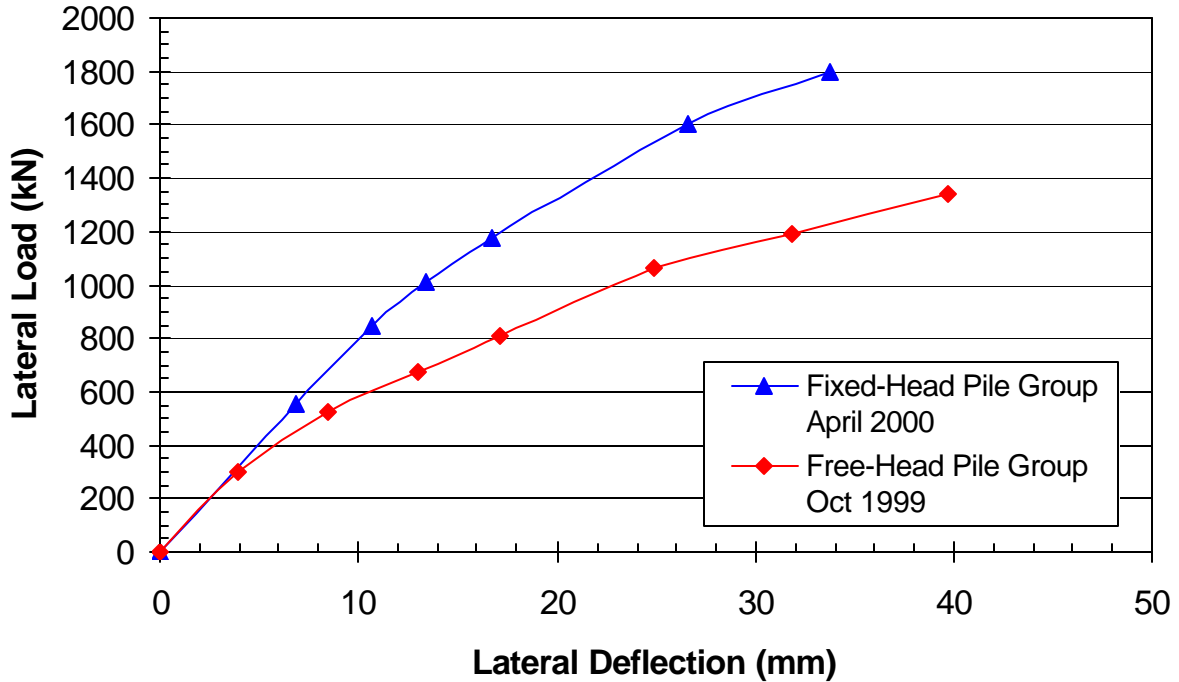
Figure 6.25 Comparison of the load versus deflection curves for the 12 pile group in the fixed- and free-head conditions.

increased structural stiffness provided when a pile cap enforces a relatively fixed-head boundary condition. The load-deflection curve for the fixed-head test is relatively linear for the load range involved but does become non-linear at the higher deflections. This suggests that much of the resistance at small deflections may have been provided by the structural element rather than the

soil. This is consistent with the fact that gaps had developed around the piles due to the previous free-head load test.

Lateral Test (September 2000). Measured lateral load versus deflection curves for the fixed-head pile group and the geopier group during the September 2000 lateral load tests are shown in Figure 6.26. Some of the unload cycles have been removed for the pile group to improve clarity. The results indicate that the load-deflection curve for the pile group is about three times stiffer than that for the geopier group for deflections less than 40 mm. At the maximum load level, the deflection of the geopier foundation was about 7.5 times greater than

that for the pile group. A comparison of the initial load-displacement curve for the geopier

shown in shown in Figure 6.23 with that in Figure 6.26 indicates that the stiffness has

significantly degraded with repeated load cycles. For example, at a deflection of 20 mm the

stiffness of the geopier is only about one-third of the stiffness measured during the initial load

cycle. The geopier load-deflection curve in Figure 6.26 also lies midway between the tension and

compression curves for the geopier shown in Figure 6.24. This again indicates the influence of

the normal force on the lateral resistance for the geopier foundation. In contrast, the load-

deflection curve for the fixed-head pile group during the lateral load test with no axial force is

nearly identical to the curve obtained during the bent test as shown in Figure 6.26.
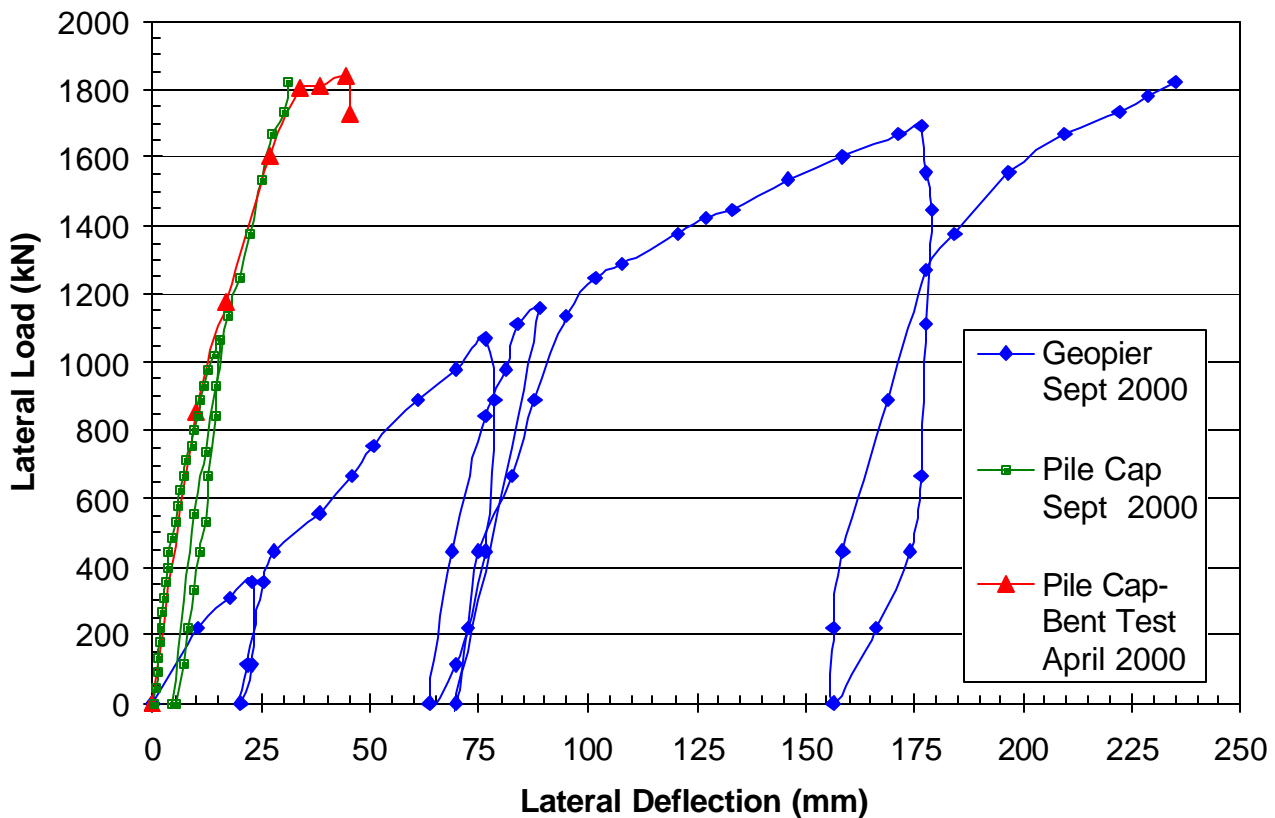
**Figure 6.26 Comparison of the load versus deflection curves from the bent test (April 2000) and the
lateral load test (September 2000) involving the geopier cap and pile cap.**

CHAPTER 7 STATIC LATERAL LOAD TESTS ON FIFTEEN-PILE GROUP AT 3.3 DIAMETER SPACING

INTRODUCTION

In order to quantify the pile-soil-pile interactions within a large pile group, static lateral load tests were performed on a 15-pile group. With row spacing at 3.3 pile diameters, group interaction effects were expected to be significant. Because this pile group also had five rows, the test also provided data on whether or not row loads continue to decrease when more than three rows are involved in a group of piles.

In the first lateral load test, the group was loaded toward the south using the adjacent geopier foundation cap as a reaction. Because the geopier cap was to be used as the footing for the load frame in the bent test described in Chapter 6, the deflection of the geopier cap had to be limited to about 50 mm or less. Unfortunately, this deflection limit was reached when the 15-pile group had deflected only 12.5 mm. Subsequently, dynamic load tests were carried out on the 15-pile group which moved the 15-pile group over 90 mm toward the south and precluded additional virgin static load testing in that direction.

Following the completion of the bent test, there were no restrictions on deflection of the geopier. Therefore, the geopier could be used as a reaction to load the 15-pile group in the opposite direction to the initial load test. Prior to conducting the test, a 2.5 m-high box was built on top of the geopier cap and filled with sand to increase the normal force on the cap and increase its lateral resistance. In addition, sand was back-filled behind the geopier cap to provide increased lateral resistance due to passive force on the cap.

TEST SETUP FOR VIRGIN LOADING (SOUTH DIRECTION)

The piles in the pile group had an outside diameter of 324 mm (12.75 in) and a wall thickness of 9.53 mm (0.375 in). The end of each pile was closed off by welding a 38.1 mm (1.5 in) thick circular steel plate to the bottom of the pile. The properties of the pipe piles were identical to that described for the single pile test in Chapter 4. The piles were driven to a depth of approximately 12 m (39 ft) which caused the soil in the interior of the group to heave approximately 0.15 to 0.2 m. The piles were driven in a 3x5 arrangement with five rows consisting of three piles in each row. The center-to-center spacing between each row and between piles within each row was 1.07 m (3.5 ft). The piles were driven of the 25th of August 1999. The middle row of piles was driven first, followed by rows of piles on the east side and the west sides. A steel-loading frame was designed to allow the simultaneous loading of all 15 piles. The stiffness of the frame relative to the pile-soil resistance was great enough that all the piles deflected the same amount. The frame and reaction beams were supported by lubricated steel wheels which ran on the web of a steel W section placed on the soil surface to minimize friction forces.

Static loads were applied with two 1.3 MN (150 ton) hydraulic jacks. The jacks were located on the opposite side of the reaction foundation from the pile group as shown in Figure 7.1. Steel swivel plates were placed between the loading jacks and the reaction foundation to minimize eccentricities in the load application. Load was transferred from the jacks to the loading frame via two W762mm x 848 N (W30in x 191 lb) reaction beams connected by eight 30.48 mm (1.2 in) diameter DYWIDAG bars. As the jacks pushed against the reaction foundation, and thus the reaction beam, the DYWIDAG bars were put in tension and the whole pile group was pulled towards the geopier reaction foundation. This arrangement was designed so that the subsequent
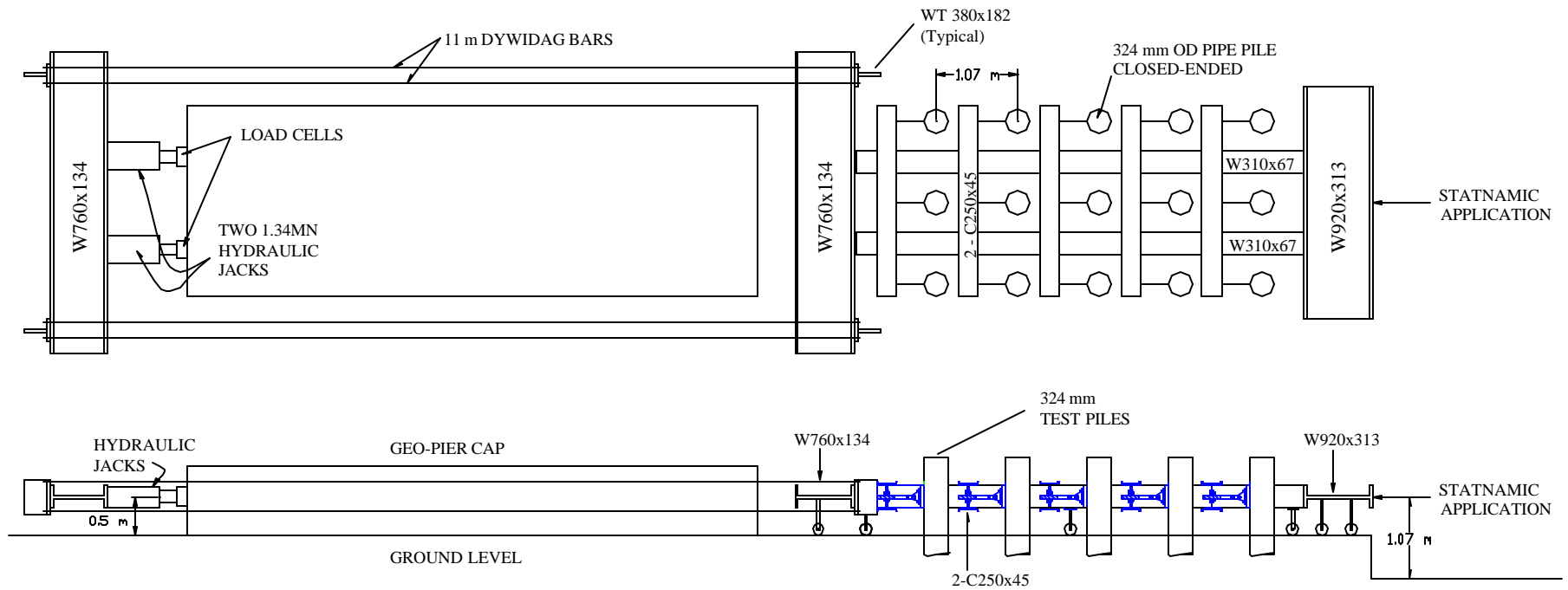
Figure 7.1: Plan and profile view of static test setup for 15-pile group during loading in virgin soil conditions.

Statnamic load applications, described in Chapter 11, would be in the same direction as the static load. Two photographs for the load set-up at the time of the test are shown in Figure 7.2.

Instrumentation

The center pile of each row was instrumented with strain gauges on both the tension and compression sides down the length of the pile. The gauges were located at 0.55 m (1.8 ft), 1.16 m (3.8 ft), 1.77 m (5.8 ft), 2.68 m (8.8 ft), 3.59 m (11.8 ft), 4.51 m (14.8 ft), 6.03 m (19.8 ft), 7.56 m (24.8 ft), and 9.08 m (29.8 ft) below the soil surface. The strain gauges were 120-ohm electrical resistance type gauges (model WFLA-6-120) manufactured by Texas Measurements, Inc. These gauges were coated in a waterproof wafer and the lead wires were also coated with a waterproof material. To protect the strain gauges during driving, a 5.08 mm (0.2 in) thick angle iron with 38.1 mm (1.5 in) legs was connected to the pile so as to cover the gauges. The angle iron was spot welded to the pile at intervals halfway between each strain gauge and extended 0.914 m (3 ft) below the last gauge. An expanding foam insulation was injected into the cavity over the strain gauges created by the angle iron through holes that had been drilled prior to welding. The foam helped to protect the gauges against shock damage during driving.

The piles were pin-connected to the loading frame using 50.8 mm (2 in) diameter solid steel tie rod/load cells as described for previous pile groups (see Figure 6.3). The tie rod/load cells were instrumented with two full-bridge strain gauges to measure loads taken by each individual pile, while eliminating any strain due to bending stresses.

Deflection was measured by eight linear variable displacement transducers (LVDT) placed on each pile of the front and back rows and on two other piles within the group. The LVDT rods were pin-connected to eyehole screws that were attached to brackets glued to the pile with epoxy. All LVDTs were placed at the load point, approximately 495.3 mm (19.5 in) above

Figure 7.2 Photographs of test setup for static lateral load tests on 15 pile group; (a) test pile group with statnamic rocket and (b) hydraulic jacks reacting against geopier cap.

the ground surface. The LVDT housings were clamped to an independent reference frame. The deflections measured by all the LVDTs were averaged together to obtain a single value of group deflection.

An Optim Megadac 5414AC version 7.0.0 data acquisition system was used to record data throughout the testing. During this test, the system utilized 90 data channels for strain gauges, 17 channels for load cells, and 8 LVDT channels recording at a rate of 1 sample per second. A gasoline generator provided power for the data acquisition system. A UPS device was used to condition the power supply and provide a temporary backup supply.

Procedure

The loading procedure was designed to bring the pile group to a target deflection. Once a target deflection was achieved, cycles of corresponding load were applied and the group response was recorded. Fifteen single amplitude cycles were applied to the group at target deflections of 6.35 mm (0.25 in) and 12.7 mm (0.50 in). During the course of the test, a single LVDT was monitored to determine when the target deflection had been reached. The plan was to systematically bring the group deflection up to 76 mm (3 in) in increments of 12.7 mm (0.5 in). However, once the pile group had reached the 12.7 mm target deflection the reaction foundation had been displaced approximately 50.8 mm. This was an unexpected problem that could not have been foreseen. The geopier foundation had previously provided approximately twice as much resistance at this displacement.

Testing of the pile group commenced on December 4, 1999. At that time the pile group received one load cycle at the 6.35 mm (0.25 in) deflection increment. This allowed approximately three months for excess pore pressures to dissipate. Data acquisition problems halted additional testing until December 7th.

Test Results

Load-Deflection

The pile group was subjected to a peak load of 756 kN (170 kips), as measured by the tie rod/load cells during the first cycle of the 12.7 mm (0.50 in) deflection increment. This resulted in a 12.7 mm (0.50 in) average deflection of the entire pile group as measured by the load point LVDTs. The results of the first and last cycles of each deflection increment for the entire group are shown in Figure 7.3. The average load per pile for the group was determined by summing the tie rod/load cell readings and dividing by the number of piles in the group. The pile group deflected approximately 1.6 times as much as the single pile at the same average load.

The reduction in soil strength as a result of the cyclic loading was approximately 4% for the 6.35 mm deflection increment and rose to over 15% for the 12.7 mm. It is estimated that if the pile group deflection had been able to proceed to the maximum target value this strength reduction trend would have continued. This reduction in strength due to cycling is consistent with the findings of earlier full scale load testing (Brown et al., 1988). Figures 7.4 and 7.5 provide plots of the average load in the group rows compared with the single pile for the 1st and 15th cycles at each deflection increment. Trailing rows for the first cycle carry a very similar percentage of the total load. This may be due to the fact that the failure zones in the soil are just beginning to form. After the fifteenth cycle, the load distribution shows more variation and group effects are more evident. As observed in other full-scale lateral load tests (Rollins et al,1998) and in centrifuge testing (Kotthaus et al, 1994 and McVay et al, 1998) the percentage of load carried by a row declines from the front to the back rows with the exception of the back which showed an increase, especially at the higher deflection.
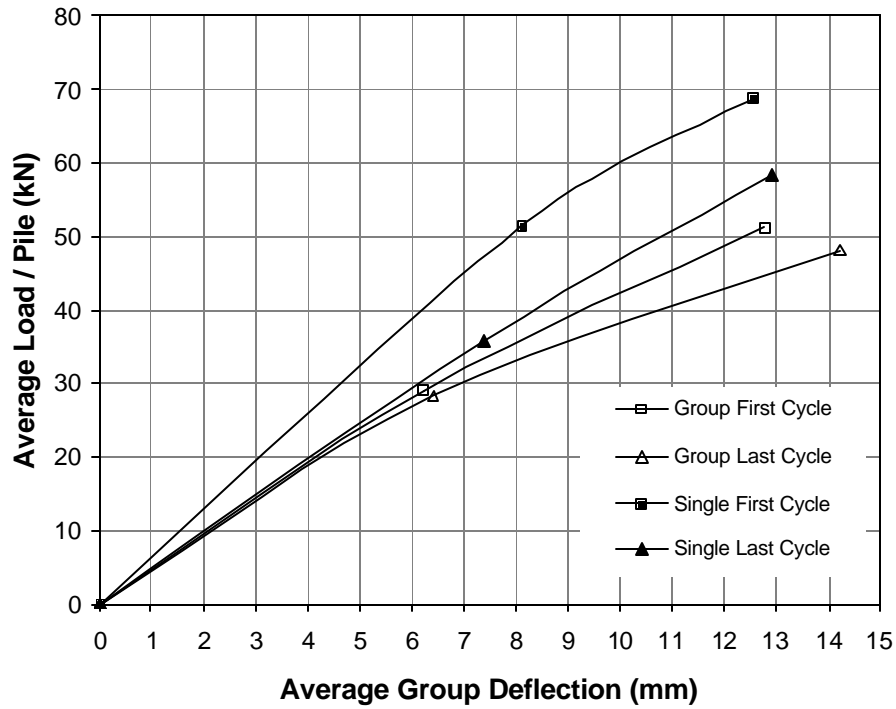
Figure 7.3 Comparison of load-deflection curves for the pile group to that for the single pile for the first and last cycles of loading.
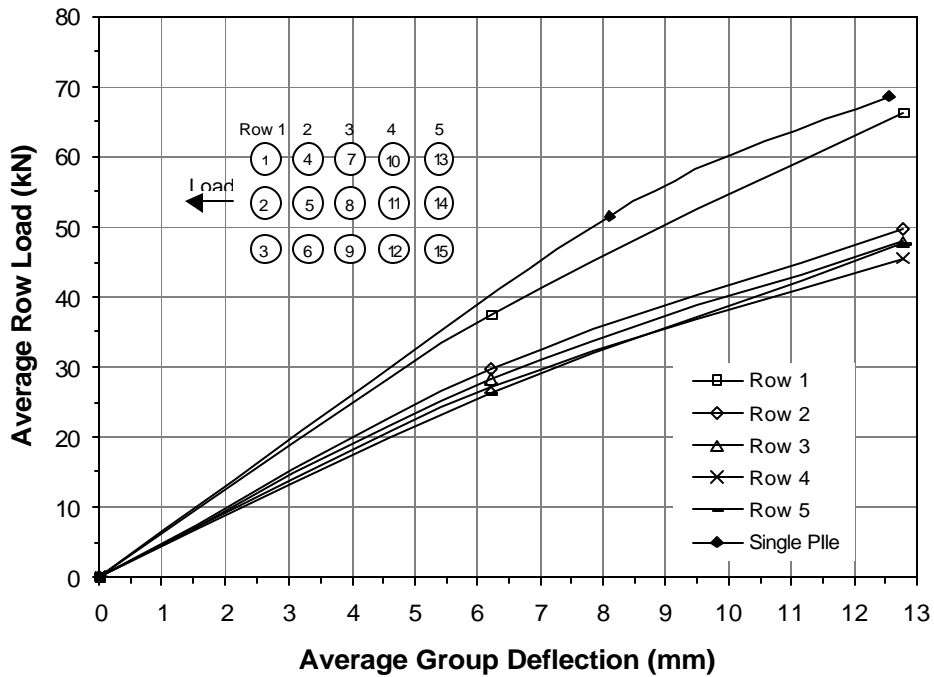
**Figure 7.4 Comparison of average row load vs deflection for the pile group relative to the single pile during the first deflection cycle.**

By cycling the load, the stiffness of the soil in the direction of the load is increased by compaction. This also causes the formation of gaps between the soil and the pile. The total effect is a reduction in the load required to achieve the same deflection because resistance is initially provided by the pile alone before the stiffened soil is encountered. In an attempt to quantify this reduction in overall stiffness as a result of gap formation, the normalized pile stiffness was calculated using the following formula

$$\frac{K_n}{K_i} = \frac{\left(\dfrac{\Delta F}{\Delta L}\right)_n}{\left(\dfrac{\Delta F}{\Delta L}\right)_i} \tag{7.1}$$

where

$$\left(\frac{\Delta F}{\Delta L}\right)_n = \text{change in load for } n^{th} \text{ cycle / change in deflection for the } n^{th} \text{ cycle}$$

$$\left(\frac{\Delta F}{\Delta L}\right)_i = \text{change in load for the initial cycle / change in deflection for the initial cycle}$$

The results of these calculations were plotted and then a curve was fitted to approximate the trend as shown in Figure 7.6. The general trend on the graph is for the stiffness of the pile to decrease as the number of load cycles increases, eventually leveling off. This trend is harder to distinguish at the 6.35 mm deflection increment with a decrease of only about 4%. At the 12.7 mm increment the stiffness decreased by 15% between the first and fifteenth cycles. There was a considerable amount of variation in the 6.35 mm results as can be seen from the R^2 value for the 3rd order polynomial equation used to approximate the results. These fluctuations could be due
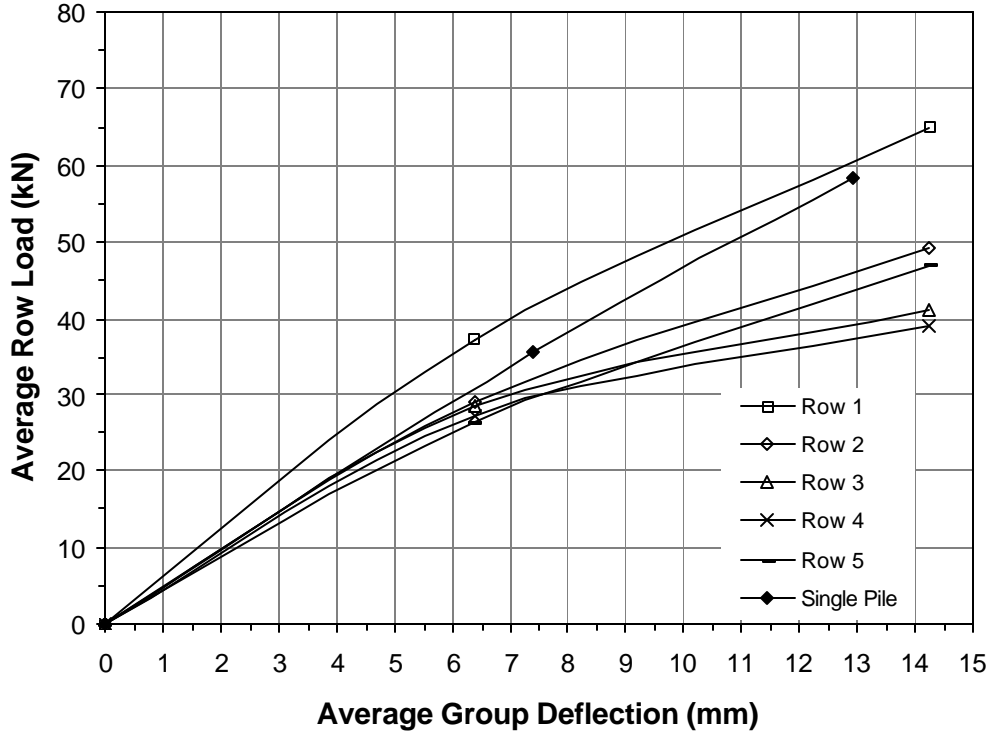
Figure 7.5 Comparison of average row load versus deflection for the pile group relative to that for the single pile for the fifteenth deflection cycle.
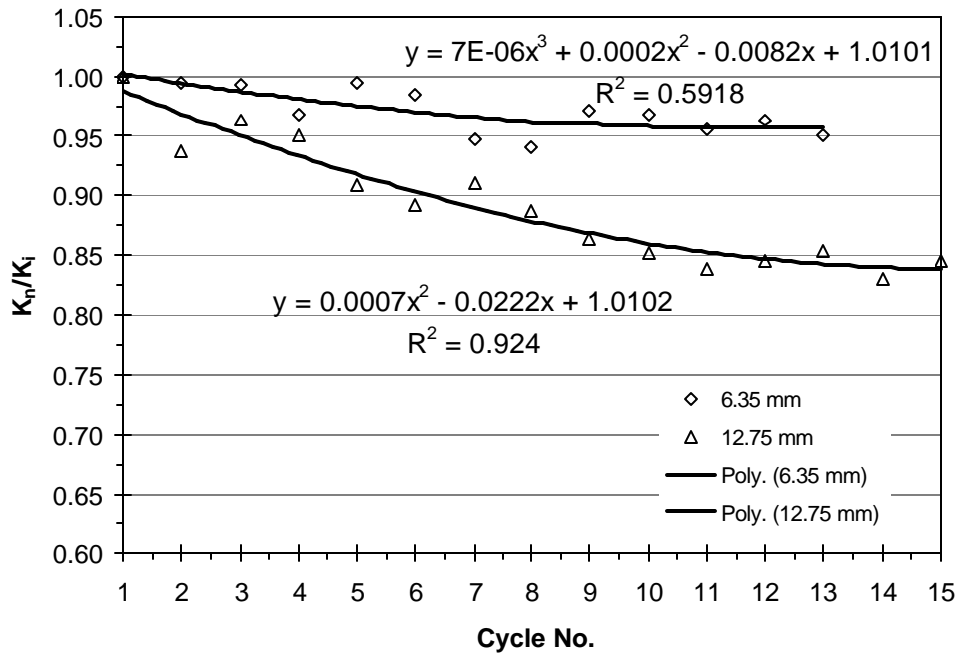
Figure 7.6 Reduction in normalized soil-pile stiffness as a result of cyclic loading.
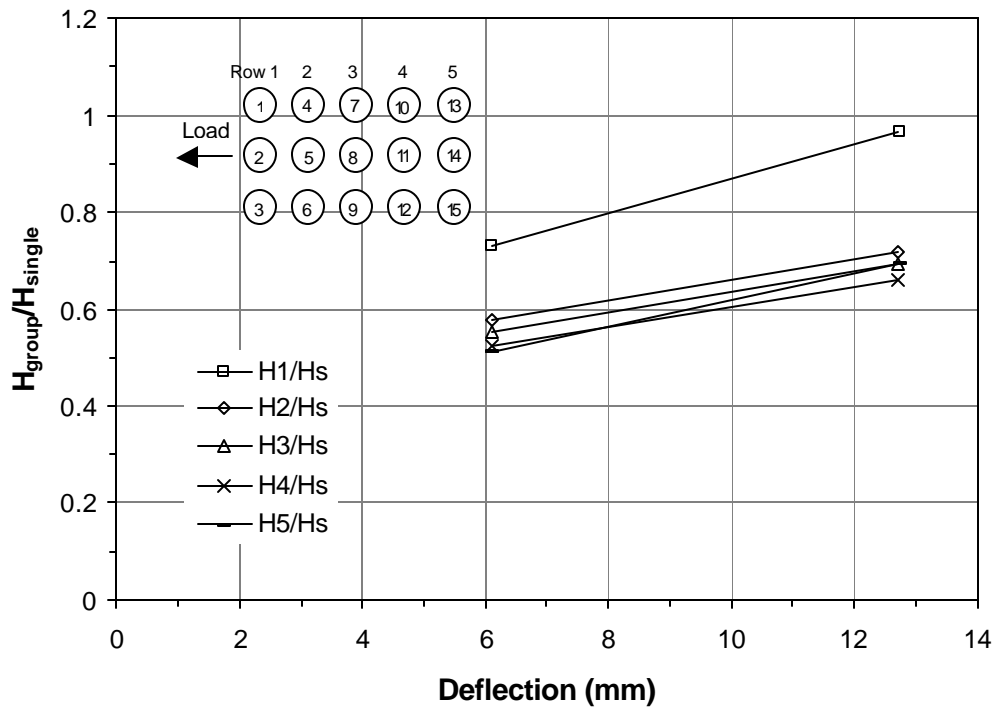
Figure 7.7 Ratio of average load carried by each row in the group relative to that carried by the single pile at the same deflection level.

to local variations in soil properties and variations in gap widths around the piles that were created during driving.

Ratios of the loads carried by individual rows of the pile group during the first cycle of each deflection increment to that of the single pile are shown in Figure 7.7. The front row carried an average of 85% percent of the single pile load between the two deflections. The trailing rows carried a lower, and very similar percentage of the single pile load. The averages of the four trailing rows were 65%, 62%, 59%, and 60% for rows 2 through 5 respectively.

Elastic theory predicts that outer piles in a row should carry a higher percentage of the load than pile(s) in the middle of a row at a given deflection. However, this prediction is not consistent with field test results reported by Brown et al (1988) and Rollins et al (1998).

The results from this test are also inconsistent with elastic theory predictions. The load-deflection curves for the three piles in the first, third, and fifth rows are presented in Figure 7.8 and are representative of load distribution within the entire group. As shown in Figure 7.8, there is no discernable pattern to the load distribution in a given row.

Bending Moment vs. Depth

The bending moments developed in the piles during the static load testing were calculated from the data provided by the strain gauges attached to the piles. Calculations and equations used were described in Chapter 4. Moment versus depth curves are plotted in Figure 7.9 for each row in the pile group. Data for these curves were taken at the time of maximum load during the first cycle of each deflection increment. Each row is plotted separately and the moment differences from the first cycle of the two deflection increments are compared. The maximum bending moment occurred approximately 1.7 m (5.6 ft), or 5.3 pile diameters, below the excavated surface for each row. This is approximately equal to the depth at which the maximum moments occurred in the single pile, accounting for slight differences in the elevation of the strain gauge.

The largest moment developed in Row 1 (45.5 kN m) followed by Rows 5, 2, 3, and 4. This result seems to be inconsistent with the load distribution curves. Presumably, group effects caused a softening of the soil and thus allowed the trailing row to develop a moment higher than the moment in the second row, which carried a larger load. For the 6.35 mm (0.25 in) deflection increment, the moments approached zero at a depth of 4.5 m (14.8 ft). At the 12.7 mm (0.50 in) increment, with the exception of the front row, the moments approached zero at a depth of 6 m (19.7 ft) as shown in Figure 7.9.
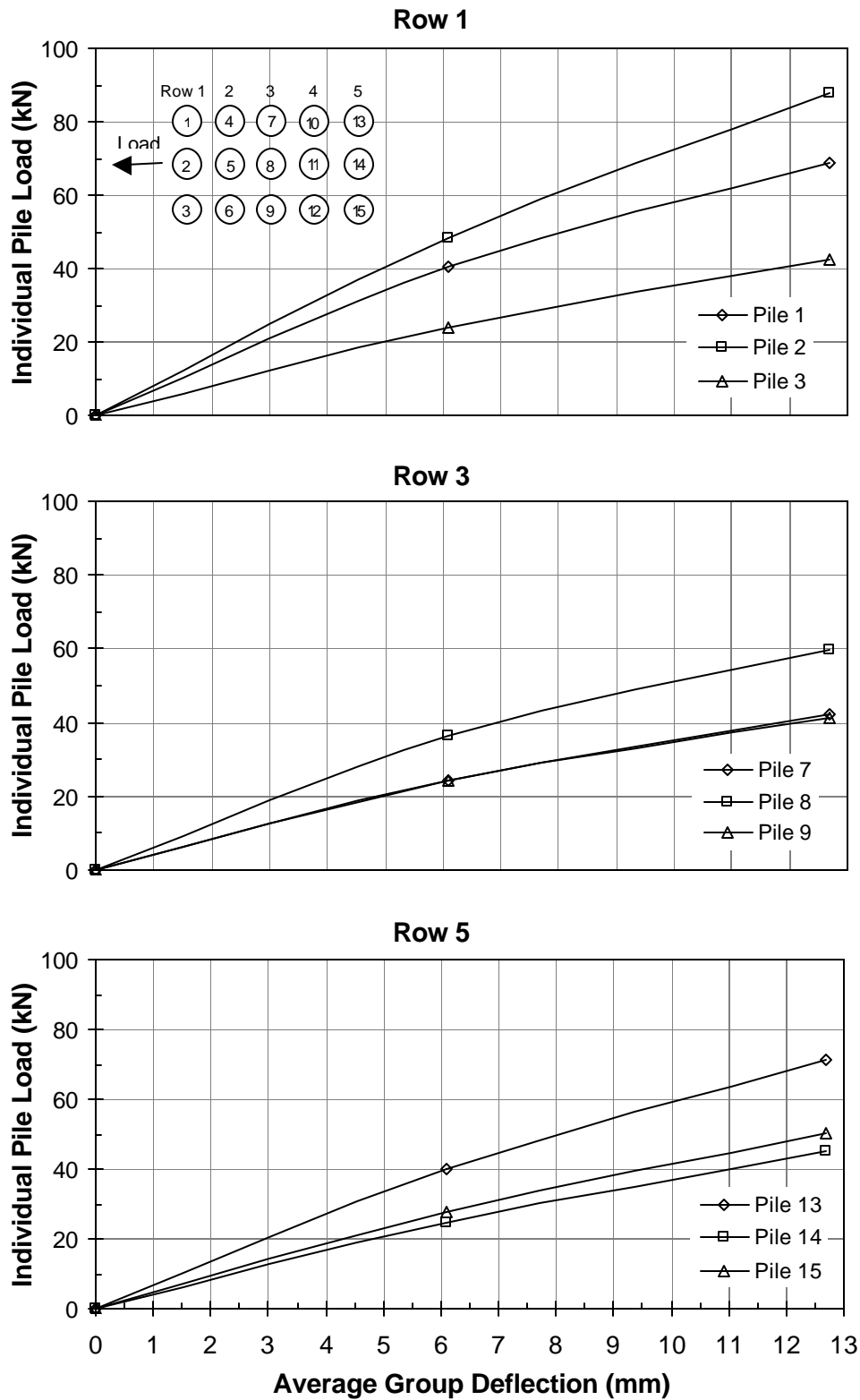
Figure 7.8 Load vs. deflection curves for individual piles within rows 1, 3, and 5 of the pile group.
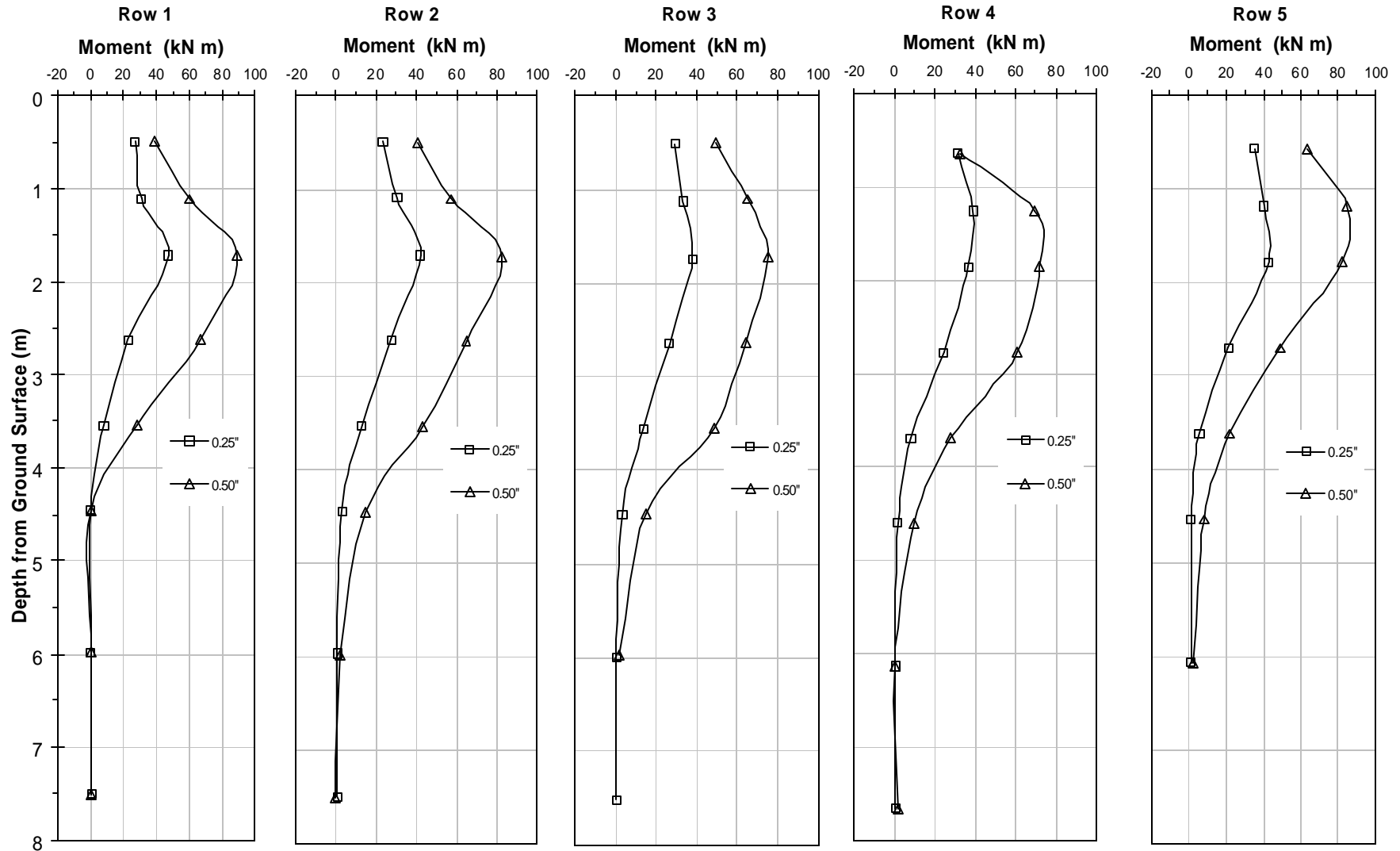
Figure 7.9 Bending moment versus depth curves for one pile in each row of the 15 pile group.

7-14

Figure 7.10 compares the moment vs. depth curve for the single pile at two pile head deflections with similar curves for a pile in each row of the pile group. For the first deflection increment, the maximum moment for piles in the group is much lower than that for single pile. This could be a result of densification due to the pile driving or just due to minor local soil variations at this small deflection level. For the second deflection increment, group effects begin to control pile response and the moments increase. For this increment rows 1, 2, and 5 have higher maximum moments than the single pile (15, 11, and 9% higher, respectively) while the remaining rows are slightly lower (about 4%) than the single pile. The bending moment for the single pile also appears to drop off more rapidly with depth than it does for piles in the group.

Maximum Moment versus Load

Maximum bending moment vs. the average load per pile for the first and last cycle of loading are shown in Figure 7.11 along with the respective single pile curves. The average pile load was obtained by summing the total group load from the tie rod/load cells and dividing by the number of piles. At similar loads, the moments in each row of the group are higher than that of the single pile. The front row moment is approximately 27% higher. For the last cycle of each deflection increment, the group effects are more evident. The moments in the group piles remain essentially the same for a given deflection, but the moments occur at a lower load while the single pile requires an increased load to achieve the same moment.

Figure 7.12 depicts the maximum moments as a function of the average load for each row in the group (i.e. the sum of the load cells in the row divided by the number of piles in the row). Again, the first and last cycles are shown on separate charts. The trailing rows clearly have higher moments at the same loads than the leading row. The moment in row five is

approximately 38% higher than the front row at a load of 47 kN (10.6 kips). Group effects again control row response by softening the soil.
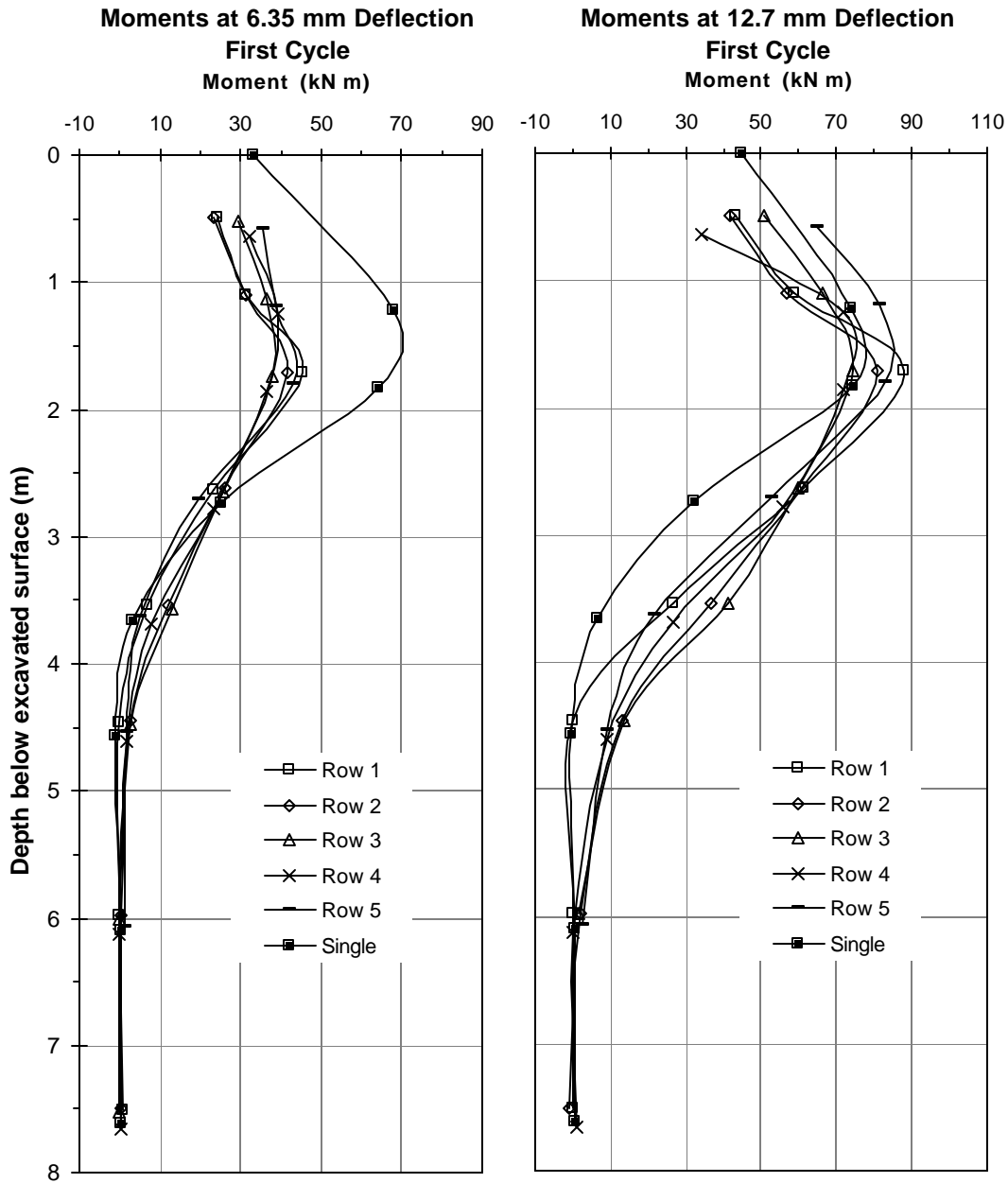
Figure 7.10 Group row and single pile moments vs. depth.
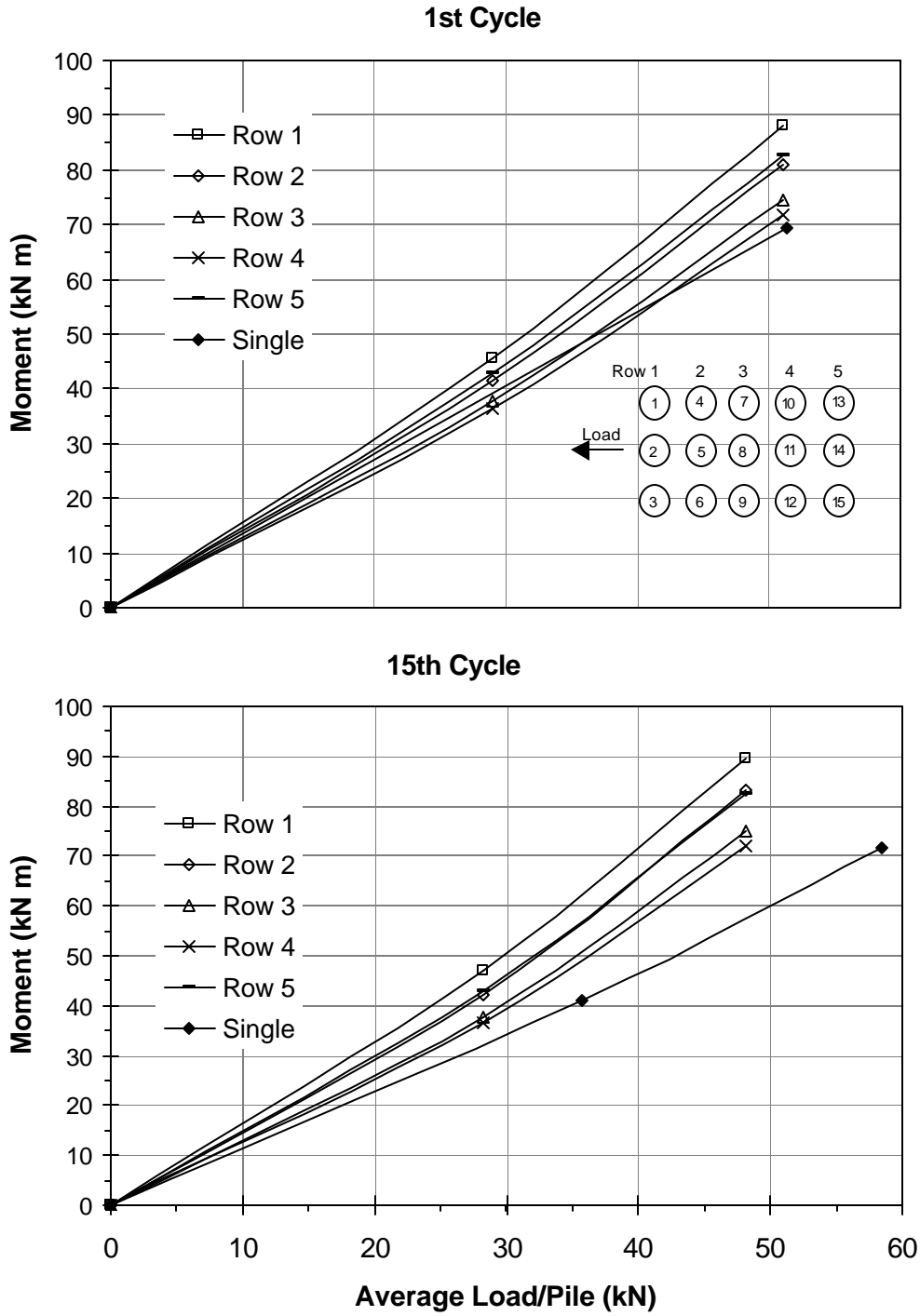
Figure 7.11 Curves showing the maximum moment versus average load for the single pile and one pile in each row of the group for the first and fifteenth load cycles.
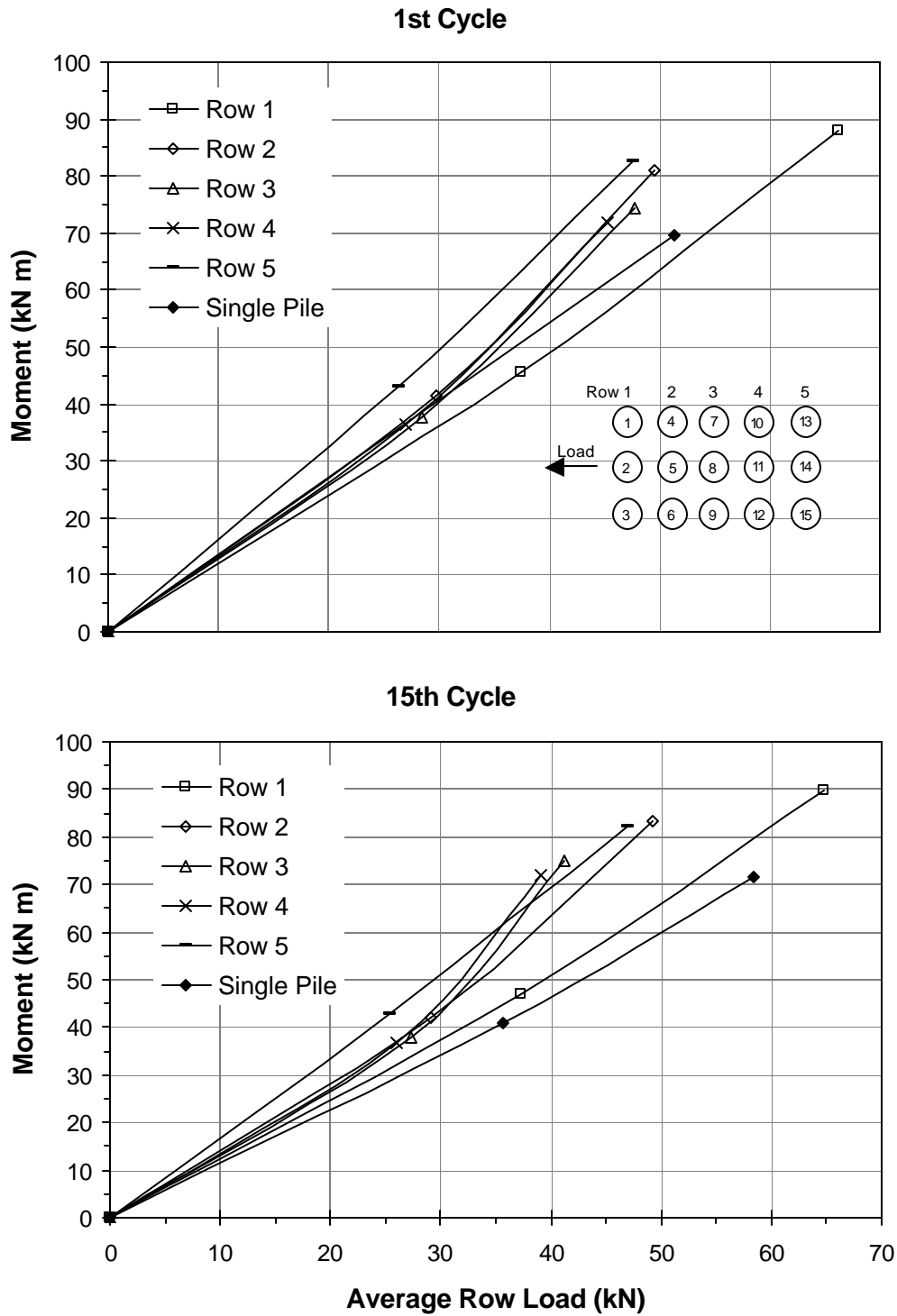
Figure 7.12 Maximum moment versus average pile load in each row of the group along with the moment versus load curve for a single pile during the first and fifteenth cycles.

TEST SETUP FOR RE-LOADING (NORTH DIRECTION)

The test setup for the re-loading of the 15-pile group in the north direction is shown in Figure 7.13 and a photo of the set-up is provided in Figure 7.14. Two 1.3 MN hydraulic jacks were placed between the load frame and the adjacent geopier footing which was used as a reaction as described previously. The jacks were attached to a manifold system so that the load applied by each jack was approximately equal. Steel swivel plates were placed between the jacks and the reaction foundation to minimize eccentricities in the load application. The load was applied at a height of 495 mm (19.5 in) above the ground surface.

Instrumentation

The instrumentation used for the re-load test was identical to that for the first load test with one exception. Instead of using eight LVDTs to monitor deflection, each of the fifteen piles was instrumented with a string potentiometer at the elevation of the load point. The string pots were attached to an independent reference frame. These string pots provided greater accuracy at the higher deflection levels when the rods in the LVDT sometimes had the potential to bind due to the rotation of the pile head.

During this test, the tie-rod load cells attached to each pile were loaded in compression rather than tension. For the load levels involved, this did not cause any problems with buckling and the sum of the loads measured by the tie-rods was usually close to that measured by the two load cells attached to the hydraulic jacks.

Procedure

The load procedure was designed to bring the pile group to a series of target deflections. Once a target deflection was achieved, 14 additional cycles were applied at that same deflection level and then deflection was increased to the next level. The target deflections for this
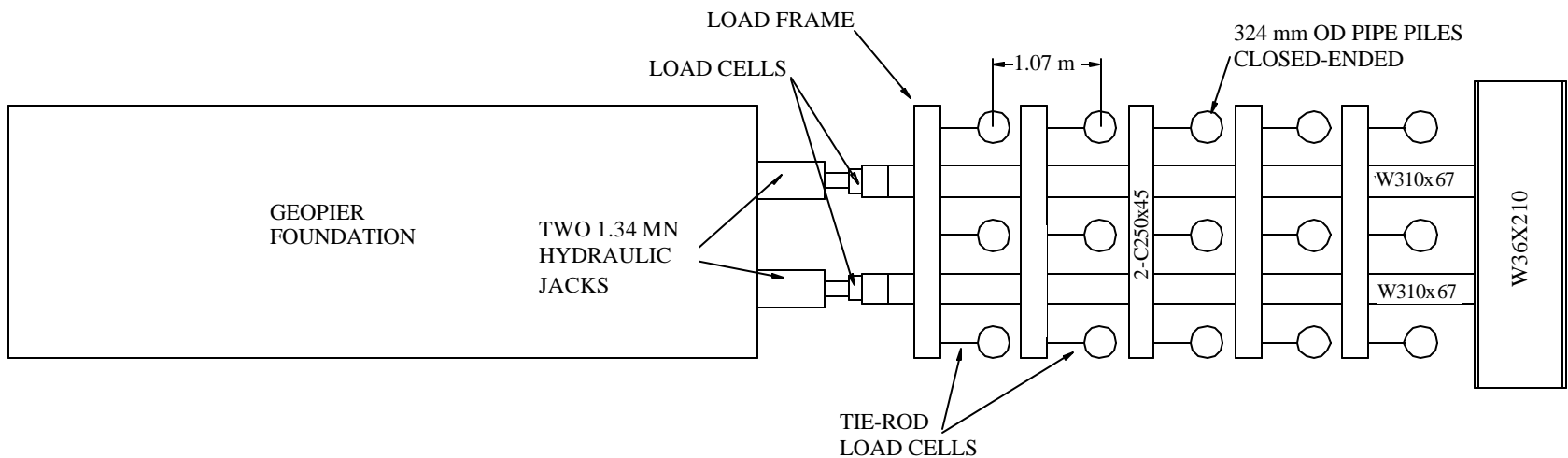
Figure 7.13 Schematic plan view drawing of setup for re-load test of 15-pile group in direction opposite to the statnamic loading.

Figure 7.14 Photograph of setup for re-load test of 15-pile group in direction opposite to the statnamic.

test were 3.1, 6.4, 12.7, 19.l, 25.4, 38.1, 50.8, 63.5, 76.2, and 88.9 mm (0.125, 0.25, 0.50, 0.75, 1.0, 1.5, 2.0, 2.5, 3.0 and 3.5 inches). The re-load test was performed on September 26, 2000.

Test Results

Load-Deflection

The average load versus deflection curve for the re-loaded pile group is shown in Figure 7.15 along with the reloaded single pile curve. Comparisons for this test were made with the reloaded single pile because it matched the loading history for the pile group. The average load in this case is the total group load divided by the 15 piles in the group. The two curves are fairly close to one another until the deflection exceeds about 10 mm. Beyond this deflection, the curves diverge substantially and at the ultimate deflection of about 90 mm the average load on the single pile is 50% higher than that for the average group pile. The reduction in lateral resistance is a result of group interaction effects within this closely spaced pile group.
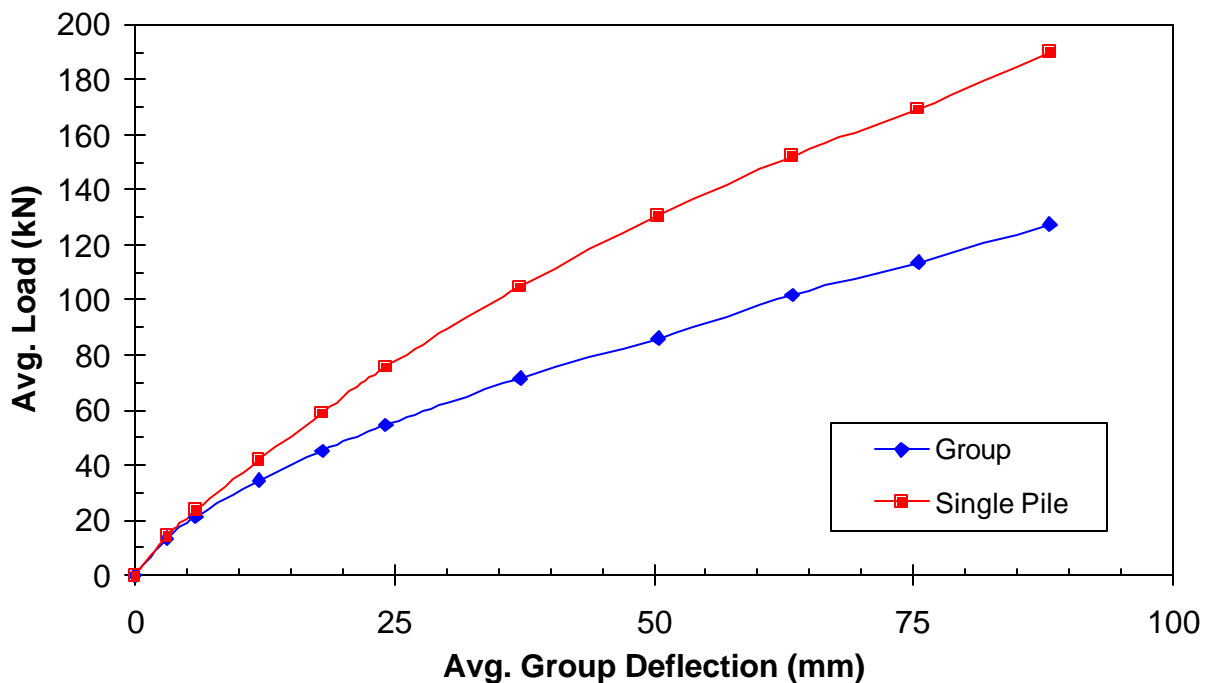
Figure 7.15 Comparison of average load-deflection curves for single pile and pile group.

Figure 7.16 shows the load-deflection curves for the left, middle and right piles in each of the five rows in the group. In this case, row 1 is the front or leading row and row 5 is the back row. This is reversed from the virgin loading case. Although the load carried by each pile within a row is not generally equal, the variation is typically less than about 15% of the average. There is no consistent pattern of load distribution within a row. For example, in three rows the middle pile carries the highest load, in one row it carries the lowest load, and in another row it carries a load between that carried by the left and right piles. This result is consistent with observations from previous full-scale lateral pile group load tests. The fact that the middle piles do not consistently carry lower loads than the exterior piles, as predicted by the elastic theory, could be attributable to strength increases in the interior of the group due to pile driving effects. However, there is presently no physical evidence to support this contention.

A review of the load-deflection curves in Figure 7.16 indicates that the load carrying capacity in the group is a function of the row number. Figure 7.17 shows the average load-deflection curves for each row in the group. In this case, the average load is the sum of the measured load in each pile divided by three. The load-deflection curve for the leading row or front row piles (row 1) is close to, but somewhat less than, that for the single pile. The curves for the second and third row piles drop progressively lower, but the curve for the fourth row is about the same as that for the third row. The load-deflection curve for the fifth or back row piles is initially higher than that for the third and fourth row piles but then becomes about the same at deflections greater than about 50 mm.

These results suggest that group reduction effects for additional rows of piles in a group will not be significantly different than those observed for the third row in the group. In fact, the back row of piles may even carry a somewhat higher load than the other trailing rows. These
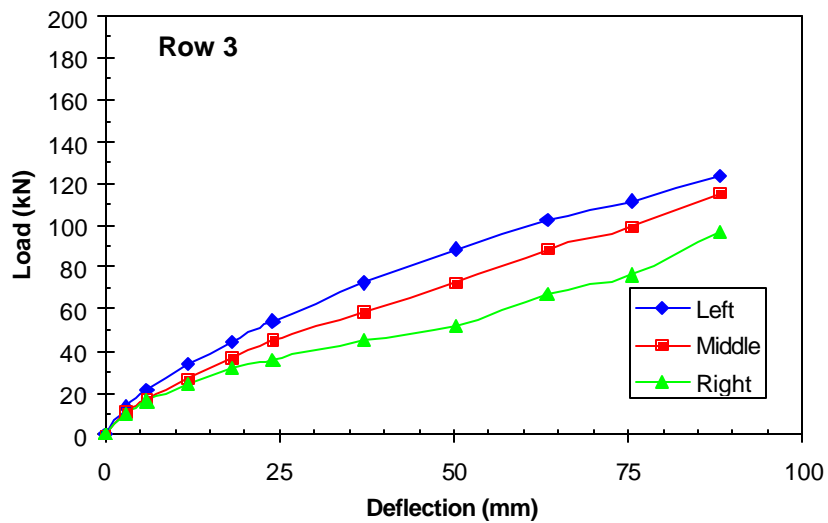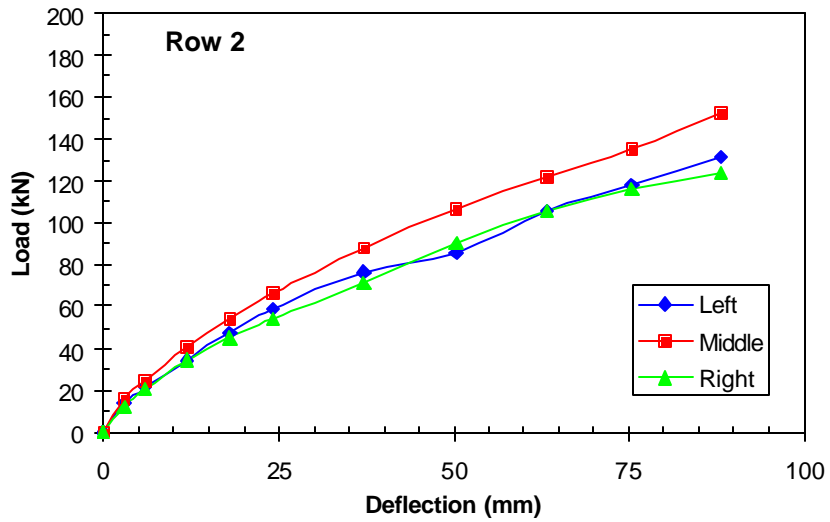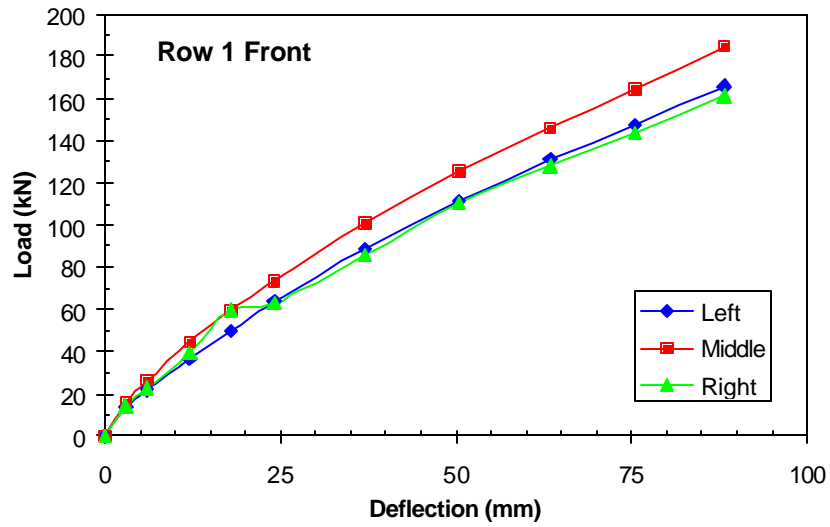
Figure 7.16 Load-deflection curves for left, middle and right piles in each row of group.
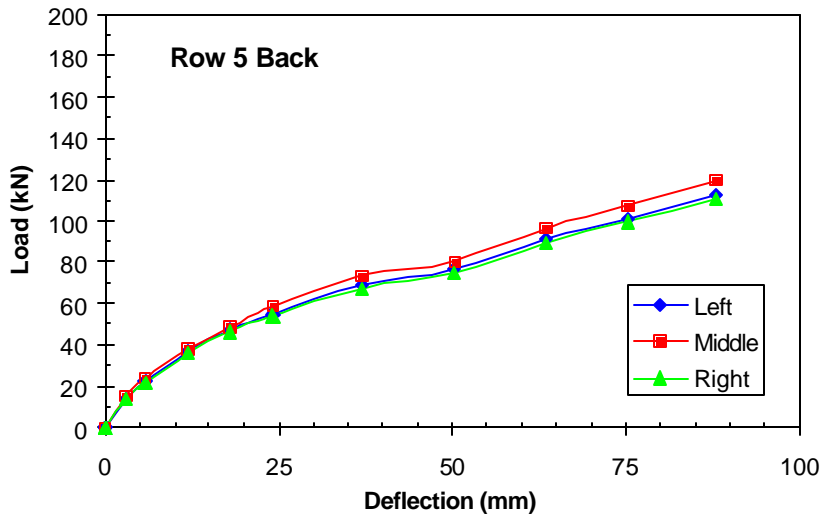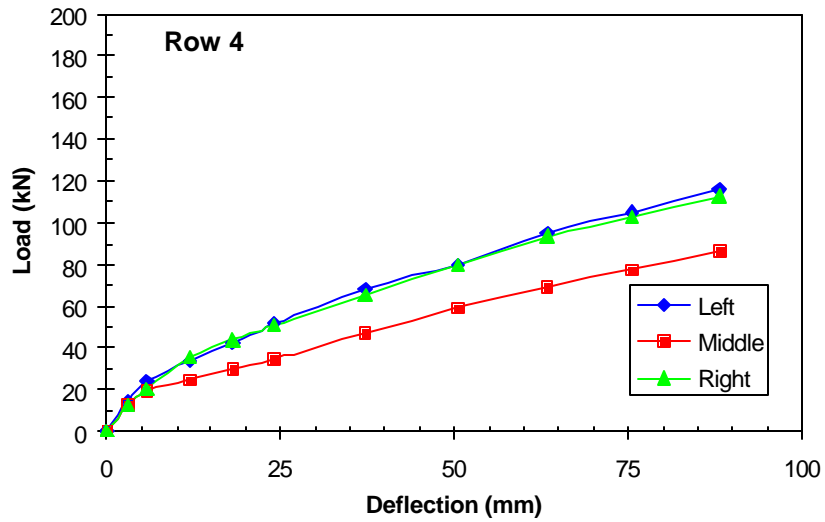
Figure 7.16 (continued) Load-deflection curves for left, middle, and right piles in each row of the group.
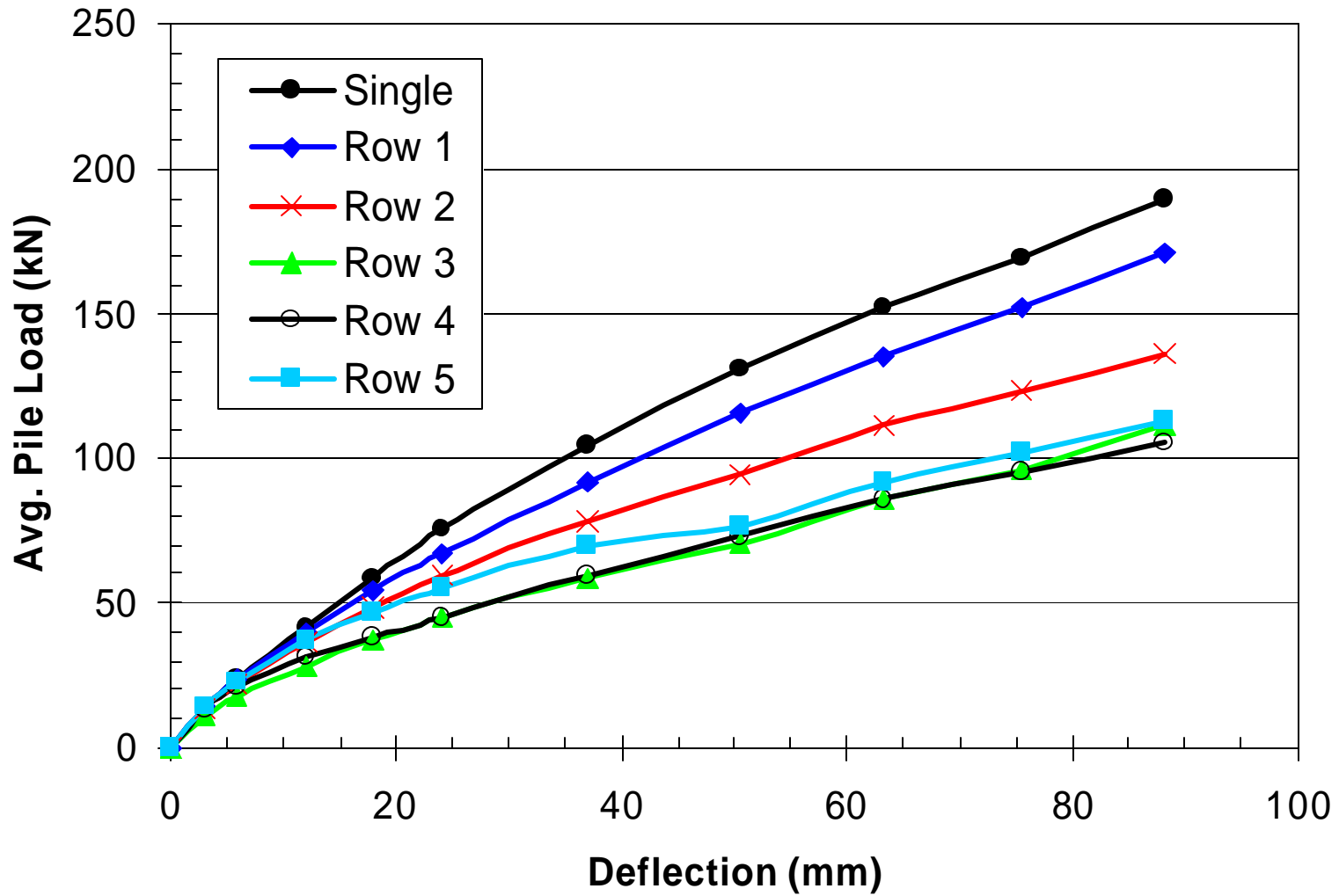
Figure 7.17 Average load-deflection curves for each row in the pile group relative to the single pile.
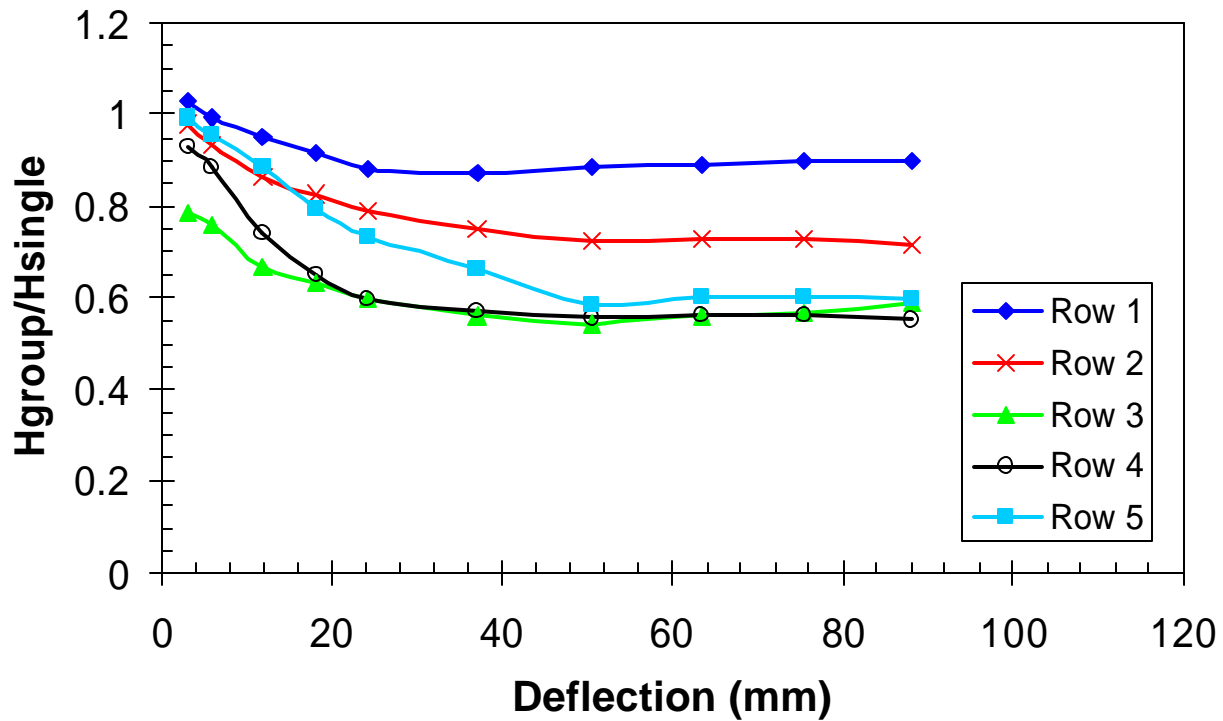
Figure 7.18 Load in each row of the pile group normalized by the load in the single pile at the same deflection

.

observations are consistent with results from the testing of the four row (12 pile) group discussed

in Chapter 6 and with results from centrifuge tests on larger pile groups (Kotthaus et al, 1994;

McVay et al, 1998).

Figure 7.18 shows the ratios of the average load carried by a pile in each row to the load

carried by a single pile at the same deflection. Generally, the ratios for each row decline until a

deflection of about 25 mm is reached, at which point they remain relatively constant. However,

the ratio for the fifth row continued to decline up to a deflection of 50 mm. These deflection

levels are somewhat greater than what was observed for the pile groups during the virgin load

tests and are likely due to the fact that more movement is required to fully engage the soil around

the pile due to the presence of gaps. The average ratio of the five rows after stabilization was

0.89, 0.74, 0.57, 0.57, and 0.63 for rows 1 through 5, respectively.

Bending Moment vs. Load.

The maximum bending moment versus load curves for the five rows in the group are shown in Figure 7.19 along with the curve for the 15th cycle of the single pile. The maximum moment is the largest moment along the length of the pile and the load is the average load for the three piles in a row. The curve for the front or leading row (row 1) is about the same as that for the single pile as is the curve for the second row. The curves for the third, fourth and eventually the fifth row piles are higher than those for the single or lead row piles primarily as a result of group effects which soften the soil response and lead to greater bending at a given pile head load.
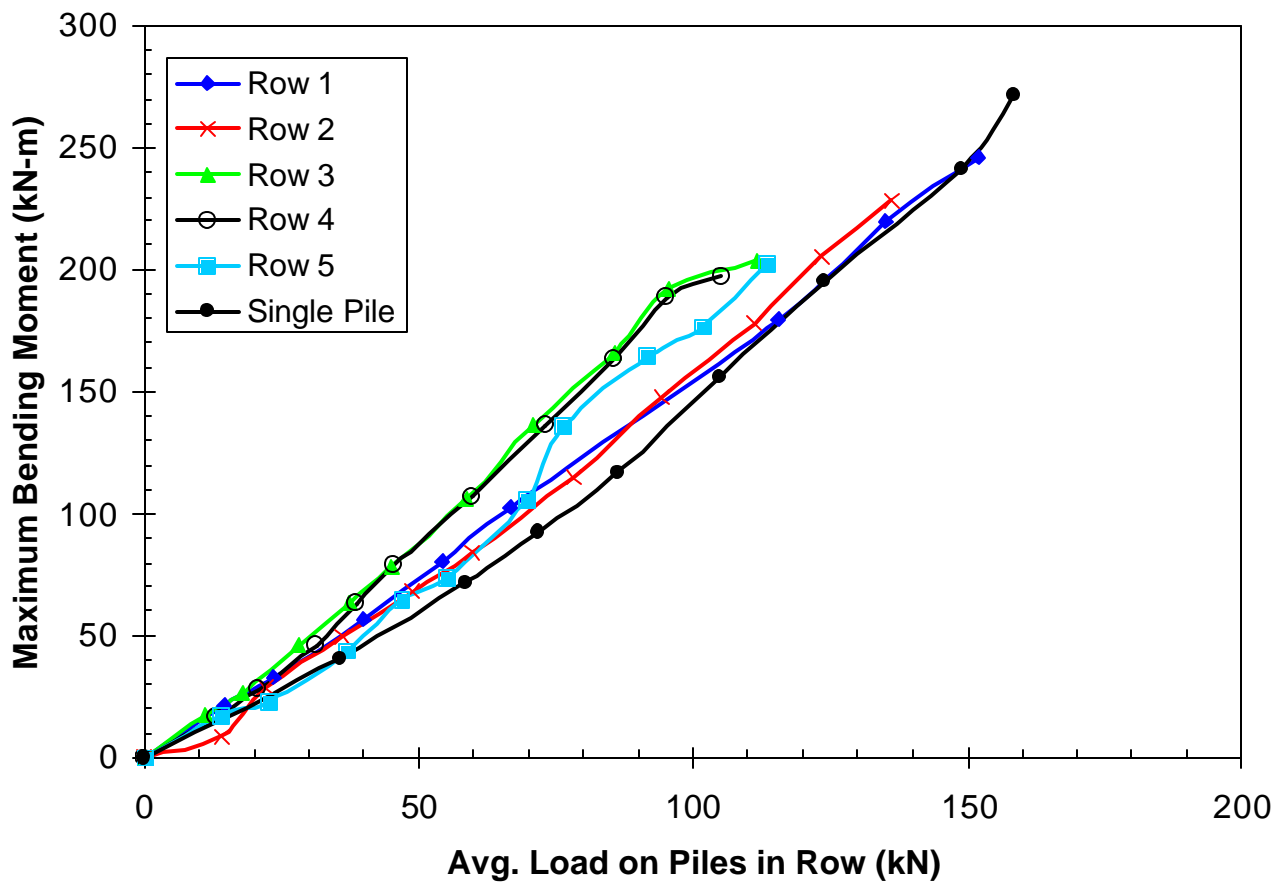
Figure 7.19 Maximum bending moment versus average pile load for each row in the 15 pile group.

Bending Moment vs. Depth

Bending moment versus depth curves for the instrumented piles in each row in the group are presented in Figure 7.20. Curves are shown for a series of maximum deflection levels. Because the re-test was performed over a year after the piles were driven, some of the strain gauges were no longer functioning properly. For example, the strain gauges for the pile in row 5 were not functioning at the two locations near the maximum. Nevertheless, reasonable bending moment vs. depth curves could be obtained for most of the rows. In most cases, the maximum moment occurred at a depth of 1.89 m below the excavated ground surface, which is approximately 6.3 pile diameters. This depth is similar to what was observed for the other tests on the groups with 324 mm piles. However, there does appear to be some tendency for the maximum moment to occur at slightly greater depths for the trailing row piles. In addition, the moments for the trailing row piles are somewhat higher than for the lead row pile at greater depths.

A comparison of the bending moment versus depth curves for each row in the group relative to that for the 15th cycle of the single pile at four deflection levels is presented in Figure 7.21. In each case, the single pile curve has a higher maximum than the piles in the group at the same deflection. This occurs because group effects soften the soil resistance for piles in the group. Therefore, the piles in the group develop the same deflection as the single pile at lower load levels. Because the load level is smaller, the maximum bending moments for piles in the group are also smaller than that for the single pile at the same deflection. In summary, softening due to group interaction leads to higher bending moments in the group piles relative to the single pile for the same <u>load</u> level. Group interaction effects also lead to lower bending moments in the group piles relative to the single pile for the same <u>deflection</u> level.
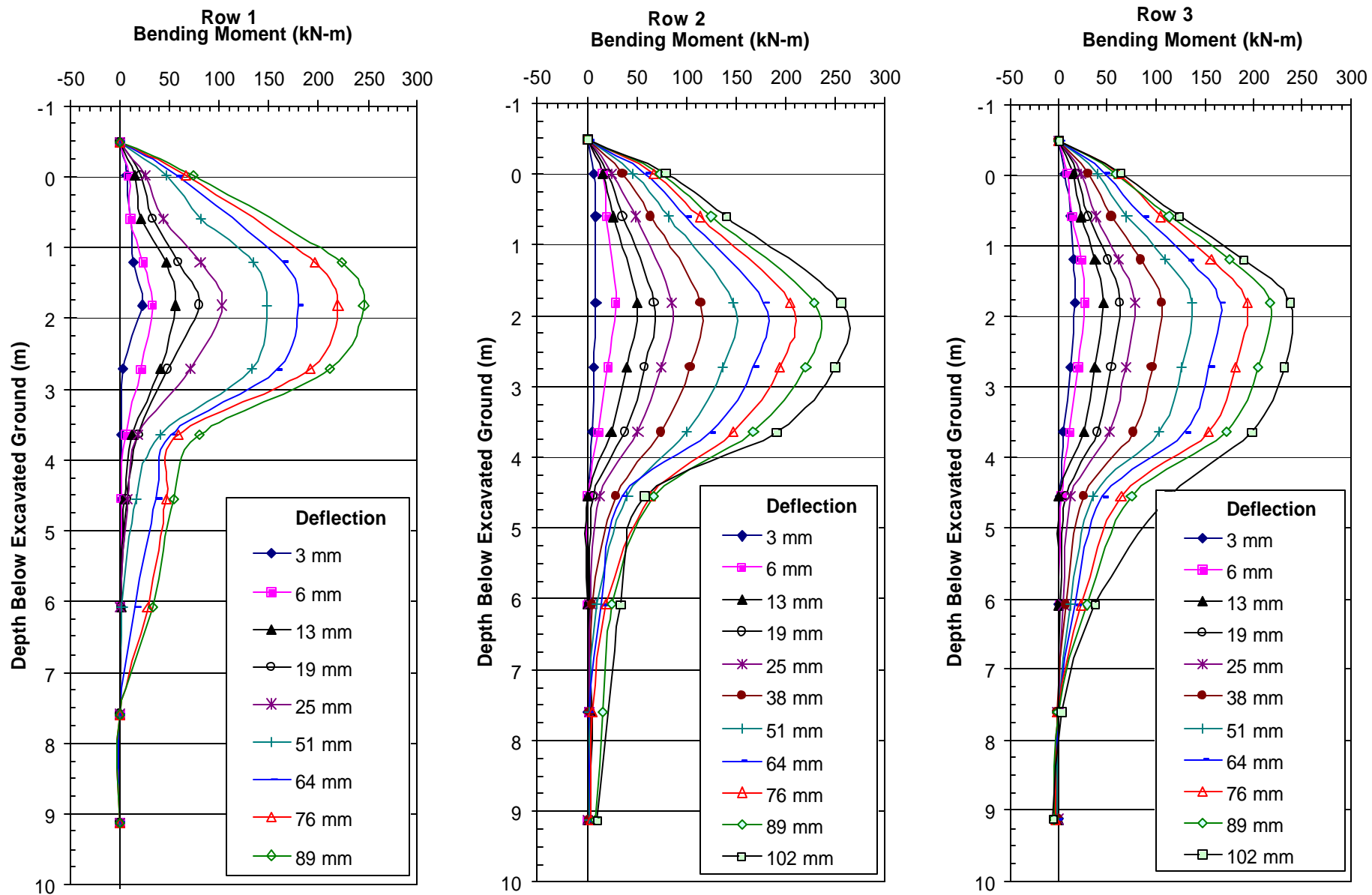
Figure 7.20 Bending moment versus depth curves for the five rows in the 15-pile group at specified displacement increments.
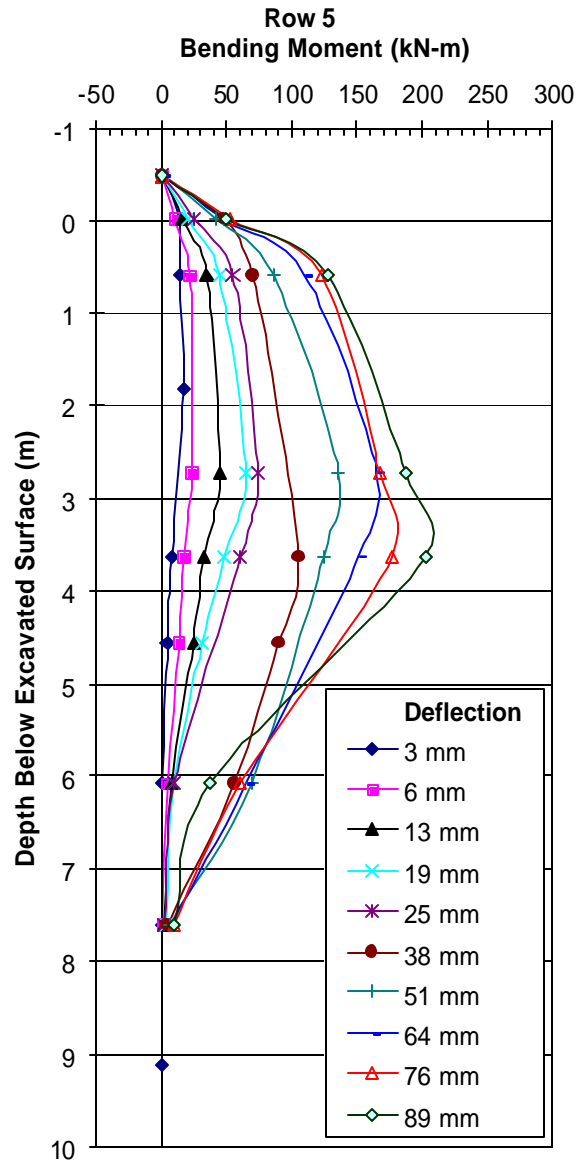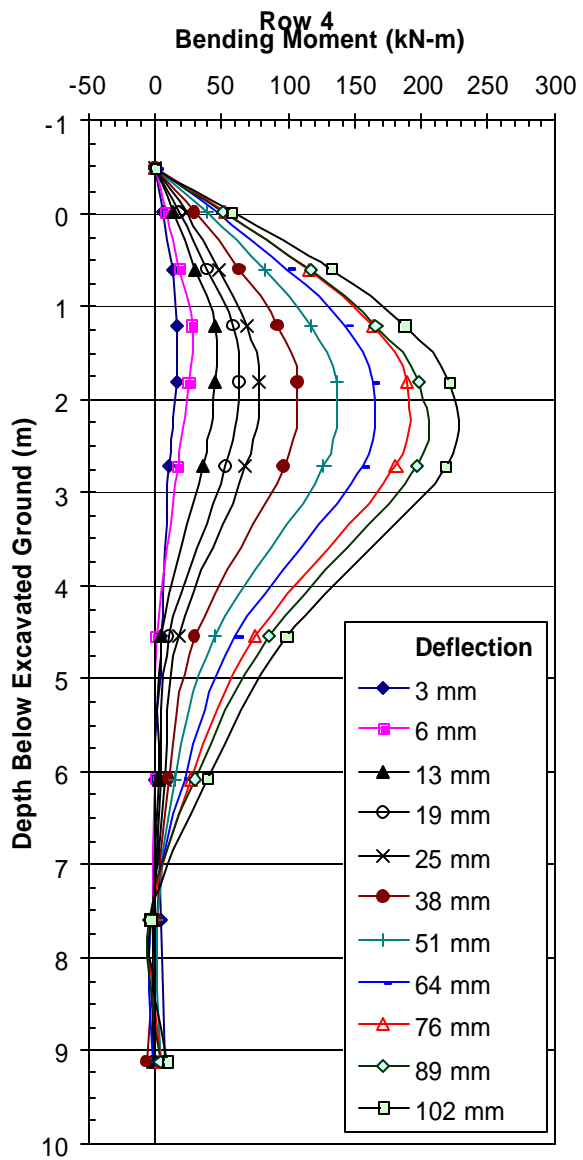
Figure 7.20(Continued) Bending moment versus depth curves for the five rows in the 15-pile group at specified displacement increments.
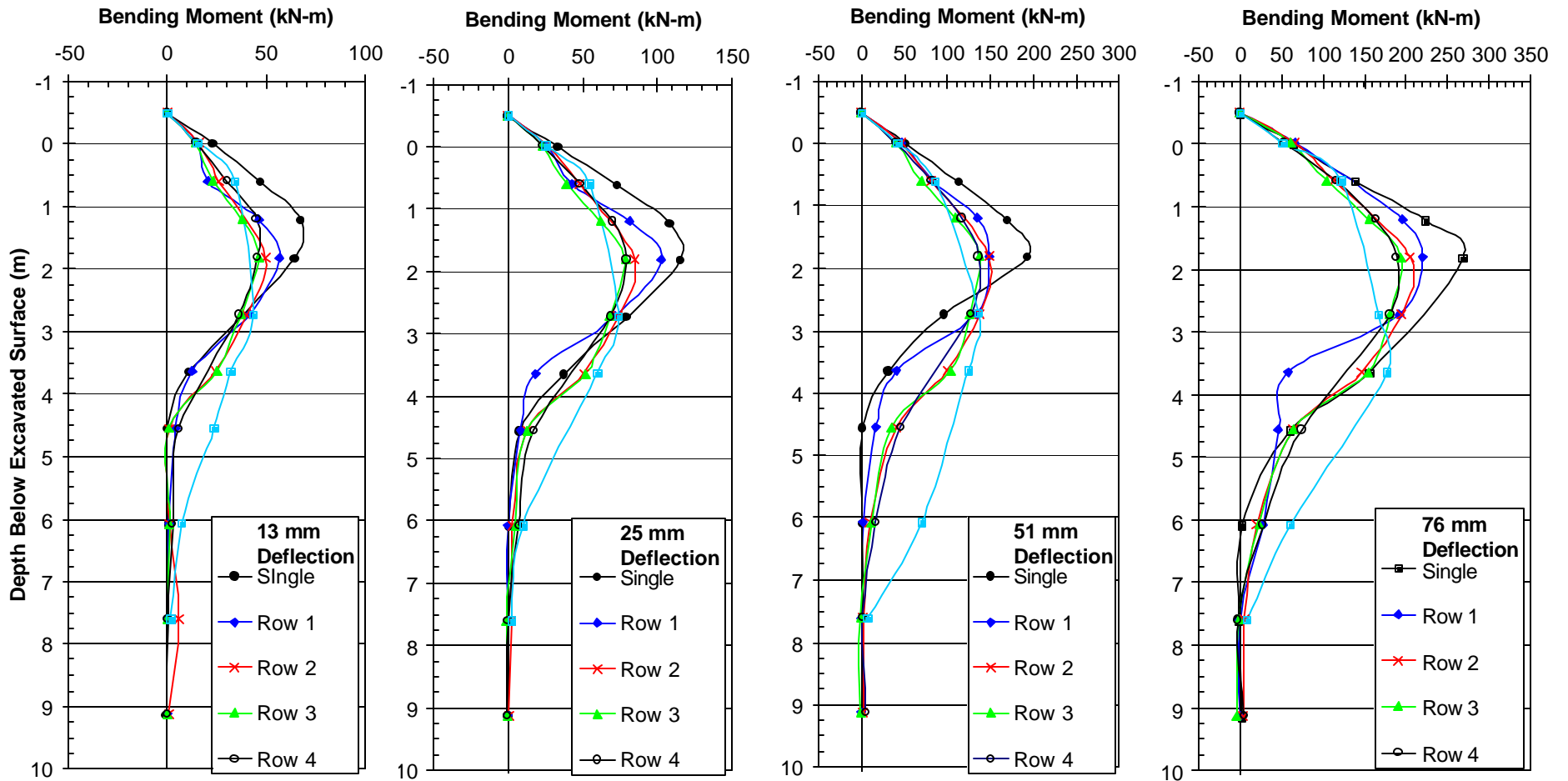
Figure 7.21 Bending moment versus depth curves for the five rows in the 15 pile group in comparison with the single pile curve at four deflection levels.

7-32

CHAPTER 8 STATIC LATERAL LOAD TESTS ON NINE-PILE GROUP AT 3 DIAMETER SPACING

INTRODUCTION

The nine pile group was tested to evaluate the pile -soil- pile interaction that occurs in pile groups involving larger diameter steel pipe pile (610 mm or 24 in.) spaced at three diameters on centers. At this relatively small spacing, significant group effects were expected. However, most previous full -scale testing has involved relatively small diameter piles (254 to 324 mm in diameter) and the difference in pile stiffne ss could influence the results. The behavior of the piles in the group have been compared to, and normalized by, the results of the test on the 610 mm diameter single pipe as described in Chapter 4. The group testing was conducted on December 10, 11, and 23, 1999.

TEST LAYOUT

Nine piles, identical to the single pile, were driven on the west side of the research site in undisturbed soil on August 24, 1999 as shown in Figure 1.3. Since the testing began on December 11, 1999, about 3 1/2 months had been allowed for excess pore water pressures to dissipate.

The nine piles in the group were arranged in three rows of three, as shown in Figure 8.1. Center-to-center spacing of the piles in the group was 1.83 m (6 ft) between rows, as well as between piles within each row. Each of the piles was numbered to aid in identification, as shown in Figure 8.1. The piles were driven in the following order: 2, 5, 8, 3, 1, 6, 9, 4, and 7.

The load was applied using two 1.34 MN (150 ton) hydraulic jacks. A pile cap, constructed on the twelve-pile group that was tested previously as described in Chapter 6, was used to react the jacks. To prevent eccentric loadings, spherical end plates were placed between
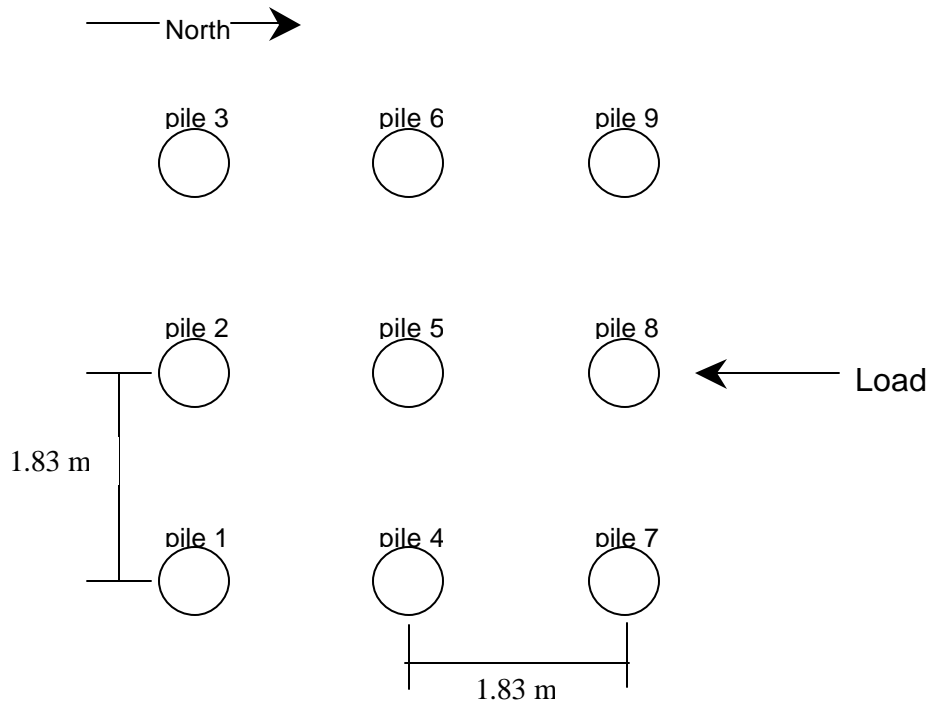
Figure 8.1 Layout of test piles.

the base of the jacks and the reaction pile cap. A steel load frame was attached to the piles by zero - moment, pin-connected tie rods. These tie rods were located 0.46 m (18.1 in.) above the ground surface. The frame was essentially rigid in comparison with the stiffness of the piles and the soil. Therefore, each pile was constrained to have essentially the same deflection. As shown in Figure 8.2, the jacks and the pile group were on opposite sides of the reaction pile cap. The jacks applied a load to a reaction beam that was connected to the pile group by DYWIDAG bars. The applied load placed the connecting bars in tension, thus pulling the load frame towards the reaction pile cap. This setup is sketched in the plan view drawing in Figure 8.2. To minimize all friction fo rces, lubricated steel casters supported the load frame. These casters rolled freely on steel beams resting on the groun **d.**

PILE CAP

WT380 x 142
(Typical)

W760x284

Two
1.33
MN
Jacks

LOAD CELLS

W760x284

2 - MC460x77.2

W920x313

4-40 mm DYWIDAG
BARS (6 m LONG) IN
50 mm PVC SLEEVE

1.82 m

610 mm OD PIPE PILE
OPEN-ENDED
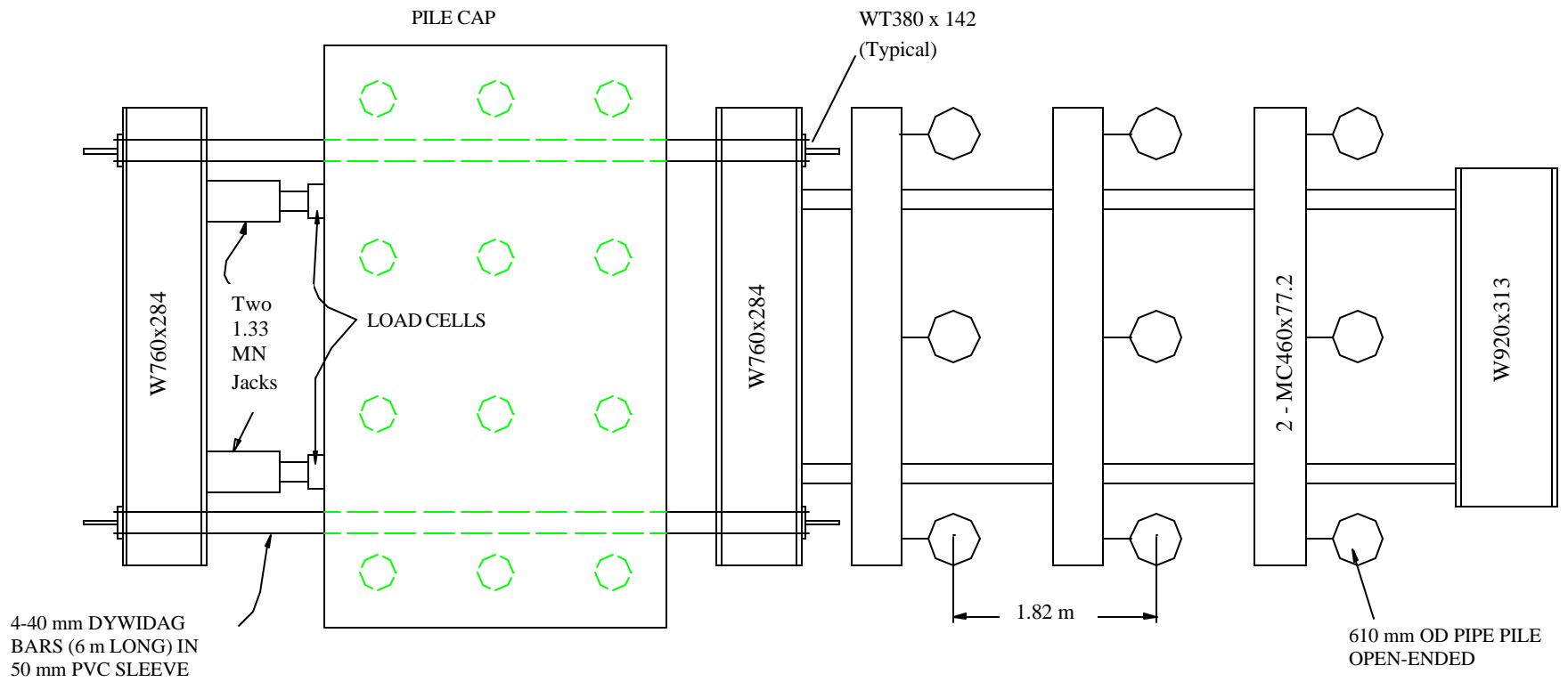
Figure 8.2 Plan view of test setup for lateral load test on 610 mm nine-pile group.

INSTRUMENTATION

The instrumentation for the pile group testing was very similar to that used for the single pile test. Tie-rod load cells were attached to each individual pile. The tie-rods were used to measure the load applied to each pile and were instrumented with electrical resistance type strain gauges on opposite faces, eliminating contributions due to bending. An electrical resistance type strain gauge load cell was also attached to each of the two hydraulic jacks, which could be used to measure the total group load. The sum of the tie-rod load cells was used when reporting total load. The total load from the tie-rod load cells was typically within 10% of that measured by the load cells attached to the hydraulic jacks.

Pile-head displacement was measured by nine LVDTs. These were attached to each pile in the leading and trailing rows (piles 1-3 and 7-9) at the load-point elevation. The center piles in these two rows (piles 2 and 8) also had an LVDT placed 0.305 meters (1 ft) above the load point. The remaining LVDT was placed on the center pile of the group (pile 5) at the load-point elevation. As with the single pile, the LVDTs were attached to an independent reference frame. Supports for the reference frame were located approximately 2.4 m (8 ft) from the edge of the outer piles.

Piles instrumented with strain gauges were driven as the center pile in each row, allowing a row-by-row analysis of bending moments. These piles were instrumented in an identical manner to the single 610 mm pile, with gauges placed on the tension and compression sides of the piles at 12 depths (see Figure 4.14). An angle iron, identical to that used in the single pile test and described in the previous chapter, was used to protect the gauges.

The same Optim Megadac data acquisition system used in the single pile test was used during the pile group testing. The system was controlled with a Pentium II desktop computer

housed in a portable lab trailer. Power was supplied by a portable generator and conditioned with a UPS unit. The system read a total of 92 channels of data, including 72 strain-gauge channels, 11 load-cell channels and 9 LVDT channels. Measurements were recorded at one-second intervals during the static pile group test.

PROCEDURE

During testing, the pile group was loaded to progressively higher deflection levels. At each level, the pile was cycled fifteen times. A sufficient load was applied to the group to produce the desired deflection and then removed, bringing the load back to zero after each cycle. The piles were loaded in one direction only. Target deflections of 6.35 mm (0.25 in.), 12.70 mm (0.50 in.), and 21.59 mm (0.85 in.) were cycled. Finally, one cycle at 28.70 mm (1.13 in.) deflection was conducted. Additional cycles were not possible because of damage to the jack and load cell during that final load increment. At the end of each cycle, the load was held constant for approximately 10 seconds while the readings stabilized.

After cycling the loading of the pile group up to target deflection, a Statnamic test was performed to the same deflection level as will be described in Chapter 11. A static load was then applied to produce the next higher target deflection. This procedure was followed for the first two target deflections, up to 12.70 mm (0.50 inches), so that the first two static tests were performed on virgin soil. At this time, a problem with the load frame prevented further static tests from being conducted. Therefore, the remaining statnamic tests were run consecutively, and the last two static tests, with deflections of 21.59 mm (0.85 in.) and 28.70 mm (1.13 in.), were conducted later, but not on virgin soil.

As the static testing of the pile group was performed using a deflection-control approach, one LVDT was monitored to achieve the target deflection. However, every load-point LVDT

was used to determine the average group deflections shown in subsequent plots. As a result, there are minor discrepancies between the target and average deflections.

TEST RESULTS

Load-Deflection at the Pile Head

Group load versus deflection curves for the first and fifteenth cycles of each load increment are plotted in Figure 8.3. These curves were taken from the sum of the tie-rod load cells and the average of the load-point LVDTs. Each data point corresponds to the peak load and the deflection at that instant.

As plotted in Figure 8.3, there was a reduction in load resistance between the first and fifteenth cycle. The magnitude of this reduction increased somewhat with increasing applied load, causing a greater separation between the two curves. Between the first and fifteenth cycles, the load reduction was about 13% at 6.35 mm (0.25 in.) of deflection and increased to about 16% at both 12.7 mm (0.5 in.) and 21.59 mm (0.85 in.) of deflection.

Figure 8.4 indicates how soil stiffness changed over the 15 load cycles. Stiffness (K) was calculated using the equation

$$K = \Delta F / \Delta L \tag{8.1}$$

where: ΔF = the force applied to the pile group for a given cycle, and
ΔL = the deflection of the pile group for that same cycle.
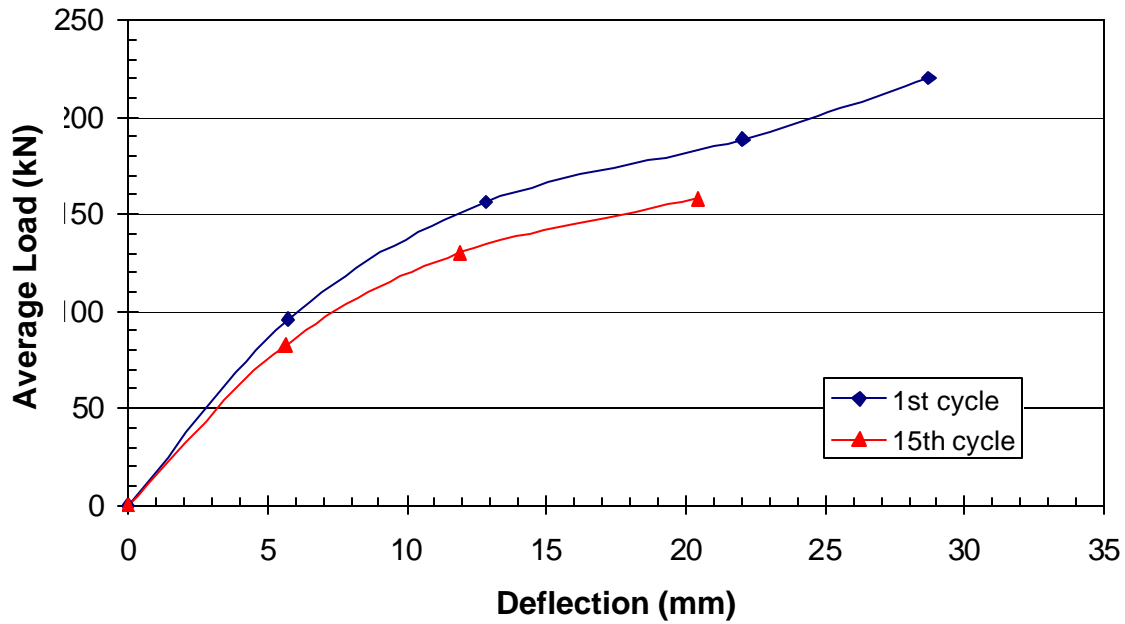
Figure 8.3 Peak load versus deflection curves for the 1st and 15th load cycle during lateral load test on 610 mm nine-pile group.
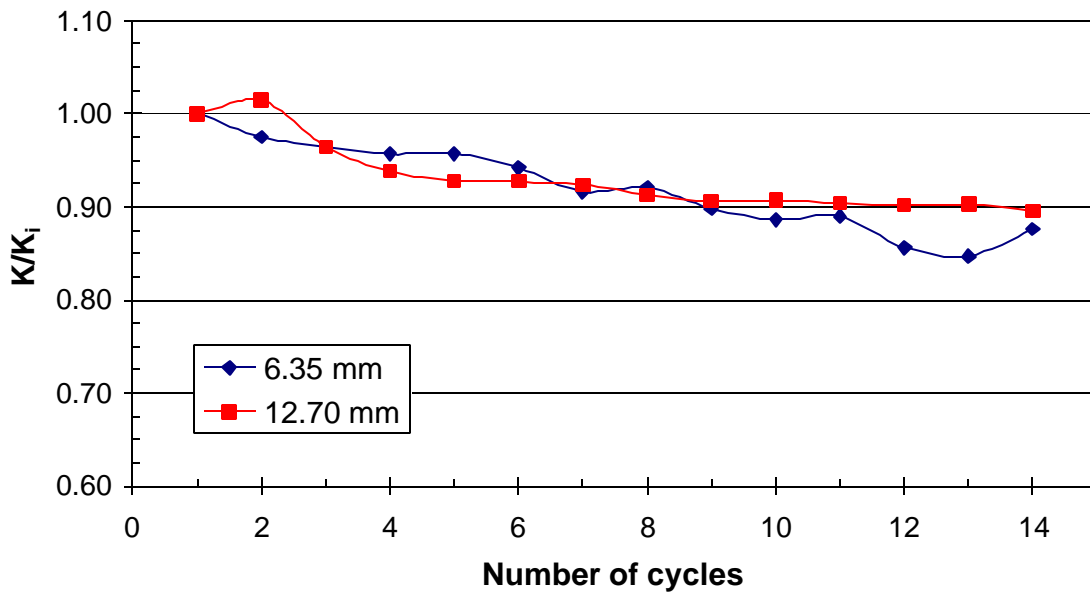
Figure 8.4 Normalized stiffness versus number of load cycles for lateral load test on 610 mm nine-pile group.

The lateral stiffness of the piles during each cycle was normalized by the initial stiffness (K_i) at the first cycle of each displacement increment. As was observed in other group tests, most of the reduction in stiffness occurs during the first few cycles, and the curves gradually approach a horizontal line. It appears that the stiffness reduction converges on a K/K_i ratio of about 0.90. For example, after the final cycle at 6.35 mm (0.25 in.) deflection, the stiffness is 88% of its initial value, after the fifteen cycles at 12.7 mm (0.5 in.) deflection the stiffness is 90% of its initial value.

With a load cell attached to each pile, comparisons can be made of the load distribution within each row during testing. Load-deflection curves for the left, middle and right piles in each row of the group are shown in Figure 8.5. Within each row, the load varies less than 10% between the lowest and the highest loads carried by the piles. The tie-rod load cell attached to pile 7 (Figure 8.1) malfunctioned during the testing; therefore, the load measured by that load cell is not shown in Figure 8.5. Because the variation in load between piles in each row is small, the load carried by pile 7 was assumed to be equal to the average of piles 8 and 9, the other two piles in the trailing row.

There does not appear to be any consistent pattern in the distribution of load on piles within a row. As shown in Figure 8.5, the middle pile carries the highest load of the piles in the back row. In the middle row, the middle pile carries the least load of the three piles. In the lead row, the middle pile carries the second highest load of the three piles. This lack of consistency is in agreement with results reported by Brown et al (1988) and Rollins et al (1998) and with other testing described in earlier chapters. Elastic theory, however, predicts that the corner piles in a row will carry higher loads than the middle pile.

In contrast, the test results suggest that load variation within a row is likely a function of local variation in soil density and strength.

a) Front Row Piles (1st cycle)
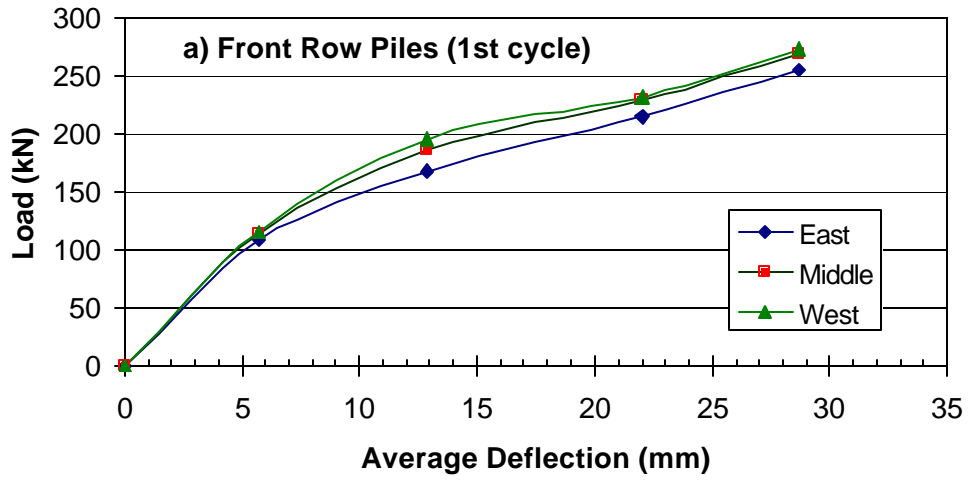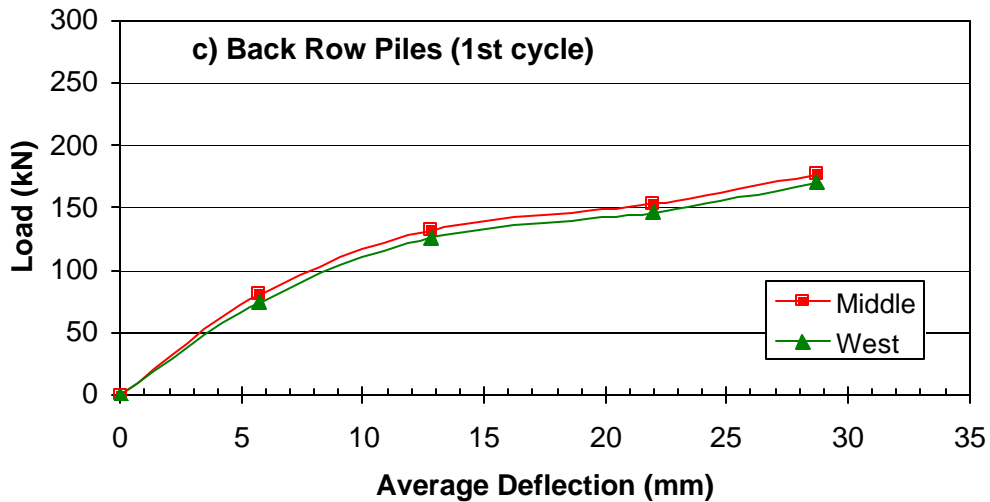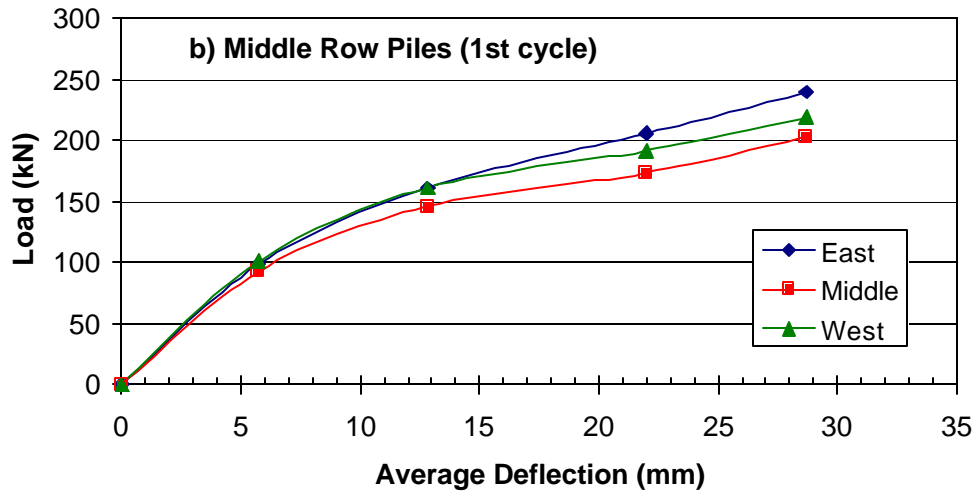
Figure 8.5 Load versus deflection curve (1st cycle) for each pile grouped by row.

As the load carried by a pile is mainly a function of its row location within the group, results of these tests will be presented in terms of the average behavior of the piles in each row.

The first cycle load versus deflection curves for each row in the group and for the companion single pile are plotted in Figure 8.6. The row load is the average load of the piles making up that row, and the average deflection is the average of the entire pile group. As was expected based on the findings discussed in the literature review, the front row piles carry a load that is similar to the single pile, while trailing rows carry a reduced load for the same deflection. Figure 8.7 shows that by the fifteenth cycle, the row-to-row load differences are still apparent;

however, they are slightly reduced from that shown in Fig. 8.6. Meimon et al (1986) reported that row to row load differences became insignificant after application of cyclic loads. However, in that study, the pile group was subjected to between 1,000 and 10,000 cycles. Similar results might have developed had as many cycles been applied in this test.

Ratios of the average row load to the single pile load are plotted as a function of the average pile -group deflection in Figure 8.8. The load ratios initially decrease as pile -head deflection increases, but they level off after about 22 mm of deflection. This deflection level at whic h the load ratios stabilize is somewhat higher than has been observed in previous testing. For example, Rollins et al (1998) reported that after a rapid, initial decrease, the row load to single pile load ratio remained relatively constant after only about 13 mm of deflection. Rollins et al (1998) tested 324 mm (12.75 in.) outside diameter piles spaced at 0.97 m (38.25 in.), whereas this investigation involved piles with an outside diameter of 610 mm (24 in.) with a spacing of 1.83 m (72 in). Both tests had center-to-center spacings of approximately three pile diameters. The difference in deflection required to stabilize the load ratios may be attributed to this 0.86 mm (33.75 in.) difference in spacing.
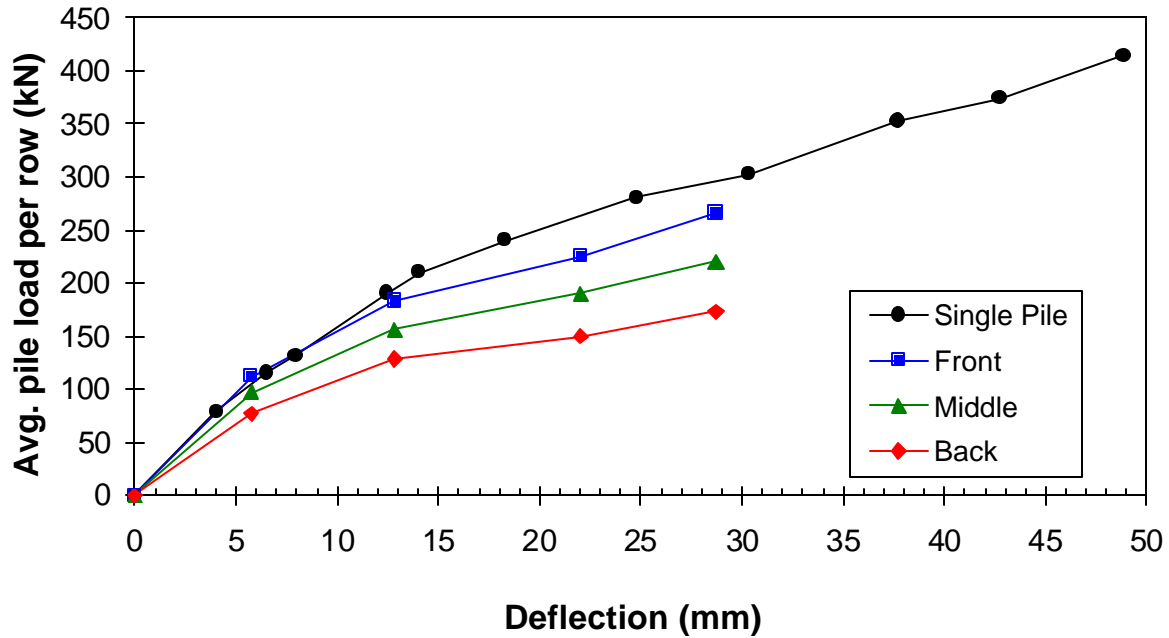
Figure 8.6 Average load versus deflection curves for each row in the group relative to the single pile curve during the first cycle.
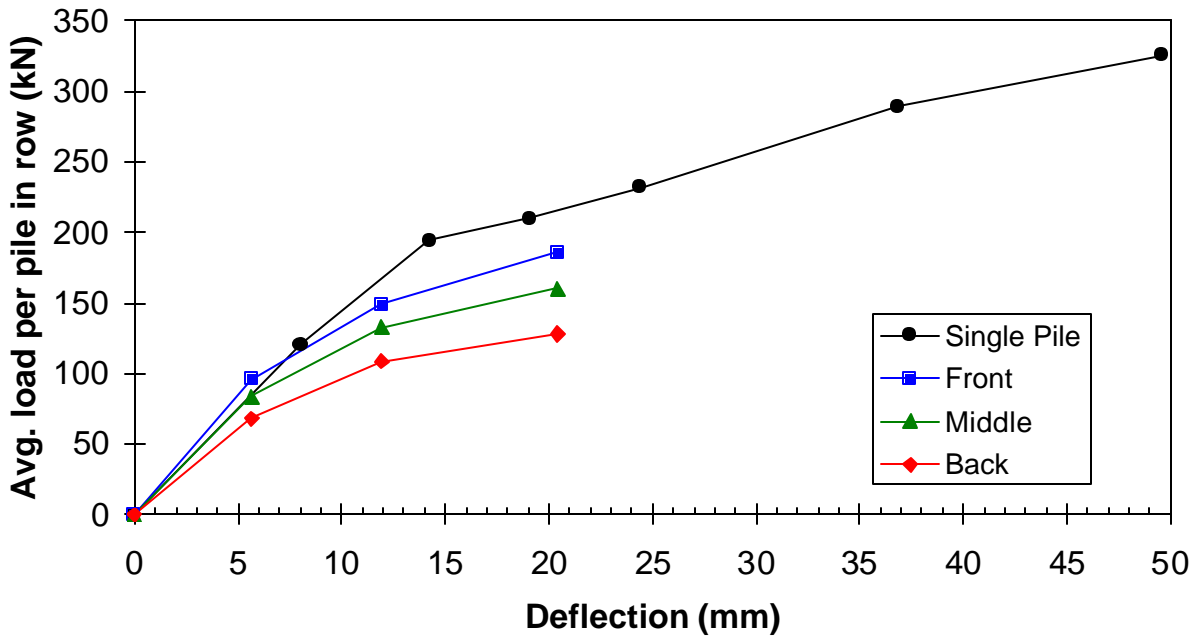
Figure 8.7 Average load versus deflection curves for each row in the group relative to the single pile curve during the fifteenth cycle.
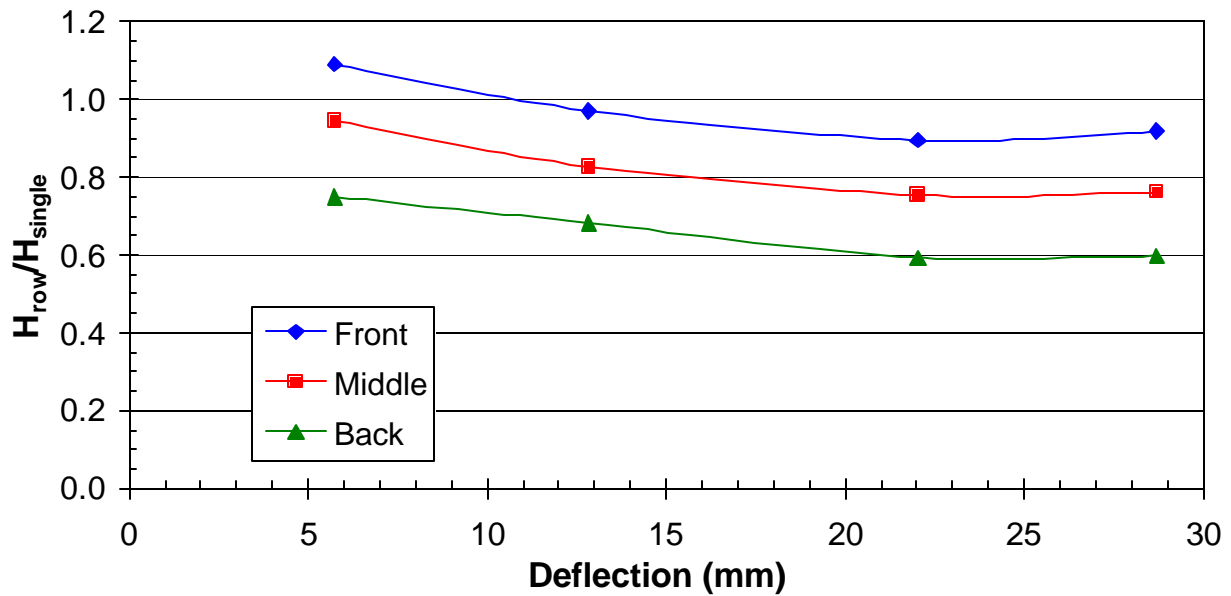
Figure 8.8 Ratios of average row load to the single pile load for each row during the first cycle of loading.

More movement would be expected to develop the overlapping shear zones for the greater spacing distance even though the spacing to diameter ratios were about the same.

After the load ratios level off at 22 mm, the average load ratios are 0.91, 0.76, and 0.60 for the piles in the front, middle, and back row, respectively. These ratios are higher than were observed by Rollins et al (1998) for smaller piles, where load ratios were measured to be 0.7, 0.5, and 0.4 for the front, middle, and back row piles, respectively.

Bending Moment
Bending Moment versus Depth.

Using the strain-gauge data, the bending-moment curves were calculated following the same procedure described in the single pile chapter. Bending moment versus depth curves for the front, middle, and back row piles are compared to the single pile curves in Figure 8.9. These curves correspond to average group displacements of 5.74, 12.83, 22.02, and 28.70 mm for the
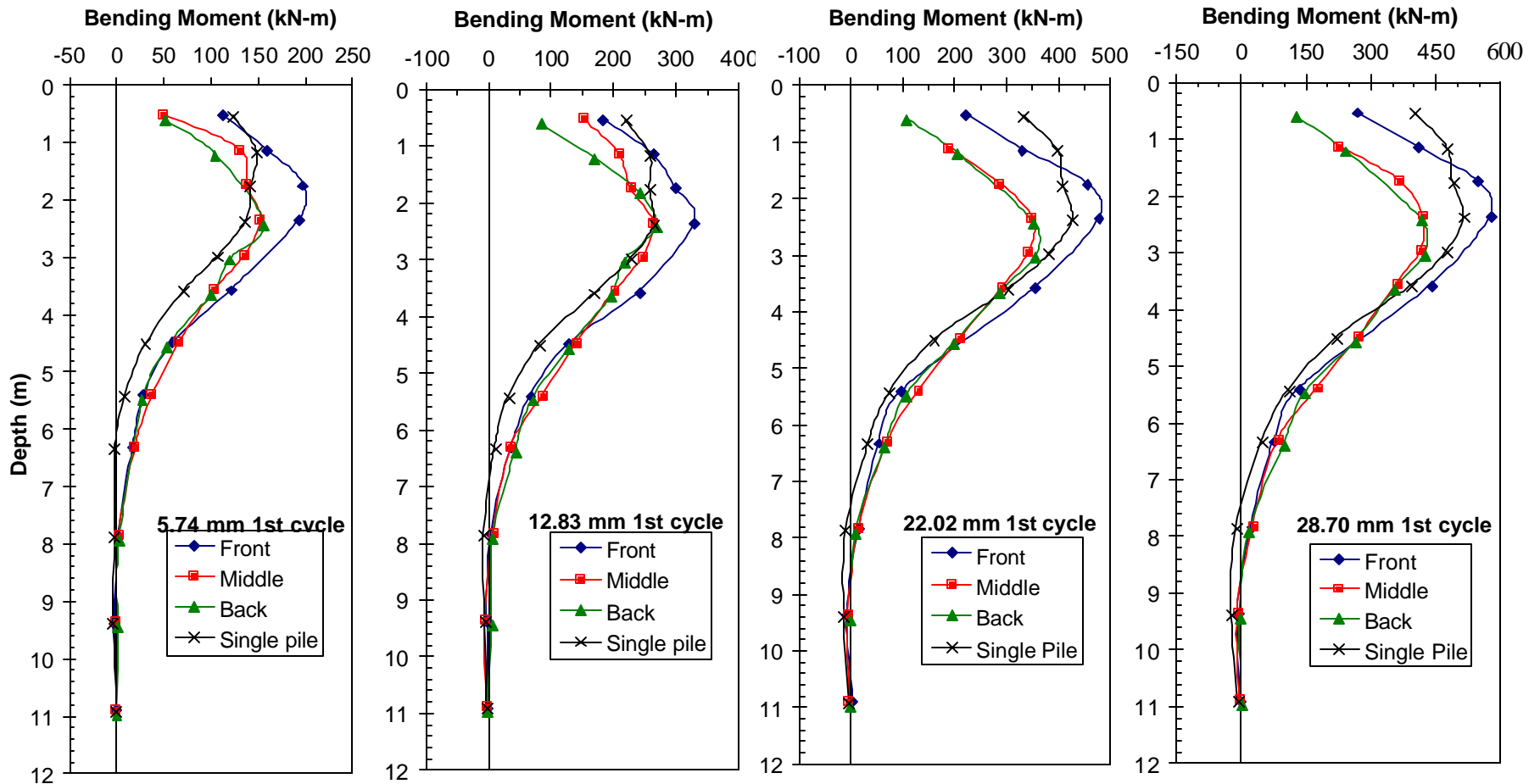
Figure 8.9 Bending moment versus depth curves for each row at four deflection levels during first cycle in comparison with single pile bending moment curves.

first cycle of loading. The single pile, bending-moment curve corresponds to the same pile-head deflections as the group moment curves. In all cases, the moment curves are for the first cycle of loading. However, due to differences in the deflection levels to which the single and group piles were loaded, the single pile deflection level shown in these plots does not always correspond to the peak loads. Therefore, the single pile curves in Figure 8.9 are not the same as those shown in Figure 4.17.

The leading-row pile had a considerably higher maximum moment than the piles in the middle and trailing rows, which had nearly identical moments. As depth increased, however, the moments for the three rows came relatively close together. Maximum bending moments generally occurred at the gauge located 2.38 m (7.8 ft) below the ground surface for the front, middle, and back rows. This corresponds to about 3.9 times the pile diameter. Below about 5 m (8.2 pile diameters) depth, there was little variation in moment among the three rows. As the load increment increased, the maximum moment migrated to a slightly greater depth. The maximum moment in the single pile was typically somewhat less than in the leading row group piles, but equal to or greater than in the trailing row group piles.

Each pile in the group had reversals in the moment, from positive to negative, occurring at depths that increased with deflection.   This reversal appeared at a depth of about 8 m for the smallest deflection, and increased to approximately 9 m for the largest deflection.

The single pile moments decreased at a greater rate with depth than the group piles and reached zero moment at shallower depths. This point of moment reversal, as with the pile group, occurred at increasingly greater depths as the load increased. For example, the point of moment reversal increased from a depth of 6 m at the 5.74 mm deflection to 7.5 m (still above the point where the group piles reached zero moment) at the 28.70 mm deflection.

Maximum Moment versus. Load

The maximum bending moment for the center pile in each row is plotted against the average group pile load in Figure 8.10. Results for the single pile are also plotted. The average load plotted was the total load divided by the nine piles in the group. The pile in the lead row had a higher moment than the middle and back-row piles, which were quite similar. This similarity was because of the higher loads carried by the lead row in reaching the target deflection. The single pile moment was consistently lower than that in each of the three rows; however, as the load increased, the single pile moments drew closer in value to the middle and trailing row moments. Group effects caused the soil to act as a softer material and were likely responsible for the higher moment observed in the group piles relative to the single pile. In Figure 8.11, maximum moments for the fifteenth cycle were plotted in a similar manner against the average pile load for the entire group. In this plot, group affects were again quite pronounced, as moments in the group were still greater than those of the single pile.

The maximum moment versus the average pile load for each row was plotted in Figure 8.12 for the first cycle. This load was the average of the three piles in the row from which the moment measurement was taken. Plotting the results in this way provides a more meaningful comparison of the bending moment relative to the actual applied force. The bending moment curve for the front and middle row piles, for this condition, plotted essentially on top of each other while the trailing row had the greatest moment for a given force. This change in the relative position of the moment curves was likely due to group effects. Group effects cause a softening of soil in the back-row piles relative to the front-row pile. Similar results were seen after cycling the piles, as plotted in Figure 8.13. Figures 8.12 and 8.13 show that due to group effects, moments in the group were again higher than the moments in the single pile and that trailing row piles developed greater moment per load.
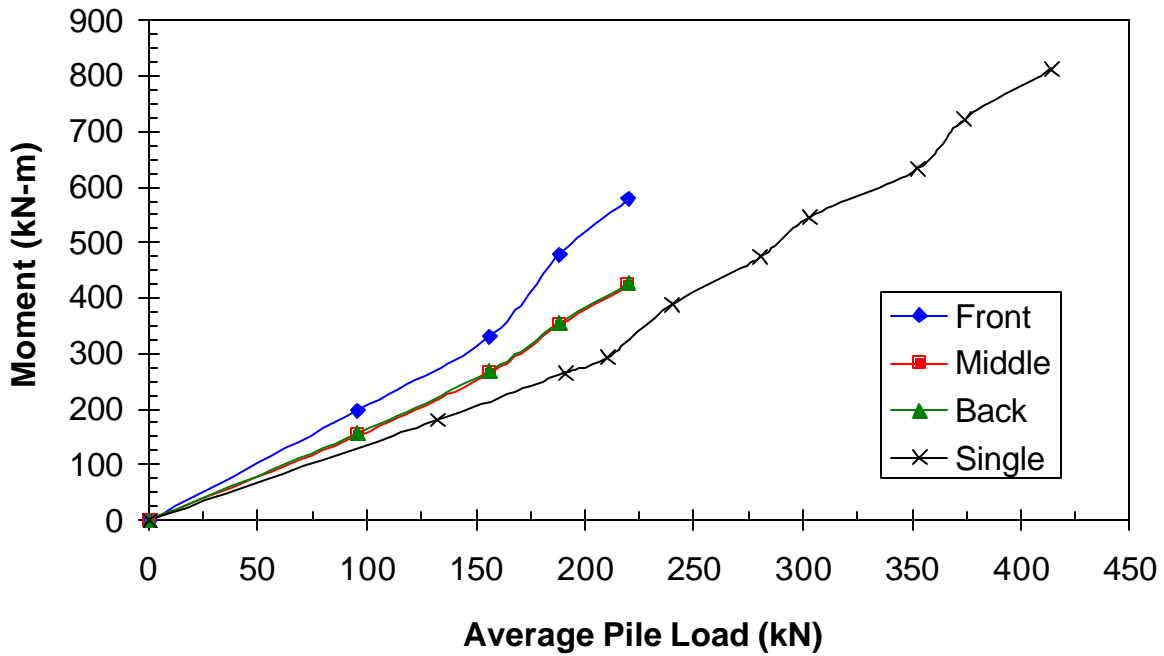
Figure 8.10 Maximum bending moment versus average pile load in the group for the 1st cycle of load relative to that for the single pile.
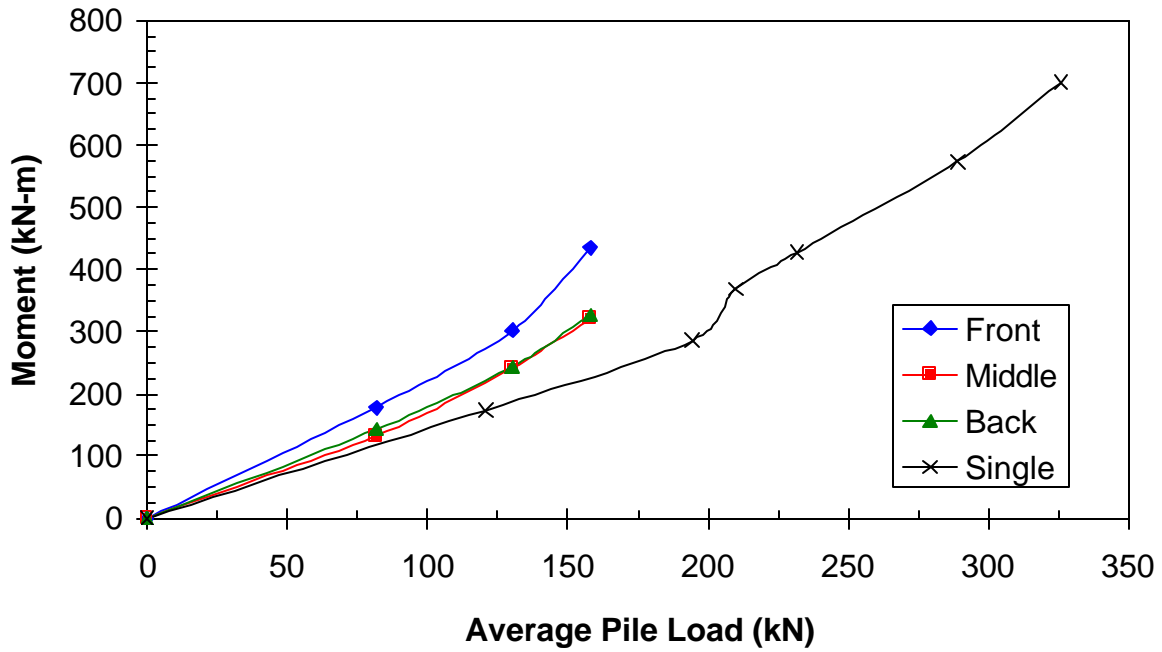

Figure 8.11 Maximum bending moment versus average pile load in the group for the 15th cycle of load relative to that for the single pile.
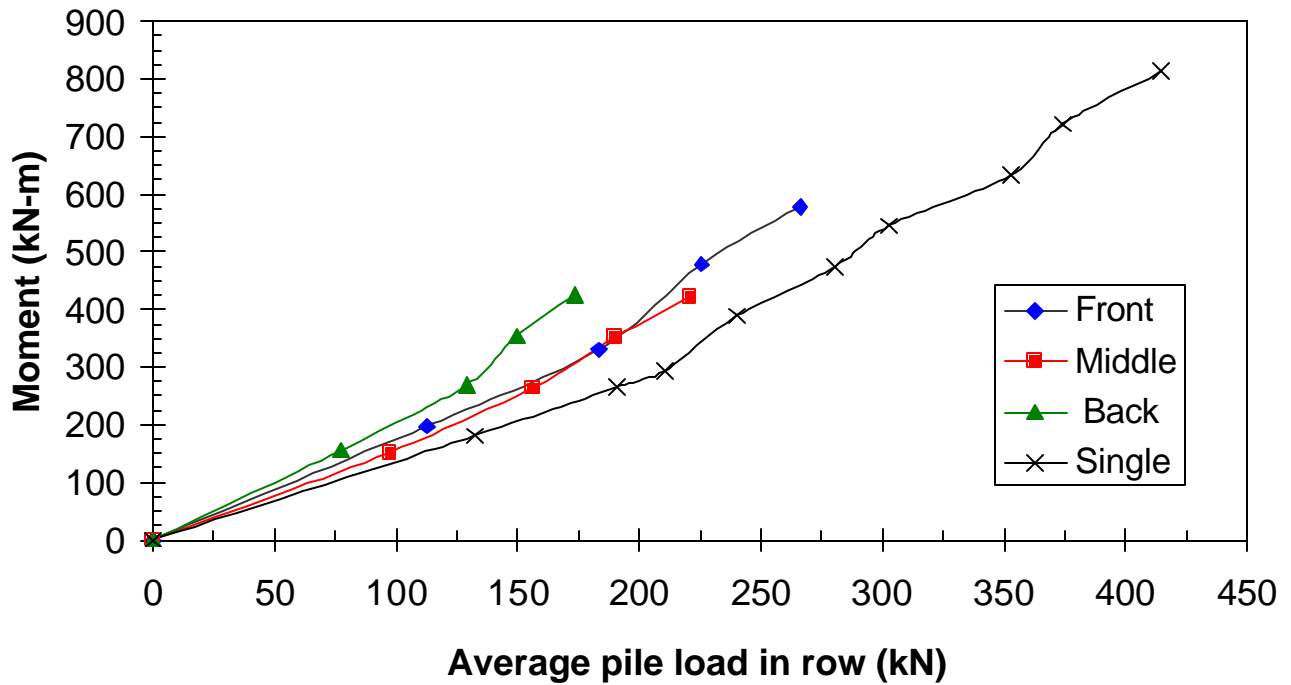
Figure 8.12 Maximum bending moment versus average pile load in each row for the 1st cycle of load relative to that for the single pile.
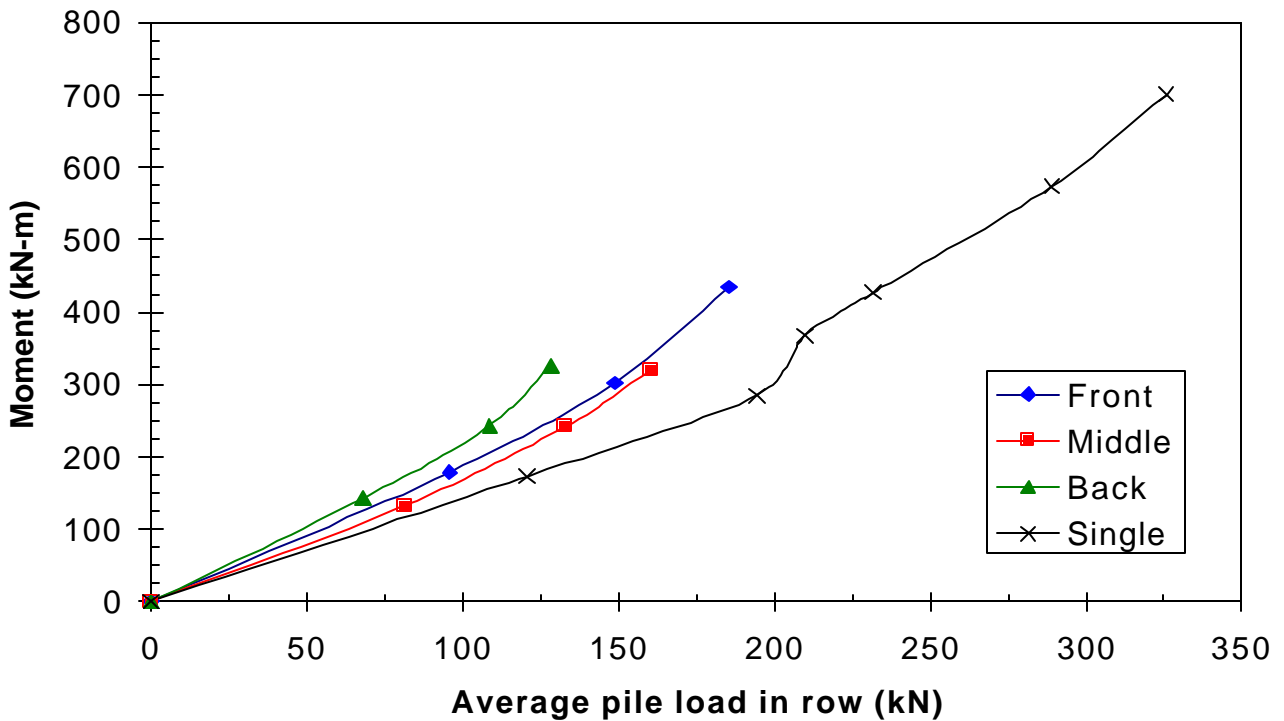
Figure 8.13 Maximum bending moment versus average pile load in each row for the 15th cycle of load relative to that for the single pile.

CHAPTER 9 COMPUTER ANALYSIS OF LATERAL SINGLE PILE LOAD TESTS
INTRODUCTION

The computer analysis of the single pile tests was conducted using two analysis programs: (1) LPILE Plus version 3.0 (Reese and Wang, 1997) and (2) Florida Pier (FLPIER) (Hoit et al, 1997). LPILE and FLPIER are soil-structure interaction programs in that they account for the resistance to lateral movement provided by both the pile and the surrounding soil. LPILE, developed by ENSOFT, Inc. of Austin, Texas, is the commercial version of the computer program COM624. COM624 was developed at the University of Texas at Austin and is used extensively in both the academic as well as consulting arenas to analyze the behavior of laterally loaded piles. Florida Pier was developed at the University of Florida for the Florida Department of Transportation. FLPIER is made available free of charge through the Florida Department of Transportation web page.

Some similar assumptions are made when using FLPIER and LPILE to analyze the lateral soil-pile interaction problem. For example, each program considers the pile as if it were a beam. The deflection, moment, and shear in the pile are calculated using a finite difference approach in LPILE and a finite element approach in FLPIER. The stiffness of the pile is computed using the modulus of elasticity as well as the moment of inertia of the steel pile. The stiffness may be either a linear or non-linear function of pile curvature. The analyses conducted in this study were performed using a linear analysis approach.

LPILE and FLPIER use non-linear springs (p-y curves) attached at nodal points along the length of the pile to model the lateral resistance provided by the soil that surrounds the pile. LPILE and FLPIER contain p-y curves, which can be selected by the user for different soil types.

ANALYSIS OF 324 mm SINGLE PILE TEST IN VIRGIN SOIL

Pile Properties

LPILE and FLPIER require several parameters and pile properties to be specified for the program to run. For LPILE, the pile length was set as 12.19 m (480 inches) and then divided into 100 increments of 0.12 m (4.8 inches) length. The load point was set at 0.39 m (15.5 inches) above the ground surface. The slope of the soil surface was specified as zero.

The pile section had to be defined prior to analysis for both programs. The outside diameter of the pile was 0.324 meters (12.75 inches) and the cross-sectional area, including the angle irons, was 0.0094 m^2 (16.07 in^2). The modulus of elasticity (E) of the steel was 200 Gpa (29,000 ksi) and the moment of inertia (I) of the pile with the angle irons attached was 1.43×10^8 mm^4 (344 in^4). It was necessary to include the angle irons in the calculation of the moment of inertia because the attachment caused them to bend with the pile section.

Soil Properties

The soil stratigraphy was defined based on the results of the geotechnical investigations of the site described in Chapter 3. An idealized soil profile was created and utilized in the computer analysis as shown in Figure 9.1. As described in Chapter 3, the soil profile consisted of stiff clays with some sand layers underlain by soft clays. At the time of the test, the water table was located 1.13 m (3.71 ft) below the excavated surface. The average unit weight of the soil was specified as 14.93 kN/m^3 (95 lb/ft^3).

The total stress method was used to define the strength of the clay layers. The vane shear tests and a correlation with the CPT cone tip resistance, described in Chapter 3, were used to establish the undrained shear strength for each layer. The agreement between the measured and correlated undrained strength from the CPT is relatively good.
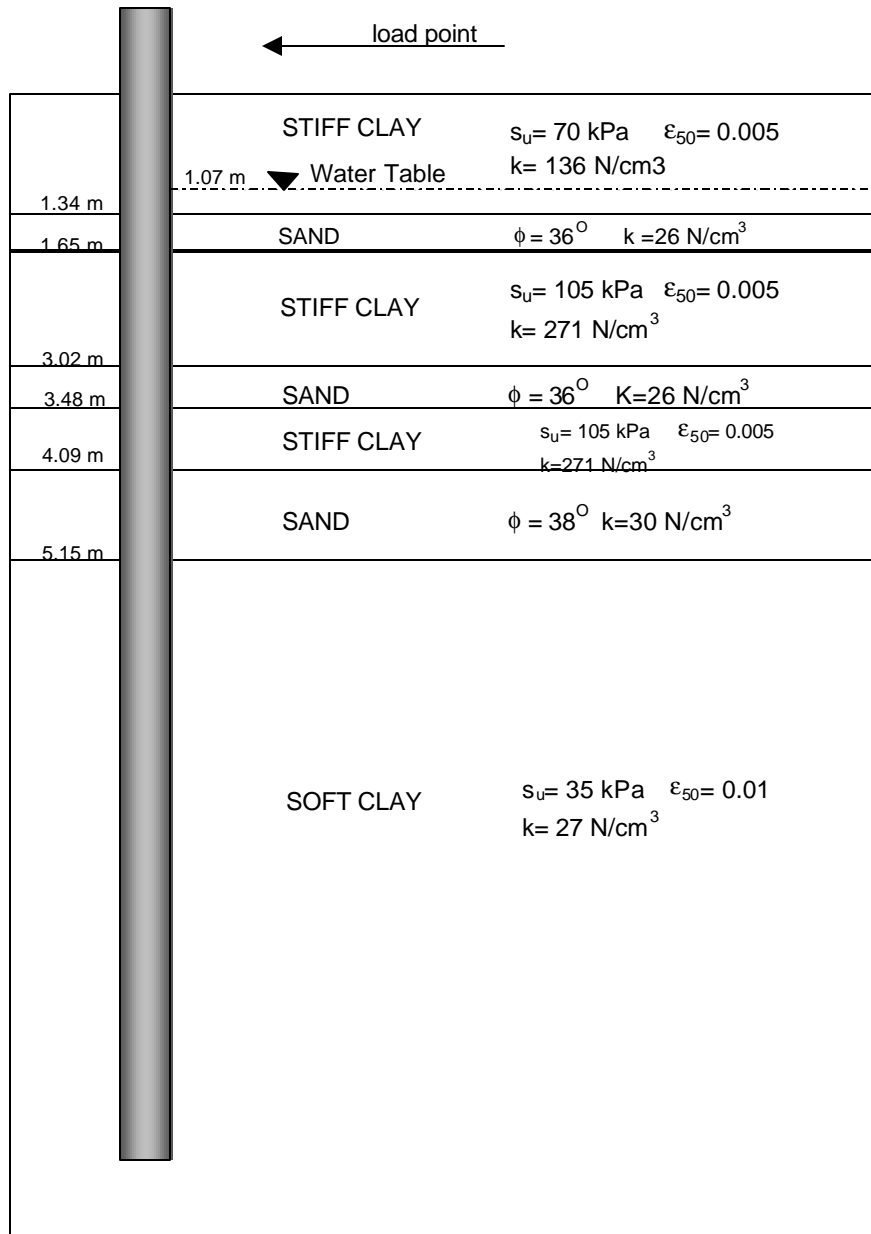
Figure 9.1 Idealized soil profile with soil properties used in the computer analysis.

For the stiff clay layers, p-y curve shapes developed by Reese and Welch (1975) were specified in both programs. Although some of the stiff clay layers are below the water table, the strength testing did not indicate that a large drop in strength would occur with strain. Therefore, the stiff clay curves proposed by Reese et al (1975) were not used in the analysis. The equations for the p-y curve shape proposed by Reese and Welch (1975) require the input of a lateral subgrade modulus (k) and the strain required to develop 50% of the ultimate shear strength (ε_{50}). The values of k and ε_{50} were based on soil strength and were chosen using correlations developed by Reese and Wang (1997). The values that were chosen are also listed in Figure 9.1.

The effective stress method was employed to define the strength of the inter-bedded sand layers. The cohesion was assumed to be zero for these layers and the results of the borehole shear tests were used to obtain the friction angles. The friction angles for the sand layers were either 36 or 38 degrees. The p-y curve shape developed by Reese et al (1974) was used for the sand layers; however, comparative analyses indicate that little difference would result from the use of the API sand p-y curves developed by O'Neill and Murchison (1983). The equations for the p-y curve in sand require an estimation of the subgrade modulus (k). The k value was chosen from a correlation involving the relative density derived from the CPT data and the friction angle of the sand (Reese et al. 1997) which is shown in Figure 9.2. The p-y curve shape in the underlying soft clay was based on recommendations given by Matlock (1970).

Pile Head Load vs. Deflection

Figure 9.3 shows the measured peak load versus deflection curves for the 1st cycle along with the curves computed by LPILE and FLPIER using the input parameters given previously. The agreement between the measured and computed curves is excellent. Very little manipulation of the input parameters was required to achieve this match. Changes in the measured

geotechnical properties were less than about 10% of the measured values which is within the range of error expected for these properties.

Angle of Internal Friction, f'
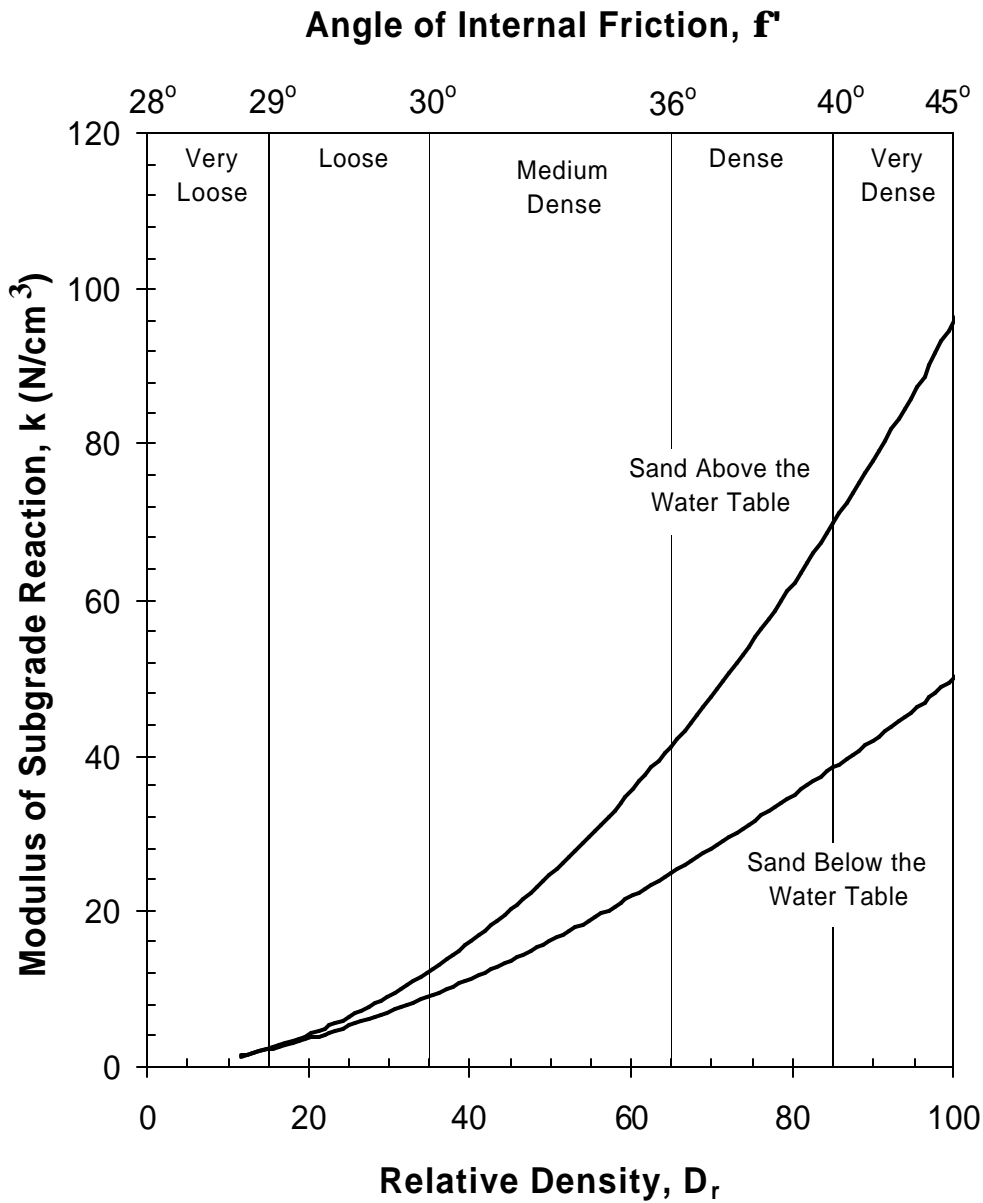
Figure 9.2 Correlations between relative density (D_r), friction angle (f'), and modulus of subgrade reaction (k) (After Reese et al, 1997).
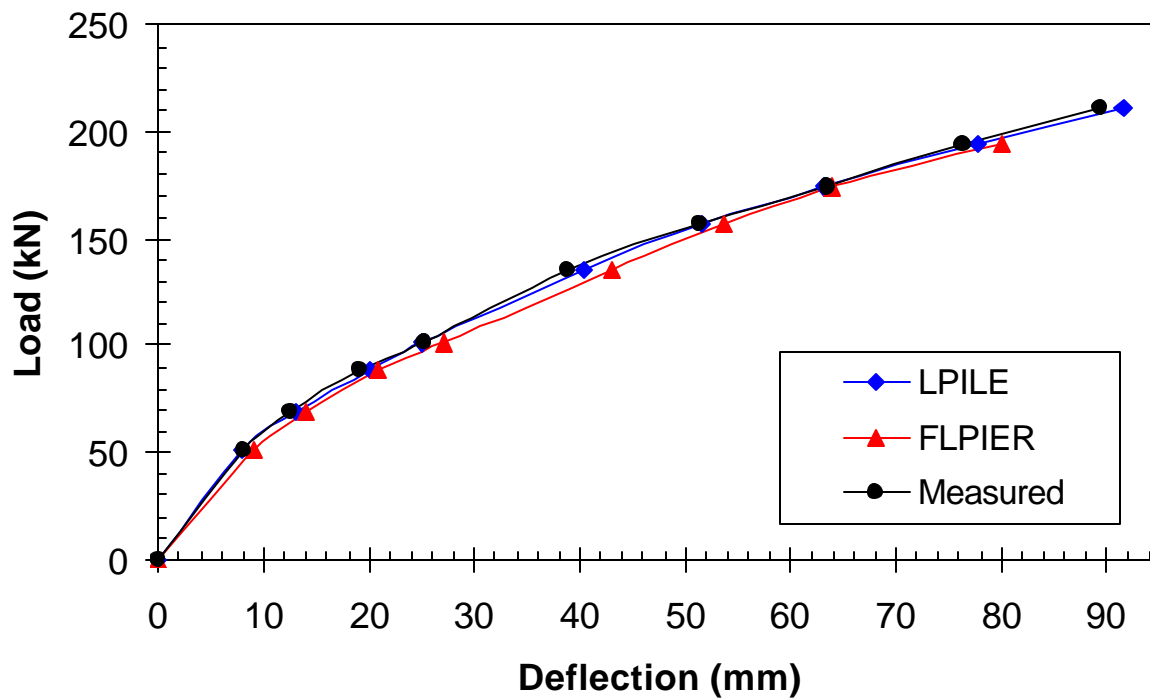
Figure 9.3 Load versus deflection comparison of the measured and computed results.

To better understand the influence of the gaps on lateral resistance, the fifteenth cycle of the 76.2 mm (3.0 inch) deflection increment was modeled using LPILE. The gap was modeled by removing part of the top layer in the soil profile until a match with the first segment of the load versus deflection curve was obtained. The strength of the remaining soil was not altered. A good fit with the initial portion of the curve was achieved after the top 0.864 m (34 inches) of the soil profile was removed (see Fig. 9.4). Measurements made at the time of the testing indicated that the gap extended to approximately this same depth. A comparison of computed and measured response is presented in Fig. 9.4. For deflections less than about 30 mm, the lateral resistance in the upper 0.86 m was primarily due to the pile itself and the agreement is good. However, at greater deflections, the pile contacted the soil and lateral resistance was due to both soil and pile stiffness. Therefore, the computed curve assuming no soil resistance becomes less and less appropriate and the measured load becomes greater than the computed curve.
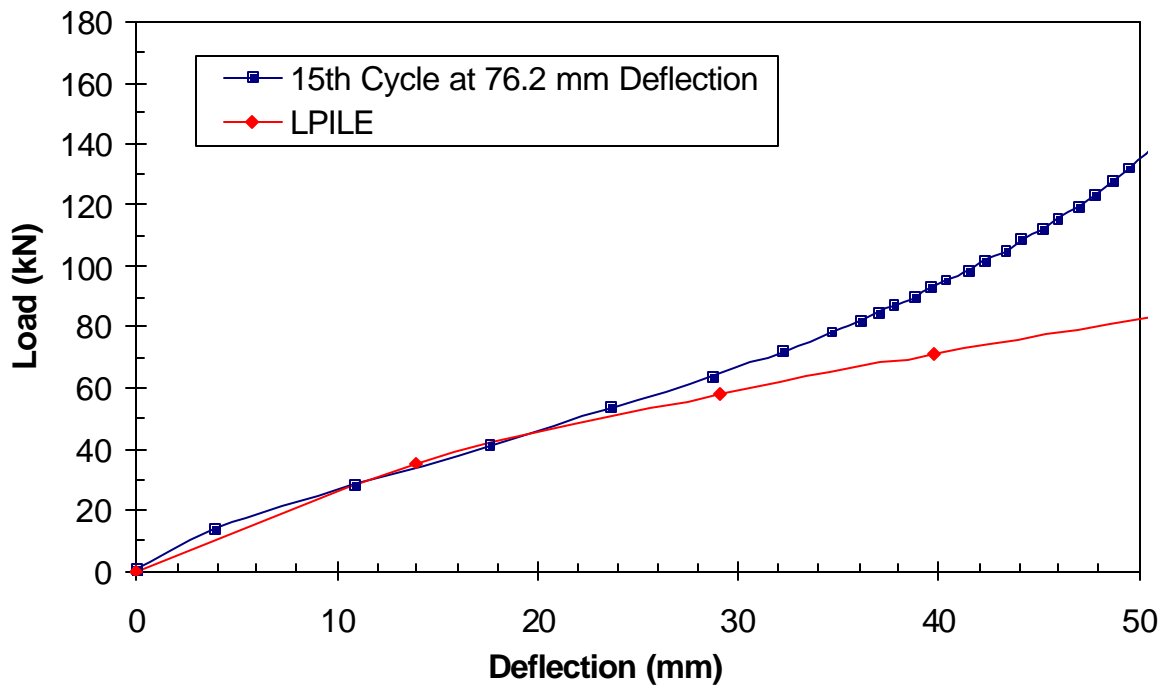
Figure 9.4 Measured load vs. deflection curve for the 15th cycle at 76.2 mm deflection along with curve computed by LPILE assuming no soil resistance in upper 0.86 m of the soil profile.
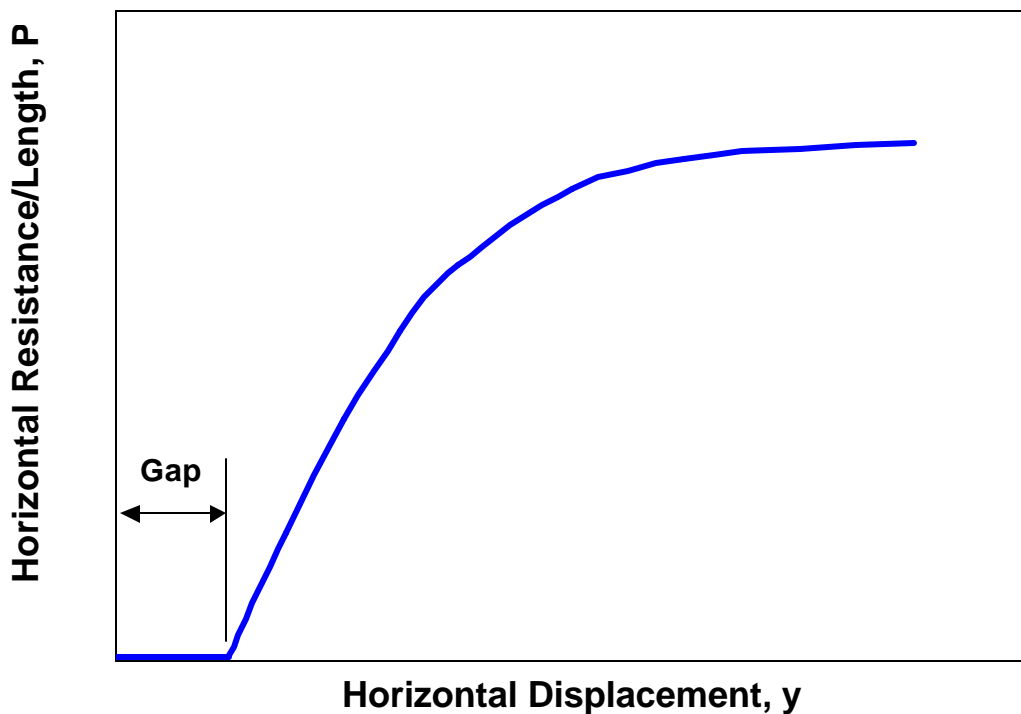
Figure 9.5 P-y curve with a zero strength section to model the drop in strength due to the presence of a gap around a pile.

To fully model the behavior of the pile during the 15th cycle of loading, it would be necessary to develop a p-y curve with a gap section as illustrated in Figure 9.5. Alternatively, one could use a variable strength soil profile for various deflection levels as described subsequently.

Bending Moment

Bending Moment vs. Load. Figure 9.6 shows the measured maximum moment vs. load curve along with the curves computed using FLPIER and LPILE. The values from LPILE are very similar to those obtained from the strain gauge data. The moments determined by FLPIER were between 5 and 10% greater than those calculated from the strain gauge data. This match between the computed and measured moments shows that these two programs can be used to model the single pile behavior.
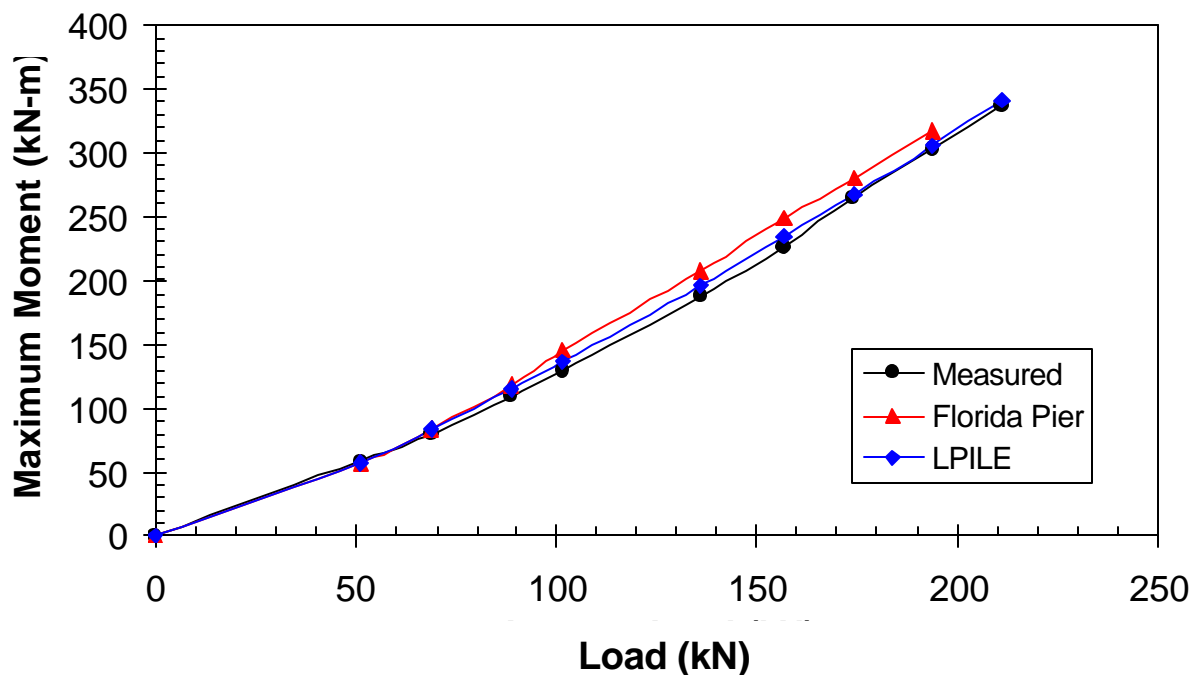
Figure 9.6 Measured maximum moment versus load curve for 1st load cycle along with curves computed using FLPIER and LPILE.

Bending Moment vs. Depth. Bending moment versus depth curves computed by LPILE for the eight load levels corresponding to the deflection increments applied during the single pile test are presented in Figure 9.7. The depth to maximum moment was 1.44 meters for the first

three increments (to 88.59 kN loading and 19.05 mm deflection), 1.81 meters for the next five increments (to 193.79 kN and 76.20 mm), and 2.17 meters for the last loading (211.11 kN and 88.90 mm). This is very close to the measured depths to maximum moment, which begin at 1.5 meters for the first load, 1.6 meters for the second load, and increase to 1.7 meters from the fifth load (135.71 kN) and subsequent deflection increments.

Figure 9.8 shows a comparison between the LPILE curves and measured values for bending moment versus depth at only four selected deflection increments for clarity. The match between the measured and computed curves response is very good.   The largest discrepancy in depth to maximum moment is about 0.5 meters, at the final deflection increment. This is also the increment in which two strain gauges at 2 and 3 m below the ground surface were no longer functioning properly.   Therefore, the discrepancy in this case may result from an inaccurate interpolation between the strain gauge locations.
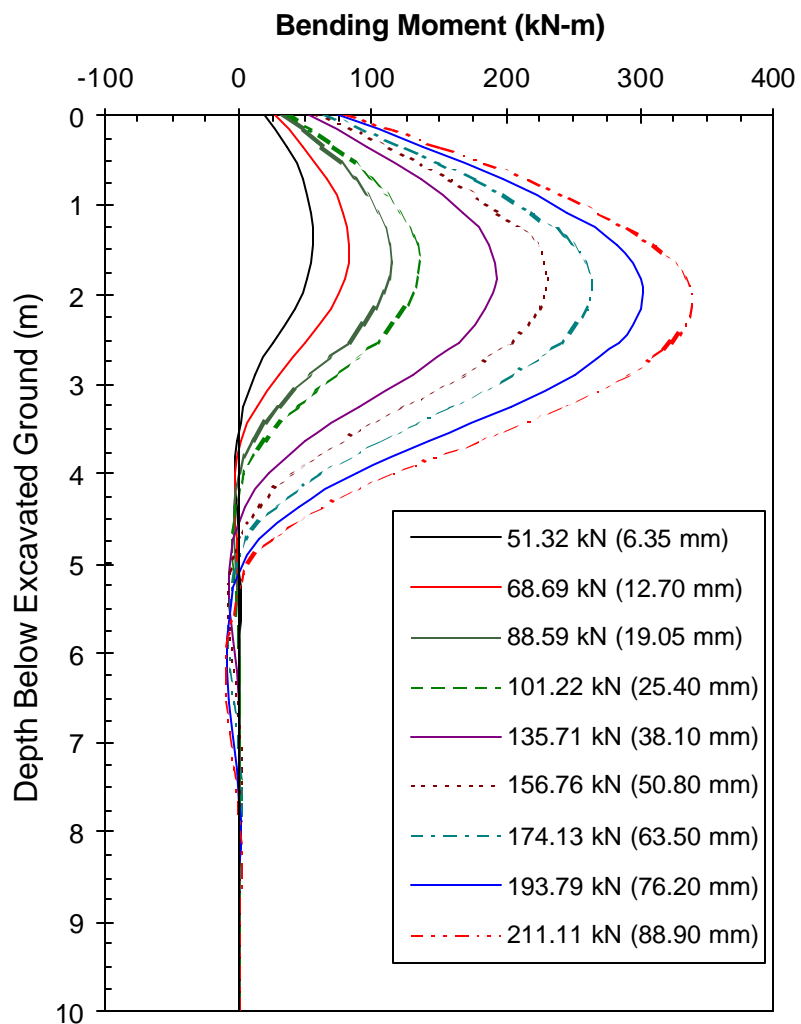
Figure 9.7 Bending moment versus depth curves for the 610 mm single pile computed using LPILE.
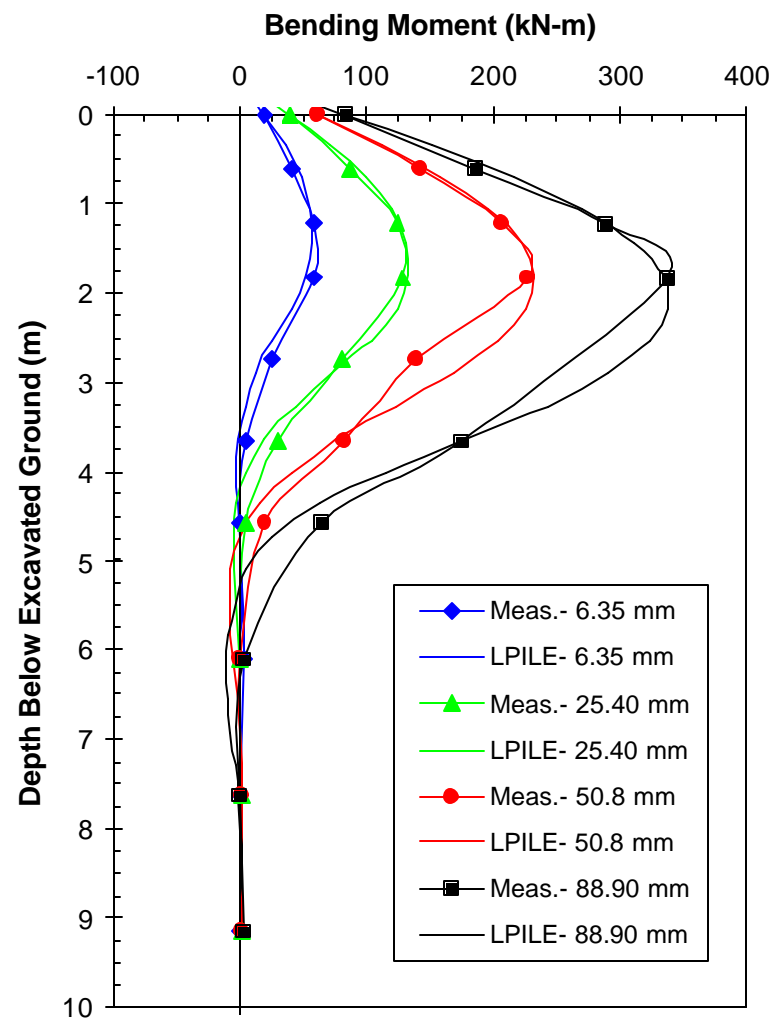
Figure 9.8 Measured moment versus depth curves along with curves computed using LPILE at four load levels.

ANALYSIS OF 324 mm SINGLE PILE TEST IN RE-LOADED SOIL

The lateral load test on the single pile located within the 12-pile group was conducted perpendicular to the direction that the pile was originally loaded during the group test as described in Chapter 4. Analyses of this test were also undertaken using the computer program LPILE. Attempts were made to model the load versus deflection curve with a single soil profile. This proved impossible to achieve because of the gapping behavior, which has been described previously. To model the measured load versus deflection curve, it was necessary to use three different soil strength profiles shown in Figure 9.9. The soil resistance is each model was progressively increased as the deflection increased and the pile came into contact with the soil. The properties of all other layers below the top of the stiff clay layer remained unchanged. In addition, the pile properties were kept the same as described in the previous section of this chapter.
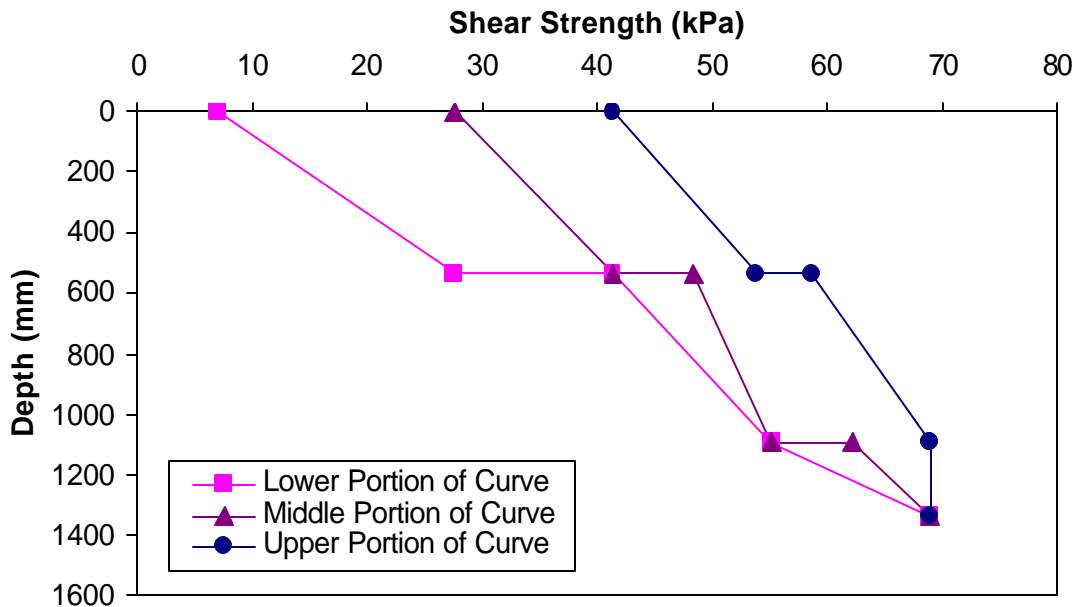
Figure 9.9 Three soil strength profiles used in LPILE to model the increasing resistance around the single pile as the gap between the pile and soil closed with increased deflection.
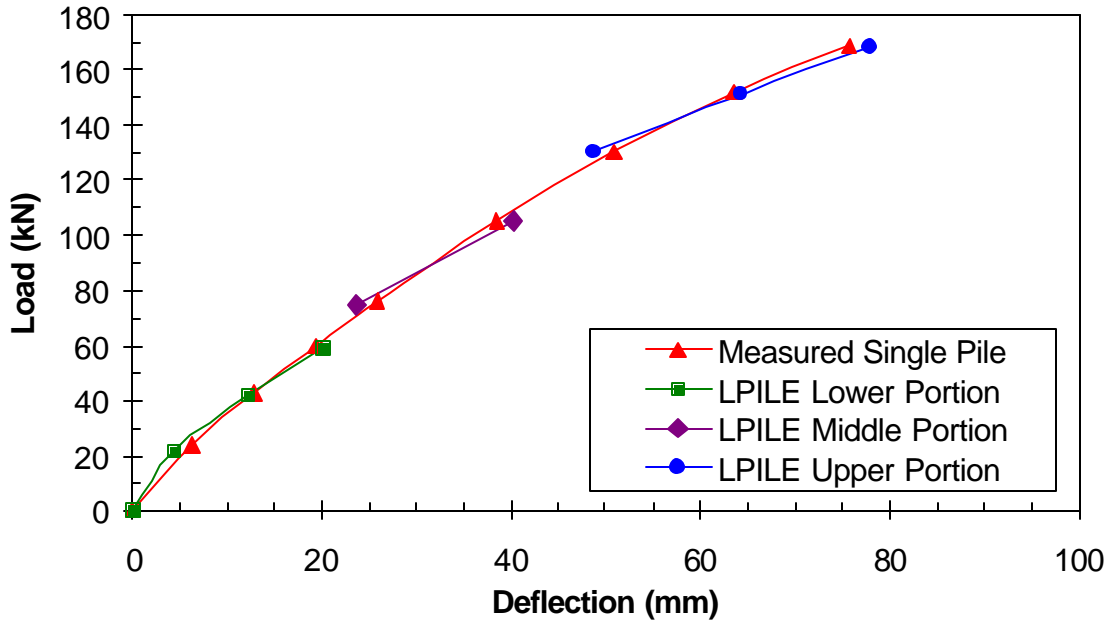
Fig 9.10 Measured load versus deflection curves along with computed load versus deflection curves obtained using the three soil strength profiles shown in Figure 9.9

Using the three profiles shown in Figure 9.9, three separate segments of the load versus deflection curve were computed to match the measured load versus deflection curve as shown in

Figure 9.10. Although this match was obtained by trial and error, the results will be useful in back-calculating p-multipliers as will be discussed subsequently in Chapter 10. No comparisons with computed and measured bending moments are provided because strain gauges were not present on the reloaded test pile.

ANALYSIS OF 610 mm SINGLE PILE TEST IN VIRGIN SOIL

Pile Properties

For the LPILE analysis, the pile properties specified previously in Chapter 4 were used. Pile length was set at 12.19 m (480 in.), with the load applied 0.46 m (18 in.) above the ground surface. The ground slope was set at zero and the pile was divided into 110 increments of 0.11 m (4.36 in.) length for the analysis. In the full-scale test, angle irons were attached to both sides of the pile with approximately 76.2 mm (3 in.) welds positioned halfway between each strain gauge. The cross-sectional pile properties that were used in the LPILE analysis included the attached angle iron. The pile section was defined as having an outside diameter of 610 mm (24 in.) and a combined cross-sectional area of 0.0248 m^2 (38.41 in.^{2}). The elastic modulus, E, of the steel pipe pile was specified as 200 GPa (29,000 ksi), and the combined moment of inertia, I, of the pile and angle iron was 1.15 x 10^9 mm^4 (2764 in^4). Yield strength was specified as 397,500 kN/m^2 (57,661 psi).

Soil Properties

The same soil stratigraphy defined for the analysis of the 324 mm single pile was also used for the analysis of the 610 mm single pile. This generalized soil profile and the soil properties used in the analysis of the

610 mm pile are presented in Figure 9.11. There are only two differences

in the soil models for the 610 mm and 324 mm diameter piles. First, the

water table during the 610 mm test was slightly higher (0.98 m versus 1.0   7

m) and second, the undrained shear strength in the top stiff clay layer was

also slightly higher (77 vs. 70 kN/m 2).   The strength in the top layer was

increased about 10% to improve the agreement with the measured load -

deflection curve.   This strength is still within the range of interpreted

strength values (see Figure 3.8); however, the requirement for a higher

strength suggests that the current equations for p-y curve shape, which

involve corrections for pile width, are somewhat conservative.

The p-y curve shapes used for each layer in the LPILE model are listed in Table 9.1 along

with the location of the top and bottom of the layers relative to the loading point. References to

the original authors proposing the p-y curve shapes are also provided in Table 9.1.

Figure 9.11 Idealized soil profile and soil properties used in the analysis of the lateral load test for the 610 mm diameter steel pipe piles.

Table 9.1 P-y curve shape models and layer thicknesses used in LPILE for analysis of the 610 mm diameter pipe pile.

Layer	Soil Type	Layer Top (m)	Layer Bottom (m)
1	Stiff Clay w/o free water (Reese and Welch, 1975)	0.46 (18")	1.80 (70.8")
2	Sand (Reese et al, 1974)	1.80 (70.8")	2.08 (82.8")
3	Stiff Clay w/o free water (Reese and Welch, 1975)	2.08 (82.8")	3.45 (135.8")
4	Sand (Reese et al, 1974)	3.45 (135.8")	3.93 (154.8")
5	Stiff Clay w/o free water (Reese and Welch, 1975)	3.93 (154.8")	4.54 (178.8")
6	Sand (Reese et al, 1974)	4.54 (178.8")	5.61 (220.8")
7	Soft Clay (Matlock, 1970)	5.61 (220.8")	12.70 (500")

Pile Head Load versus Deflection

The load versus deflection curve computed using LPILE is compared to the measured curve for the 1st cycld load on the single pile test in Figure 9.12. At deflections less then 12 mm, the LPILE curve is somewhat higher than the measured results. For example, there is a 16% difference between the two curves at a deflection of 6.5 mm. However, at deflections higher than 12 mm, the two curves are quite similar and the discrepancies are typically less than 5%. Overall, the agreement between measured and computed response is very good.   The discrepancies at small deflections could possibly be due to thin gaps around the pile produced by the pile driving.

THIS PAGE LEFT BLANK INTENTIONALLY
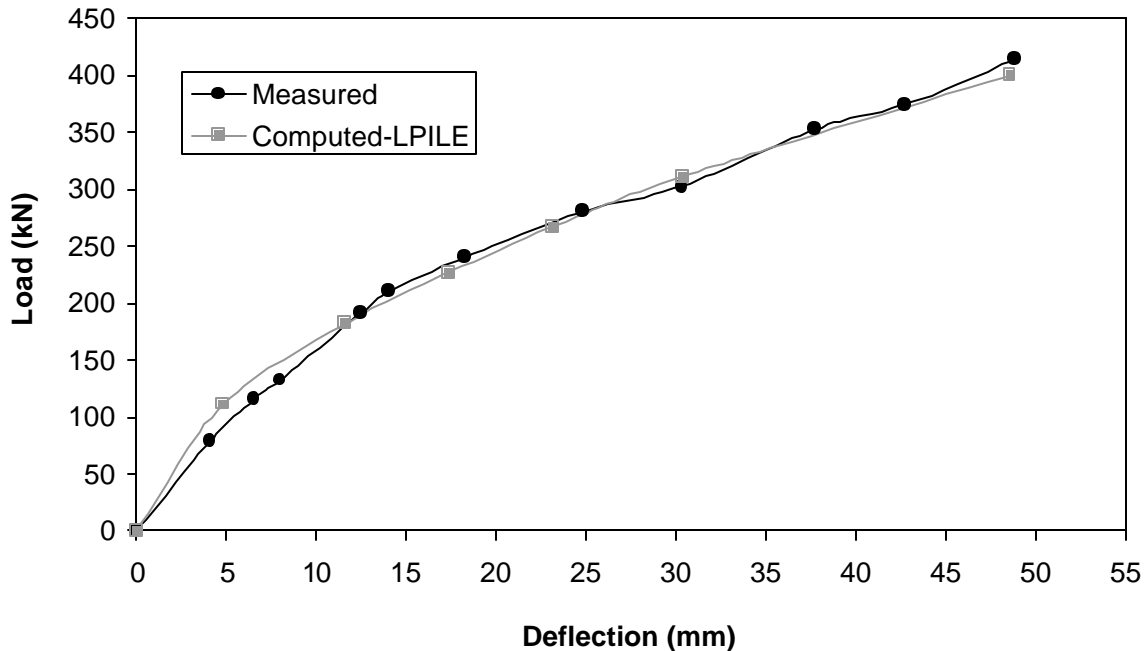
Figure 9.12 Comparison of the measured load vs. deflection curve for the 1st cycle of load with the curve computed using LPILE for the 610 mm diameter single pipe pile.

Bending moment

Bending moment vs. Depth. The single-pile bending moment versus depth curves, based on the results from LPILE, are plotted in Figure 9.13. Each curve, in this figure, represents a load equal to the load increment placed on the single pile during the test. In the LPILE analysis, the depth of the maximum moment increased with load, as plotted in Figure 9.l3, whereas the observed depth of maximum load did not appear to increase significantly with load. However, the average depth to the maximum computed moment corresponds to the measured, single-pile maximum moment depth at 2.38 m below the ground surface. This discrepancy may result from insufficient strain gauges. Moment reversals occurred in the LPILE analysis between 5.2 and 7.5 m, compared to the measured value of 6.7 to 7.6 m below the ground surface.

Several of the LPILE moment vs. depth curves are plotted along with the corresponding measured single pile test curves in Figure 9.14. The shapes are generally very similar and the depths to the maximum moment in the LPILE analysis are close to the measured depths.
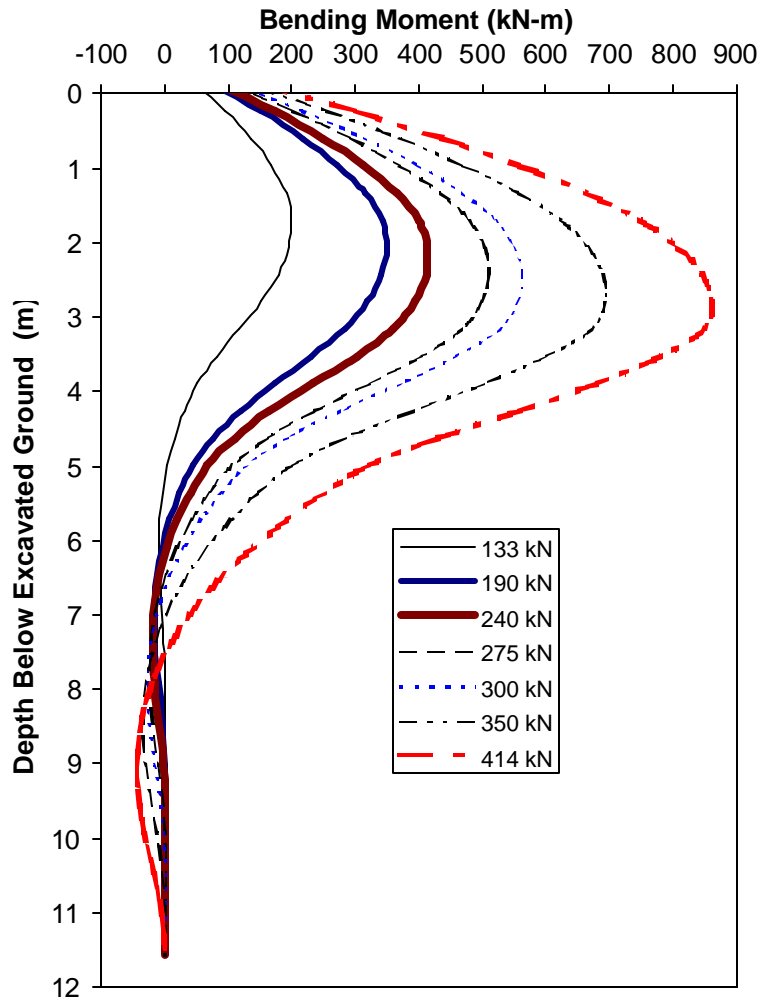
Figure 9.13 Bending moment versus depth curves for the 610 mm single pile computed using LPILE.
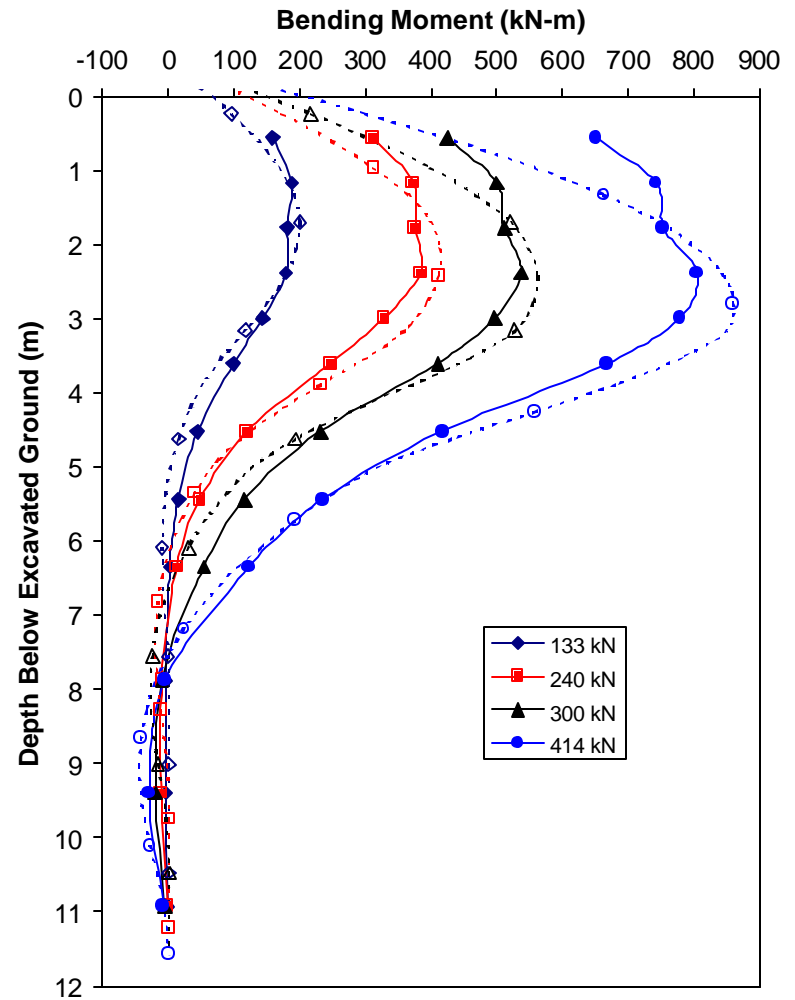
Figure 9.14 Measured moment versus depth curves for the 1st cycle (solid line) along with curves computed using LPILE (dashed line) at four load levels.

A review of the measured moment vs. depth curves suggests that the strain gauges at a depth of 1.78 m read a slightly smaller strain, leading to a smaller moment than was actually present in the pile. The LPILE analysis computed slightly higher maximum moments; however, if in fact the gauges at 1.78 m depth were recording a lower moment than was actually present, the LPILE and measured maximum moments would be even more similar, especially at the lower load levels. In each case, the LPILE moments return to zero at a slightly shallower depth than the measured moments.

Maximum moment vs. load. The maximum moments versus load curves comp uted by LPILE are plotted in Figure 9.15 along with the measured single pile test results. LPILE computed a higher moment for a given load than was actually observed. However, the difference was typically 15% or less, which is reasonable accuracy. Some of the discrepancy may result from strain gauge spacing which might not have picked up the maximum value.
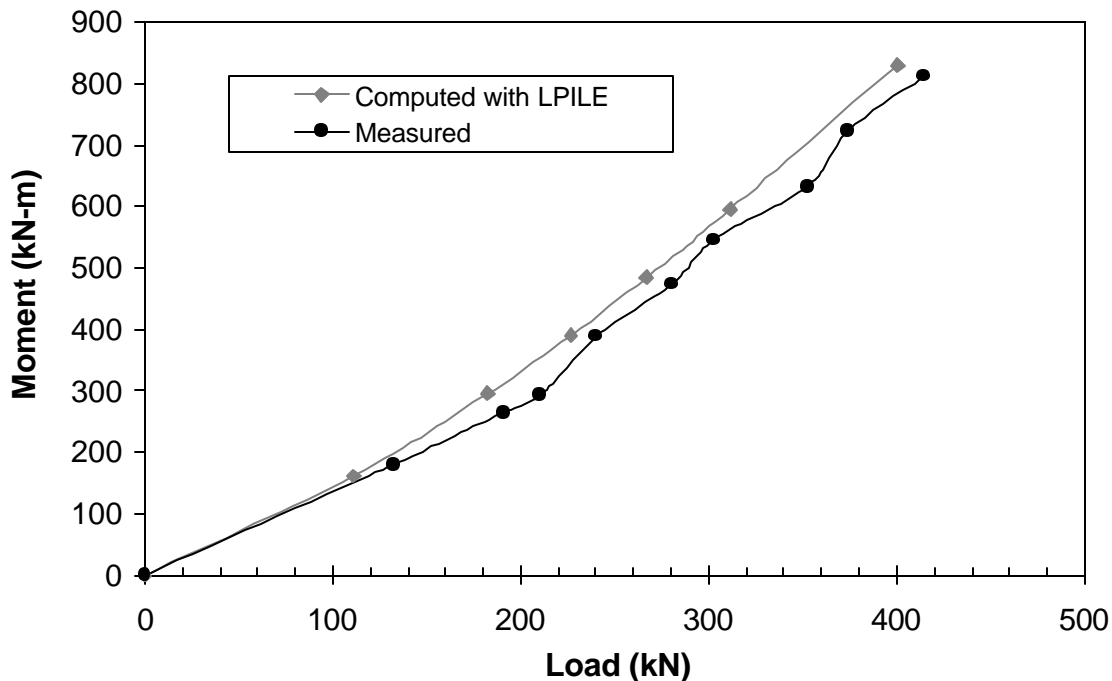
Figure 9.15 Measured maximum bending moment versus pile head load in comparison with curve computed using LPILE (1996).

CHAPTER 10 COMPUTER ANALYSIS OF LATERAL PILE GROUP TESTS

ANALYSIS PROCEDURE

GROUP version 4.0 (Reese and Wang, 1996) was used to perform the computer analysis all of the lateral pile group tests conducted in this study. GROUP is essentially an extension of the finite difference model used in LPILE; however, there are some additional factors that have to be considered. For example, GROUP considers the reduction in pile capacity for closely spaced groups with the use of p-multipliers as described in Chapter 1. The p-multiplier adjusts the horizontal resistance value, p, that would be used for a single isolated pile, by a constant factor. The user may specify p-multipliers for each row in the group or select default p-multipliers that are defined as a function of pile spacing for leading row and trailing row piles. In addition, GROUP also considers other factors such as pile group rotation in performing the lateral load analysis. For example, when a pile group is loaded laterally, the group may tend to rock, creating a compressive force on the front row piles and a tensile force on the back row piles. Side friction and end bearing from the piles resist these forces and stiffen the pile group against rotation. To account for these forces, the user must supply values for unit side friction and end bearing.

Florida Pier (FLPIER) version 1.71 NT (Hoit et al, 1997) was also used to analyze the 12 pile group along with the GROUP program. FLPIER also uses the p-multiplier concept to take into account the reduction in pile capacity due to the closely spaced piles. In addition to the parameters required in the GROUP analysis, FLPIER requires the input of a shear modulus value to account for shear deformations in the soil within the pile group.

SOIL PROPERTIES

The same soil profile and soil properties used in the companion single pile test were used in the GROUP analysis of the companion group. However, additional parameters such as side friction and end-bearing resistance were also specified based on the CPT cone resistance and undrained shear strength. For example, the unit side friction, q_s, for the sand layers was defined by the equation

$$q_s = q_c/200 \tag{10.1}$$

where q_c is the cone tip resistance. In clay, the unit side friction was taken as

$$q_s = 0.75 \, S_u \tag{10.2}$$

where s_u is the undrained shear strength. The unit end-bearing resistance, q_p, was defined by the equation

$$q_b = 9 \, s_u \tag{10.3}$$

PILE PROPERTIES

The pile properties used in GROUP were the same as those described in Chapter 9 for use in LPILE; however, the spacing in both directions was specified in the input. In some cases, the height of the load for the group tests involving the 324 mm diameter piles was somewhat higher than for the companion single pile test. Computer analyses using LPILE suggest that for the soil and pile properties involved in these tests, the load versus deflection curves are not very sensitive to these small variations. For example, the load versus deflection curves for the single 324 mm pipe computed assuming load heights of 0.39 and 0.495 m (15.5 and 19.5 in) are compared in Figure 10.1. While there is slightly more deflection for the pile with the 0.49 m load height, the two curves are almost indistinguishable. Therefore, no special adjustments have been made to account for these minor variations.

DETERMINATION OF P-MULTIPLIERS

Because the soil profile at each test pile group had already been defined based on the LPILE analysis of the companion single pile, the GROUP analysis could be used to back-calculate appropriate p-multipliers. Analysis options such as the number of iterations, convergence criteria and pile increments were also chosen to match the LPILE setup. In addition, sensitivity analyses using a range of side friction and end-bearing values suggested that the computed deflections were relatively insensitive to these parameters. In fact, analyses indicated that LPILE and GROUP computed the same average load versus deflection curves when group effects were ignored (p-multipliers equal to 1.0).

Initially p-multiplier values were set as the row multiplier values. The row multiplier values are the ratios of the average load carried by piles in a row in the group divided by the load carried by the single isolated pile at the same deflection. The GROUP analysis was then run for the total loads applied to the pile group. P-multipliers were adjusted, generally using a common factor, until the calculated deflections matched the field measurements at each load increment.

The p-multipliers are always smaller than the row multipliers because the row multipliers account for the reduction in resistance of the combined pile-soil system, whereas the p-multipliers only account for the reduction in soil resistance. Since the pile resistance remains essentially constant, the soil resistance must account for all the reduced resistance, hence the p-multiplier must be smaller than the row multiplier. Once the p-multipliers had been back-calculated based on the load-deflection curve, GROUP was used to compute load versus deflection curves for each row along with bending moment curves for each row. Comparisons were made between the computed and measured pile head load versus deflection curves and the computed and measured bending moments for each row.

RESULTS OF ANALYSIS FOR 9-PILE GROUP AT 5.6 DIAMETER SPACING

P- Multipliers and Pile Head Load versus Deflection.

The load-deflection curves for each row in the 9 pile group were compared with the load-deflection curve from the lateral load test on the 324 mm diameter pile tested in virgin soil. The average row load multipliers were found to be 1.00, 0.94, and 0.82 for the front, middle and back rows, respectively. Using GROUP, the back-calculated p-multipliers for this relatively widely spaced pile group were found to be 0.94, 0.88 and 0.77 for the front, middle and back rows, respectively. Figure 10.1 compares the measured total load versus average group deflection curve for this pile group with that computed using the p-multipliers found in this study. When the decreased soil resistance is accounted for by p-multipliers, the overall average difference in
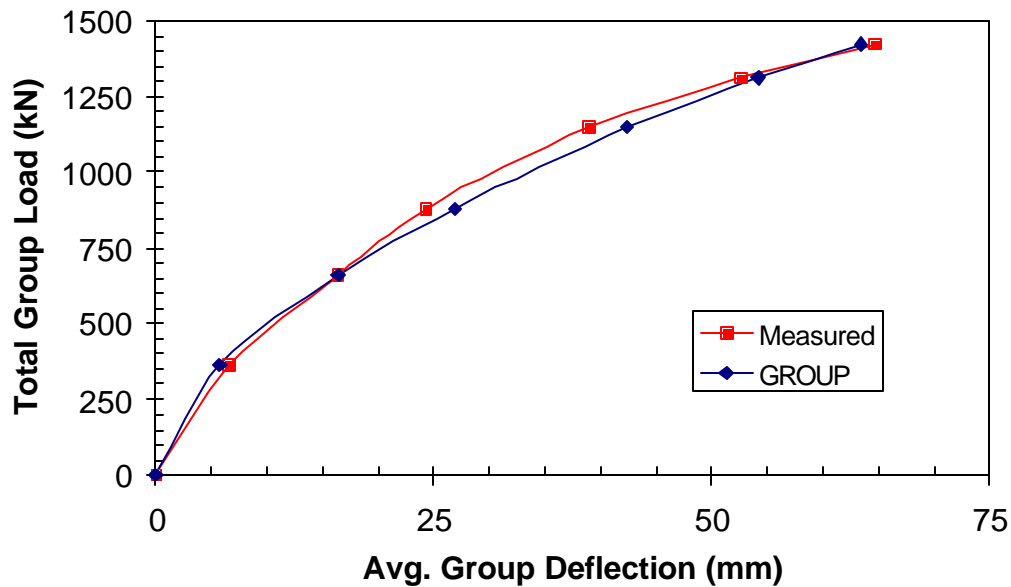
Figure 10.1 Measured total load versus deflection curve for 324 mm nine-pile group relative to curve computed by GROUP using p-multipliers developed in this study.
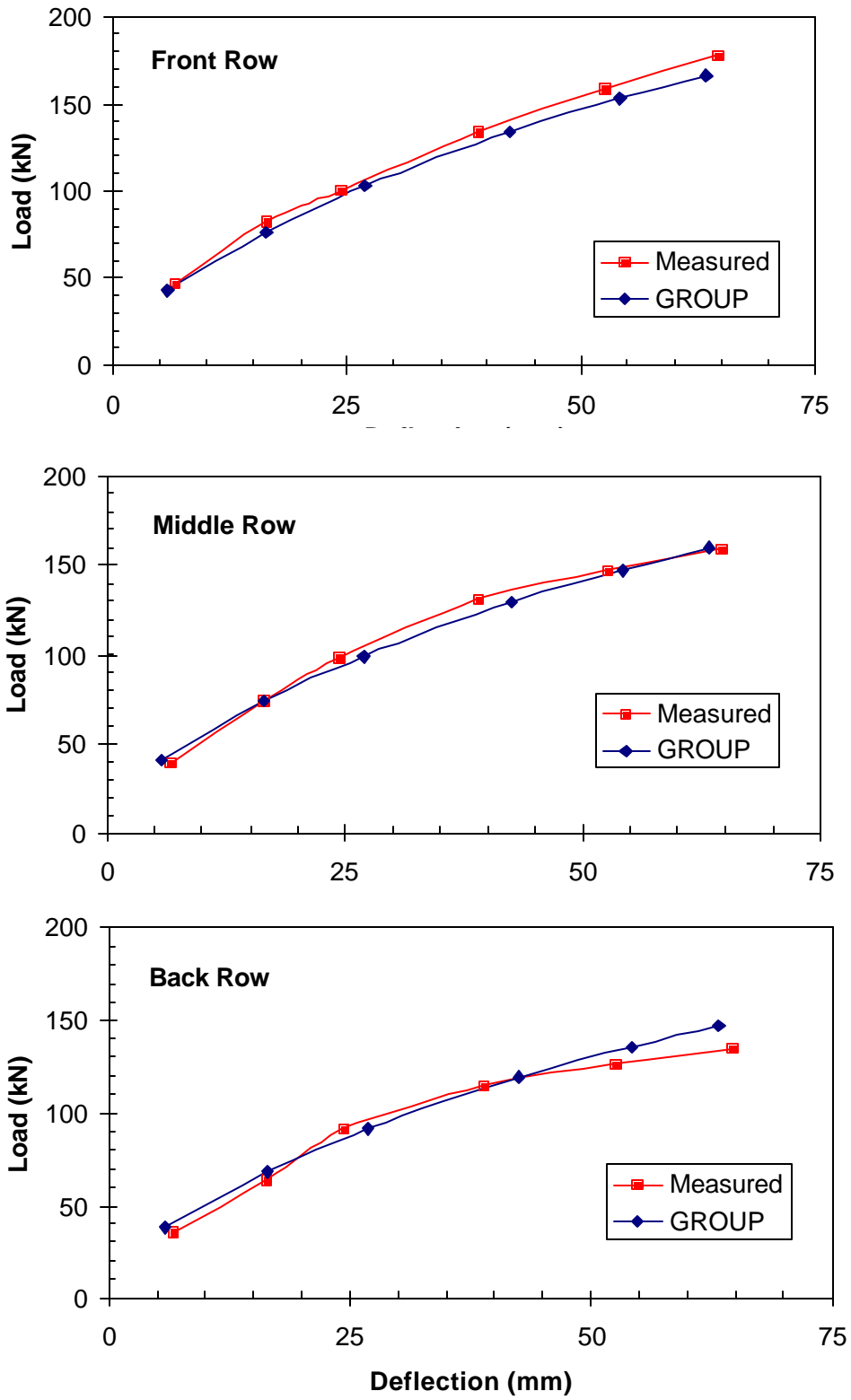
Figure 10.2 Measured load vs. deflection curves relative to curves computed by GROUP using p-multupliers developed in this study.

THIS PAGE LEFT BLANK INTENTIONALLY

computed deflection for a given load is within 6% of the measured deflection. In most cases, the computed deflection is slightly higher than the measured value.

Average measured load versus deflection curves for the three rows in the group are shown in Figure 10.2 in comparison with the curves computed using GROUP with the new p-multipliers developed in this study. The match between measured and computed response is very good in each case with a maximum difference in computed and measured load of less than about 10% for a given deflection.

Bending Moment versus Load.

Curves showing the computed maximum bending moment versus average row load are shown in Figure 10.3. As with the measured curves presented in Figure 5.16, the back row has the highest moment for a given load and the front and middle curves are close together. The difference between the back and front rows increases slowly with increasing load, reaching about 13% at 135 kN in comparison with a 23% difference for the measured values.

Figure 10.4 compares the bending moment versus load curves computed by GROUP with the measured curves for each row. The computed and measured curves match very well on the back row and are within about 10% on the front and middle rows. The conservative estimate of the maximum moment for the front and middle rows suggests that the p-multiplier may be slightly conservative.
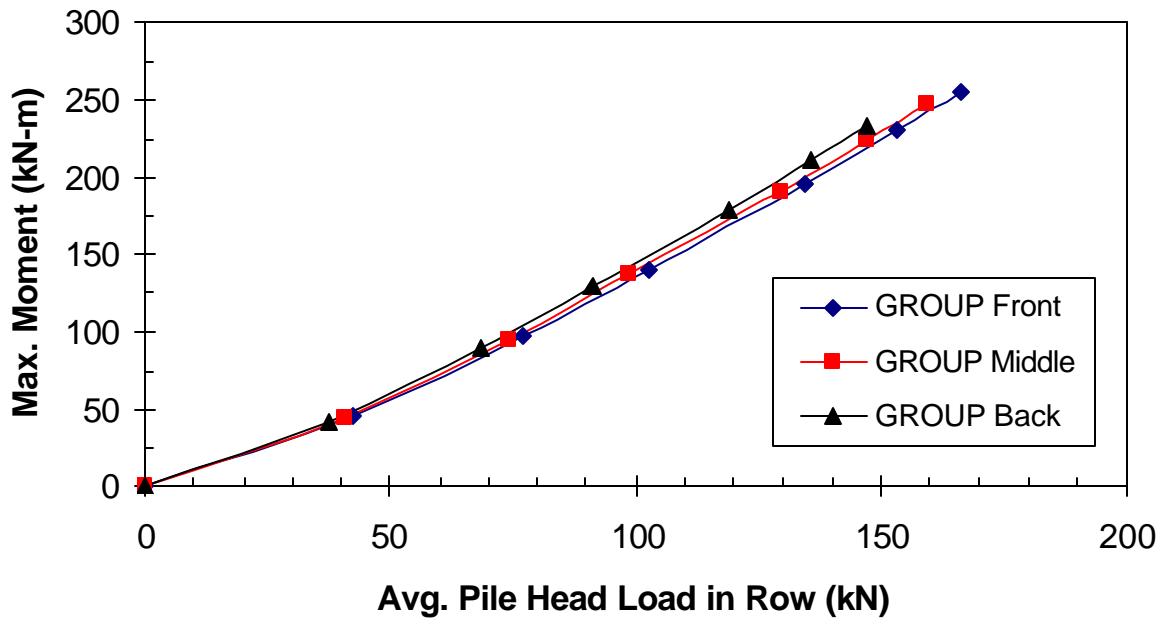
Figure 10.3 Computed maximum moment versus load curves for each row in the group computed by GROUP using the p-multipliers developed in this study.

Bending Moment versus Depth.

Computed bending moment versus depth curves are presented in Figures 10.5 and 10.6 for two load increments along with corresponding measured curves for the three rows in the pile group. The depths to the maximum moment computed by GROUP appear to be approximately correct although somewhat shallower than the measured depth in one case. The general shape of the computed curves is also approximately correct; however, GROUP tends to predict a more rapid drop-off in bending moment with depth than was measured during this test. For example, the average depth to zero moment was about 4.5 m, compared to 6.10 meters in the measured results.
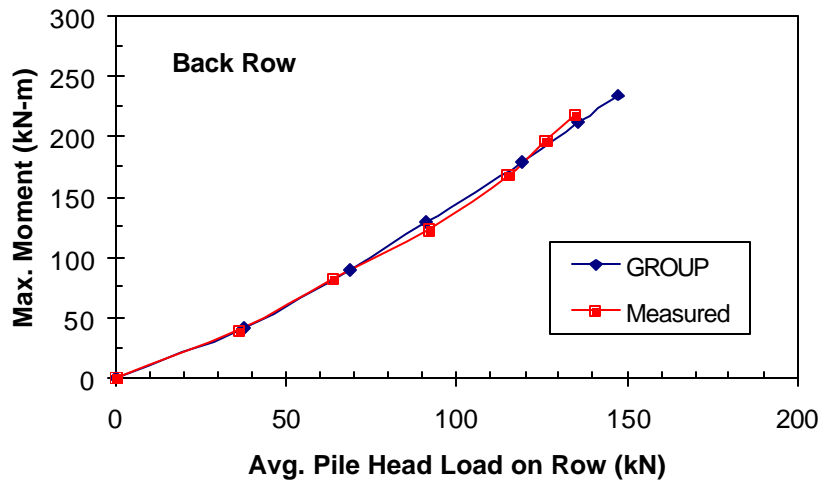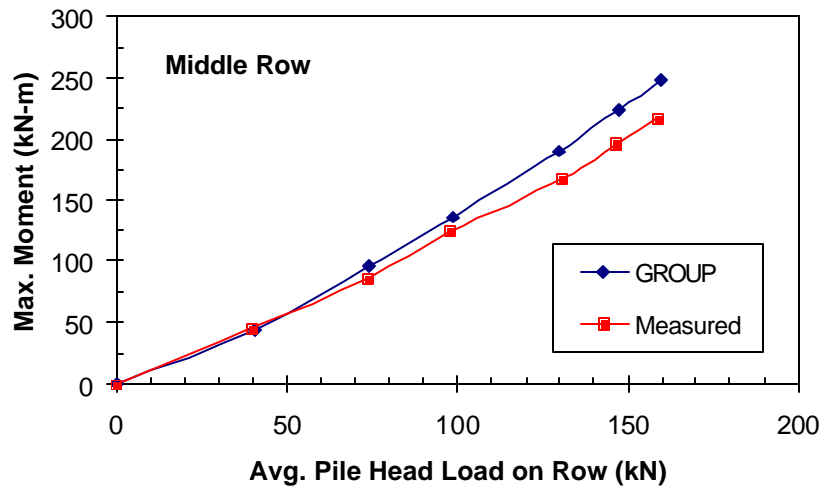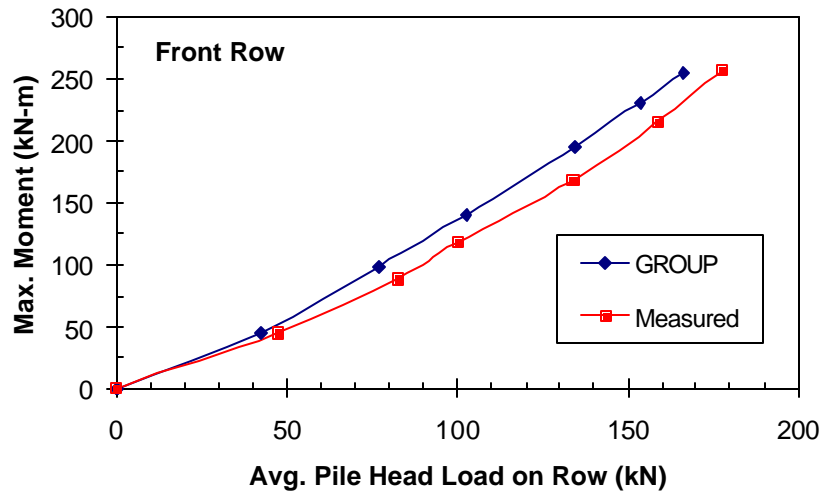
Figure 10.4 Measured maximum bending moment curves for each row relative to curves computed using GROUP with P-multipliers developed in this study.
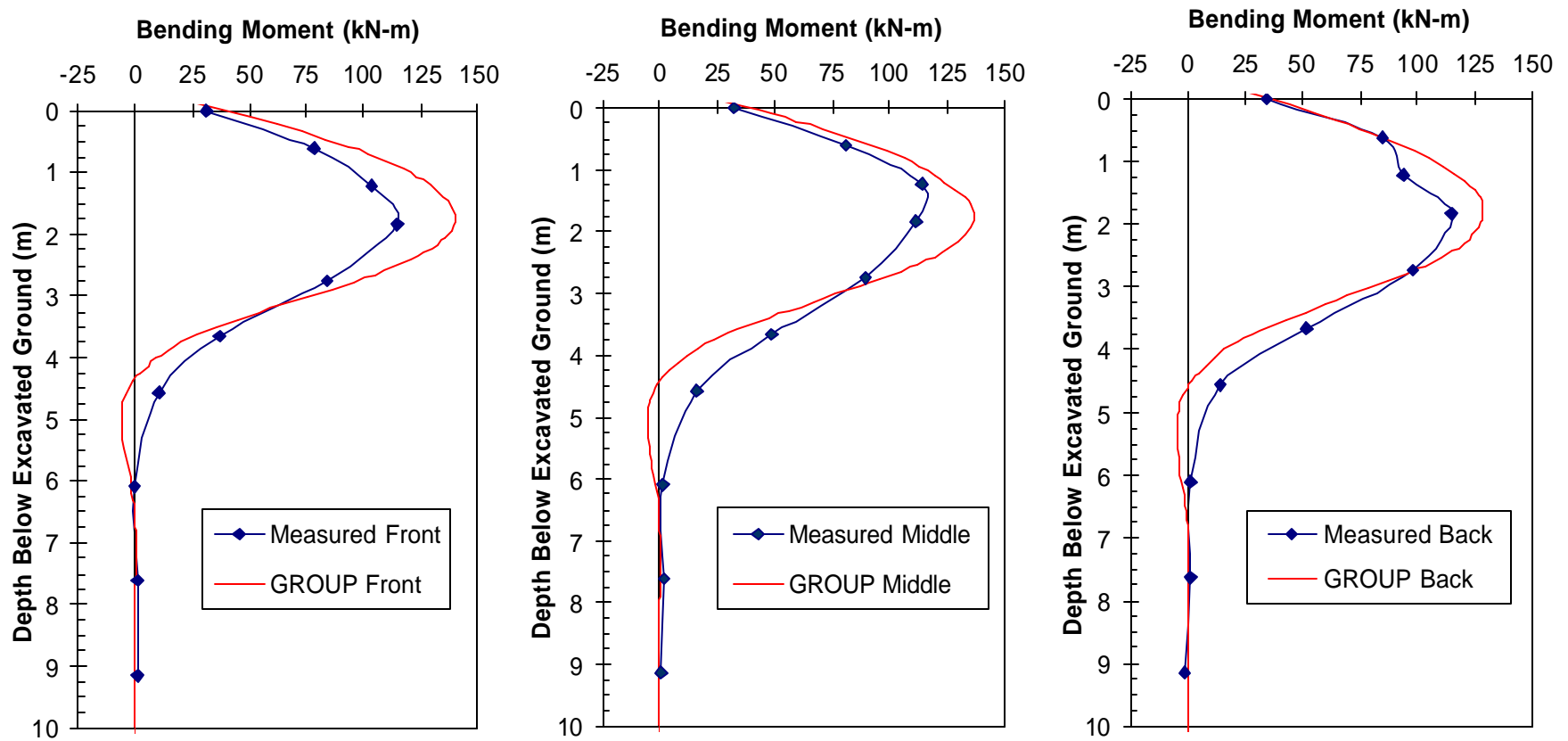
Figure 10.5 Comparison by row of measured bending moment versus depth curves and curves computed using GROUP for the 24 mm deflection.
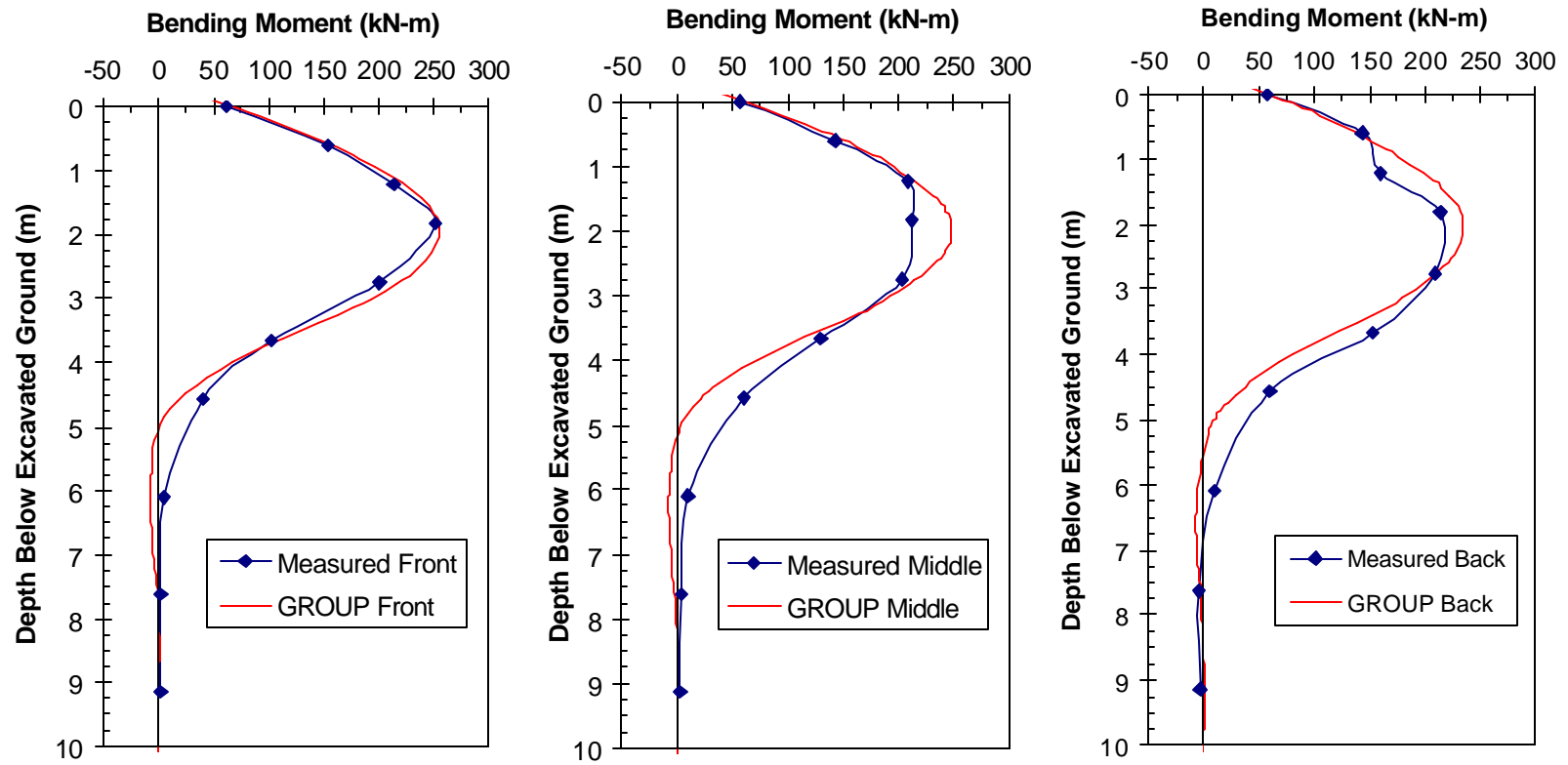
Figur 10.6 Comparison by row of measured bending moment versus depth curves and curves computed using GROUP for the 63.5 mm deflection.

RESULTS OF ANALYSIS FOR 12-PILE GROUP AT 4.3 DIAMETER SPACING

P- Multipliers and Pile Head Load versus Deflection.

The load-deflection curves for each row in the 12 pile group were compared with the load-deflection curve from the lateral load test on the 324 mm diameter pile tested in virgin soil. The average row load multipliers were found to be 1.00, 0.89, and 0.77 and 0.81 for rows 1 (front), 2, 3, and 4 (back), respectively. Using an iterative process with GROUP, the back-calculated p-multipliers for this pile group were found to be 0.90, 0.81, 0.69, and 0.73 for rows 1, 2, 3, and 4, respectively. When these p-multipliers were used in FLPIER, the computed load versus deflection curve was very similar to that obtained with GROUP.

The GROUP and Florida Pier programs allowed the user to (1) specify the p-multipliers, (2) use default p-multipliers chosen by the program, or (3) ignore the group effect altogether. Figure 10.7 show the measured total group load versus average group deflection curve with the
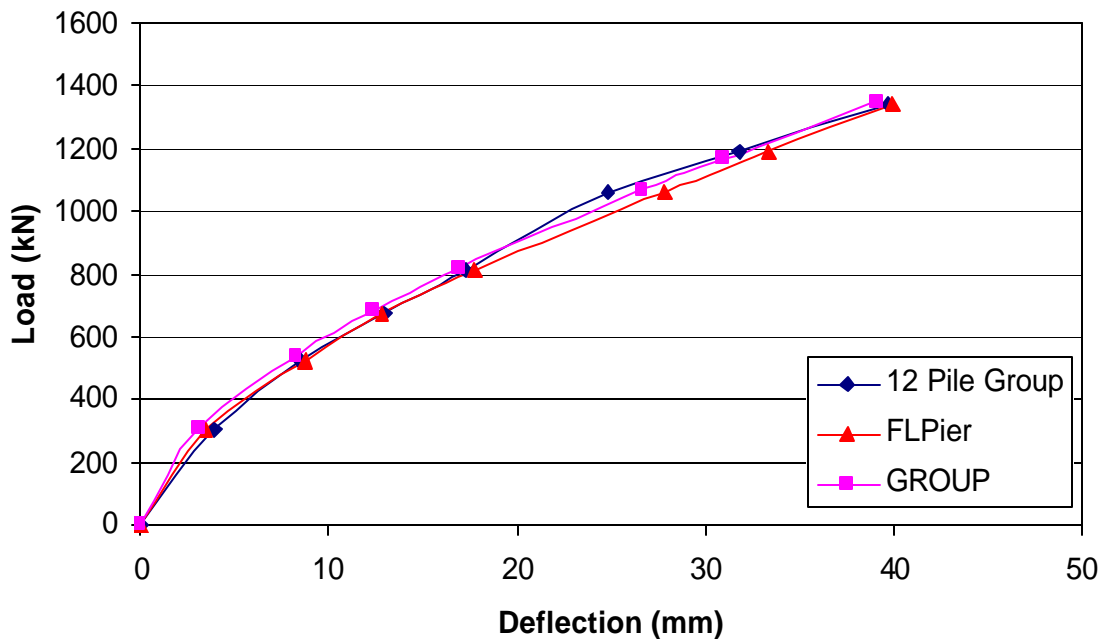

Figure 10.7 Comparison of measured total load versus deflection curves with curves computed by GROUP and FLPIER using p-multipliers developed during this study.

curves computed using GROUP and FLPIER with the p-multipliers developed during this study. The agreement in both cases is very good; however, FLPIER tended to compute somewhat higher deflections for a given load relative to GROUP.

Figure 10.8 presents the load versus deflection curves computed using the default p-multipliers chosen by GROUP and FLPIER based on the spacing and the same soil profile. The default p-multipliers chosen by GROUP were 1.0 for the leading row and 0.93 for the trailing rows. The deflections that were measured in the field tests were, on average, 23% greater than those predicted by GROUP using the default p-multipliers. Florida Pier used default p-multipliers of 0.8 for the leading row and 0.4, 0.2, and 0.3 for the three trailing rows. The deflections calculated by Florida Pier were on average 100% greater than those measured in the field. This was due to the very low default p-multipliers chosen by the program.
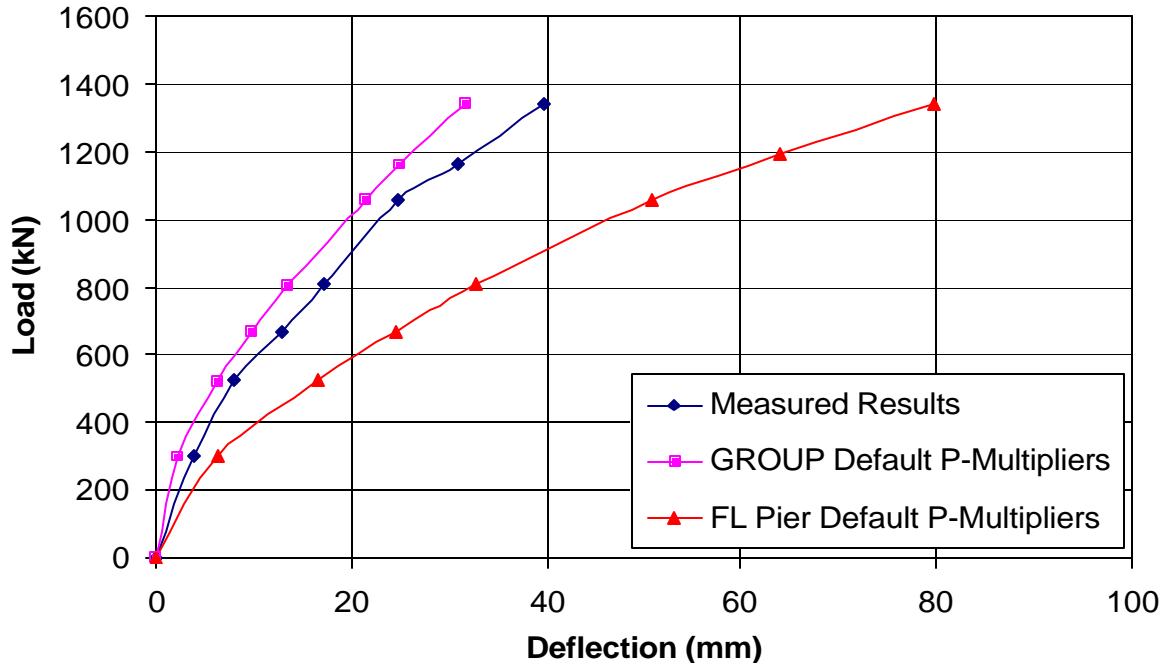
Figure10.8 Comparison of measured total load versus deflection curve with curves computed by GROUP and FLPIER using their respective default p-multipliers.

When the group effects were completely ignored, (the p-multipliers set to 1.0 for each row) there was a better correlation between Florida Pier and GROUP than when respective default p-multipliers were used. However, the computed load versus deflection curves were stiffer than the measured results. Figure 10.9 shows the measured total load versus deflection curve and the curves calculated by GROUP and FLPIER using the same soil profile and p-multipliers of 1.0 for each row. The deflections that were measured in the field tests were on average 27% greater than those predicted by GROUP and 22% greater than those predicted by FLPIER.
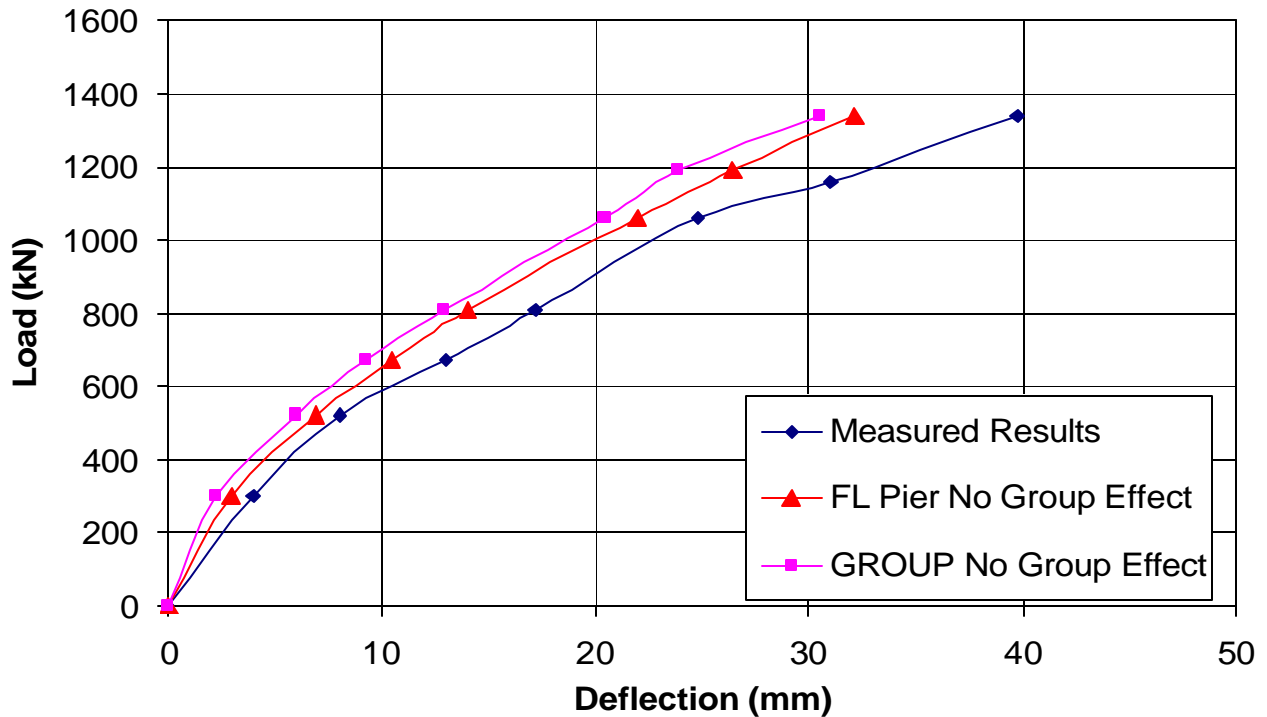
Figure 10.9 Comparison of measured total load versus deflection curves with curves computed by GROUP and FLPIER when the group effect is ignored (P-mult=1.0).

Row 1
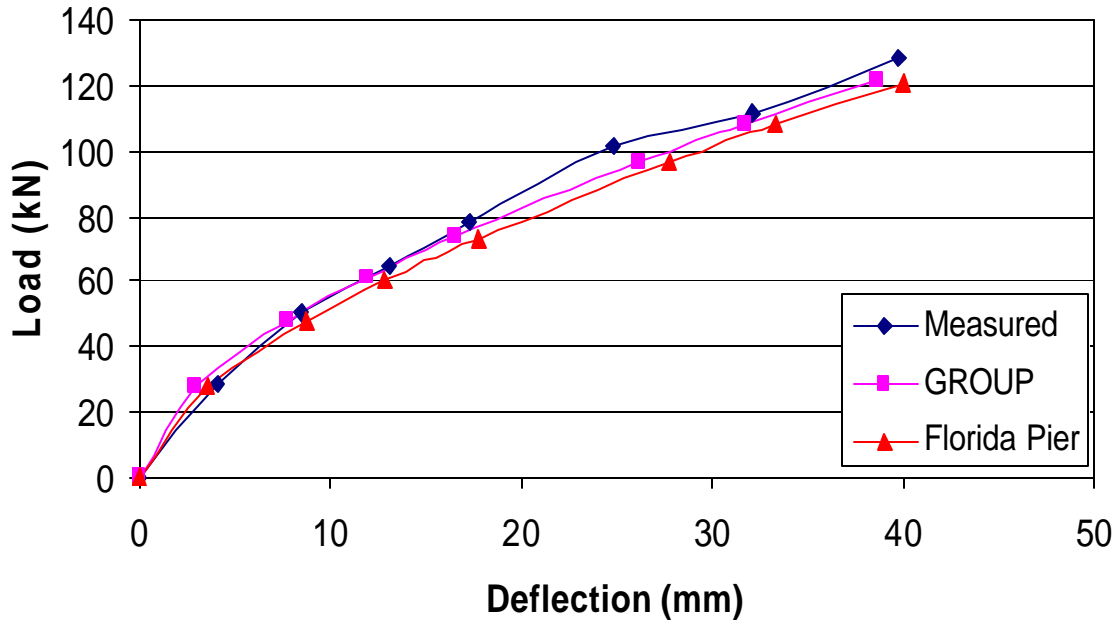
Row 2
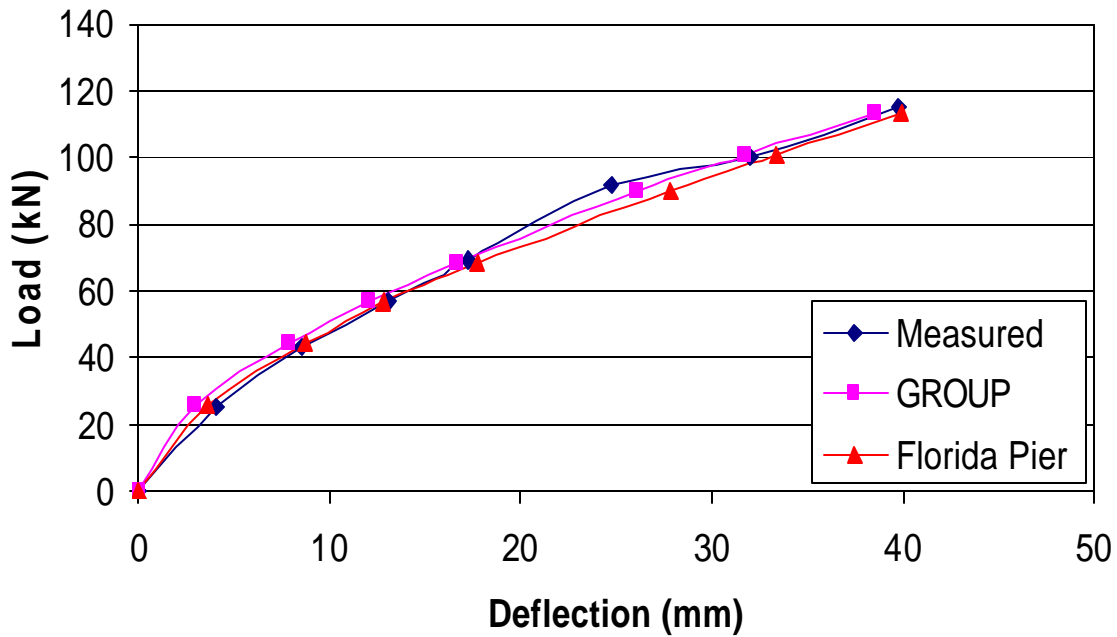
Figure 10.10 Comparison of the measured load versus deflection curves for each row with curves calculated by GROUP and FLPIER using the p-multipliers developed in this study.
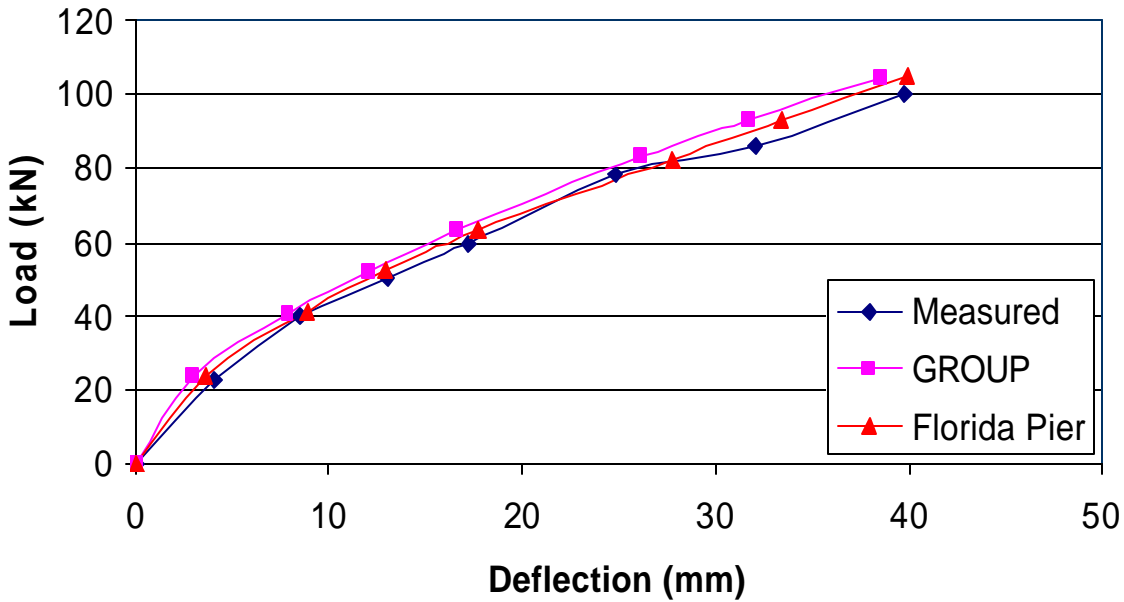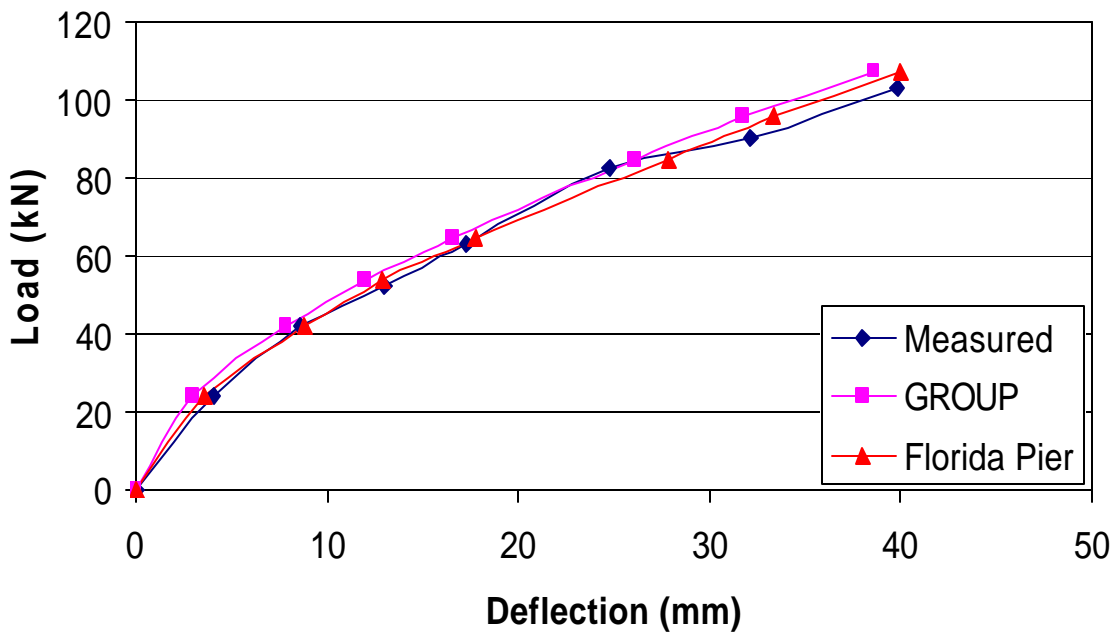
Figure 10.10 (Cont.) Comparison of the measured load versus deflection curves for each row with curves calculated by GROUP and FLPIER using the p-multipliers developed in this study.

Figure 10.10 shows the measured and calculated average pile load in each row versus deflection curves for each row of the pile group. The calculated loads were obtained using the p-multipliers developed in this study. The agreement is excellent. The calculated loads from the GROUP and FLPIER programs differed from the measured loads by less than ten percent. In the previous plots, p- multipliers were back calculated to match the first cycle of loading at each target deflection. However, the behavior of the group had changed by the 15th cycle of each target deflection and the resistance was typically 18% lower than **it** was initially. To verify that the p- multipliers developed for the first cycle were still adequate for modeling the peak load deflection curve for the 15th cycle, another computer analysis was conducted.

The three soil profiles that were used to match the load versus deflection curve for the re -loaded single pile (see Figure 9.9) were used to check the applicability of the p-multipliers
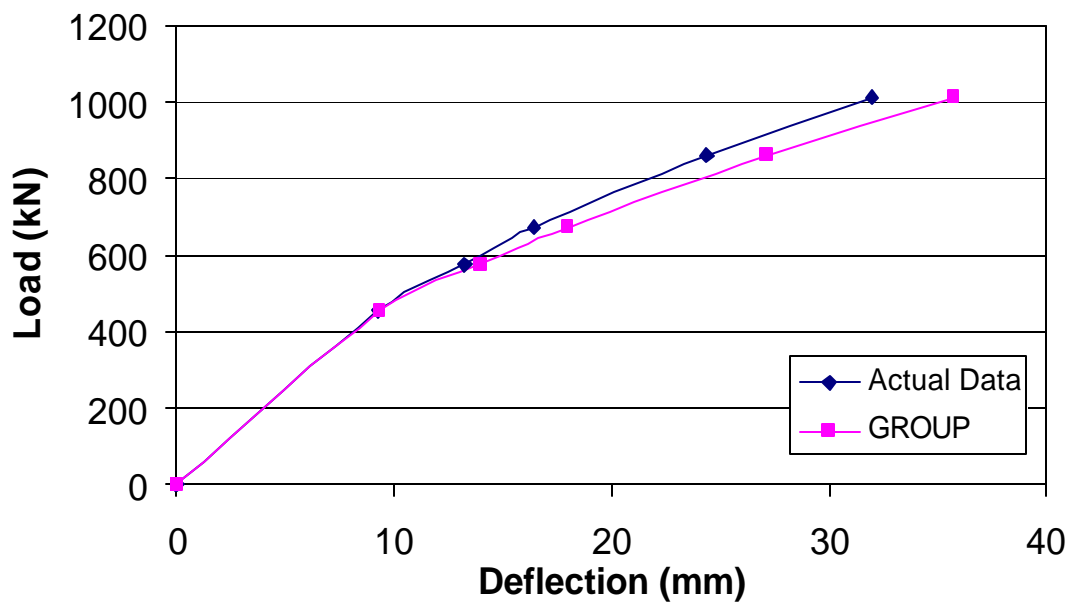
Figure 10.11 Measured fifteenth cycle load vs. deflection curve in comparison with curve computed by GROUP using reduced strength and p-multipliers developed during this study.

10-17

during the 15th cycle. Once again, p- multipliers of 0.9, 0.8, 0.69, and 0.73 were used for the first, second, third, and fourth rows, respectively. Figure 10.11 presents the measured fifteenth cycle total load versus average deflection curve with that generated by GROUP using the p- multipliers.   The difference in the measured deflection and the computed deflection at a given load was approximately 10%.

The maximum moment versus the average pile head load per row is shown in Figures 10.12 and 10.13 for the GROUP and the FLPIER analyses, respectively. The results from both computer analyses were similar to those shown in Figure 6.18 for the measured field results. The third row was shown to have the highest moments while the first row had the least for a given average load. This is due to the reduced soil resistance in the trailing rows relative to that in front of the lead row.

The difference between the first and third row moments increased as the load increased in both the measured and computed results. The computer solutions, however, showed much less variation in the maximum moments for the four rows than was measured in the test. The maximum moment of the third row obtained in the field results was 24% greater than the moment in the first row for an equivalent load. In the GROUP calculations, this difference was only 8%. The FLPIER results showed a difference between the third and first row of about 7%. Both GROUP and FLPIER underpredict the measured variation in moment observed in the testing.

Figures 10.14 and 10.15 show the maximum moment versus average load within a row for the first and third rows of the pile group. The models fit the front row quite well with a small amount of divergence as the moments and loads reached peak values. The models overpredicted
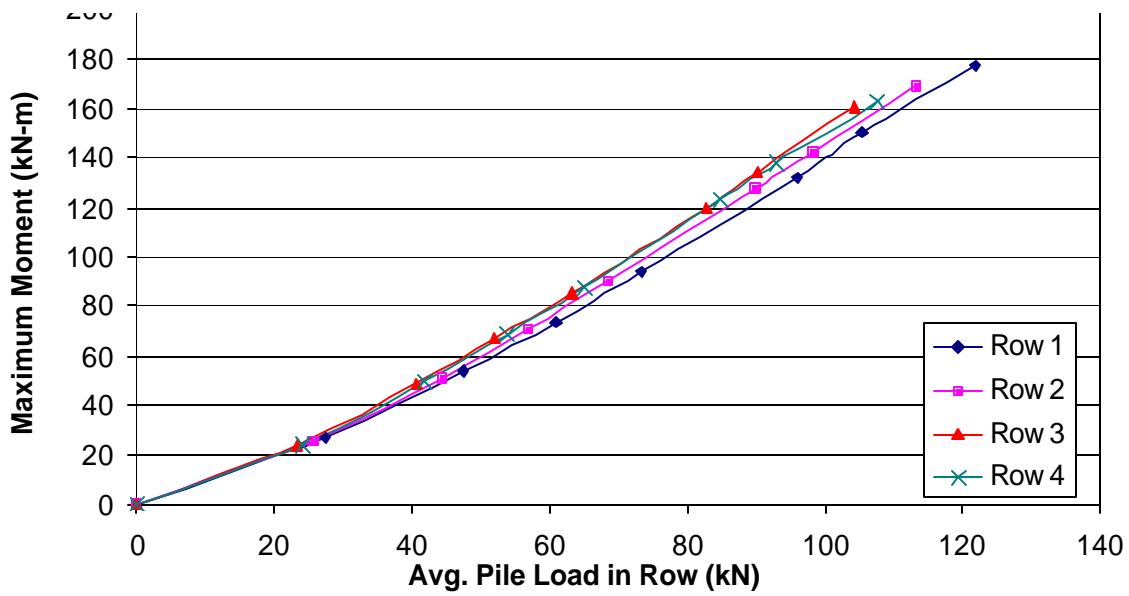
**Figure 10.12 Maximum moment versus average pile load in row computed by GROUP.**
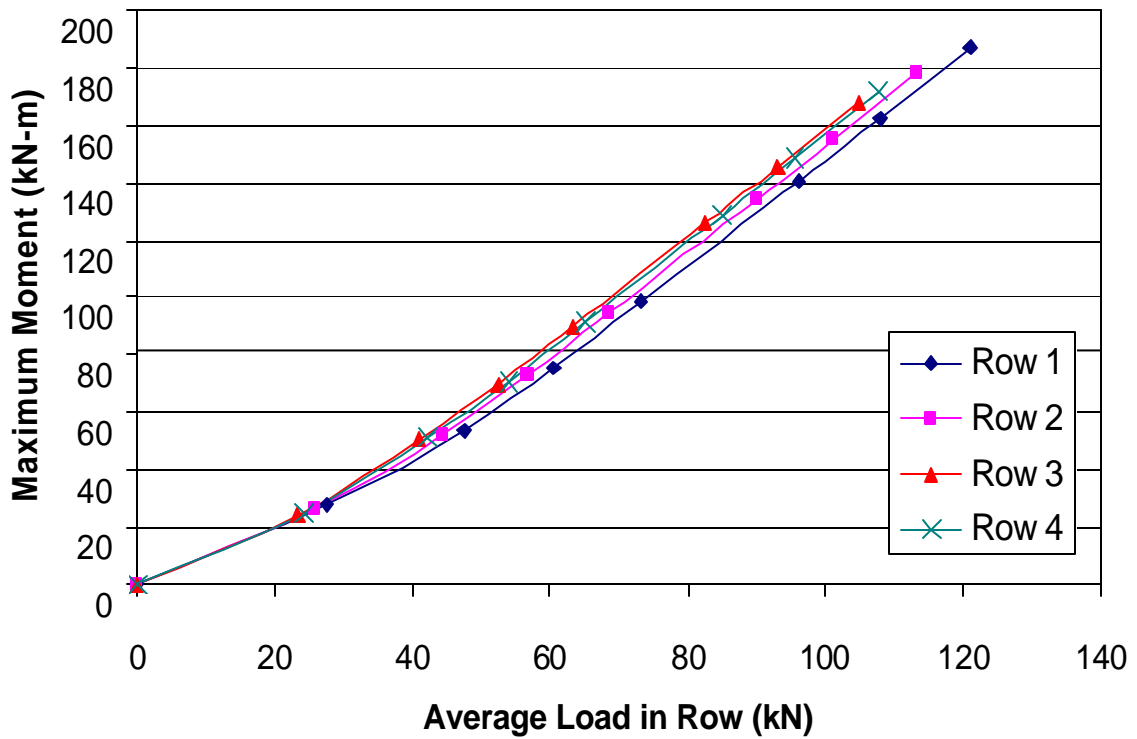
Figure 10.13 Maximum moment versus average pile load in row computed by FLPIER.

10-19
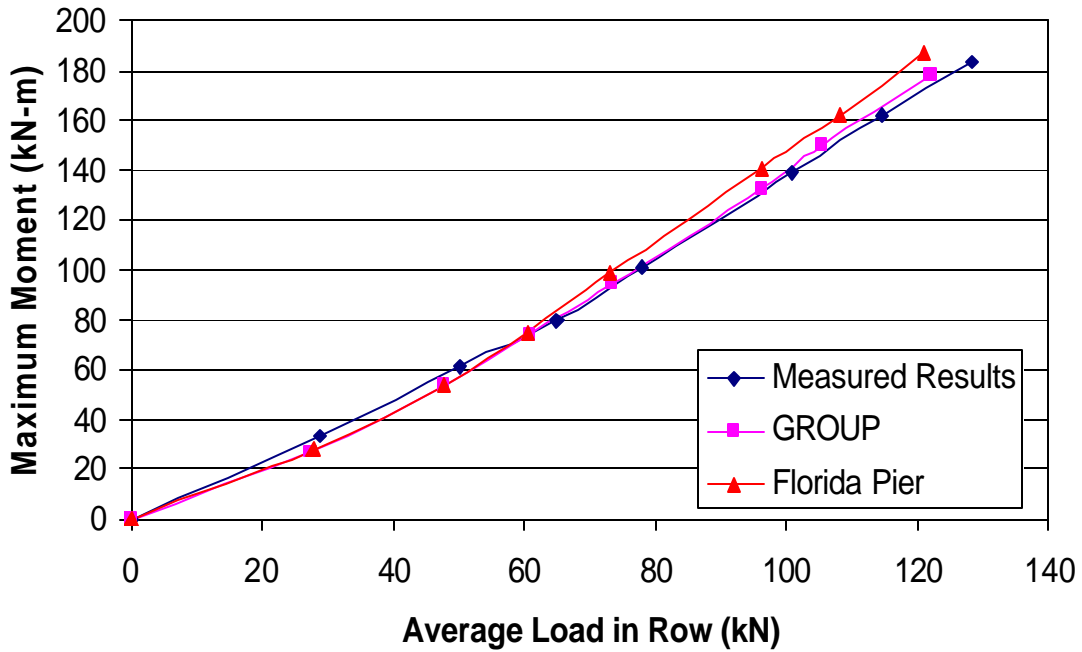
**Figure 10.14 Maximum moment versus average load per pile for the front row.**
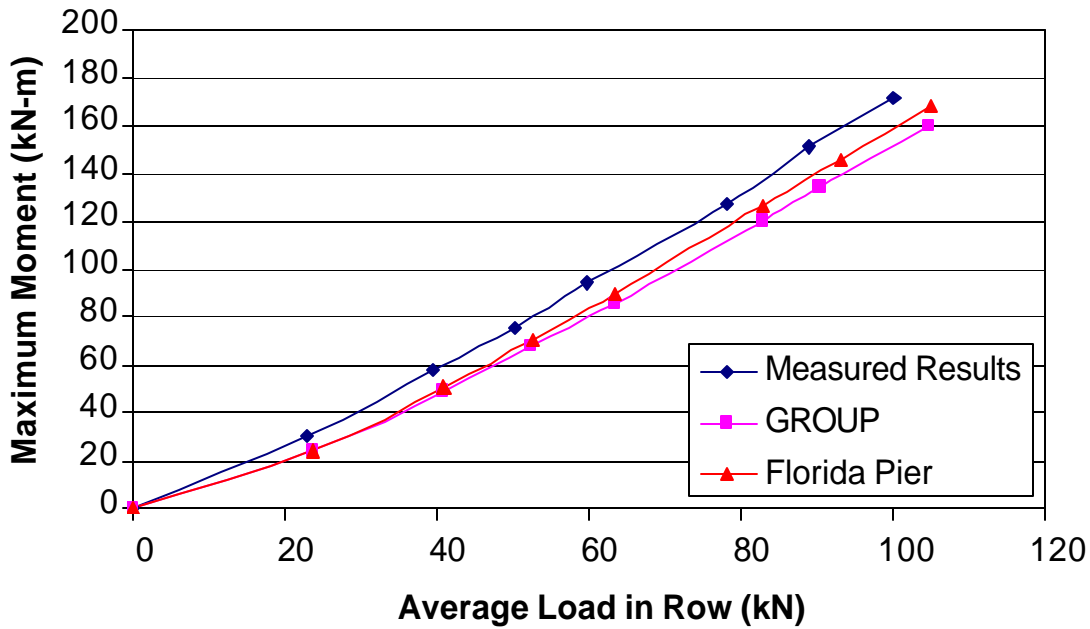
Figure 10.15 Maximum moment versus average load in row for third row of piles

the load required to get the maximum moment in the third row by about 4%. This is probably

due to less soil resistance around the third row than anticipated by the model.s

    Figures 10.16 and 10.19 provide comparisons between the measured bending moment versus

depth curves and the curves calculated using GROUP and FLPIER at three specific

deflections of 8.5, 24.2, and 39.5 mm (0.33, 0.95, and 1.55 inches). The maximum bending moments in the front row were calculated by GROUP to occur at depths of 1.95, 2.07, and 2.32 meters (6.4, 6.8, and 7.6 ft) for the three chosen deflections. The depths to the maximum bending moment calculated by FLPIER were all at 2.13 m (7.0 ft). This discrepancy may be due to differences in the node spacing in the two models. For example, GROUP had nodes every 122 mm (4.8 in) along the length of the pile, while Florida Pier only had nodes at increments of 787 mm (32.3 in). This node spacing can be adjusted by the user in GROUP but is fixed in the FLPIER program.

The GROUP analysis showed that the maximum moment in the trailing rows occurred slightly deeper than in the leading row. As stated in Chapter 6, the measured bending moments for the trailing rows appeared to occur deeper than the leading row due to the group effect that reduces the shear strength of the upper soil layers. The FLPIER results showed the maximum moment occurring at the same depth for each row. This is likely due to the relatively large gaps between nodes where the pile behavior was analyzed. There was a good correlation between the measured and calculated results. In most cases, however, the depth to the maximum moment calculated from the strain gauge measurements appeared to occur slightly deeper than those predicted by the models. Nevertheless, the agreement is still relatively good.

The computer models tend to underpredict the bending moment values below the depth where the maximum moment occurs. The programs predict a more rapid drop off in bending moment than actually occurs. In addition, the moment reversal that was measured is less significant than that predicted by the computer models.

A comparison of the maximum moments reveals that for the higher deflections, the difference between the measured and computed values is generally less than 10%. For the 39.5

mm deflection, the computed maximum moment was within ± 2% of the measured value. The agreement seemed to get better as the deflection of the pile group increased. At small deflections, local variations around the pile may be more important than they would be at large deflection levels. For example, during driving, small gaps can be created due to wobbling of the pile that may influence lateral pile response at small deflections but not at large deflections.
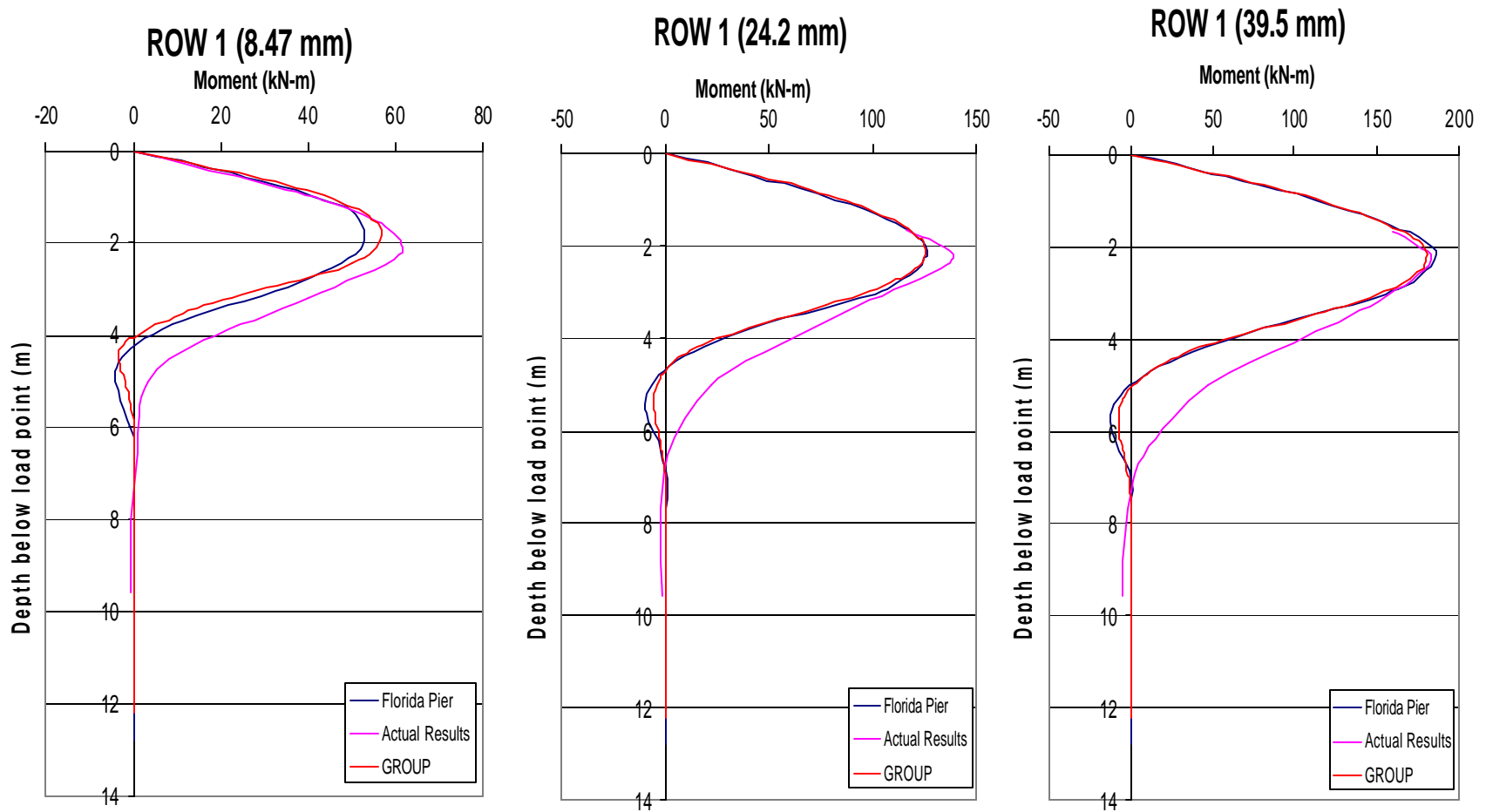
Figure 10.16 Comparison of measured bending moment vs. depth curves with curves computed using GROUP and Florida Pier for row 1 (front row) at three deflection levels.

10-23
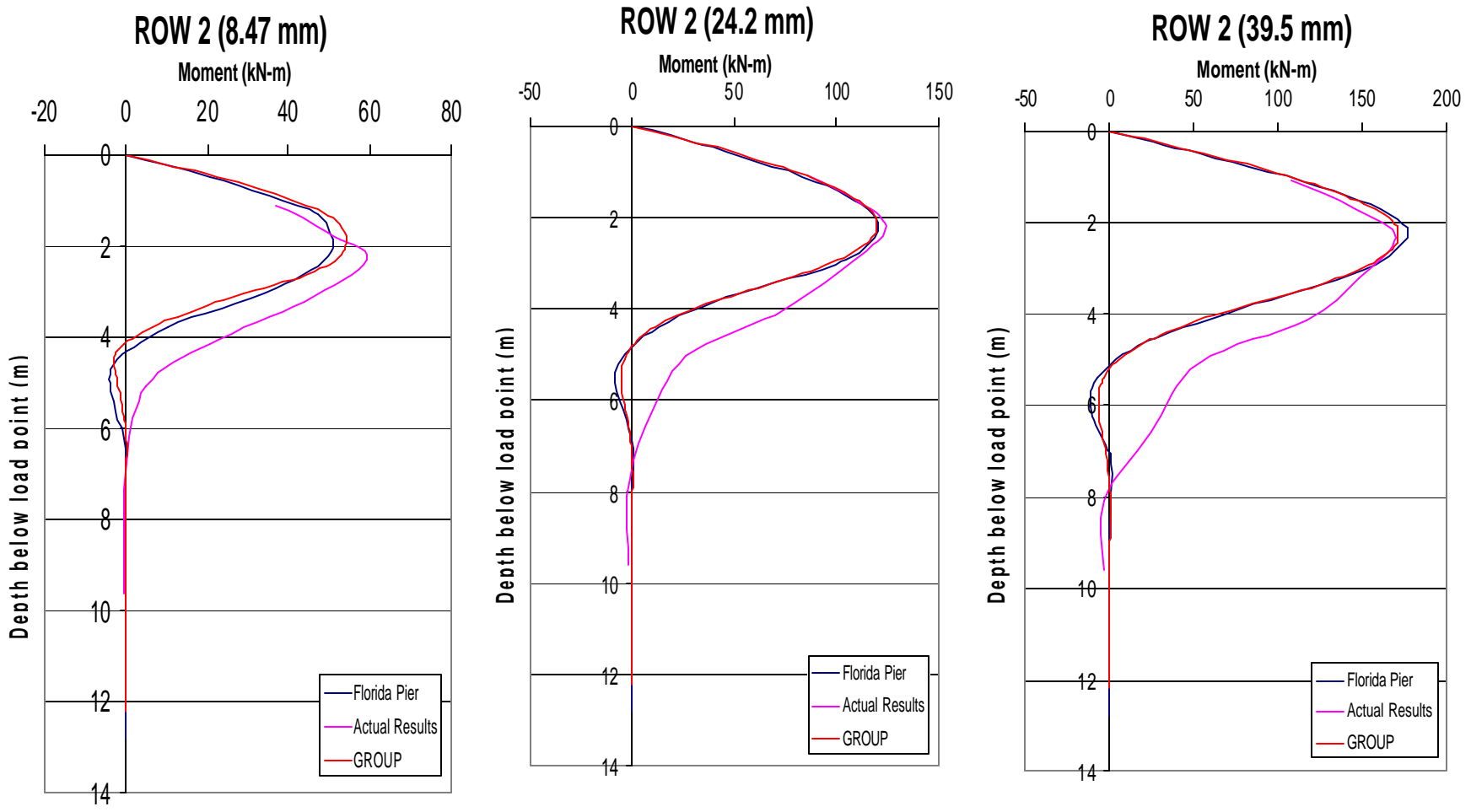
Figure 10.17 Comparison of measured bending moment vs. depth curves with curves computed using GROUP and Florida Pier for row 2 piles at three deflection levels.
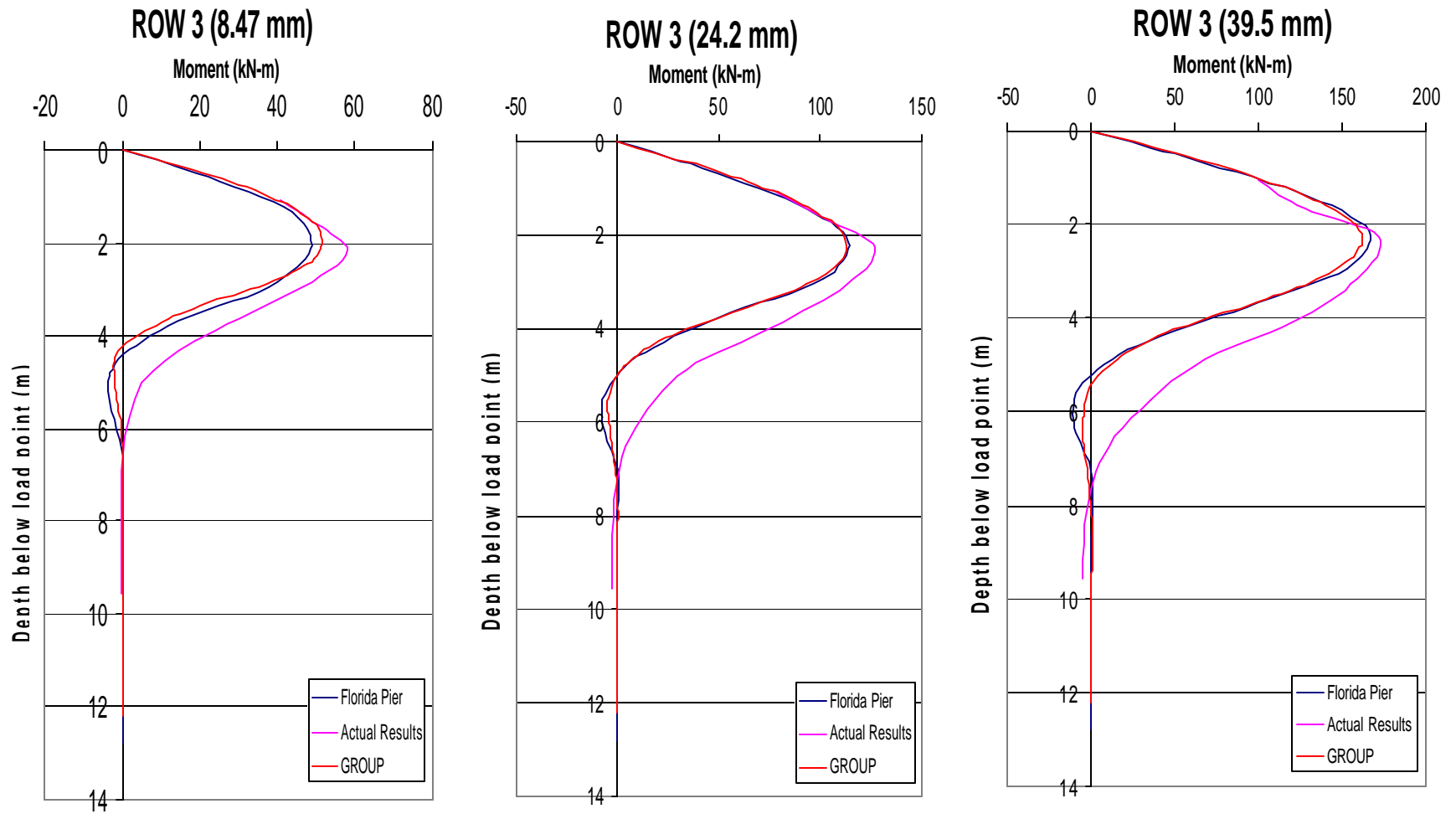
Figure 10.18 Comparison of measured bending moment vs. depth curves with curves computed using GROUP and Florida Pier for row 3 piles at three deflection levels.
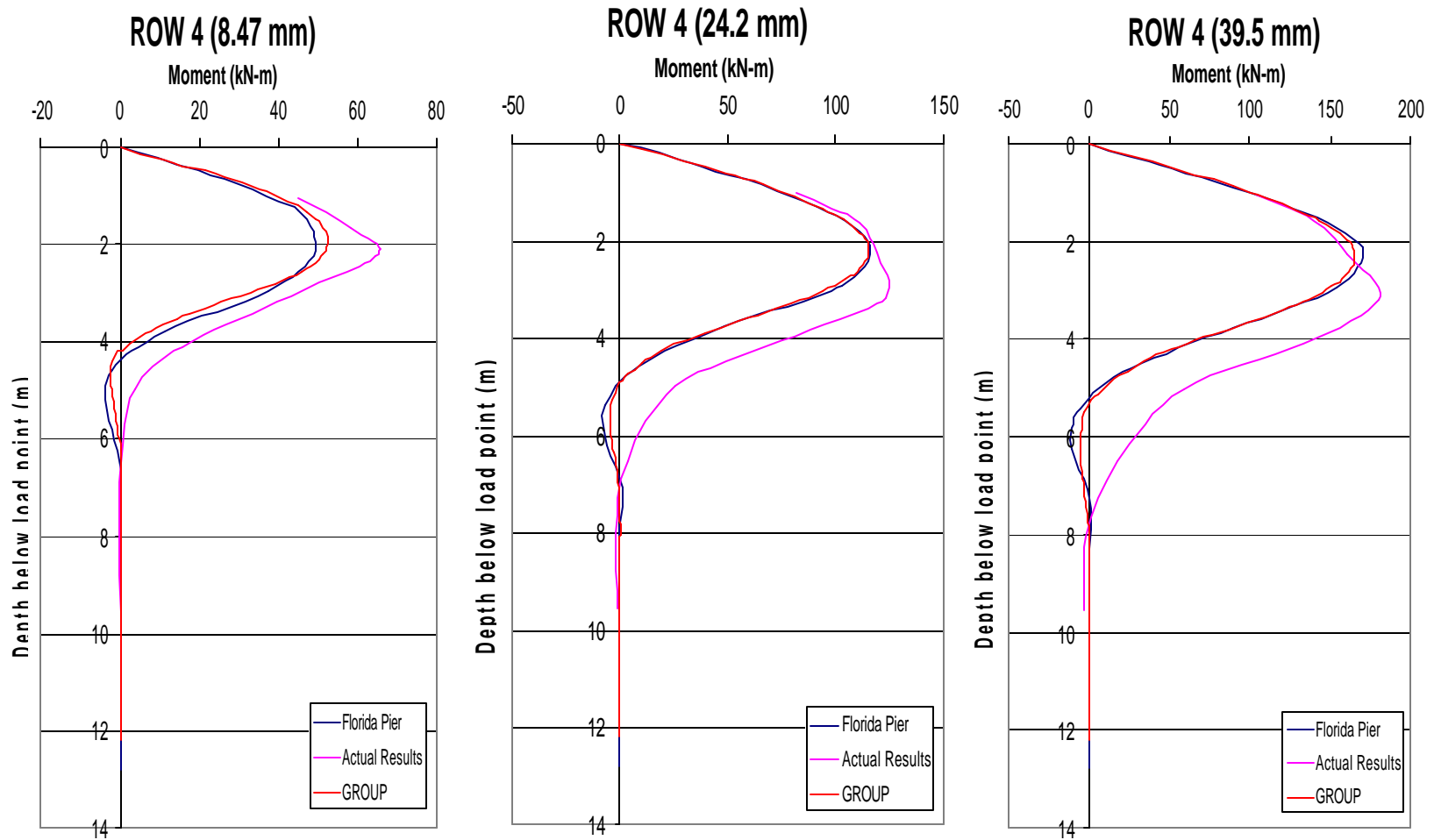
Figure 10.19 Comparison of measured bending moment vs. depth curves with curves computed using GROUP and Florida Pier for row 4 (back row) piles at three deflection levels.

Rotation

GROUP and LPILE can compute a pile head rotation as part of the model computations. FLPIER did not provide rotational calculations in its output files. The measured rotation of the isolated single pile and the free-head pile group are shown in Figure 10.20 along with the rotations computed using LPILE for the single pile and GROUP for the pile group. The measured rotation of the pile group was approximately 50% greater than predicted by GROUP. The measured rotation of the single pile was approximately 70% smaller than those predicted by LPILE. Although the percentage difference seems quite large, it should be noted that we are dealing with small differences in rotation. The difference between the maximum measured pile group result and that predicted by GROUP is 0.0151 radians or 0.87 degrees. Future attempts to study pile head rotation should be conducted using LVDTs spaced further apart so that the measured rotation will not be so sensitive to errors.
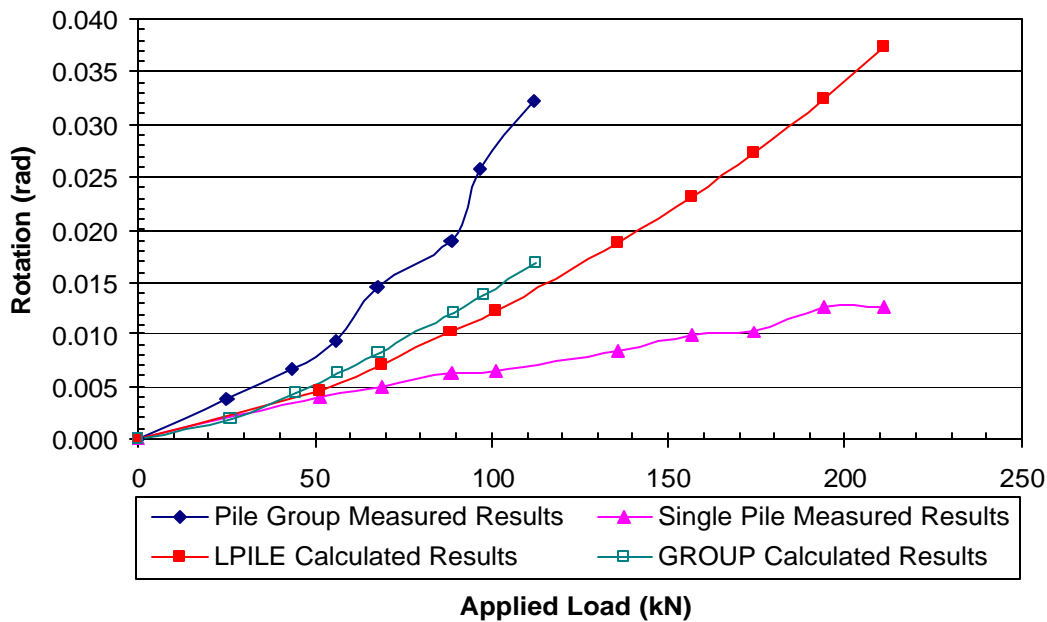
Figure 10.20 Comparison of measured and computed rotations.

ANALYSIS OF TEST RESULTS FOR 12 -PILE GROUP UNDER FIXED-HEAD CONDITIONS

After the free-head testing, a reinforced concrete pile cap was poured around the 12 pile group as described in Chapter 6. The measured load versus deflection curve obtained during the "fixed-head" testing conducted on September 20, 2000 is shown in Figure 10.21. In addition, this graph contains the curves computed using GROUP and FLPIER models.

The idealized soil profile and p-multipliers that were developed to model the free head pile test were initially used to model the fixed-head group. All the properties of the model remained unchanged except that a fixed-head boundary condition was imposed at the pile head. The computed response was significantly stiffer than the measured response. The top layer of the idealized soil profile (see Figure 9.1) used in the initial comparisons had to be softened to account for the gaps that had developed due to the prior tests. In the idealized soil profile, the top clay layer, with a thickness of 1.34 m (4.4 ft), had a shear strength of 68.95 kPa (10 psi). In order to match the measured response, the shear strength of this layer had to be reduced to 27.6 kPa (4 psi), with other factors remaining constant.

Using the reduced strength in the upper layer, the measured load-deflection curves could be approximated using the computer programs GROUP and FLPIER. Both Florida Pier and GROUP over-predict the load for a given deflection at small deflections (< 20 mm); however, at greater deflections the agreement with the measured response was very good. Overall, using the p-multipliers and the modified soil profile that accounted for the gaps, the measured load versus deflection curve could be modeled quite well by the two programs.
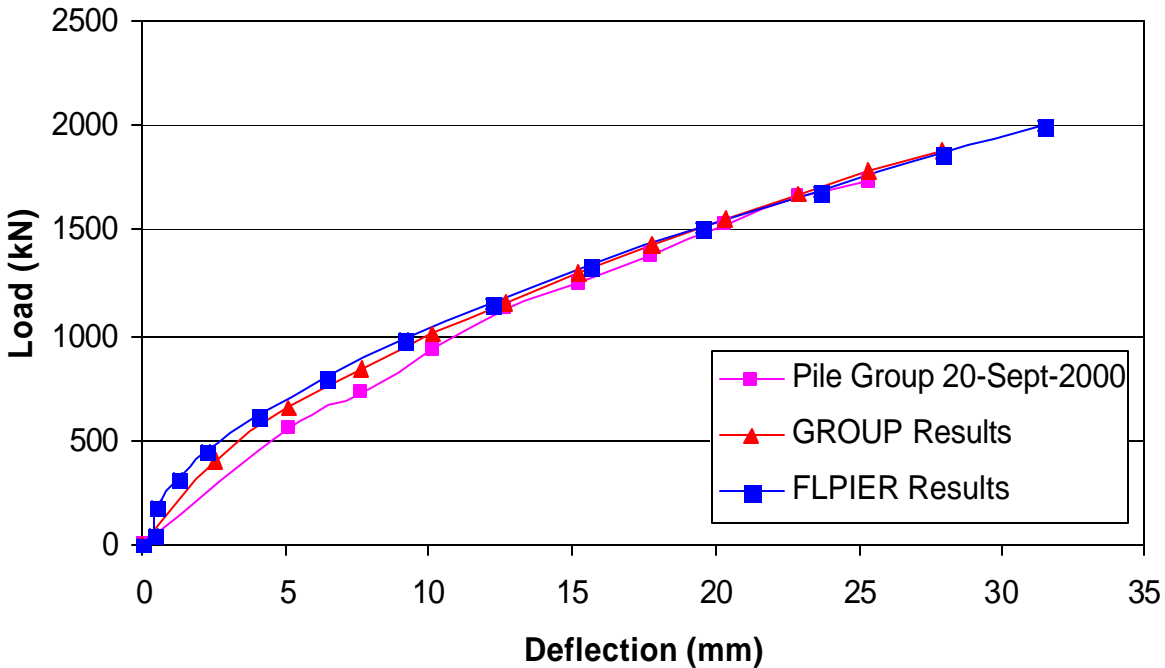
Figure 10.21 Measured load versus deflection curve for fixed-head pile group relative to curves computed using GROUP and FLPIER.

RESULTS OF ANALYSIS FOR 15-PILE GROUP AT 3.3 DIAMETER SPACING

P- Multipliers and Pile Head Load versus Deflection.

The load versus deflection curves for each row in the 15 pile group were compared with the load-deflection curve from the re-load test on the single 324 mm diameter single pile described in Chapter 4. Using GROUP, the back-calculated p-multipliers for this relatively closely spaced pile group were found to be 0.82, 0.61, 0.45, 0.45, and 0.46 for rows 1 through 5, respectively. However, at smaller deflections, the p-multiplier for the back row was found to be 0.51 to match the measured response of the pile. In computing the p-multipliers, three soil models were used, but none of the properties were changed in any of the models other than the p-multipliers, which were kept constant for each soil model. Figure 10.22 compares the measured
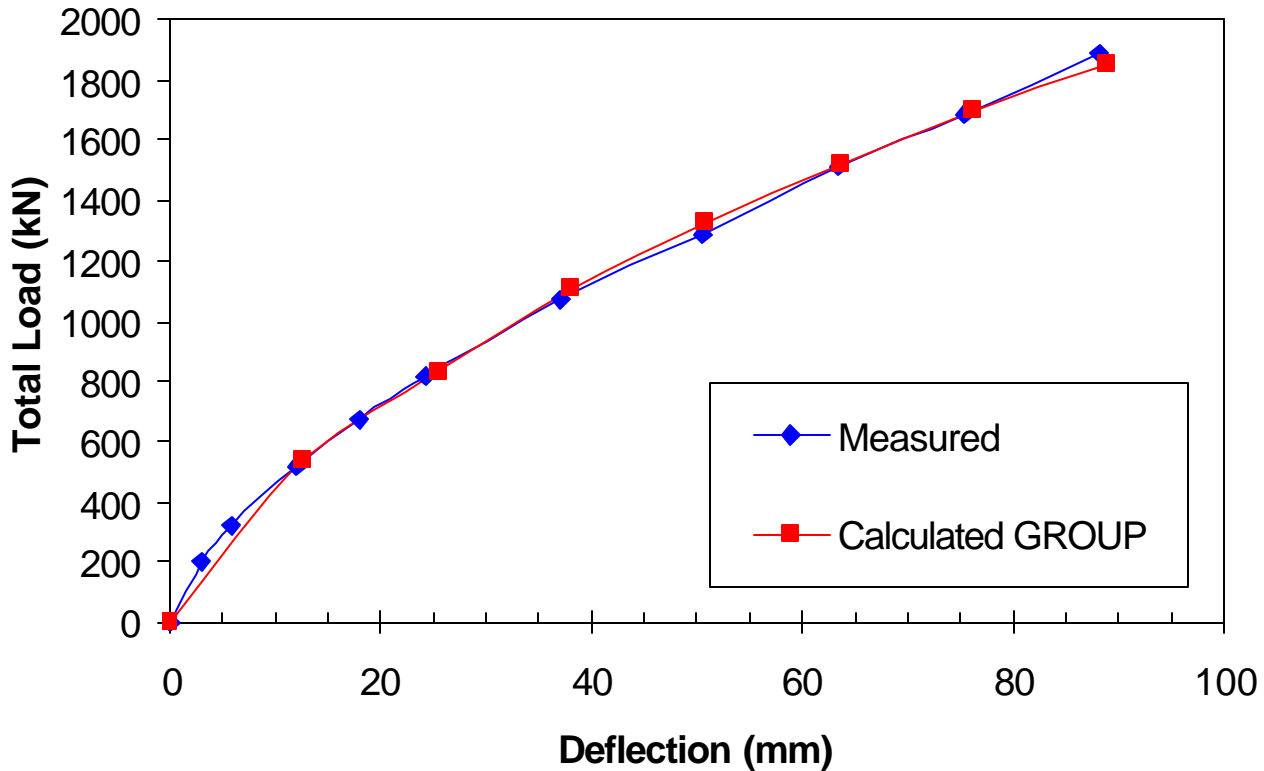
**Figure 10.22 Measured total load versus deflection curve for 15 pile group along with curve computed using GROUP with p-multipliers developed in this study.**

total load versus average group deflection curve for this pile group with that computed using the p-multipliers developed in this study. When the decreased soil resistance is accounted for with the p-multipliers developed in this study, the difference in computed deflection for a given load is typically within 5% of the measured deflection. In most cases, the computed deflection is slightly higher than the measured value.

Figure 10.23 shows average load versus deflection curves for the five rows in the group in comparison with the curves computed using GROUP with the p-multipliers developed in this study. The match between measured and computed response is very good in each case with a maximum difference in computed and measured load of less than about 10%.
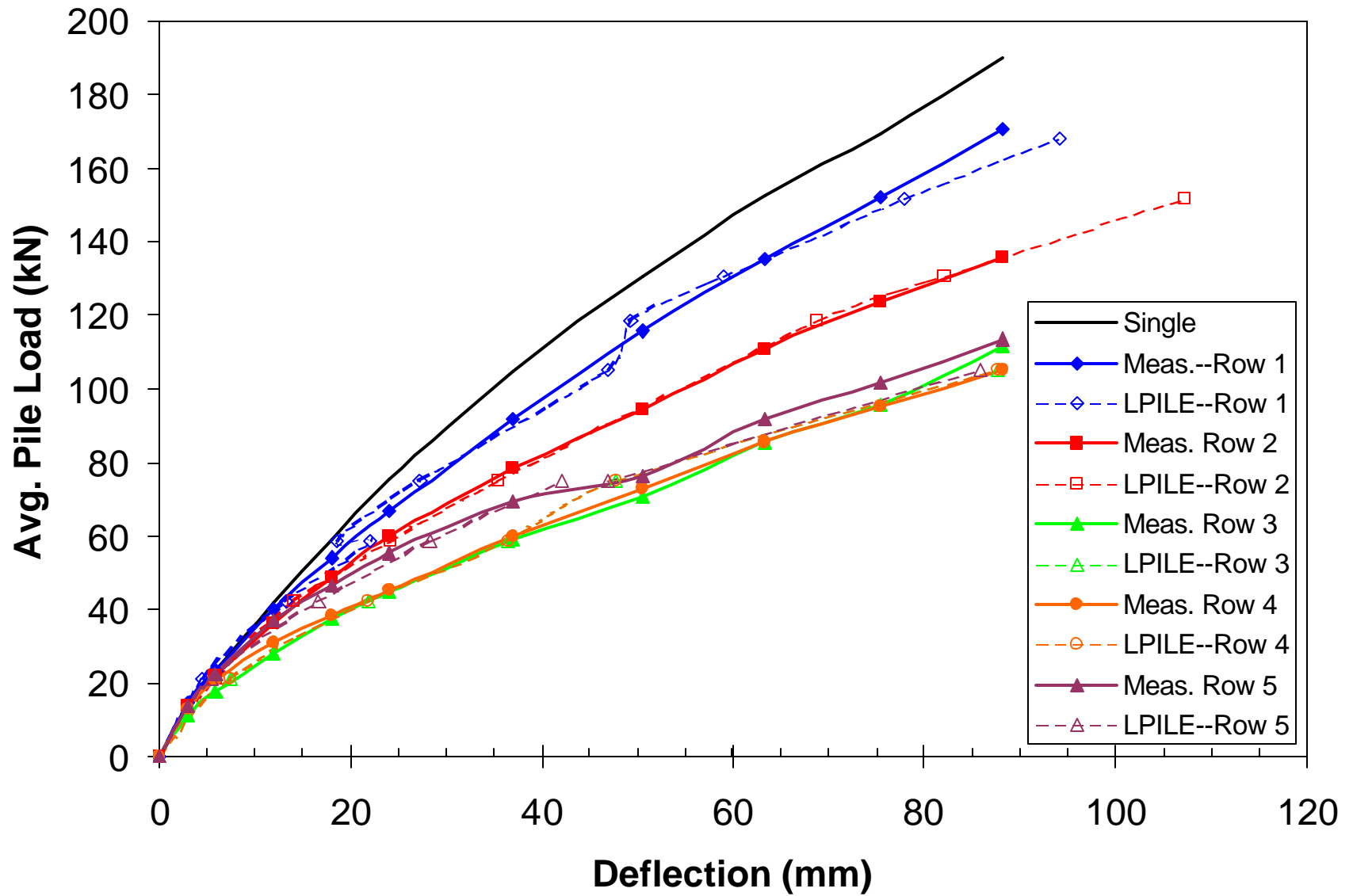
Figure 10.23 Measured load versus deflection curves for each row in the 15-pile group along with curves computed using the GROUP with the p-multipliers developed in this study.

THIS PAGE LEFT BLANK INTENTIONALLY

Bending Moment vs. Load

Curves showing the computed maximum bending moment versus average row load are presented in Figure 10.24. As with the measured curves presented in Figure 7.19, the trailing row piles typically have the highest moment for a given load while the leading row piles show the lowest moment for a given load. The difference between the back and front rows increases with increasing load, reaching about 15% at an applied load of 125 kN. This difference is smaller than that for the measured moments.
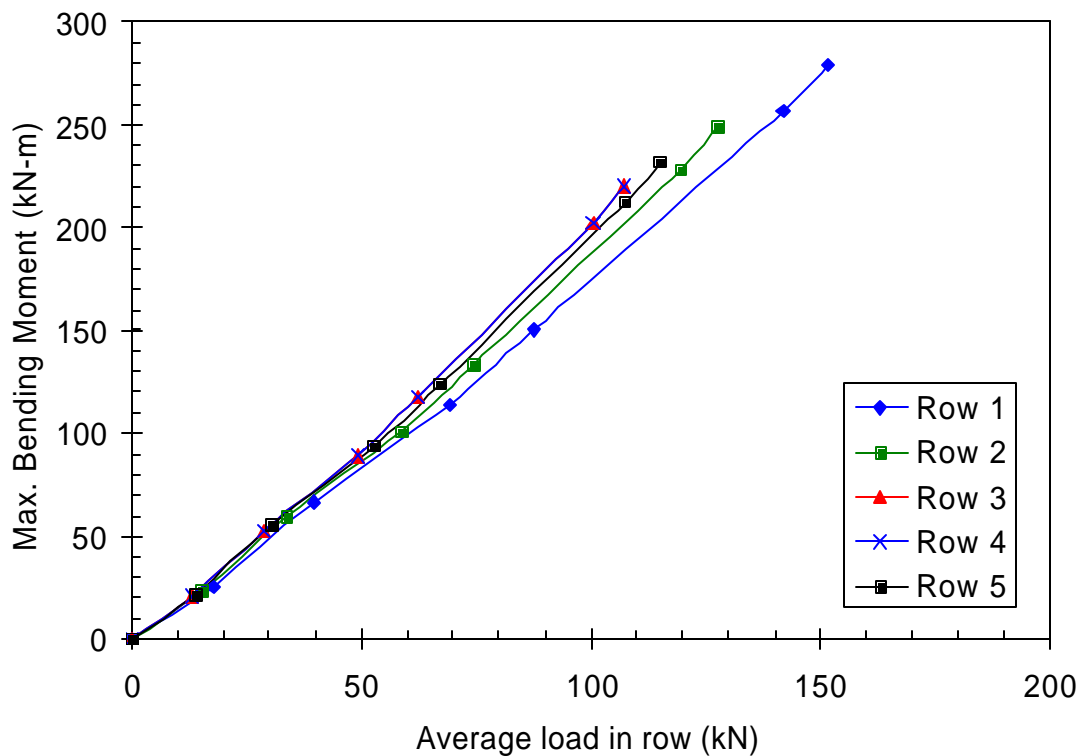
Figure 10.24   Maximum bending moment versus average pile load in each row of the 15 pile group computed using GROUP with p-multipliers developed during this study.
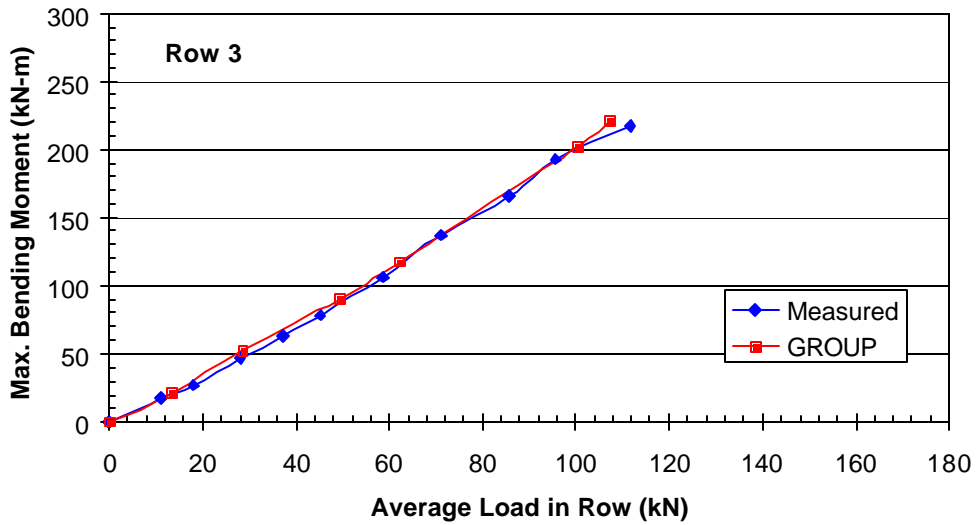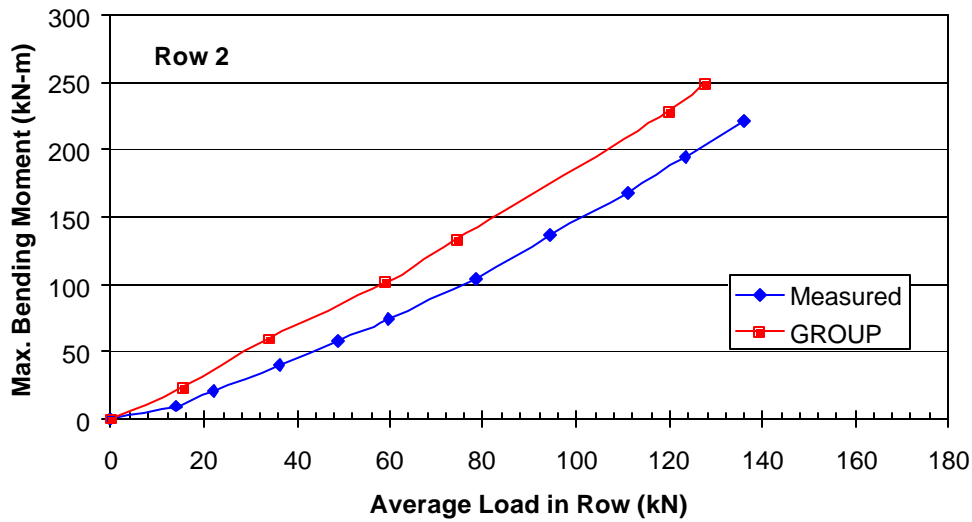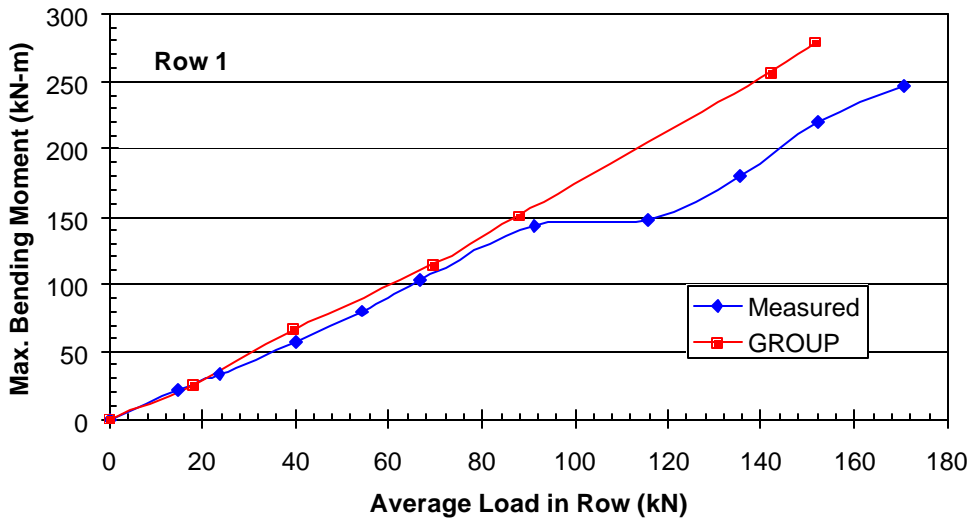
Figure 10.25 Comparison of computed and measured bending moment versus load for each row in the 15 pile group.
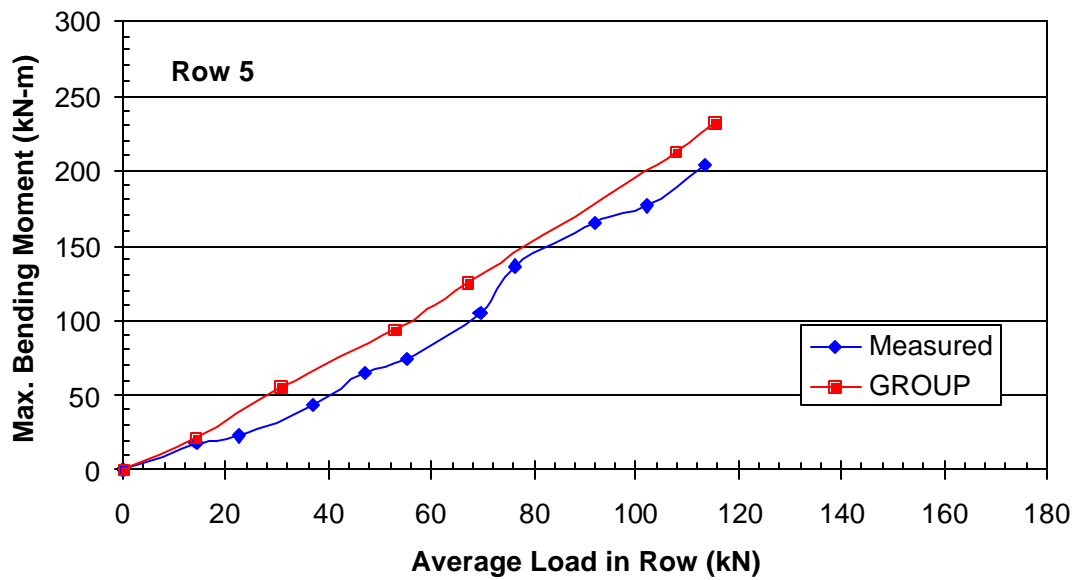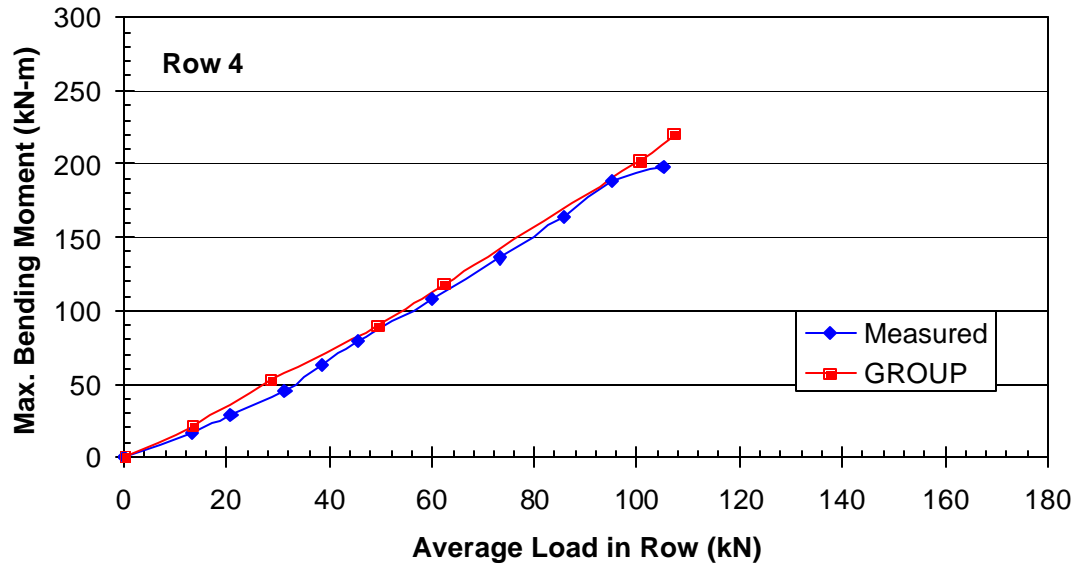
Figure 10.25 Comparison of computed and measured bending moment versus load for each row in the 15 pile group (Continued).

Figure 10.25 compares the bending moment versus average row load curves computed by GROUP along with the measured curves for each row. The computed and measured curves match very well for rows 3 and 4 and for row 1 up to a load of about 80 kN. For loads above 80 kN there is a distinct change in the shape of the bending moment versus load curve which is different than that observed for the all the other curve shapes. This discrepancy suggests that there may be a problem with the strain measurements at the higher load levels. For rows 2 and 5 the computed moment is 15 to 40% higher than the measured moment. The difference between the measured and computed response decreases as the load level increases.

Bending Moment versus Depth.

Computed bending moment versus depth curves are presented in Figures 10.26 through 10.29 for four load increments along with corresponding measured curves for the five rows in the pile group. The computed curves were developed using the p-multipliers back-calculated for the pile group based on the measured load versus deflection curves. With the exception of row 5, the depths to maximum moment computed by GROUP appear to match the measured depths reasonably well. In addition, the curves computed using GROUP generally match the overall shape of the measured bending moment curves, although the absolute values are lower in some rows as discussed previously.
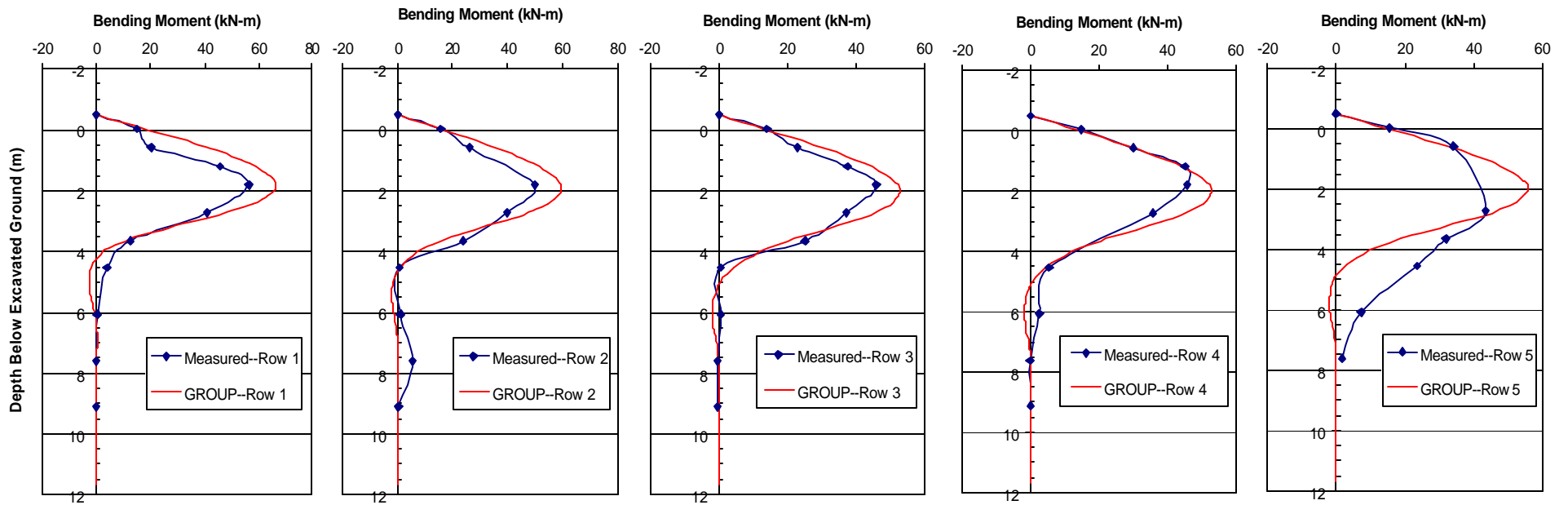
Figure 10.26   Comparison of measured and computed bending moment versus depth curves for each row in the 15 pile group at an average group deflection of 13 mm.
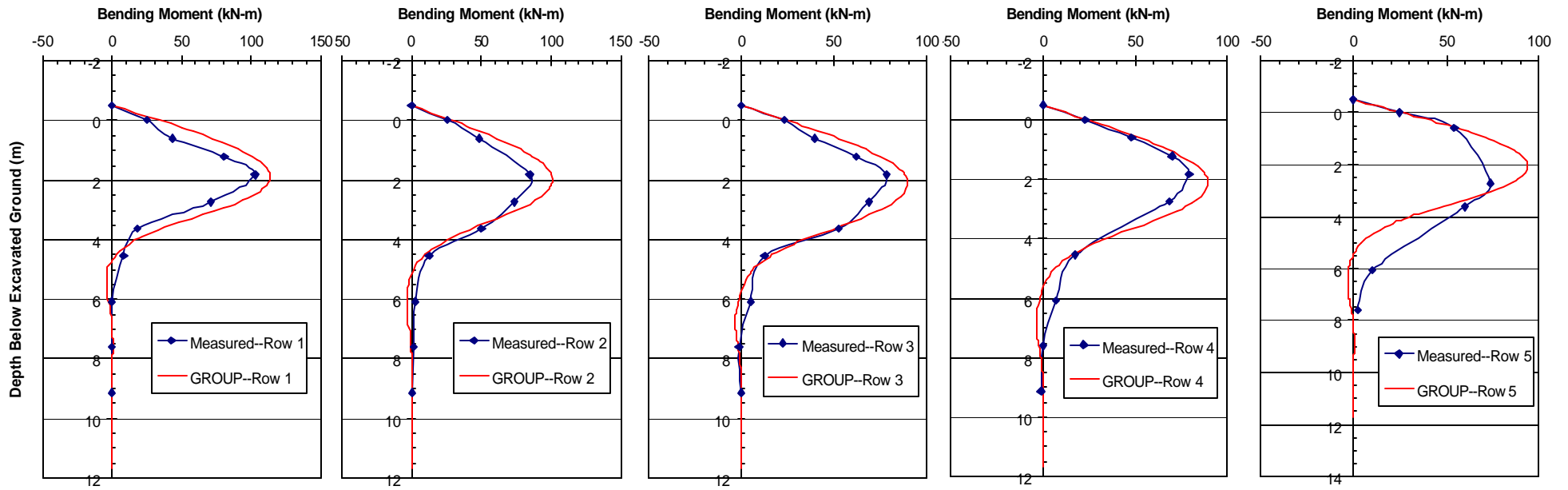
Figure 10.27   Comparison of measured and computed bending moment versus depth curves for each row in the 15 pile group at an average group deflection of 26 mm.
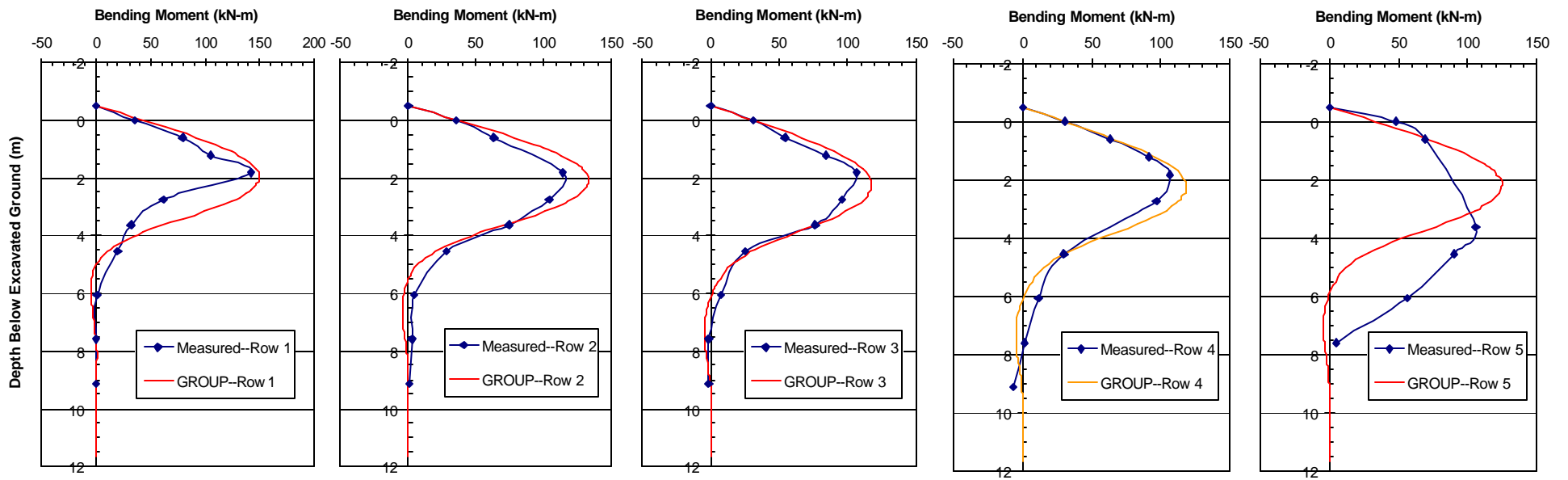
Figure 10.28 Comparison of measured and computed bending moment versus depth curves for each row in the 15 pile group at an average group deflection of 38 mm.
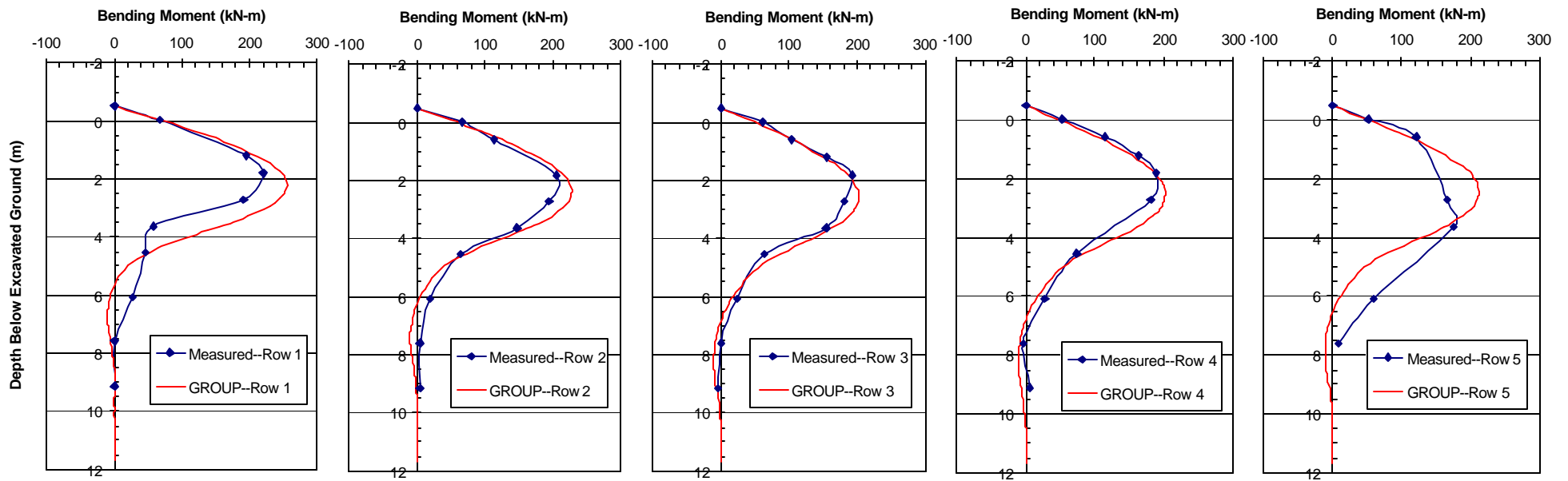
Figure 10.29 Comparison of measured and computed bending moment versus depth curves for each row in the 15 pile group at an average group deflection of 38 mm.

RESULTS OF ANALYSIS FOR 9-PILE GROUP AT 3.0 DIAMETER SPACING

P-Multipliers and Pile Head Load vs. Deflection

Once again, a series of analyses were run using GROUP to determine the appropriate p-multipliers. The p-multipliers were adjusted until the results for each row matched those observed during the pile-group tests. The p-multipliers that best described the behavior of the pile group are 0.82, 0.61, and 0.45 for the front, middle, and back row piles, respectively. These p-multipliers are identical to those for the first three rows of the 15-pile group at 3.3 pile diameter spacing. This result suggests that the p-multipliers are reasonably similar for piles with diameters ranging from 0.3 to 0.6 m.
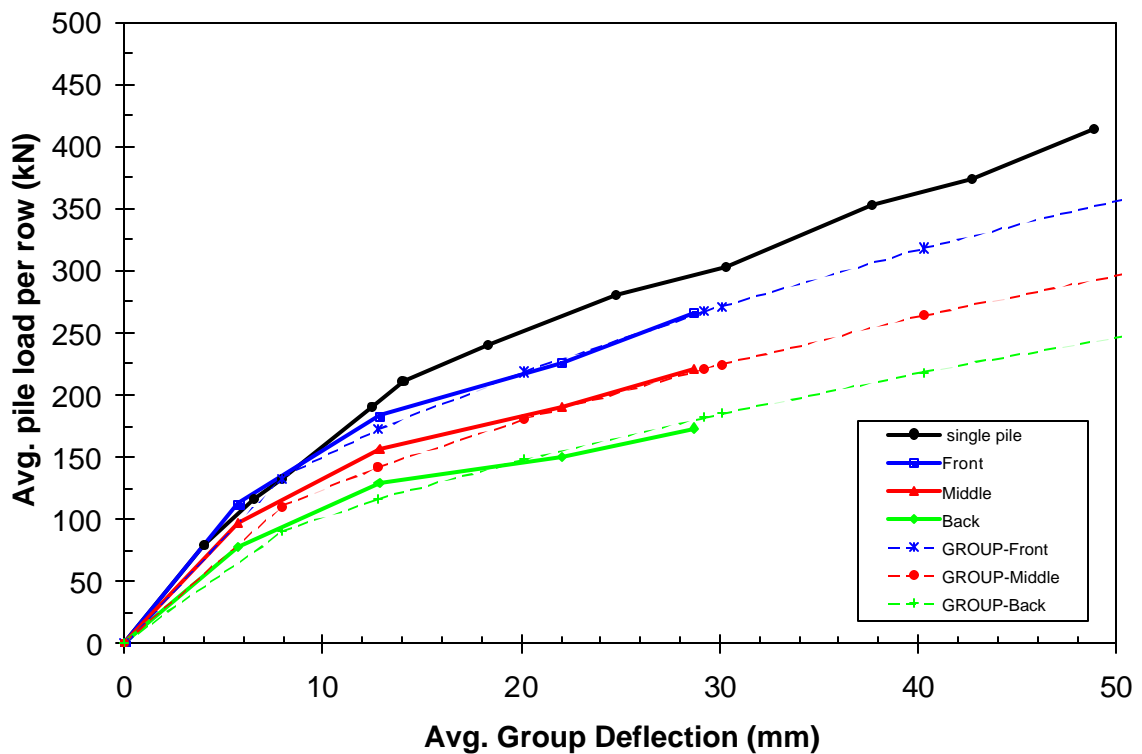

Figure 10.30 Measured load vs. deflection curves for three rows in the 610 mm nine-pile group relative to curves computed using GROUP with p-multipliers developed in this study.

The load versus deflection curves for each of the three rows in the nine-pile group are shown in Figure 10.30 compared to the curves computed by GROUP using the back-calculated p-multipliers. At the lower deflection levels, the GROUP results tend to underestimate the measured lateral resistance somewhat, but the computed and measured curves match very well at the higher deflection levels.

Bending Moment versus Depth

Bending moment versus depth plots are shown in Figures 10.31 and 10.32 for each row. Figure 10.31 compares the GROUP and full-scale test data at a deflection of 12.75 mm, and Figure 10.32 compares the measured and computed moments at 29.2 mm of deflection. In general, the shape of the computed curve is relatively close to the measured curve shape; however, in each row, the curve computed by GROUP returns to zero at a shallower depth than the actual results. Figure 10.32 shows that in the lead and trailing rows of the pile group the measured maximum moments were higher than the GROUP moments by 9% and 12%, respectively, but the GROUP maximum moment was only 3% higher than the measured values for the middle row. The computed and measured moments in the trailing row in Figure 10.31 align well as they approach zero, but the measured moments for the lead and middle rows reach zero at a shallower depth than predicted by GROUP. In both Figures 10.31 and 10.32, the depth to moment reversals computed by GROUP are much greater than those that were observed.
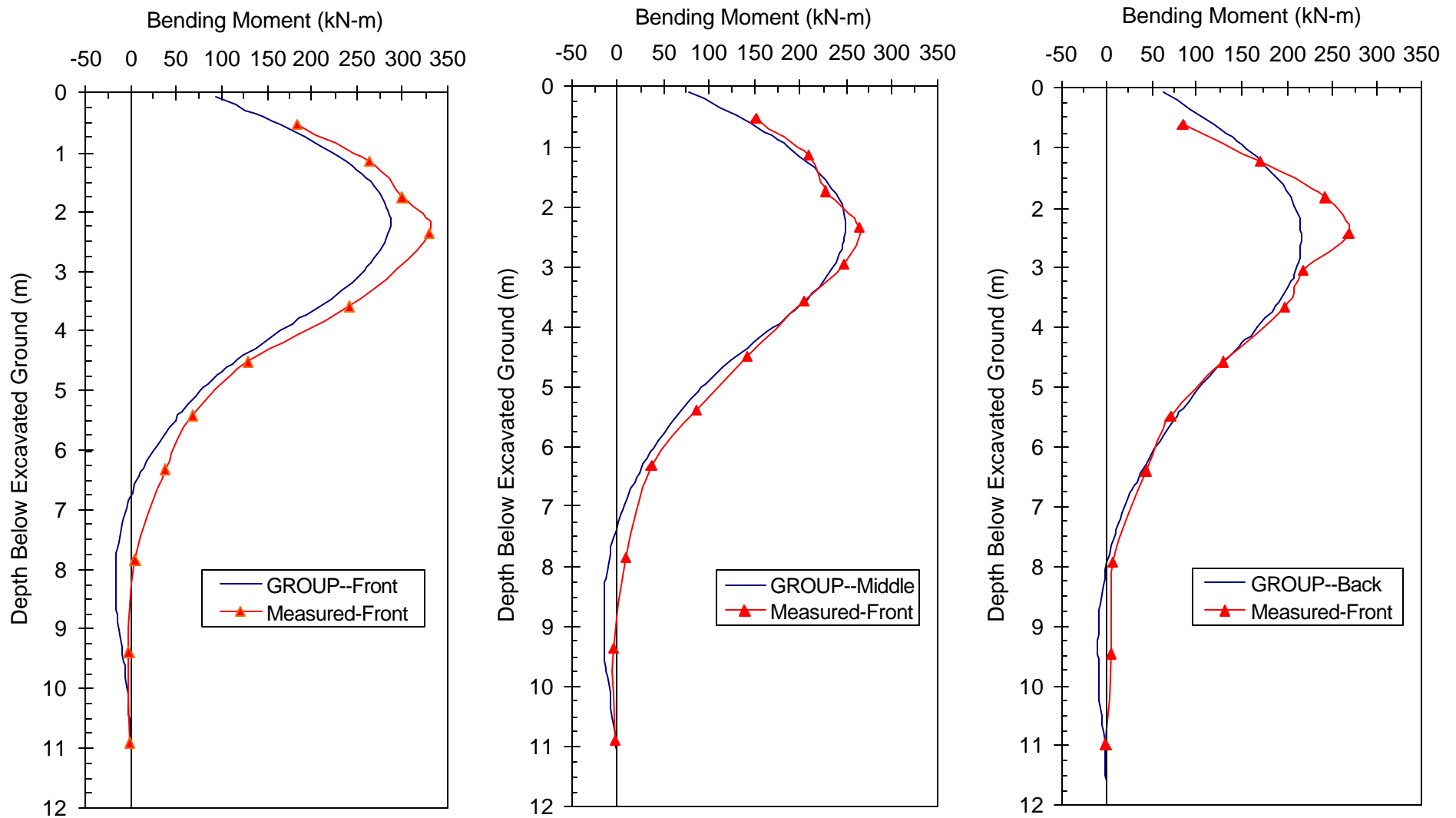
Figure 10.31 Measured bending moment vs. depth plots for 610 mm nine-pile group at a deflection of 12.75 mm along with curves computed using GROUP with p-multipliers developed during this study.

THIS PAGE LEFT BLANK INTENTIONALLY
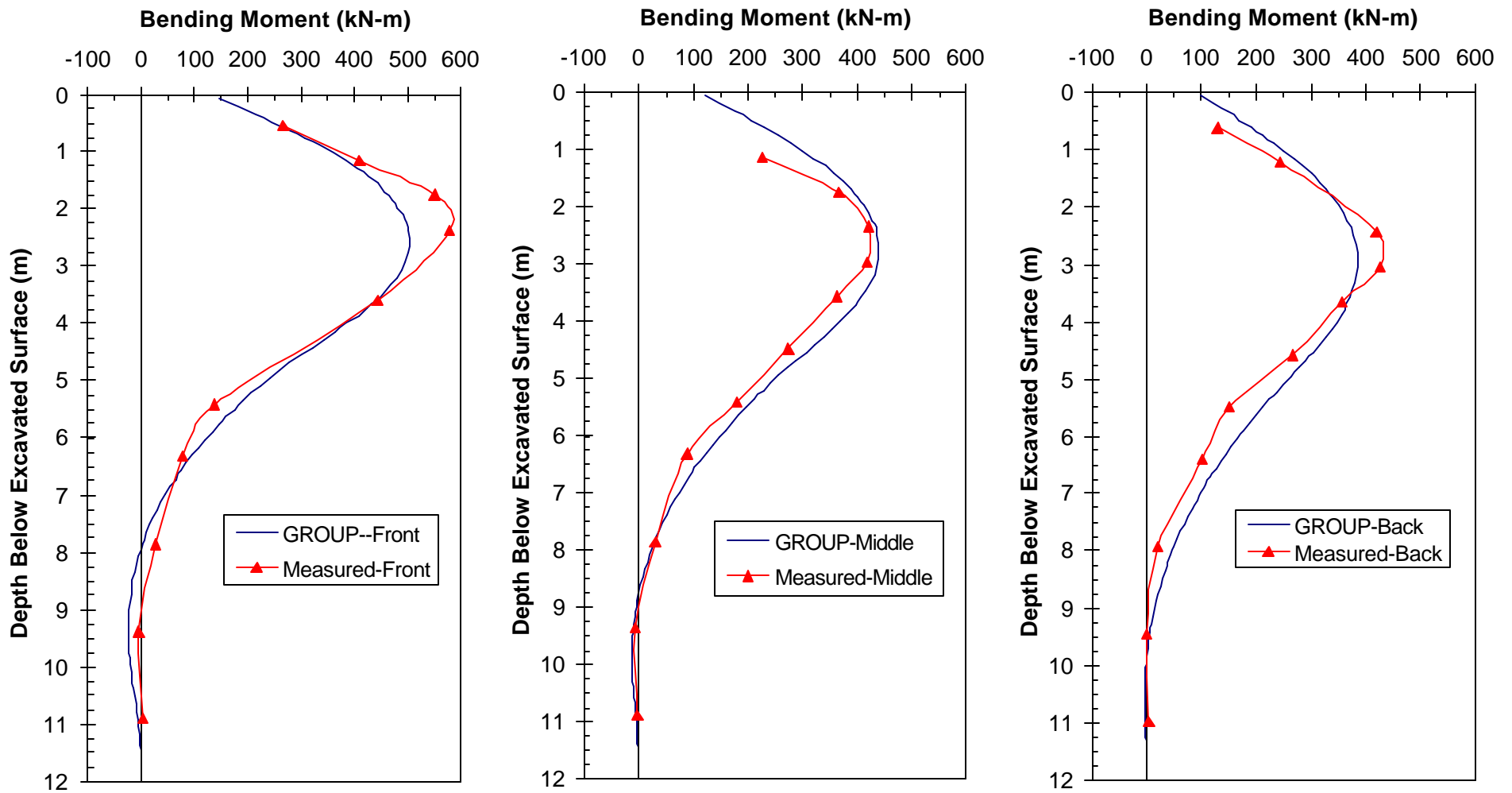
Figure 10.32 Measured bending moment vs. depth plots for 610 mm nine-pile group at a deflection of 29.2 mm along with curves computed using GROUP with p-multipliers developed during this study
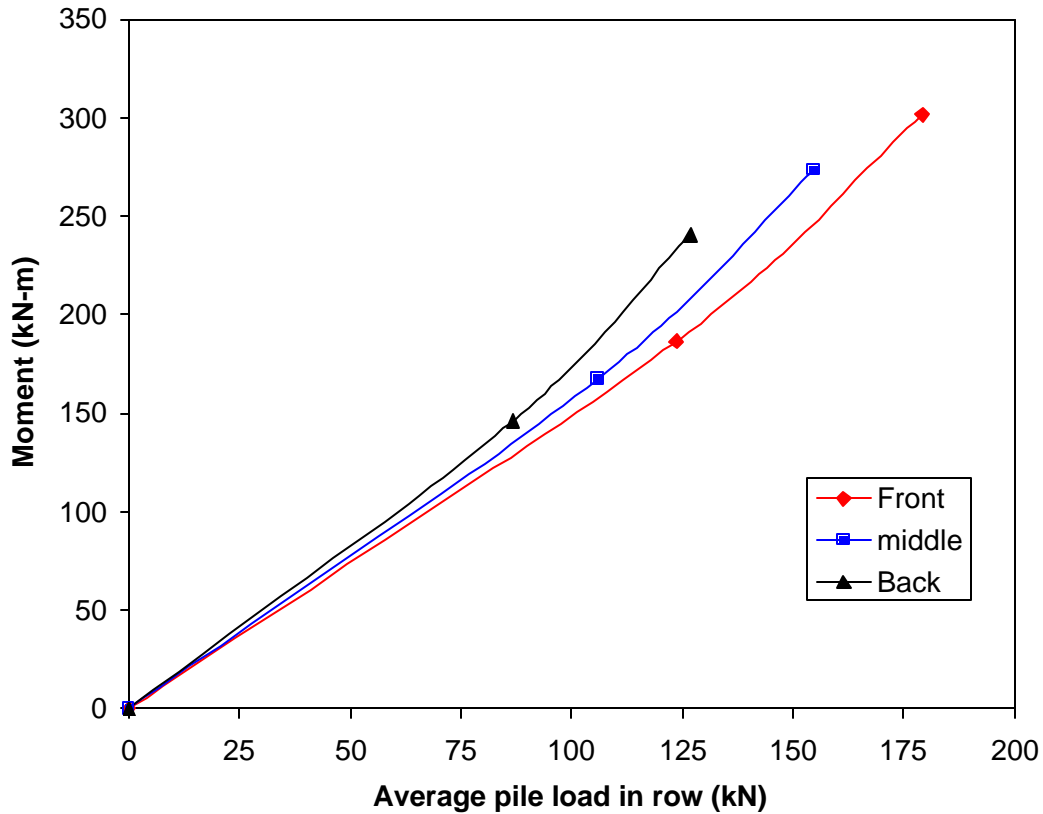
Figure 10.33 Maximum bending moment vs average pile load in each row computed using GROUP.

Maximum Moment versus Load

The maximum moment calculated by the GROUP analysis is plotted against the average row load in Figure 10.33. These plots show results quite similar to those for the other full-scale group lateral load tests. For example, due to the group effects, which cause a decrease in soil strength around the trailing row piles, these piles show the highest bending moment for a given load. In addition, the curves for each row separate more with increasing load and the slope of the trailing rows increases more rapidly than that for the leading row.

The moment vs. load curves computed using GROUP are compared with the measured curves for each row in Figure 10.34. The curves in this figure represent the first loading of
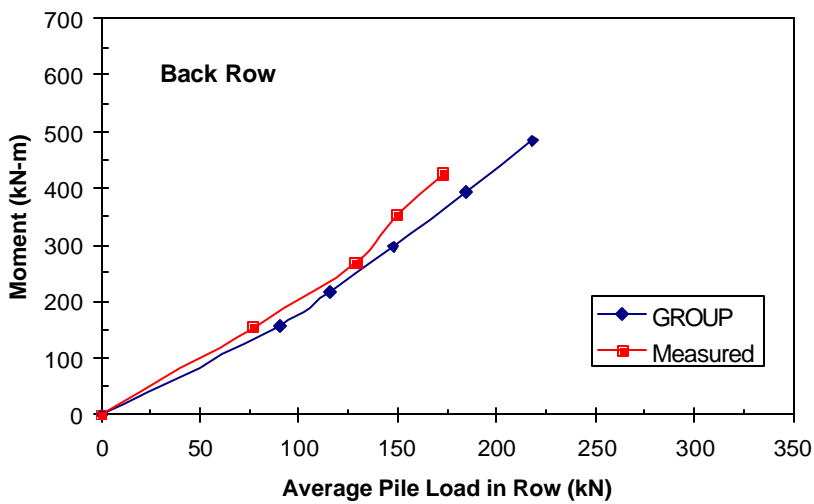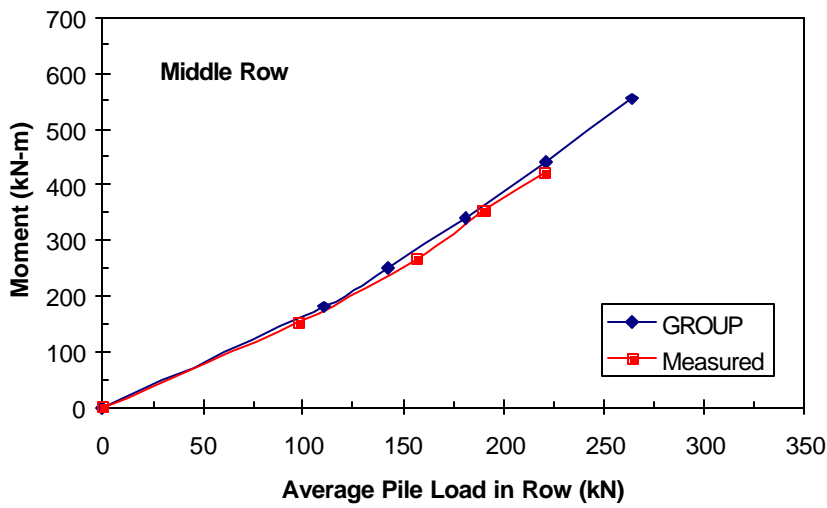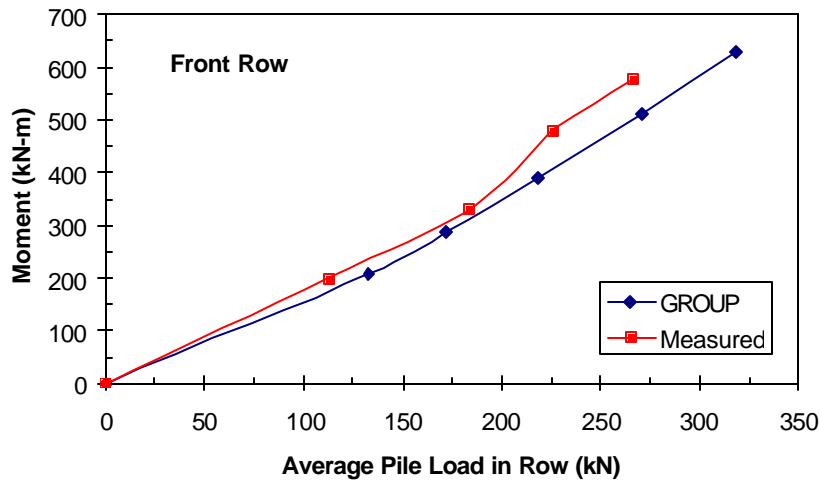
Figure 10.34 Comparison of the measured maximum bending moment vs load curves with the curves computed using GROUP.

the soil; therefore, the full-scale results shown in this figure are the first-cycle results that were performed before the statnamic tests only. As the statnamic test was performed before the last two static load levels were cycled, the data points representing those tests are not shown in this figure. The GROUP results show somewhat lower moments than the measured moments for the lead and trailing rows. The middle row, however, shows nearly identical moments for much of the curve, with the GROUP data being slightly higher than the measured values at the highest load. The difference between the GROUP and full-scale results for the lead-row pile at 124 kN is 16%, this difference decreased to 7% at 179 kN, but then the difference increases somewhat. The middle row has a maximum separation of about 4% between the GROUP computation and the actual test results. At a load of 78 kN, a 20% difference is observed in the trailing row; however, the two curves converge slightly to a 9% difference at 127 kN before diverge again.

P-MULTIPLIERS VERSUS PILE SPACING

Based on the full-scale testing and numerical analyses conducted during this study, p-multipliers have been developed for piles in groups at four different spacings. The back-calculated p-multipliers for all the tests are summarized in Table 10.1

Table 10.1 Summary of row spacing, pile diameter and p-multipliers back-calculated for each pile group during this study.

Row Spacing Center-to-Center	Pile Diameter	P-Multipliers				
		Row 1	Row 2	Row 3	Row 4	Row 5
5.6	324 mm	0.94	0.88	0.77	--	--
4.4	324 mm	0.90	0.80	0.69	0.73	--
3.3	324 mm	0.82	0.61	0.45	0.45	0.51 to 0.46
3.0	610 mm	0.82	0.61	0.45	--	--

A review of the results in Table 10.1 and those for other full-scale load tests indicates that the p-multipliers for the leading row piles are significantly higher than those for the trailing row piles. In addition, the results from this study suggest that the p-multipliers for the second row of piles are also noticeably higher than those for the third and subsequent rows. The p-multipliers tend to remain about the same for the third and subsequent rows.

The back-calculated p-multipliers for the leading row piles in each group are plotted versus pile spacing in Figure 10.35 (a) while the p-multipliers for the trailing row piles are shown in Figure 10.35 (b). P-multipliers obtained from previous full-scale load testing are also shown in Figure 10.35 for comparison. The p-multipliers from this series of tests are within the middle of the range from previous tests at the closest spacings.

Proposed design curves, which show p-multiplier values as a function of pile spacing, have been developed based on the results from this study and the curves for leading and trailing row pile are presented in Figure 10.35 (a) and (b), respectively. For both leading and trailing row piles, there is a clear trend for the p-multipliers to increase as the spacing increases; however, the relationship does not appear to be linear. The p-multipliers tend to change more gradually as the spacing increases. Extrapolation of the curves suggests that the p-multiplers will go to one at a spacing of 6.5 diameters for the leading row and 7 to 8 diameters for the trailing rows. Two curves are provided for trailing row piles in Figure 10.35 (b). The upper curve gives p-multipliers for the second row (or first trailing row) in the group, while the lower curve gives the p-multiplier for all other trailing rows in the group.

The p-multiplier versus pile spacing curves currently used in GROUP (Reese et al, 1996) are also presented in Figures 10.35 (a) and (b) for comparison. The p-multipliers based on the results from this and previous full-scale group load tests are significantly lower than the curves used in GROUP, particularly for the closest spacing. In addition, the curves used in GROUP assume that group interaction effects are eliminated at much smaller spacings than are
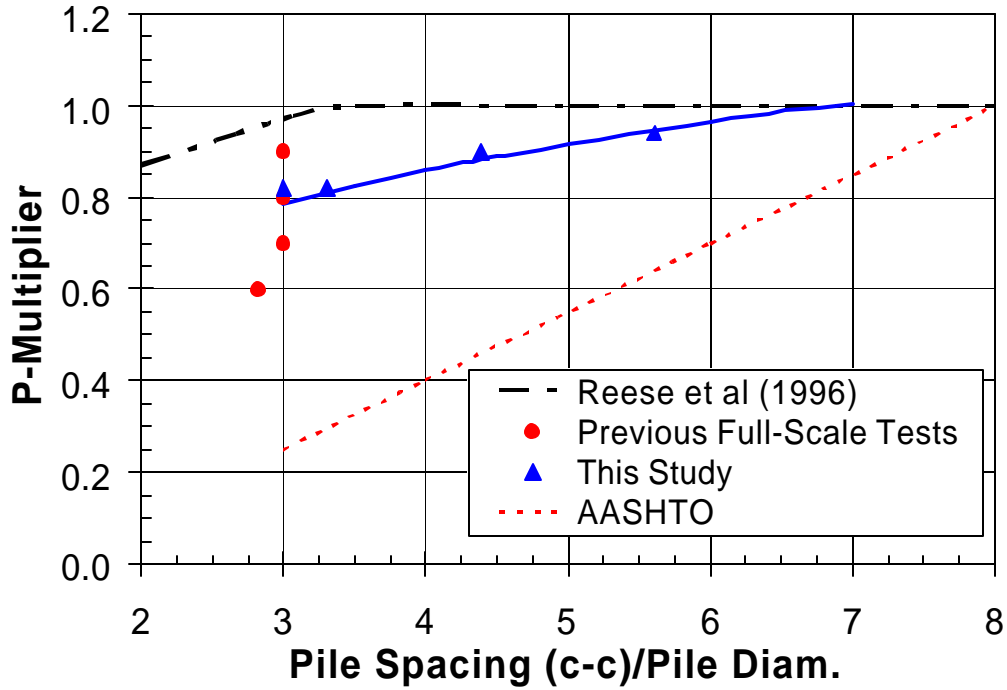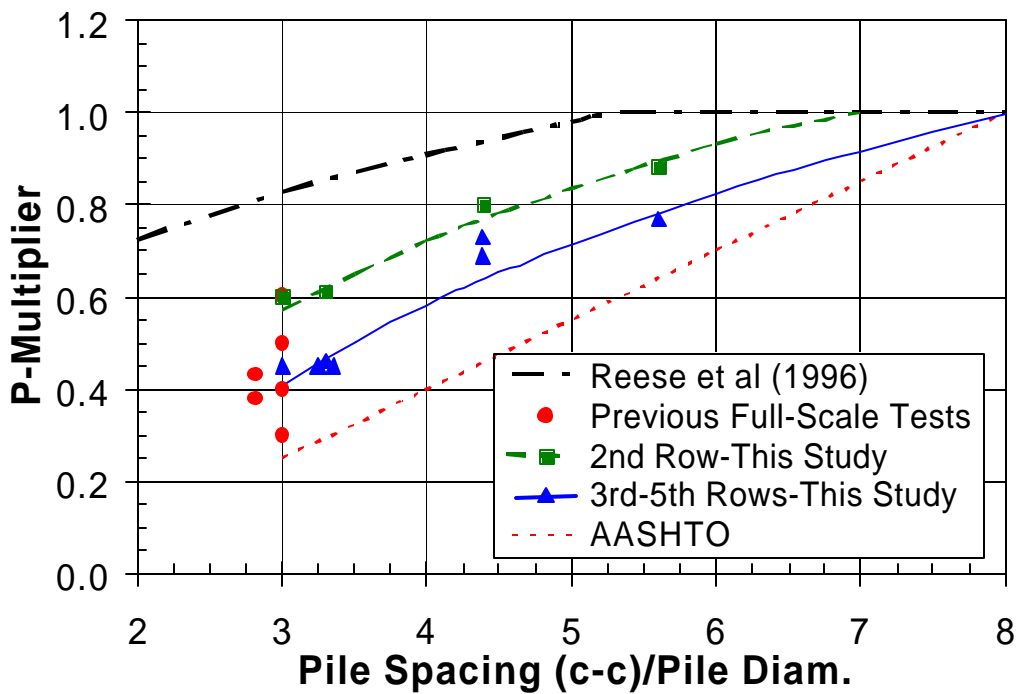
Figure 10.35 Back-calculated p-multipliers for (a) leading row and (b) trailing row piles from this study and previous full-scale load tests along with recommended design curves.

indicated by the current series of tests. Therefore, use of the default p-multiplier curves in GROUP will generally produce non-conservative estimates of the lateral resistance of closely spaced pile groups.

The AASHTO p-multiplier versus pile spacing curve is also shown in Figure 10.35. The AASHTO curve consistently underestimates the back-calculated p-mulipliers determined from this study. The error is greatest for the front row piles, however, there is still significant error for the trailing row piles.

SUMMARY OF P-MULTIPLIER DESIGN CURVES

A summary plot of the curves recommended for determining p-multipliers for pile groups based on the results of this study is provided in Figure 10.36. Curves are provided for three separate cases, namely: (1) first row piles sometimes referred to as leading row piles, (2) second row piles, and (3) third or higher row piles. The AASHTO curve is also provide in Figure 10.36 for comparison purposes only.

Equations have also been developed to compute the p-multiplier (P_m) for each of the curves shown in Figure 10.36. The equations for each condition are:

$$\text{First (Lead) Row Piles:} \qquad P_m = 0.26\ln(s/d) + 0.5 \ = 1.0 \qquad (10.1)$$

$$\text{Second Row Piles:} \qquad P_m = 0.52\ln(s/d) \ = 1.0 \qquad (10.2)$$

$$\text{Third or Higher Row Piles:} \quad P_m = 0.60\ln(s/d) - 0.25 = 1.0 \qquad (10.3)$$

Where s is the center to center spacing between piles in the direction of loading and d is the width or outside diameter of the pile. The upper limit of the computed P_m for each equation is 1.0.
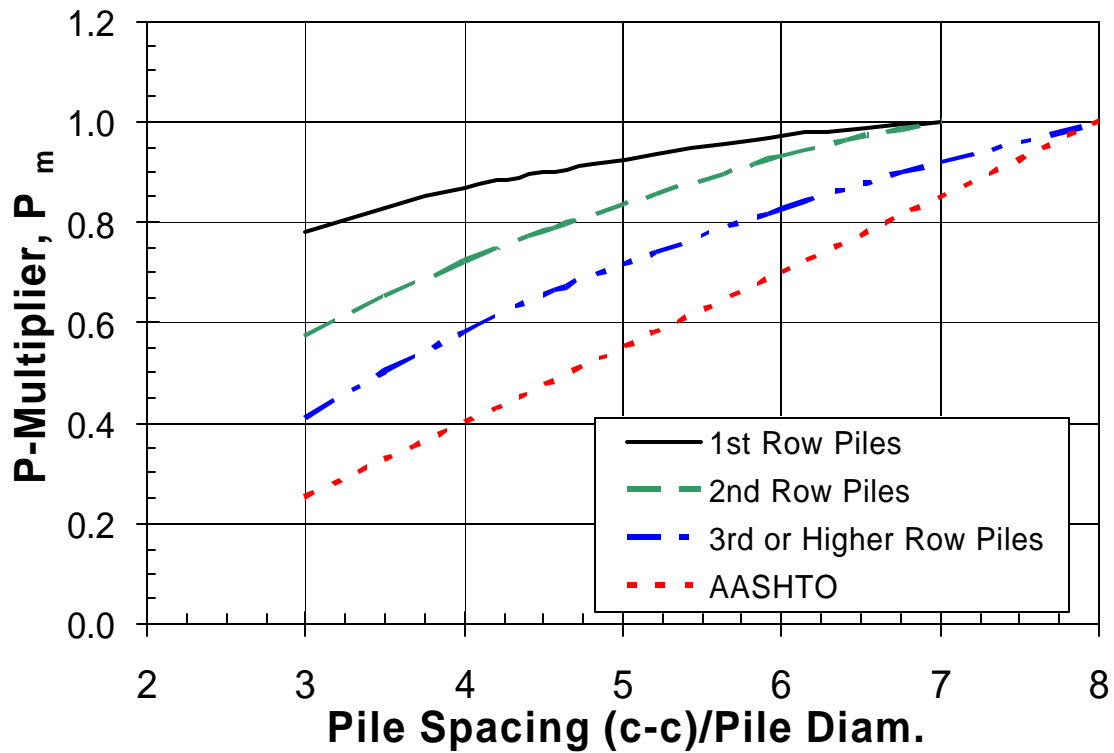
Figure 10.36 Recommended design curves for selecting p-multipliers (P_m) as a function of normalized pile spacing for 1st row piles, 2nd row piles and 3rd row or higher row piles.

CHAPTER 11 STATNAMIC LATERAL PILE GROUP TESTS

INTRODUCTION

Because many pile foundations are subjected to dynamic loadings produced by earthquakes and impact loads, there is a need to understand pile group response under these conditions. There are, at present, very few dynamic load test results that can tell whether or not group effects are the same for dynamic loads and static loads. To assess the response of the pile group to these conditions, a series of dynamic lateral loads was applied to two full-scale pile groups. Previous dynamic lateral load tests conducted on a full-scale pile group suggested damping resistance could produce significant increases in lateral resistance (Rollins, et al. 1998). However, these tests typically involved only one cycle of loading and gaps were not generally present while the tests were conducted. Therefore, testing in this study was also designed to ascertain if damping would still be significant when gaps in the soil were present prior to the dynamic loading. However, as a consequence of the premature failure of the reaction foundations, there were both virgin dynamic loadings as well as dynamic reloadings. Statnamic tests were performed on the nine pile group of 610 mm diameters piles and the 15 pile group of 324 mm diameter piles.

STATNAMIC LOAD TESTS ON NINE PILE GROUP

Test Layout

The statnamic load tests were conducted on the same pile group described in Chapter 8. The same load frame and tie-rod load cells were used to transfer the load to the piles. The nuts on the DYWIDAG bars were loosened so that forces were not transferred between the reaction beams on each side of the reaction pile cap used during the static tests. In this manner, the hydraulic jacks used in the static tests were independent of the load frame and had no influence on the pile group during the statnamic test.

Directly to the north of the pile group, a trench was dug in which the statnamic device was set and fired. This trench was of sufficient depth to allow the statnamic force to be applied at the level of the tie-rod load cells. This excavation was also a sufficient length to allow the statnamic device to move horizontally until it stopped by friction, without colliding with the end of the trench.

The statnamic device, operated by Applied Foundation Testing, Inc., was capable of providing a 14 MN vertical load or a 7.1 MN lateral load. Fuel pellets ignited in the fuel chamber generated a gas, which expanded and caused the 31,750 kg (70 kip) reaction mass to accelerate the away from the statnamic piston that was resting against the north beam of the load frame. The force generated would be transferred from the statnamic piston through the load frame and tie-rod load cells to the piles in the group. A drawing of the statnamic device in position with the pile group is shown in Figure 11.1.

Instrumentation

Most of the instrumentation for the statnamic tests was the same as described previously in Chapter 8 for the static tests. All differences in the instrumentation between the two tests are noted below.

Acceleration measurement.

Piezoelectric accelerometers were placed on several piles to record accelerations that occurred during the statnamic testing. This type of meter is an AC coupled device which can not be used to measure constant (DC) accelerations. Therefore, the accelerometers were only

PILE CAP

W310x74
BEAMS

STATNAMIC
DEVICE

W760x184

2-1.34 MN
JACKS

LOAD CELLS

W760x184

MC460x77.2

W920x313

STATNAMIC
PISTON

41 mm
DYWIDAG BARS

1.83m

600 mm OD PIPE PILE
OPEN-ENDED
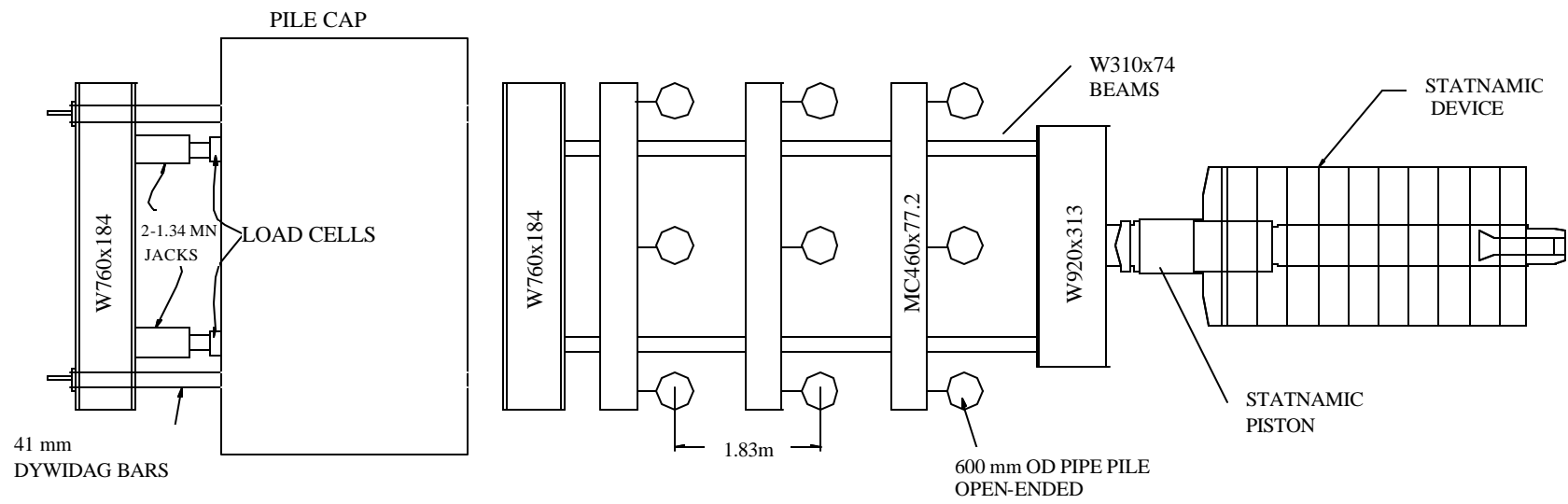
Figure 11.1: Plan view of the statnamic device which loads the pile group toward the left.

11-3

useful for obtaining the time history while the accelerations were changing rapidly. Generally, the acceleration measurements are reasonable for the first load and unload cycle, but they drift considerably as the acceleration becomes relatively constant. Accelerometers were attached at the elevation of the load point for the lead-row piles and the two outside piles of the trailing row (piles 1, 2,3,7, and 9 in Figure 8.1).

Load measurement.

Tie-rod load cells were used to measure the load response of each pile in the group. As the nuts on the DYWIDAG bars were loosened, the hydraulic jacks were independent of the pile group, and the load cells attached to the hydraulic jacks, though attached, were not used to measure loads. However, a load cell was attached to the statnamic device, allowing the total statnamic force to be measured.

Displacement measurements.

The setup of the LVDTs used in the statnamic test was unchanged from that of the pile group test. Although the LVDTs were attached to an independent reference frame with supports located 3 m away from the piles, the reference frame was also expected to be subjected to some vibration due to the statnamic firing. To provide an independent check on the displacement measurements, the acceleration time histories were double integrated to obtain displacement time histories. These calculated deflections were then compared to the deflections measured by the LVDTs.

Data acquisition.

The same Optim Megadac data acquisition system used in the single pile and static-group tests was used during the statnamic testing of the pile group. However, data was acquired at a sampling rate of 1500 readings per second during the statnamic pile-group test. During the test,

the system recorded 96 channels of data including 10 load cell channels, five acceleration channels, nine LVDT channels, and 72 strain gauge channels.

PROCEDURE

Five statnamic tests were conducted on December 11, 1999. After statically cycling the pile group at a target deflection, this deflection was then used as the target for a statnamic test. Next, a static test was conducted for an increased deflection level. The objective of this test procedure was to evaluate damping resistance once gaps had formed around the piles due to static cyclic loading. This procedure was followed for the first two target deflections, up to 12.7 mm (0.50 inches). At that time, a problem with the load frame prevented further static tests from being conducted. Therefore, the final statnamic tests were run consecutively. For this reason, the last three statnamic tests were conducted without the pile group being first cycled statically. These three tests should provide an indication of the damping resistance in a virgin load condition. As the static test pulled the load frame from the south side of the pile group, the statnamic device pushed the frame from the north; therefore, the piles were loaded in one direction only regardless of the test.

Tests with target deflections of 6.35 mm (0.25 in.), 12.70 mm (0.50 in.), 19.05 mm (0.75 in.), 25.4 mm (1.0 in.), and 38.1 mm (1.5 in.) were run. However, these target deflections were not exactly met, as precise control of the statnamic loading is impossible. Actual peak deflections for the five tests were 3, 11.5, 21, 32, and 38 mm, respectively.

Test Results

Time histories of measured load, acceleration, and deflections along with velocities calculated from accelerometer data are shown in Figures 11.2 to 11.6 for each statnamic test. The deflections in these figures are the average deflections measured by the LVDTs.

The characteristics of the loading and the peak pile response values are summarized in Table 11.1.

Table 11.1 Summary of load characteristics and pile group response for statnamic tests on nine pile group.

Test	Maximum Load (kN)	Rise Time (sec)	Maximum Deflection (mm)		Maximum Velocity (m/sec)		Maximum Acceleration (m/sec^2)	
			(+)	(-)	(+)	(-)	(+)	(-)
1	413	0.20	3	0.7	0.06	0.10	11	10.5
2	1080	0.15	11.5	3	0.18	0.38	30	14
3	1800	0.09	21	3.5	0.4	0.6	32	28
4	2650	0.09	32	3	0.75	0.80	42	50
5	3200	0.07	38	3	1.2	1.2	60	90

As the maximum load increased, the rise time (time to develop the peak load) decreased. The rise time was 0.2 for the smallest load pulse and decreased to 0.07 for the largest load. However, these rise times are reasonable approximations of what might be produced by an earthquake. The peak velocities and accelerations were typically somewhat greater in the negative direction due to the fact that there was no soil resistance restraining pile movement as it rebounded in contrast to the initial loading. The ratio of peak velocity to peak acceleration for earthquake motions is typically about 1 m/sec/g (Seed and Idriss, 1982). Therefore, the peak velocities, particularly those for the last three tests, are similar to what would be expected for a large magnitude earthquake which would have peak accelerations ranging from 0.5 to 1.2 g. However, the maximum accelerations measured in these tests (3 to 9 g's) are significantly higher than what would be produced by an earthquake. Therefore, the damping resistance, which is proportional to velocity, will likely be similar to what would be expected in an earthquake, but

the inertia force, which is proportional to acceleration, would likely be excessive. Nevertheless,

the inertia force is relatively small and can be easily adjusted for expected earthquake motions.
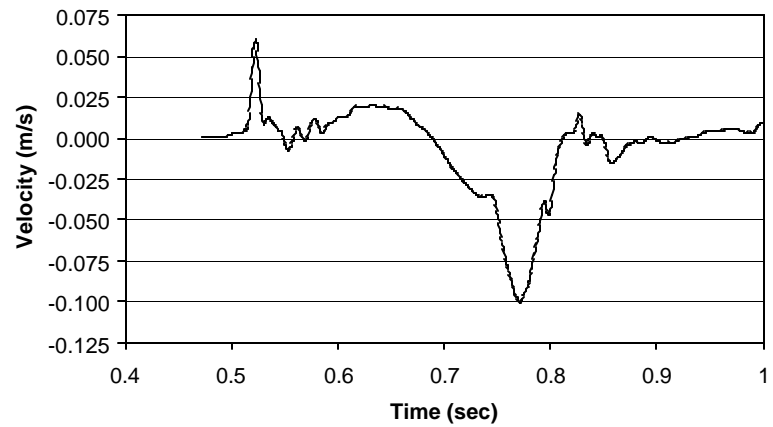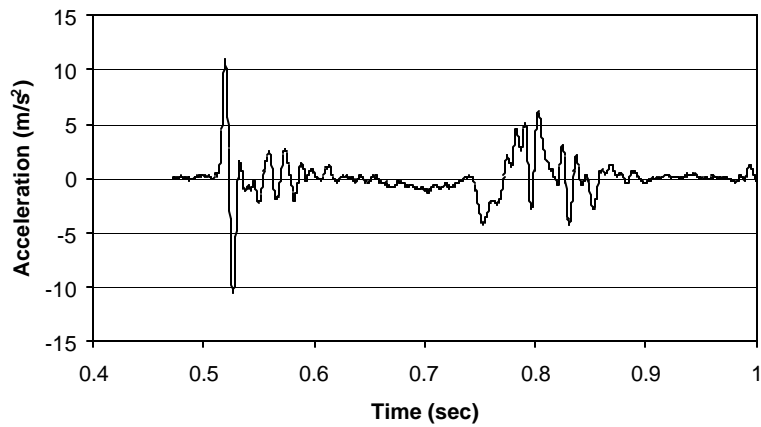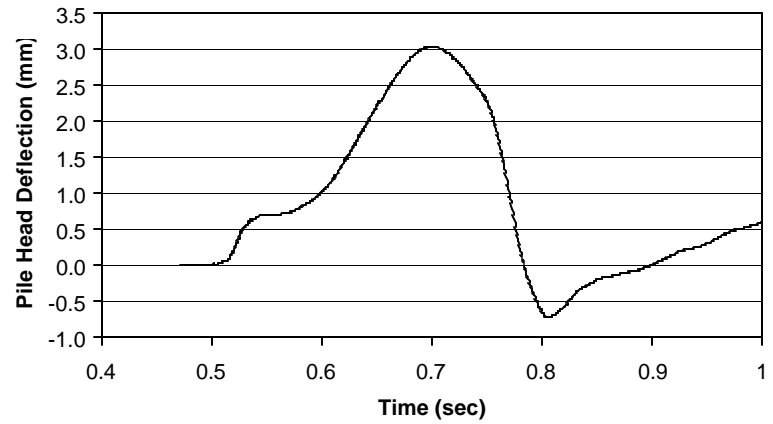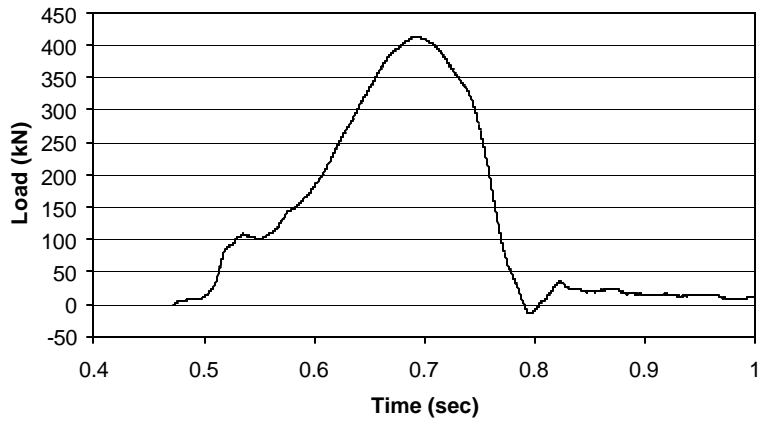
Figure 11.2 Time histories of load, displacement, velocity and acceleration of the pile group for statnamic test one.
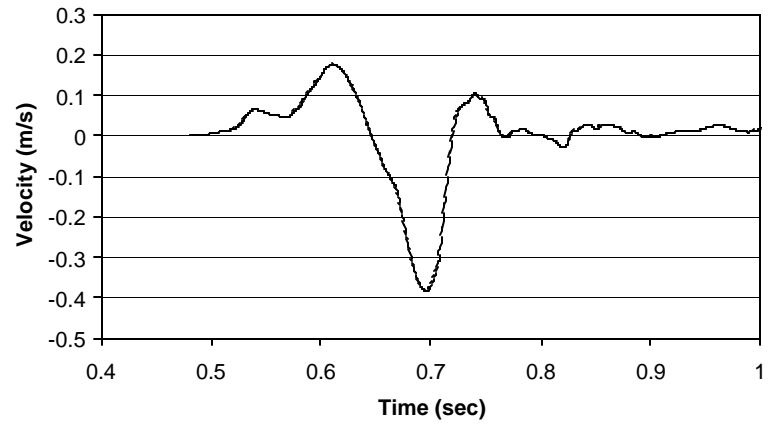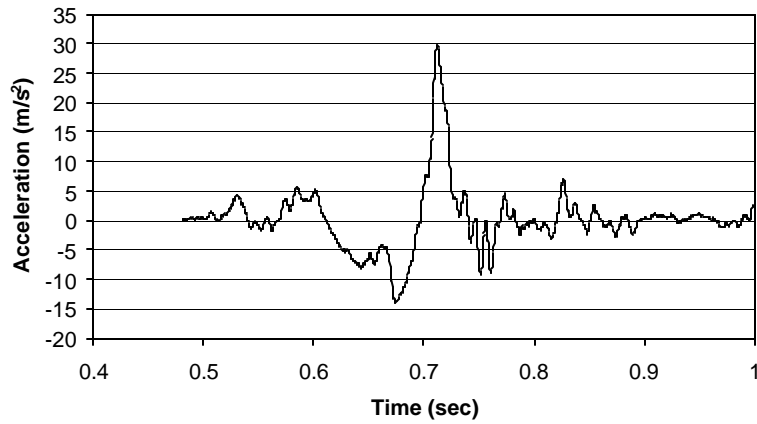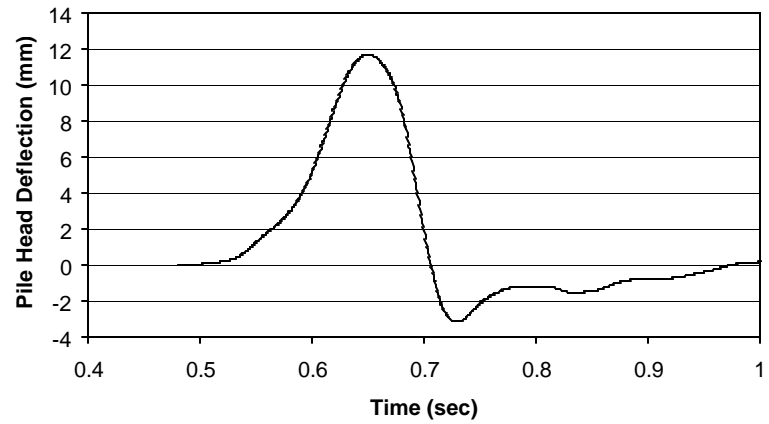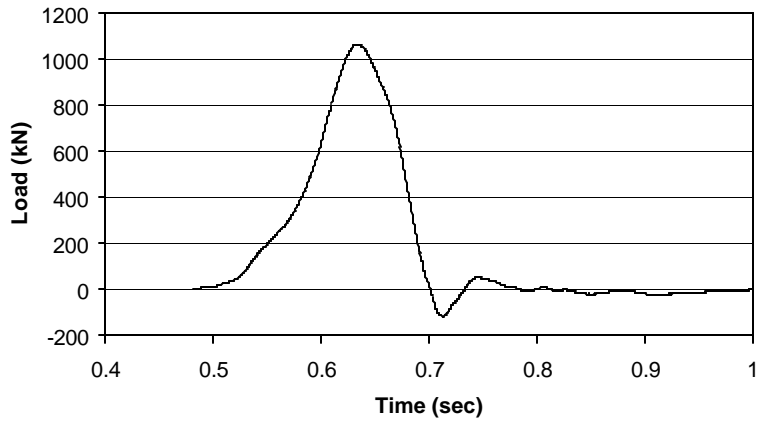
Figure 11.3 Time histories of load, displacement, velocity and acceleration of the pile group for statnamic test two.
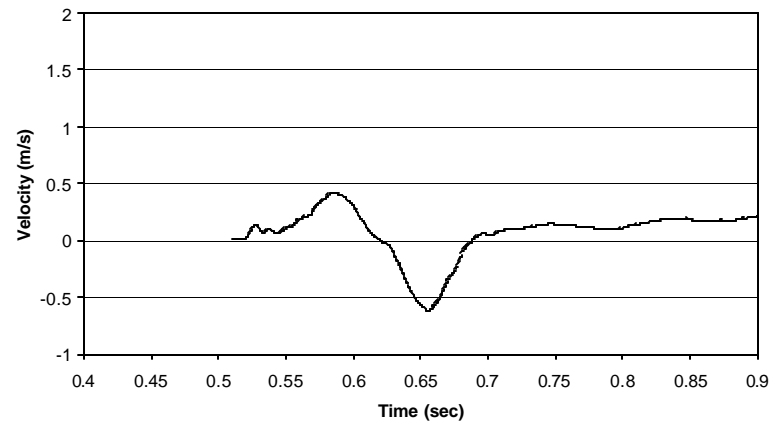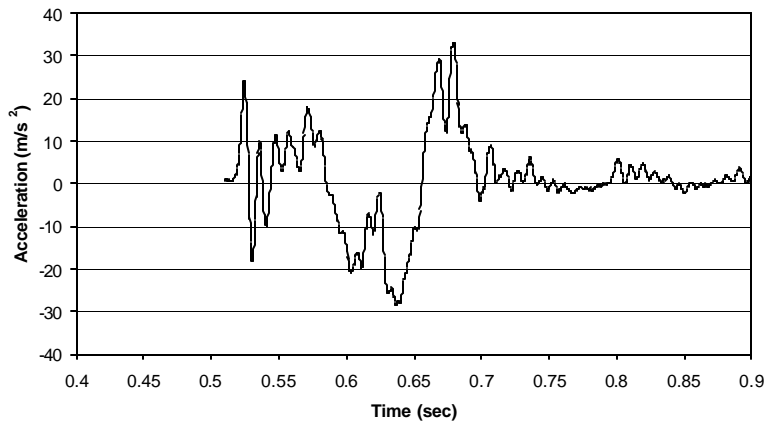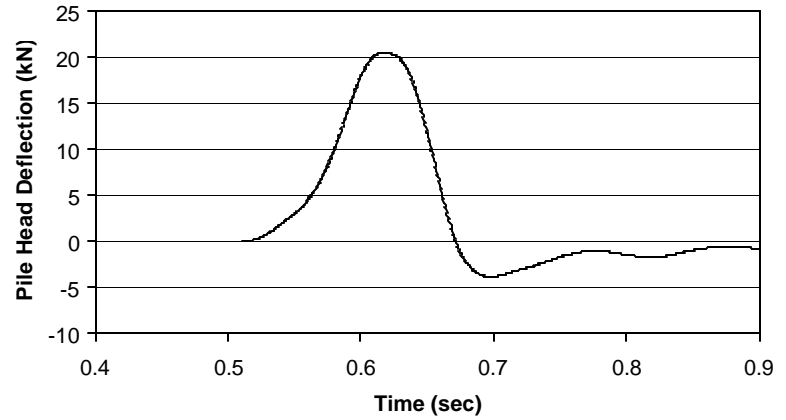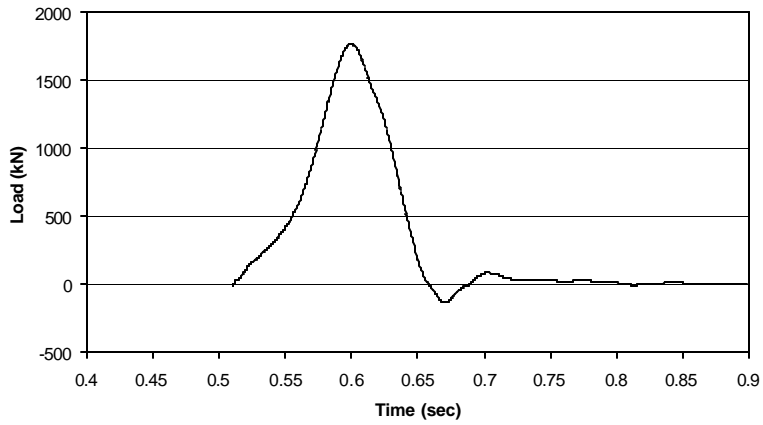
Figure 11.4 Time histories of load, displacement, velocity and acceleration of the pile group for statnamic test three.
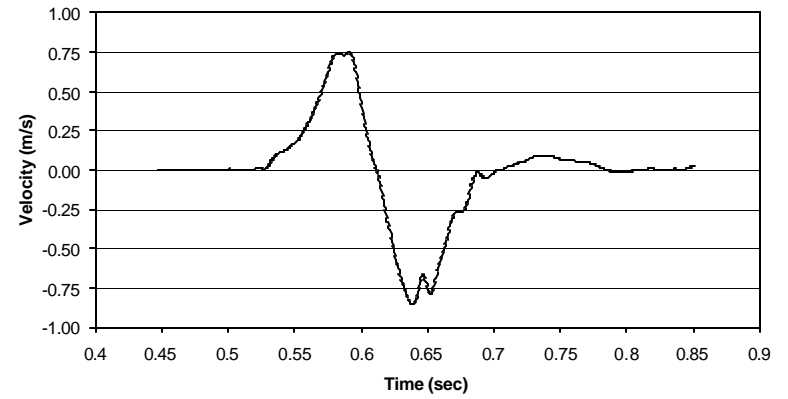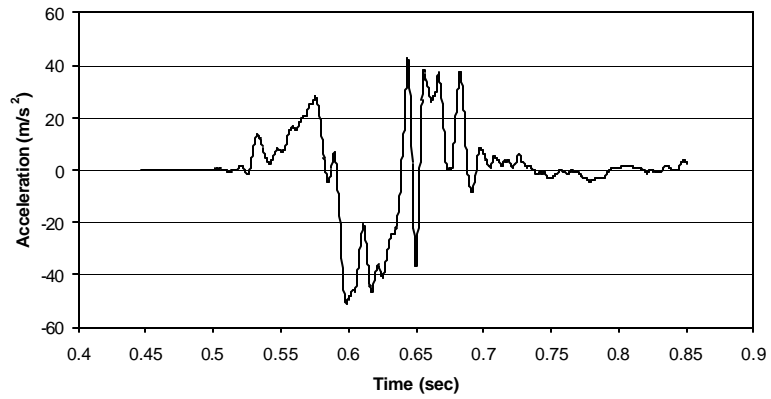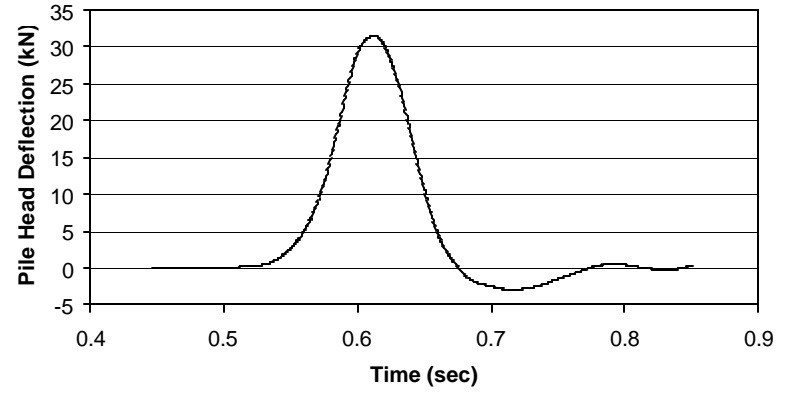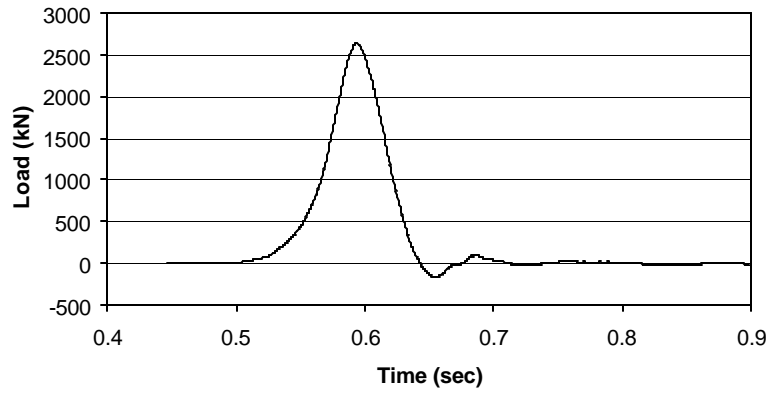
Figure 11.5 Time histories of load, displacement, velocity and acceleration of the pile group for statnamic test four.
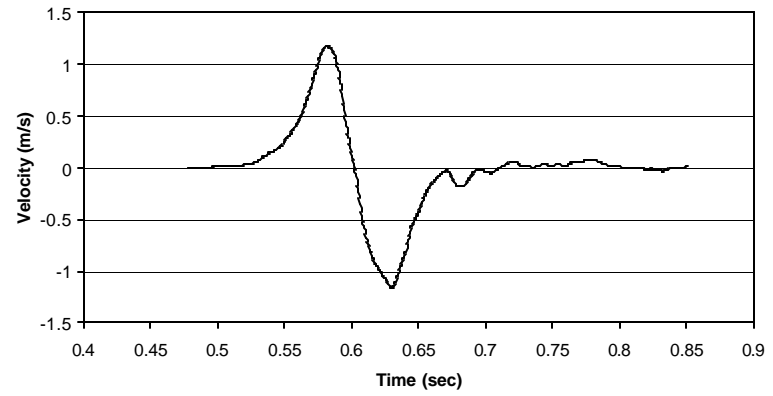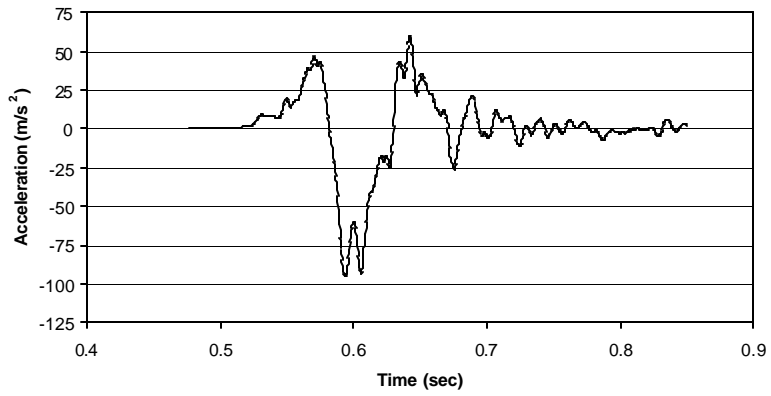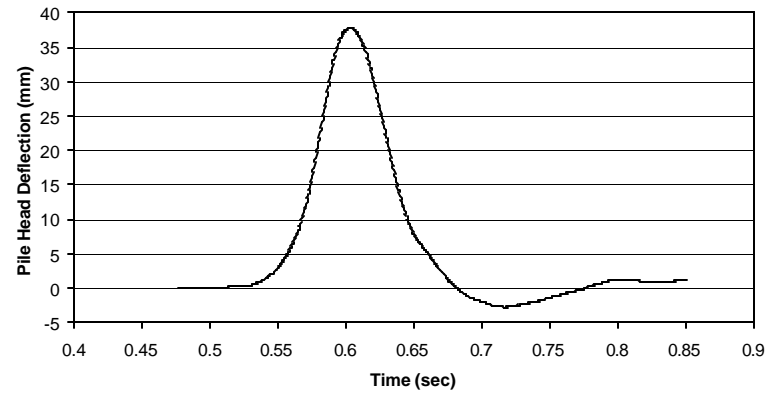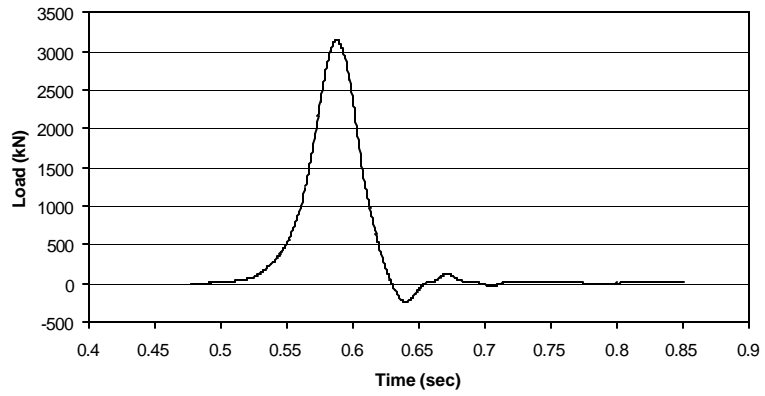
Figure 11.6 Time histories of load, displacement, velocity and acceleration of the pile group for statnamic test five.
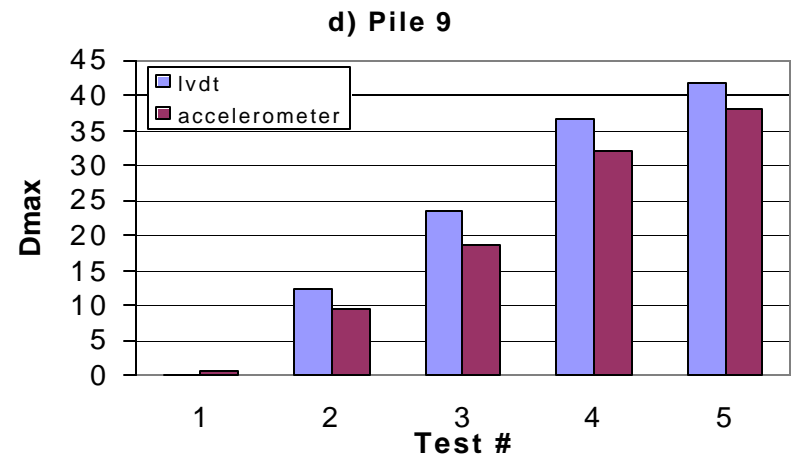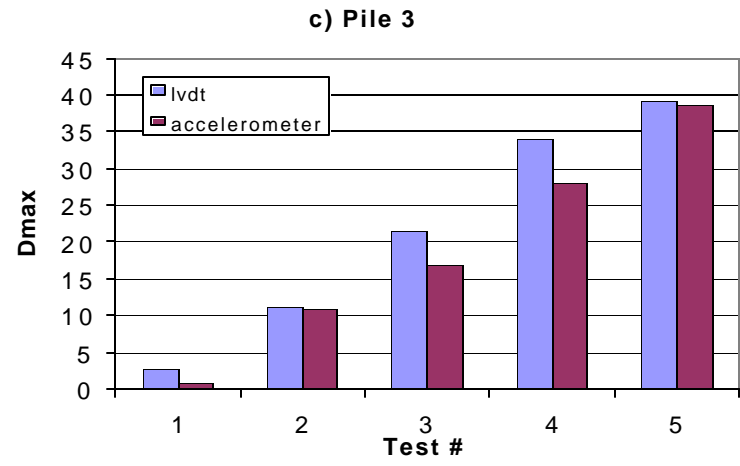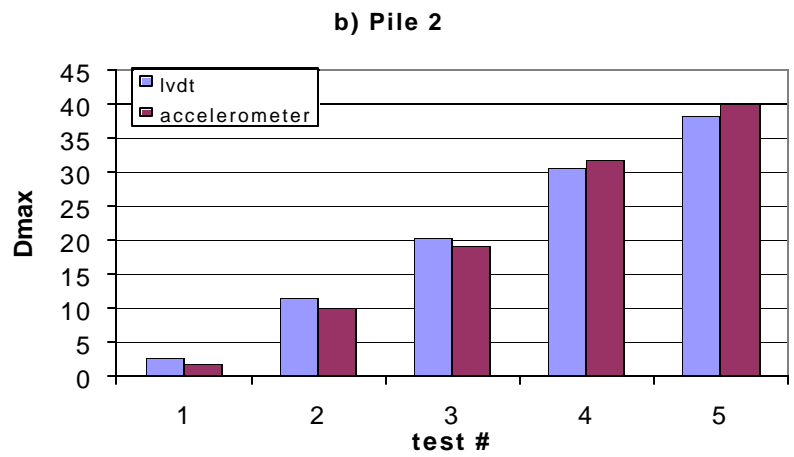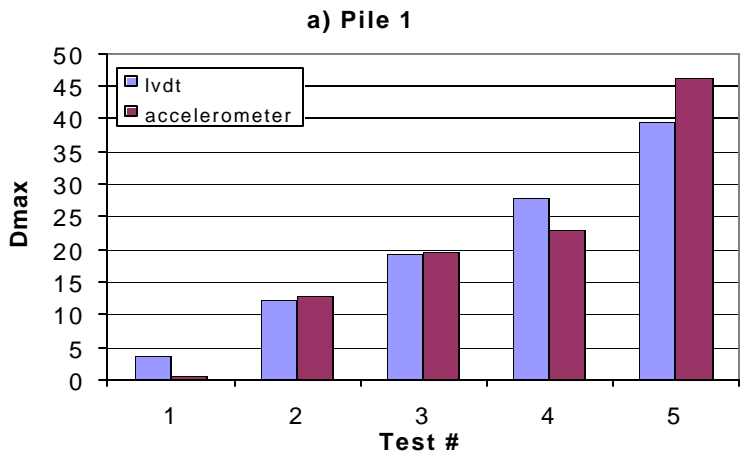
Figure 11.7 Comparison of the maximum deflections measured by the LVDTs and calculated from the accelerometer data.

Load- deflection at the pile head.

Figure 11.7 shows the peak-deflections measured by the LVDTs compared to those calculated by double integration of the accelerometer records. In most cases, the LVDTs measured higher deflections than the accelerometers. The difference between the deflections measured by the LVDTs and those calculated from the accelerometers was quite high for the first statnamic test; however, during the other four tests there was a 10.2% mean difference between the LVDT and the accelerometer deflections, with a standard deviation of 10.1%. Throughout the discussion and in all subsequent plots the deflections used were obtained from the LVDTs.

The total load used in this discussion was the sum of the individual loads measured by the tie-rod load cells that were attached to the piles. A load cell attached to the statnamic device was used to make comparisons with the sum of the measured pile loads. In every case, the statnamic load cell measured a larger force than the sum of the tie-rod load cells. Generally, as the load increased, the error between the two load measurements decreased. It was observed that there was a maximum difference of 29.2% at the lowest load level and the minimum difference of 13.5% was recorded during the fourth test. Discrepancies between the two methods of load measurement can be at least partially attributed to friction in the load frame that would cause a loss in force between the statnamic device and the piles. The load from the tie-rods was preferred for two reasons. First, these cells had a better resolution, particularly at the small loads, and second, these cells give the load actually transferred to the piles, neglecting potential energy losses in the frame.

The average load is plotted against the average deflection for the pile group in Figures 11.8 and 11.9 for both the statnamic and static tests. Figure 11.8 contains the results of the first
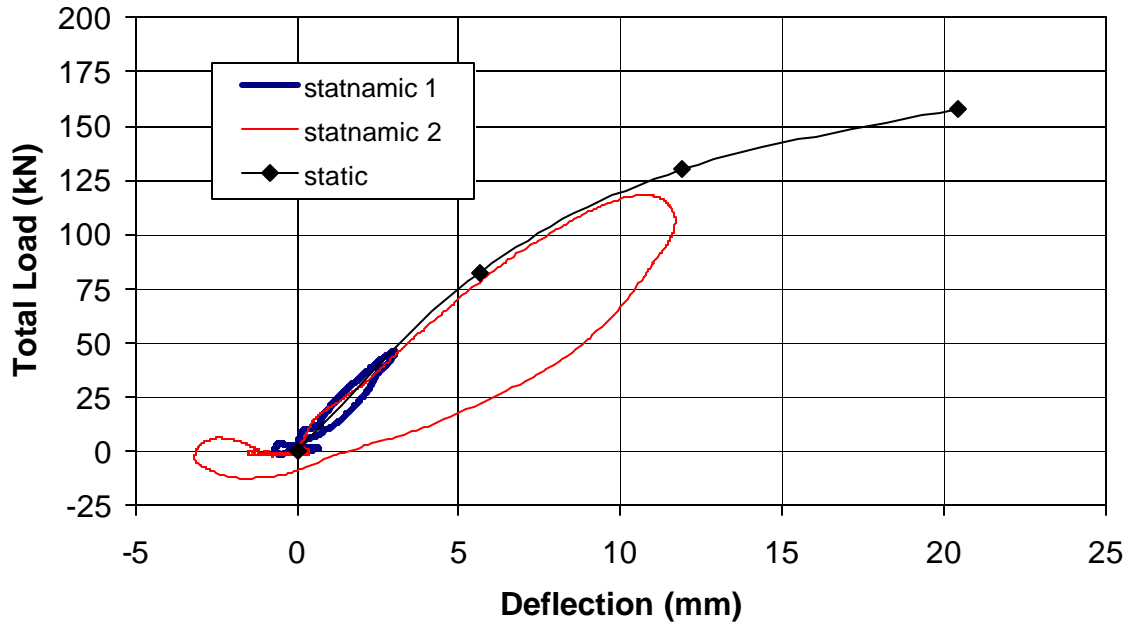
Figure 11.8 Load vs. deflection curves for statnamic tests conducted after previous cyclic static loadings relative to static load vs. deflection curve.
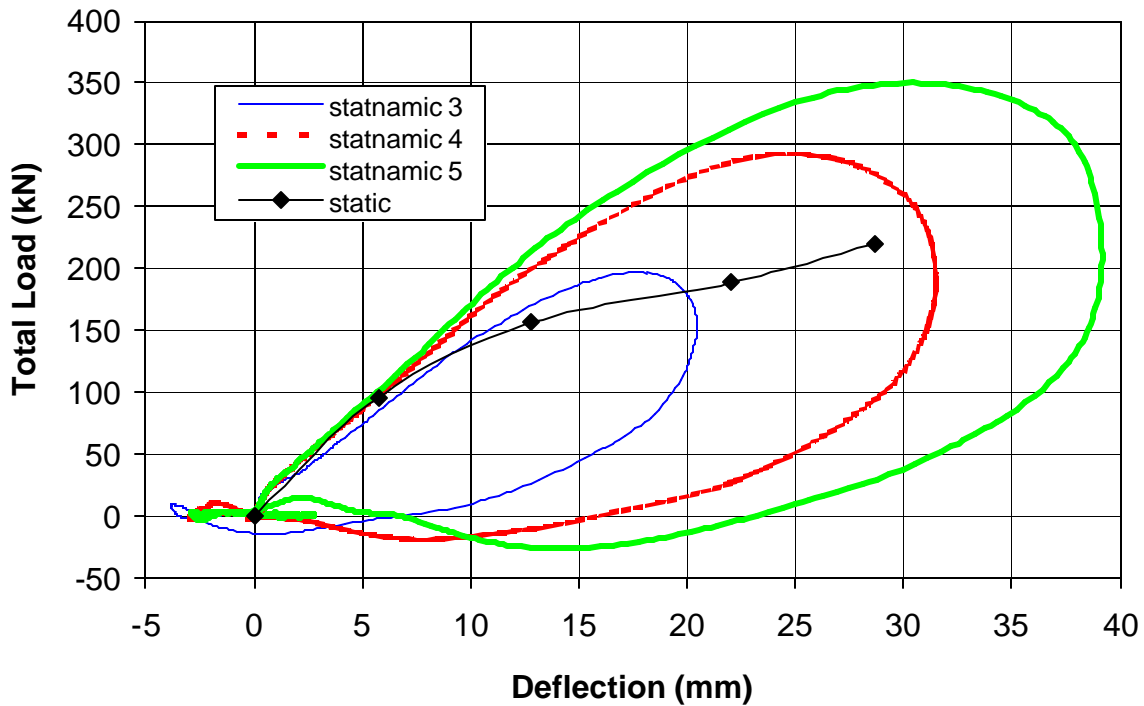

Figure 11.9 Load vs. deflection curves for statnamic tests conducted before static loading along with subsequent static load vs. deflection curve

THIS PAGE LEFT BLANK INTENTIONALLY

two statnamic tests, which were performed after 15 static load cycles. Also plotted in Figure 11.8 is load-deflection curve for the fifteenth cycle of the static group test for comparison. The last three statnamic tests are shown in Figure 11.9. These tests were conducted before the group was statically cycled to these higher deflections; therefore, the first cycle static group results are shown in comparison.

Especially in the higher load levels shown in Figure 11.9, but also in Figure 11.8, the maximum deflection occurred significantly later than the maximum load in the statnamic cycles. This was due to momentum generated during the rapid loading of the pile group. The maximum loads and the deflections that occurred at these loads have been used in the subsequent figures and the discussion of the statnamic testing.

As plotted in Figure 11.8, the load-deflection curves for the two statnamic tests are very similar to the load-deflection curve for the 15th cycle of the static test. These statnamic tests were performed after gaps had been formed in the soil due to static load cycling. Therefore, inertia and damping forces associated with the movement of the soil would likely be relatively small. In contrast, the load-deflection curves for the statnamic tests performed on virgin soil, shown in Figure 11.9, indicate much greater lateral resistance than the static load-deflection curves particularly after the deflection exceeds the previous maximum deflection. This higher statnamic load required to produce a given deflection can be attributed to resistance from inertial and damping forces. The hystersis loops for the statnamic load-deflection curves in Figure 11.9 are much larger than those in Figure 11.8 indicating greater energy dissipation for the virgin loading condition relative to that after cyclic loading.

As with the static tests results, comparisons of the load variation within a row were made during the statnamic tests and the load-deflection curves for each row are plotted in Figure 11.10.

11-17
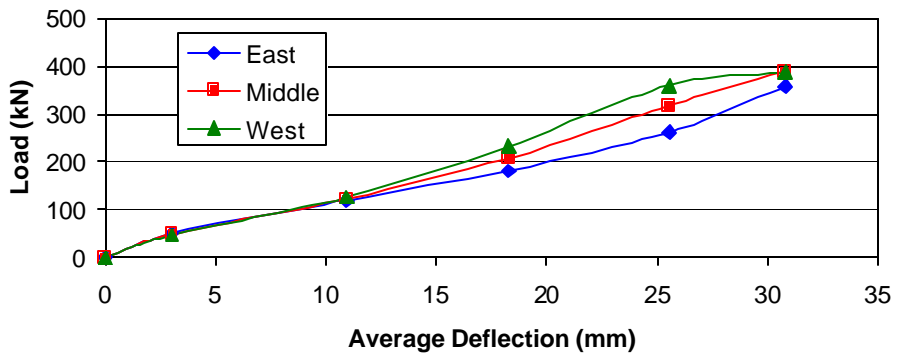
a) Front Row Piles

b) Middle Row Piles
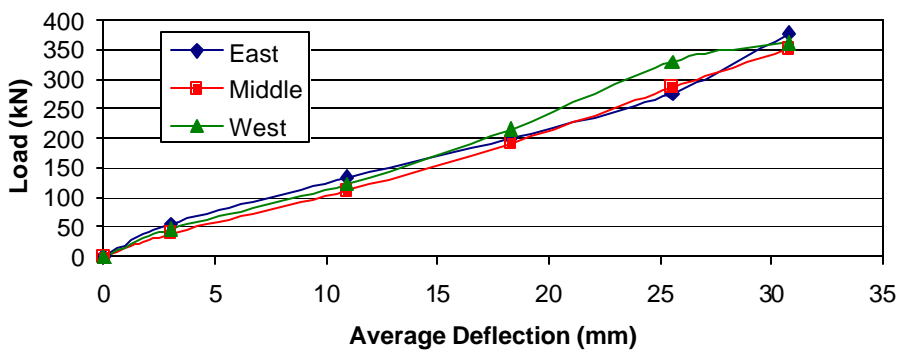

c) Back Row Piles
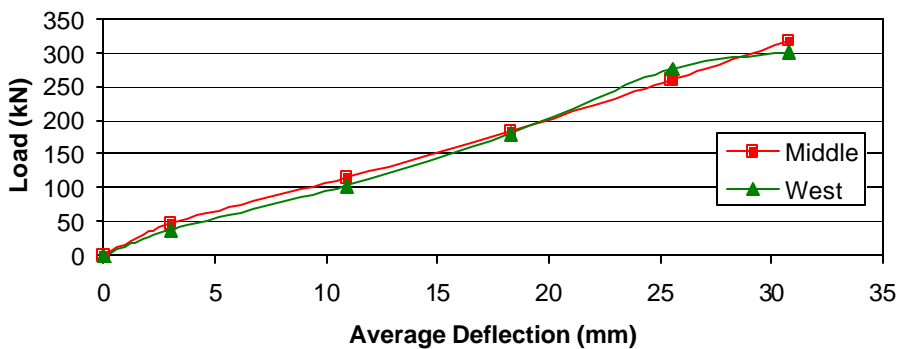
Figure 11.10 Load vs. deflection curves for piles in the front (a), middle (b) and back (c) rows of the pile group.
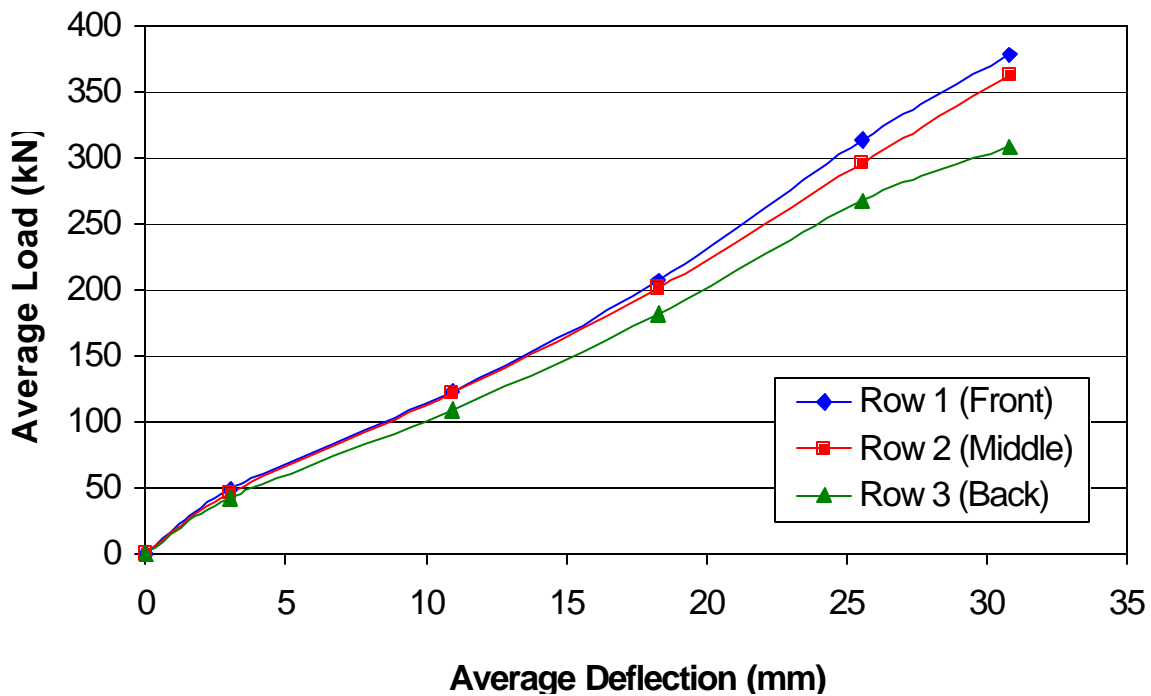
Figure 11.11 Average load vs. deflection curves for the front, middle and back row piles in the group during the five statnamic loadings.

Group effects are small for the first two tests involving reloading, but increase for the last three tests involving virgin loading.

The average variation of load, within each row, was less than 9% between the lowest and the highest loads carried by the piles. The tie-rod load cell attached to pile 7 was not functioning properly and is not shown in the figure. For all total load measurement, the load value used for this pile was again taken as the average between the remaining two piles in that row. As observed in the static test, there is no consistent load distribution pattern within a given row.

The average load per pile at the peak load is plotted for each row with the corresponding deflections in Figure 11.11. As stated previously, the first two statnamic tests were performed after the static load cycles had been run. Gaps were formed during the static tests, which prevented group effects from being a factor. When the lateral pile deflection was less than the gap width, the lateral resistance was provided primarily by the pile itself. Since there was little soil resistance, there was also little, if any, group effect. Group effects were especially absent

between the first and second rows on these first two tests, as these curves are nearly equal. Group effects were, however, more pronounced on the last three tests, which were performed before the soil gaps were formed by static cycling. Nevertheless, the variation in load carrying capacity between rows was considerably smaller than was observed during the static testing.

Bending Moment

Bending Moment vs. Depth. Using the strain-gauge data, the bending-moments were calculated following the same procedure described for the single-pile tests in Chapter 4. Bending moment versus depth curves for the front, middle, and back row piles are shown in Figures 11.12 and 11.13. These curves correspond to the average group displacements of 3.0, 10.9, 18.3, 25.5, and 30.8 mm. These displacements occurred at the maximum loadings on the pile group for each of the five statnamic tests. Similar to the static test results, the maximum moment for each statnamic test was generally highest in the lead row, while the second and trailing rows developed nearly equal moments. The only exception to this occurred during the first statnamic test, when the moments in the second row were significantly higher than the trailing row. The maximum moment in the leading row typically occurred at a shallower depth than the maximum moment in the middle and trailing rows. Though there are significant differences in moments near the top of each pile, at greater depths the moments in each row are essentially the same.

Figure 11.14 presents the bending moment versus depth curves of each row for the static and statnamic tests at nearly equal loads and deflections. The statnamic results plotted in this figure were taken at the maximum load for the second statnamic test with deflections of 10.9 mm. The moments are compared at this deflection because of the close alignment of the static and statnamic results, as plotted in Figure 11.9. The solid lines represent the statnamic moments for the middle pile of each row while the dashed lines represent the static test results.
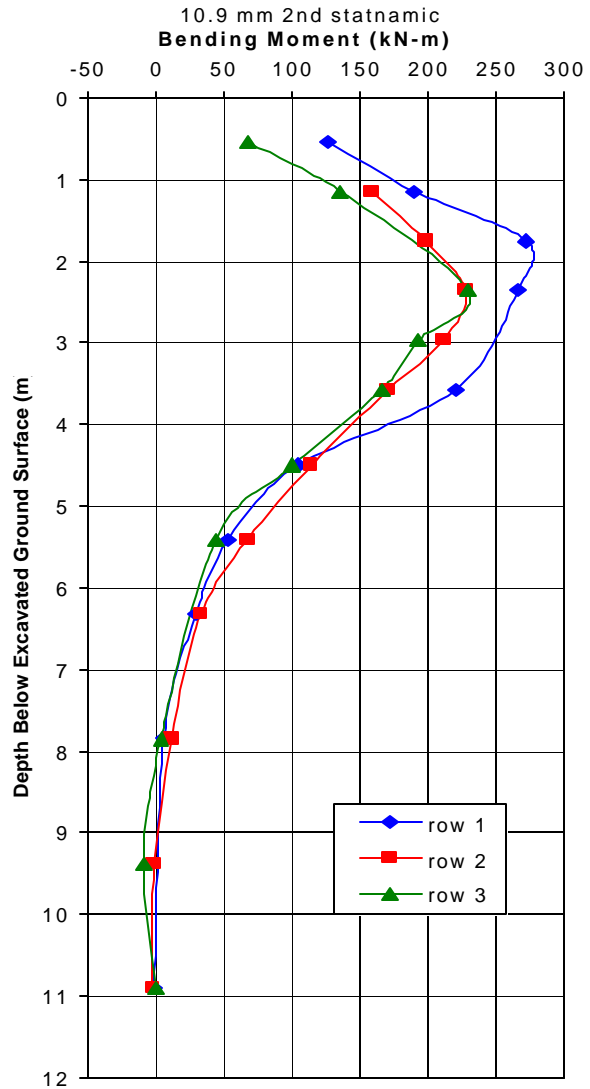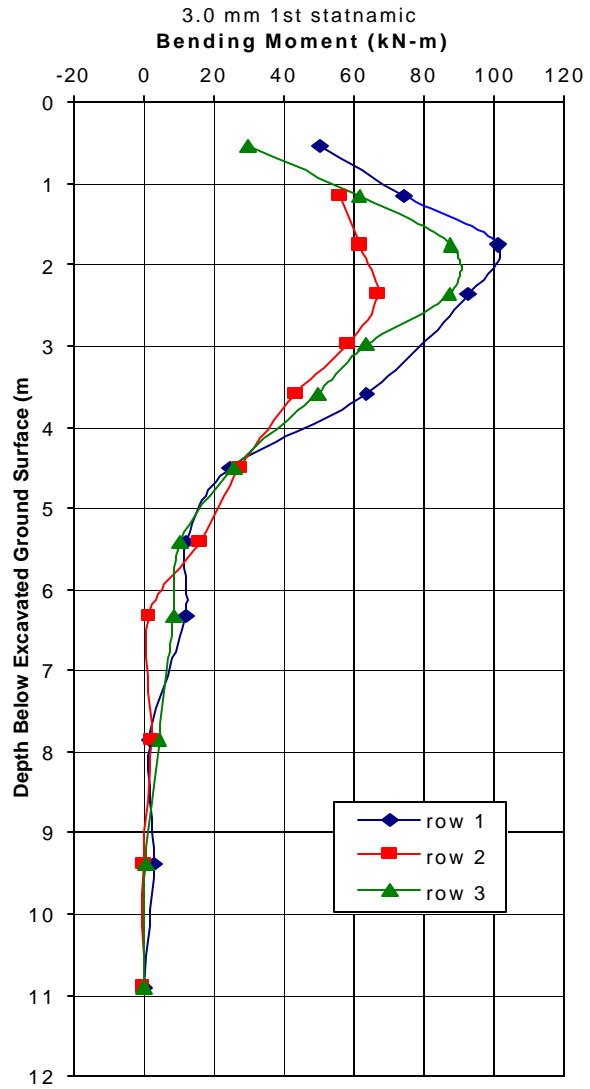
Figure 11.12 Bending moments versus depth curves for each row at the maximum load during statnamic tests one and two. Corresponding deflection levels are indicated.

11-21
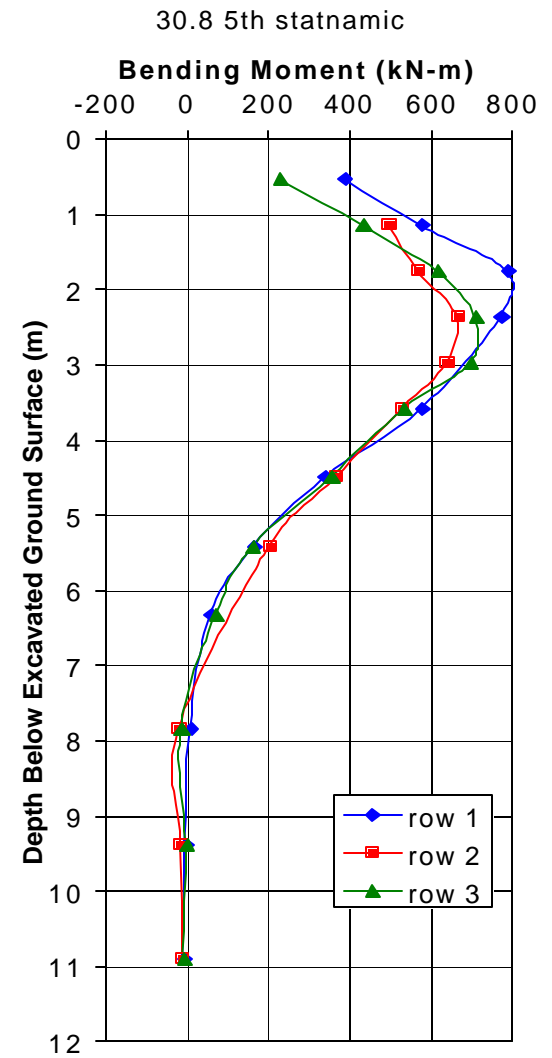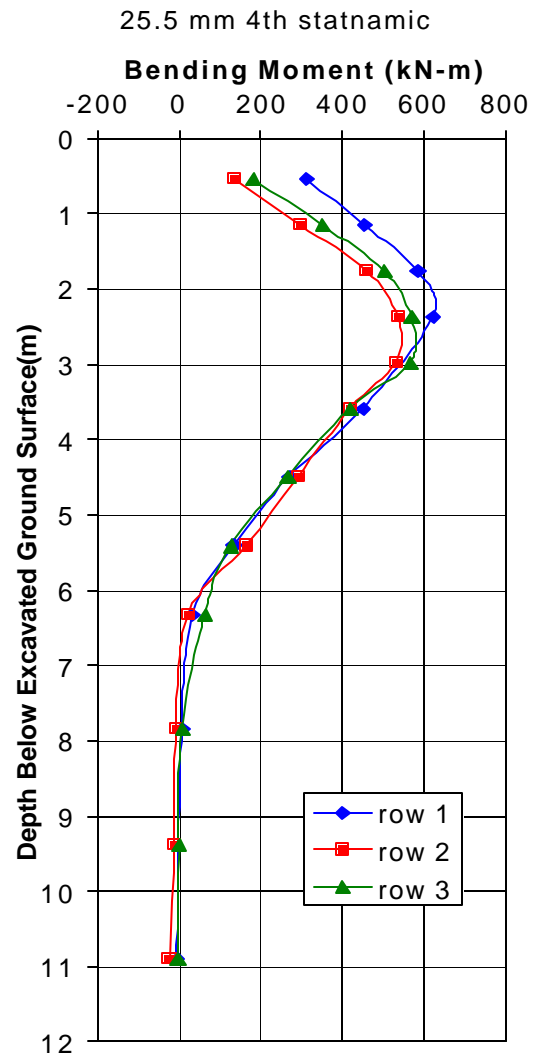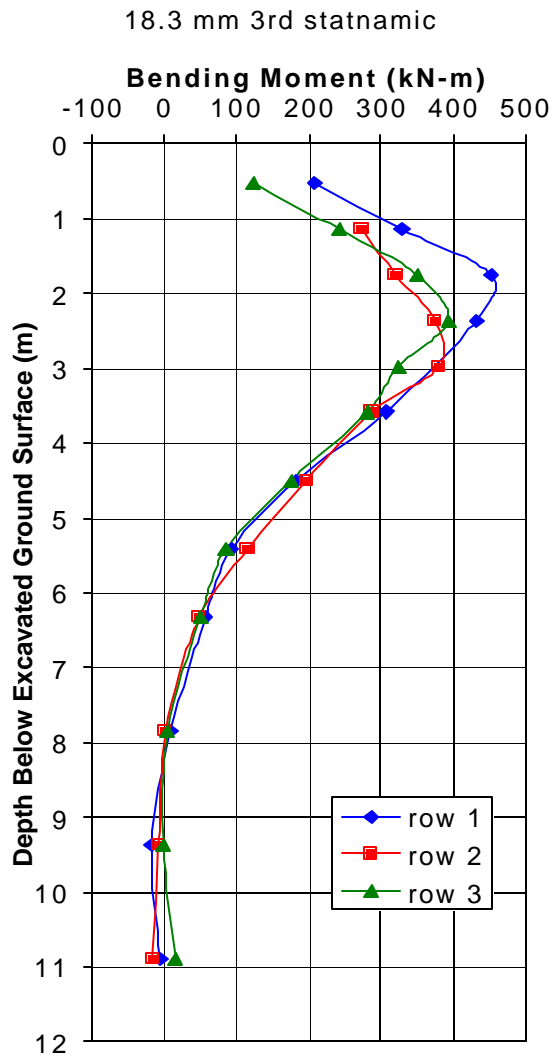
Figure 11.13 Bending moment versus depth curves for each row at the maximum load during statnamic tests three through five. Corresponding deflection levels are shown.
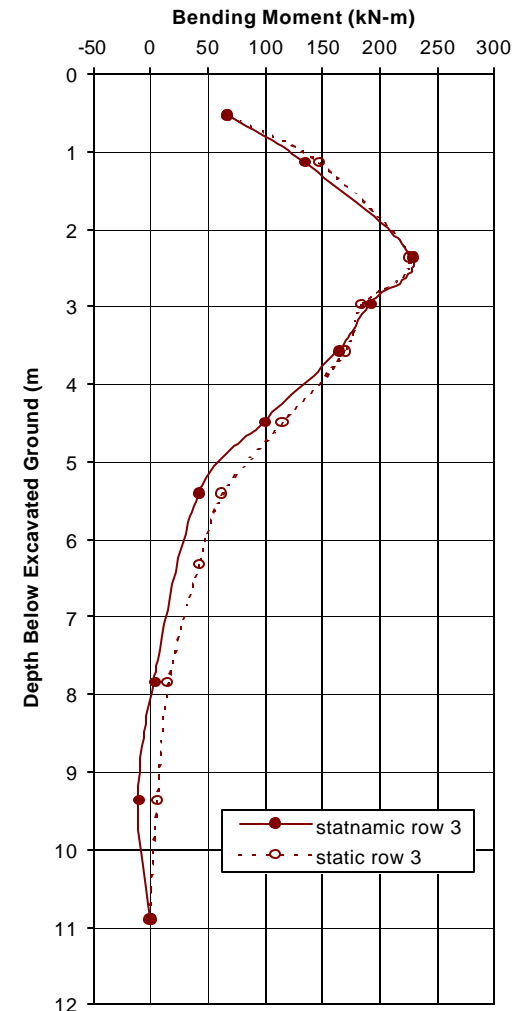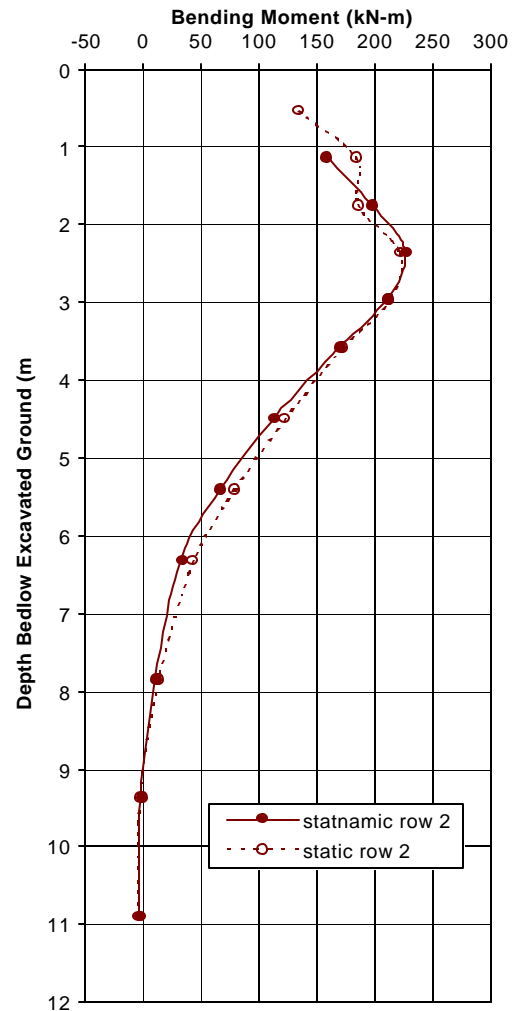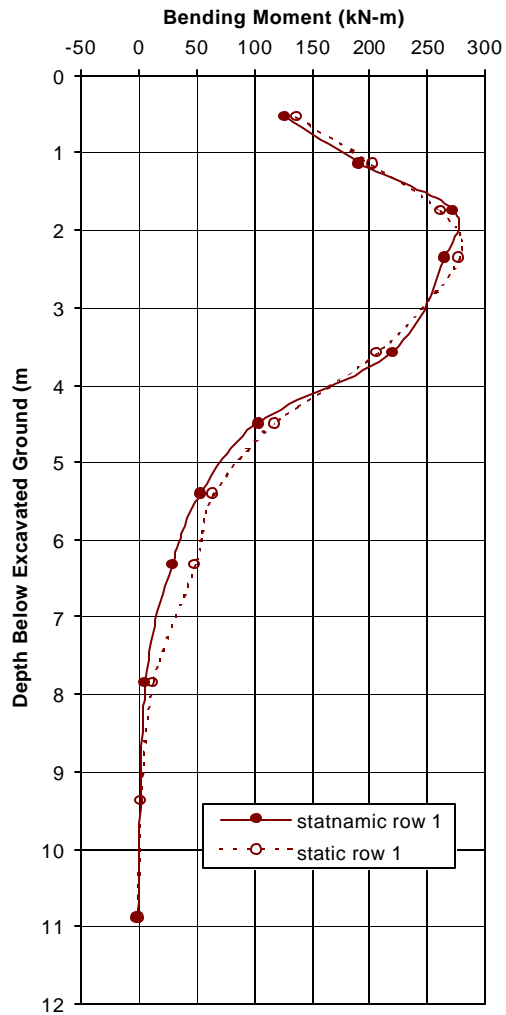
Figure 11.14 Bending moments vs. depth curves for static and statnamic tests for each row at near equal load and deflection

The moments from the two tests match very well. The only discrepancies appear to be that the maximum moment on the lead row during the statnamic test developed slightly higher on the pile than during the static test and the statnamic moments appear to return to zero at a somewhat shallower depth than during the static tests.

Maximum moment vs. load. The maximum bending moment for the center pile in each row is shown in Figure 11.15 plotted against the average pile load for the entire group. The average in this case is the total load divided by nine. This approach neglects the fact that the lead row piles carry greater loads. Because of the higher loads carried by the lead row in the group tests, the pile in that row has a higher moment than the middle and back row piles, whose response is quite similar.

The maximum moment versus the average pile load of each row is plotted in Figure 11.16 for the statnamic tests. The load shown in this figure is the average of the three piles in the row from which the moment measurement was taken. Plotting the moment against this load results in the trailing row recording the greatest moment at a given load. The higher moment is due to a softening of the soil around the trailing row due to group effects. Similar results were observed during the static test, as seen in Figures 8.12 and 8.13.
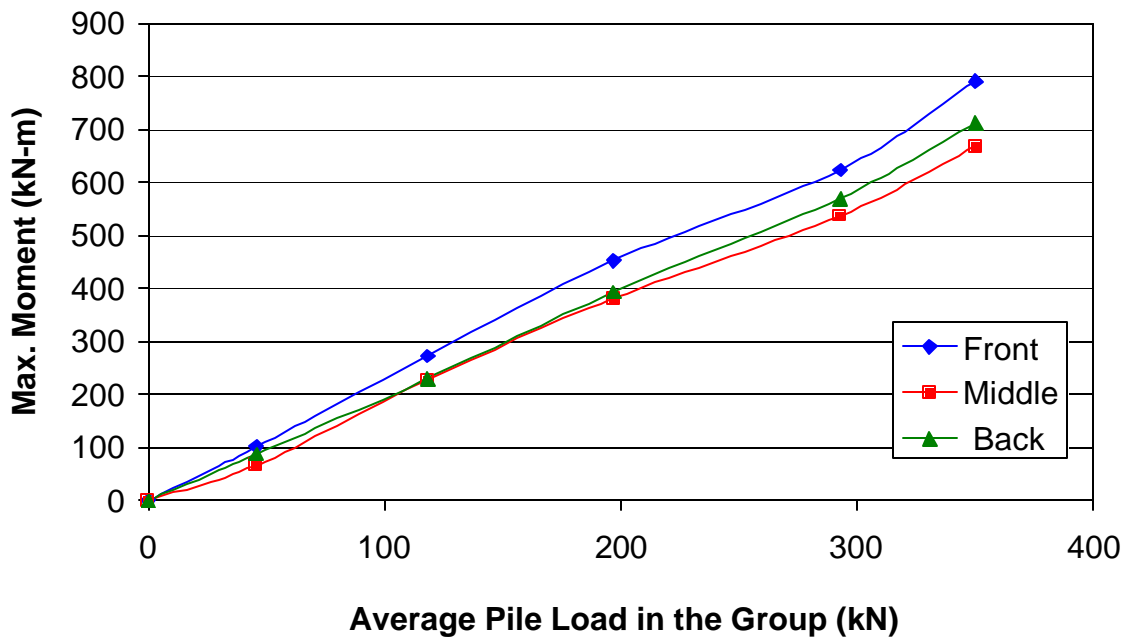

Figure 11.15 Maximum moment vs. average group load for each row in the group during the statnamic testing. Average load is total load divided by nine.
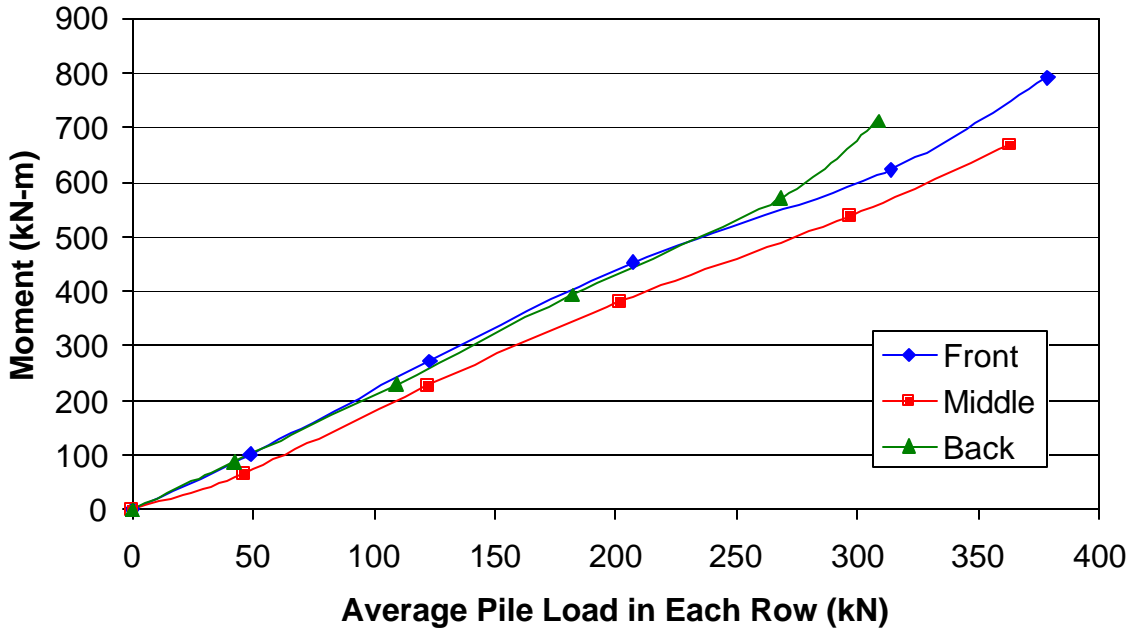
Figure 11.16 Maximum moment vs. average row load curves for the three rows in the pile group during the statnamic testing. Average load is total load in a row divided by three.

STATNAMIC LOAD TESTS ON FIFTEEN PILE GROUP
Test Setup

The piles and instrumentation to measure pile load, deflection, and strain vs. depth are the same as described in Chapter 7. In addition, instrumentation for the statnamic tests on the fifteen pile group included accelerometers to measure pile acceleration. Pile 2 was equipped with seven accelerometers at depths equivalent to the depths of the strain gauges down to 7.01 m (23 ft) below the top of the pile. These accelerometers were magnetically attached to the inside wall of the pile. Additionally, there were accelerometers at the load points of piles 1 and 3, which were used to compare with the LVDT readings, and one on the reference frame near pile 5 to measure any acceleration of the frame from the statnamic blast.

The statnamic load was applied in the same direction as the static loading but from the opposite side of the pile group as shown in Figure 11.17. Load was transferred from the device to the test piles by a large (W36X 210) reaction beam attached to the frame. During the

statnamic testing the nuts on the DYWIDAG bars used during the static test were loosened so that the statnamic load was only applied to the pile group.

Procedure

The statnamic testing was done in a series of six blasts. Don Robertson, P.E. of Applied Foundation Testing, Inc., calculated the amount of fuel for each blast based upon previous test experience. Each blast was intended to increase the deflection of the pile group 12.7 mm (0.50 in) over the previous blast. Because of the very short duration of each test, data acquisition was triggered just prior to the ignition of the fuel and data samples were collected at a rate of 1500 samples per second.
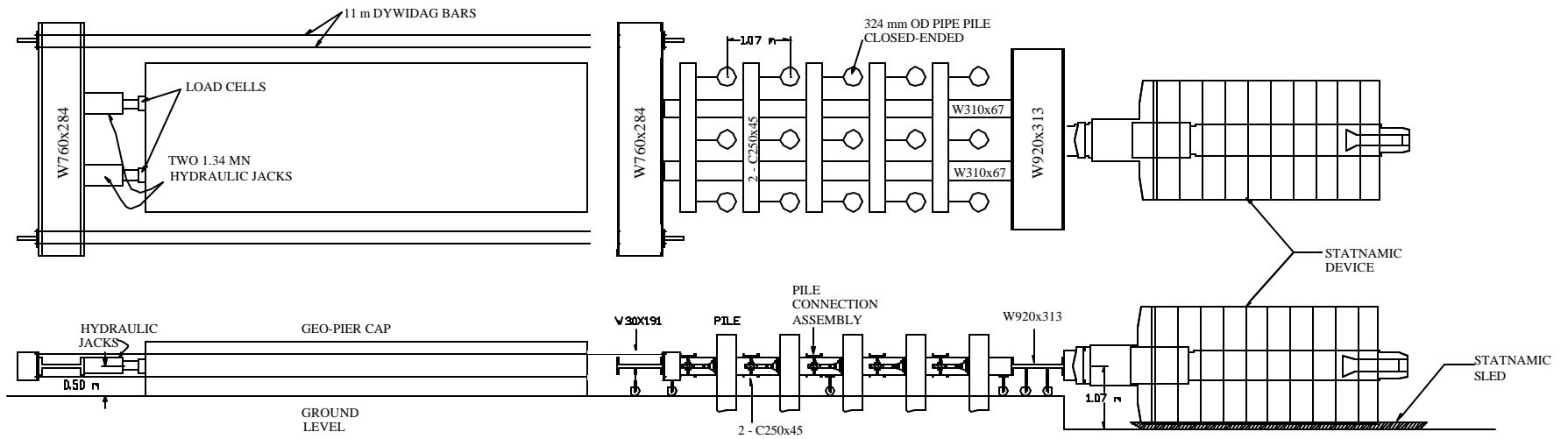
Figure 11.17 Schematic plan and profile drawing of the test setup for the statnamic lateral load test on the 15 pile group.

Statnamic testing of the pile group commenced on December 7, 1999 after the pile group had previously been brought to a maximum deflection of 14.0 mm (0.55 in) during the static testing. Premature failure of the Geopier cap prevented additional static tests prior to each statnamic test. On December 7th one statnamic test firing was made after the completion of the 14 mm series of static loadings. The remaining five test firings were performed on December 8, 1999.

Test Results
The load characteristics and the peak response for the pile group are summarized in Table 11.2. Once again, the rise times decreased as the maximum loads increased and the range is similar to that observed for the nine pile group. The maximum velocities for tests 2 through 5 are very similar to what would be produced by a large magnitude earthquake which would have acceleration levels between 0.4 and 1.6 g, but the maximum accelerations is these tests are much higher than would be expected for an earthquake.

Table 11.2 Summary of load characteristics and pile group response for statnamic tests on 15 pile group.

Test	Maximum Load (kN)	Rise Time (sec)	Maximum Deflection (mm)		Maximum Velocity (m/sec)		Maximum Acceleration (m/sec^2)	
			(+)	(-)	(+)	(-)	(+)	(-)
1	320	0.30	6.5	1.7	0.07	0.15	4	6
2	1020	0.14	28	10	0.36	0.72	43	36
3	1400	0.13	43	12	0.65	1.06	60	64
4	1700	0.12	57	16	0.90	1.3	76	75
5	2200	0.9	80	10	1.6	1.6	135	110
6	2558	0.075	95	12	2.7	2.1	120	195

Pile Head Load-Deflection
        The continuous load vs. deflection curves for each of the statnamic tests are shown in Figure 11.18. The pile group was subjected to a peak load of 2558 kN (575 kips) with a corresponding deflection of 72.04 mm (2.84 in), as measured by the tie rod load cells and load

point LVDT, during the sixth statnamic test. Though hard to distinguish, the static load vs. deflection curve is also shown on the graph for comparison. The last cycle from the static test was used because the soil had already been sheared when the statnamic testing began. For test 1, the LVDTs recorded a maximum deflection of approximately 2 mm (0.07 in) while deflection calculated from the acceleration record gave a 6.5 mm (0.26 in) average deflection between the three load point accelerometers. The deflection calculated from the acceleration record was used as the deflection at peak load for this test because vibration of the frame appears to have affected the measurement.

Figure 11.19 compares the peak statnamic response of the pile group with the static response. The average load per pile is the sum of the load measured by the tie-rod load cells divided by the number of piles in the group. The data points are from the peak load of each statnamic test and the corresponding average group deflection at that peak load. The static and statnamic curves appear to match reasonably well in both load and deflection for the small deflection levels involved where reloading is occurring rather than virgin loading. The last cycle of the static tests was again used to compare with the statnamic results.
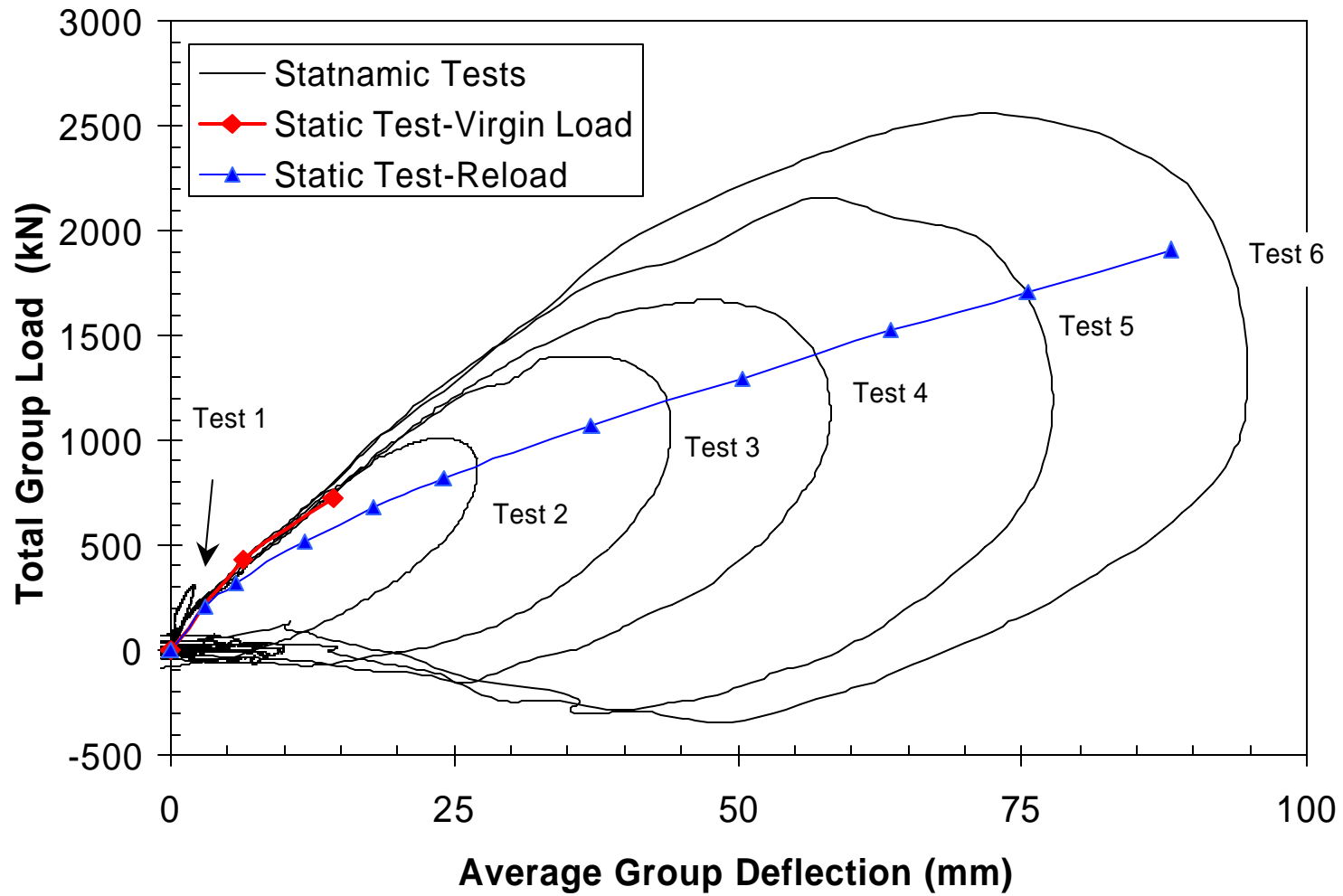
Figure 11.18   Load-deflection for each statnamic test of the pile group compared with the 15th cycle of each static test.
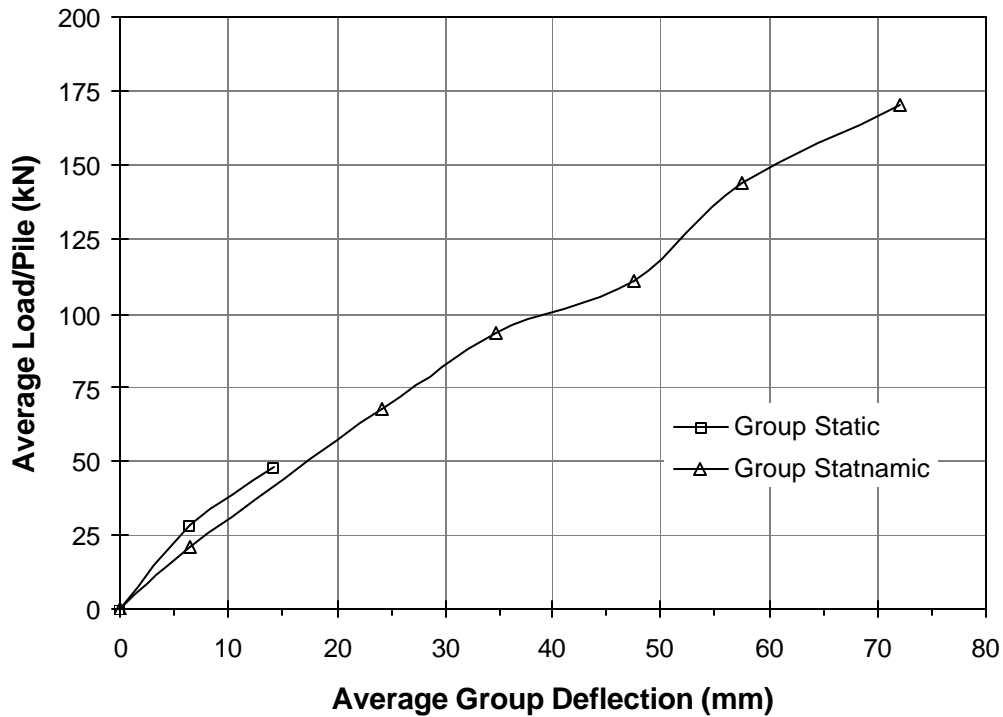
Figure 11.19 Comparison of statnamic and static peak average load/pile vs. average group deflection.

Figures 11.20 through 11.25 are plots of the entire load deflection curve of each pile for each statnamic test. Figure 11.26 is a plot of the peak average row load vs. deflection curves for individual rows of the pile group during each of the statnamic tests. Generally, the highest loads were taken by row 1 followed by rows 5, 3, 2, and 4. The fifth row closely mimics the first row throughout the statnamic testing until the last test in which the fifth row carried a slightly (4%) higher load. The trend of the fifth row not to follow the continuously reduced load from front to back rows is similar to the static test, though the overall load distribution is not consistent. Figure 11.27 compares the static row response to the first two statnamic tests. The static load distribution was 1st row, 2nd, 5th, 3rd, and 4th respectively, for each of the two deflection increments.
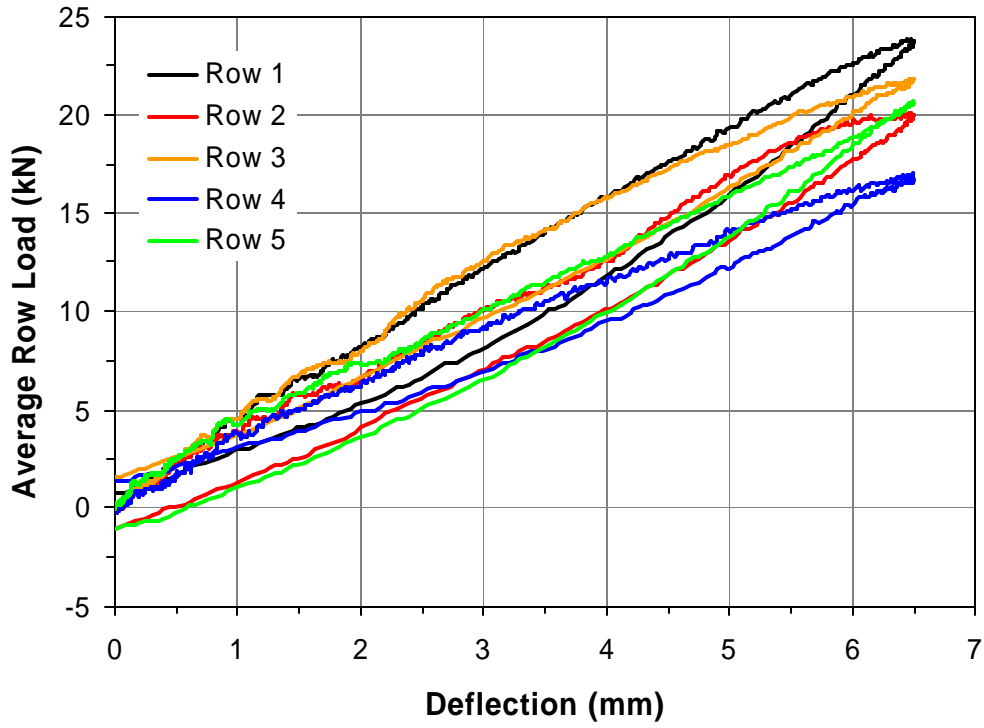
Figure 11.20 Average row load vs. deflection curve of each pile row for statnamic test 1.
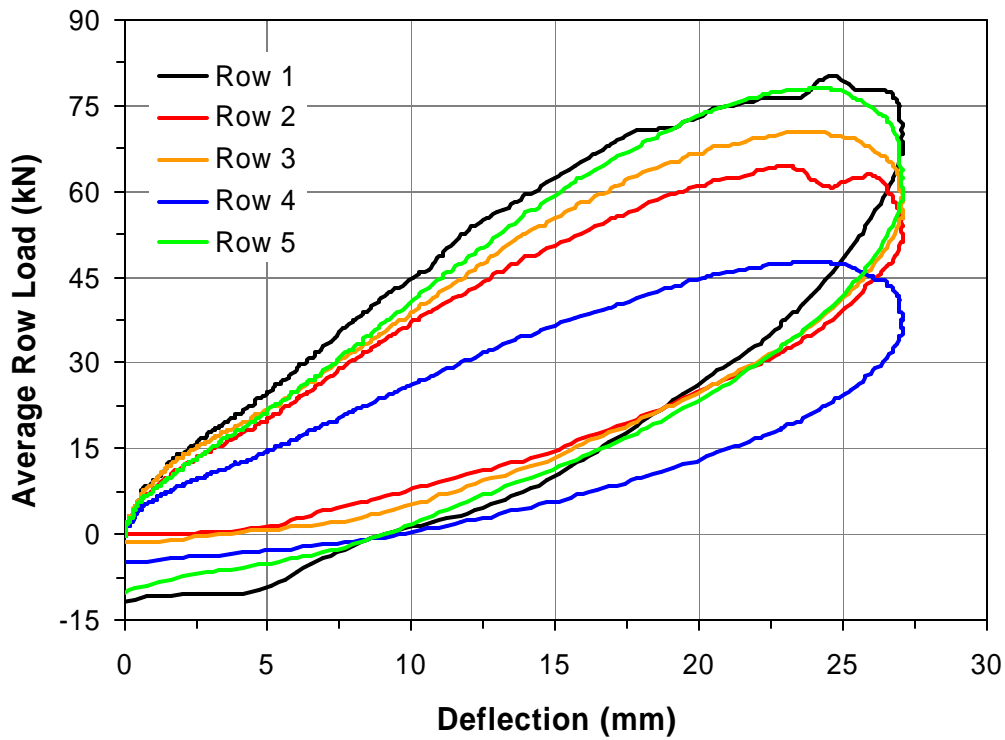

Figure 11.21 Average row load vs. deflection curve of each pile row for statnamic test 2.
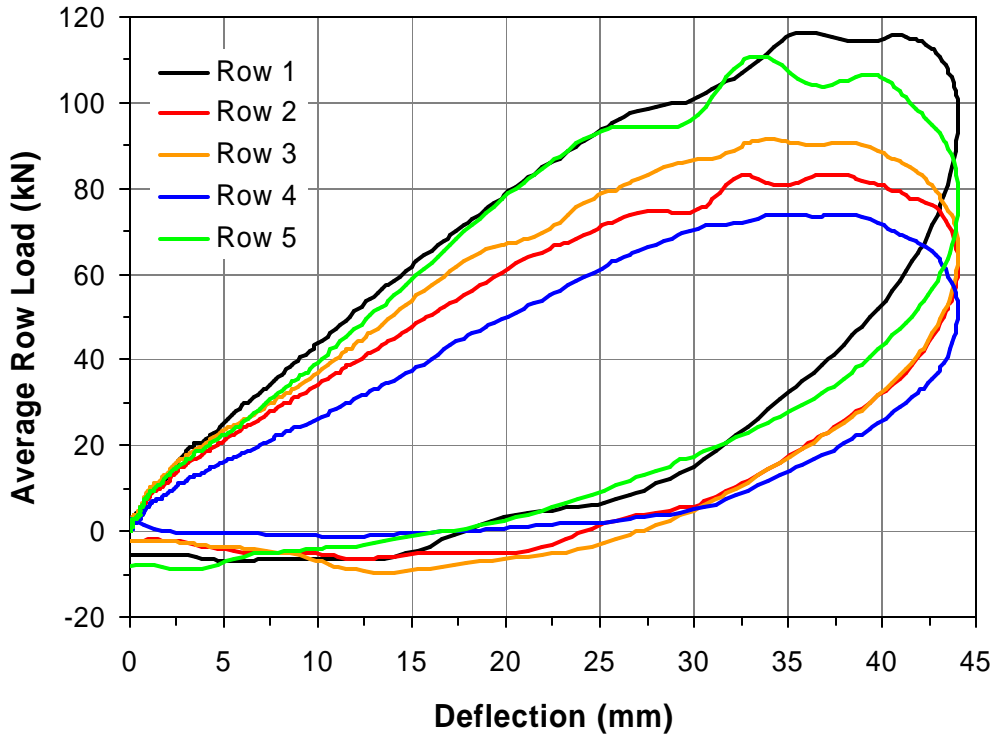
**Figure 11.22 Average row load vs. deflection curve of each pile row for statnamic test 3.**
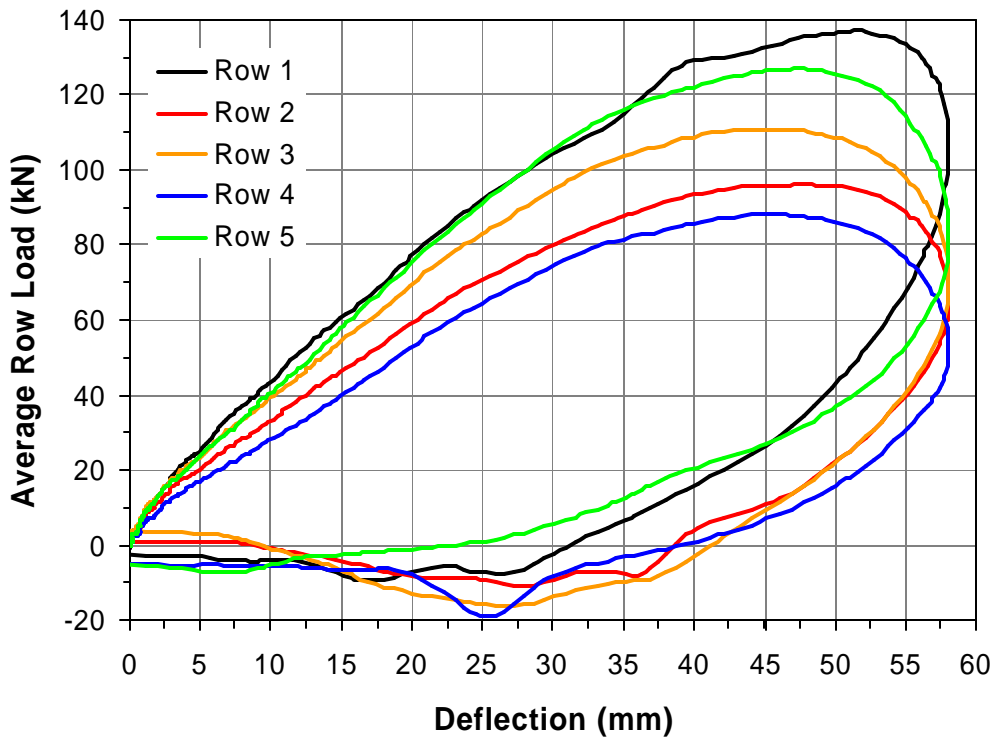
Figure 11.23 Average row load vs. deflection curve of each pile row for statnamic test 4.

11-33
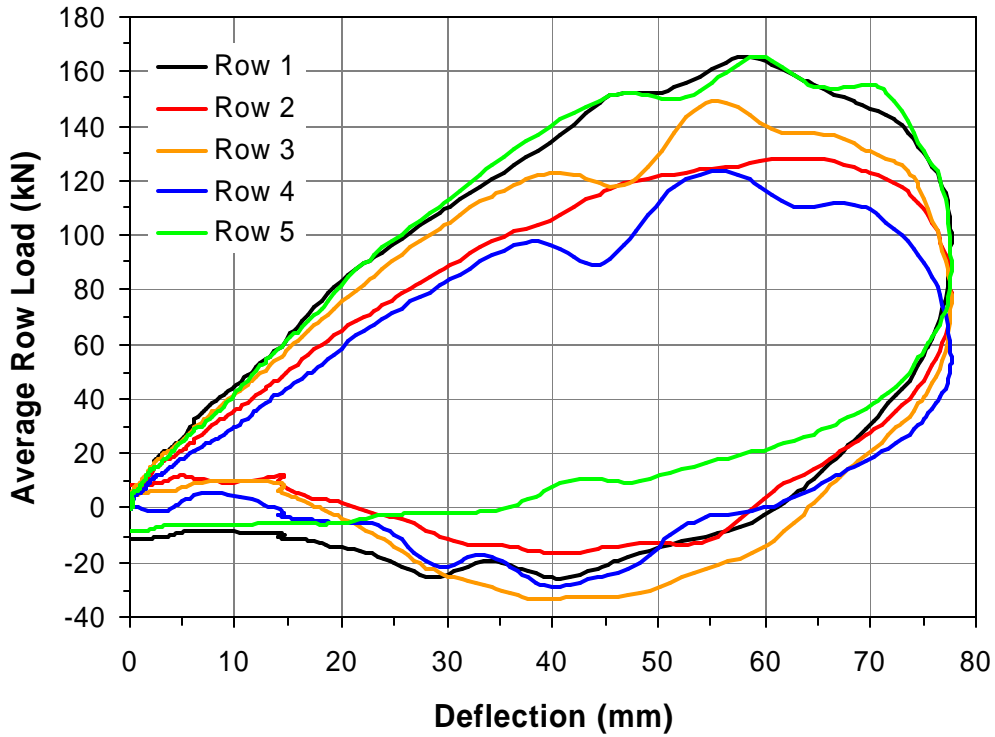
Figure 11.24 Average row load vs. deflection curve of each pile row for statnamic test 5.
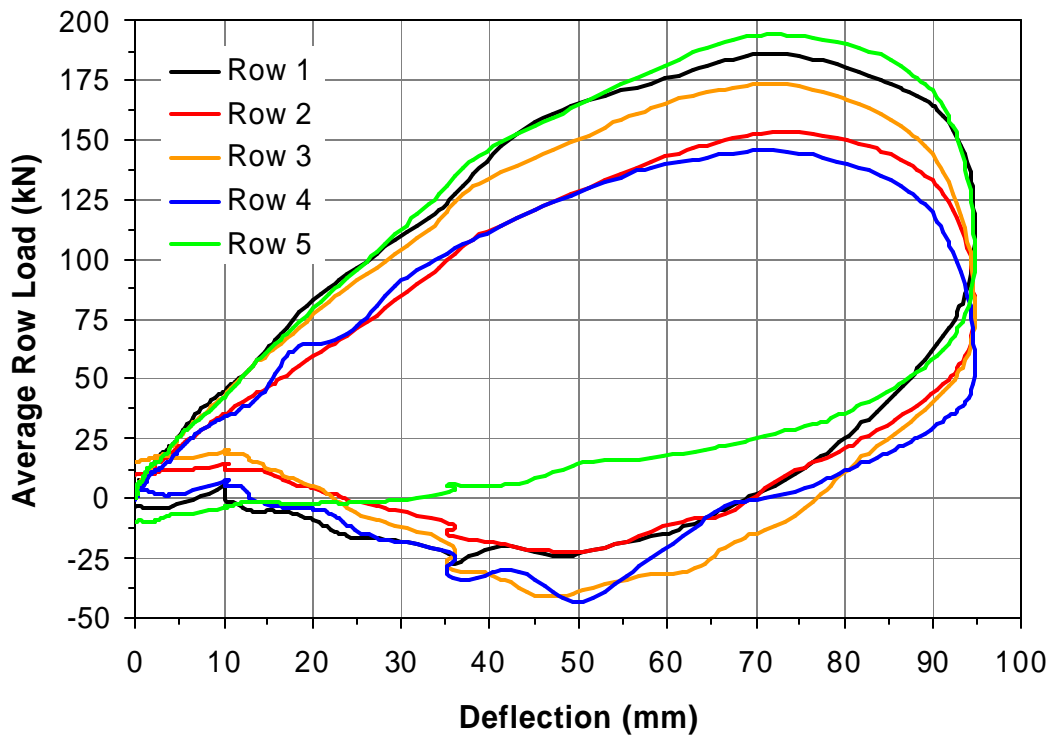

Figure 11.25 Average row load vs. deflection curve of each pile row for statnamic test 6.
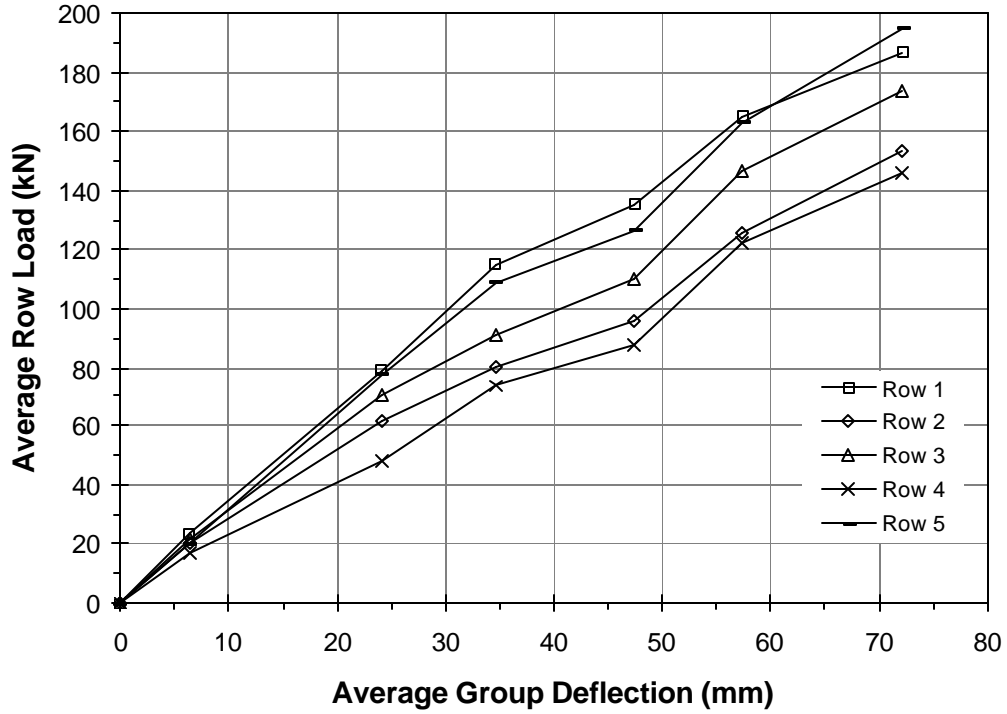
Figure 11.26 Average peak row load vs. deflection for statnamic tests 1- 6.
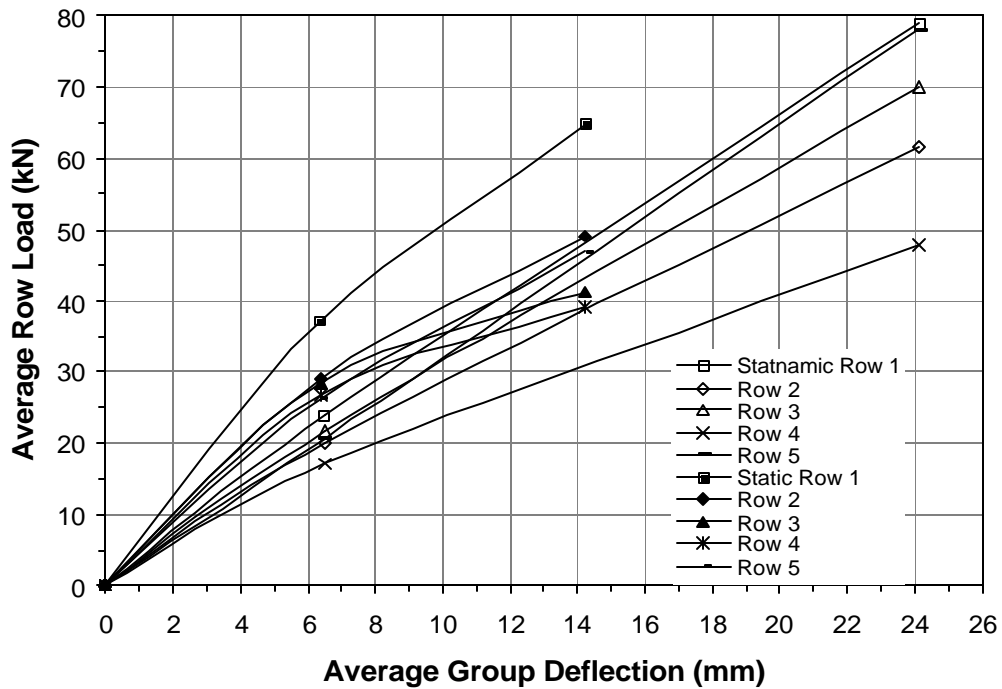

Figure 11.27 Average row loads and deflections for statnamic tests 1&2 and static tests.

Close examination of Figure 11.27 reveals the following load distribution for the first statnamic test: 1st, 3rd, 5th, 2nd, and 4th. This distribution is closer to the static results, but rows 2 and 3 are switched. Perhaps the static load distribution, at higher deflections, would more closely resemble the statnamic results if the static tests had been able to proceed to the maximum target deflection of 50 mm (2 in).

Another possible explanation as to why the statnamic load distribution does not mimic the static response could be in the rapid nature of the statnamic loading process. During the statnamic tests, data was recorded at approximately 0.0007 second intervals. When summing the load from the load cells, a peak load for the group would be reached at a specific time. Upon close examination of the loading record for each pile, the peak loads were not achieved on each pile at exactly the same time interval as that for the maximum load on the group. For some piles there was as much as five times this interval, a mere 0.0035 seconds, between their peak load and the peak load of the whole group. Some piles reached peak load before the group, some afterwards. For example, in test 6, two of the piles in row 2 achieved peak load after the group as a whole, whereas in row three, two of the piles reached peak load at the same instant as the group. Also, after the first statnamic test, the piles were loading against virgin soil and new conditions could have been encountered.

As with the static testing, the loads carried by individual piles in a row did not follow any specific pattern as shown in Figure 11.28. Rows 1 and 3 reacted the same as in the static testing, but row 5 had a different distribution. In row 5, unlike the static test, pile 14 carried a larger load than pile 15.
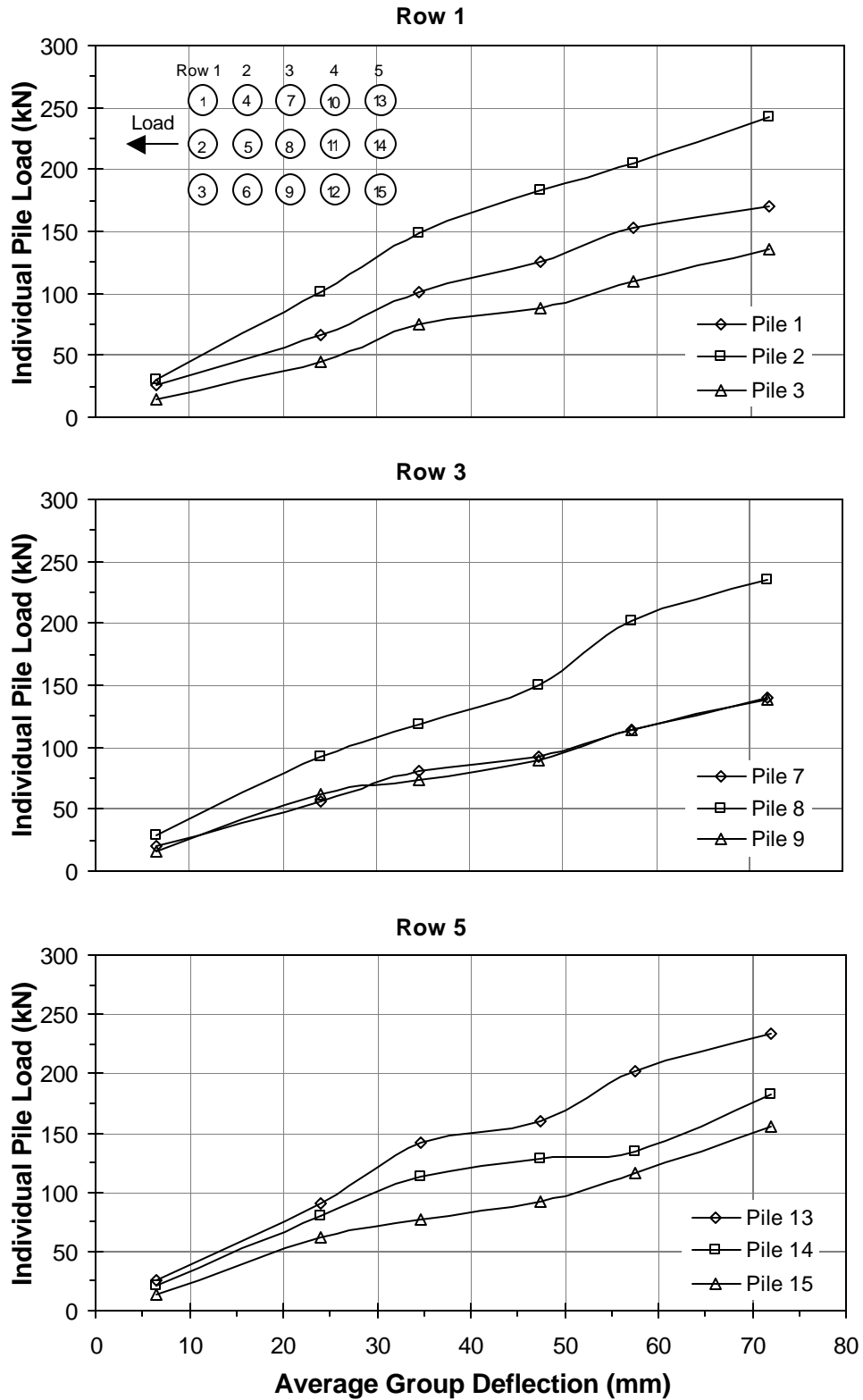
Figure 11.28 Individual pile loads within a row for statnamic tests 1-6.

Bending Moments vs. Depth

The bending moments developed in the rows during the statnamic load testing were calculated from data provided by the strain gauges attached to the center pile of each row. Calculations were performed using equation 4.1, as described previously. In cases where a gauge at a particular depth was clearly malfunctioning, the reading from the corresponding gauge on the opposite side of the pile was doubled for use in the moment calculations. Moment vs. depth curves are plotted in Figure 11.29 for the center pile of each row. Data for these curves were taken at the time of maximum group load during each of the statnamic tests. Each row is plotted separately and the moment differences from the first to sixth statnamic tests are compared. The maximum bending moment occurred approximately 1.7 m (5.6 ft), or 5.3 pile diameters, below the excavated surface. This is the same depth at which the maximum moments occurred during the static testing sequences.

The largest moment developed in row 5 (201.3 kN-m {148.5 kip-ft}), during test six, followed by rows 4, 2, 1, and 3. The moments approached zero at a depth of approximately 4.5 m (14.8 ft), which is consistent with the static tests. As can be seen, some of the strain gauge data was lost because of moisture (snow) at the site during testing. Load distribution and bending moments within the pile group showed the results of group effects causing a softer soil response and higher moments in the rows most influenced.
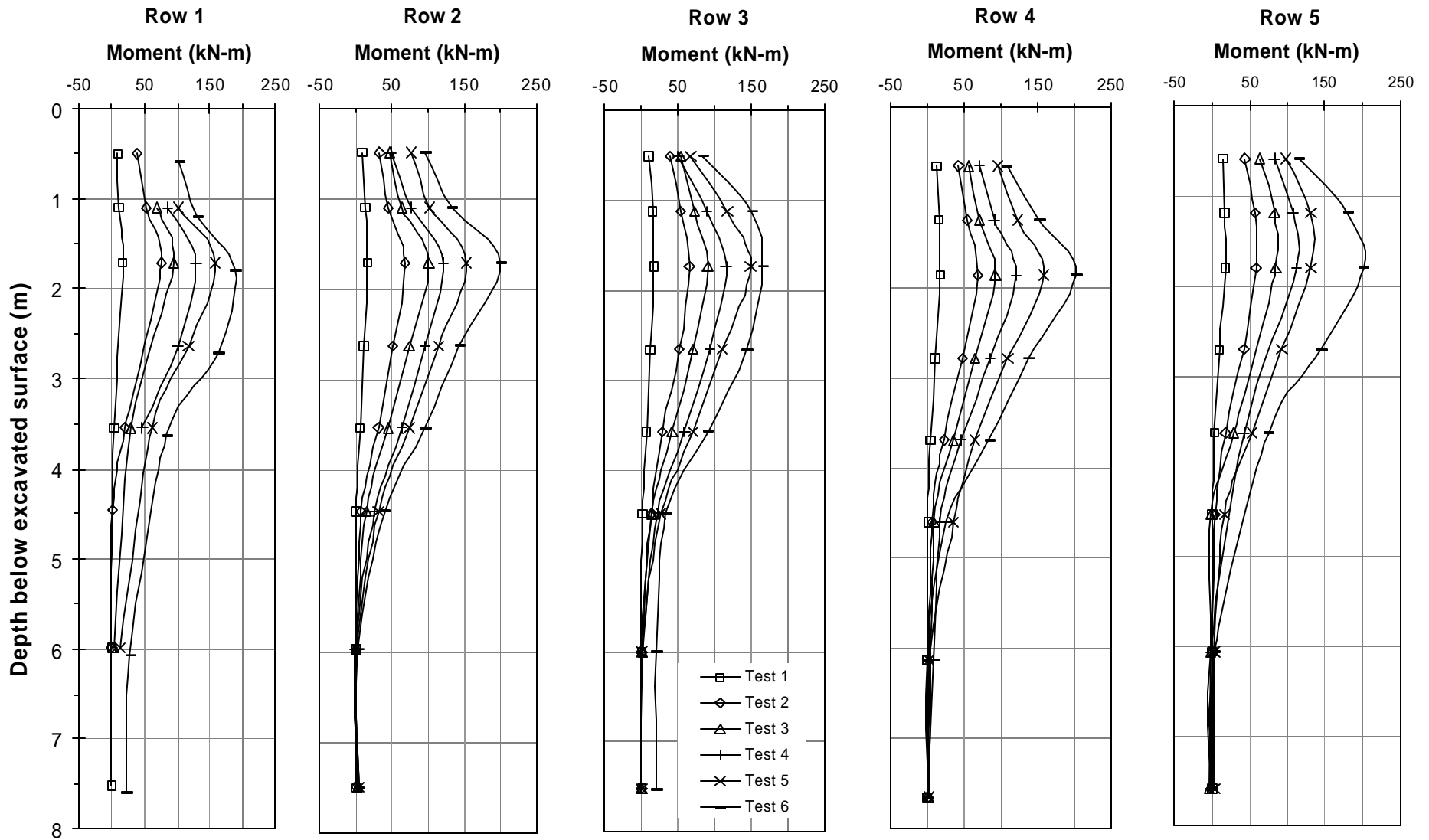
Figure 11.29 Bending moment vs. depth for statnamic tests 1 – 6 on the 15 pile group.
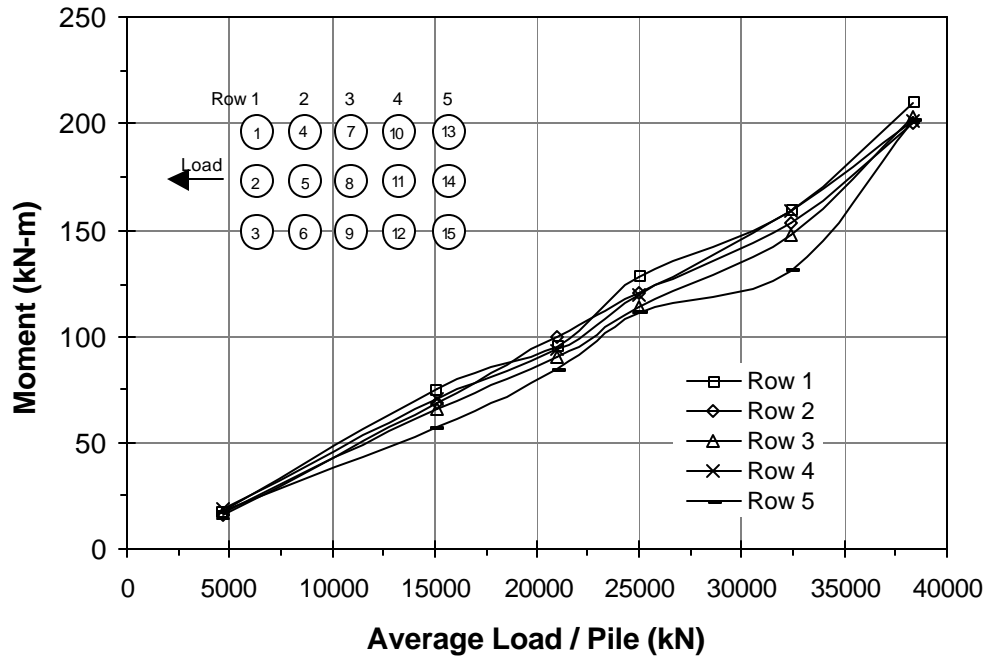
Figure 11.30 Maximum moment vs. average load per pile in the group for statnamic tests 1 through 6 on the 15 pile group.
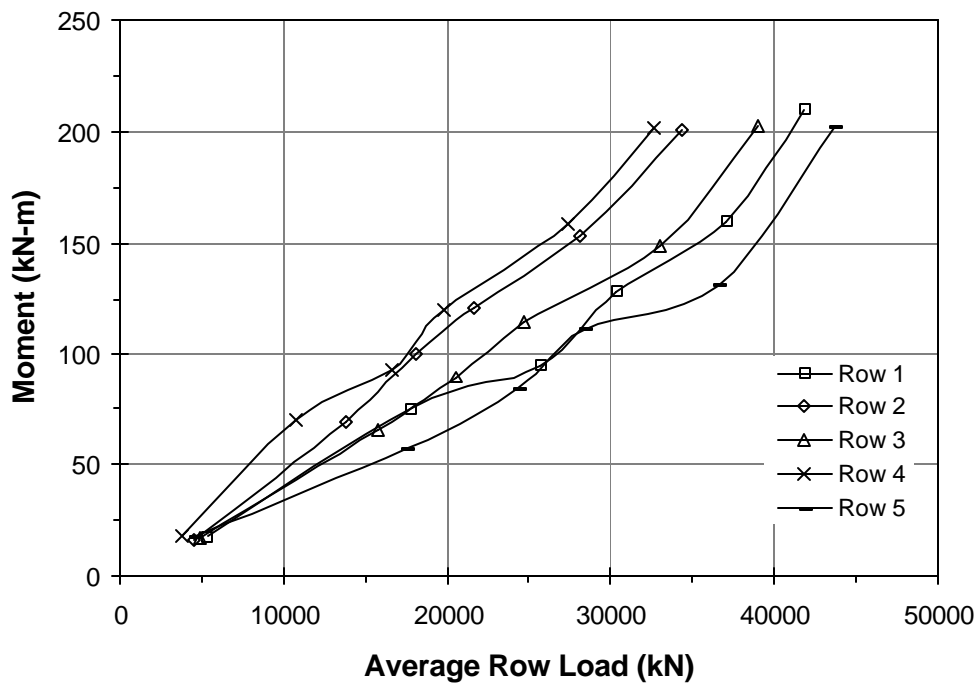

Figure 11.31 Maximum moment vs. average load in each row for statnamic tests 1 through 6 on the 15 pile group.

Maximum Moment vs. Load

Curves showing the maximum moment vs. the average load per pile for each row in the group are presented in Figure 11.30 for all of the statnamic tests. The average load/pile was obtained by summing the readings from the tie rod/load cells and dividing by the number of piles. However, the moments are very similar for each of the rows during all the statnamic tests.

Figure 11.31 depicts the maximum moments vs. the average load for each row in the group during the statnamic testing. The average load for a row was obtained by summing the load cells in the row and dividing by the number of piles in the row. The trailing rows clearly have higher moments at the same loads than the leading row. The maximum moment for a given load is generally higher for rows 2, 3, and 4 relative to rows 1 and 5. This is not fully consistent with observations on group effects seen in the static testing, but the observations are consistent with the observed load distribution during the statnamic testing.

Time Histories of Pile Group Response

Time histories of measured load, deflection and acceleration at the load point elevation are presented in Figures 11.32 through 11.37 for each statnamic test. The velocity and deflection time histories derived from the acceleration time history are also presented. The load time histories in each figure provide a comparison between the total load as measured by the load cell attached to the statnamic device and the sum of the load cells attached to each individual pile. The statnamic load cell consistently provided a slightly higher load measurement than the load obtain from the sum of the load cells. This difference may be due in part to friction losses within the loading frame as the statnamic load was transferred from the frame to the individual piles. Differences in the loads from the two measurements range from a high of approximately 10% for test 1 to a low of approximately 2% in test 3.
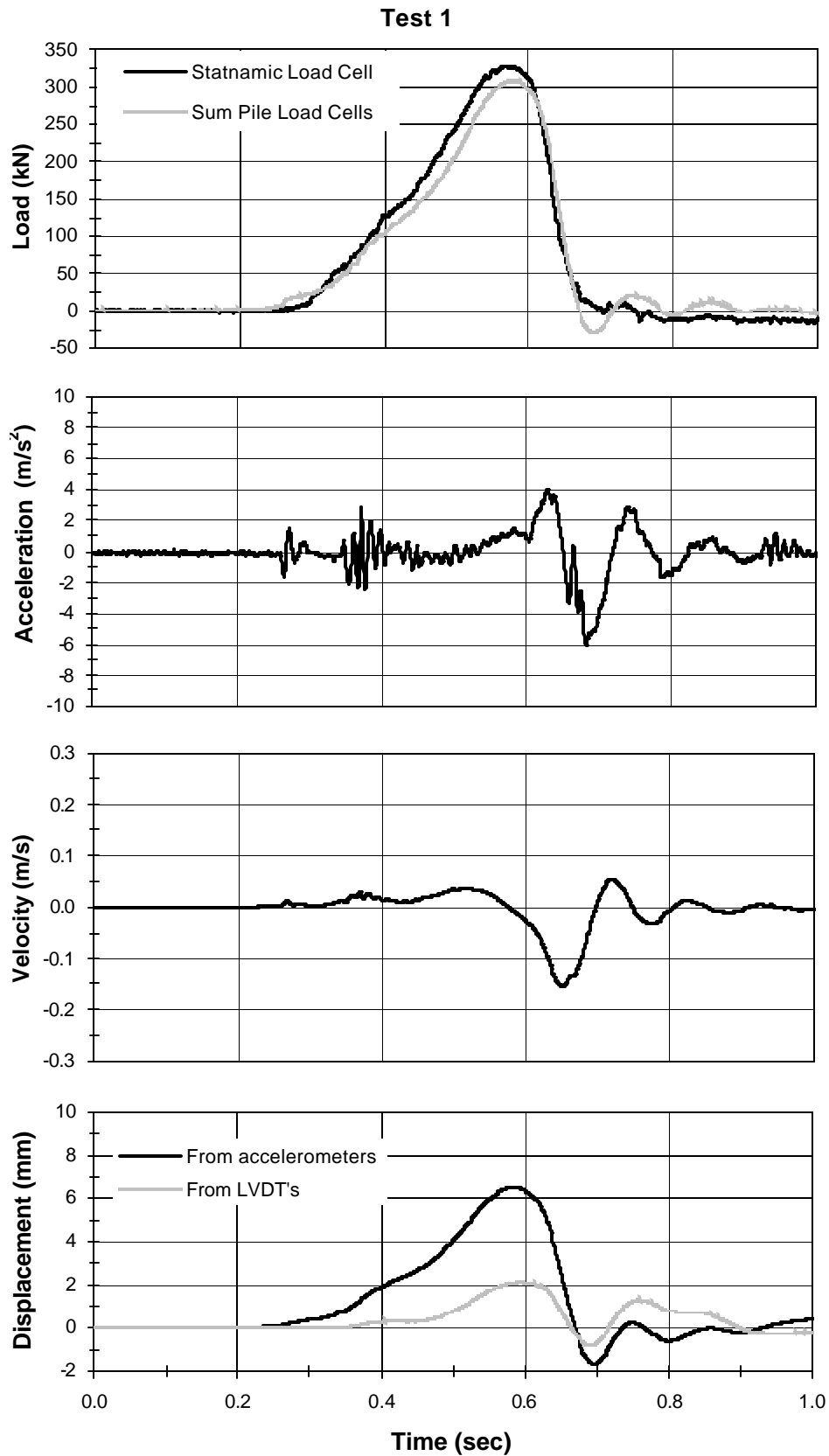
Figure 11.32 Load, acceleration, velocity, and displacement vs. time for statnamic test 1.
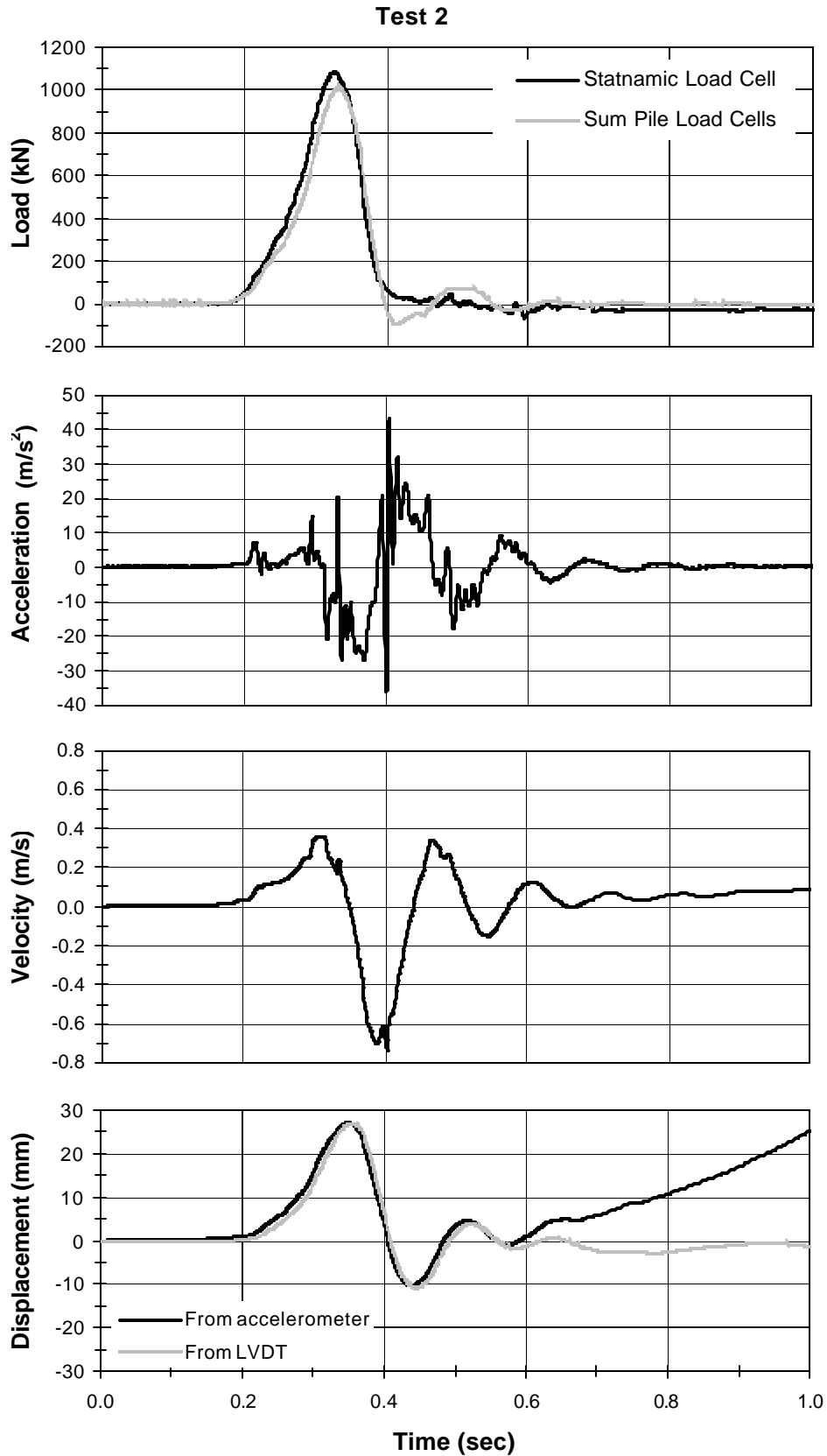
Figure 11.33 Load, acceleration, velocity, and displacement vs. time for statnamic test 2.

11-43
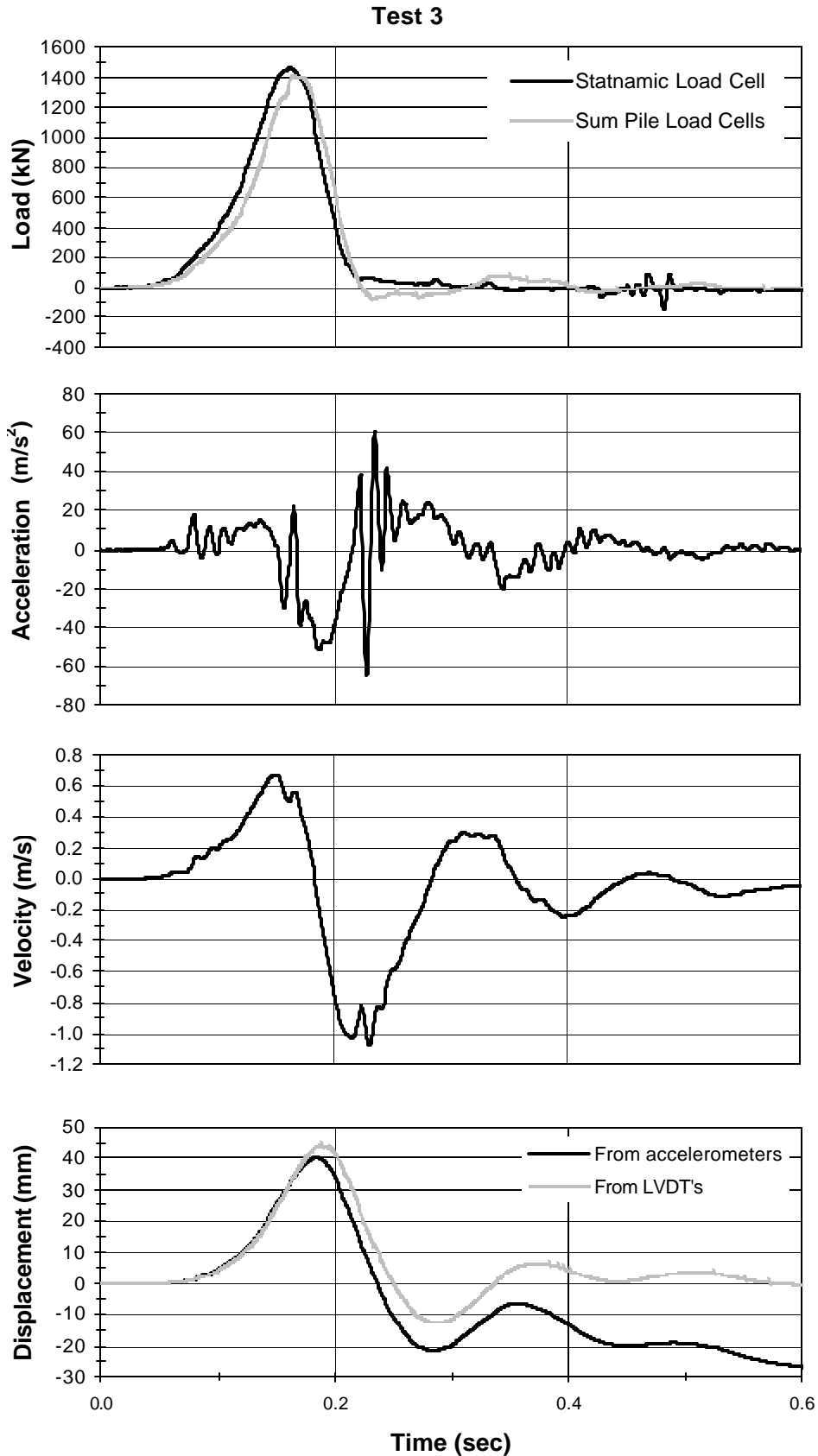
**Figure 11.34 Load, acceleration, velocity, and displacement vs. time for statnamic test 3.**
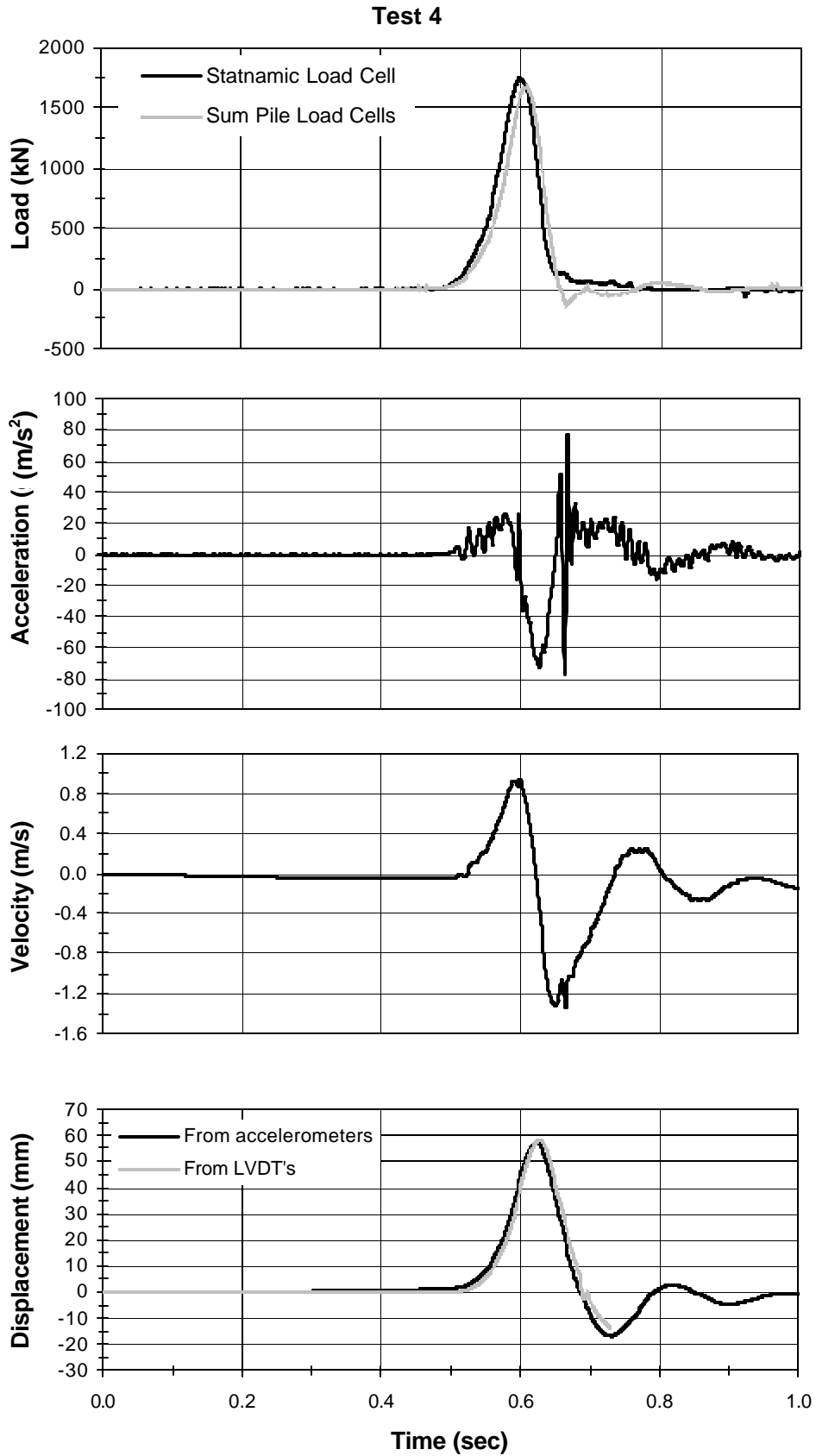
Figure 11.35 Load, acceleration, velocity, and displacement vs. time for statnamic test 4.
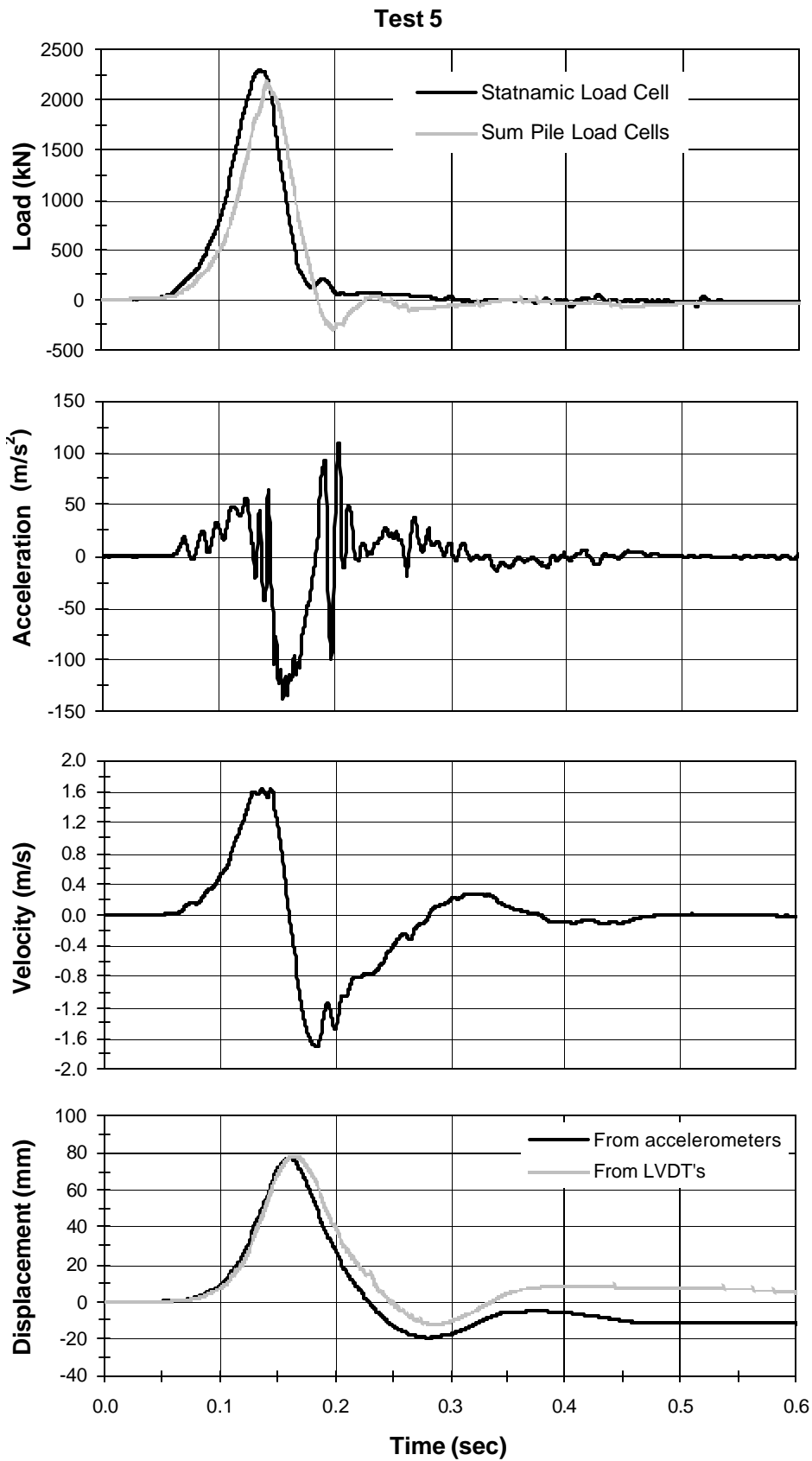
**Figure 11.36 Load, acceleration, velocity, and displacement vs. time for statnamic test 5.**
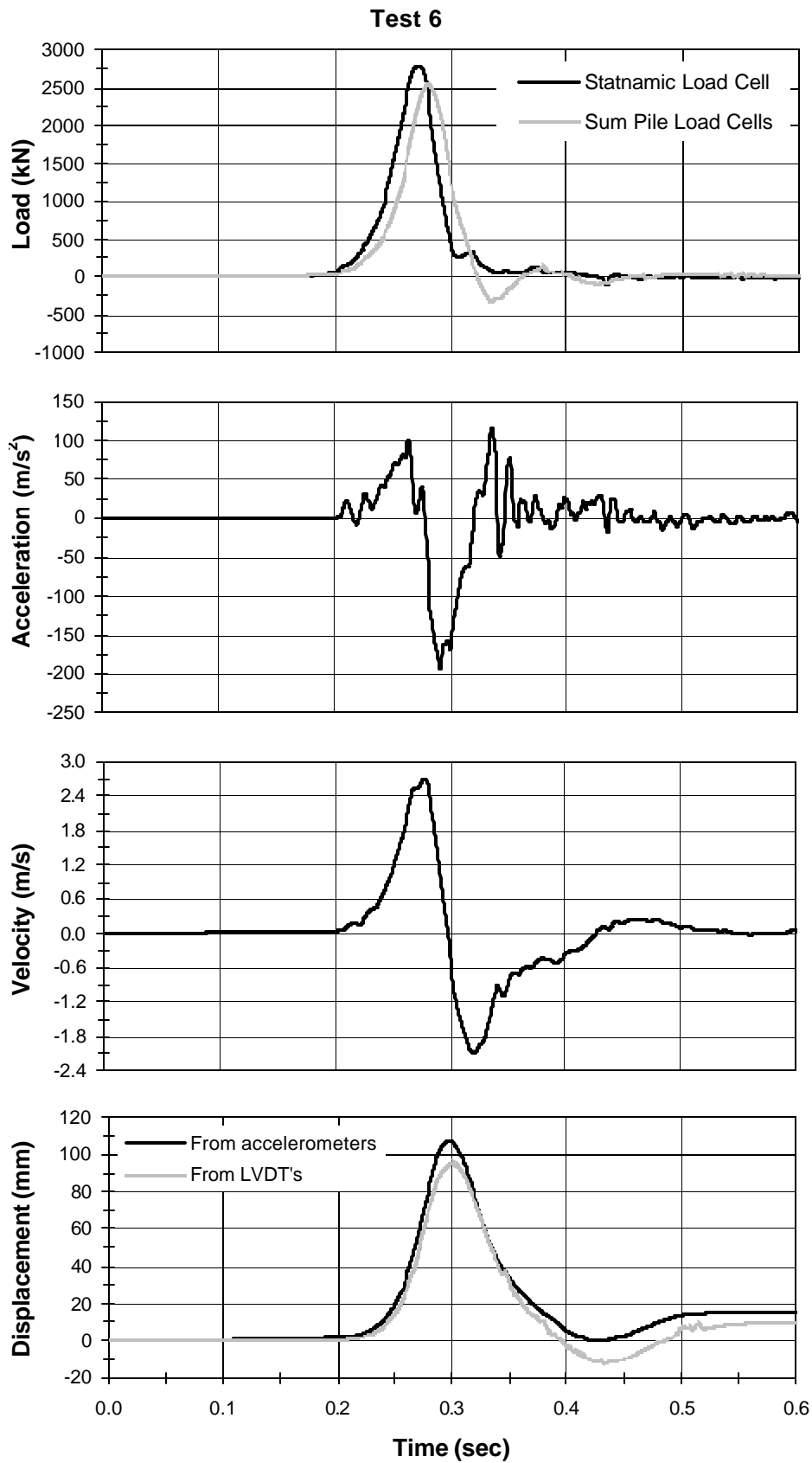
Figure 11.37 Load, acceleration, velocity, and displacement vs. time for statnamic test 6.

Deflections calculated from the accelerometer records are compared with those measured by the LVDT's in each figure. The deflections generally matched well, with the exception of the deflections for statnamic test 1. The average value calculated from the three load point accelerometers was used as the maximum deflection for test 1 in all load deflection plots.

Pile Response versus Depth Measurements

During the statnamic testing, pile 2 was equipped with accelerometers attached to the inside wall of the pile at locations matching the strain gauge locations down the length of the pile to a depth of 7.01 m (23 ft) from the top of the pile. Using the acceleration time history, the velocity and displacement time histories were computed using numerical integration. The peak measured accelerations, along with the peak computed velocities and deflections, are shown in Figure 11.38.

Electronic noise and drift were a problem with a few of the accelerometer recordings. Corrections were made to eliminate as much of the drift as possible by fitting a curve to the data, finding its slope and then subtracting the slope out so as to bring the drifting reading back to a base line. In some cases this drift was too great and was unable to be corrected out. For this reason, there are missing points for some of the plots.

As statnamic testing progressed and loads increased, the depth at which pile acceleration approached zero gradually increased. Velocity and displacement were similarly affected.
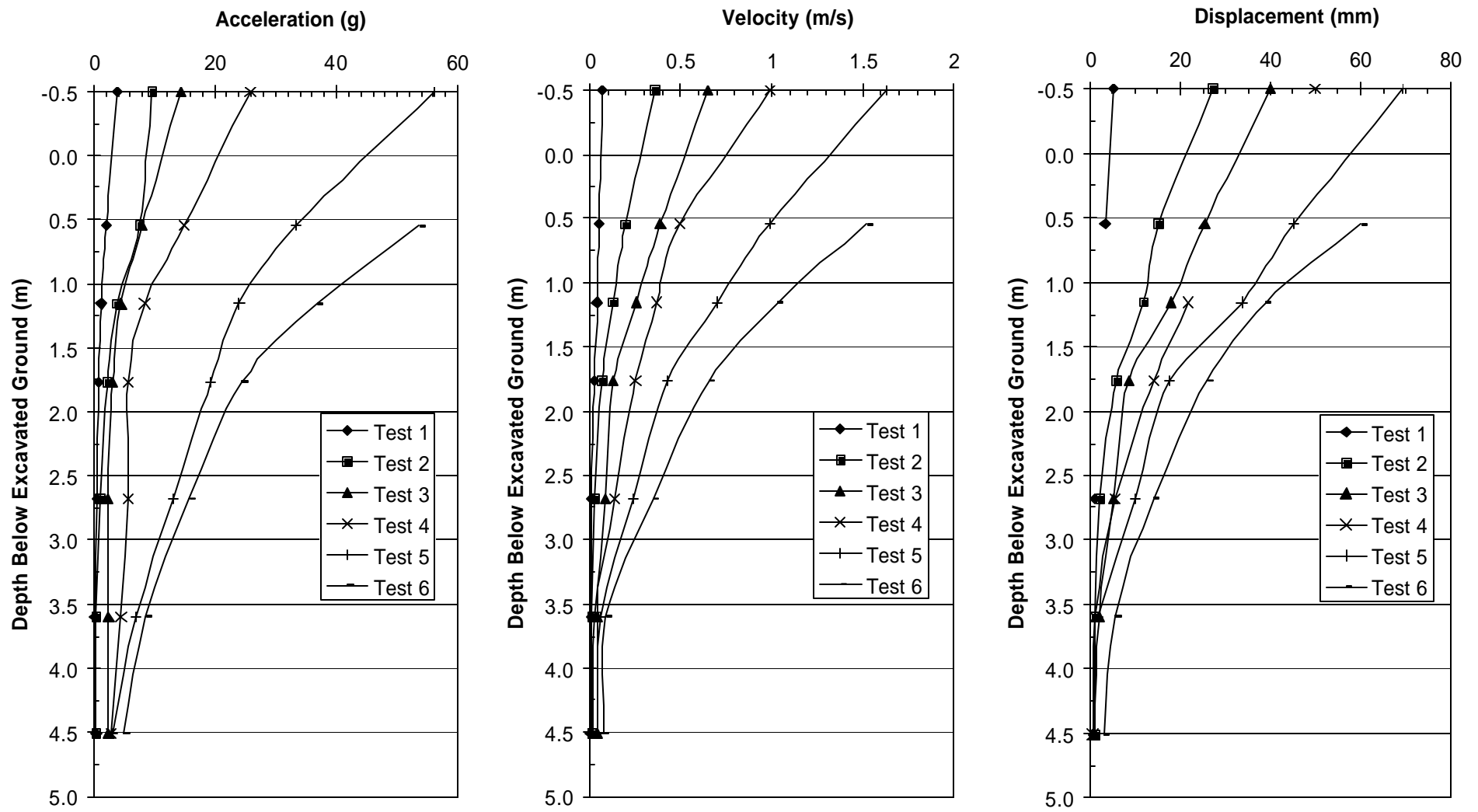
Figure 11.38 Peak acceleration, velocity and displacement versus depth for six statnamic tests on 15 pile group.

CHAPTER 12 ANALYSIS OF THE STATNAMIC TEST RESULTS

The results of the statnamic tests, including the load versus displacement curves, may in some cases be directly applicable. These cases may include ship impacts or earthquakes where load is applied rapidly. However, it is often useful to separate and analyze the components of lateral resistance. These components include static "spring" stiffness, damping, and inertia forces. The unloading point method, introduced by Middendorp et al (1992), was used to analyze the statnamic tests that were performed on the 9 pile and 15 pile groups.

UNLOADING POINT METHOD

Although this method was developed for the analysis of axial statnamic tests, the Unloading point method has been modified to estimate the static resistance in several lateral pile load tests. This method carries the assumption that each pile moves as a rigid body so that it can be treated as a concentrated mass. However, this assumption is only valid when stress waves are negligible. In long piles and very short duration statnamic loadings ($<$ 0.05 sec), stress waves become more significant (Middendorp and Daniels, 1996).

The forces acting on a pile during a statnamic load test are illustrated schematically in Figure 12.1. The soil-pile system is treated as a single-degree-of-freedom, damped oscillator. Admittedly, this is a simplification of a much more complicated physical reality. The static soil resistance, F_u, is represented by the spring. The dashpot represents the damping force (dynamic soil resistance), F_v. The solid circle represents the inertial force, F_a, which consists of the mass of the pile multiplied by the acceleration of the pile mass. The vector represents the applied

statnamic force, F_{stn}. The total soil response, F_{soil}, is the sum of the static and dynamic soil

resistance, F_u and F_v, respectively (Nishimura and Matsumoto, 1995). This can be defined by the

equation

$$F_{soil} = F_u + F_v = F_u + C \cdot v \qquad (12.1)$$

where C is the coefficient of damping of the soil-pile system and v is the velocity. Summing

forces in the horizontal direction, it can be written that

$$F_{stn} = F_{soil} + F_a = F_u + F_v + F_a = F_u + C \cdot v + m \cdot a \qquad (12.2)$$

or

$$F_{soil} = F_{stn} - F_a = F_{stn} - m \cdot a. \qquad (12.3)$$

Static soil resistance can now be expressed as

$$F_u = F_{stn} - F_v - F_a \qquad (12.4)$$
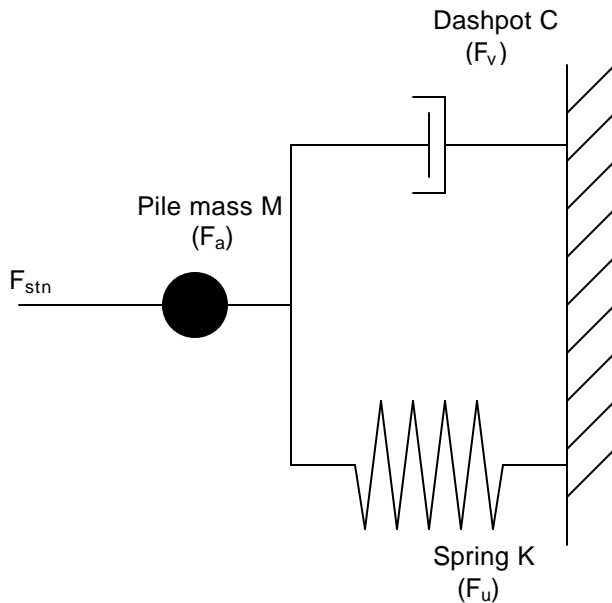
Figure 12.1 Schematic representation of forces acting on the pile group during a statnamic loading treating the pile group as a single-degree-fo-freedom dampled oscillator. Adapted from Nishimura and Matusmoto (1995).

Figure 12.2 Typical statnamic load versus deflection curve.

One of the basic assumptions of this method is that the static soil resistance remains essentially the same at point A (see Figure 12.2) as it is at point B on the statnamic load vs. deflection curve. The difference in force between point A and B is primarily due to the dynamic resistance provided by material damping. At point B, when the velocity of the mass is equal to zero, the static soil resistance is at a maximum, $F_{u(max)}$. At this instant, the damping forces are zero because the piles are not in motion. Using the measured statnamic force along with the mass and measured acceleration of the pile group, equation 12.4 can be used to calculate the maximum static soil resistance, $F_{u(max)}$, at point B because F_v is equal to zero. The coefficient of damping can then be determined using

$$C = \frac{F_{soil(max)} - F_{u(max)}}{v} \tag{12.5}$$

where $F_{soil(max)}$ is the maximum value obtained using Equation 12.4, and v is the velocity the instant $F_{soil(max)}$ occurs at point A. Brown (1993) suggested the following variation to this damping equation:

$$C = \frac{F_{stn}(A) - F_u(\max) - ma(A)}{v(A)} \qquad (12.6)$$

where A is the time of the maximum statnamic force instead of the time of the maximum soil force. $F_{u(max)}$ is the same as in Equation 12.5. $F_{soil(max)}$ does not always occur at the maximum statnamic force because of inertial effects, so the damping coefficients calculated by these two equations may be slightly different.

When applied to lateral loadings, there are several difficulties associated with the Unloading Point method. First, laterally loaded piles move gradually slower as depth below the ground surface increases; therefore, the assumption that the piles act as a rigid body is not valid. Next, although damping is probably dependant on the strain levels in the soil and thereby varies with depth, one value of damping coefficient must be selected to represent the damping resistance for the entire length of the pile. When used to analyze lateral loads, the Unloading Point method also requires an unknown equivalent mass of the foundation or the pile-soil system.

Previous lateral statnamic tests on large diameter drilled shafts (Berminghammer, Inc., 1994, 1995) and on a pile group tested under fixed head and free head conditions (Weaver et al, 1998) estimated the equivalent mass to be equal to the mass of the piles to a depth of five pile diameters plus 30% of the mass of the soil within the pile group to a depth of five pile diameters plus the mass of the pile cap. Instead of estimating the mass of the pile-soil system, Brown

(2000) estimated a mass of the foundation only. He estimated this to be the mass of the piles above the mud-line plus the mass of the pile cap.

Three different cases were analyzed in applying the Unloading Point method to the statnamic tests on the nine-pile group. In case one, the equivalent mass was set equal to the mass of the load frame plus the mass of the piles to a depth of five pile diameters, including the portion of the pile that was above the ground. In case two, the equivalent mass was the mass of the piles that were above the ground surface. Finally, for case three zero mass was used.

ANALYSIS OF STATNAMIC TESTS ON THE NINE PILE GROUP USING UNLOADING POINT METHOD

Using the Unloading Point method, static load vs. deflection curves were derived from the statnamic lateral load tests on the nine pile group of 610 mm diameter piles. Equation 12.6 was used to compute the coefficient of damping for each test. The derived static force is dependent upon the mass used in the calculations. Figure 12.3 presents the measured statnamic force, the corresponding measured static force, and the derived static force for the second statnamic test. The derived static force in each of the plots of this figure was computed using the different estimations of mass. A mass of 0 kg was used with the Unloading Point method to derive the static curve in Figure 12.3(a). The estimated mass used to derive the static curve in Figure 12.3(b) was the mass of the piles above the excavated ground level. The mass estimation used for the curve shown in Figure 12.3(c) was the mass of the piles to a depth of five pile diameters, including the mass of the pile above the ground, plus the mass of the load frame. Figures 12.4 and 12.5 contain the force components associated with the various calculated static forces of the second statnamic test. Figure 12.4 contains the damping forces that resulted from the different masses used in the Unloading Point method analysis of the second statnamic test,

and Figure 12.5 shows the inertial forces for those mass levels. When zero mass was used, the inertial force was equal to zero. Figures 12.6 to 12.8 contain similar plots for the third statnamic test, while Figures 12.9 to 12.11 and Figures 12.12 to 12.14 correspond to the forth and fifth statnamic tests, respectively.
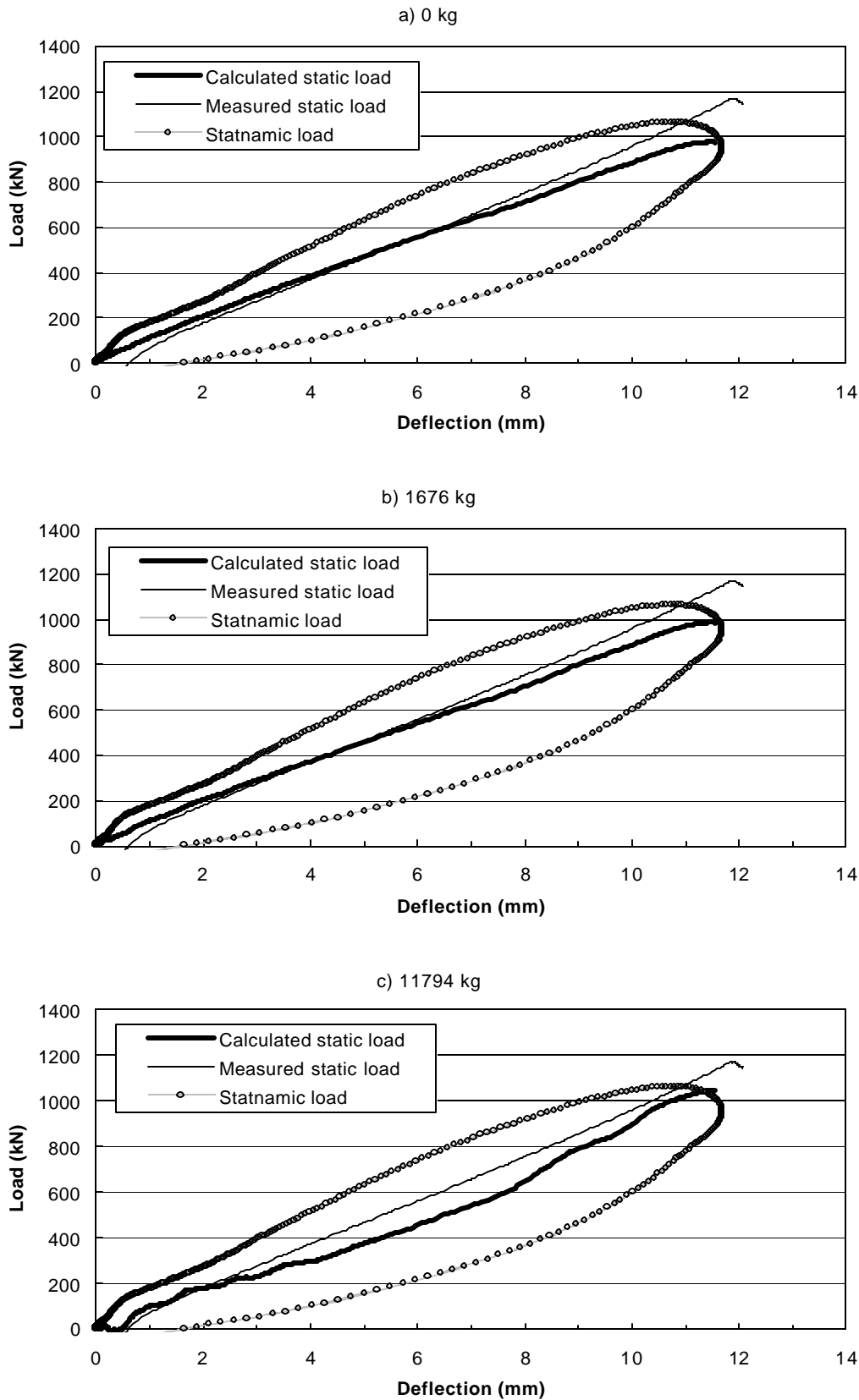
Figure 12.3 Measured Statnamic, measured static and computed static load-displacement curves for test two with three mass assumptions.
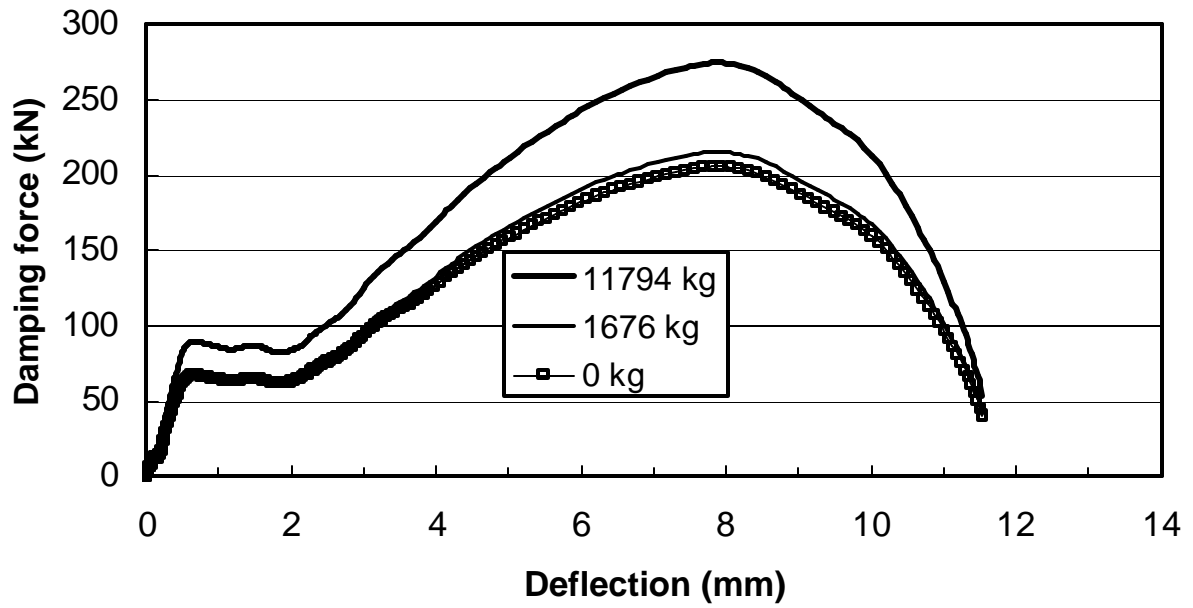
Figure 12.4 Calculated damping forces from statnamic test two with three mass assumptions.
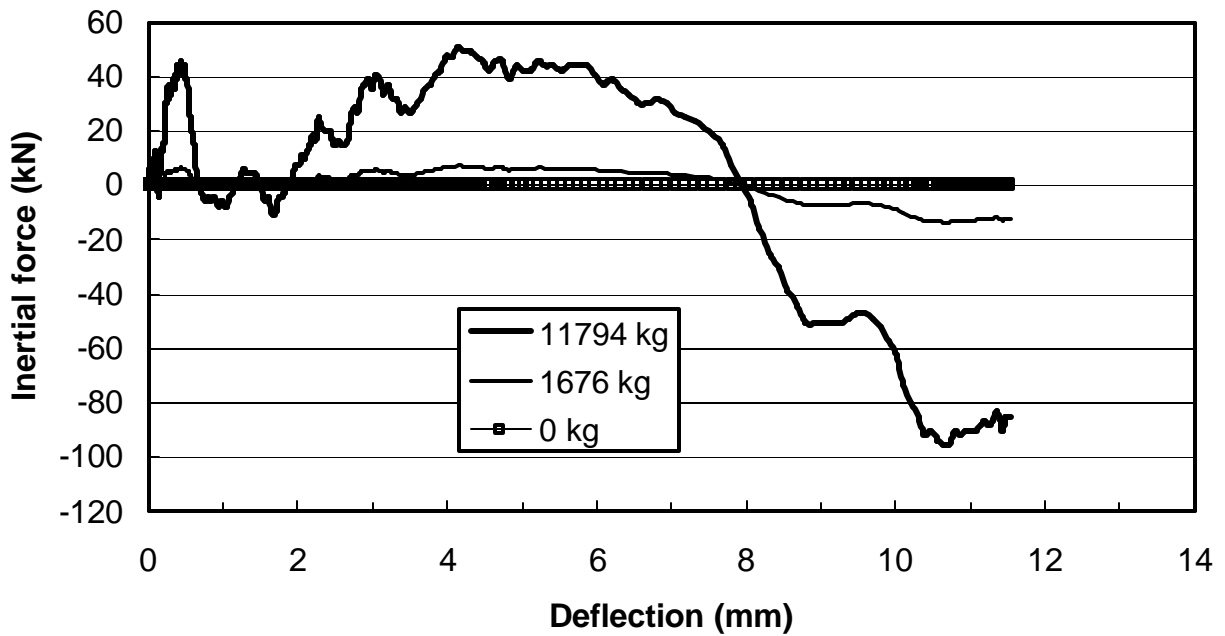
Figure 12.5 Calculated inertial forces from statnamic test two with three mass assumptions.
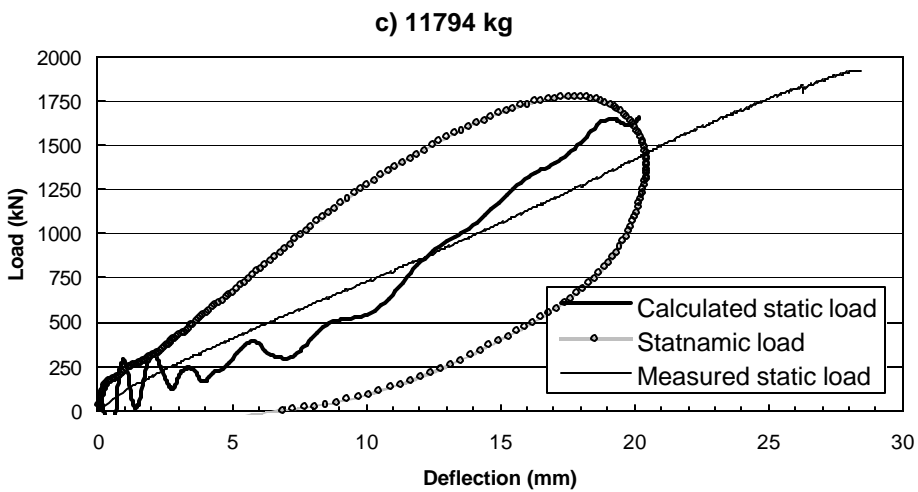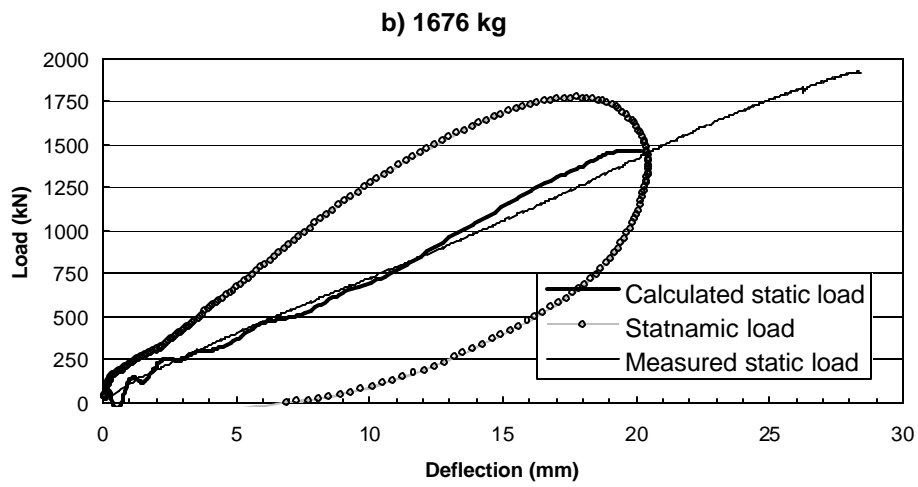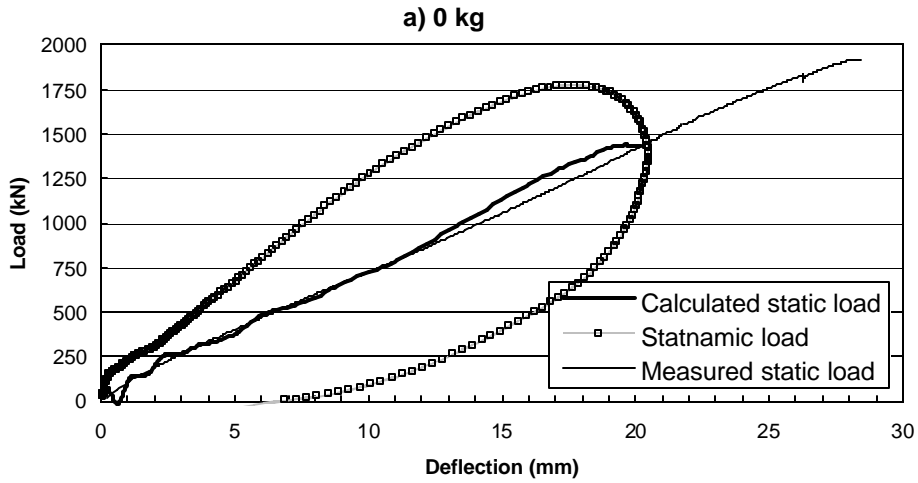
Figure 12.6 Measured Statnamic, measured static and computed static load-displacement curves for test three with three mass assumptions.
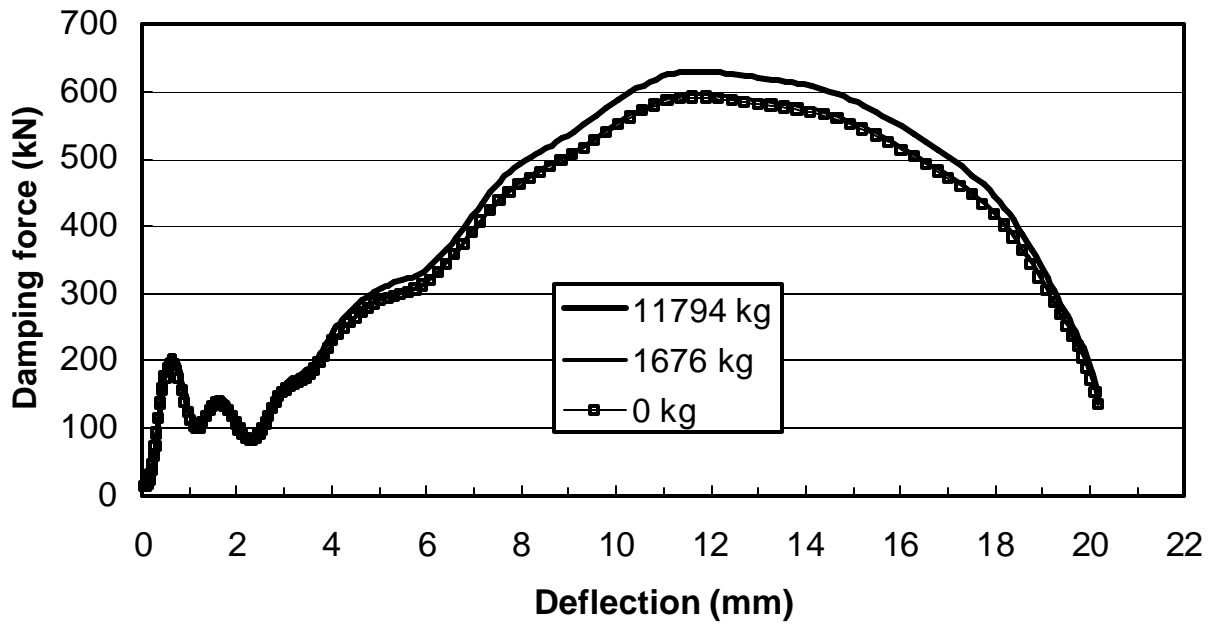
Figure 12.7   Calculated damping forces from statnamic test three with three mass assumptions.
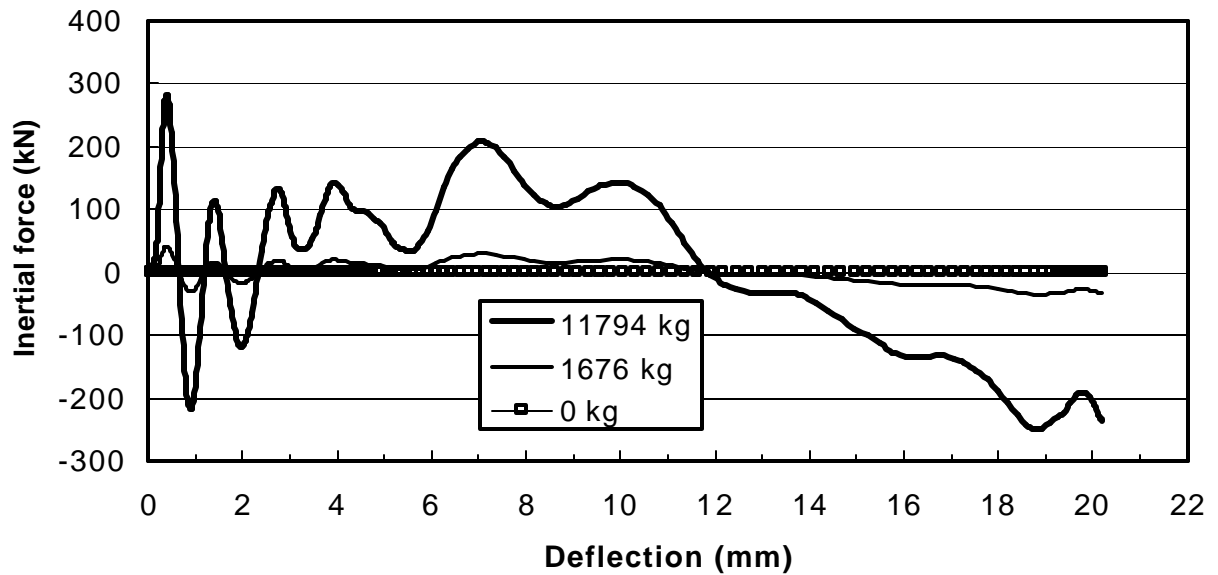
Figure 12.8   Calculated inertial forces from statnamic test three with three mass assumptions.
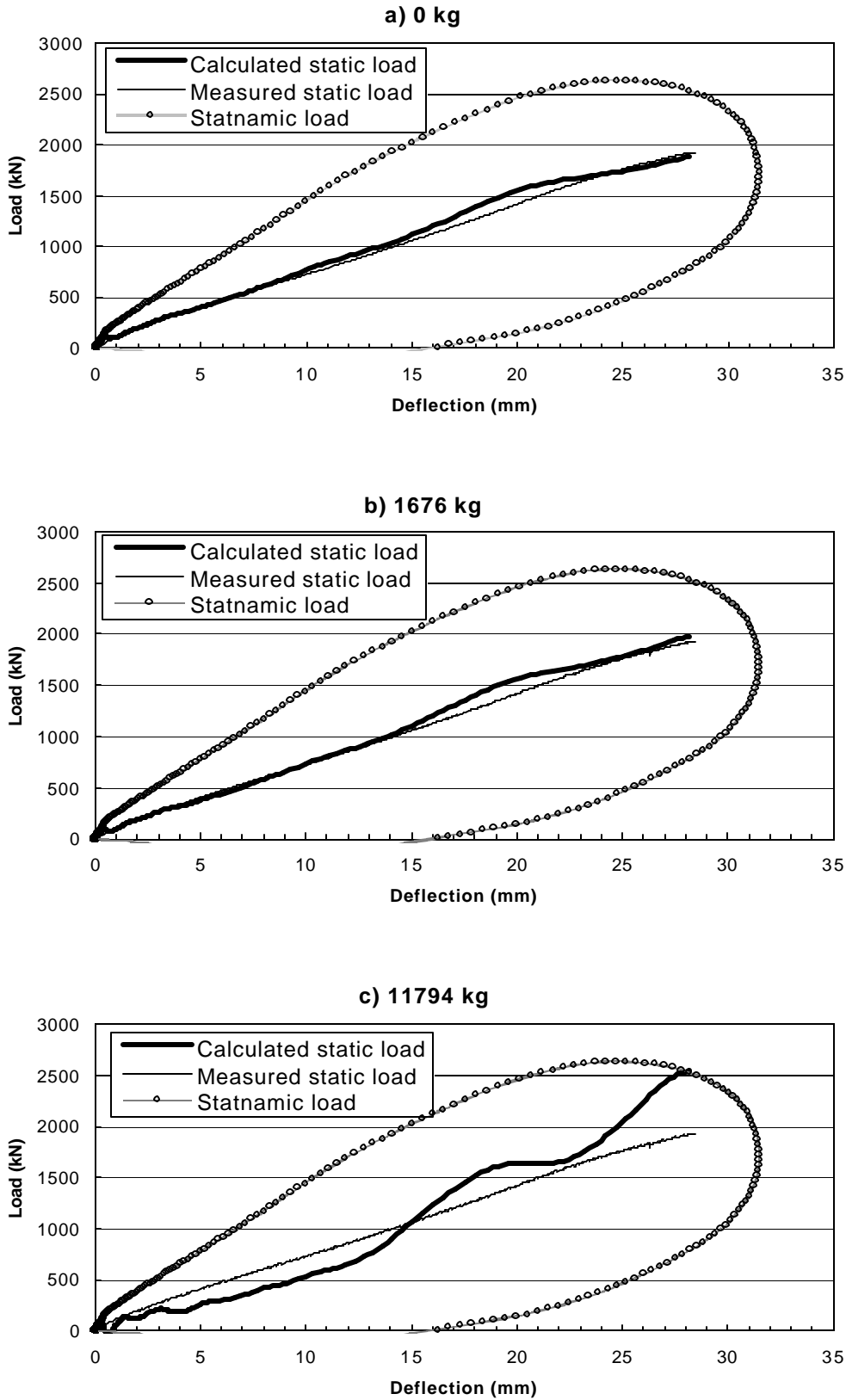
Figure 12.9 Measured Statnamic, measured static and computed static load-displacement curves for test four with three mass assumptions.
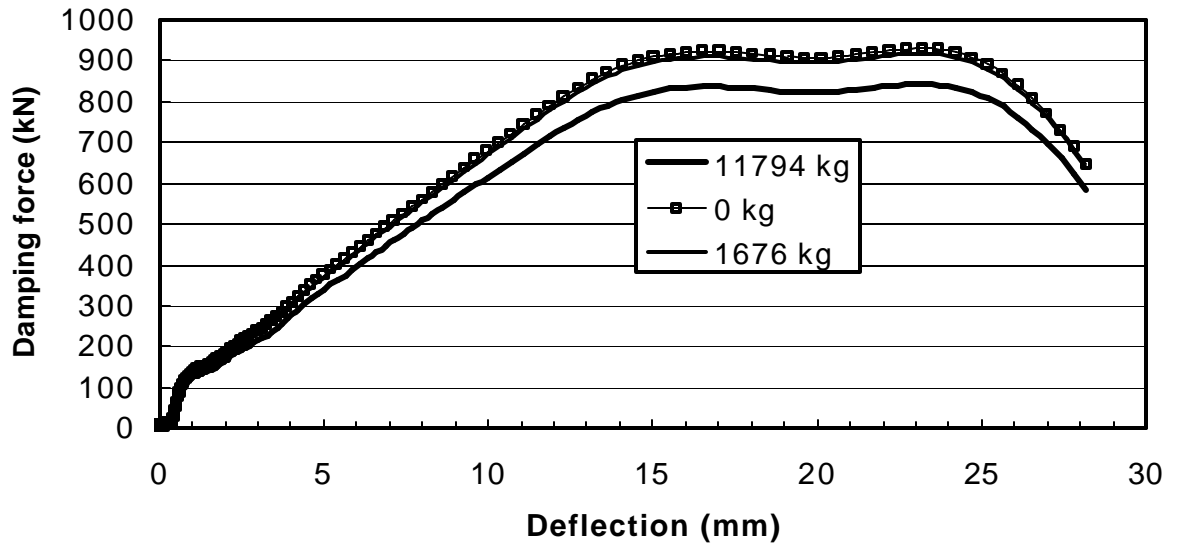
Figure 12.10: Calculated damping forces from statnamic test four with three mass assumptions.
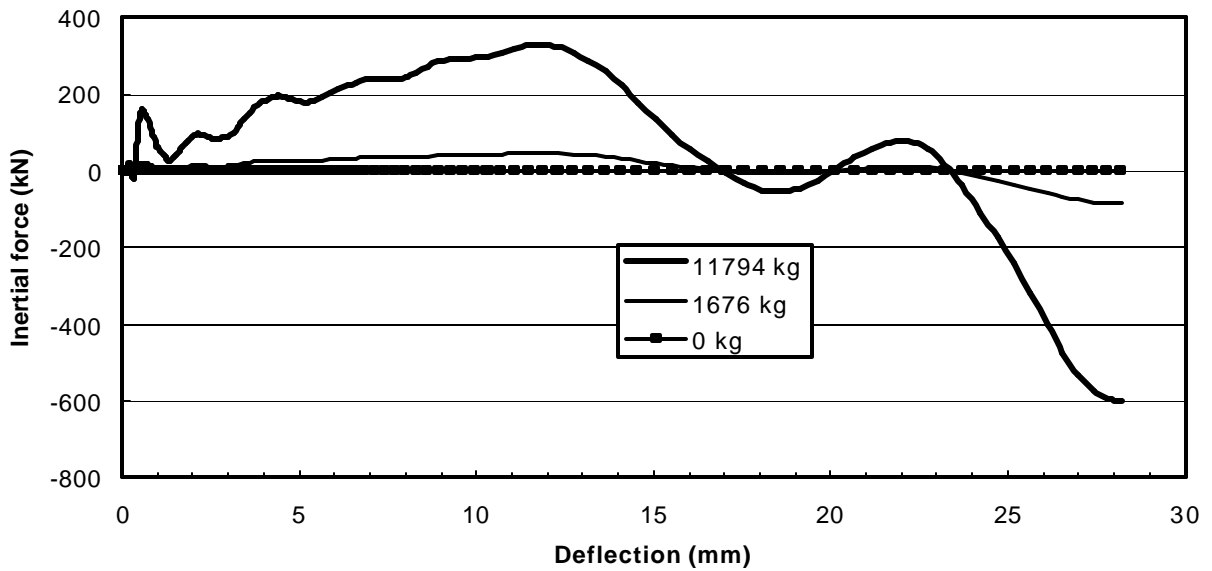
Figure 12.11: Calculated inertial forces from statnamic test four with three mass assumptions.

a) 0 kg

b) 1676 kg

c) 11794 kg
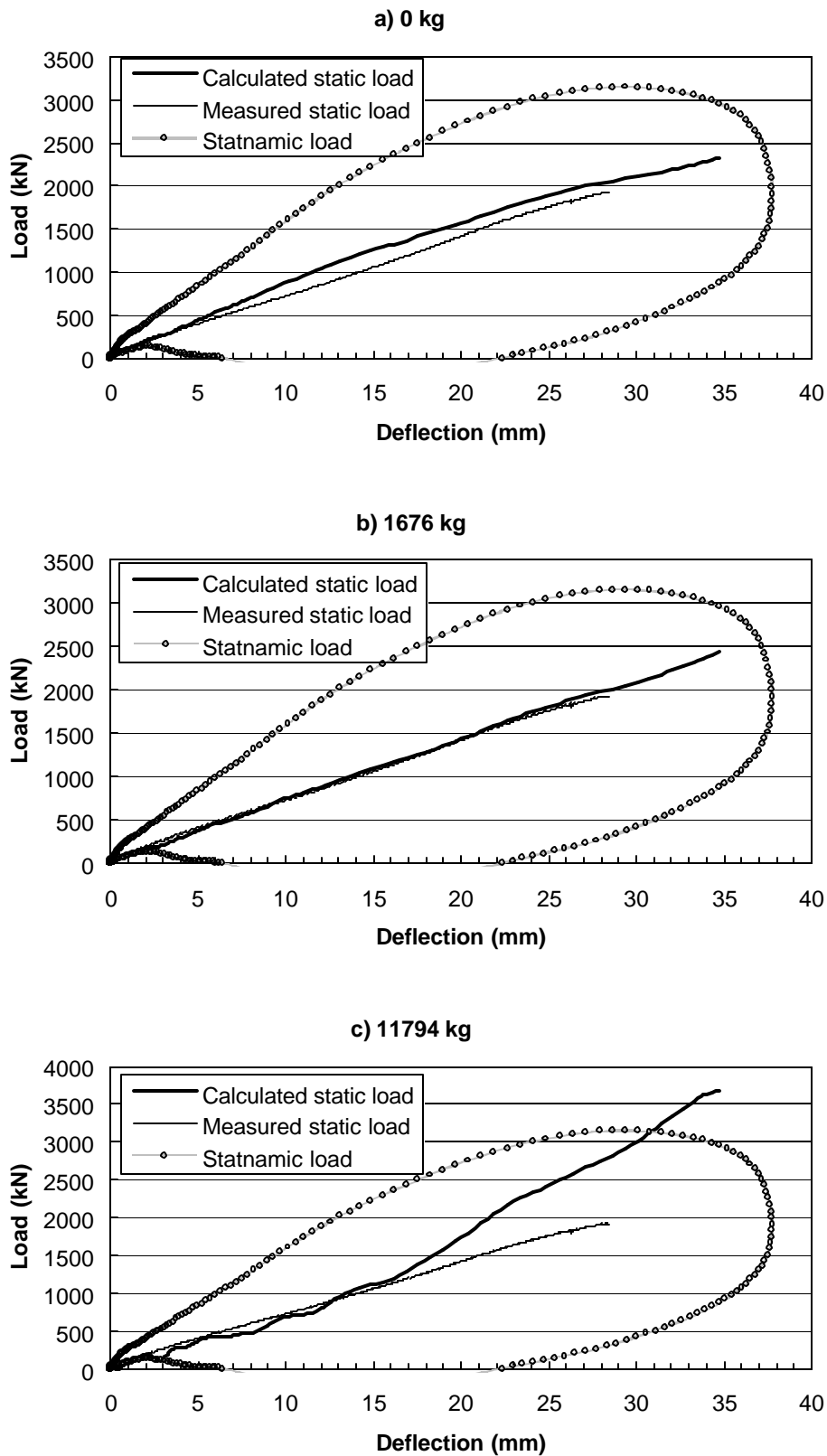
Figure 12.12 Measured Statnamic, measured static and computed static load-displacement curves for test five with three mass assumptions.
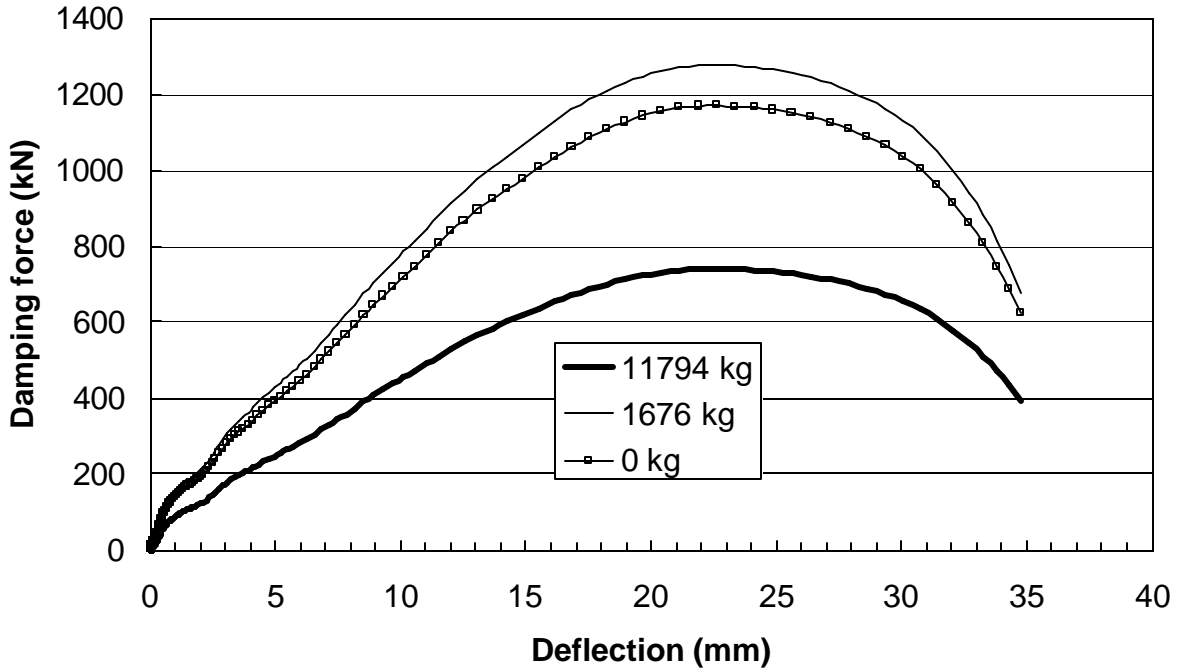
Figure 12.13   Calculated damping forces from statnamic test five with three mass assumptions.
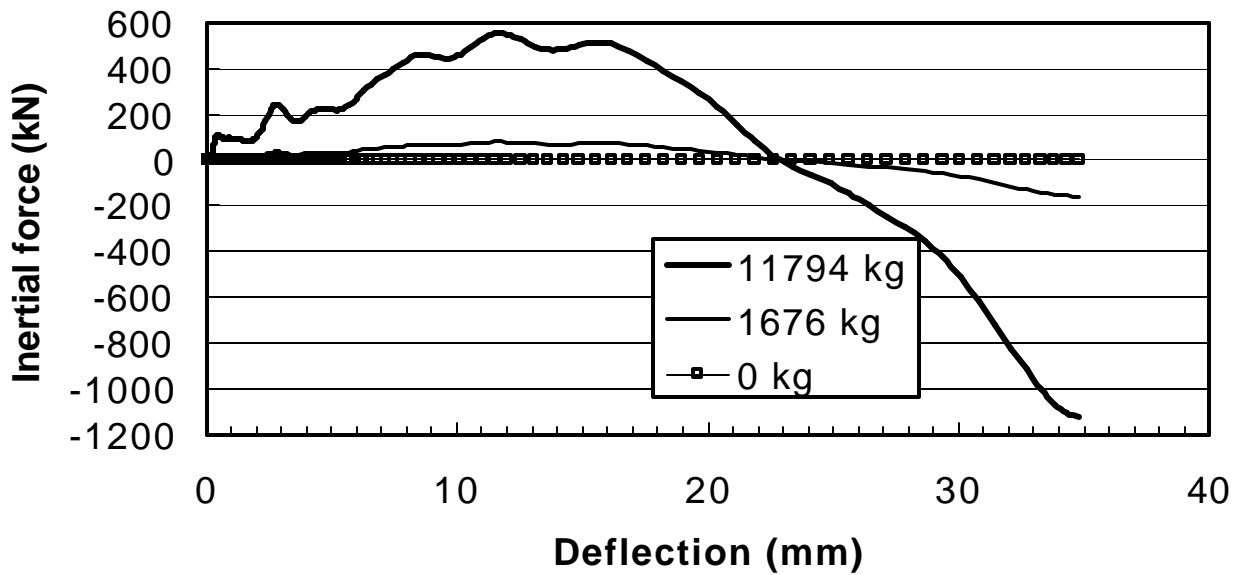

Figure 12.14   Calculated inertial forces form statnamic test five with three mass assumptions.

Equation 12.6 resulted in a negative coefficient of damping for the first statnamic test. As a negative damping coefficient is unreasonable, these results are not shown. As previously stated, the Unloading Point method is generally not accurate for long piles and very short duration statnamic loadings because stress waves are not negligible (Middendorp and Daniels, 1996). In the case of the first statnamic test, the duration of the statnamic loading may have been too short to negate the stress waves, eliminating the possibility of an accurate analysis.

As the first two statnamic tests were conducted after the static loads were cycled, the measured static force shown in Figure 12.3 is the fifteenth-cycle load vs. deflection curve. The third, forth, and fifth statnamic tests, however, were performed on virgin soil, and the measured static forces shown in Figures 12.6, 12.9, and 12.12 correspond to the first-cycle loading.

At the highest mass level, the calculated inertial force for each test fluctuated considerably with deflection. This is observed in Figures 12.5, 12.8, 12.11, and 12.14. The inertial force fluctuation led to oscillations in the calculated static forces. Reducing the mass used in the Unloading Point analysis directly reduced the calculated inertial force, resulting in a more linear, calculated static force. The resulting near-linear, calculated static forces were in much better agreement with the measured static forces. Parts (a) and (b) of Figures 12.3, 12.6, 12.9, and 12.12 show that the calculated static forces align remarkably well with the measured static force where the mass is small.

The static forces calculated using the highest mass level also match quite well with the measured static forces. This is especially noted to a deflection level of 3 mm in the second statnamic test, Figure 12.3(c), and to 17 mm of deflection in the fifth statnamic test, Figure 12.12(c). However, at greater deflections in these tests, and at almost all deflections in the other tests, there is a greater discrepancy between the static forces calculated with the highest mass

level and the measured static force. Since the mass cannot be zero and the results using the highest mass were clearly unsuitable, the best approach to interpreting the static resistance in this case would be to use the mass of the piles above the ground.

As was the case with the inertial force, the damping force was also dependent upon the mass. Figures 12.4, 12.7, 12.10, and 12.13 show how the damping force changed with mass. As the statnamic load increased, the damping force computed with the higher mass levels fell in relation to the damping force computed with lower masses. For example, in Figure 12.4, the damping force calculated with the highest mass is about 28% higher than the damping force calculated with the next highest mass, which is about 5% higher than the damping force calculated with zero mass. However, the relationship between these forces gradually changes until, in Figure 12.14, the damping force calculated with zero mass is about 6% higher than the damping force computed with the next lowest load, which in turn, is about 50% higher than the damping force calculated with the highest mass.

The statnamic force was considerably higher than the static force for each test but the differences were more pronounced for virgin loading than for reloading. For example, the load from statnamic test two, which was a reload test, was about 30% higher than the corresponding static load (see Figure 12.3). In contrast, for statnamic tests 3, 4 and 5 which involved virgin loading, the statnamic force was 55%, 70% and 70% higher, respectively, than the static force. Based on the inertia and damping forces computed using the unloading point method, the difference between the statnamic forces and the static force was primarily due to the damping force. For example, the maximum damping force for the second statnamic test was about thirty times greater than the maximum inertia force for the same test (see Figures 12.4 and 12.5). The relative difference between the maximum damping force and the maximum inertia force

decreased as the maximum statnamic load increased. Nevertheless, even for the fifth statnamic test, where the accelerations were the largest, the maximum damping force was still 10 times greater than the maximum inertia force.

Table 12.1 provides a summary of the natural frequency, natural period, static stiffness, damping coefficient, critical damping coefficient and damping ratio for each statnamic test. These results were obtained using the mass of the piles (1676 kg) above the ground level for each test. As the measured static force was quite linear, the stiffness, K, was approximated by the slope of the static load-deflection line, as seen in part (b) of Figures 12.3, 12.6, 12.9, and 12.12. The damping coefficient, C, shown in Table 12.1, was obtained from the unloading point analysis for each test. The natural frequency, f, of the foundation in cycles per second (Hz) was computed using the equation

$$f = \frac{1}{2p} \sqrt{K/m} \tag{12.7}$$

where K is the static spring stiffness and m is the mass of the piles above the ground surface. The natural period, T, in seconds, was then computed using the equation

$$T = \frac{1}{f} \tag{12.8}$$

As shown in Table 12.1, the natural frequency for the nine pile group was typically about 33 Hz which is equivalent to a natural period of 0.03 seconds. Based on the data in Table 11.1, the rise time of the loading had a duration that was 2 to 7 times longer than the natural period. Therefore, the load was more akin to what would be produced by an earthquake motion rather than what would be produced by pile hammer impact.

As the load applied by the statnamic device increased, both the spring stiffness and the damping coefficient decreased due to the non-linearity of the soil. While the absolute value of

the damping coefficient does not have much physical meaning, the damping ratio provides some basis for comparison between different foundation systems. The damping ratio is the ratio of the damping coefficient to the critical damping coefficient. With a critical damping ratio above one, the system will essentially stop oscillating in one cycle. The critical damping coefficient, C_c, was calculated using the equation

$$C_c = 2(K \cdot m)^{1/2} \tag{12.9}$$

where K is the static spring stiffness and m is the mass of the system. The damping ratio for the second test involving reloading was lower than that for the tests involving virgin loading. For the virgin statnamic loadings, the damping ratio decreased as the load increased but was in the range of 1.6 to 1.9, which indicates that the system is still heavily damped.

Table 12.1: Summary of the statnamic analysis for the nine pile group.

Test Number	Load Condition	Naural Frequency, f Hz	Natural Period, T sec	Spring Stiffness, K kN/mm	Damping Coef., C kN-sec/m	Critical Damping, C_c KN-sec/m	Damping Ratio, C/C_c
2	Reload	36.5	0.027	88	1096	768	1.43
3	Virgin	33.2	0.030	73	1303	700	1.86
4	Virgin	32.5	0.031	70	1225	685	1.79
5	Virgin	32.1	0.031	68	941	675	1.61

In Figure 12.15 all of the derived load (F_u) -deflection curves from the four statnamic tests are plotted together along with the measured static load-deflection curve for the maximum static load application. The consistency in the curve shapes for the various statnamic tests is very good. During the virgin loading segment of a given load-deflection curve, there is a clear indication of greater resistance. However, for repeated loadings, the load-deflection curves for the various testss lie nearly on top of each other. The derived load-deflection curves are also in very good agreement with the measured load-deflection curve.
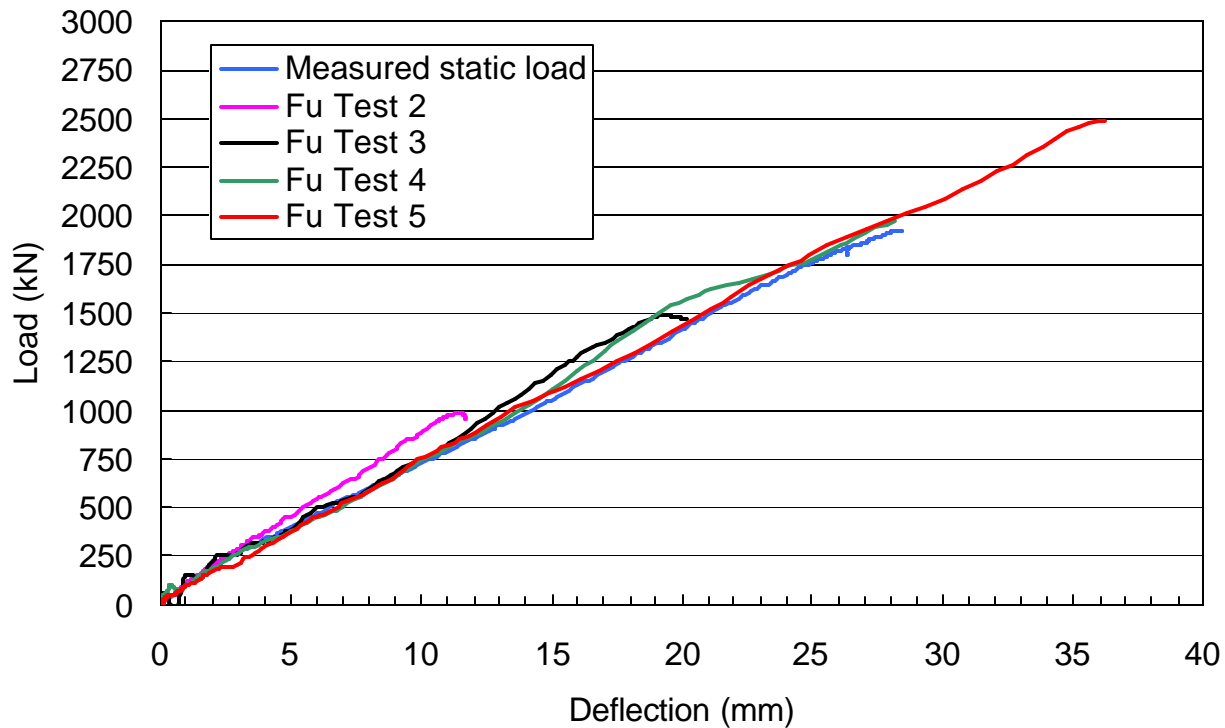
Figure 12.15 Comparison of derived static load-deflection curves from four statnamic tests with measured static load-deflection curve.

ANALYSIS OF STATNAMIC TESTS ON 15 PILE GROUP USING THE UNLOADING POINT METHOD

Based on the success of the Unloading Point Method in analyzing the response of the nine pile group, the same analysis procedure was used to analyze the response of the 15 pile group. Once again, the mass used in the analysis was only the mass of the 15 pile segments above the ground surface. This mass was determined to be 1092 kg (2407 lbs).

Figures 12.16 through 12.21 present the results of the Unloading Point Method analysis of the statnamic testing. The upper plot (a) in each figure compares the derived static load (F_u) versus deflection curve with the measured static load versus deflection curve. The measured statnamic load versus deflection curve is also shown for comparison purposes. For tests 1 and 2, the static load versus deflection curve is that obtained from the peak points for the 15th cycle of

loading. Because the static testing was halted on the 15 pile group after the 12.7 mm deflection cycle, due to the premature failure of the geopier reaction foundation, the derived static load versus deflection curves for statnamic tests 3 through 6 are compared to the measured peak load versus deflection curve obtained from loading the 15 pile group in the opposite direction from the earlier statnamic testing. The derived static resistance is generally somewhat lower than the measured resistance for cases where the pile group is being re-loaded. This lower resistance is explained by the fact that gaps had developed in front of the pile during the previous statnamic loading leading to less resistance at the same deflection for the subsequent statnamic test. In the region of virgin loading for each test, the agreement with the measured load versus deflection curve is generally very good.

The lower curve (b) in Figures 12.16 through 12.21 shows the variation in the measured and derived forces from the statnamic testing and the Unloading Point Method analysis over time. These forces include the measured statnamic force from the sum of the load cells attached to each pile, and the derived static, damping, and inertia forces as calculated with equations 12.3 through 12.6.

Because the mass of the system is relatively small, the inertia force was also small and never exceeded a few percentage points of the maximum statnamic force. The damping force time history has a major positive and negative pulse. During the positive pulse the pile is moving into the soil which produces the damping resistance, however, as the pile moves backwards there is no soil behind the pile until it returns to its original position. Therefore, the computed negative damping force is probably not real. The ratio of the maximum positive damping force to the maximum static force is 0, 0.22, 0.34, 0.45, 0.48, and 0.53 in statnamic
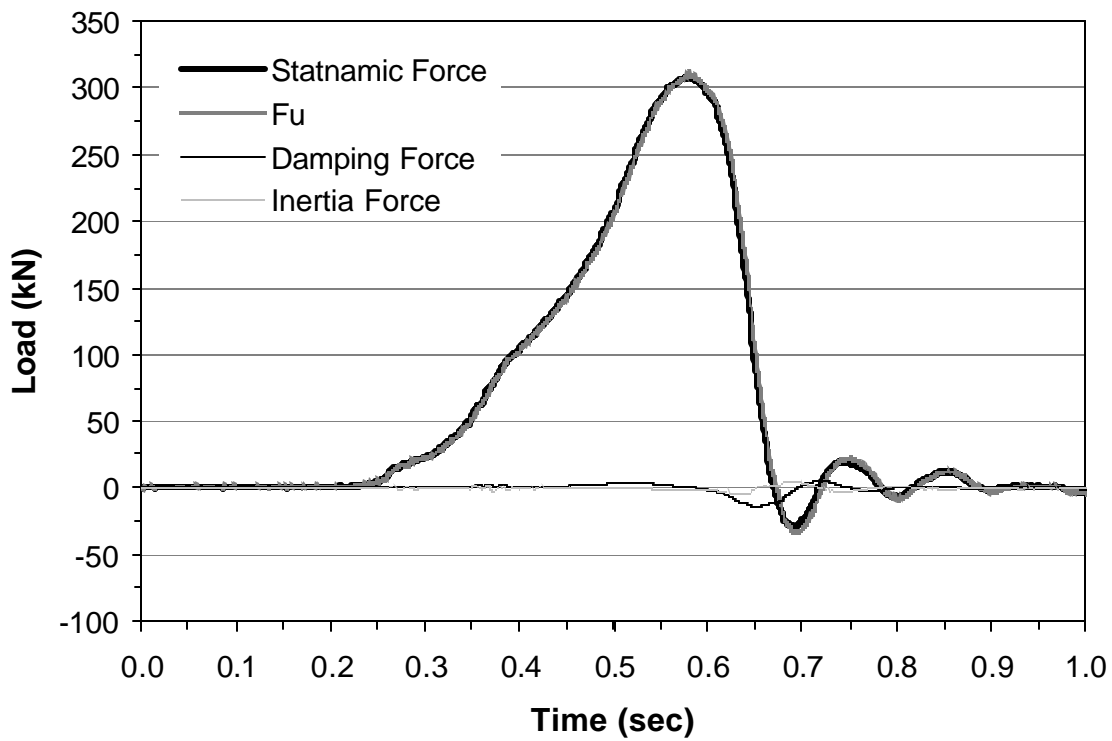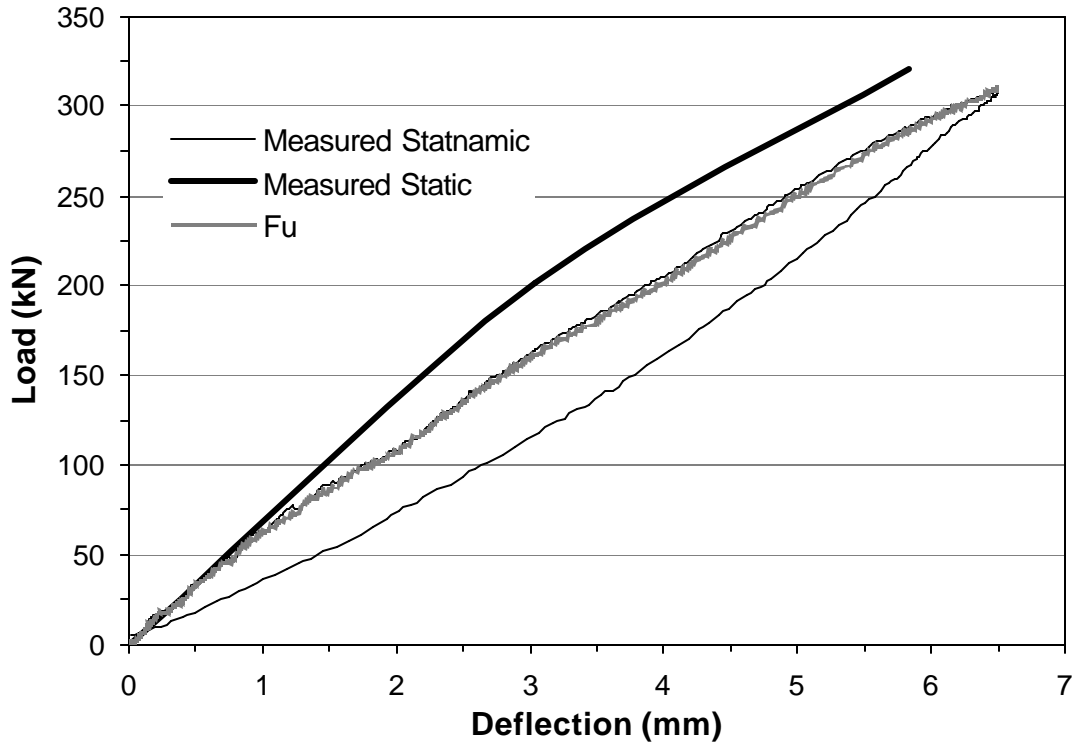
Figure 12.16 Measured statnamic results and derived results from the Unloading Point Method analysis of statnamic test 1 for the 15 pile group.
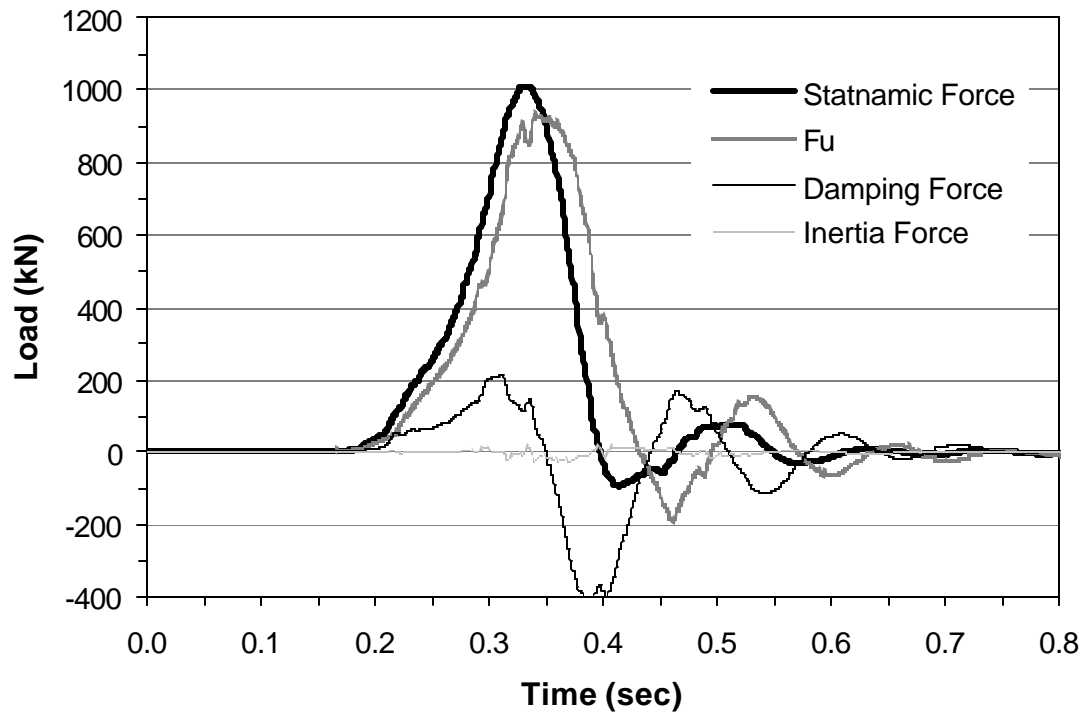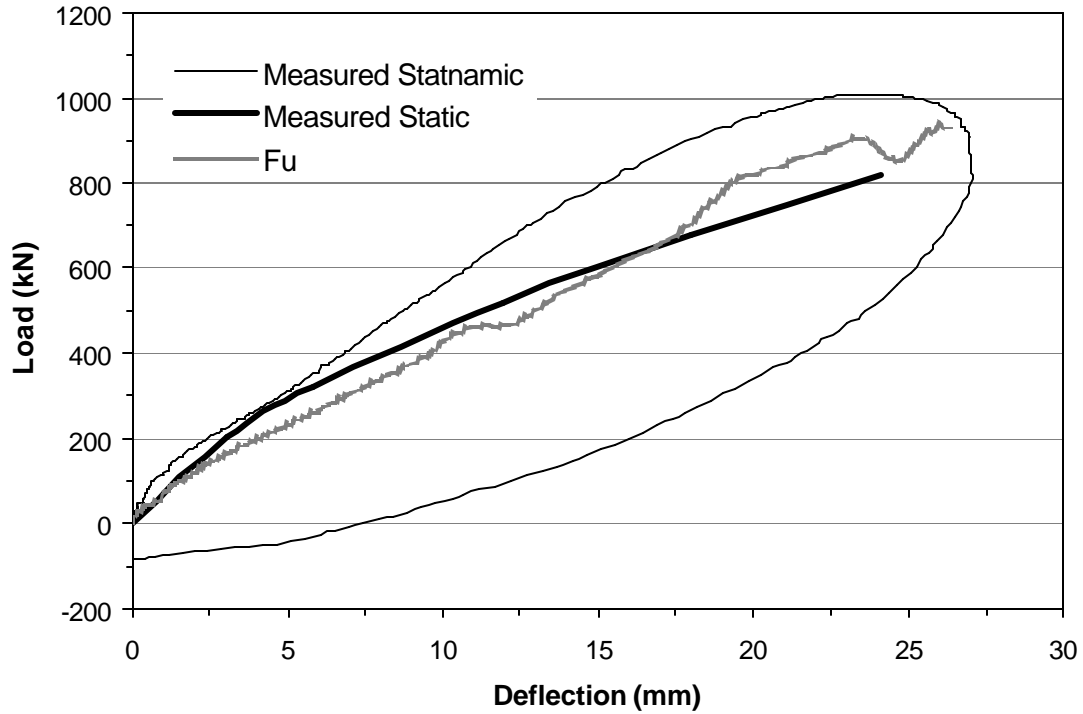
Figure 12.17 Measured statnamic results and derived results from the Unloading Point Method analysis of statnamic test 2 for the 15 pile group.
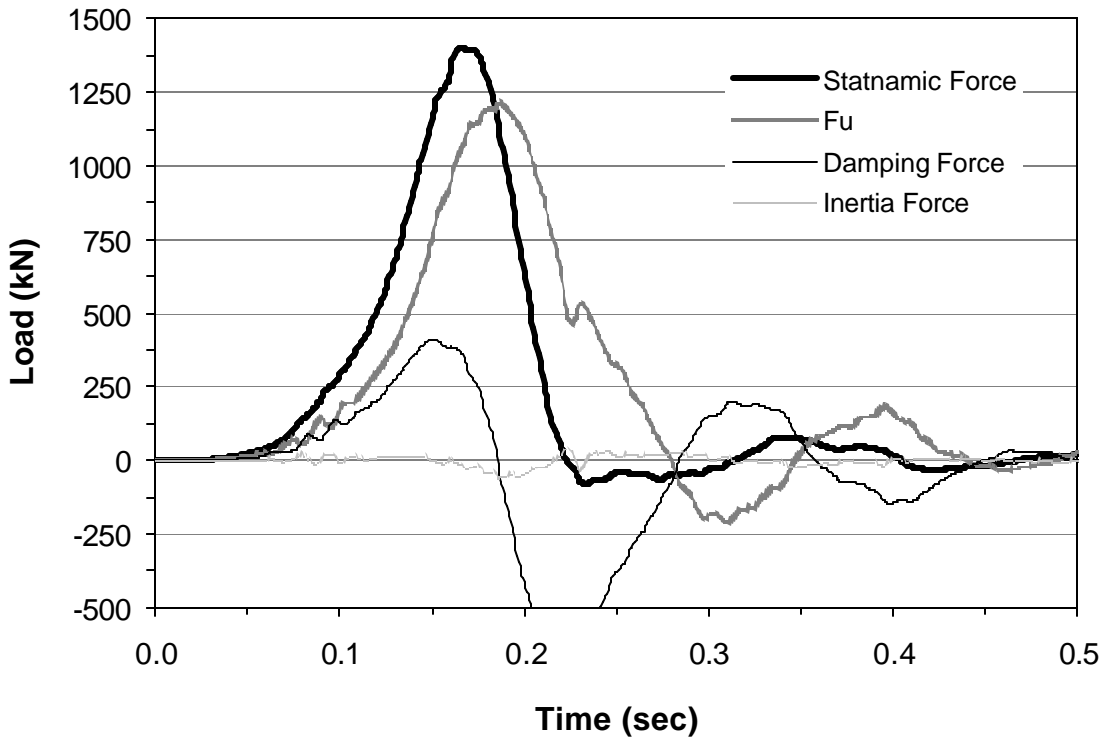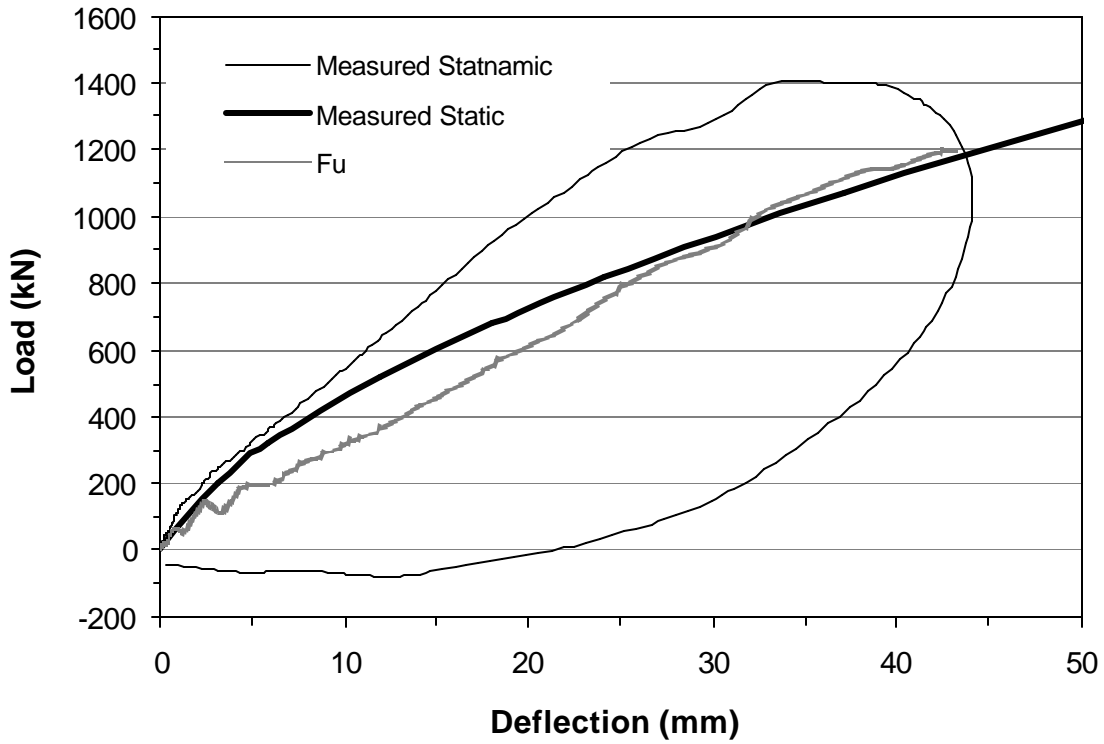
Figure 12.18 Measured statnamic results and derived results from the Unloading Point Method analysis of statnamic test 3 for the 15 pile group.
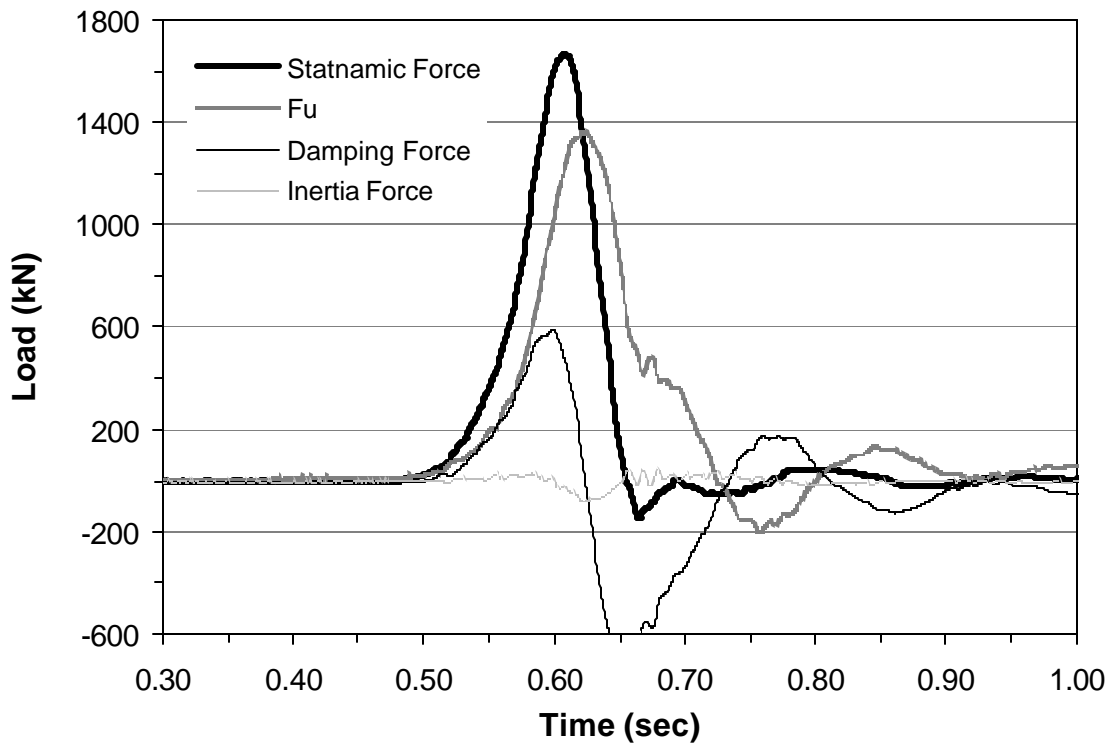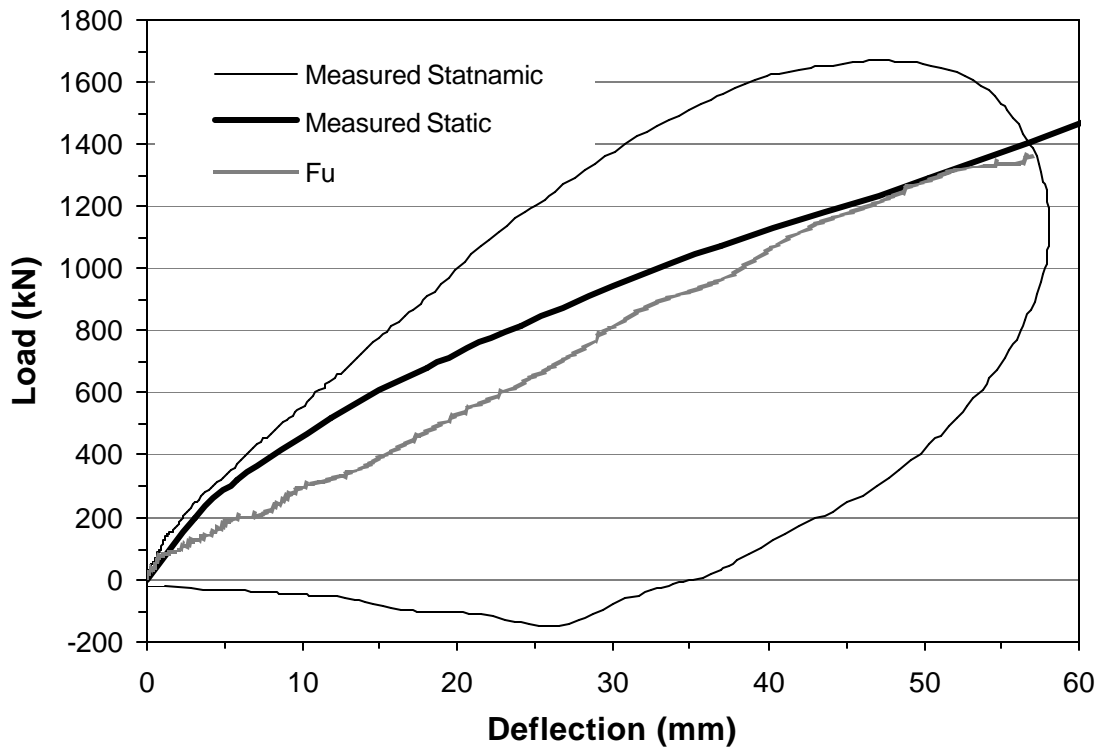
Figure 12.19 Measured statnamic results and derived results from the Unloading Point Method analysis of statnamic test 4 for the 15 pile group.
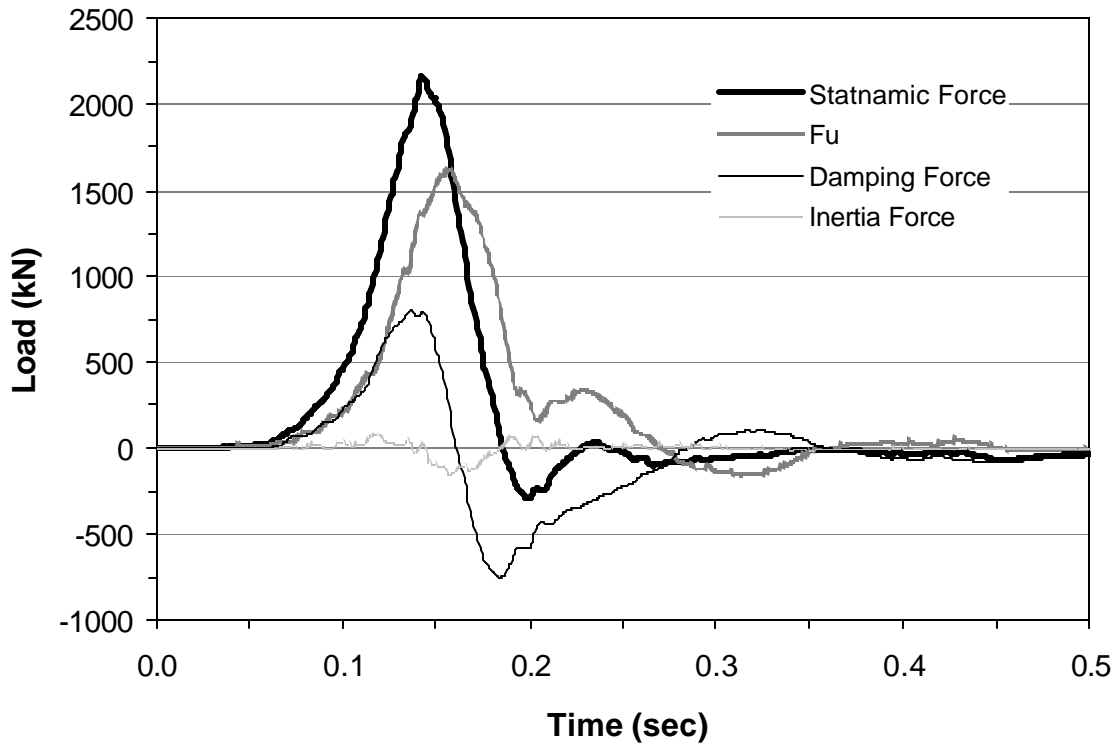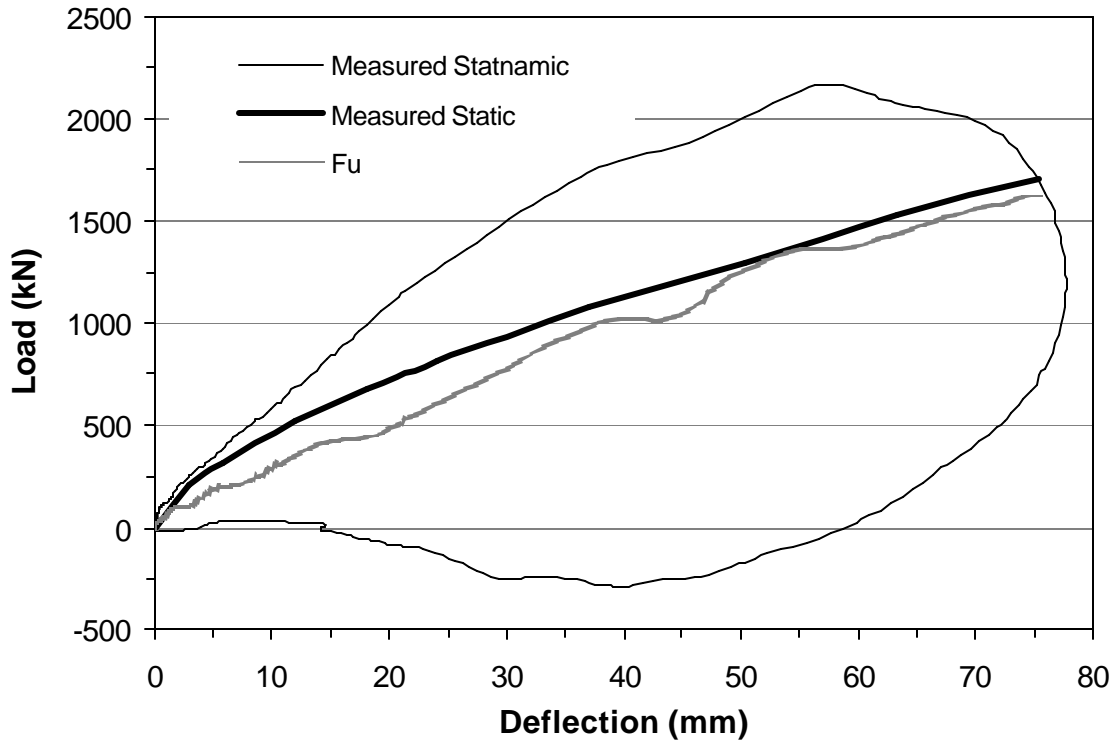
Figure 12.20 Measured statnamic results and derived results from the Unloading Point Method analysis of statnamic test 5 for the 15 pile group.
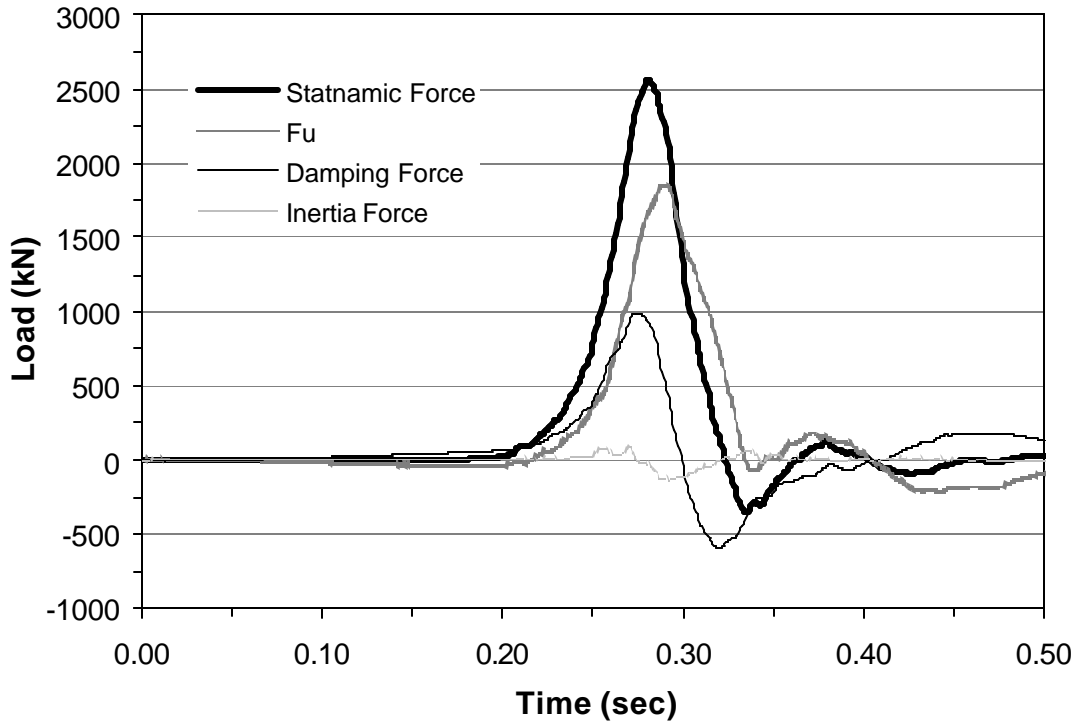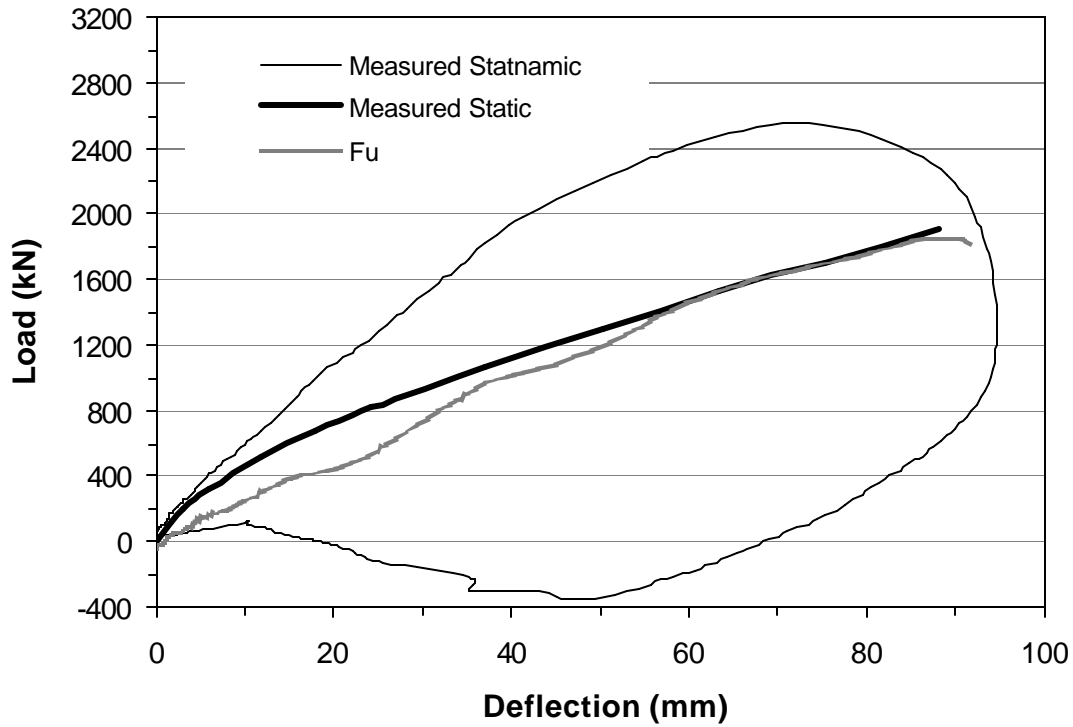
Figure 12.21 Measured statnamic results and derived results from the Unloading Point Method analysis of statnamic test 6 for the 15 pile group.

tests 1 through 6 indicating that damping resistance produces a considerable force which is greater for virgin loading than for reloading conditions.

Table 12.2 provides a summary of the natural frequency, natural period, static stiffness, damping coefficient, critical damping coefficient and damping ratio for each statnamic test. The natural frequency and period were computed using equations 12.7 and 12.8, respectively. The natural period for the 15 pile group ranged from 0.026 to 0.045 seconds, which is quite similar to that for the nine pile group (approximately 0.027 to 0.31 seconds). The rise times are still considerably longer than the natural period of the structure.

The value of k was estimated as the slope of the static load deflection line and was considerably less than that for the nine pile group. The damping coefficient was also 50 to 80% of that computed for the nine pile group. The critical damping coefficient for each statnamic test was again calculated using equation 12.9 to provide a better comparison of the damping in each pile group. While the damping ratio was essentially zero for the first test involving reloading, the damping ratio was typically between 1.62 and 1.70 for the virgin loading cases. These high damping ratios are very similar to the range of damping ratios (1.61 to 1.86) computed previously for the nine pile group. The exception to this rule was the fifth test where the computed damping ratio was only 1.36.

Table 12.2: Summary of statnamic analysis data for 15 pile group.

Test	Load Condition	Natural Frequency, f Hz	Natural Period, T Sec.	Spring Stiffness K kN/mm	Damping Coeff. C kN-sec/m	Critical Damping Cc kN-sec/m	Damping Ratio, C/Cc kN-sec/m
1	Reload	39.0	0.026	66	0	0	0
2	Virgin	34.5	0.029	51	800	471	1.70
3	Virgin	27.5	0.036	33	621	382	1.63
4	Virgin	25.9	0.039	29	579	357	1.62
5	Virgin	24.6	0.041	26	456	336	1.36
6	Virgin	22.4	0.045	21	509	299	1.70

In Figure 12.22, all of the derived load (F_u)-deflection curves from the six statnamic tests are plotted together along with the measured static load-deflection curve. The static curve is the peak load-deflection curve obtained from the test conducted in the opposite direction to that for the statnamic tests as described in Chapter 7. The consistency in the curve shapes for the various statnamic tests is very good. During the virgin loading segment of a given load-deflection test, there is a clear indication of greater resistance and the derived static load-deflection curves plot close to the measured static curve. However, for re-loadings, the resistance drops considerably due to the formation of gaps in front of the piles. The load-deflection curves for the various statnamic tests for reloading conditions lie nearly on top of each other, although there is some drop-off in resistance with each load cycle as was also observed during the static cyclic testing.
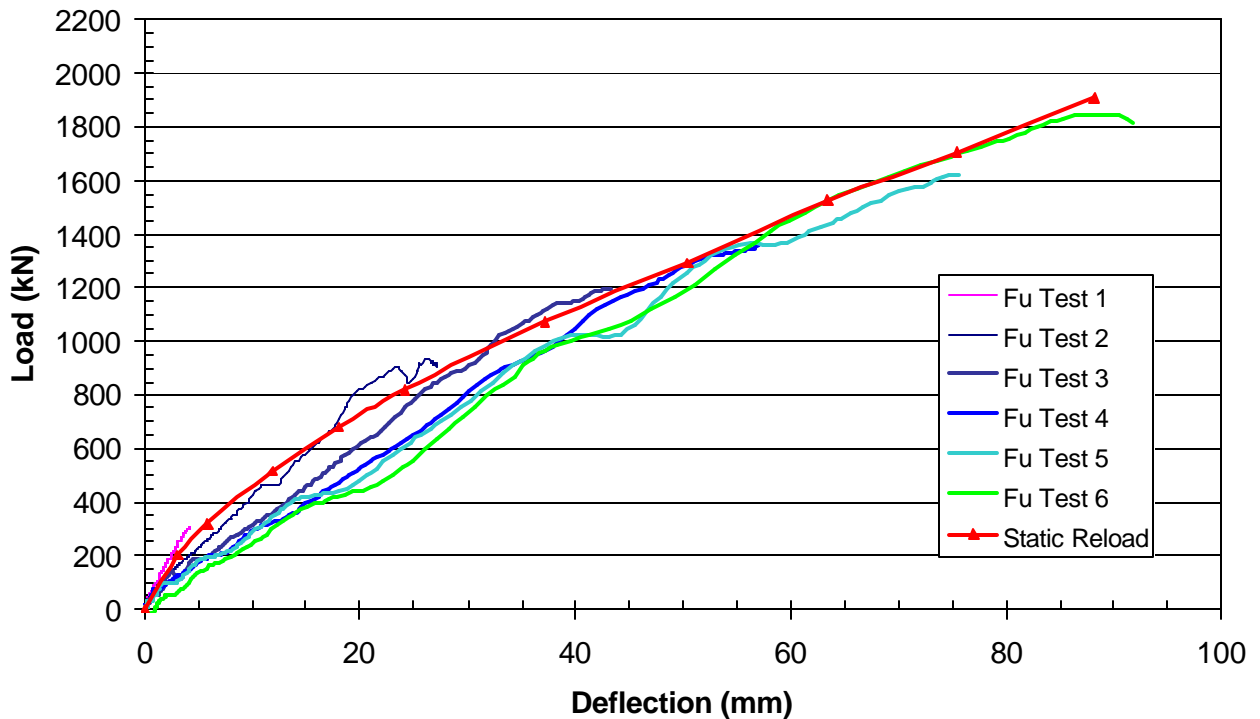
Figure 12.22 Comparison of derived static load-deflection curves from six statnamic tests with measured static load-deflection curve.

CHAPTER 13 SUMMARY AND CONCLUSIONS

SUMMARY

Static lateral load tests were conducted on three single piles and four pile groups at center-to-center spacings of 3.0, 3.3, 4.4 and 5.6 pile diameters. The pile groups had three to five rows with three piles in each row and the test piles consisted of 0.61 m and 0.324m OD steel pipe piles. Fifteen cycles of loading were applied at each deflection increment to evaluate the effect of cyclic loading and gap formation on lateral resistance. The load carried by each pile was measured along with deflection, rotation and strain along the length of the pile during each of the tests to allow comparisons between the behavior of the pile group and the single pile. In addition, comparisons were made between the measured and calculated model values using the computer programs LPILE (Reese and Wang, 1997), GROUP (Reese and Wang, 1996), and FLPIER (Hoit et al, 2000). An idealized soil profile based on the geotechnical investigation was used in the computer analysis. Once the measured load versus deflection curve for the single pile was successfully modeled with LPILE, the same soil profile was used in GROUP to back-calculate appropriate p-multipliers for each group.

In addition to the static load tests, dynamic load tests were performed on two pile groups using the Statnamic loading system. Comparisons between static and dynamic performance were made and the unloading point method was employed to separate the measured resistance into static spring stiffness, damping, and inertia force components. The interpreted static resistance was compared with measured static resistance to evaluate the analysis method.

CONCLUSIONS BASED ON THE STATIC SINGLE PILE TESTING AND ANALYSIS
  - ➢ When the lateral load resistance was divided by the pile cost, the 324 mm pipe pile was slightly more economical than the 610 mm pipe pile.

➢ The formation of a gap due to cyclic loading led to a decrease in the stiffness of both the single piles tested in virgin soil as they were repeatedly loaded. The maximum load in the first and fifteenth cycle differed on average by only about 15%; however, at deflections less than the peak value, differences were over 70% and the load-deflection curve was substantially altered.

➢ Loading of a pile in a direction that is 90 degrees to a previous loading resulted in a significant drop in resistance and a more linear load-deflection curve than the initial curve due to the formation of gaps.

➢ On average, the bending moments of the fifteenth cycle were 15% greater than those of the first cycle due to the softening of the profile and formation of a gap around the pile.

➢ The load versus deflection, load versus maximum moment, and bending moment versus depth profiles computed using LPILE (Reese and Wang, 1997) and FLPIER (Hoit et al., 2000) compared very well with measurements made during the full-scale tests for virgin loading conditions; however, poor agreement was obtained for the reloading conditions.

➢ FLPIER and LPILE do not have an option to account for the gap that develops as a pile is cyclically loaded. Three soil profiles with varied shear strengths in the upper portions of the profile were necessary to adequately model the behavior of the pile loaded in the presence of the gap.

➢ Improvement in p-y curves to account for soil gapping are essential to accurately model the response of piles and pile groups subjected to cyclic lateral loads and additional research should be directed at this important problem.

**CONCLUSIONS BASED ON THE STATIC FREE -HEAD PILE GROUP
TESTING AND ANALYSIS**

➢ The lateral resistance of the piles in the group was a function of row location within the group, rather than location within a row. Contrary to expectations based on the elastic theory, the piles located on the edges of the group did not consistently carry more load than those located within the group.

➢ The front row piles in the groups carried the greatest load, while the second and third row piles carried successively smaller loads for a given displacement. However, the fourth and fifth row piles, when present, carried about the same load as the third row piles. The back row piles often carried a slightly higher load than that in the piles in the preceding row. This finding is consistent with test results reported by Rollins et al (1998) and McVay et al (1998).

➢ Average lateral load resistance was a function of pile spacing. Very little decrease in lateral resistance due to group effects was observed for the pile group spaced at 5.6 pile diameters; however, the lateral resistance consistently decreased for pile groups spaced at 4.4, 3.3 and 3.0 pile diameters on centers.

➢ Group reduction effects typically increased as the load and deflections increased up to a given deflection but then remained relatively constant beyond this deflection. The deflection necessary to fully develop the group effects increased as the pile spacing increased. This increase in required deflection is likely related to the increased movement necessary to cause interaction between failure zones.

➢ For a given load, the maximum bending moments in the trailing row piles were greater than those in the lead row and occurred at somewhat greater depths due to group interaction effects, which essentially softened the lateral soil resistance against the

trailing row piles relative to the leading row piles. This effect was also observed in full-scale group tests conducted by Brown et al (1988).

➤ For a given deflection, the maximum bending moments in the trailing row piles were lower than those in the lead row due to group interaction effects. This occurs because the load carried by the trailing row piles is lower than that carried by the lead row piles for a given deflection level.

➤ The reduction in maximum lateral resistance due to cyclic loading of the pile group was similar to that of the single isolated pile. For the free-head group tests, the average reduction in load between the first and fifteenth cycle was about 16%.

➤ Back-calculated p-multipliers based on the test results increased as the pile spacing increased from 3 diameters to 5.6 diameters. Extrapolation of the test results suggests that group reduction effects can be neglected for spacings greater than about 7 to 8 pile diameters.

➤ The p-multipliers back-calculated for the 610 mm diameter piles at a 3.0 pile diameter spacing were essentially the same as the p-multipliers for the 324 mm diameter piles at a 3.3 pile diameter spacing. These results suggest that pile stiffness does not significantly affect p-multipliers.

➤ Current recommendations for p-multipliers in GROUP (Reese et al, 1996) are unconservative and overestimate the lateral resistance for closely spaced pile groups. Based on the full-scale test results, more accurate design curves have been developed for three general cases: (a) front piles, (b) second row piles and (c) other trailing row piles, as shown in Fig. 10.35.

- The results generated using GROUP (Reese et al, 1996) and Florida Pier version 1.71 NT (Hoit et al., 2000) correlated well with those of the full-scale test when the p-multipliers developed in this test program were employed. Use of the default p-multipliers chosen by the programs led to an under-prediction of the deflection by GROUP and an over prediction of the deflection by FLPIER at a given load.

- The behavior of the pile group for the fifteenth cycle could be reasonably modeled using the same p-multipliers developed for the first cycle once the soil profile was softened to account for the gap that formed during the cyclic testing.

CONCLUSIONS BASED ON THE FIXED-HEAD TESTING AND ANALYSIS

- The stiffness of the fixed-head pile group was 60 to 70% greater than that for the same pile group under free-head conditions even though gaps had formed around the piles due to previous loadings. The restraint provided by the boundary conditions is an important factor in evaluating the lateral resistance of a pile group.

- The measured load-deflection curve for the fixed-head pile group correlated well with the curves computed using GROUP (Reese and Wang, 1996) and Florida Pier version 1.71 NT (Hoit et al., 2000) when the p-multipliers that were back-calculated during the free-head test were used in modeling the behavior of the fixed-head group. Use of the default p-multipliers would, however, lead to errors.

- Tests involving both the geopier footing and the fixed-head pile group indicated that the pile group carried approximately 85% of the lateral load when the pile group was in compression and the geopier group was in tension. When the pile group was in tension and the geopier group was in compression, the pile group carried approximately 60% of the lateral load.

13-5

➢ The lateral load-deflection relationship for the pile group remained essentially the same even when significant axial compression or tension forces were applied to the group. In contrast, the lateral resistance of the geopier group increased when an axial compressive force was applied and decreased when an axial tensile force was applied.

CONCLUSIONS BASED ON THE STATNAMIC FREE- HEAD PILE GROUP TESTING AND ANALYSIS

➢ The statnamic loading system was able to produce displacement, velocity and frequency content similar to what might be produced by a large magnitude earthquake, but the pile group acceleration (3 to 10 g's) was significantly higher than would be produced by an earthquake. In addition, the load pulse duration was significantly longer than the natural period of the pile group.

➢ For virgin soil conditions, the lateral resistance during dynamic (statnamic) loading was significantly higher than for static loading at a given deflection. However, for reloading conditions, the dynamic resistance was about the same or only slightly higher than the static resistance.

➢ Group effects clearly influenced the lateral response during the statnamic testing under virgin soil conditions and lateral resistance was still a function of row location. The lead row piles nearly always carried the highest loads with trailing row piles carrying lesser loads. Nevertheless, for the 15 pile group, the back row piles often carried loads similar to those carried by the front row piles at a given deflection. In addition, group reduction effects were less significant for the statnamic loading relative to the static loadings.

➢ Group effects were much less pronounced during the statnamic tests involving reloading because of the gaps that formed in front of the piles. When the lateral pile deflection was less than the gap width, the lateral resistance was provided primarily by the pile only. Since there was little soil resistance, there was also little group effect.

➢ As with the static testing, no consistent pattern was observed in the load distribution within a row.

➢ The depths to the maximum bending moment and to zero moment were approximately the same during the statnamic testing as they were during the static testing.

➢ Although the dynamic response of a pile group is a complex, non-linear, three-dimensional problem, the unloading point method, which employs a one-dimensional mass-spring-dashpot analogy with a constant damping coefficient, provided a remarkably good estimate of the measured static load-displacement curves in most cases.

➢ Based on sensitivity studies, the equivalent mass used in the unloading point method should be set equal to the mass of the piles above the ground surface.

➢ The analysis of the response of both pile groups strongly suggests that the difference in the static and dynamic response is primarily attributable to damping resistance and that inertia forces are relatively minor. Damping was relatively small for reloading conditions, but the foundation was heavily damped (damping ratios greater than one) for virgin loading conditions.

➢ Based on the test results, soil damping at large displacement levels appears to have a significant influence on the lateral load response of piles and pile groups. Additional research funding should be directed at better understanding this phenomenon and how damping may decrease for cyclic loadings.

REFERENCES

Applied Technology Council (1996). ATC-32, Improved Seismic Design Criteria for California Bridges: Provisional Recommendations, Arlington, Virginia, 215 p.

AASHTO (2000). *Bridge Design Specifications*, American Association of State Highway and Transportation Officials, Washington, D.C.

Baguelin, F., Jezequel, J.F., and Shields, D.H. (1978). *The Pressuremeter and Foundation Engineering*, TransTech Publications, Clausthal-Zellerfeld, W. Germany,

Berminghammer, Inc. (1994). "Nuese River foundation testing site,

Jacksonville, North Carolina", North Carolina Department of

Transportation, S9410.

Berminghammer, Inc. (1995). "Camp Johnson testing site,

Jacksonville, North Carolina.", North Carolina Departmen *t of*

Transportation, S9413.

Bjerrum, L. (1974). "Problems of soil mechanics and construction on soft clays," Norwegian Geotechnical Institute, Publication No. 110, Oslo, Norway

Briaud, J-L, (1992). *The Pressuremeter*, Balkema, Rotterdam, The Netherlands, 321 p.

Brown, D.A. (1993). "Evaluation of static capacity of deep foundations from statnamic testing." *Geotechnical Testing Journal*, ASTM, Vol.17, No. 14.

Brown, D.A., (2000). "STATNAMIC lateral load response of two deep

foundations." STATNAMIC Loading Test '98. Kusakabe, Kuwabara &

Matsumoto (eds), Balkema, Rotterdam, pp. 415 -422.

Brown, D.A., Morrison, C., and Resse, L.C. (1988). "Lateral load behavior of a pile group in sand." *Journal of Geotechnical Engineering.* ASCE, Vol.114, No. 11, pp. 1261-1276.

Brown, D.A., Resse, L.C., and O'Neill, M.W. (1987). "Cyclic lateral loading of a large-scale pile group." *Journal of Geotechnical Engineering.* ASCE, Vol.113, No. 11, pp.1326-1343.

Brown, D.A., and Shie, C. F. (1991). "Modification of p-y curves to account for group effects on laterally loaded piles." *Geotechnical Engineering Congress Volume 1*, pp. 479-490.

Brungraber, R.J. and Kim, J.B. (1976). "Full-scale lateral load tests of pile groups." *Journal of Geotechnical Engineering.* ASCE, Vol.102, No. GT1, pp. 87-105.

Canadian Geotechnical Society (1985). *Canadian Foundation Engineering Manual,* 2nd Edition, BiTech Publishers Ltd.

Cox, W.R., Dixon, D.A., and Murphy, B.S. (1984). "Lateral load tests of 25.4 mm diameter piles in very soft clay in side-by-side and in-line groups*" Procs. of Laterally Loaded Deep Foundations; Analysis and Performance*, ASTM, SPT 835.

Dunnavant, T.W. and O'Neill, M.W. (1986). "Methodology for analysis of laterally loaded pile groups," *Third Intl. Conf. on Numerical Methods in Offshore Piling*, IFDP/LCPC, Nantes, France, p. 303-316.

Hoit, M., Hays, C., and McVay, M. (1997). "The Florida Pier analysis program methods and models for pier analysis and design." *Transportation Research Record 1569*, Transportation Research Board, National Research Council, Washington, D.C., 1-7.

Kotthaus, M., Grundhoff, T., Jessberger, H. L. (1994). "Single piles and pile rows subjected to static and dynamic lateral loads." *Proc., Int. Conf. Centrifuge '94*, C. F. Leung, F. H. Lee, and T. S. Tan, eds., A. A. Balkema, Rotterdam, The Netherlands, 497-502.

Kulhawy, F. H. and Mayne, P. W. (1990). *Manual on Estimating Soil Properties for Foundation Design*, Electric Power Research Institute, Palo Alto, California, Research Report EERI EL-6800.

Lawton, E. (2003). "Performance of Geopier-supported foundations during simulated seismic tests on Northbound Interstate 15 bridge over South Temple, Salt Lake City, Utah", Research Division, Utah Department of Transportation,

McClelland, B., and Focht, J.A., Jr. (1958). "Soil modulus for laterally

*l*oaded piles." Transactions , ASCE, Vol. 123, p. 1049-1086.

McVay, M., Bloomquist, D., Vanderline, D., and Clausen, J. (1994).

"Centrifuge modeling of laterally loaded pile groups in sands."

Geotechnical Testing Journal, GTJODJ, Vol. 17, No. 2, p. 129-137   .

McVay, M., Casper, R., and Shang, T. (1995). "Lateral r esponse of

three-row groups in loose to dense sands at 3D and 5D pile spacing.   "

Journal of Geotechnical Engineering, ASCE Vol. 121, No. 5, pp. 436-

441.

McVay, M., Shang, T., and Casper, R. (1996). "Centrifuge Testing of Fixed-Head Laterally Loaded Battered and Plumb Pile Groups in Sand," *Geotechnical Testing Journal*, GTJODJ, Vol. 19, No. 1, pp. 41-50.

McVay, M., Zhang, L., Molnit, T., and Lai, P. (1998). "Centrifuge testing of large laterally loaded pile groups in sands." *Journal of Geotechnical and Geoenvironmental Engineering*, ASCE, Vol. 124, No. 10, p. 1016-1026.

Meimon, Y., Baguelin, F. and Jezequel, J.F. (1986). "Pile group behavior under long term lateral monotonic and cyclic loading." *Proc., Third Int'l Conf. on Numerical Methods in Offshore Piling*, Inst. Francais Du Petrole, Nantes, p. 286-302.

Middendorp, P., Bermingham, P., and Kuiper, B. (1992). "Statnamic load testing of foundation piles," *Proc., Fourth Int'l Conf. on the Application of Stress-Wave Theory to Piles*, The Hague, The Netherlands, p. 581-588.
Middendorp, P. and Daniels, B. (1996). "The influence of stress wave phenomenon during load testing," *Proc., Fifth Intl. Conf. on the Application of Stress-Wave Theory to Piles*, TNO Building and Construction Research, Orlando, Florida.

Nishimura, S. and Matsumoto, T. (1995). "Wave propagation analysis during statnamic loading of a steel pipe pile," *Proc., First Intl. Statnamic Seminar*, Vancouver, British Columbia, Canada.

O'Neill, M.W. and Murchison, J.M. (1983). "An evaluation of p-y relationships in sands" A Report to the American Petroleum Institute, PRAC 82-41-1. University of Houston, Texas

Prakash, S. and Sharan, S. (1967) "Behavior of laterally-loaded piles in cohesive soil." *Third Asian Conference on Soil Mechanics and Foundation Engineering*, Vol. 1, p. 235-238.

Prakash, S. and Sharan, S. (1990) *Pile Foundations in Engineering Practice*, John Wiley and Sons, p. 392-393.

Resse, L.C. (1986). *Handbook on the design of piles and drilled shafts under lateral load*, Report No. FHWA-IP-84-11, Federal Highway Administration.

Resse, L.C. (1986). *Behavior of piles and pile groups under lateral load*, Report No. FHWA/RD-85/106, Federal Highway Administration.

Reese, L.C., Cox, W.R., and Koop, F.D. (1974). "Analysis of laterally loaded piles in sand," *Proceedings, VI Annual Offshore Technology Conference*, Houston Texas, 2(OTC 2080) p. 473-485.

Reese, L.C., Cox, W.R., and Koop, F.D. (1975). "Field testing and analysis of laterally loaded piles in stiff clay." *Proceedings,VII Annual Offshore Technology Conference*, Houston, Texas, 2(OTC 2312), p. 672-690.

Reese, L.C. and Wang, S.T. (1997). *LPILE plus 3.0 for Windows technical manual*, Ensoft, Inc. Austin, Texas.

Reese, L.C., Wang, S.T., Arrellaga, J.A., and Hendrix, J. (1996). *GROUP version 4.0 for Windows users manual*, Ensoft, Inc. Austin, Texas.

Reese, L.C. and Welch, R.C. (1975). "Lateral loading of deep foundations in stiff clay," *J. of Geotechnical Engineering Division*, ASCE, Vol. 101, No. GT7, p. 633-649.

Remaud, D., Garnier, J., and Frank, R. (1998). "Laterally loaded piles: investigation of group effects." *Proc., Int. Conf. Centrifuge '98*, C. F. Leung, F. H. Lee, and T. S. Tan, eds., A. A. Balkema, Rotterdam, The Netherlands, p. 497-502.

Robertson, P.K. and Campanella, R.G. (1988). *Guidelines for using the CPT, CPTU and Marchetti DMT for geotechnical design*, U.S. Department of Transportation, Federal Highway Administration, Office of Research and Special Studies, Report No. FHWA-PA-87-023+84-24.

Rollins, K. M., Peterson, K. T., and Weaver, T. J. (1998). "Lateral load behavior of full-scale pile group in clay." *J. of Geotechnical and Geoenvironmental Engineering*, ASCE, Vol. 124, No. 6, p. 468–478.

Ruesta, P.F. and Townsend, F.C. (1997). "Evaluation of laterally loaded pile group at Roosevelt Bridge.", *J. of Geotechnical and Geoenvironmental Engineering*, ASCE, Vol. 123, No. 12, pp. 1153-1161.

Seed, H.B., Idriss, I.M., Makdisi, F., and Banerjee, J. (1975). "Representation of Irregular Stress Time Histories by Equivalent Uniform Stress Series in Liquefaction Analysis", *Report No. EERC 75-29,* Earthquake Engineering Research Ctr., Univ. of Calif., Berkeley, CA.

Seed, H.B. and Idriss, I.M. (1982). *Ground Motions and Soil Liquefaction*, Monograph, Earthquake Engineering Research Institute, Oakland, California.

US Army (1993). *Design of Pile Foundations,* Technical Engineering and Design Guides No. 1, U.S. Army Corps of Engineers, Washington, D.C.

US Navy (1982). *Foundations and Earth Structures-Design Manual 7.2*, NAVFAC DM-7.2., Naval Facilities Engineering Command, Department of the Navy, Washington, D.C.

Weaver, T.J., Rollins, K.M., and Peterson, K.T. (1998). "Lateral statnamic load testing and analysis of a pile group." *Geotechnical Earthquake Engineering and Soil Dynamics III*, ASCE, Vol. 2, Geotechnical Special Publication No. 75, pp. 1319-1330.

WSDOT (2000) *Bridge Design Manual*, Washington State Department of Transportation, Olympia, WA.

Zhang, L., McVay, M., and Lai, P. (1999). "Numerical analysis of laterally loaded 3 X 3 to 7 X 3 pile groups in sands." *J. of Geotechnical and Geoenvironmental Engineering*, ASCE, Vol. 125, No. 11, pp. 936-946.
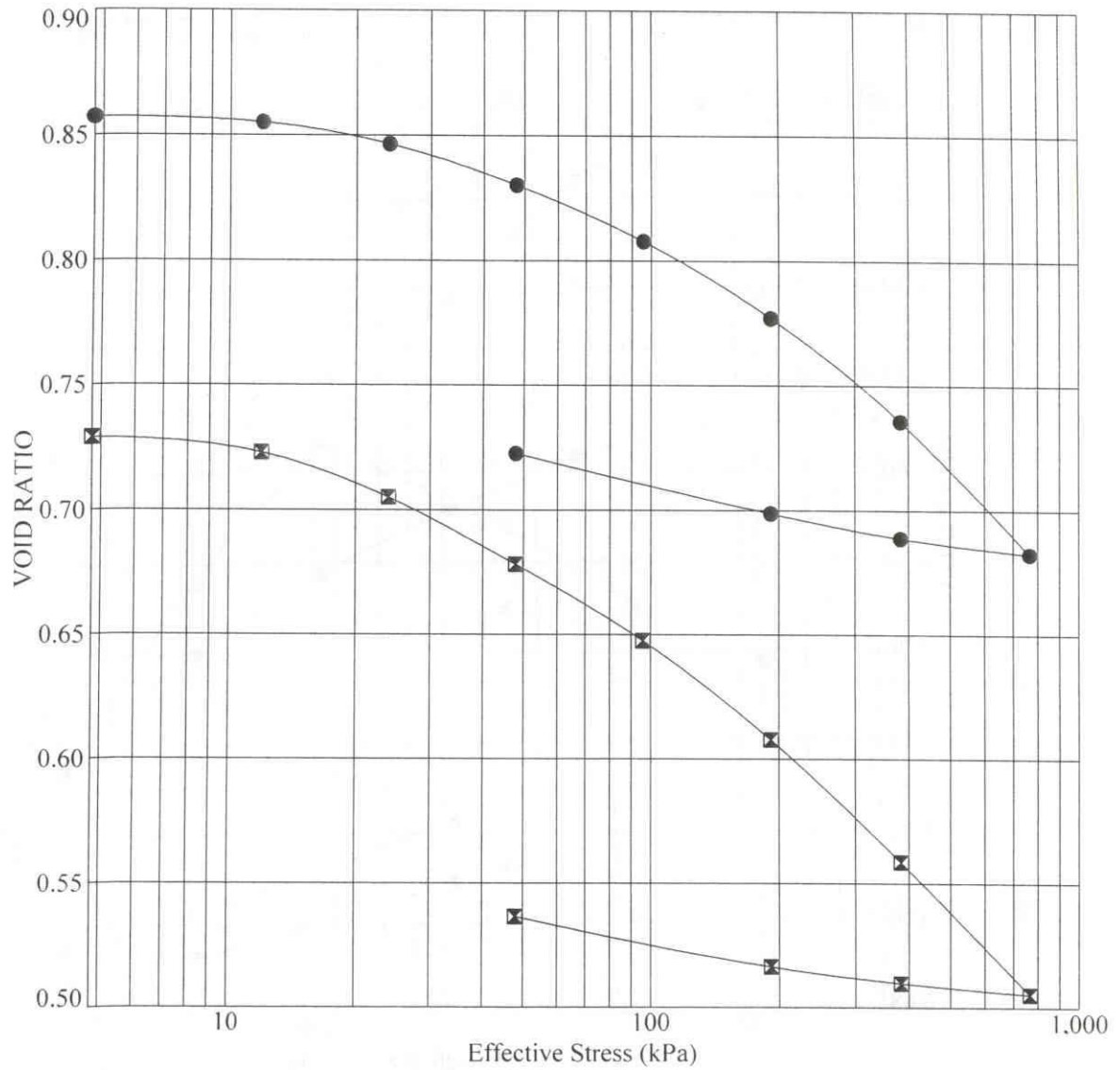
	Sample	Depth	USCS				Dry Unit Weight (kN/m³)		Moisture Content (%)	
ID		(m)	Classification	C_C	C_r	OCR	Initial	Final	Initial	Final
●	DH- 1	0.24	Lean CLAY (CL)	0.185	0.03	29.7	14.0	15.1	31.7	29.0
⊠	DH- 1	1.92	Lean CLAY (CL)	0.2	0.025	2.4	15.3	17.2	23.9	23.0

ONE-DIMENSIONAL CONSOLIDATION TEST
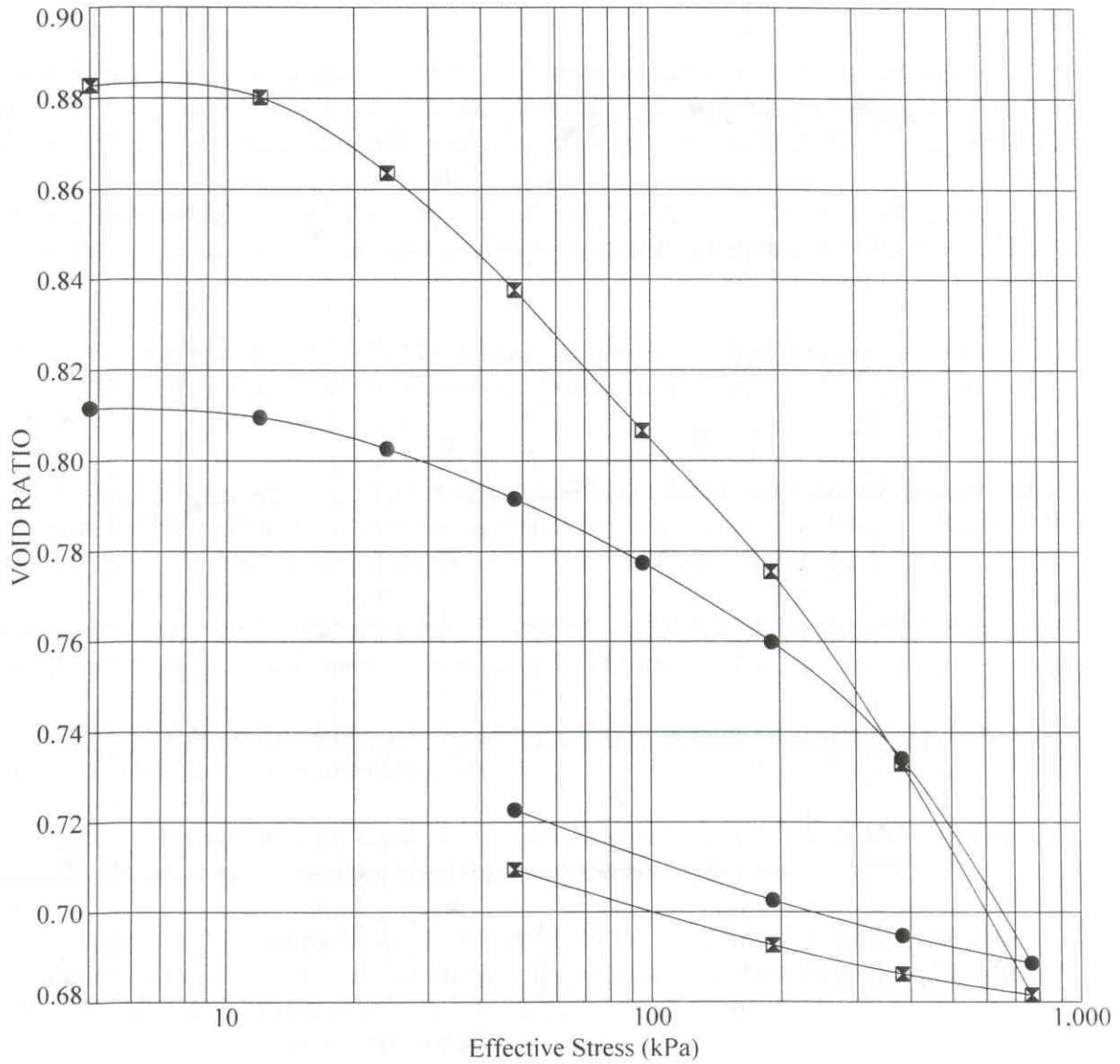
	Sample	Depth	USCS				Dry Unit Weight (kN/m³)		Moisture Content (%)	
	ID	(m)	Classification	C_c	C_r	OCR	Initial	Final	Initial	Final
●	DH-1	2.47	Lean CLAY (CL)	0.19	0.025	2.8	14.8	15.6	28.6	27.7
⊠	DH-1	3.60	Lean CLAY (CL)	0.19	0.025	1.6	14.0	15.4	30.4	27.4

ONE-DIMENSIONAL CONSOLIDATION TEST
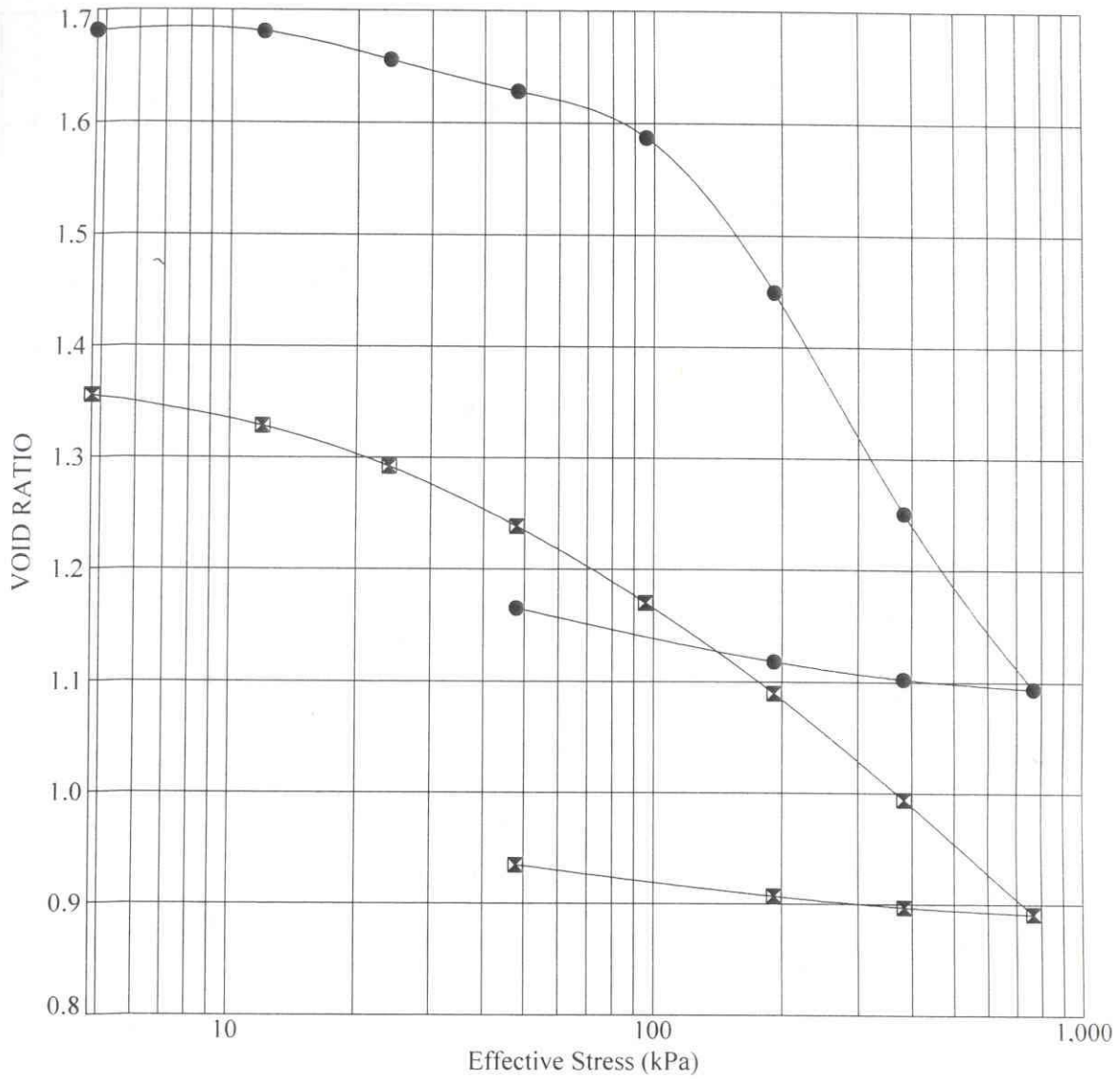
	Sample	Depth	USCS				Dry Unit Weight (kN/m^3)		Moisture Content (%)	
	ID	(m)	Classification	C_C	C_r	OCR	Initial	Final	Initial	Final
●	DH- 1	5.36	Fat CLAY (CH)	0.57	0.06	1.3	10.1	12.5	59.3	41.4
⊠	DH- 1	6.34	Fat CLAY (CH)	0.42	0.04	1.3	11.0	13.4	51.9	36.3

ONE-DIMENSIONAL CONSOLIDATION TEST
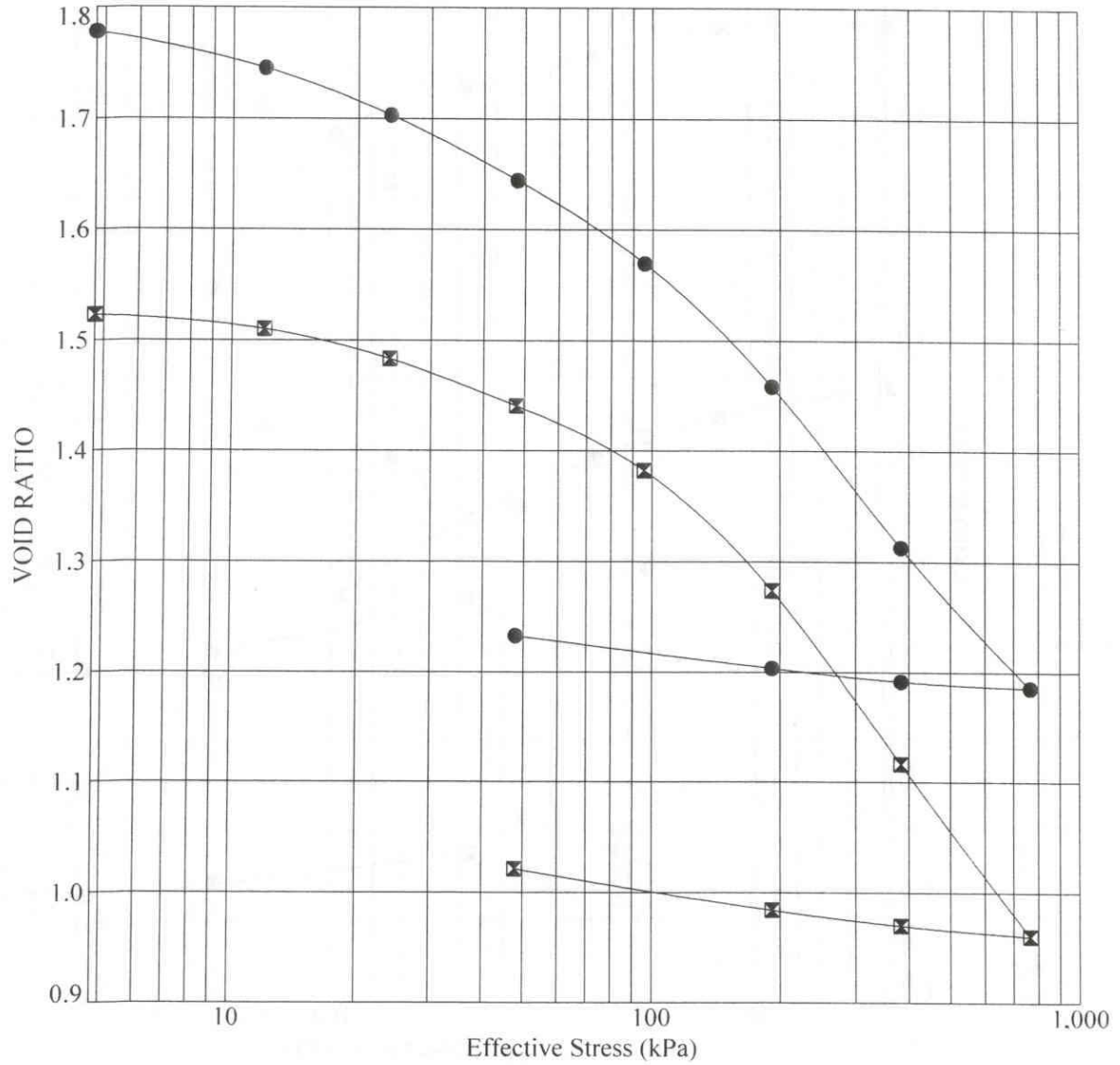
Sample	Depth	USCS				Dry Unit Weight (kN/m³)		Moisture Content (%)	
ID	(m)	Classification	C_c	C_r	OCR	Initial	Final	Initial	Final
● DH-1	8.93	Fat CLAY (CH)	0.535	0.04	1.1	9.8	12.2	62.2	42.5
⊠ DH-1	10.30	Fat CLAY (CH)	0.62	0.05	1.1	10.7	13.3	53.7	36.8

ONE-DIMENSIONAL CONSOLIDATION TEST